C by Thesis.

REACTIVITY OF SOME COMPLEX HYDROCARBONS ON CONSTANT AND VARIABLE ACTIVITY REFORMING CATALYSTS

BY

O. D. ONUKWULI

B.Sc. (CHEM. ENG.); M.Sc. (CHEM. ENG.)

VESZPREM UNIVERSITY OF CHEMICAL ENGINEERING, HUNGARY

A THESIS SUBMITTED TO THE SCHOOL OF POSTGRADUATE STUDIES
IN PARTIAL FULFILMENT OF THE REQUIREMENTS FOR THE DEGREE OF
DOCTOR OF PHILOSOPHY
IN THE DEPARTMENT OF CHEMICAL ENGINEERING
UNIVERSITY OF LAGOS, NIGERIA

APRIL, 1988.

D E D I C A T I O N

To my Dad Chief M. N. Onukwuli (1908-1983):

Mum Mrs. Mercilina Onukwuli

and

To Chief Simeon N. Akukalia

ABSTRACT

The product distributions, kinetics and catalyst mortality of the reforming reactions of n-octane, iso-octane and methylcyclopentane (MCP) were investigated on constant and variable activity Pt/Al_2O_3 and $Pt-Re/Al_2O_3$ catalysts. The Berty CSTR was used for data collection at total pressure of 1atm, various reactant and H_2 diluent partial pressures, W/F and temperatures, depending on the reactant.

The dehydrocyclization of n-octane on $0.3\%Pt/Al_2O_3$ catalyst was investigated at temperatures between 400°C and 460°C in H_2. The products of the reaction were: hydrocracked products, iso-octane, ethylbenzene, m-xylene, p-xylene, o-xylene and toluene. Experimental data showed that the yields of cracked products and aromatics generally increase with increase in W/F and temperature, but the aromatic yield decreased with increase in n-octane partial pressure. Results obtained with varying hydrogen partial pressures showed that, at constant temperature, the total conversion and the yield of aromatics each passed through a maximum.

Another n-octane isomer (1,1,3- trimethylpentane) was the sole product of the reaction of 2,2,4 trimethyl-pentane (iso-octane) on Pt/Al_2O_3 catalysts at temperatures between 390°C and 430°C. The conversion of iso-octane on $0.6\%Pt/Al_2O_3$ catalyst was found to be approximately the same as that obtained with $0.3\%Pt/Al_2O_3$ catalyst at the same conditions.

The reactions of MCP on $0.3\%Pt/Al_2O_3$ and $0.3\%Pt-0.3\%Re/Al_2O_3$ catalysts were studied at temperatures between 370°C and 410°C and MCP partial pressures between 0.058atm and

0.1816atm. At these conditions, the products of reaction were: hydrogenolysis products, cyclohexane and benzene. The beneficial effect of rhenium in Pt-Re/Al_2O_3 catalyst was clear from the total conversion and benzene yield obtained with Pt-Re /Al_2O_3 (DRIED) catalyst. Experimental results showed that the total conversion and benzene yield obtained with the Pt-Re/Al_2O_3 (DIRED) catalyst was about 1.5 times greater than that obtained when the bimetallic catalyst was not dried before reduction. In addition to the high conversion and high benzene yield, the dried bimetallic catalyst was found to be more stable than both the Pt/Al_2O_3 catalyst and Pt-Re/Al_2O_3 (UNDRIED) catalyst.

Mechanistic kinetic equations of these reactions were developed on both steady and unsteady state catalyst surfaces. The development of mechanistic rate equations for the steady state kinetics of n-octane conversion was based on the mechanisms obtained from the modified reaction network proposed by Ako and Susu[1]. Nineteen rate equations were derived and discrimination among rival models was based on positiveness of rate and equilibrium constants, on the goodness of fit and also on the increase of the value of the rate constants with increase in temperature. The rate models that best fitted the data were based on:

1. Dissociative adsorption of hydrogen and conversion of adsorbed n-octane to adsorbed iso-octane as rate limiting step (Eqn. 3.1.5).

2. Dissociative adsorption of hydrogen and desorption of adsorbed iso-octane (Eqn.3.1.6).

3. Dissociative adsorption of hydrogen and conversion of adsorbed iso-octane to adsorbed ethylbenzene as rate limiting step (Eqn.3.1.7)

4. Dissociative adsorption of hydrogen and conversion of adsorbed iso-octane to adsorbed o-xylene as rate limiting step (Eqn.3.1.8)

5. Molecular desorption of hydrogen and conversion of adsorbed n-octane to adsorbed iso-octane as rate limiting step (Eqn.3.1.13)

Good fit and positive values of rate and equilibrium constants were obtained when model Eqns.(3.1.7) and (3.1.8) were used to predict the conversion obtained with varying hydrogen partial pressures at constant temperature.

The kinetic rate equations for the isomerization of iso-octane in the absence of coking (steady-state kinetics) were derived on the basis of the generally accepted mechanism for skeletal isomerization. The rate models that best fitted the data were based on:

1. Reaction of adsorbed unsaturated iso-octane on the acidic site to adsorbed iso-octene as the rate determining step (Eqn.3.1.25)

2. Desorption of iso-octene from the acidic site as the rate determining step (Eqn.3.1.27).

Kinetic rate equations for the aromatization of MCP in the absence of coking (steady state kinetics) were derived on the basis of the reaction network proposed by this author (see chapter 6, section 6.1.3). Eleven rate equations were derived and tested. Five out of the eleven models satisfied the set criteria when Pt/Al_2O_3 catalyst was used for the conversion of MCP. The five rate equations that best fitted the data were based on:

1. The rate model is based on the dehydrogenation of adsorbed methylcyclopentane as the rate determining step (Eqn.3.1.44)

2. The rate model is based on the conversion of adsorbed methylcyclopentene to adsorbed olefinic hydrogenolysis products as the rate determining step. (Eqn.3.1.46)

3. The rate model is based on the hydrogenation of adsorbed olefinic hydrogenolysis products to adsorbed hydrogenolysis products as the rate determining step (Eqn.3.1.48)

4. The rate model is based on the hydrogenation of adsorbed cyclohexene to adsorbed cyclohexane as the rate determining step (Eqn.3.1.49)

5. The rate model is based on the desorption of hydrogenolysis products as the rate determining step (Eqn.3.1.50)

Using the $Pt\text{-}Re/Al_2O_3$(DRIED) catalyst, however, only two rate equations (Eqns 3.1.48 and 3.1.49) satisfied the set criteria.

For deactivation kinetic studies of Pt/Al_2O_3 catalyst iso-octane and MCP were used as reactants while for the deactivation kinetic studies of $Pt-Re/Al_2O_3$ catalyst only MCP reactant was used. The reactant and hydrogen partial pressures were varied. To describe the distribution of products with time, an activity and a deactivation function of the non-separable type was used. Model equations 3.2.11 and 3.2.19 were used to evaluate the constants of deactivation at various values of n(0,1, and 2).

Catalyst mortality experiments were also carried out with all the reactants investigated. Seven deactivation - regeneration cycles were carried out using iso-octane on fresh Pt/Al_2O_3 while forty deactivation - regeneration cycles were carried out with MCP on the Pt/Al_2O_3 catalyst used previously for the mortality study with iso-octane. Twelve deactivation-regeneration cycles were carried out on dried and undried $Pt-Re/Al_2O_3$ catalyst using MCP. Two stability states, characterized by the difference in the coke levels, were established in the life of Pt/Al_2O_3 during the mortality investigation with MCP. The transition from the first state to the second state occured in the 6th cycle. The coke level in the first state was about 0.045gC while the coke level in the second state was about 0.09gC. The coking levels of the reactants investigated were in the order MCP > N-Octane ∿ Iso-Octane.

A C K N O W L E D G E M E N T S

I wish to express wholeheartedly my profound gratitude and sincere appreciation to my supervisor, Professor A.A.Susu, for his invaluable assistance, encouragement and patience throughout the period of this program. The friendly relationship that existed between us is highly appreciated.

My profound gratitude goes to Messrs A.O.F. Williams, E.C.Anumonwo, J.A. Osaheni, Dosunmu and A.R. Olabisi for their help with the computer.

The assistance of Messrs A. Kolaru, S. Ganeshalingam, A. Ajetumobi, Sqm Bamigbetan and A. Reju in the laboratory is highly appreciated.

I need to express my satisfaction with the friendly attitude of all members of academic staff of the Department of Chemical Engineering, University of Lagos. Their friendliness made the atmosphere around the Department conducive for effective study.

My sincere appreciation goes to the following people: Mr. Charles Ekumankama, Kolawole Olajumoke, Nna Ochili, J. Onyeme, A. Okoye, Frank Uzondu, Horace Ngomo, J.T.O.Nwosu, Ifeoma Onwuka, Ijeoma Agbai, Remi Arowomiwura, Angela Udoye, Charles Onyegbado, Frank Ejike, Mike Ejike, Ifeanyi Mbanefo, Eric Nwosu and A. Amaechi. They were all instrumental to the success of this work.

Many thanks to my mother, brothers, sisters and other relations for their concern, patience and understanding during the course of this work.

Special thanks are due to Mr. Mark Anya for the excellent typing of this thesis and to Mr. E.A.Nnenji, for the neat tracing of the graphs.

TABLE OF CONTENTS

LIST OF TABLES

LIST OF FIGURES

LIST OF APPENDICES

CHAPTER ONE

I N T R O D U C T I O N

The catalytic reforming of naphtha is one of the major refinery processes designed to increase the octane number of naphtha or to produce aromatics for the petrochemical industry. In catalytic reforming several reactions occur simultaneously: isomerization, hydrogenation, dehydrogenation, dehydrocyclization and hydrocracking. An undesirable side reaction that occurs simultaneous with reforming reaction is coking. The reforming reactions have been widely studied on chromia-alumina and platinum - alumina catalysts using different C_6-C_8 alkanes, naphthenes and aromatics as model reactions[1-13].

The concept of bifunctional catalysis consists of combining two different functions in one catalyst. The catalyst contains a metal which catalyzes (de) hydrogenation reactions of paraffins into olefins or naphthenes into aromatics and an acidic function which catalyzes skeletal rearrangements of the olefins formed on the metal through carbocation mechanisms. This picture seems to be consistent with the macroscopic phenomena observed in the catalytic reforming. However each of the two catalytic functions are known to catalyze several of the reactions. For example, dehydrocyclization, skeletal isomerization, closure and opening of five and six membered rings as well as the hydrogenolysis of n-alkanes can be catalyzed by the metallic function only. Similarly the acidic function alone can catalyze ring opening, ring closure, isomerization and ring expansion reactions.

Paraffin isomerization can take place on acid sites of the Pt/Al_2O_3 catalyst and on the metal surfaces of the catalyst. When isomerization reactions are catalyzed by the acid component of the catalyst, the mechanism is via a carbonium ion intermediate, but requires a hydride ion abstraction as a first step as illustrated below for n-pentane[14].

$$CH_3CH_2CH_2CH_2CH_3 + Hx \rightleftharpoons CH_3CH_2\overset{+}{C}HCH_2CH_3 + x^- + H_2 \quad (1)$$

$$CH_3CH_2\overset{+}{C}HCH_2CH_3 \rightleftharpoons CH_3\overset{+}{C}H\overset{CH_3}{C}HCH_3 \quad (2)$$

$$CH_3\overset{+}{C}H\overset{CH_3}{C}HCH_3 \rightleftharpoons CH_3\overset{+}{C}HCH_2CH_2CH_3 \quad (3)$$

$$CH_3\overset{+}{C}HCH_2CH_2CH_3 + H_2 + x^- \rightleftharpoons CH_3\overset{CH_3}{C}HCH_2CH_3 + Hx \quad (4)$$

On the other hand, when isomerization reaction occurs on the metal component of the catalyst[16], the paraffin splits off two hydrogen atoms and adsorbs as an olefinic species. Desorption without readdition of the hydrogen gives gas phase olefin:

$$H_3CCH_2CH_2CH_2CH_2CH_3 + 4Pt \rightleftharpoons H_3C\text{-}\overset{H}{\overset{|}{C}}\text{-}\overset{H}{\overset{|}{C}}\text{-}CH_2\text{-}CH_2\text{-}CH_3 + 2Pt$$

$$\text{(Pt, Pt)} \rightleftharpoons 4Pt + H_3C\,CH = CHCH_2CH_2CH_3 + H_2$$

The above mechanism occurs when the paraffin concerned has two adjacent carbon atoms. If the carbon atoms are not

adjacent, an alternative to desorption is the formation of a new C- C bond leading to a five or six membered ring species[105-107].

n-hexane ⟶ Five membered ring ⟶ methylcyclopentane

Species on metal surface

Most of the earlier works on the dehydrocyclization of paraffins were carried out largely on supported non-acidic metal oxide or metal catalysts in continuous vapor phase reactors. The mechanisms of dehyrocyclization of normal and branched chain octanes and trimethylpentanes are now reasonably well understood on chromia - alumina. However, there appears to be some controversy with regard to the mechanism of these aromatization reactions on platinum - alumina, especially when the acidity of the alumina is retained[1].

The kinetics of the isomerization - dehydroisomerization of methylcyclopentane has been considered at low hydrogen pressure[15]. It has been suggested that the rate limiting step is the formation of intermediate methylcyclopentenes via the reaction scheme:[15]

$$MCP \underset{[H]}{\rightleftharpoons} [MCP^{=}] \underset{MCP^{=}}{\rightleftharpoons} [R] \xrightarrow[k_2]{[H]} R'$$

in which the brackets refer to species on the surface and [R] represents surface residue. According to this scheme, methylcyclopentane dehydrogenates on platinum sites to form

methylcyclopentenes, which in turn either desorbs or undergoes further dehydrogenation and polymerization reaction to form the residue [R]. The surface residue is continuously being removed by reaction with adsorbed hydrogen to form gaseous hydrocarbons. Numerous studies have shown that the selectivity of platinum catalysts for the hydrogenolysis of MCP depends on the structure of the catalyst[17,18], on the reaction temperature[17] as well as on the hydrogen pressure.

In catalytic reactions, the catalyst activity is not always constant with time - on - stream. In industrial practice as well as in kinetic measurements, it is desirable to restrict the variations of activities to the possible minimum. On the other hand, a careful examination of the changes of the catalytic activity may greatly contribute to a better understanding of catalytic phenomenon, which might be important in the operation of a commercial plant and also in the future development of more stable catalysts. In addition, a better understanding of catalyst deactivation could lead to catalyst of longer life and can contribute to the basic knowledge on active centres and reaction mechanisms. According to B. Delmon[19] about 50% of the time of professionals working on research and development in catalysis is devoted to deactivation and 90% of the total expenditure concerns this problem.

Catalyst deactivation can occur through several routes and the most common are impurity poisoning, sintering and coking. Impurity poisoning is generally eliminated by purification of the feed to levels below which economic catalyst activity of the catalyst is maintained for the expected

lifetime of the catalyst. Sintering is the effect of a very high temperature on the catalyst whereby there is an agglomeration of the catalyst's active sites due to the free movement of the active elements. This agglomeration of the active sites results in a loss of surface area and consequently, reduction of available active sites for reaction. Sintering of the catalyst is avoidable if the catalyst is not exposed to excessively high temperatures. At the operating conditions of reforming reactors, however, catalyst deactivation due to coke formation posses the greatest economic and technological problems in petroleum refining and petrochemical industry. Coking has the effect of covering the active sites of the catalyst and blocking the catalyst pores. Such coverage or blockage makes the active sites inaccessible for reaction, hence, there is a fall in the activity of the catalyst. A deactivated catalyst is normally regenerated by burning off the coke in air at a high temperature. Care is particularly excercised during the regeneration of the coked catalyst to eliminate run-away temperatures during oxidation. This is assured by using low concentration of oxygen in an inert stream (N_2) for oxidizing the carbonaceous residue on the catalyst surface. Most studies indicate that coke deposits consist of hydrogen deficient mono and polycyclic aromatic rings connected by aliphatic and alicyclic fragments[20]. The rate proportion of each depends on catalyst reaction system. The groups are interconnected to form a pseudographitic structure with different degrees of crystallinity and cross linking which varies with reaction conditions. Hydrogen

plays a key role in decreasing the rate of coke deposition by hydrogenating unsaturated fragments and producing desorbable paraffinic fragments.

At the refinery the gradual loss in activity with time on stream due to deactivation by coke is compensated for by either decreasing the feed flow rate at a given temperature and/or increasing the temperature to ensure specified product quality. However, when the catalyst activity falls below an economically viable level, the coked catalyst is regenerated in an oxygen containing carrier gas. The cycle of deactivation and regeneration is repeated until the catalyst can no longer be revived to an acceptable level of activity. At this point, the catalyst is dead, and it is discarded.

In an attempt to solve the problem of catalyst mortality by coking, the bimetallic platinum - rhenium alumina catalyst ($Pt-Re/Al_2O_3$) catalyst was introduced to the reforming process in 1969. Even though the life and the process condition tolerance of the catalyst have been improved, the problem of mortality is yet to be eradicated. It is not clear why reforming catalysts deactivated by coke cannot be reused for as long as the catalyst pelletts retain their mechanical properties.

From my discussion it has become compelling to investigate more thoroughly the reforming reactions on monometallic Pt/Al_2O_3 and bimetallic $Pt-Re/Al_2O_3$ using a model paraffin (n-octane), a model isoparaffin (iso-octane) and a model naphthene (methylcyclopentane). As is obvious from the literature survey section, these reactions have been little studied even on steady-state catalyst (constant activity catalysis). No significant publication has addressed non

steady-state catalysis (variable activity catalysis) of these reactions. The only significant work on the mortality of Pt/Al_2O_3 and $Pt-Re/Al_2O_3$ catalysts was done in our laboratory and only addressed catalyst mortality from the point of view of the metallic function (cyclohexane dehydrogenation to benzene). For, if catalyst deactivation and mortality studies are to enhance and extend our fundamental catalysis knowledge and contribute to the prolongation of reforming catalyst lifetime, the deactivation and mortality studies must be investigated for those reactions where both catalytic functions are important and several of the reforming reactions are occuring.

The selected model reactions satisfy the above criteria. First, n-octane onversion includes dehydrogenation, isomerization, dehydrocyclization and hydrogenation reactions that require both the metallic and acidic functions of the supported platinum catalyst. Secondly iso-octane conversion further enhances our knowledge of the complex n-octane reaction as it contains a subset (isomerization) of the network of reactions occuring during n-octane conversion. Thirdly, the methylcyclopentane reaction is of special interest because of its enhanced propensity to for coke formation.

In order to understand deactivation catalysis, however, it becomes necessary to thoroughly understand steady-state kinetic behavior of each of the reacting systems selected for investigation. This is because the deactivation rate models must contain kinetic parameters that match those of steady-state kinetics at zero time as deactivation must start on a surface at constant activity.

In view of the above, therefore, our objectives for this investigation are enumerated below. They follow the normal progression from the constant activity catalysis to deactivation catalysis and finally catalyst mortality.

1. To determine the product distributions of the reactions of n-octane, iso-octane and MCP on supported monometallic Pt/Al_2O_3 and supported bimetallic $Pt\text{-}Re/Al_2O_3$ catalysts.

2. To determine the influence of the process variables (temperature, reactant partial pressure, hydrogen partial pressure and W/F) on the product distribution of the hydrocarbons enumerated above on steady (constant activity) and unsteady state (variable activity) catalyst surfaces.

3. To develop mechanistic kinetic and deactivation models for the enumerated hydrocarbon reactions under investigation in this work.

4. To evaluate the rate and equilibrium constants of the models and hence the determination of the activation energies and adsorption energies.

5. To investigate the principles of deactivation by coking leading to the mortality of Pt/Al_2O_3 and $Pt\text{-}Re/Al_2O_3$ catalyst and evaluate the constants of deactivation.

CHAPTER TWO

2.0 LITERATURE REVIEW

The subject of this thesis relates to the reactivity of some hydrocarbons (n-octane, iso-octane and methylcyclopentane) on bifunctional monometallic Pt/Al_2O_3 and bimetallic $Pt-Re/Al_2O_3$ reforming catalysts. These reactivity studies were made on constant activity catalysts, i.e. catalysts on which the activity did not change with time throughout the period of investigation. They were also studied on variable activity catalysts i.e. catalysts on which coke was progressively deposited with time. Thus, the literature review must exhaustively discuss past works on this subject so as to address the need for doing this work and also expose the issues that were resolved as a result of this investigation.

Unfortunately, the issues addressed in this thesis have been studied to varying degrees in the past although some are little studied, especially with specific reference to the particular systems studied. In the literature review, therefore, we have elaborated on those works that relate specifically to the subject matter. Other related works, especially in the experimental investigations, were also discussed for a thorough perspective on the same subject matter.

2.1 Kinetic Studies on Constant Activity Reforming Catalysts.

Kinetic studies are important for accurate reactor design and also for understanding the phenomenon of catalysis. The literature available on the kinetic studies of n-octane, iso-octane and MCP will be presented in this section. Of the

three compounds much more literature is available for MCP.

2.1.1 N-Octane

Generally, the literature on n-octane conversions on Pt/Al_2O_3 catalysts are relatively sparce. However, Davis et al [4,9,22,23], Christoffel et al[21] and Susu et al[1] had done some work on the kinetics of the dehydrocyclization of n-octane. We shall now consider details of these contributions.

Davis and Venuto[9] studied the dehydrocyclization of different C_8 paraffin carbon skeleton structures using non-acidic Pt/Al_2O_3 catalyst. A vycor glass reaction tube wound with nichrome heater wire and fitted with a thermocouple well, a water cooled condenser, liquid collector, and glass flow meters was used for the investigation. All the runs were made at atmospheric pressure with no added carrier gas. The hydrocarbon flow of 1.5 ml/hr was used at a temperature of 482°C. The result of their investigation shows that the aromatic products obtained are those predicted by a direct six-membered ring closure. In all the cases investigated, very small amounts of the isomers not expected for direct six-membered ring closure were obtained. They explained the probable source of the small amount of aromatic isomers not allowed by direct six membered ring formation to be from the isomerization of the reactant by a small residual acidity, not neutralized by the alkali prior to or during the cyclization step.

Davis and Venuto[9] found that in contrast to the non-acidic Pt/Al_2O_3, where more than 95% of the aromatic products were those predicted by direct six member ring formation, the

acidic Pt/Al_2O_3 catalyst produced more than 50% of the m - and P - xylene isomers. The acidic alumina did not cause any appreciable xylene isomerization under the same reaction conditions as described when non-acidic Pt/Al_2O_3 catalyst was used. Consequently, they suggested that the aromatic isomers, not allowed by direct six-member ring formation, are formed from isoparaffins which result from dual functional catalytic reaction as shown below.

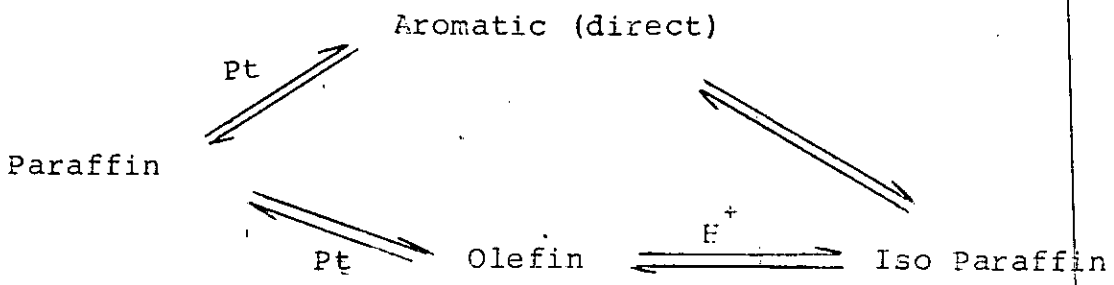

Davis[24] working at the same reaction condition as described above found no considerable variation in the o-xylene/ethylbenzene ratio as a function of hydrogen pressure. He also observed that the selective amount of 0-xylene from n-octane icreased:

(a) With decreasing Pt-loading of the catalyst[22]

(b) With the poisoning of the catalyst with thiophene[23]

(c) With increasing tin addition[23,24]

(d) If octanes and octynes were used as starting hydrocarbons[23].

Davis explained aromatization by "direct" C_6 ring closure. He offered an explanation in terms of the electronic

factor: when the catalyst is electron deficient, the probability of the adsorption of primary and secondary carbon atoms would be almost equal (with o-xylene/ethylbenzene ratio being nearly equal). Over catalysts that are not very electron deficient, the adsorption of secondary carbon atoms (and hence, 0-xylene formation) would predominate[23] because of the lower bond energy of the secondary C-H bond.

Christoffel and Paal[21] studied the dehydrocyclization of n-octane on 0.35Pt/Al_2O_3 and 0.5 Pt/zeolite catalyst. The reaction was carried out in a pulse reactor, H_2 carrier gas, pressure of 18bar and temperature of 400°C. They revealed that only C_8 - aromatics (ethylbenzene and o-xylene) which are expected from 1,6 ring closure are formed. The C_5 - ring naphthenes (which were also observed) will not react yielding C_6- ring naphthenes under the applied reaction conditions on the Pt/Al_2O_3 catalyst. On the Pt/zeolite catalyst, however the same C_8 aromatic distribution is obtained which corresponds to the thermodynamic equilibrium concentrations and no C_5 - ring naphthenes could be detected among the dehydrocyclization products. They argued that, in contrast with the Al_2O_3 - carrier, the zeolite carrier sets up thermodynamic equilibrium among C_5 and C_6- ring naphthenes. Since the zeolite carrier of the Pt/zeolite catalyst exhibits no ring closure activity, the rate determining steps in the reaction sequence should be 1,5 and 1,6 ring closures on platinum sites. Due to the high (de) hydrogenation activity of the platinum by which C_6- ring naphthenes are immediately dehydrogenated no C_5 - ring naphthene intermediates will occur among the products.

Susu et al[1] investigated the dehydrocyclization of n-octane to iso-octane, ethylbenzene, 0 - m - and p-xylene on monofunctional (non acidic) and bifunctional (acidic) Pt/Al_2O_3 catalyst in a microcatalytic reactor with hydrogen carrier at 1.8 atom and 300°C - 400°C. On bifunctional Pt/Al_2O_3 catalyst, they reported that the total conversion of n-octane started from a high value and decreased with increasing temperature for all the pulse sizes investigated. The primary product of n-octane conversion on acidic Pt/Al_2O_3 was iso-octane. The product yield - temperature profiles showed a large initial production of iso-octane which decreased, to a minimum as the catalyst temperature increased due to its conversion to ethylbenzene and o-xylene. On non-acidic Pt/Al_2O_3, the total conversion of n-octane increased initially and then went through a maximum as the catalyst temperature increased. The primary products of reaction were found to be ethylbenzene and o-xylene, indicative of the activity of the metal to effect ring closure reactions. The authors suggested the following sequence of single reactions on the bifunctional Pt/Al_2O_3 catalyst.

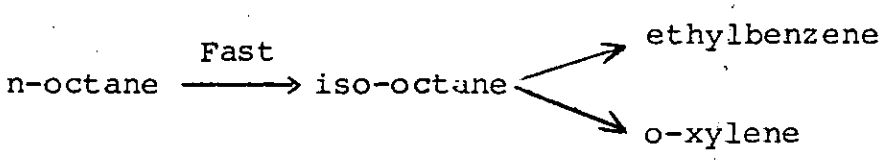

2.1.2 Iso-Octane (2,2,4 Trimethylpentane)

The kinetic data for the reactions of iso-octane are sparce. However, Lester[25], Dautzenberg[26] and Ako[27] have reported some results on the reactions of iso-octane using different

catalysts. In addition to the contributions of these researchers, we shall present the works of some others who worked on the kinetics of isomerization of n-pentane as the knowledge gathered from it is applicable to the kinetic investigation of iso-octane.

Lester[25] studied the product distribution obtained in aromatization of iso-octane on $k_2O - Cr_2O_3 - Al_2O_3$ and non-acidic Pt/Al_2O_3 at 400°- 500°C. He used a microreactor - chromatographic apparatus for the investigation. The hydrogen carries gas rate was 140cc(STP)/min for a residence time of about 0.1sec. The pressure employed was slightly above atmospheric. He showed that different mechanisms are required for iso-octane aromatization on the different types of catalysts. The composition of effluent compositions, on both catalysts is shown in Table 2.1.1.

Table 2.1.1. Composition of Effluents from Reactions of 2,2,4 trimethylpentane over $k_2O-Cr_2O_3-Al_2O_3$ at 500°C and non-acidic Pt/Al_2O_3 catalyst at 425°C.

Catalyst	$k_2O-Cr_2O_3-Al_2O_3$	Pt/Al_2O_3
$C_1 - C_7$	6.6	21.0
$2_1 2_1 4$ TMP	74.8	37.4
1,1,3 TMP	0.0	32.4
C_8H_{16}(Total)	16.1	-
C_7H_8	0.4	1.3
P-xylene	2.1	3.2
m-xylene	0.0	4.7
o-xylene	0.0	0.0

Lester[25] found that cyclogentanes are important intermediates of iso-octane aromatization over non-acidic Pt/Al_2O_3 but not over k_2O-Cr_2O_3- Al_2O_3. Weak Lewis acid character was attributed to Pt to explain the ability of the otherwise nonacidic catalyst to cause ring expansion of cyclopenthyl species to cyclohexyl species.

Dautzenberg and Platteeuw[26] studied the aromatization of iso-octane in a micropulse reactor at 480°c, hydrogen carrier gas at 1.2atm and 4.5 liters/hr using 500mg 1% wt Pt on inert alumina catalyst and found the total aromatic conversion to be 20 mole%. M-xylene and P-xylene accounted for 49.7 and 41.6%, respectively of the total aromatics formed while o-xylene and ethylbenzene were only 7.1 and 1.6% respectively.

Ako[27] studied the aromatization of iso-octane on acidic Pt/Al_2O_3 catalyst at temperatures between 300° and 400°C. He found out that the major products of iso-octane dehydrocyclization on bifunctional catalysts were ethylbenzene and P-xylene at 300°C. The initial P-xylene produced isomerized to ethylbenzene. At higher temperatures however, (320°C) there was simultaneous production of ethylbenzene and o-xylene, but at 400°C the reaction pattern was again

Iso-octane $\longrightarrow$ P-xylene $\longrightarrow$ ethylbenzene.

A study of the kinetics of isomerization of n-pentane at 372°C over a platinum on alumina catalyst (0.3% platinum) has been reported by Sinfelt et al[28]. The rate measurements were made in a flow system at low conversion levels (4-18%). The n-pentane was passed over the catalyst in the presence of hydrogen at total pressures ranging from 7.7 to 27.7atm and.

at hydrogen to n-pentane ratios varying from 1.4 to 18. Over this range of conditions, the rate was found to be independent of total pressure and to increase with increasing n-pentane to hydrogen ratio. The rate data were correlated by an expression of the form:

$$r = K \left(\frac{P_{nC_5}}{P_{H_2}} \right)^n \qquad 2.1.1$$

where r represents the rate in gram moles isomerized per hour per gram of catalyst and the parameters k and n have the values 0.040 and 0.5, respectively for the catalyst used in the study.

The kinetic data were interpreted in terms of a mechanism involving n-pentane intermediates:

$$nC_5 \overset{Pt}{\rightleftharpoons} nC_5 = + H_2$$

$$nC_5 = \xrightarrow[site]{Acid} iC_5 =$$

$$H_2 + iC_5 = \overset{Pt}{\rightleftharpoons} iC_5$$

According to this mechanism, n-pentane dehydrogenates to n-pentenes on platinum sites. The n-pentenes are then adsorbed on acidic sites, where they are isomerized to isopentenes. The latter are then hydrogenated to isopentane on platinum sites, thus completing the reaction.

The isomerization step on the acidic sites presumably takes place via a carbonium ion mechanism[29] :

$$n\,C_5^{=} + H^{+} \rightleftharpoons nC_5^{+}$$

$$nC_5^{+} \rightleftharpoons iC_5^{+}$$

$$iC_5^{+} \rightleftharpoons iC_5^{=} + H^{+}$$

They pictured the initial formation of the ion as taking place by protonation of the n-pentenes. The n-pentyl ion then rearranges to an isopentyl ion, which in turn can eliminate a proton to form isopentenes.

They postulated that at their conditions of study, the isomerization of the n-pentenes on the acidic sites was the rate limiting step, so that the rate is given by

$$r = k' \; (n\,C_5^{=}) \qquad (2.1.2)$$

where k' is the rate constant and $(nC_5^{=})$ represents the concentration of the n-pentenes on the acidic sites. They assumed that an equilibrium is effectively established between n-pentenes, n-pentane, and hydrogen in the initial dehydrogenation step with the partial pressure of n-pentenes given by:

$$P_{nC_5^{=}} = K \frac{P_{nC_5}}{P_{H_2}} \qquad (2.1.3)$$

where K is an equilibrium constant. They further assumed

that an adsorption equilibrium is established between n-pentenes in the gas phase and on the acid sites and that the equilibrium can be expressed simply by:

$$(nC_5^{=}) = b\, P_{nC_5}^{n} \qquad (2.1.4)$$

the rate expression becomes, after substituting(2.1.3) and(2.1.4) (2.1.2):

$$r = k' b K_n^n \left(\frac{P_{nC_5}}{P_{H_2}}\right)^n = K\left(\frac{P_{nC_5}}{P_{H_2}}\right)^n \qquad (2.1.5)$$

This is identical to equation 2 derived from the data. The data they obtained on the rate of skeletal isomerization of 1-pentene over a sample of catalyst containing only the acidic function (no platinum) provided additional strong support for the proposed mechanism.

Starnes and Zabor[30] proposed an alternative mechanism, based on the studies of n-pentane isomerization over platinum-alumina - halogen catalysts. They postulated that the paraffin is adsorbed on platinum sites with dissociation of a hydrogen atom, followed by polarization of the adsorbed species

$$R - CH_2 - CH_2 \rightleftharpoons R-\overset{+}{C}H - CH_3 + \underset{Pt}{\overset{+}{H}}$$

The authors suggested that the support confers Lewis acid properties on the platinum, which in turn accounts for the polarization of the adsorbed alkyl group to a carbonium ion

type structure. The latter then undergoes the usual carbonium ion reactions. The mechanism involves a single type of catalyst site instead of two different types of sites as envisioned in the previously discussed mechanism. The objections raised by Starnes and Zabor to the two - site mechanism are based on several experimental observations: (a) When n-pentane was isomerized over a mixture of pellets of Pt - alumina and HF - promoted alumina, the rate increased with time on stream, coinciding with transfer of the flouride to the Pt containing pellets. (b) Although the olefin content of the products remained constant at equilibrium level, the rate suddenly increased about 7- or 8-fold when the platinum of the catalyst was increased from 0.3 to 0.4%. (c) The rate was propotional to the olefin partial pressure to a power somewhat lower than unity. These objections have been answered by Keulemans and Schuit[31] who suggested that (a) and (b) do not refute a two site mechanism, but simply reflect diffusion limitations in the experiments of Starnes and Zabor.

Hosten and Froment[32] studied the isomerization of n-pentane on a commercial reforming catalyst (Pt/Al_2O_3) in an isothermal, bench-scale, fixedbed reactor. The influence of total pressure, molar ratio hydrogen/hydrocarbon, chlorine content in a feed, and space time was investigated in the temperature range of 375° to 425°C. Reaction rate equations of the Hougen - Watson type were derived on the basis of the generally accepted mechanism for skeletal isomerization. Eleven rate equations were developed. Discrimination between these eleven rate models was based upon the following experimental evidence: (i) The rate is independent of total pressure

(ii) the rate is influenced by the chlorine concentration. They observed that when one of the steps of the dehydrogenation or hydrogenation stages is considered to be rate determining, the corresponding overall rate equation is always total pressure dependent. Since the dehydrogenation or hydrogenation steps are incompatible with the experimental results, they concluded that the isomerization sequence determines the rate of the overall process. Their conclusion is confirmed by the observation that the reaction rate is affected by the chlorine concentration. The three models of the isomerization sequence were then subjected to discrimination based upon significance tests for the overall regression and for each parameter separately. From the results they obtained, they concluded that the adsorption step of the isomerization sequence is the rate limiting step.

2.1.3 Methylcyclopentane (MCP)

Christoffel and Paal[11] studied the activity and selectivity of bifunctional platinum catalysts in hydrocarbon reactions. In particular, they looked at the conversions of a number of C_6 - C_8 alkanes, naphthenes and aromatics on bifunctional Pt/carrier catalyst, on Pt black and on the acidic carriers of the bifunctional catalysts in the temperature range 300-500°C and hydrogen partial pressures of 0-45 bars in a continuously operated fixed bed reactor and microcatalytic pulse reactors. Among other things, they confirmed the previous finding that methylcyclopentane ring opening yields selectively on acidic catalysts, n-hexane/ 2 methyl pentane/ 3 methyl pentane in a ratio of 2:2:1 on

small platinum crystallites and selective ring opening producing methyl pentanes only over large platinum crystallites[17]. Using pulse technique, their own product distribution from MCP reaction on a laboratory 0.5 Pt/Al_2O_3 catalyst showed that the primary ring opening products -n - hexane, 2 methyl pentane and 3 methyl pentane - are formed nearly in the ratio 2:2:1 over fresh supported catalyst whereas over partially deactivated catalyst and the Al_2O_3 carrier, n-hexane is the main product. Thus, over the fresh catalyst, mainly platinum reactions contribute to the measured ring opening products, while on partially deactivated catalyst, mainly the acidic sites of the carrier catalyze the ring opening reactions. On platinum black with rather large crystallites, mainly selective ring opening occurs.

The results of MCP conversions in differently pretreated Pt/Al_2O_3 catalysts clearly indicate that by the employed pretreatment, the platinum function is partially deactivated in asmuch as it has lost its isomerization and hydrogenolysis activity while the (de) hydrogenation activity remained unchanged.

Typical product distribution of MCP conversion on partially deactivated $0.5Pt/Al_2O_3$ catalyst was reported by Christoffel and Paal[11] as:

Reactant	MCP	
Products	%	
$C_1 - C_5$	0.03	Hydrogenolysis products
hexanes	0.15	
MCP	98.4	
Benzene	0.3	

Methylcyclopentene (MCP^{2-})	1.03
Cyclohexane and Cyclohexene	0.08

Jossens and Peterson[33] used the dehydrogenation of methylcyclohexane to toluene and the dehydroisomerization of methylcyclopentane to benzene as the model reforming reactions in their study of fouling of a Pt-Re reforming catalyst. The fouling characteristics by MCP dehydroisomerization of a platinum catalyst was monitored by measuring the catalytic activity as the ratio of benzene production rate R to initial benzene production rate R_o. The contribution of the acidic site on a Pt and Pt-Re catalyst (sulfided and unsulfided) at 475°C and 70 torr in the dehydro-isomerization of MCP was also studied. It was found that the conversion of MCP to benzene was less than 20%.

Though Pt and Pt-Re equally calatyzed the dehydroisomerization of MCP, the ring opening activity of the sulfided and unsulfided Pt catalyst, the initial distribution of secondary products from either sulfided or unsulfided catalyst was found roughly to be in the propotion of 2,1 and 2 parts for methylcyclopentane, 3 methyl pentane and normal hexane respectively.

Dartigues et al[34] in their investigation of the structure sensitivity for the ring opening of MCP, found an equal probability of breaking all five cyclic carbon - carbon bonds for a highly dispersed Pt-on alumina catalyst. Similarly de Jougeste et al[35] found that a copper rich Pt-Cu catalyst supported on silica also gave non-selective ring opening of

MCP. Ring opening of MCP catalyzed by gamma alumina yielded predominantly n-hexane[36]. This suggests that the highly dispersed metal function of a Pt or Pt-Re catalyst is responsible for the ring opening activity of these catalysts.

Dehydrogenation of the cyclohexane ring uses only the metallic Pt-function of these bimetallic catalysts[37,38] and is thought to be structure insensitive for a supported Pt catalyst. The dehydroisomerization of MCP to benzene utilizes both metallic and acidic sites of a bifunctional reforming catalyst and proceeds through a methylcyclopentene MCP^{2-} intermediate[16,34,36].

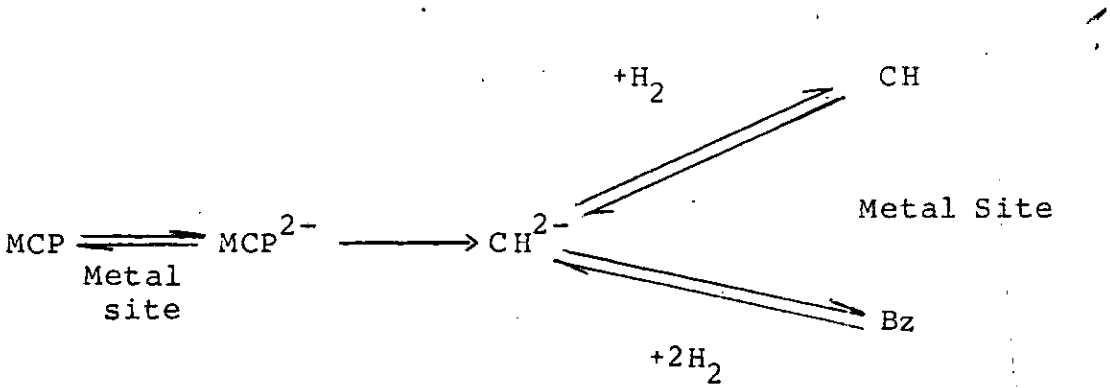

Ring enlargement from MCP^{2-} to cyclohexene, CH^{2-}, on an acidic site is thought to be the controlling step in this sequential reaction[36,41,42]. This is viewed as a means to detect the effect of rhenium on the support.

Kramer and Zuegg[43] as well as numerous other authors[44-48] studied the hydrogenolysis of methylcyclopentane and the results confirmed what has already been reported above.

2.2 Kinetic Studies on Variable Activity Reforming Catalysts.

The literature available on the deactivation kinetics of n-octane, iso-octane or MCP are sparce. However, some studies have been reported on the deactivation kinetics of Pt/Al_2O_3 catalyst by C_6 hydrocarbons by Cooper and Trimm[49]. Also the kinetics of isobutene oxidation on 5% $HgCl_2$/active charcoal by parallel reaction has been reported by Corella and Asua[50]. The methods used in their studies can be applied to the studies of the deactivation kinetics of reforming catalyst using n-octane, iso-octane and MCP as reactants.

2.2.1 Kinetics of Deactivation of Pt/Al_2O_3 Catalyst by C_6 Hydrocarbons.

Cooper and Trimm studied the kinetics of coking of a Pt/Al_2O_3 catalyst by the dehydrogenation, dehydrocyclization, dehydroisomerization and isomerization of C_6 hydrocarbons between the temperatures of 450°C and 550°C under 10 bar pressure. The reactions were carried out in a tubular reactor suspended from one arm of a microbalance. The results were analysed using the general coking scheme of Froment[51].

$$A + * \rightleftharpoons A* \quad (1)$$

$$A* \longrightarrow B*(r.d.s) \quad (2)$$

$$B* \rightleftharpoons B + * \quad (3)$$

Cooper and Trimm obtained the modelling equations shown in Table 2.2.1.

Table 2.2.1: Deactivation Functions for various order of Coking reactions of Cooper and Trimm.

Order of Coking(n)	Single Site(h)	Dual Site (h)
0	$r_t = r_o(1 - \alpha_1 C_k)$	$r_t = r_o(1-\alpha_4 C_k)^2$
1	$r_t = r_o(\exp(-\alpha_2 C_k))$	$r_t = r_o(\exp -2\alpha_5 C_k))$
2	$r_t = r_o(1 -\alpha_3 C_k)^{-1}$	$r_t = r_o(1-\alpha_6 C_k)^{-2}$

Generally,

$$r = r_o\phi \qquad (2.1.6)$$

where ϕ is the activity of the coking reaction since the variable used in this modeling is the number of coked sites.

The quantity of coke in milligrams deposited on the catalyst with respect to the time on stream was monitored for each hydrocarbon reaction at various temperatures. The quantity of coke deposited per gram of catalyst was plotted against the time on stream for each reaction. At various coke levels, the coking rate (dC_k/dt) was determined and a table of rate of coking versus coke content obtained. The modelling equation of Table 2.2.1 were tested with each set of data, and the equation that best fits the data was determined for each reaction.

From these results, Cooper and Trimm found that one molecule of cyclohexane reacted with one adsorbed coke precusor molecule during the reaction of benzene and cyclohexane. Hence they concluded that the mechanism of reaction of benzene and cyclohexane on Pt/Al_2O_3 catalyst

was bimolecular condensation on the metal function of the catalyst. This implies that a single site exponential form of activity decay can best describe the coke formation due to the dehydrogenation of cyclohexane and the hydrogenation of benzene on Pt/Al_2O_3 catalyst. The deactivation function was given by

$$\phi = \exp(-\alpha C_k) \qquad (2.1.7)$$

where C_k is the number of coked sites. The rate controlling step was represented as:

$$A^* \longrightarrow C + A \longrightarrow \text{Coke} \qquad (4)$$

For other compounds, because more than one free molecule was involved in the formation of the coke molecule, a polymerization reaction involving acid sites on the catalyst was proposed. For example, for the fast coking reaction of n-hexane at 500°C, the deactivation function was given by

$$\phi = (1 - \alpha C_k)^{-0.33} \qquad (2.1.8)$$

Cooper and Trimm showed that temperature has a significant effect on the mechanism of coking and the deactivation function of the catalyst. The summary of the effect of temperature on the deactivation of Pt/Al_2O_3 for n-hexane reaction is shown in Table 2.2.2.

Table 2.2.2: Deactivation Function and Mechanism by Cooper and Trimm (Experimental)

Temperature (°C)	Model	n	Reaction Controlling Step
450°	$r_t = r_o(1-\alpha C_k)$	0	$A^* \longrightarrow C \longrightarrow$ Coke
500°	$r_t = r_o(1-\alpha C_k)^{-1}$	2	$A^* \longrightarrow C+2A \longrightarrow$ Coke
550°	$r_t = r_o(1-\alpha C_k)^{-0.33}$	4	$A^* \longrightarrow C+4A \longrightarrow$ Coke

They also found that decreasing order of coking for the various hydrocarbons investigated can be represented.

Methylcyclopentane > 3 - methylpentane ∿ n-hexane > 2 - methylpentane > benzene > cyclohexane

The relatively slow rate of coking in cyclohexane and benzene compared to other C_6 hydrocarbon studied was attributed to the bimolecular condensation which was largely unaffected by the acidity of the catalyst.

Since Cooper and Trimm used the direct quantity of primary coke deposited on the catalyst to model the deactivation of the catalyst, the deactivation function obtained is applicable to the primary coke formation reaction.

The presentation of only six modelling equations and the failure to show the procedure of development of such equations limit the applicability of the models.

2.2.2 Isobutene Oxidation on 5% $HgCl_2$/Active Charcoal by Parallel Reaction

(a) Model Development

Corella and Asua indicated a method of studying the deactivation of a catalyst when the principal reaction is not simple and when the distribution of product changes with time. The study was carried out on the oxidation of isobutene to methylacrolein on a 5% $HgCl_2$/active charcoal catalyst at 0.97 atmosphere in an isothermal and differential fixed bed reactor at 220°, 200° and 180°C.

The model proposed for the main reaction was represented by

$$A + B \longrightarrow R + V \qquad (1)$$

$$A + B \longrightarrow S + V \qquad (2)$$

$$A + 6B \longrightarrow 4U + 4V \qquad (3)$$

where A = Isobutene

B = Oxygen

R = Methylacrolein

U = Carbondioxide

V = Water

The mechanism of catalyst deactivation by coking was represented by

$$(n+h)\ A \longrightarrow P$$

where n can be 0, 1, 2 and h can be 1,2 due to the improbability of three free-body collisions.

For a parallel main reaction network, the kinetic of deactivation was represented for each of the products by

$$r_{Ro} = (r_{Ro})_o \, a_1 \tag{2.2.1}$$

$$-da_1/dt = \psi_{o1}(P_i,T) a^{d_1} \tag{2.2.2}$$

$$r_{so} = (r_{so})_o \, a_2 \tag{2.2.3}$$

$$-da_2/dt = \psi_{02}(P_i,T) \, a_2^{d_2} \tag{2.2.4}$$

$$r_{uo} = (r_{uo})_o \, a_3 \tag{2.2.5}$$

$$-da_3/dt = \psi_{03}(P_i,T) a_3^{d_3} \tag{2.2.6}$$

Generally, for reaction j,

$$r_j = (r_j)_o \, a_j \tag{2.2.7}$$

$$da_j/dt = \psi_{0j}(P_i,T) a_j^{d_j} \tag{2.2.8}$$

There is a possibility that $a_1 \neq a_2 \neq a_3$.

Defining yield of product R as

$$Y_{R/A} = Y_R = \frac{\text{moles of R obtained}}{\text{moles of A fed}} \tag{2.2.9}$$

the activity a, was given by

$$a_1 = r_{Ro}/(r_{Ro})_o = \frac{Y_R/W/F_{Ao}}{Y_{Ro}/W/F_{Ao}} = \frac{Y_R}{Y_{Ro}} \tag{2.2.10}$$

For differential reactor system and dj = 1 from (2.2.8)

$$a_j = ajo \exp \int_o^t (-\psi_{oj}\ (P_i,T))\ dt$$

$$\therefore aj = a_{jo} \exp(-\psi_{oj}\ (P_i,T)t) \qquad (2.2.11)$$

where ajo = 1 (initial activity

$$\therefore \ln a_j = -\psi_o(P_i,T)t \qquad (2.2.12)$$

If dj ≠1

$$(a_j^{(1 - dj)} - 1) = (1 - dj)\psi_{oj}(P_i,T)t \qquad (2.2.13)$$

To determine the value of dj, the data of the activity aj versus time, t is required.

For the main product R, consideration has been given to four different kinetic equations from two out of the six different mechanisms depicted in Table (2.5.1). The d - 1 and d - 2 mechanisms with the second and third step controlling in each case were tested because they were the simplest to us. Corella and Asua however cautioned that the fact that one of the two mechanisms tested fitted a set of data does not make it the right one since other mechanisms were not tested. The same approach was followed with respect to the second product S. Because of the complex form of the stoichiometry of the third product U i.e

$$A + 6B \longrightarrow 4U + 4V$$

no mechanistic expression for its deactivation equation was derived. Its deactivation equation was represented by the empirical equation of the type:

$$-da/dt = \psi_{03}(P_i,T)\ a_3^{\ d_3} \qquad (2.2.14)$$

For a differential operation, when $d_3 = 1$ after integration equation (2.2.14) was obtained

$$\ell n a_3 = -\psi_{03}(P_i,T)t = K_{d_3} P_A^{\ n_1}\ t \qquad (2.2.15)$$

when $d_3 \neq 1$

$$(a_3^{\ 1-d_3} - 1) = (d_3 - 1)K_{d_3} P_A^{\ n_1}\ t \qquad (2.2.16)$$

(b) Data Collection:

In order to identify the influence of each reactant on deactivation order dj, two separate sets of experiments were performed keeping the pressure of one of the reactants constant and varying the pressure of the other reactants (equation (2.2.6) was used).

Sample Data Analysis for the First Product R

A table of the yield of R, y_R, and time on stream t, was obtained at each temperature y_R was plotted against time t and the activity y_R/y_{Ro}, was obtained at various times on streams. $\ell na = \ell n(y_R/y_{Ro})$ was then plotted against t as in equation (2.2.13) to verify the value of d or h. At 220°C with the assumption that d=1, a graph of ℓna_1 vs t was linear indicating that d= h=1. This was confirmed also at 180°C and 200°C. The same result was obtained regardless of which of the two reactants was held constant. In an earlier work, Corella and Asua had found that m=1. Hence, the four equations

to be tested for n with m=1 and h=1 from Table 2.1.1. after linearization were reduced to:

d - 1 mechanism, 2nd step

$$\frac{P_A^{n+1}}{\psi_{01}(P_i,T)} = (1/k_{d_1} K_{A1}) + \frac{1}{k_d} P_A + (K_{B1}/k_{d1} K_{A1}) P_B \quad (2.2.17)$$

d - 1 mechanism, 3rd step

$$\frac{P_A^{n+1}}{\psi_{01}(P_i,T)} = 1/k_{d1} K'_{A1} + (K_{A_1}/k_{d1} K'_{A_1}) P_A +$$

$$+ K_{B1}/k_{d1} K'_{A1} P_B + \frac{K''_{A1}}{k_{d1} K'_{A1}}, P_A^{n+1} \quad (2.2.18)$$

d - 2 mechanism, 2nd step

$$\frac{P^{n+1}}{\psi_{01}(P_i,T)} = \frac{1}{k_{d1} K^*_{A1}} + \frac{(K_{A1} + K^*_{A1})}{k_{d1} K_{A1}} P_A + \frac{K_{B1}}{k_{d1} K^*_{A1}} P_B \quad (2.2.19)$$

d - 2 mechanism, 3rd step

$$\frac{P^{n+1}}{\psi_{01}(P_i,T)} = \frac{1}{k_{d_1} K^*_{A1}}, + \frac{K_{A1}}{k_{d_1} K^*_A}, P_A + \frac{K_{B1}}{k_{d_1} K^*_{A_1}}, P_B + \frac{K^*_A}{k_{d_1} K^*_{A1}}, P_A^{n+1} \quad (2.2.20)$$

where $\psi_{01} = 1/t \ \ell n a_1$

To determine which of the four equations would give the correct mechanism of reaction, the following criteria were set for the parameters:

(a) the values of the deactivation parameters k_{d_1} K^*_{A1} $k^{*\prime}_{A1}$ must be positive

(b) the values of the K_{A1} and K_{B1} obtained from the equation must agree with those obtained from the kinetic study of the fresh catalyst without deactivation.

Using the data of $\psi_{01}(P_i,T)$ at different P_A and P_B at each temperature and adjusting the linearized equations by the least square method, Corella and Asua found that equation (2.2.18) gave the best fit with n=1. Hence the main reaction and the rate of activity decay of the catalyst in the formation of methylacrolein are given by:

$$r_R = (r_R)_o \, a_1 \qquad (2.2.21)$$

$$-da/dt = \frac{k_{d_1} K_{A1} P_A^2}{1+(k_{A1}+ k_{A1})P_A + K_{B1}P_B} a_1 \qquad (2.2.22)$$

The same procedure was followed for the modelling of the reactions of the second product, and the same set of deactivation kinetic parameters were obtained for m,n and h.

The value of d_3 was found to be 1 and that of n found to be zero with respect to the third product (CO_2). Its rate

of activity was therefore given by:

$$-da_3/dt = k_{d3}\, a_3 \qquad (2.2.23)$$

While the deactivation kinetic parameters m,n,h were found to be independent of temperature, the kinetic constants k_d and K^*_{A1} vary with temperature in accordance with Arrhenius relationship.

The model of Corella and Asua has demonstrated a method of modelling the activity decay of the catalyst with respect to each product of a non-simple reaction. The approach of solving the equations of deactivation makes it possible to determine both the deactivation kinetic parameters m, n, h as well as the fresh catalyst kinetic constants k_d and K^*_{A1}.

It was observed that the deactivation equation was solved for the parameters m, n and h stepwise with m already determined from a previous experiment. Previous determination of m made the solution of the equation less rigorous. Also, the solution would have been impossible under an integral reactor system since the assumption of a constant ψ_{oj} with respect to the concentration in equation (2.2.12) would have been wrong. Hence, the approach of Corella and Asua for solving deactivation kinetic equations is more directly applicable to a differential reactor system.

2.3 Mortality Studies On Reforming Catalysts

The progression of the reforming catalysts to the mortal state using the dehydrogenation of cyclohexane to benzene in an 0_2 free N_2 and 1 atm system total pressure has been studied by Omoleye[52]. A CSTR reactor packed with 5g of catalyst was

used. The N_2 atmosphere ensured accelerated aging of the catalyst. Deactivated catalyst was regenerated by burning off the coke in air for 3 hrs at 673k. The regenerated catalyst was then reduced in H_2 for 2 hr to prepare the catalyst for the next cycle of deactivation - regeneration cycle. Twenty-six deactivation - regeneration cycles were performed on commercial Pt/Al_2O_3 catalyst until catalyst mortality occured and the results obtained were as follows:

A plot of cycle life versus cycle number (figure 2.3.1) shows three stability states with respect to the cycle life as the cycle was increased from 1 to 24. Cycles 1 to 8 had life expectancy ranging from 20 to 50 min. From the 9th cycle, there was a sudden increase in the cycle life to 120 mins., and cycles 9, 10 and probably cycle 11 served as the transition states for the second stability state. The cycle life expectancy for the second stability state ranges from 75 - 130 min., and it covers cycles 12 to 18. The third stability state also started with a transition state from the 19th cycle where the cycle life also increased suddenly to 200min. From the 20th cycle, there was a consistent rise in the cycle life up to the 22nd cycle. Cycle 22 lasted 260min, and after this cycle, the catalyst no longer responded to normal regeneration procedures.

Figures (2.3.2 - 2.3.4) show the deactivation profiles for Pt/Al_2O_3 from the 1st cycle to the last cycle. Figure (2.3.2) shows the first stability state of cycles 1 to 8 of the catalyst while figures 2.3.3 - 2.3.4 show the profiles for the second cycles 9 to 18 and the third cycles 19 to 22 states. For the first and second states, the lenght of the cycle life was random while in the third state, cycle life

increased with the cycle number.

When Pt-Re/Al_2O_3 catalyst was used for the mortality studies the following differences in the character of the profiles for Pt-Re/Al_2O_3 was observed.

(a) A general decrease in cycle life of Pt-Re/Al_2O_3 catalyst starting from the first cycle till the 16th cycle was observed. This is in contrast with the result obtained with Pt/Al_2O_3 where there was a general increase in the cycle life of Pt/Al_2O_3 from the first to the 22nd cycle.

(b) While the cycle life of fresh Pt-Re/Al_2O_3 is the longest of all the cycles in the bimetallic catalyst, the cycle life of fresh Pt/Al_2O_3 is one of the shortest.

(c) The continuous decrease in the cycle life of Pt-Re/Al_2O_3 starting from the second cycle indicated a gradual death of the catalyst while the change in the cycle life of Pt/Al_2O_3 at the 23rd cycle marked the point of death of the catalyst.

(d) The behaviour of the cycle life with cycle number for Pt-Re/Al_2O_3 is cyclical with decreasing amplitude as cycle number increases (see figure 2.3.5). This manifests itself in the manner in which it falls from the first cycle up till the 7th cycle and rises from the 7th cycle up till the 9th cycle, then falls again till the 11th cycle, and finally rising and falling to a low value on the 15th cycle with the maximum on the 12th cycle. This type of systematic cyclic behaviour was not found with Pt/Al_2O_3.

(e) 16 cycles of deactivation - regeneration processes were done on Pt-Re/Al_2O_3 before it could no longer react for any reasonable period of time while with Pt/Al_2O_3, 26 deactivation regeneration cycles were performed.

The coke content after each cycle was plotted against the cycle number. The coking level on the Pt/Al_2O_3 catalyst surface exhibited definite discontinuities indicative of the existence of pseudo-stability states on the catalyst surface. The first pseudo stability state exists up to the 9th cycle; from the first to the 9th cycle, a fairly constant level of coking at between 0.4 to 0.5 x 10^{-2} moles CO_2 is maintained. Beyond the 9th cycle, the level of coking makes a discontinous jump to the second pseudo stability state where a coking level of 1.4 x 10^{-2} moles CO_2 is maintained. The life time of the second pseudo-stability state extends from the 10th to the 19th cycle. Beyond the 19th cycle, the coke level accelerates to a value of about 3.0x10^{-2} moles CO_2 (See Figure 2.3.6). On the 23rd cycle, there was a huge fall in the amount of coke deposited on the catalyst to as little as 1/8th of the coke deposited at the 22nd cycle. This decline continued on the 24th cycle to a very low value of about 0.003 mole CO_2. It can be observed in Figure (2.3.6) that the coking level equally reflected the three stability states previously indicated on the cycle life profiles (Figures 2.3.2 - 2.3.4).

Figure (2.3.6) also show the coke content of Pt-Re/Al_2O_3 againist the cycle number after each reaction period. The coking level on Pt-Re/Al_2O_3 also showed three distinct levels of coking. The first coking level of Pt-Re/Al_2O_3 has higher

coke deposit than Pt-Re/Al_2O_3. However both the second and the third normal coking levels of Pt-Re/Al_2O_3 deposited much less coke than the Pt-Re/Al_2O_3. In the first stability state of each catalyst, the quantity of coke deposited per cycle remained fairly constant. From the beginning of the second stability state, both catalysts experienced a sudden increase in the quantity of coke deposited per cycle. The quantity of coke deposited on Pt/Al_2O_3 catalyst was maintained throughout the second state. However, the increase in the quantity of coke deposited on Pt-Re/Al_2O_3 catalyst on the 7th cycle did not apply to the other cycles within the state. Rather,there was a continuous decline in the amount of coke deposited up to the 12th cycle. There was an increase in the quantity of coke deposited on the catalysts at the 13th cycle for Pt-Re/Al_2O_3 and 19th cycle for Pt/Al_2O_3, thus, marking the beginning of the third coking state. While the coke content on Pt/Al_2O_3 increases from one cycle to another up to the last cycle, it increased to a maximum deposit at the 14th cycle and then declined steadily to the 16th cycle on Pt-Re/Al_2O_3.

2.4 General Kinetic Modelling Studies

In a kinetic investigation, it is not known a priori which is the rate controlling step and therefore the form of the rate equation or model. Also unknown, are values of rate constants and adsorption equilibrium constants which are parameters of the models.

The rate equations can be developed following-the procedure outlined by Hougen and Watson[53] i.e.

1. Propose a mechanism

2. Consider that one of its steps is the slowest so it will be controlling of the process, the rest being in equilibrium.

3. Deduce the kinetic equation for this controlling step.

4. Repeat this procedure for all possible controlling steps and for different mechanisms and

5. Select experimentally the best equation among the different possible equations obtained theoretically by estimation of their parameters.

Estimation of parameters in linear or linearized non-linear equations can be accomplished using linear regression. Linearized non-linear equations, however contain constants formed from group of rate and adsorption equilibrium constants. It is usually difficult in most cases, to evaluate the rate and adsorption equilibrium constants from the results obtained using linear regression. Itereative method is required with non-linear equations.

Any estimation starts with the definition of a suitable objective function. Let the model equation be represented by

$$y = f(C,k) \qquad (2.4.1)$$

where y represents the m vector or dependent variables, C the n vector of independent variables (also called states) like concentration, temperature or W/F_{AO} and K the P vector of unknown parameters. R experiments are carried out, and

y is measured for known C, with certain random experimental errors. If the difference between the model prediction and the data is called residual

$$e_r(k) = y_r - f(C_r, K) \qquad (2.4.2)$$

and the moment matrix of the residual is given by

$$M(k) = \sum_{r=1}^{R} e_r(k)\, e_r(k)^T \qquad (2.4.3)$$

then the estimation aims at minimizing some function of this moment matrix, generally called objective function, by the suitable choice of k. The most common objective function is the weighted least square criterion $S = \text{Trace}\,[QM(k)]$ (2.4.4) where Q is an mxm weighting matrix, whose elements are selected to reflect the knowledge about the relative precision of the residuals. Q is a diagonal matrix when only sums of squares of residuals are considered and a full matrix when the sum of cross products are also taken into account.

The objective function can also be based upon the maximum likelihood principle. The likelihood function is the conditional probability relating the dependent variable y (also called output) to the parameters K. When the variance-covariance matrix of the responses V is known, maximizing the likelihood is equivalent to minimizing

$$S = \text{Trace}[V^{-1} M(k)] \qquad (2.4.5)$$

where Q in equation (2.4.4) equals V^{-1}, the weighted least squares estimates are also the maximum likelihood estimates. When the variance - covariance matrix of the responses is unknown, it turns out, from a Bayesian analysis,

that the maximum likelihood estimates are obtained from the minimization, with respect to the parameters, of

$$S = \det M(k) \qquad (2.4.6)$$

As already mentioned, estimation in algebraic equations which are non-linear generally requires extensive iteration involving some hill descending procedure. The numerous procedures which have been proposed can be classified into three categories. The first category could be called function methods, the second is gradient methods and the third group, Newton methods. The basic procedures in these categories are, respectively, the univariable, the steepest descent, and the Newton - Raphson method. The principal characteristics of these three basic methods are shown in Table (2.4.1).

Table 2.4.1: Characteristics of Basic Methods of Three Categories of Hill Descending Procedures[54]

Category	Required	Basic Procedure	Iteration cycle
Function	S	Univariable	$k^{(i+1)} = k^{(i)} + \sum_{j=1}^{P} \lambda_j^o e_j$
Gradient	S and $\frac{\partial s}{\partial k}$	Steepest descent	$k^{(i+1)} = k^{(i)} - \lambda_j^o \left(\frac{\partial s}{\partial k}\right)_{k^{(i)}}$
Newton	S, $\frac{\partial s}{\partial k}$ and $\frac{\partial^2 s}{\partial k^2}$	Newton-Raphson	$K^{(i+1)} = k^{(i)} - \left[\left(\frac{\partial^2 s}{\partial k^2}\right)_{k^{(i)}}\right]^{-1} \left(\frac{\partial s}{\partial k}\right)_{k^{(i}}$

In the univariable procedure, the search directions are parallel to the axes. λ_j^o is the value of the scalar λ_j corresponding to the minimum of S in the j^{th} direction in the cycle leading from $k^{(i)}$ to the next approximation $k^{(i+1)}$. The steepest descent procedure calculates S in the opposite direction of the gradient and changes direction when a minimum is attained. λ_j^o is the value of λ corresponding to the minimum of S in the direction followed between the i^{th} and (i+1)th iteration.

The Newton-Raphson procedure develops the objectives function $S[k^{(i+1)}]$ in a Taylor series around a starting value $k^{(i)}$ which contains no terms beyond second order. $S[k^{(i+1)}]$ is then considered as the minimum of the objective function, so that a system of P linear equations is obtained, from which $k^{(i+1)}$ is easily calculated. The method generates simultaneously the search direction and the distance in that direction. The method converges quite rapidly in the vicinity of the minimum of S, but it is more complicated, since it requires the calculation of second order derivatives and inversion of matrices. For quadratic objective functions, this method leads to the minimum of S in one single step.

The univariable and steepest descent methods do not account for information gathered in the previous steps and therefore may converge slowly. For this reason more elaborate methods have been developed. Some of the better known are the Hooke - Jeeves method, which is based on pattern search that progresses in the successful direction and has ridge following properties; Rosenbrock's method, which involves rotation and

orthogonalization of search directions; the simplicial method which proceeds over regular simplexes produced by reflection; and the Nelder and Mead method which allows expansion and contraction of the simplexes. More efficient gradient methods have been developed to avoid oscillation in the vicinity of the minimum, to account for past information, and to take advantage of the fact that many objective functions are approximately quadratic in the vicinity of the minimum. The idea of the Fletcher - Powell and Fletcher - Reeves methods is that the minimum of an n dimensional quadratic function is found by n one - dimensional searches along conjugated directions. The Fletcher-Reeves method proceeds along conjugated directions after starting in the opposite direction of the gradient. With non quadratic objective functions, the method switches after P+1 one - dimenstional searches along conjugated directions, again to an initial search opposite to the gradient.

The algorithm of the Newton-Gauss method is derived from a quadratic approximation of the objective function; $Z_r(k)$ is developed in a Taylor series, neglecting all derivatives of second and higher orders. This linearization may lead to Δk which are too large, so that the method becomes unstable. To overcome this, Levenberg and later Marquardt developed very similar modifications of the method. The algorithm is derived from constrained application of the Newton-Gauss approximation. λ is a lagrangian multiplier, restricting the step lenght and continuously adjusting the search direction. At the start λ has to be large, and as the direction of search is close to that of steepest descient.

λ is gradually decreased until, in the vicinity of the minimum, the constraint upon the Newton-Gauss procedure is no longer necessary, and λ is set equal to zero.

The Powell method is a function method which does not make use of gradients, except at the start. $\bar{U}^{(i)}$ is the matrix of the normalized search directions. At the start, these coincide with the coordinate axes. $\bar{\Gamma}$ is the matrix of the normalized derivatives of the Z(k) with respect to the parameters. This matrix is updated continuously, without recalculating the derivatives.

Table 2.4.2. Algorithm of methods for minimizing objective functions that are of the sum of squares type[54]

Method	Algorithm
Gauss-Newton	$k^{i+1} = k^{i} - [k^{(i)})J(k^{(i)})]^{-1} J^{T}[k^{(i)}]Z[k^{(i)}]$
Levenberg-Marquardt	$= k^{(i)} - [J^{T}(k^{(i)})J(k^{(i)}) + \lambda^{(i)} D^{(i)}]^{-1} J^{T}[k^{(i)}]Z[k^{(i)}]$
Powell	$= k^{i} + \lambda_{i}^{o} U^{(i)} [\bar{\Gamma}^{T}(k^{(i)})\bar{\Gamma}(k^{(i)})]^{-1} \bar{\Gamma}^{T}[k^{(i)}] Z[k^{(i)}]$

The method of Nelder and Mead[55,56] minimizes a function of n independent variables using (n+1) vertices of a flexible polyhedron in E^n. Each vertex can be defined by a vector x. The vertex (point) in E^n which yields the highest value of f(x) is projected through the center of gravity (centroid)

of the remaining vertices. Improved (lower) values of the objective function are found by successively replacing the point with the highest value of f(x) by better points until the minimum of f(x) is found.

The details of the algorithm are as follows:

Let $x_i^k = [x_{i1}^{(k)}, \ldots, x_{ij}^{(k)}, \ldots, x_{in}^{(k)}]^T$, where i = 1,..., (2.4.7)

n+1, be the ith vertex (point) in E^n on the kth stage of the search, k=o,1..., and let the value of the objective function at $x_i^{(k)}$ be $f(x_i^{(k)})$. In addition, we need to label x vectors in the polyhedron that give the maximum and minimum values of f(x).

Define

$$f(x_h^{(k)}) = \max\{f(x_1^{(k)}), \ldots f(x_{n+1}^{(k)})\} \qquad (2.4.8)$$

with the corresponding

$$x_i^{(k)} = x_h^{(k)}, \text{ and} \qquad (2.4.9)$$

$$f(x_i^{(k)}) = \min\{f(x_1^{(k)}), \ldots, f(x_{n+1}^{(k)})\} \qquad (2.4.10)$$

with the corresponding $x_i^{(k)} = x_l^{(k)}$. Since the polyhedron in E^n is made up of (n+1) vertices, $x_1, \ldots x_{n+1}$, let x_{n+2} be the centroid of all the vertices excluding x_h. The ccordinates of the centroid are given by

$$x_{n+2,j}^{(k)} = \frac{1}{n}\left[\left(\sum_{i=1}^{n+1} x_{ij}^{(k)}\right) - x_{kj}^{(k)}\right] \qquad (2.4.11)$$

$$j = 1, \ldots n$$

where the index j designates each coordinate direction.

The initial polyhedron usually is selected by a regular simplex (it does not have to be), with point 1 as the origin, or perhaps the centroid as the origin. The procedure of finding a vertex in E^n at which f(x) has a better value involves four operations:

1. Reflection:

Reflect $x_h^{(k)}$ through the centroid by computing

$$x_{n+3}^{(k)} = x_{n+2}^{(k)} + \alpha(x_{n+2}^{(k)} - x_h^{(k)}) \qquad (2.4.12)$$

where $\alpha > 0$ is the reflection coefficient,

$x_{n+2}^{(k)}$ = centroid computed by equation

$x_h^{(k)}$ = vertex at which f(x) is the largest of (n+1) values of f(x) on kth stage

2. Expansion

If $f(x_{n+3}^{(k)}) \leq f(x_l^{(k)})$, expand the vector $(x_{n+3}^{(k)} - x_{n+2}^{(k)})$ by computing

$$x_{n+4}^{(k)} = x_{n+2}^{(k)} + \gamma(x_{n+3}^{(k)} - x_{n+2}^{(k)}) \qquad (2.4.13)$$

where $\gamma > 1$ is the expansion coefficient. If $f(x_{n+4}^{(k)}) < f(x_l^{(k)})$, replace $x_h^{(k)}$ by $x_{n+4}^{(k)}$ and continue from step 1 with k = k + 1. Otherwise, replace $x_h^{(k)}$ by $x_{n+3}^{(k)}$ and continue from step 1 with k = k+1.

3. Contractions

If $f(x_{n+3}^{(k)}) > f(x_i^{(k)})$ for all $i \neq h$, contract the vector

$(x_h^{(k)} - x_{n+2}^{(k)})$ by computing

$$x_{n+5}^{(k)} = x_{n+2}^{(k)} + \beta(x_h^{(k)} - x_{n+2}^{(k)}) \qquad (2.4.14)$$

where $o<\beta<1$ is the contraction coefficient. Replace $x_h^{(k)}$ by $x_{n+5}^{(k)}$ and return to step 1 to continue the search on the (k+1) st stage.

4. Reduction

If $f(x_{n+3}^{(k)}) > f(x_h^{(k)})$, reduce all the vectors,

$(x_i^{(k)} - x_L^{(k)})$, $i = 1, \ldots, n+1$, by one half from $x_L^{(k)}$ by computing

$$x_i^{(k)} = x_L^{(k)} + 0.5(x_i^{(k)} - x_L^{(k)}) \quad i = 1, \ldots n+1 \qquad (2.4.15)$$

and return to step 1 to continue the search on the (k+1)st stage.

The criterion used by Nelder and Mead to terminate the search was to test to determine if

$$\{\frac{1}{n+1} \sum_{i=1}^{n+1} [f(x_i^{(k)}) - f(x_{n+2}^{(k)})]^2\}^{\frac{1}{2}} \leq \varepsilon \qquad (2.4.16)$$

where ε is an arbitrary small number, and $f(x_{n+2}^{(k)})$ is the value of the objective function at the centroid $x_{n+2}^{(k)}$.

Figure 2.4.1 is an information flow diagram of the flexible polygon method. The flexible polyhedron, as opposed to the rigid simplex, is designed to adapt itself to the topography of the objective function, elongating down long inclined planes, changing direction in curving valleys, and contracting in the neighbourhood of a minimum.

The reflection coefficient α is used to project the vertex with the largest value of f(x) through the centroid of the flexible polyhedron. The expansion coefficient γ is used to elongate the search vector if the reflection has produced a vertex with a value of f(x) smaller than the smallest f(x) obtained prior to the reflection. The contraction coefficient β is used to reduce the search vector if the reflection has not produced a vertex with a value of f(x) smaller than the second largest value of f(x) obtained prior to the reflection. Therefore, by means of either expansions or contractions, the size and shape of the flexible polyhedron are scaled to fit into the particular topology of the problem being solved.

Lewis et at[57] estimated kinetic parameters for propylene dispropotionation. Numerous Hougen and Watson[53] type rate expression were simplified to the initial rate form which assumes products to be present in negligible amount. Of the rate expression considered only the following dual site surface expression gave satisfactory correlation of the initial rate data

$$r = \frac{k(P_p^2 - P_E P_B / K_{eq})}{(1 + K_E P_E + K_P P_P + K_B P_B)^2} \qquad (2.4.17)$$

when reduced to the initial rate form equation (2.4.17) become

$$r = kP_p^2/(1 + K_P P_P)^2 \qquad (2.4.18)$$

Equation (2.4.18) was rewritten in the form

$$Y = a + bP_P \qquad (2.4.18a)$$

where $Y = P_p/\sqrt{r}$, $a = 1/\sqrt{k}$ and $b = K_p/\sqrt{k}$

values of a and b were determined from equation (2.4.18a) by linear least squares treatment of the initial rate data at each of three temperatures investigated. Values of k and K_P determined solely from initial rate data gave preliminary estimates of K_P and k, two of the four parameters which were to be determined in equation (2.4.17). The fifth was calculated from data by Rossini[58] assuming cis and trans 2-butene to be in equilibrium at each temperature.

They assumed that the remaining adsorption coefficients K_E, K_P and K_B appearing in equation (2.4.17) would be the same order of magnitude at a given temperature. Using this assumption, an iterative non-linear least - squares computer program was written which utilized the initial rate correlation value of K_P at each temperature as initial estimates for K_E and K_B as well.

Hosten and Froment[32] studied the isomerization of n-pentane on a commercial reforming catalyst (Pt/Al_2O_3) in an isothermal, bench scale, fixed bed reactor. Reaction rate equations of the Hougen - Watson type were derived on the basis of the generally accepted mechanism for skeletal isomerizations. The rate equations derived were non-linear in the parameters. For example when the surface reaction of isomerization of n-pentene into i-pentene is postulated to be the slowest step, the overall rate equation is given by

$$r = \frac{k\, K_5 \left(P_m - \frac{P_N}{K_5 K_6 K_7}\right)}{1 + K_5\, P_m + \frac{1}{K_7} P_N} \qquad (2.4.19)$$

Using linear regression approach, the equation was transformed into a relation which is linear in groups of combinations of the kinetic parameters. Replacing $K_5 K_d$ by K_A and $1/K_7 k_h$ by K_B, equation (4) was then rearranged to give

$$y = \frac{P_A - P_B/K}{r} = \frac{1}{k} P_A + \frac{K_B}{kK_A} P_B + \frac{1}{kK_A} P_{H_2} \qquad (2.4.20)$$

The rate equation now takes a form which allows estimation of the groups $1/k$, $1/kK_A$ and K_B/kK_A by linear regression. Subsequently, the parameters are easily calculated.

Some objections may be formulated concerning the method of the preceding paragraph involving rearrangement of the terms of the rate equation. Indeed, the statistical theory requires that the experimental error is normally distributed with zero mean and constant variance. These conditions are generally fulfilled for the error associated with the real

dependent variable. The error on the group y, however, does not necessarily meet these conditions, since y is a combination of the dependent and independent variables. Moreover, the parameter estimates can be influenced by the fact that the residual sum of squares of the group y is minimized, instead of the sum based on the reaction rate itself.

Therefore, they decided also to minimize

$$\Sigma (r - \hat{r})^2$$

where $\hat{r}$ is the calculated reaction rate. Since equation (2.4.19) is not linear in the parameters, search techniques are involved. The rate expression (equation (2.4.19)was developed in a Taylor series retaining only the partial derivatives of the first order

$$r[x,K^{(j+1)}] = r[x,K^{(j)}] + \Sigma \frac{\partial r}{\partial K_i}\bigg|_{K^{(j)}} \Delta K_i^{(j)} \qquad (2.4.21)$$

The method of linear least squares applied to this linear equation provides successive approximations for the parameters.

A comparison of the parameter values obtained using the different methods show that, $1/kK_A$ and K_B/kK_A are nearly independent of the method. In most cases, however $1/k$ values are not comparable.

2.5 Modelling Studies on Variable Activity Catalysts

The development of deactivation kinetic models for solid catalyst is a very important aspect in the study of catalysts and some problems regarding their development have

been highlighted for instance by Butt[59,60], Froment[51] and Hegedus and McCabe[62].

Two broad forms of catalyst deactivation models can be classified as separable and non separable forms. Modelling done under the principle of separability results in a rate equation that incorporates a term that represents the activity of the catalyst. Such term can be separately determined. On the other hand, modelling following the non-separability approach results in a rate equation that incorporates the activity of the catalyst, but such activity term can neither be isolated nor determined separately[63].

Most models of catalyst deactivation by coking are of the separable form as will be discussed below.

Voorhie's[64] model:

$$N_C = at^n$$

The model expresses the quantity of coke N_C deposited on the catalyst as a function of time of deactivation, t raised to a power n where both a and n are constants. The expression was used to model the deactivation by coking in the hydroisomerization and hydrocracking of n-paraffins using Mordrnite bifunctional catalyst. For a conversion of cracking process below 15% and for constant deactivation rate, n was found to be constant.

Other researchers like Eberly et al[65] and Dumez and Froment[66] showed the inconsistency of the model with respect to the constant n. Eberly et al[65] found that the constants

depend on the reaction conditions: n varied between 0.41 to 0.82 as the feed rate decreased from 20v/v/hr to 0.2v/v/hr while the conversion decreased from 0.29 to 0.049. Dumez and Froment[66] found that n decreased from 0.55 to 0.35 with increasing time on stream. Even though the model can predict the coke content with respect to time of deactivation, it is not a rate law from which mechanisms of coke formation can be derived and cannot be used to study the kinetics of deactivation.

Levenspiel[67] proposed a model for the conversion of reactant A to product R based on the separability approach. A summary of the model is as follows:

2.5.1 Levenspiel's Model

For the conversion of reactant A to product R, Levenspiel[67] proposed the following reaction paths for deactivation based on separability approach.

$$A \longrightarrow R + P \qquad (1)$$

or

$$A \longrightarrow R \quad \text{(Parallel reaction)}$$
$$\searrow P \qquad (2)$$

$$A \longrightarrow R \longrightarrow P \quad \text{(Series reaction)} \qquad (3)$$

$$A \longrightarrow R \quad \text{(Side by side)} \qquad (4)$$

$$A \longrightarrow P \qquad (5)$$

where P is the coke.

The rate equations for the main and coking reactions are given by:

Reaction rate = $F_1\left(\begin{matrix}\text{main stream}\\ \text{temperature}\end{matrix}\right) \cdot F_3\left(\begin{matrix}\text{main stream}\\ \text{concentration}\end{matrix}\right) \cdot$

$$F_5\left(\begin{matrix}\text{activity of}\\ \text{catalyst}\end{matrix}\right) \qquad (2.5.1)$$

$$-r_A = k\, C_A^n\, a = k_o\, (\exp(-E/RT))\, C_A^n\, a \qquad (2.5.2)$$

Deactivation rate = $F_2\left(\begin{matrix}\text{main stream}\\ \text{temperature}\end{matrix}\right) \cdot F_4\left(\begin{matrix}\text{main stream}\\ \text{concentration}\end{matrix}\right) \cdot$

$$F_6\left(\begin{matrix}\text{Present state}\\ \text{of catalyst}\end{matrix}\right) \qquad (2.5.3)$$

$$\frac{-da}{dt} = k_d\, C_i^{n1}\, a^d = k_{d_o}(\exp(-E_d/RT))\, C_i^{n1}\, a^d \qquad (2.5.4)$$

For parallel and consecutive reactions:

$$\begin{array}{l} A \longrightarrow R \longrightarrow P \downarrow \\ \qquad\searrow \\ \qquad\quad P\downarrow \end{array} \qquad (6)$$

$$\frac{-da}{dt} = k_d (C_A + C_R)^{n'}\, a^d \qquad (2.5.5)$$

Since $C_A + C_R$ is a constant for specific concentration

$$\frac{-da}{dt} = k_d\, a^d \text{ (independent rate of deactivation)} \qquad (2.5.6)$$

Solution to rate equations for specific conditions.

A. Conditions;

(a) Activity independent of concentration $\Longrightarrow n^1 = o$

(b) 1st order reaction $\Longrightarrow n=1$

(c) 1st order of deactivation $\Longrightarrow d=1$

(i) For reactions performed with batch - solids and batch fluid:

$$a = a_o \exp(-k_d t) \tag{2.5.7}$$

$$\ell n \frac{C_{Ao}}{C_A} = \frac{k_w}{k_d V} [1 - \exp(-k_d t)] \tag{2.5.8}$$

(ii) For reactions performed with batch-solids, mixed constant flow of fluid:

$$a = a_o \exp(-k_d t) \tag{2.5.9}$$

$$\ell n \left[\frac{C_{Ao}}{C_A} - 1 \right] = \ell n(k\tau) - k_d t \tag{2.5.10}$$

where

$$\tau = WC_{Ao} \mid F_{Ao} \tag{2.5.11}$$

(iii) For reactions performed with batch solid, plug constant flow of fluid:

$$a = a_o \exp(-k_d t) \tag{2.5.12}$$

$$\ell n \left[\ell n \left(\frac{C_{Ao}}{C_A} \right) \right] = \ell n(\tau k) - k_d t \tag{2.5.13}$$

(iv) For reactions performed with batch solid, mixed changing flow of fluid (keeping C_A fixed)

$$\ell n \, \tau' = k_d t + \ell n(C_{Ao} - C_A)/kC_A \tag{2.5.14}$$

where the feed flow rate is varied to keep final concentration of reactant constant.

(v) For reactions performed with batch solid, plug changing flow of fluid (keeping C_A, out fixed)

$$\ell n\ \tau^{1} = k_d t + \ell n\left(\frac{1}{k}\ \ell n\left(\frac{C_{Ao}}{C_A}\right)\right) \qquad (2.5.15)$$

The above method for the prediction of the activity of the catalyst with respect to time of deactivation can be extended to any reaction order n and deactivation order d if activity is concentration independent, i.e $n^i = o$.

B. Conditions:

(a) Activity made independent of concentration by keeping concentration of reactant C_A, constant

(b) nth order of reaction

(c) dth order of deactivation

For parallel deactivation in a mixed reactor,

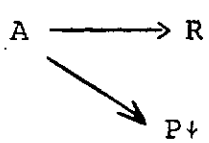

$$-r'_A = kC_A^{\,n}\, a = (kC_A^{\,n})a = k'_d a \qquad (2.5.16)$$

$$\frac{-da}{dt} = k_d C_A^{\,n'} a^d = (k_d\, C_A^{\,n'})a^d = k'_d\, a^d \qquad (2.5.17)$$

where C_A is kept constant

From the equations above

$$\tau'^{d-1} = C_1 + C_2 t \qquad (2.5.18)$$

Where:

$$C_1 = \frac{(C_{Ao} - C_A)^{d-1}}{k'} \qquad (2.5.19)$$

$$C_2 = \frac{(C_{Ao} - C_A)^{d-1}}{k'} \cdot (d-1)k_d' \qquad (2.5.20)$$

$$\tau' = WC_{Ao}/F_{Ao} \qquad (2.5.21)$$

For zeroth order of deactivation:

$$\frac{1}{\tau'} = -\frac{k'k_d}{(C_{Ao}-C_A)} t + \frac{k'}{(C_{Ao}-C_A)} \qquad (2.5.22)$$

1st order of deactivation:

$$\ell n\ \tau' = \ell n\frac{(C_{Ao} - C_A)}{k'} + k_d t \qquad (2.5.23)$$

2nd order of deactivation

$$\tau' = \frac{C_{Ao} - C_A}{k'} + \frac{(C_{Ao} - C_A)}{k'} k_d' t \qquad (2.5.24)$$

3rd order of deactivation

$$(\tau')^2 = \frac{(C_{Ao}-C_A)}{k'} + 2\frac{(C_{Ao} - C_A)^2}{k'} k_d' t \qquad (2.5.25)$$

With the right order of deactivation d, a plot of τ^{d-1} versus t will be linear in accordance with equation (2.5.18). While Levenspiel's model is based on sound theoritical principles, it cannot be used in this work due to the following reasons:

(a) The rate equation is based on a simple reaction system.

(b) In most cases, the activity of a deactivating catalyst is dependent on the concentration of the reactant.

Levenspiel's method of keeping the reactant concentration constant during deactivation for such cases is difficult to attain in reality. A time consuming experimental scheme is necessary to attain this condition in the laboratory. A series of experiments are performed at various space times τ with each experiment serving as a data point at a given reactant concentration C_A in order to obtain a single model of the set conditions.

(c) While Levenspiel's model will give information about the orders of deactivation and reaction, it will not provide any information about the number of active sites involved in the main and coking reactions.

(d) Furthermore, the model does not take into consideration, the mechanism leading to deactivation. Hence all information in the types of coking that has been observed in catalyst deactivation is lost.

2.5.2 Model of Froment

Froment[63] developed two models for the catalyst deactivation by coking, one describing catalyst deactivation by purely site coverage and another describing the deactivation by both active site coverage and pore blockage by coke.

A. Site Coverage

For a single site: If the conversion of A to B is rate controlling for the reaction:

$$A \rightleftharpoons B \qquad (1)$$

The rate equation is given by:

$$r_A = k_r K_A C_1 (C_A - C_B/K) \qquad (2.5.26)$$

The irreversible adsorption of the coke precusor C is represented by:

$$C + 1 \longrightarrow C1 \qquad (2)$$

The total number of sites is given by:

$$C_t = C_1 + C_{A_1} + C_{B_1} + C_{c_1} \qquad (2.5.27)$$

but $C_{A_1} = C_A k_A C_1$ and $C_{B_1} = k_B C_B C_1$ (2.5.28)

Substitute in (2.5.27) and divide by C_1.

$$C_t = C_1 (1 + K_A C_A + K_B C_B + C_{c_1} / C_1) \qquad (2.5.29)$$

Substitute (2.5.29) into (2.5.26) and rearrange

$$-r_A = \frac{k_r C_t K_A (C_A - C_B/k)}{1 + K_A C_A + K_B C_B + C_{c_1} / C_1} \qquad (2.5.30)$$

$$\text{or} \quad r_A = \frac{C_t - C_{c_1}}{C_t} \quad \frac{k_r C_t K_A (C_A - C_B/K)}{1 + K_A C_A + K_B C_B} \qquad (2.5.31)$$

eqn.(2.5.30) is non-separable while equation (2.5.31) is separable with $\frac{C_t - C_{c_1}}{C_t}$ being the fraction of active sites

for single main reaction. For an M_A sites of the main reaction the activity of the catalyst is given by:

$$\phi_A = \frac{(C_t - C_{c1})^{M_A}}{C_t} \qquad 0 \leq \phi_A \leq 1 \qquad (2.5.32)$$

If the coke precusor is formed by a reaction in parallel to the main reaction i.e $A1 \longrightarrow C1$
the rate equation for the coking reaction is given by

$$r_c = \frac{dC_{c1}}{dt} = \frac{k_c C_t K_A \phi_c C_A}{1+K_A C_A + K_B C_B} = r_c^{\circ} \phi_c \qquad (2.5.33)$$

and if the coke precusor is formed by a reaction in series with the main reaction, i.e. $B1 \longrightarrow C1$

$$r_c = \frac{dC_{c_1}}{dt} = \frac{k_c C_t K_B \phi_c C_B}{1 + K_A C_A + K_B C_B} = r_c^{\circ} \phi_c \qquad (2.5.34)$$

Following the same procedure as in the main reaction and for m_c coking sites, the coking activity is given by:

$$\phi_c = \frac{(C_t - C_{c_1})^{m_c}}{C_t} \quad - 0 \leq \phi_c \leq 1 \qquad (2.5.35)$$

The rate of coke formation r_c and the rate of fractional site coverage, r_s^o, is given by:

$$r_s^o \phi_c = \frac{r_c^o}{C_t M_c} \phi_c \qquad (2.5.36)$$

Froment[63] related the activity ϕ to the rate of fractional site coverage r_s by the equation:

$$\phi_A = \phi_C = \exp\left(-\int_o^t r_s^o \, dt\right) \qquad (2.5.37)$$

and for differential operation,

$$\phi_A = \phi_C = \exp(-r_s^o t) \qquad (2.5.38)$$

B. Site Coverage and Pore Blockage

1. Deactivation in a Single Pore

For deactivation by coking in pores through site coverage and pore blockage, Froment[63] made the following assumptions:

1. Single site mechanism for both the main and the coking reactions.
2. The size of a molecule of coke depends on the reaction conditions and may become large enough to block the pores
3. The coke precusor deposits in a random manner on the active sites,
4. The rate of coke growth is extremely fast compared to the rate of formation of the coke precusor on an active site
5. There are no diffusional limitations.
6. Catalyst has single ended pores
7. No concentration gradients in the catalyst pore and the gas phase composition is kept constant with time.

Based on the above assumptions, Froment[63] derived an expression for the local deactivation function $\phi(t)$ as the

product of two probabilities: the probability that a site is accessible at time t and the conditional probability that an accessible site is not covered

$$\hat{\phi}(t) = \left(\frac{2}{N_s} \sum_{n=1}^{N_s} \exp(-n r_s^o t) - \exp(-N_s r_s^o t)\right) \qquad (2.5.39)$$

$$r_A = (r_A)_o \, \phi(t) \qquad (2.5.40)$$

2. Deactivation in a network of pores

For deactivation in a network of pores, the following assumptions were made:

1. A micro - macro pore network with micropores and macropores branching into two macropores
2. The rate of growth intrinsically much faster than the rate of formation of the coke precusor
3. The coke can grow to a size that can block the micropore but not the macropores.
4. There are no concentration gradients in the pores.

Based on the above assumption, Froment[63] presented the following model:

$$\phi(t) = \gamma s(t)(1-q^2) + (1-\gamma)s(t) \qquad (2.5.41)$$

$$q = \sigma/V \, (1-s(t))/1 + \sigma/V(1-s(t))) \qquad (2.5.42)$$

$$S(t) = \exp(-r_s^o t) \qquad (2.5.43)$$

$$r_A = (r_A)_o \, \phi(t) \qquad (2.5.44)$$

Froments approach offer quite a lot of information useful in the study of the changes in the physical properties of the catalyst with the time of deactivation. However, the model, as far as I know, has not been used by anybody else. The model, if successfully used, offers some advantages over the other models in providing information on some properties of the catalysts structure like the number of active sites per micropore and the ratio of micropore and macropore in the catalyst and how they affect the deactivation of the catalyst.

2.5.3 Cooper and Trimm[49] followed Froment's approach[63] and represented the main reaction as

$$A + * \rightleftharpoons A^* \quad (1)$$

$$A^* \longrightarrow B^* \text{ (rate determining step)} \quad (2)$$

$$B^* \rightleftharpoons B + * \quad (3)$$

The coking side reaction may involve either A* or B* and will result in the total number of active sites (C_t) being reduced by the number of coked sites (C_k). Both the main reaction and the coking reaction will slow as the number of coked sites increases, and Froment expressed this in terms of the equation:

$$\frac{-dC_*}{dC_k} = \alpha F(C_*) \quad (2.5.41)$$

where α is a constant, $\frac{-dC^*}{dt}$ is the rate of loss of active sites, C_*, and $\frac{dC_k}{dt}$ is the coking reactions. Then for

different order coking reactions, we may write:

Zero Order:

$$\frac{-dC_*}{dC_k} = \alpha \ , \quad C_* = C_t \ (1 - \alpha C_k) \tag{2.5.42}$$

1st Order

$$-\frac{dC_*}{dC_k} = \alpha C_* \ , \ C_* = C_t (e^{-\alpha C_k}) \tag{2.5.43}$$

2nd Order

$$-\frac{dC_*}{dC_k} = \alpha C_*^2 \ ; \ C_* = C_t \frac{1}{1 + \alpha C_k} \tag{2.5.44}$$

or in general

$$C_* = C_t \ \phi_i \tag{2.5.45}$$

where ϕ_i is the deactivation function. Expressing the kinetics of coking in terms of the Langmuir - Hinshelwood approach for the coking sequence of the type

$$hA_* \xrightarrow{r.d.s} C + nA \longrightarrow \text{Coke} \tag{2.5.46}$$

(h^{th} site mechanism)

$$\frac{dC_k}{dt} = k[A_*]^h = \frac{k(K_A C_A)^h \ C_*^h}{(1 + \Sigma K_j C_j)^h} \tag{2.5.47}$$

or

$$\frac{dC_k}{dt} = \frac{k(K_A C_A)^h \ C_t^h \ \phi_i^h}{(1 + \Sigma K_j C_j)^h} \tag{2.5.48}$$

where k_j is the adsorption coefficient and C_j is the concentration of the species. Or in terms of the various deactivation

functions.

$$\frac{dC_k}{dt} = r_o \phi_i \qquad (2.5.49)$$

where r_o is the reaction rate in the absence of deactivation.

2.5.4 The model of Corella and Asua:

The model of Corella and Asua[50] is based on parallel coking system which for a non simple reaction, they are represented by:

$$A + B \longrightarrow R + V \qquad (1)$$

$$A + B \longrightarrow S + V \qquad (2)$$

$$A + 6B \longrightarrow 4U + 4V \qquad (3)$$

$$(n+h)A \longrightarrow P \qquad (4)$$

or for simple reactions, represented by Froment's equation:

$$A \longrightarrow R + S \qquad (5)$$

$$M \longrightarrow P \qquad (6)$$

Reactions (1) to (3) and (5) are the main reactions while reactions (4) and (6) are the coking reactions. M is the substance causing deactivation and it is adsorbed on the catalyst surface.

Corella and Asua[50,68] represented the rate of activity decay by

$$-\frac{da}{dt} = \frac{(\text{kinetic term})\ (\text{Pressure term})^{n+h}}{(\text{chemisorption term})^{h}}\ xa^{d} \qquad (2.5.50)$$

where d, the order of deactivation is given by

$$d = \frac{m + h - m}{m} \qquad (2.5.51)$$

The different mechanisms of the model of Corella and Asua are given by:

Mechanism d-1: M is adsorbed in the coking reaction the same way it is adsorbed in the main reaction

$$M + I \rightleftharpoons MI \qquad K_m = C_m/P_m C_I \tag{7}$$

adsorption step

$$nM(g) + hMI \rightleftharpoons P_1I_h \tag{8}$$

coke precusor formation step

$$P_1I_h \rightleftharpoons P_2I_h \rightleftharpoons P_3I_h \tag{9}$$

coking sequence step

when coke precusor formation step is rate controlling, (i)

for h = 1

$$a^{1/m} = \exp\left(-\int_o^t \frac{k_d K_m P_m^{n+1}}{1+ K_A P_A + K_R P_R + K_s P_s (m-1)} dt\right) \tag{2.5.52}$$

(ii) for h ≠1

$$a^{(1-h)/m} = \frac{-h(1-h)}{\lfloor 1-h} \int_o^t \frac{k_d K_m^h P_m^{h+n}}{(1+K_A P_A + K_R P_R + (m-1) K_s P_s)^h} dt+1 \tag{2.5.53}$$

$$-\frac{da}{dt} = (mhL^{h-1} k_d K_m^h P_m^{h+n} / ((1+K_A P_A + K_R P_R + (m-1) K_s P_s)))^h \times a^{m+h-1/m} \tag{2.5.54}$$

The order of deactivation

$$d = (m + h - 1)/m \tag{2.5.55}$$

Mechanism d-2: M is adsorbed in a different way in the main reaction as M1, and adsorbed in the coking reaction as M*1. This indicates a different energy of adsorption

$$M+1 \underset{}{\overset{k_m^*}{\rightleftharpoons}} M^*1 \; ; \quad K_m^* = C_{m^*1}/C_1 P_m \qquad \text{(adsorption step)} \tag{2.5.56}$$

$$nM(g) + hM^*1 \overset{K}{\rightleftharpoons} P_1 1_h ; \; k_d = C_{P_1}/C_{m^*1} P_m^{\,n} \tag{2.5.57}$$

(coke precusor formation step)

$$P_1 1_h \rightleftharpoons P_2 1_h \rightleftharpoons P_3 1_h$$

(Coking sequence step)

when the coke precusor formation step is rate controlling, for $h \neq 1$,

$$a^{(1-h)/m} = \frac{-h(1-h)}{L^{1-h}} \int_o^t \frac{k_d K_m^{*h} P_m^{h+n}}{(1+K_A P_A + K_R P_R + (m-1)K_s P_s + K_m^* P_m)^h} dt + 1 \tag{2.5.58}$$

The summary of the different mechanisms and the corresponding deactivation functions $\psi(P_i, T)$ are shown in Table (2.5.1).

The models by Corella and Asua[50] are very comprehensive and informative. Deactivation parameters useful in analysing the specific mechanism of catalyst deactivation can be obtained from them. However, some of the models will be difficult to use due to insufficient information on some of the constants, like K_m^* necessary to model the catalyst deactivation. The assumption that h is both the number of active sites involved in the rate controlling step of the deactivation reaction

Table 2.5.1 : Mechanism and model of deactivation by Corella and Asua

Deactivation function, $\Psi(P_1,T)$	
Mechanism	Controlling step; 2nd
d-1 $nM_{(g)} + hM1 \longrightarrow P_1 1_h$	$\dfrac{mhL^{h-1}k_d K_m^h P_m^{n+h}}{(1+K_A P_A + K_R P_R (M-1) K_s P_s)^h}$ (1)
d-2 $nM_{(g)} + hM^*1 \longrightarrow P_1 1_h$	$\dfrac{mnL^{h-1}k_d K_m^{*h} P_m^{n+h}}{(1+K_A P_A + K_R P_R + (m-1)K_s P_s + K_m^* P_m)^h}$ (2)
d-3 $nM_{(g)} + hM1 \longrightarrow P_1 1_h$ (same as equation (1)	
d-4 $nM + hM^*1 \longrightarrow P_1 1_h$ (same as equation (2)	

Controlling step; 3rd	
d-1 $\rightleftharpoons P_2 1_h \rightleftharpoons P_3 1_h \rightleftharpoons$ for h=1	$\dfrac{mk_d K'^* P_m^{n+1}}{1+K_A P_A + K_R P_R + (m-1)K_s P_s k'' P_m^{n+1}}$ (4)
d-2 $\rightleftharpoons P_n 1_h \rightleftharpoons P_3 1_h \rightleftharpoons$ for h=1	$\dfrac{mk_d K^{*\prime}{}_m P_m^{n+1}}{1+K_A P_A + K_R P_R + (m-1)K_s P_s + K_m^* P_m + K_m^{*\prime\prime} P_m^{n+1}}$ (5)
d-3 $P_1 1_n \overset{+M}{\rightleftharpoons} (g) \rightleftharpoons P_2 1_h \overset{+M}{\rightleftharpoons} (g) \longrightarrow P_3 1_h$ for h=1	$\dfrac{mk_d K_m P_m^{n+3}}{1+K_A P_A + K_R P_R + (m-1)K_s P_s + K_1 K_m P_m^{n+1} + K_1 k_2 K_m P_m^{n+2}}$ (6)
d-4 $P_1 1_h \overset{+M}{\rightleftharpoons} (g) P_2 1_h \overset{+M}{\longrightarrow} (g) P_3 1_h$ for h=1	$\dfrac{mk_d K'^* P_m^{n+3}}{1+K_A P_A + K_R P_R + (m-1)K_s P_s + K_1 K_m^* P_m^{n+1} + K_1 K_2 K_m^* P_m^{n+2}}$ (7)

Table 2.5.1 (Contd.)

Mechanism	Deactivation function, $\psi(P_iT)$ Controlling step: 2nd	Controlling step: 3rd
d-5	$nM_{(g)} + hM1 \longrightarrow P_1{}^1{}_h$ (same as equation (1)	$P_1{}^1{}_h \underset{}{\overset{+M1}{\rightleftharpoons}} P_2{}^1{}_{h+1} \xrightarrow{+M1} P_3{}^1{}_{h+2} \rightleftharpoons$ $-da/dt \neq \psi_{(P_iT)} \cdot a^d$ (8)
d-6	$nM_{(g)} + hM1 \longrightarrow P_1{}^1{}_h$ $\frac{mL^{h-1}(h+1)k_d K_m^h P_m^{h+n}}{(1+K_A P_A + K_R P_R + (m-1)K_s P_s)^h}$ (3)	$P_1{}^1{}_h \rightleftharpoons P_2{}^1{}_{h+1}{}_b \longrightarrow P_3{}^1{}_{n+1}{}_b \rightleftharpoons$ $-da/dt \neq \psi_{(P_iT)} . a^d$ (9)

as well as the number of adsorbed reactant molecules involved in the same rate controlling step of the deactivation reaction, presupposes that one adsorbed reactant molecule occupies only one active site.

2.6 Coking Level On Pt/Al_2O_3 Catalyst

Barbier et al[69] established that two temperatures exists at which two peaks of coke formation on Pt/Al_2O_3 can be identified. At the lower temperature of 200°C having the smaller peak, the quantity of coke formed on the platinum metal site can be burnt off fastest, while at the higher temperature of 380°C with the higher peak, the quantity of coke deposited on the alumina support can be burnt off at the fastest rate. They also found that the greater the metal dispersion, the greater the amount of coke deposited per equal amount of accessible platinum metal site. In other words, the total amount of coke deposited on a given quantity of catalyst is a function of the number of platinum metal sites accessible for reaction. In agreement with the work of Tarnam and Kriz[70] they reported that the amount of coke deposited is a function of the catalyst composition. They observed that coking is more extensive on Pt/Al_2O_3 with large platinum loading.

Cooper and Trimm (49) in their contribution to the study of coke deposited on Pt/Al_2O_3 measured the rate of uptake of carbon by the catalyst using pressurized microbalance for n-hexane, cyclohexane, benzene, 2- and 3- methylpentane and MCP at standard conditions. Typical results show that coking induced by benzene and cyclohexane occurs at a low rate, while every other hydrocarbon produces relatively high coking.

The tendency to coke formation decreases in the order

MCP > 3 - methyl pentane ∿ n-hexane >

> 2 methyl pentane > benzene > cyclohexane

Using n-hexane as typical of a high coking hydrocarbon and benzene as typical of a low coking feed, they carried out various tests on the assumption that coking was connected with acidity. Coking was compared in the absence and presence of Cl^- in the feed. Coke formation from benzene remained approximately the same. They then examined the effect of temperature on coking for two hydrocarbons and found that the relative rate of coking were maintained at all temperatures.

By comparing the coking of Pt/Al_2O_3 catalyst by C_6 hydrocarbons, Cooper and Trimm[49] concluded that the rate of coke formation may be fast (n-hexane, methyl pentanes) or slow (benzene, cyclohexanes). The activity of the catalyst appears to affect fast coking but not slow coking. Coke, involving carbon and high molecular weight carbonlike polymers, can be formed on metals[71] and on acidic catalyst[72]. As a result, slow coke formation from benzene and cyclohexane could be attributed to the inert nature of the hydrocarbons or to the fact that reactions involving these hydrocarbons occur predominantly on the metal function.

Lankhorst et al[73] reported the possibility of hydrogenating coke deposited between the temperatures 210 and 310°C in the hexane reforming reaction, and the failure to hydrogenate the coke formed at high temperatures like 450°C due to the massive deposit of the coke at such temperatures. The result

of Lankhorst et al[73] showed that the rate of coke deposition on a naphtha reforming catalyst depends on the surface concentration of coke precusors (mainly olefins) and the H_2 that hydrogenates them to harmless paraffins.

2.7 The Role of Rhenium in Bimetallic Pt-Re/Al_2O_3 Catalyst

Despite the fact that Pt-Re/Al_2O_3 catalyst was introduced into the reforming industry in the late sixties, the role of rhenium in the bimetallic catalyst is still unclear.

Whether Pt and Re form an alloy when supported on alumina as they do when they are bulk metals has attracted the attention of many researchers. Evidence for some substantial interaction, possibly alloy formation, comes from the shift to lower temperature of the H_2 uptake corresponding to Re reduction when Pt is present[74]. H_2/O_2 titrations have provided evidence about Pt-Re interactions. Compared to the separately supported metals, the bimetallics showed reduced H_2 and increased O_2 uptake, suggestive of alloy formation in the Pt/Re/Al_2O_3 catalyst[75].

Reaction studies were also used to probe alloy formation. Laboratory investigation of several reactions revealed complex behaviour[76]. Activity for 1,1,3 trimethyl cyclohexane hydrogenolysis declined monotonically as Re was added to a level less than that obtained when the two metals were supported separately. Activity in benzene hydrogenation, cyclopentane hydrogenolysis, butane hydrogenolysis and benzene - deuterium exchange was a maximum near 70% Re. This behaviour was understood as the combination of the monometallic activities with a subtle (undefined) electronic interaction between the

metals. The same investigators later confirmed their findings for cyclopentane hydrogenolysis and showed that the magnitude of activity enhancement was correlated with the extent of Re reduction temperature decrease[74]. Subsequently, they found no activity increase for n-heptane decomposition, but increasing selectivity towards aromatics as Re was added[77]. More recently an extensive study of the effect of Re addition on reactions related to reforming[78] showed that rates of production of benzene from methylcyclopentane and of toluene from methylcyclohexane and the rate of self deactivation by methylcyclohexane (short term) were unaffected. In contrast, the rate for methylcyclopentane ring opening decreased, as did the rates for toluene dealkylation and self deactivation by methylcyclohexane(long term). The latter reactions are believed to be structure sensitive while the former are not, suggesting that Re directly affects Pt, as would be expected if Pt-Re alloys formed.

Surface area measurement has been used to examine the effects of catalyst pretreatment on reduced $Pt/Re/Al_2O_3$ catalysts[79]. The results indicate significant alloy formation in reduced $Pt/Re/Al_2O_3$ for all drying temperatures of 500°C or less. While the surface amount of unalloyed Pt-Re is insensitive to the drying temperature, the surface amount of unalloyed Re varies significantly with the drying temperature. Reduction of the $Pt/Re/Al_2O_3$ catalyst dried at 100°C, which contains no unalloyed Re, is complete after 1hr of 500°C H_2 reduction. Reduction of the $Pt/Re/Al_2O_3$ catalyst dried at 500°C H_2 which does contain unalloyed Re, is not complete until after 15h of 500°C H_2 reduction. For both drying

temperature, alloy formation is complete after 1h of 500°C H_2 reduction.

The works of Dowell[80], Cooper and Trimm[49] showed that one of the advantages of rhenium in the catalyst is the operation at low pressures and high temperatures without the excessive coke deposit that characterize those conditions with monometallic catalysts.

Bertolocini and Pellet[81] explained how rhenium prevents cyclopentane dimerization to naphthalene, which is a strong coke precusor, by promoting the ring opening reactions to harmless paraffins. They also pointed out the inability of rhenium to prevent deactivation in cases where naphthalene is formed from some other sources. They observed that rhenium does not have to stay together with platinum on the same support to function. However, they must be close and mixed together (especially if the coke precusor is formed in the reactor).

2.8 Model Used for Catalyst Mortality:

Following the method of Cooper and Trimm[49] and Correla and Asua[50,68] a model which makes use of both concentration–time data and the data required by the model of Cooper and Trimm was derived by Omoleye[52] for the modelling of the deactivation of Pt/Al_2O_3 catalyst by the dehydrogenation of cyclohexane to benzene.

Consider the general coking reaction scheme

$$A \rightleftharpoons A^* \qquad (1)$$

$$nA + hA^* \longrightarrow P_1^* \quad (\text{slow}) \qquad (2)$$

$$P_1^* \rightleftharpoons P_2^* \rightleftharpoons P_3^* \rightleftharpoons \ldots \qquad (3)$$

In the above scheme, provision is made for the reaction of free reactants with adsorbed reactants for the production of coke precusor. The method of Cooper and Trimm made no such provision as it only accounted for the interaction of adsorbed reactants for the formation of the coke precusor.

The rate of growth of number of coked sites is given by:

$$\frac{dC_k}{dt} = kC_A^n \; C_{A^*}^h \qquad (2.8.1a)$$

$$= r\phi_i \qquad (2.8.1b)$$

where r_o is the kinetic equation of the main reaction determined from the kinetic data at zero time or in the absence of coke. r_o is of the form:

$$r_o = \frac{kK_jC_j - kK'\pi_iC_i}{1 + \Sigma K_jC_j} \qquad (2.8.2)$$

Therefore

$$\frac{dC_k}{dt} = \frac{kK_j^h \; C_j^{n+h} - (K')^h(\pi C_j)^{n+h}}{(1 + \Sigma K_jC_j)^h} \qquad (2.8.3)$$

The change in the number of active sites with respect to the number of coked sites is given by:

$$- \frac{dC_*}{dC_k} - \alpha \; C_*^n \qquad (2.8.4)$$

$$\int_{C_t}^{C_*} \frac{dC_*}{C_*^n} = -\alpha \int_{o}^{C_k} dC_k \qquad (2.8.5)$$

Since at t=0, $C_* = C_t$, $C_k = 0$

Case I, n=1

Equation (2.8.5) becomes

$$C_* = C_t\, e^{-\alpha C_k} \qquad (2.8.6)$$

For m-th site mechanism of the main reaction the activity a is given by

$$a = \left(\frac{C_*}{C_t}\right)m \qquad (2.8.7)$$

Substituting equation (2.8.6) into equation (2.8.7) yields

$$a = [\exp(-\alpha C_k)]^m \qquad (2.8.8)$$

Equation (2.8.3) becomes

$$\frac{dC_k}{dt} = \frac{kK_j^h C_j^{1+h} - (K')^h (\pi C_i)^{1+h}}{(1 + \Sigma K_j C_j)^h} \times C_t^h (\exp(-\alpha C_k)^h \qquad (2.8.9)$$

From equation (2.8.8) and (2.8.9)

$$a = \left[\alpha hk C_t^h \int_o^t \frac{K_j^h C_j^{1+h} - (K')^h (\pi C_i)^{1+h}}{(1 + \Sigma K_j C_j)^h} dt + 1\right] \qquad (2.8.10)$$

Equation 2.8.10 implies that a plot of

$$a^{-\frac{h}{m}} \text{ versus } \int_o^t \frac{K_j^h C_i^{1+h} - (K')^h (\pi C_i)^{1+h}}{(1 + \Sigma K_j C_j)^h} dt$$

should yield a straight line with an intercept of unity for the right value of h and m.

Case II, $n \neq 1$

$$C_* = [C_t^{1-n} - (1-n)\alpha C_k]^{\frac{1}{1-n}} \qquad (2.8.11)$$

$$\frac{dC_k}{dt} = \frac{k\{K_j^h C_j^{n+h} - (K')^h (\pi C_i)^{n+h}\}}{(1 + \Sigma K_j C_j)^h} \cdot \left[C_t^{1-n} - (1-n)\alpha C_k\right]^{\frac{h}{1-h}} \qquad (2.8.12)$$

Finally

$$a = \left[\frac{\alpha(h-n+1)k}{C_t^{n-h-1}} \int_o^t \frac{K_j^h C_j^{n+h} - (K')^h (\pi C_i)^{n+h}}{(1 + \Sigma K_j C_j)^h} dt + 1\right]^{\frac{m}{n-h-1}} \qquad (2.8.13)$$

Equation 2.8.13 implies that a plot of

$$a^{\frac{n-h-1}{m}} \text{ versus } \int_o^t \frac{K_j^h C_j^{n+h} - (K')^h (\pi C_i)^{n+h}}{(1 + \Sigma K_j C_j)^h} dt \qquad (2.8.14)$$

should yield a straight line with an intercept of unity for the right values of n,m and h.

Although the equations look complicated, the experimental data (concentration - time) data required to determine its parameters are quite easy to get. Again, the use of computers makes numerical solution to problems of this nature very easy as the algorithm required is so well known - least square fit for a linear plot and Simpson's rule or any other rule for numerical integration. The n, m and h values obtained from this model have mechanistic implications just like those of Corella and Asua[50,68].

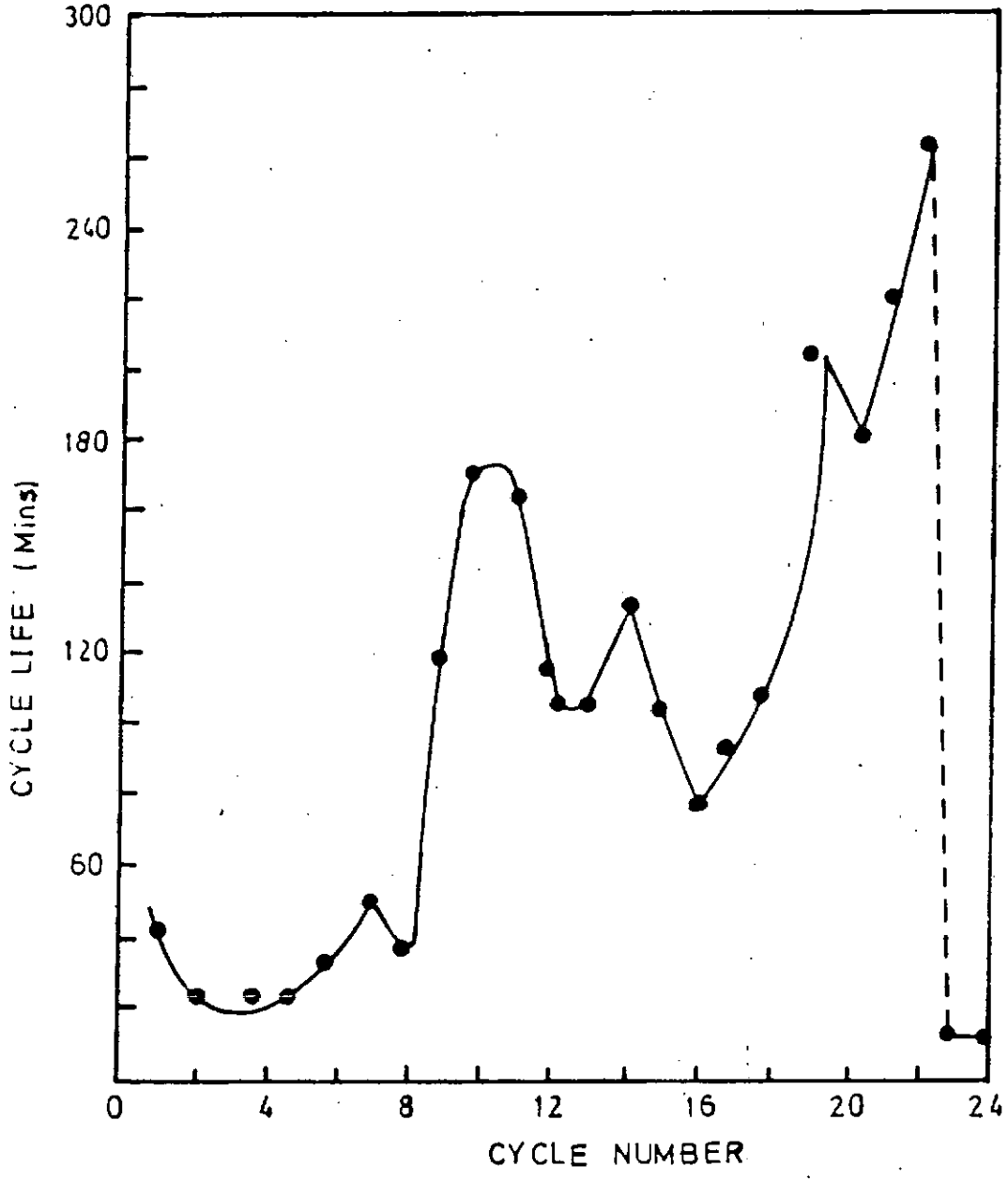

Fig. 2.3.1: Cycle Life Time Versus cycle number (Pt/Al_2O_3, 430°C)

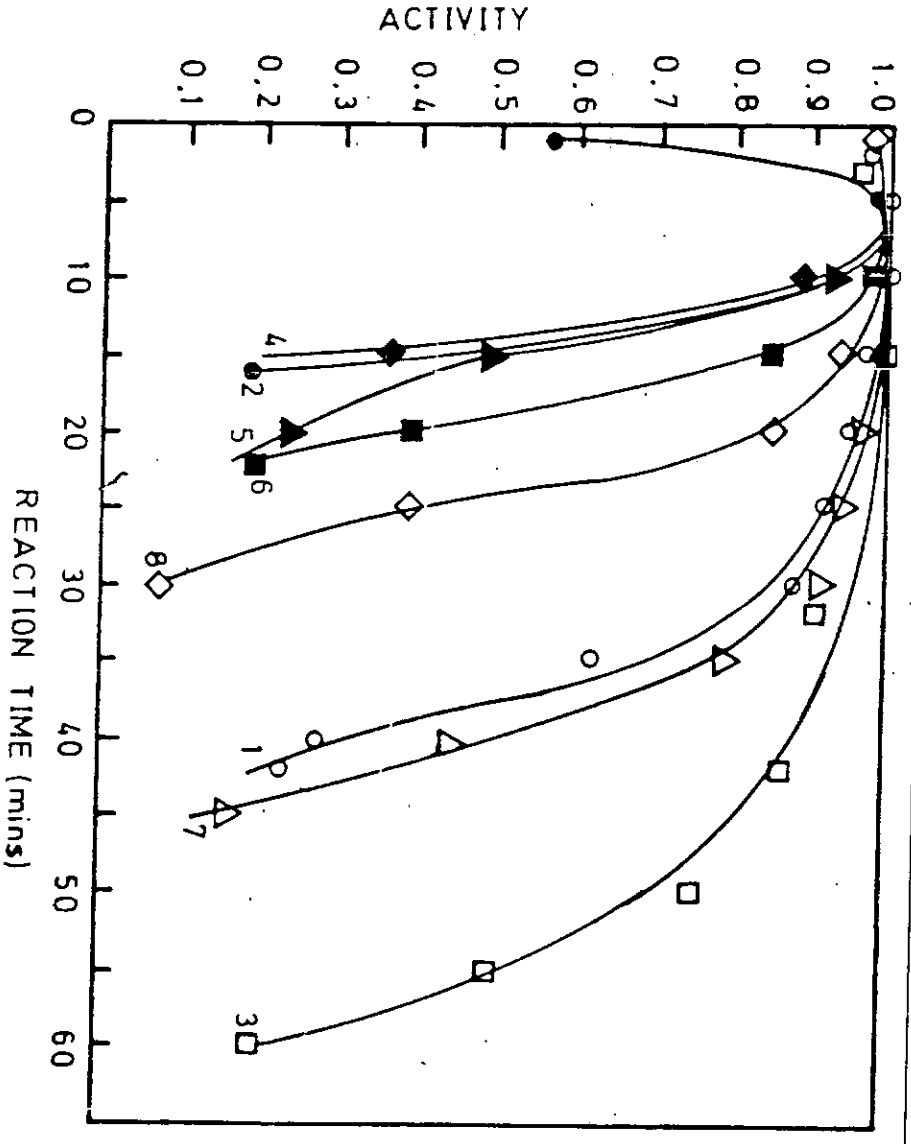

Fig. 2.3.2: Activity versus reaction time for the first stability state of Pt/Al_2O_3 (430°C)

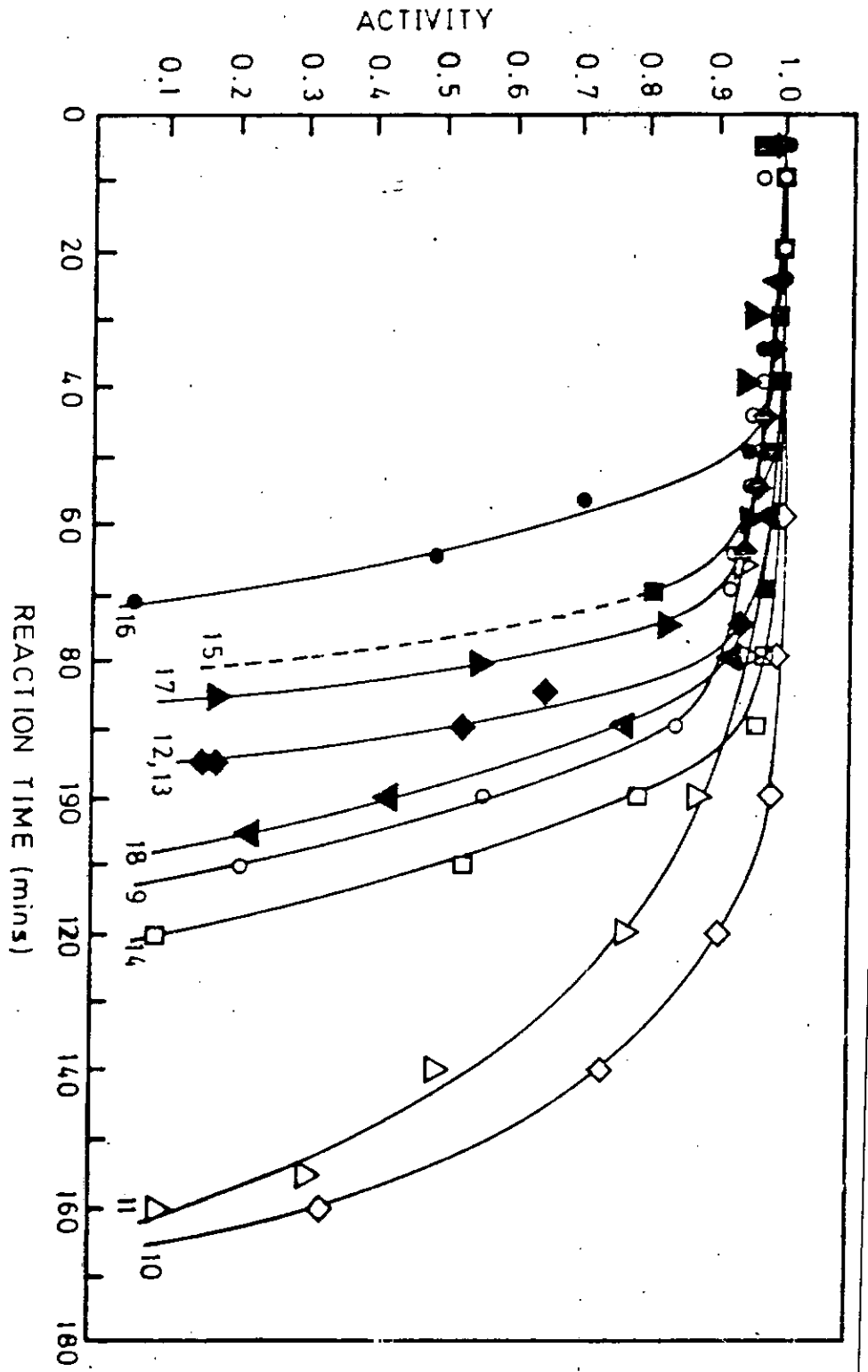

Fig.2.3.3: Activity versus reaction time for the second stability state of Pt/Al_2O_3 (430°C)

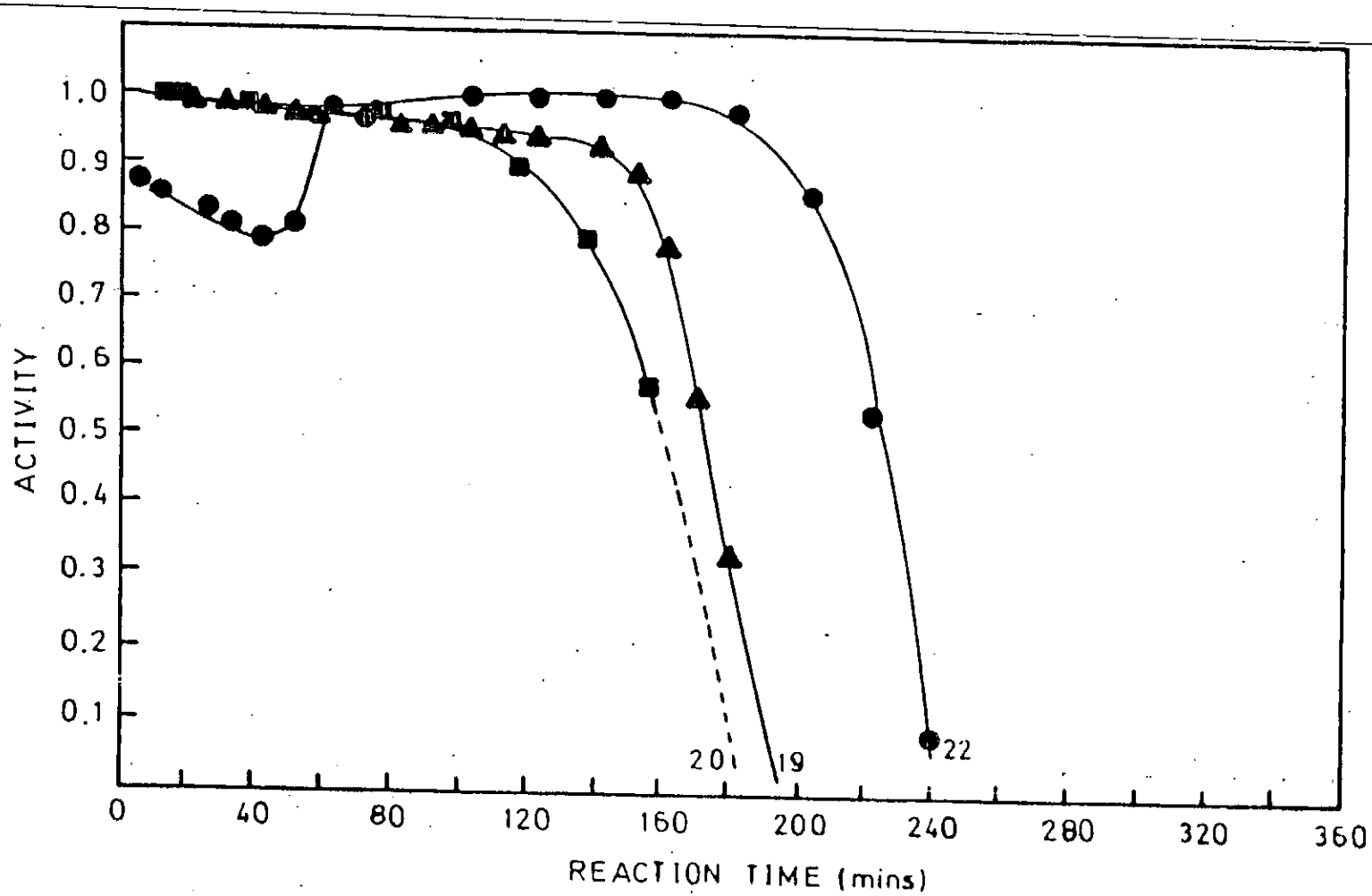

Fig.2.3.4: Activity versus reaction time for the third stability state of Pt/Al_2O_3 (430°C)

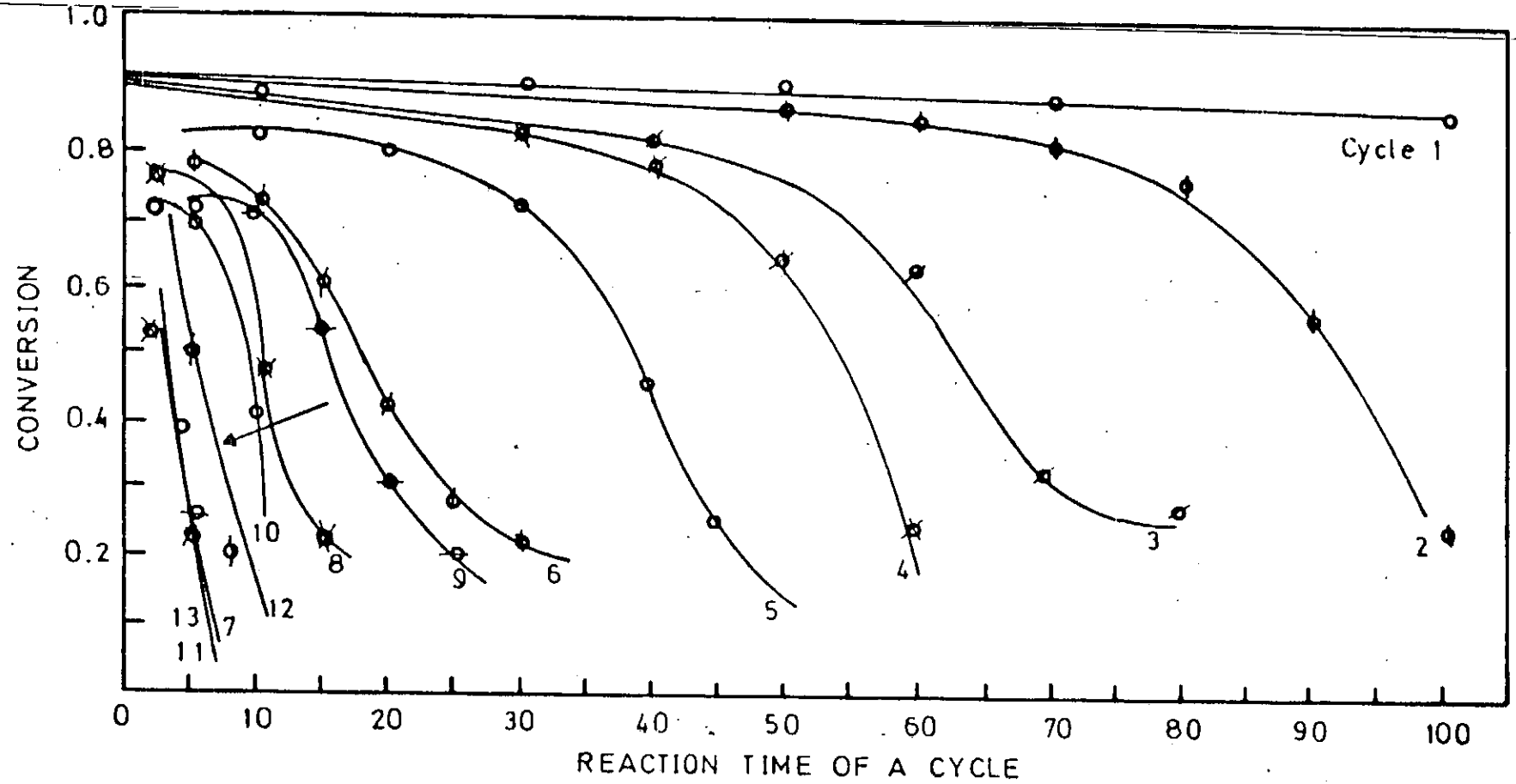

Fig.2.3.5: Conversion versus time of reaction ($Pt-Re/Al_2O_3$ 430°C)

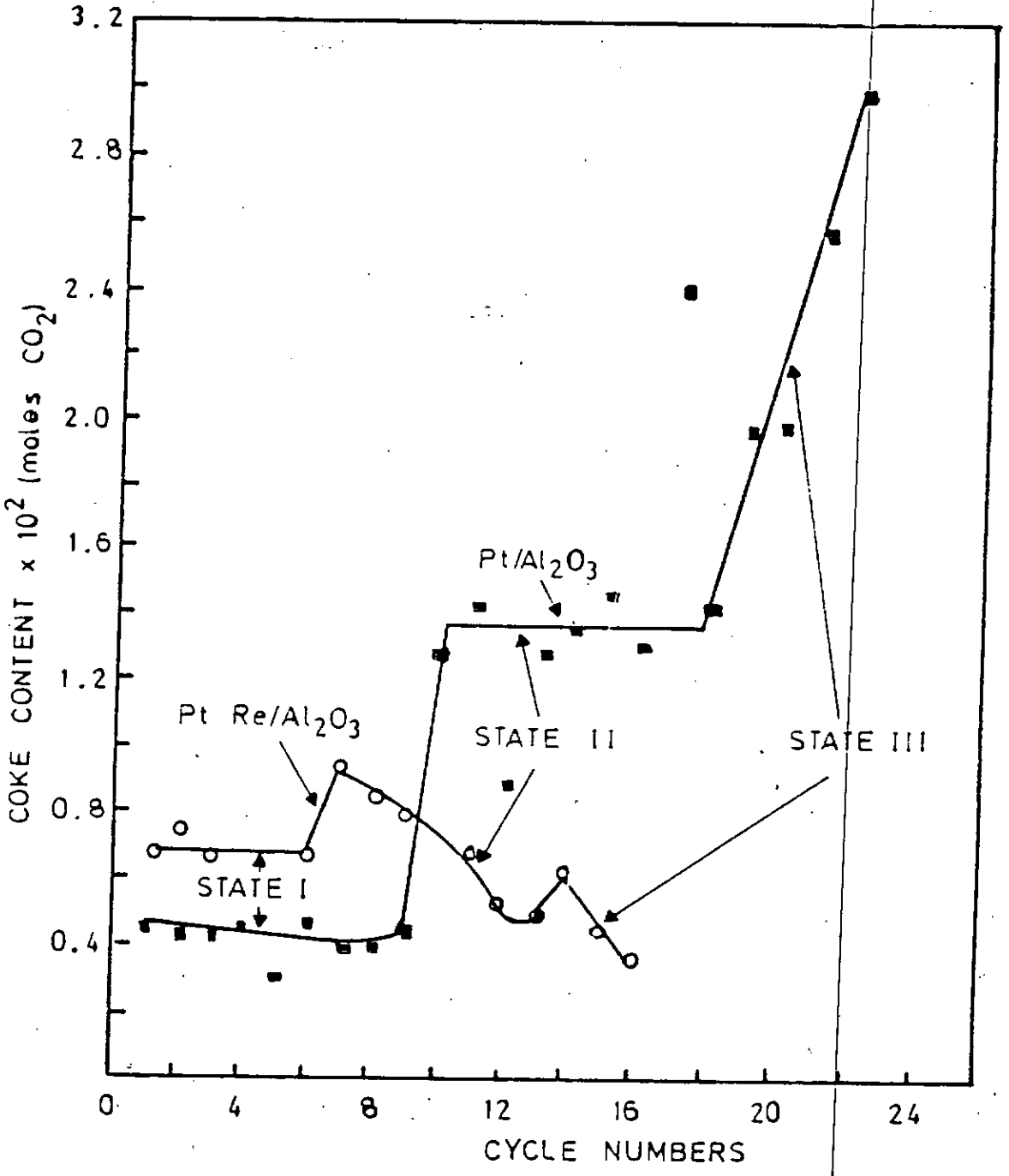

Fig.2.3.6: Coke content versus cycle numbers for Pt/Al_2O_3 and Pt-Re/Al_2O_3 at 430°C

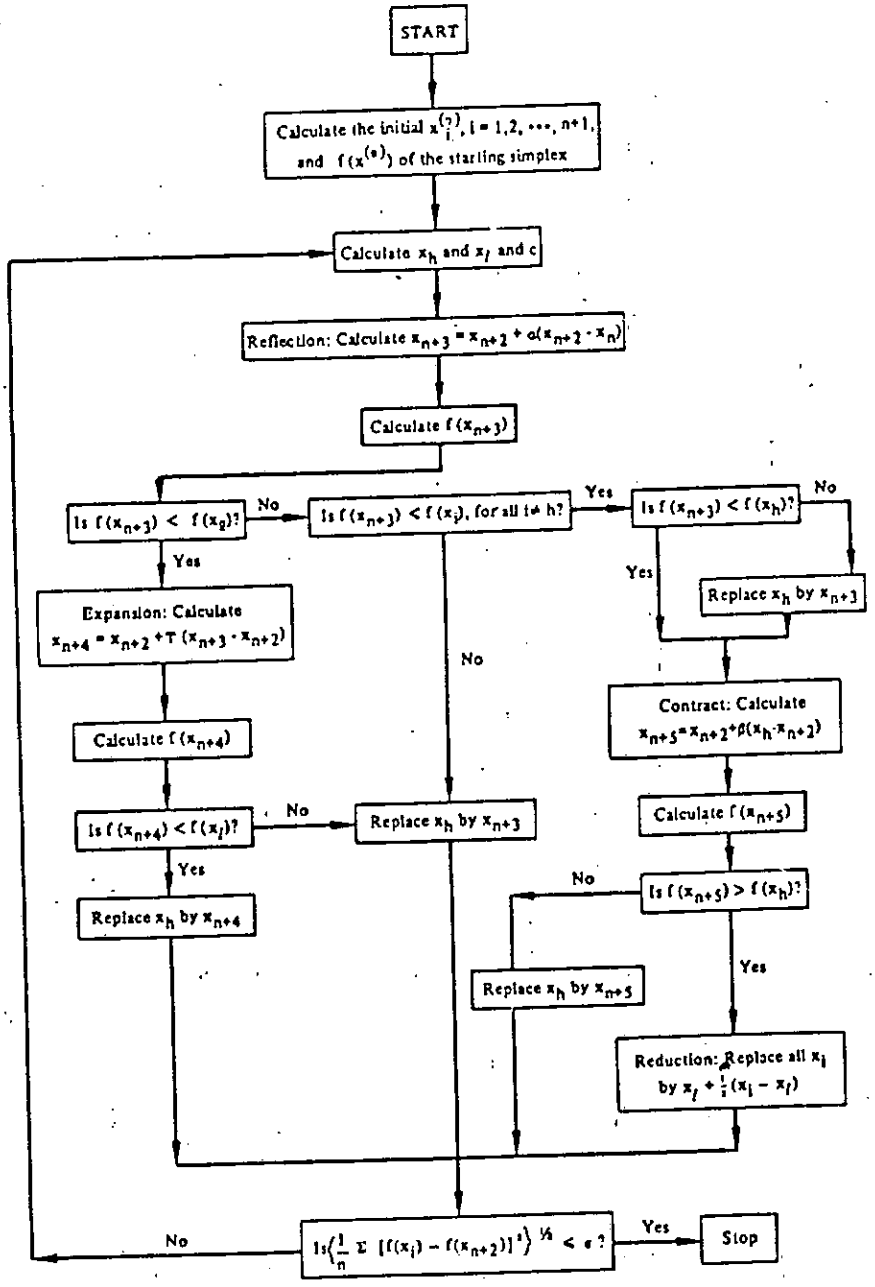

Fig.2.4.1: Information flow chart for the flexible polygon search of Nelder and Mead.

CHAPTER 3

DEVELOPMENT OF MECHANISTIC KINETIC MODELS

3.1 Constant Activity Kinetic Models

3.1.1 N - Octane

In a recent publication, Ako and Susu[1] used the pulse microcatalytic reactor to determine the reaction network for n-octane dehydrocyclization on acidic and nonacidic Pt/Al_2O_3 catalyst in H_2 carrier at 1.8 atm pressure and temperatures between 563 - 673k. The use of the pulse microcatalytic reactor minimized coking and enhanced the identification of the primary products. In that work, the following sequence of single reactions was identified as occuring on bifunctional Pt/Al_2O_3:

$$\text{n - Octane} \xrightarrow{\text{fast}} \text{iso octane} \begin{cases} \nearrow \text{ethylbenzene} \\ \searrow \text{o-xylene} \end{cases} \qquad (1)$$

P - and m - xylene were found to be secondary products.

In the pulse microcatalytic reactor, the dehydrocyctization reaction was relatively clean as no significant hydrocraked products were detected. With the CSTR however, the yield of hydrocracked products was high and this has to be accounted for in the kinetic scheme. The network was therefore modified for the CSTR as:

$$\text{n-octane} \begin{cases} \nearrow \text{HCP} \\ \xrightarrow{\text{fast}} \end{cases} \text{iso octane} \begin{cases} \nearrow \text{ethylbenzene} \\ \searrow \text{o-xylene} \end{cases} \qquad (2)$$

REACTION MECHANISM

The classical bifunctional mechanism is assumed to account for the products of n-octane conversion. The major aromatic products of n-octane dehydrocyclization were those predicted by direct 1,6 - ring closure. The sequence of elementary steps for two reaction schemes is shown in Tables 3.1 and 3.2. The dehydrogenation - hydrogenation steps occuring during the bifunctional mechanism have been omitted for ease of development of the rate equation. In Scheme I, n-octane is adsorbed on metal sites and the dehydrogenated species migrated to the acidic sites where it is hydroisomerized or hydrocracked. The iso-octane then migrates to the metal sites for hydrogenation prior to desorption (reaction 5). Hydrocracked products are desorbed (reaction 4) after formation (reaction 3). The predominant source of ethylbenzene and o-xylene is iso-octane, p - and m- xylene are then formed from any of the preceding products. Since the secondary products are probably not rate-determining, they are ignored in the kinetic sense although their coverages are accounted for in the site balance. The only difference between Schemes I and II is that hydrogen coverage is assumed to be sparce on the catalyst surface in Scheme II while it is incorporated into Scheme I.

In either scheme, each of the elementary steps could be rate determining in principle although some of the steps are unlikely candidates. In Scheme I, if the adsorption of n-octane is rate determining, the rate of the reaction is given by:

$$r_1 = k_1 C_N(S) - k_2(NS) \qquad (3.1.1)$$

The site balance is given by:

$$1 = (S) + (NS) + (IS) + (HCPS) + (EBS) + (OXS) + (PXS) + (MXS) + (HS) \qquad (3.1.2)$$

In the concept of the rate determining step, all other steps are in quasi - equilibrium and the unknown surface coverages (S), (NS) in equation (3.1) are expressed in terms of fluid phase species concentrations. In this manner, equation 3.1 becomes:

$$r_1 = \frac{k_1 C_N - \frac{k_2}{K_4 K_5} C_I}{1 + \left(\frac{1+K_5}{K_4 K_5}\right) C_I + \frac{C_{cp}}{K_3} + \frac{C_{EB}}{K_8} + \frac{C_{ox}}{K_9} + \frac{C_{mx}}{K_{11}} + \frac{C_{Px}}{K_{12}} + \frac{(C_{H_2})^{\frac{1}{2}}}{K_{10}}} \qquad (3.1.3)$$

where

$$K_3 = \frac{k_5}{k_6}$$

$$K_4 = \frac{k_7}{k_8}$$

$$K_5 = \frac{k_9}{k_{10}}$$

$$K_8 = \frac{k_{15}}{k_{16}}$$

$$K_9 = \frac{k_{17}}{k_{18}}$$

$$K_{10} = \frac{k_{19}}{k_{20}}$$

K_{11}, K_{12} = adsorption constants for m - and p - xylene, respectively.

It is unlikely that the production of hydrocracked products will be rate - determining and hence reactions 2 and 3 are ignored. A summary of the 8 derived rate equations for Scheme I are shown in Table 3 while those for Scheme II are shown in Table 4.

Table 3.1: Sequence of Elementary Steps for N-Octane Reaction (Reaction Scheme I)

$$N + S \underset{2}{\overset{1}{\rightleftharpoons}} NS \qquad (1)$$

$$NS \underset{4}{\overset{3}{\rightleftharpoons}} HCPS \qquad (2)$$

$$CPS \underset{6}{\overset{5}{\rightleftharpoons}} HCP + S \qquad (3)$$

$$NS \underset{8}{\overset{7}{\rightleftharpoons}} IS \qquad (4)$$

$$IS \underset{10}{\overset{9}{\rightleftharpoons}} I + S \qquad (5)$$

$$IS + S^* \underset{12}{\overset{11}{\rightleftharpoons}} EBS + HS^* \qquad (6)$$

$$IS + S^* \underset{14}{\overset{13}{\rightleftharpoons}} OXS + HS^* \qquad (7)$$

$$EBS \underset{16}{\overset{15}{\rightleftharpoons}} EB + S \qquad (8)$$

$$OXS \underset{18}{\overset{17}{\rightleftharpoons}} OX + S \qquad (9)$$

$$H\,S \underset{20}{\overset{19}{\rightleftharpoons}} \tfrac{1}{2}H_2 + S \qquad (10)$$

* For the stoichiometric balance of steps 6 and 7, six adsorbed hydrogen atoms are necessary for the formation of adsorbed ethylbenzene and o-xylene. However this will result in an exponent of 7 for the denominator of r_6 and r_7 (Scheme I) which is considered kinetically unacceptable. Hence, only one type of adsorbed hydrogen is considered to yield a more acceptable exponent of 2. The kinetic implication of this assumption is that hydrogen atoms are adsorbed in patches on the catalysts surface.

Table 3.2: Sequence of Elementary Steps for N-Octane Reaction (Reaction Scheme II)

$$N + S \underset{2}{\overset{1}{\rightleftharpoons}} NS \qquad (1)$$

$$N\,S \underset{4}{\overset{3}{\rightleftharpoons}} CPS \qquad (2)$$

$$CPS \underset{6}{\overset{5}{\rightleftharpoons}} CP + S \qquad (3)$$

$$N\,S \underset{8}{\overset{7}{\rightleftharpoons}} I\,S \qquad (4)$$

$$I\,S \underset{10}{\overset{9}{\rightleftharpoons}} I + S \qquad (5)$$

$$I\,S \underset{12}{\overset{11}{\rightleftharpoons}} EBS + 3H_2 \qquad (6)$$

$$I\,S \underset{14}{\overset{13}{\rightleftharpoons}} OXS + 3H_2 \qquad (7)$$

$$EBS \underset{16}{\overset{15}{\rightleftharpoons}} EB + S \qquad (8)$$

$$OXS \underset{18}{\overset{17}{\rightleftharpoons}} OX + S \qquad (9)$$

Table 3.3: Derived Rate Equations for Scheme I

RATE DETERMINING STEPS

1. Adsorption of n-octane (reaction 1)

$$r_1 = \frac{k_1 C_N - \frac{k_2}{K_4 K_5} C_I}{1 + \left(\frac{1+K_5}{K_4 K_5}\right) C_I + \frac{C_{CP}}{K_3} + \frac{C_{EB}}{K_8} + \frac{C_{ox}}{K_9} + \frac{C_{mx}}{K_{11}} + \frac{C_{Px}}{K_{12}} + \frac{(C_{H_2})^{\frac{1}{2}}}{K_{10}}}$$

2. Conversion of adsorbed n-octane to adsorbed iso octane (reaction 4)

$$r_4 = \frac{k_7 K_1 C_N - \frac{k_8}{K_5} C_I}{1 + K_1 C_N + \frac{C_I}{K_5} + \frac{C_{cP}}{K_3} + \frac{C_{EB}}{K_8} + \frac{C_{ox}}{K_9} + \frac{C_{Mx}}{K_{11}} + \frac{C_{Px}}{K_{12}} + \frac{(C_{H_2})^{\frac{1}{2}}}{K_{10}}} \qquad (3.1.5)$$

3. Desorption of adsorbed isooctane (reaction 5)

$$r_5 = \frac{k_9 K_1 K_4 C_N - k_{10} C_I}{1 + (K_1 + K_4 K_1) C_N + \frac{C_{cP}}{K_3} + \frac{C_{EB}}{K_8} + \frac{C_{ox}}{K_9} + \frac{C_{Mx}}{K_{11}} + \frac{C_{Px}}{K_{12}} + \frac{(C_{H_2})^{\frac{1}{2}}}{K_{10}}} \qquad (3.1.6)$$

4. Conversion of adsorbed isooctane to adsorbed ethylbenzene (reaction 6)

$$r_6 = \frac{k_{11} K_1 K_4 C_N - \frac{k_{12}}{K_8 K_{10}} C_{EB} C_{H_2}^{\frac{1}{2}}}{\left(1 + K_1 C_N + \frac{C_I}{K_5} + \frac{C_{cP}}{K_3} + \frac{C_{EB}}{K_8} + \frac{C_{Mx}}{K_{11}} + \frac{C_{Px}}{K_{12}} + \frac{C_{H_2}^{\frac{1}{2}}}{K_{10}} + \frac{C_{ox}}{K_9}\right)^2} \qquad (3.1.7)$$

5. The conversion of adsorbed iso octane to adsorbed o xylene (reaction 7)

$$r_7 = \frac{k_{13} K_4 K_1 C_N - k_{14} C_{ox} C_{H_2}^{\frac{1}{2}}}{\left(1 + K_1 C_N + \frac{C_1}{K_5} + \frac{C_{cP}}{K_3} + \frac{C_{EB}}{K_8} + \frac{C_{ox}}{K_9} + \frac{C_{Mx}}{K_{11}} + \frac{C_{Px}}{K_{12}} + \frac{C_{H_2}^{\frac{1}{2}}}{K_{10}}\right)^2} \qquad (3.1.8)$$

6. Desorption of ethylbenzene (reaction 8)

$$r_8 = \frac{\frac{k_{15} K_{10}}{K_5} \frac{C_I}{C_{H_2}^{\frac{1}{2}}} - k_{16} C_{EB}}{1 + K_1 C_N + \frac{C_I}{K_5} + \frac{C_{cP}}{K_3} + \frac{K_6 K_{10}}{K_5} \frac{C_I}{C_{H_2}^{\frac{1}{2}}} + \frac{C_{ox}}{K_9} + \frac{C_{Mx}}{K_{11}} + \frac{C_{Px}}{K_{12}} + \frac{C_{H_2}^{\frac{1}{2}}}{K_{12}}} \quad (3.1.9)$$

7. Desorption of o-xylene (reaction 9)

$$r_9 = \frac{\frac{k_{17} K_{10}}{K_5} \frac{C_I}{C_{H_2}^{\frac{1}{2}}} - k_{18} C_{ox}}{1 + K_1 C_N + \frac{C_I}{K_5} + \frac{C_{cP}}{K_3} + \frac{C_{EB}}{K_8} + \frac{k_7 K_{10}}{K_5} \frac{C_I}{C_{H_2}^{\frac{1}{2}}} + \frac{C_{Mx}}{K_{11}} + \frac{C_{Px}}{K_{12}} + \frac{C_{H_2}^{\frac{1}{2}}}{K_{10}}} \quad (3.1.10)$$

8. Desorption of hydrogen (reaction 10)

$$r_{10} = \frac{\frac{k_9 K_6 K_8}{K_5} \frac{C_I}{C_{EB}} - k_{20} C_{H_2}^{\frac{1}{2}}}{1 + K_1 C_N + \frac{C_I}{K_5} + \frac{C_{cP}}{K_3} + \frac{C_{EB}}{K_8} + \frac{C_{ox}}{K_9} + \frac{K_6 K_8}{K_5} \frac{C_I}{C_{EB}} + \frac{C_{Mx}}{K_{11}} + \frac{C_{Px}}{K_{12}}} \quad (3.1.11)$$

Table 3.4: Derived Rate Equations for Scheme II

RATE DETERMINING STEPS

1. Adsorption of n-octane (reaction 1)

$$r_1 = \frac{k_1 C_N - \frac{k_2}{K_4 K_5} C_I}{1 + \left(\frac{1 + K_4}{K_4 K_5}\right) C_I + \frac{C_{cP}}{K_3} + \frac{C_{EB}}{K_8} + \frac{C_{ox}}{K_9} + \frac{C_{Mx}}{K_{10}} + \frac{C_{Px}}{K_{11}}} \quad (3.1.12)$$

2. Conversion of adsorbed n-octane to adsorbed isooctane (reaction 4)

$$r_4 = \frac{k_7 K_1 C_N - \frac{k_8}{K_5} C_I}{1 + \left(\frac{1+K_1K_5}{K_5}\right) C_I + \frac{C_{cP}}{K_3} + \frac{C_{EB}}{K_8} + \frac{C_{ox}}{K_9} + \frac{C_{Mx}}{K_{10}} + \frac{C_{Px}}{K_{11}}} \quad (3.1.13)$$

3. Desorption of isooctane (reaction 5)

$$r_5 = \frac{k_9 K_1 K_4 C_N - k_{10} C_I}{1 + (K_1 + K_4 K_1) C_N + \frac{C_{cP}}{K_3} + \frac{C_{EB}}{K_8} + \frac{C_{ox}}{K_9} + \frac{C_{Mx}}{K_{10}} + \frac{C_{Px}}{K_{11}}} \quad (3.1.14)$$

4. Conversion of adsorbed iso octane to adsorbed ethylbenzene (reaction 6)

$$r_6 = \frac{\frac{k_{11}}{K_5} C_I - \frac{k_{12}}{K_8} C_{EB} C_{H_2}^3}{1 + K_1 C_N + \frac{C_I}{K_5} + \frac{C_{cP}}{K_3} + \frac{C_{EB}}{K_8} + \frac{C_{ox}}{K_9} + \frac{C_{Mx}}{K_{10}} + \frac{C_{Px}}{K_{11}}} \quad (3.1.15)$$

5. Conversion of adsorbed iso octane to adsorbed o-xylene (reaction 7)

$$r_7 = \frac{\frac{k_{13}}{K_5} C_1 - \frac{k_{14}}{K_9} C_{ox} C_{H_2}^3}{1 + K_1 C_N + \frac{C_I}{K_5} + \frac{C_{cP}}{K_3} + \frac{C_{EB}}{K_8} + \frac{C_{ox}}{K_9} + \frac{C_{Mx}}{K_{10}} + \frac{C_{Px}}{K_{11}}} \quad (3.1.15)$$

6. Desorption of ethylbenzene (reaction 8)

$$r_8 = \frac{\frac{k_{15}K_6}{K_5}\frac{C_I}{C_{H_2}^3} - k_{16}}{1 + K_1C_N + \frac{C_I}{K_5} + \frac{C_{cP}}{K_3} + \frac{K_6}{K_5}\frac{KC_I}{C_H^3} + \frac{C_{ox}}{K_9} + \frac{C_{Mx}}{K_{10}} + \frac{C_{Px}}{K_{11}}} \quad (3.1.17)$$

7. Desorption of 0-xylene (reaction 9)

$$r_9 = \frac{\frac{k_{17}K_7}{K_5}\frac{C_I}{C_{H_2}^3} - k_{18}C_{ox}}{1 + K_1C_N + \frac{C_I}{K_5} + \frac{C_{cP}}{K_3} + \frac{C_{EB}}{K_8} + \frac{k_7}{K_5}\frac{C_I}{C_{H_2}^3} + \frac{C_{ox}}{K_9} + \frac{C_{Mx}}{K_{10}} + \frac{C_{Px}}{K_{11}}} \quad (3.1.18)$$

3.2 ISO OCTANE

Mechanistic rate equations were derived on the basis of the generally accepted mechanism for skeletal isomerization[32] namely:-

1. Adsorption of the reactant (paraffin) on a dehydrogenation - hydrogenation site, followed by dehydrogenation into an olefin;
2. Desorption of the olefin from the dehydrogenation - hydrogenation site and diffusion to a skeletal re-arranging site, which converts the olefin to iso-olefin via a carbonium ion mechanism, and
3. Desorption of the iso-olefin from the skeletal re-arranging site and diffusion to a hydrogenation dehydrogenation site where it is finally hydrogenated into a paraffin molecule.

For an industrial bifunctional reforming catalyst, this mechanism can be written as shown in Scheme III below:

Table 3.5

Sequence of elementary steps for the isomerization of iso-octane (Scheme III)

Dehydrogenation (metal site)

$$A + \ell \underset{2}{\overset{1}{\rightleftharpoons}} A\ell \quad ; \quad K_1 = [A\ell]/[A][\ell] \qquad (1)$$

$$A\ell + \ell \underset{4}{\overset{3}{\rightleftharpoons}} M\ell + H_2\ell \quad ; \quad K_2 = [M\ell][H_2\ell]/[A\ell][\ell] \qquad (2)$$

$$H_2\ell \underset{6}{\overset{5}{\rightleftharpoons}} H_2 + \ell \quad ; \quad K_3 = [H_2][\ell]/[H_2\ell] \qquad (3)$$

$$M\ell \underset{8}{\overset{7}{\rightleftharpoons}} M + \ell \quad ; \quad K_4 = [M][\ell]/[M\ell] \qquad (4)$$

ISOMERIZATION (acidic site)

$$M + S \underset{10}{\overset{9}{\rightleftharpoons}} MS \quad ; \quad K_5 = [MS]/[M][S] \qquad (5)$$

$$MS \underset{12}{\overset{11}{\rightleftharpoons}} NS \quad ; \quad K_6 = [NS]/[MS] \qquad (6)$$

$$NS \underset{14}{\overset{13}{\rightleftharpoons}} N + S \quad ; \quad K_7 = [N][S]/[NS] \qquad (7)$$

HYDROGENATION (Metal Site)

$$N + \ell \underset{16}{\overset{15}{\rightleftharpoons}} N\ell \quad ; \quad K_8 = [N\ell]/[N][\ell] \qquad (8)$$

$$H_2 + \ell \underset{18}{\overset{17}{\rightleftharpoons}} H_2\ell \quad ; \quad K_9 = [H_2\ell]/[H_2][\ell] \qquad (9)$$

$$N\ell + H_2\ell \underset{20}{\overset{19}{\rightleftharpoons}} B\ell + \ell \quad ; \quad K_{10} = [B\ell][\ell]/[N\ell][H_2\ell] \qquad (10)$$

$$B\ell \underset{22}{\overset{21}{\rightleftharpoons}} B + \ell \quad ; \quad K_{11} = [B][\ell]/[B] \qquad (11)$$

The rate of the overall phenomenon is determined by the slowest of these 11 consecutive reactions. Sinfelt[15] postulated in his work on n-pentane isomerization that the isomerization of the n-pentenes on the acidic sites was the rate limiting step. Hosten and Froment[32] showed experimentally that the isomerization sequence determines the rate of the overall process. In view of this, we developed rate equations for only those steps that occurs on the skeletal re-arranging sites (acidic sites).

When the adsorption of i-octene on the acidic site (i.e reaction 5 of the scheme) is postulated to be the slowest step, the overall rate equation is given by

$$r_5 = k_1[M][S] - k_2[MS] \qquad (3.1.19)$$

The acidic site balance is given by

$$1 = S + MS + NS \qquad (3.1.20)$$

In the concept of the rate determining step, all other steps are in quasi - equilibrium and the unknown surface coverages (S), (MS) in equation (3.1.20) are expressed in terms of fluid phase species concentrations.
In this manner, equation (3.1.19) becomes:

$$r_5 = \frac{\frac{k_1 K_d [C_A]}{[C_{H_2}]} - \frac{k_2 [C_B]}{K_h K_7 K_6 [C_{H_2}]}}{1 + \frac{[C_B]}{K_7 K_h [C_{H_2}]} \left(\frac{1}{K_6} + 1\right)} \qquad (3.1.21)$$

where

$$K_h = K_{11} K_{10} K_9 K_8 \qquad (3.1.22)$$

$$K_d = K_4 K_3 K_2 K_1 \qquad (3.1.23)$$

When the surface reaction of the isomerization of i-octene into i' - octene - i.e reaction 6 of the Scheme - is postulated to be the slowest step, the overall rate equation is given by:

$$r_6 = k_1 [MS] - k_2 [NS] \qquad (3.1.24)$$

Expressing the surface coverages in terms of fluid phase concentration, we obtain the expression in equation (3.1.25)

$$r_6 = \frac{\frac{k_{11} K_5 K_d [C_A]}{H_2} - \frac{k_{12} [C_B]}{K_h K_7 [C_{H_2}]}}{1 + \frac{K_5 K_d [C_A]}{[C_{H_2}]} + \frac{[C_B]}{K_7 K_h [C_{H_2}]}} \qquad (3.1.25)$$

When the desorption of an i - octene from an alumina site (i.e reaction 7) is taken as the rate determining step, then the overall rate equation is given by

$$r_7 = k_1[NS] - k_2[N][S] \qquad (3.1.26)$$

Expressing the surface converages in terms of fluid phase concentrations we obtain the expression in equation (3.1.27)

$$r_7 = \frac{\frac{k_{13}K_6K_5K_d[C_A]}{[C_{H_2}]} - \frac{k_{14}[C_B]}{K_h[C_{H_2}]}}{1 + \frac{K_5\ K_d[A]}{[C_{H_2}]} + \frac{K_6\ K_5\ K_d\ [C_A]}{[C_{H_2}]}} \qquad (3.1.27)$$

3.1.3 METHYLCYCLOPENTANE (MCP)

The sequence of elementary steps for the reaction of MCP is shown in Scheme IV. MCP is adsorbed on the catalyst site and the adsorbed species then dehydrogenates to form adsorbed methylcyclopentene. The adsorbed methylcyclopentene then reacts to form either adsorbed cyclohexene or adsorbed hydrogenolysis products (reactions 3 and 4 of the Scheme). Some of the adsorbed hydrogenolysis products form adsorbed cyclohexene while the rest are hydrogenated to form adsorbed cyclohexane (reactions 5 and 6 of the Scheme). The adsorbed cyclohexene undergoes dehydrogenation reaction to form adsorbed benzene while the remaining part forms adsorbed cyclohexane (reactions 9 and 7). Then, adsorbed cyclohexane, benzene

and hydrogenolysis products then desorb to form cyclohexane, benzene and hydrogenolysis products.

Each of the eleven elementary steps could be rate determining. If the adsorption of MCP is rate determining (reaction 1 of the Scheme IV), the rate of reaction is given by

$$r_1 = k_1[MCP][S] - k_2[MCP.S] \qquad (3.1.28)$$

The site balance is given by

$$1 = S + MCPS + MCP^{=}S + CH^{=}S + CHS + \Sigma C_6^{=}S + \Sigma C_6 S + BzS \qquad (3.1.29)$$

In the concept of the rate - determining step, all other steps are in quasi-equilibrium and the unknown surface coverages (S), (MS) in equation (1) are expressed in terms of fluid phase concentrations. In this manner, equation 1 then becomes

$$r_1 = \frac{k_1[MCP] - \dfrac{k_2[CH]}{K_8K_7K_3K_2}}{1 + \dfrac{\Sigma C_6}{K_{11}K_6K_4K_2} + \dfrac{\Sigma C_6}{K_{11}K_6K_4} + \dfrac{CH}{K_8K_7[H_2]} + \dfrac{CH}{K_8} + \dfrac{Bz}{K_{10}} + \dfrac{\Sigma C_6}{K_{11}K_6[H_2]} + \dfrac{\Sigma C_6}{K_{11}}} \qquad (3.1.30)$$

where

$$K_1 = \frac{k_1}{k_2}$$

$$K_2 = \frac{k_3}{k_4}$$

$$K_3 = \frac{k_5}{k_6} \qquad K_8 = \frac{k_{15}}{k_{16}}$$

$$K_4 = \frac{k_7}{k_8} \qquad K_9 = \frac{k_{17}}{k_{18}}$$

$$K_5 = \frac{k_9}{10} \qquad K_{10} = \frac{k_{19}}{k_{20}}$$

$$K_6 = \frac{k_{11}}{k_{12}} \qquad K_{11} = \frac{k_{21}}{k_{22}}$$

$$K_7 = \frac{k_{13}}{k_{14}}$$

Table 3.6: Scheme IV

MECHANISM FOR MCP REACTION

$$S + MCP \underset{2}{\overset{1}{\rightleftharpoons}} MCPS \qquad (1)$$

$$MCPS \underset{4}{\overset{3}{\rightleftharpoons}} MCP^{=}S + H_2 \qquad (2)$$

$$MCP^{=}S \underset{6}{\overset{5}{\rightleftharpoons}} CH^{=}S \qquad (3)$$

$$MCP^{=}S \underset{8}{\overset{7}{\rightleftharpoons}} \Sigma C_6^{=} S \qquad (4)$$

$$\Sigma C_6^{=} S \underset{10}{\overset{9}{\rightleftharpoons}} CH^{=}S \qquad (5)$$

$$\Sigma C_6^{=} S + H_2 \underset{12}{\overset{11}{\rightleftharpoons}} \Sigma C_6 S \qquad (6)$$

$$CH^{=}S + H_2 \underset{14}{\overset{13}{\rightleftharpoons}} CHS \qquad (7)$$

$$CHS \underset{16}{\overset{15}{\rightleftharpoons}} CH + S \qquad (8)$$

$$CH^{=}S \underset{18}{\overset{17}{\rightleftharpoons}} BzS + 2H_2 \qquad (9)$$

$$B\ S \underset{20}{\overset{19}{\rightleftharpoons}} Bz + S \qquad (10)$$

$$\Sigma C_6\ S \underset{22}{\overset{21}{\rightleftharpoons}} \Sigma C_6 + S \qquad (11)$$

A summary of the eleven derived rate equations for Scheme IV is shown in Table 3.7.

Table 3.7 Derived Rate Equations for Scheme IV

1. Adsorption of MCP

$$r_1 = \frac{k_1[MCP] - \frac{k_2[CH]}{K_8K_7K_3K_2}}{1 + \frac{[\Sigma C_6]}{K_{11}K_6K_4K_2} + \frac{[\Sigma C_6]}{K_{11}K_6K_4} + \frac{[CH]}{K_8K_7}[H_2] + \frac{[CH]}{K_8} + \frac{[Bz]}{K_{10}} + \frac{[\Sigma C_6]}{K_{11}K_6[H_2]} + \frac{[\Sigma C_6]}{K_{11}}} \qquad (3.1.43)$$

2. Dehydrogenation of adsorbed methylcyclopentane to adsorbed methylcyclopentene

$$r_2 = \frac{k_3 K_1 [MCP] - \frac{k_4 [CH] [H_2]}{K_8 K_7 K_3}}{1 + K_1 [MCP] + \frac{[\Sigma C_6]}{K_{11} K_6 K_4} + \frac{[CH]}{K_8 K_7 [H_2]} + \frac{[CH]}{K_8} + \frac{[Bz]}{K_{10}} + \frac{[\Sigma C_6]}{K_{11} K_6 [H_2]} + \frac{[\Sigma C_6]}{K_{11}}} \quad (3.1.44)$$

3. Conversion of adsorbed methylcyclopentene to adsorbed cyclohexene (reaction 3)

$$r_3 = \frac{\frac{k_5 K_2 [MCP]}{H_2} - \frac{k_6 [CH]}{K_8 K_7 [H_2]}}{1 + K_1 [MCP] + \frac{K_2 K_1 [MCP]}{[H_2]} + \frac{[CH]}{K_8 K_7 [H_2]} + \frac{[CH]}{K_8} + \frac{[Bz]}{K_{10}} + \frac{[\Sigma C_6]}{K_{11} K_6 [H_2]} + \frac{[\Sigma C_6]}{K_{11}}} \quad (3.1.45)$$

4. Conversion of adsorbed methylcyclopentene to adsorbed olefinic hydrogenolysis products (reaction 4)

$$r_4 = \frac{\frac{k_7 K_2 K_1 [MCP]}{[H_2]} - \frac{k_8 [\Sigma C_6]}{K_{11} K_6 [H_2]}}{1 + K_1 [MCP] + \frac{K_2 K_1 [MCP]}{[H_2]} + \frac{[CH]}{K_8 K_7 [H_2]} + \frac{[CH]}{K_8} + \frac{[Bz]}{K_{10}} + \frac{[\Sigma C_6]}{K_{11} K_6 [H_2]} + \frac{[\Sigma C_6]}{K_{11}}} \quad (3.1.46)$$

5. Conversion of adsorbed olefinic hydrogenolysis products to adsorbed cyclohexene

$$r_5 = \frac{\frac{k_9[\Sigma C_6]}{K_{11}K_6[H_2]} - \frac{k_{10}[CH]}{K_8K_7[H_2]}}{1 + K_1[MCP] + \frac{K_2K_1[MCP]}{[H_2]} + \frac{[CH]}{K_8K_7[H_2]} + \frac{[CH]}{K_8} + \frac{Bz}{K_{10}} + \frac{[\Sigma C_6]}{K_{11}K_6[H_2]} + \frac{[\Sigma C_6]}{K_{11}}} \quad (3.1.47)$$

6. Hydrogenation of adsorbed olefinic hydrogenolysis products to adsorbed hydrogenolysis products

$$r_6 = \frac{k_{11}K_4K_2K_1[MCP] - \frac{k_{12}[\Sigma C_6]}{K_{11}}}{1 + K_1[MCP] + \frac{K_2K_1[MCP]}{[H_2]} + \frac{[CH]}{K_8K_7[H_2]} + \frac{[CH]}{K_8} + \frac{Bz}{K_{10}} + \frac{K_4K_2K_1[MCP]}{[H_2]} + \frac{[\Sigma C_6]}{K_{11}}} \quad (3.1.48)$$

7. Hydrogenation of adsorbed cyclohexene to adsorbed cyclohexane (reaction 7)

$$r_7 = \frac{k_{13}K_3K_2K_1[MCP] - \frac{k_{14}[CH]}{K_8}}{1 + K_1[MCP] + \frac{K_2K_1[MCP]}{[H_2]} + \frac{K_5[\Sigma C_6^-]}{K_{11}K_6[H_2]} + \frac{[CH]}{K_8} + \frac{B_z}{K_{10}} + \frac{[\Sigma C_6]}{K_{11}K_6[H_2]} + \frac{[\Sigma C_6]}{K_{11}}} \quad (3.1.49)$$

8. Desorption of hydrogenolysis products (reaction 8)

$$r_8 = \frac{k_{15}K_7K_3K_2K_1[MCP] - k_{16}[CH]}{1 + K_1[MCP] + \frac{K_2K_1[MCP]}{[H_2]} + \frac{K_5[\Sigma C_6^-]}{K_{11}K_6} + \frac{K_7K_5[\Sigma C_6^-]}{K_{11}K_6} + \frac{[B_z]}{K_{10}} + \frac{[\Sigma C_6]}{K_{11}K_6[H_2]} + \frac{[\Sigma C_6]}{K_{11}}} \quad (3.1.50)$$

9. Conversion of adsorbed cyclohexene to adsorbed benzene (reaction 9)

$$r_9 = \frac{\frac{k_{17}[CH]}{K_8K_7[H_2]} - \frac{k_{18}[B_z]}{K_{10}}}{1 + K_1[MCP] + \frac{K_2K_1[MCP]}{[H_2]} + \frac{[CH]}{K_8K_7[H_2]} + \frac{[CH]}{K_8} + \frac{B_z}{K_{10}} + \frac{[\Sigma C_6^-]}{K_{11}K_6[H_2]} + \frac{[\Sigma C_6]}{K_{11}}} \quad (3.1.51)$$

10. Desorption of benzene (reaction 10)

$$r_{10} = \frac{\frac{k_{19}K_9[CH]}{K_8K_7[H_2]} - k_{20}[Bz]}{1 + K_1[MCP] + \frac{K_2K_1[MCP]}{(H_2)} + \frac{[CH]}{K_8K_7[H_2]} + \frac{[CH]}{K_8} + \frac{K_9K_5[\Sigma C_6]}{K_{11}K_6[H_2]^2} + \frac{[\Sigma C_6]}{K_{11}K_6} + \frac{[\Sigma C_6]}{K_{11}}} \quad (3.1.52)$$

8. Desorption of hydrogenolysis products (reaction 8)

$$r_8 = \frac{k_{15}K_7K_3K_2K_1[MCP] - k_{16}[CH]}{1 + K_1[MCP] + \frac{K_2K_1[MCP]}{[H_2]} + \frac{K_5[\Sigma C_6^-]}{K_{11}K_6} + \frac{K_7K_5[\Sigma C_6^-]}{K_{11}K_6} + \frac{[B_z]}{K_{10}} + \frac{[\Sigma C_6]}{K_{11}K_6[H_2]} + \frac{[\Sigma C_6]}{K_{11}}} \quad (3.1.50)$$

9. Conversion of adsorbed cyclohexene to adsorbed benzene (reaction 9)

$$r_9 = \frac{\frac{k_{17}[CH]}{K_8K_7[H_2]} - \frac{k_{18}[B_z]}{K_{10}}}{1 + K_1[MCP] + \frac{K_2K_1[MCP]}{[H_2]} + \frac{[CH]}{K_8K_7[H_2]} + \frac{[CH]}{K_8} + \frac{B_z}{K_{10}} + \frac{[\Sigma C_6^-]}{K_{11}K_6[H_2]} + \frac{[\Sigma C_6]}{K_{11}}} \quad (3.1.51)$$

10. Desorption of benzene (reaction 10)

$$r_{10} = \frac{\frac{k_{19}K_9[CH]}{K_8K_7[H_2]} - k_{20}[Bz]}{1 + K_1[MCP] + \frac{K_2K_1[MCP]}{(H_2]} + \frac{[CH]}{K_8K_7[H_2]} + \frac{[CH]}{K_8} + \frac{K_9K_5[\Sigma C_6]}{K_{11}K_6[H_2]^2} + \frac{[\Sigma C_6]}{K_{11}K_6} + \frac{[\Sigma C_6]}{K_{11}}} \quad (3.1.52)$$

11. Desorption of hydrogenolysis products

$$r_{11} = \frac{k_{21}K_6K_4K_2K_1[MCP] - k_{22}[\Sigma C_6^-]}{1 + K_1[MCP] + \frac{K_2K_1[MCP]}{[H_2]} + \frac{[CH]}{K_8K_7[H_2]} + \frac{[CH]}{K_8} + \frac{[Bz]}{K_{10}} + \frac{K_4K_2K_1[MCP]}{[H_2]} + K_6K_4K_2K_1[MCP]} \quad (3.1.53)$$

3.2 Variable Activity Kinetic Models

The mechanism of deactivation is supposed to be of the form

$$A \rightleftharpoons R \quad (1)$$

$$M \longrightarrow P \quad (2)$$

where A is the reactant, R is the desired product of reaction, M is the reactant and it forms the coke precusor (M=A) and P is the coke.

The first step is the adsorption on the catalyst surface of the substance that produces the deactivation (the reactant)

$$M + \ell \rightleftharpoons M\ell \quad ; \quad K_m = C_{M\ell}/P_m C_\ell \quad (3)$$

The second step is the coke precusor formation reaction of the molecule adsorbed with others of the same species adsorbed on active centers or in gaseous phase to form the first state of the molecules in its degradation.

$$nM(g) + hM\ell \rightleftharpoons P_1I_h \qquad (4)$$

n = 0,1,2 and h = 1,2. In order that this reaction be elementary $n+h \leq 3$

The third step is the coking sequence. Reaction of the coke precusor to other forms of coke until a final form is reached.

$$P_1I_h \rightleftharpoons P_2I_h \rightleftharpoons P_3I_h \qquad (5)$$

3.2.1 Kinetic Equation When the Coke Precusor Formation (Second steps) is the Controlling Step.

$$nM(g) + hM\ell \xrightarrow{\text{slow}} P_1I_h \overset{\text{fast}}{\rightleftharpoons} P_2I_h \overset{\text{fast}}{\rightleftharpoons} P_3I_h \qquad (6)$$

The degradation reactions of P_1I_h will be much faster than that of its formation, therefore validating the pseudostationary - state hypothesis, the coke precusor P_1I_h will be at equilibrium at any moment with the other coke species.

Given that the first reaction from equation (6) is elementary, the rate of coke formation will be

$$dC_{P_{\ell h}}/dt = -k_d P_m^n C_{M\ell}^h = k_d K_m^h P_m^{n+h} C_1^h \qquad (3.2.1)$$

$$PI_h = P_1I_h + P_2I_h + P_3I_h + \ldots\ldots \qquad (3.2.2)$$

The total concentration of active sites L is

$$L = C_1 + C_{A\ell} + C_{R\ell} + hC_{P_{\ell h}} \qquad (3.2.3)$$

$$C_{A\ell} = k_A P_A C_1 \qquad (3.2.4)$$

$$C_{R\ell} = k_R P_R C_1 \qquad (3.2.5)$$

Substituting equation (3.2.4) and (3.2.5) into equation (3.2.3) and eliminating C_1 gives

$$C_1 = \frac{L - hC_{P_{\ell h}}}{1 + K_A P_A + K_R P_R} \qquad (3.2.6)$$

Substituting C_1 from equation 3.2.6 into equation 3.2.1 we obtain

$$\frac{dC_{P_{\ell h}}}{dt} = \frac{k_d K_m^h P_m^{n+h} [L - hC_{PI_h}]^h}{\{1 + K_A P_A + K_R P_R\}^h} \qquad (3.2.7)$$

Regrouping and putting $a^{1/m} = \frac{L - C_{PI_h}}{L}$

the above equation becomes

$$\frac{-da}{dt} = \frac{[MhL^{h-1} k_d K_m^h P_m^{n+h}]}{[1 + K_A P_A + K_R P_R]^h} a^{(m+h-1)/m} \qquad (3.2.8)$$

$m = 1 \; ; \; h = 1$

$$\frac{-da}{dt} = \frac{k_d K_m P_m^{n+1}}{1 + K_A P_A + K_R P_R} a \qquad (3.2.9)$$

$$- \ell n\ a = \frac{k_d K_m P_m^{n+1}}{1 + K_A P_A + K_R P_R} t \qquad (3.2.10)$$

$$\frac{P_m^{n+1}}{\psi_{01}(P_i, T)} = \frac{1}{k_d K_A} + \frac{K_A}{k_d K_m} P_A \qquad (3.2.11)$$

3.2.2 Kinetic Equation when an intermediate Reaction in the Coking Sequence (3rd Step) is the Controlling Step.

The coking sequence will be

$$nM(g) + hM\ell \overset{k_1}{\rightleftharpoons} P_1 I_h \overset{k_3}{\rightleftharpoons} P_2 I_h \overset{\text{slow}}{\longrightarrow} P_3 I_h \qquad (7)$$

where

$$K_1 = C_{P_1 I_h} / P_M^n \, C_{M\ell}^h \quad ; \quad K_2 = C_{P_2 I_h} / C_{P_1 I_h} \qquad (3.2.12)$$

Then the deactivation rate will be

$$dC_{P_{I_h}}/dt = k_d C_{P_2 I_h} = k_d K_1 K_2 K_m^h P_m^{n+h} C_1^h = k_d K_m^1 P_m^{n+h} C_1^h \qquad (3.2.13)$$

where C_{PI_h} is the concentration of any of the forms of coke on the catalyst which changes with time.

$$C_{PI_h} = C_{P_3 I_h} + C_{P_4 I_h} + \ldots \qquad (3.2.14)$$

$C_{P_{I_h}}$ does not include $C_{P_{1h}}$ and $C_{P_{2h}}$ because these species are at any moment in equilibrium with the concentration of the deactivating substances in the gaseous phase and for that reason the concentrations of P_1I_h and P_2I_h on the catalyst do not vary with time.

In this case

$$L = C_1 + C_{A\ell} + C_{R\ell} + h\,C_{P_1I_h} + hC_{P_2I_h} + h\,C_{P_3I_h} \qquad (3.2.15)$$

$h = 1$; $m = 1$ similar approach to the one previously shown leads to

$$-\frac{da}{dt} = \frac{k_d K_m' P_m^{n+1}}{1 + K_A P_A + K_R P_R + K_m'' P_m^{n+1}} a \qquad (3.2.16)$$

where $K_m' = K_1 K_2 K_m$ and $K_m'' = K_1 K_A + K_1 K_2 K_A$ (3.2.17)

$$\ell n\, a = \frac{k_d K_m' P_m^{n+1}}{1 + K_A P_A + K_R P_R + K_m'' P_m^{n+1}} t \qquad (3.2.18)$$

$$P_R \approx 0$$

$$\frac{P_m^{n+1}}{\psi_{01}(P_i,T)} = \frac{1}{k_d K_m'} + \frac{K_A}{k_d K_m'} P_A + \frac{K_m''}{k_d K_m'} P_m^{n+1} \qquad (3.2.19)$$

CHAPTER 4

EXPERIMENTAL

4.1 Materials and Specifications

(i) Normal Octane (MERCK, Munich)

Assay G.C.	98%
Wt/ml (at 20°C)	0.702 - 0.703g
Molecular weight	114.23

(ii) Benzene (May & Baker Ltd, Dagenham England)

Assay G. L. C.	99.95%
Wt/ml (at 20°C)	0.875 - 0.878g
Molecular weight	78.11

(iii) O - xylene (BDH Chemicals Ltd, Poole England)

Assay G.L.C.	99%
Wt/ml (at 20°C)	0.878 - 0.88g
Molecular weight	106.17

(iv) Ethyl Benzene (Hopkins & Williams)

Assay G. L. C.	99%
Wt/ml (at 20°C)	0.866g
Molecular weight	106.17

(v) P - xylene (Hopkins & Williams)

Assay G. L. C.	99%
Wt/ml (at 20°C)	0.86g
Molecular weight	106.17

(vi) Toluene (MERCK, Munich)

Assay G. L. C.	99%
Wt/ml (at 20°C)	0.86
Molecular Weight	92.14

(vii) Meta Xylene (Hopkins & Williams,Essex England)

Assay G.L.C.	99%
Wt/ml (at 20°C)	0.866g
Molecular Weight	106.16

(viii) 2,2,4 Trimethyl Pentane (Hopkins & Williams)

Assay G. L. C.	99%
Wt/ml (at 20°C)	0.629g
Molecular Weight	114.23

(ix) Cyclohexane (Philips Petroleum Company,U.S.A)

Assay G.L.C.	99.5%
Wt/ml (at 20°C)	0.776 - 0.78g
Molecular Weight	84.16

(x) 2 Methylpentane (BDH Chemicals Ltd, England)

Assay G.L.C.	99%
Wt/ml (at 20°C)	0.65g
Molecular Weight	86.18

(xi) Methylcyclopentane (Philips Petroleum Company,U.S.A)

Assay G.L.C.	99%
Wt/ml (at 20°C)	0.74 g
Molecular Weight	84.16

(xii) $Ba(OH)_2.8H_2O$ (BDH Chemicals Ltd)

Minimum Purity	98%
Molecular Weight	315.50

(viii) HCI (MERCK, Munich)

Specific gravity	1.18
Concentration	35.4% Wt/wt
Molecular Weight	36.46

(viv) Sodium tetraborate (BDH Chemicals Ltd)

Minimum Purity	99%
Molecular Weight	381.44

(xv) 0.3% Pt/Al_2O_2 Catalyst (Commercial)

Platinum content	0.3% Pt
Chlorine content	0.6% Cl
Surface area	$180m^2\ g^{-1}$

Pore volume	$0.50 Cm^3 g^{-1}$
Pellet size	12 - 16 mm

(xvi) 0.6% Pt/Al_2O_3 Catalyst (Commercial)

Platinum content	0.6% Pt
Chlorine content	0.6 - 1% Cl
Surface area	$180 m^2 g^{-1}$
Pore volume	$0.5 cm^3 g^{-1}$

(xvii) 0.3%Pt - 0.3% Re/Al_2O_3 (Commercial)

Platinum content	0.3wt%
Rhenium content	0.3wt%
Chlorine content	0.6 - 1% Cl
Surface area	$180 m^2 g^{-1}$
Pore volume	$0.5 cm^3 g^{-1}$

(xviii) Cylinder Gases: Air, Nitrogen, Hydrogen (Industrial gases, Lagos)

The nitrogen and hydrogen gases are over 99% purity.

(xix) Phenolphthalein indicator, Methyl Red indicator, Ethylene glycol.

4.2 Equipment

The flow diagram of the equipment used for all experimentations is shown in Fig.4.2.1. The set up is made up of the following:

4.2.1 Temperature Controller

The Barber Coulman temperature controller of the Autoclave Engineer's Inc. is connected via thermocouples and is capable of monitoring the temperatures of five different systems simultaneously. The temperature controller

regulates the temperature within ±1°C of the set point.

4.2.2 Reactor

The reactor is a CSTR of the Berty-type purchased from Autoclave Engineer's, Inc. The bolted closure unit consists of a body, cover, colosure gasket and capscrews.

Reactor Specifications:

Maximum Allowable Working Pressure	- 2000Psig at 200°F
Total pressure	7000Psig

Material	
Body	SA - 182 - F316
Cover	SA - 182 - F316
Colosure gasket	316
Cap Screw	SA - 193 Cr. B 16

Body and Cover Connections

Connections are provided in the sides of the body and cover which are used for thermocouples and for introducing either gas or liquid into the reactor. Agitation is achieved by means of a turbine type magnetic stirrer. A jacket -type 3 - zone furnace is furnished with the reactor. The furnace has resistance windings and insulation enclosed in a sleeve -type jacket which slides over the body and cover of the reactor. The furnace is provided with flexible armor leads with twist lock connectors for connection to power source.

4.2.3 Air

Air cylinder was purchased from industrial gases, Lagos and was used without further purification. Air was used in the chromatography and also to burn off the polymerous carbon compound (coke) deposited on the catalyst surface in the course of experimentation.

4.2.4 Double - Stage Regulators

The gas in the cylinder were fed into the system through double - stage regulators. The maximum outlet pressure was seven atmospheres.

4.2.5 Valves

They were used to control flow paths and flow rates of gases.

4.2.6 Nitrogen

The nitrogen gas purchased from Industrial Gases was used without further purification. Nitrogen was used as carrier gas for the gas chromatograph, for deactivation studies, for partial pressure experiments in the dilution of hydrogen and for drying of Pt-Re/Al_2O_3 catalyst.

4.2.7 Hydrogen

The hydrogen gas also purchased from Industrial Gases was used without further purification. Hydrogen was used in the chromatograph, for reduction of the catalyst, for kinetic studies on clean catalyst surface and for partial pressure studies.

4.2.8 Saturator

This unit was used to prepare feed for flow experiment. A stream of gas passed through the saturator and partly vaporises the reactant in the saturator. Entrainment was avoided by using low gas flow rate and keeping the liquid reactant level in the saturator low.

4.2.9 Constant Temperature Bath

The saturator is immersed in a New Brunswick Scientific Frigid Flow bath circulator Model RF 10 which can be set between -50°C and 100°C. The concentration of the reactant in the gas stream could be varied by varying the temperature of the bath.

4.2.10 Gas Chromatograph

Reactor outlet was analyzed by use of Hitachi 164 gas chromatograph with FID containing 6ft x 1/8 in. SS 5% SR-1200/1 75% Bentone 34 on 100/120 mesh Supelcoport. The operating conditions of the chromatograph are as follows:

Column temperature	75°C
Carrier gas flow rate	20ml/min
Attenuation	64
Range	10^2
Chart Speed	5mm/min

Key to Figure 4.2.1

Unit	Description
1	Temperature Controller
2	Reactor
3	Air Cylinder
4	Double Stage Regulators
5	Valve
6	Two Way Valve
7	Nitrogen Cylinder
8	Hydrogen Cylinder
9	Ethylene glycol/Water(50/50 v%)
10	Reactants
11	Saturator
12	Bath
13	Chromatography

4.3 Experimental Procedure

4.3.1 Precautions

In general, the following precautions were taken during the experimental runs.

a. The system was leak tested from time to time in order to avoid loss of reactants and excessive pressure drop across the reactor system.

b. During the constant activity kinetic investigation experimental runs were started only after the catalyst activity was found to be constant. This state is normally achieved in H_2 stream in 10 - 15 minutes. During deactivation and mortality runs, accelerated deactivation (deactivation in N_2 or N_2 containing gas) was started only after constant activity has been achieved in H_2.

c. The saturator unit was isolated from the rest of the system in between experimental runs. This was in order to avoid contamination of the rest of the line by vapor diffusion of reactant. The system was flushed with nitrogen before the commencement of any experimental run.

d. When the temperature of the furnaces were altered, there was tendency for the temperature to oscillate initially about the set point. Experiments were carried out only after the temperature was stable.

e. Changes in the controlling variables were made in random manner.

f. In between runs, the catalyst was left in hydrogen flow (30ml/min) at 200°C.

g. For every experimental condition, replicate runs were made to ensure reproducibility.

h. During steady state kinetic studies, catalyst activity was ensured constant by checking the conversion level every 25-30 minutes. If the conversion differs from that obtained at the 15th minute (under the same conditions), then the conversion level is brought up again by burning off the coke from the catalyst surface in air (flowrate 150ml/min) for 15 minutes at 420°C. The catalyst was then reduced in H_2 stream (40ml/min) for 2 hrs at 500°C. This procedure reproduced the expected activity for further experimentation.

i. Catalyst regeneration was carried out by passing air at a flowrate of 150ml/min (by - passing the saturator) into the reactor. The high air flowrate was necessary in order to overcome the liquid ($Ba(OH)_2$ solution) pressure in the saturator. The temperature of the reactor was maintained at 420°C for 3 h during the regeneration process. The 3h was chosen sequel to the experiment performed on a Pt/Al_2O_3 catalyst deactivated during MCP reforming. In this experiment (Figure 4.3.1) the coke content removed by burning was monitored as a function of time. The figure shows that no more coke was removed after 180 minutes.

4.3.2 Catalyst Pretreatment

Every new batch of catalyst used in the investigation was reduced using H_2 at a flowrate of 40ml/min and a temperature of 500°C for 2hrs. The Pt-Re/Al_2O_3 (DRIED) catalyst, however was first dried for 2hrs in nitrogen at 110°C and flowrate of 60ml/min before reduction. In catalyst deactivation and mortality runs, drying was also performed in between deactivation for the bimetallic Pt-Re/Al_2O_3 (DRIED) catalyst.

4.3.3 Procedure

The apparatus used in this investigation is shown in Figure 4.2.1. The reactor is packed with 10g of the required catalysts. Every new batch of catalyst used was reduced in H_2 stream at 500°C for 2hrs at a flowrate of 40ml/min. The Pt-Re/Al_2O_3 (DRIED) catalyst, however was first dried in N_2 at 110°C for 2hrs at a flowrate of 60ml/min before reduction. During catalyst reduction, the saturator was bypassed to ensure that only hydrogen flows through the reactor. The concentration of the reactant was varied by varying the temperature of the bath. Saturator temperature above ambient were undesirable because this would result in condensation of the reactant in the line. Saturator temperature was varied within the range 2°C and 25°C for all the reactants studied in this investigation: n-octane, 2,2,4 trimethyl

pentane and methylcyclopentane. Steady state reactivity experiments were carried out as detailed below for the three reactants investigated.

a. N-Octane:

In the kinetic investigation of n-octane conversion, temperatures of 420°, 440° and 460°C were employed at n-octane partial pressures of 5.7×10^{-3}, 7.63×10^{-3}, 13.7×10^{-3} and 25×10^{-3} atm using Pt/Al_2O_3 catalyst. Conversion and product composition of n-octane were collected at W/F values of 0.083, 0.11, 0.166 and 0.33 gmincm^{-3}.

During H_2 partial pressure dependence studies, H_2 partial pressures of 0.11, 0.33, 0.5, 0.66 and 0.88 atms were employed at constant W/F of 0.11 gmincm^{-3}. The n-octane partial pressure employed was 7.63×10^{-3} atm at 420°, 440° and 460°C.

b. Iso-Octane:

0.3%Pt/Al_2O_3 and 0.6%Pt/Al_2O_3 catalysts were employed during the steady state kinetic studies. Temperatures of 390°, 400°, 410°, 420° and 430°C were employed at iso-octane partial pressures of 0.023, 0.0316, 0.056 and 0.081 atm. The W/F values used were 0.083, 0.11, 0.166 and 0.33 gmincm^{-3}.

c. Methylcyclopentane (MCP):

In the reactivity studies with MCP, Pt/Al_2O_3, $Pt-Re/Al_2O_3$(UNDRIED) and $Pt-Re/Al_2O_3$ (DRIED) catalysts were used for the investigation. The temperatures of 370°, 380°, 390° and 400°C were employed while MCP partial pressures of 0.058, 0.092, 0.1447 and 0.1816 atm were used. There was very low conversion of MCP below 370°C and high coking above 400°C. Conversion and product composition data were collected at 0.083, 0.11, 0.166 and 0.33 $gmincm^{-3}$ W/F values.

ii Deactivation Kinetics was studied using iso-octane and MCP as detailed below:

a. Iso-Octane

The deactivation kinetics of iso-octane was performed on both 0.3%Pt/Al_2O_3 and 0.6%Pt/Al_2O_3 catalysts. The temperatures used in this investigation were 390°, 410° and 430°C. At the different temperatures employed, the iso-octane partial pressures used were 0.11, 0.33, 0.5 and 0.778atm. The W/F value used in this investigation was 0.11$gmincm^{-3}$. The deactivation kinetics of iso-octane (at P_{H_2} = 0.5 atm) as function of iso-octane partial pressures was also investigated at a temperature of 430°C.

b. MCP

Pt/Al_2O_3 and $Pt-Re/Al_2O_3$ (DRIED) catalysts were used in the investigation. The temperatures employed were 390°,400° and 410°C. At each temperature, the decrease in conversion of MCP

reaction at H_2 partial pressures of 0.11, 0.33, 0.5 and 0.78atm was monitored as functions of time at MCP partial pressure of 0.092atm. The deactivation of the catalysts was also studied at various MCP partial pressures at a constant H_2 partial pressure of 0.778atm.

iii Catalyst Mortality Studies

Catalyst mortality studies were investigated using n-octane, iso-octane and MCP as detailed below:

a. N-Octane

The n-octane mortality experiment was performed in N_2 at 440°C, n-octane partial pressure of 13.7×10^{-3}atm and W/F of 0.166gmincm^{-3}. Seven deactivation regeneration cycles were performed. Also during regeneration the coke content (in gC) was measured after each deactivation.

b. Iso-Octane

The iso-octane mortality experiment was performed at 430°C using 0.3%Pt/Al_2O_3 catalyst. Iso-octane partial pressure of 0.0316atm and W/F of 0.11gmincm^{-3} were employed during the investigation. Twenty four deactivation - regeneration cycles were performed in N_2 stream and the coke content measured after each deactivation.

c. MCP

Three different catalysts were used: Pt/Al_2O_3 and bimetallic Pt-Re/Al_2O_3 (DRIED and UNDRIED). The temperature employed was 430°C, W/F of 0.11gmincm^{-3} and MCP partial pressure of 0.092atm. The 0.3%Pt/Al_2O_3 catalyst used for the investigation

was the one previously used for iso-octane mortality studies (24 deactivation - regeneration cycles). Forty deactivation-regeneration cycles were completed using MCP. Twelve deactivation regeneration cycles each were completed on both the dried and undried bimetallic Pt-Re/Al_2O_3 catalysts at the same conditions as the Pt/Al_2O_3 catalyst. During the mortality studies with Pt-Re/Al_2O_3 (DRIED) catalyst, the catalyst was dried at 110°C in N_2 stream (60 ml/min) for 2hrs after each regeneration.

FIGURE 4.2.1: SCHEMATIC DIAGRAM OF EXPERIMENTAL APPARATUS.

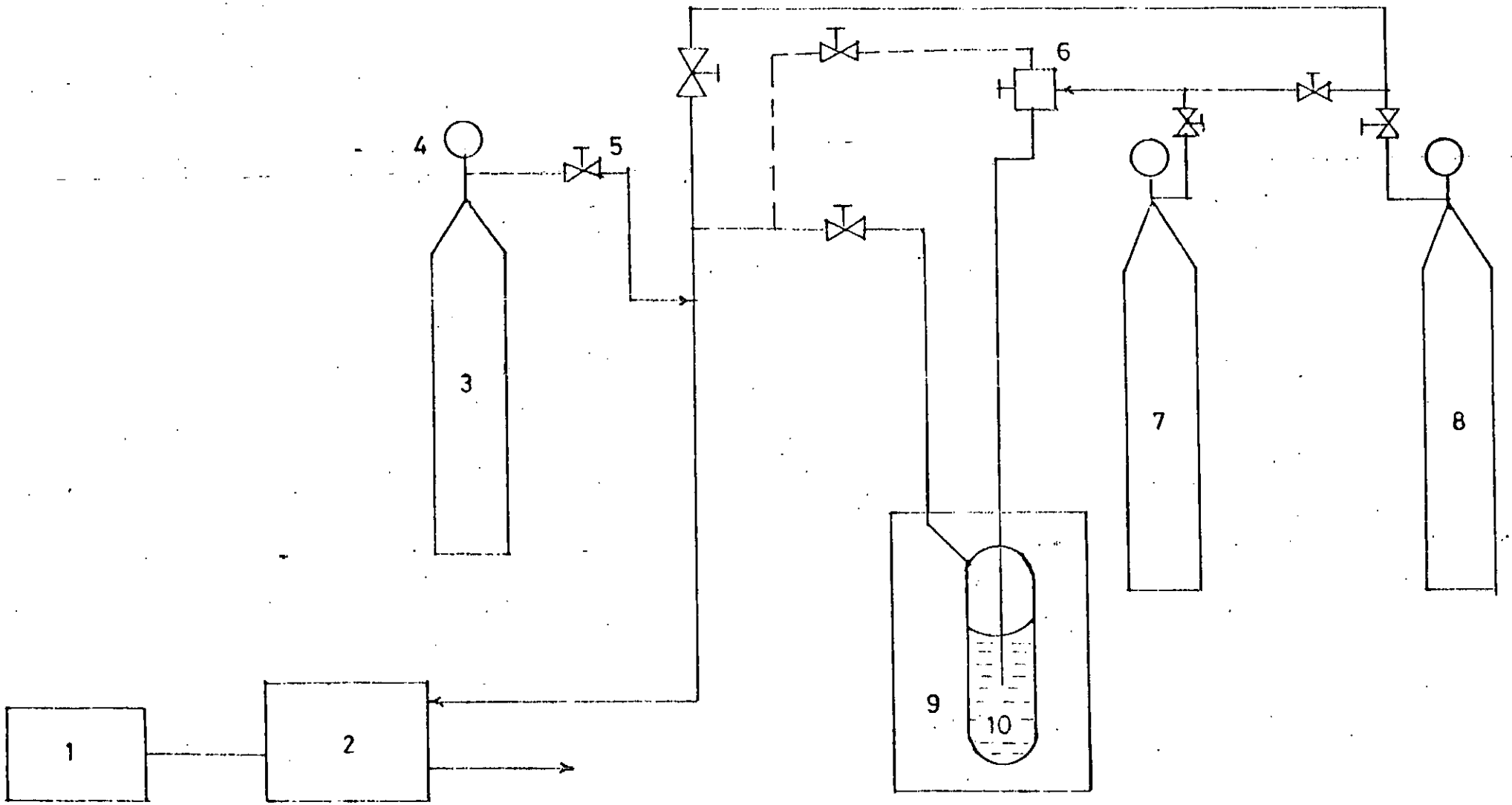

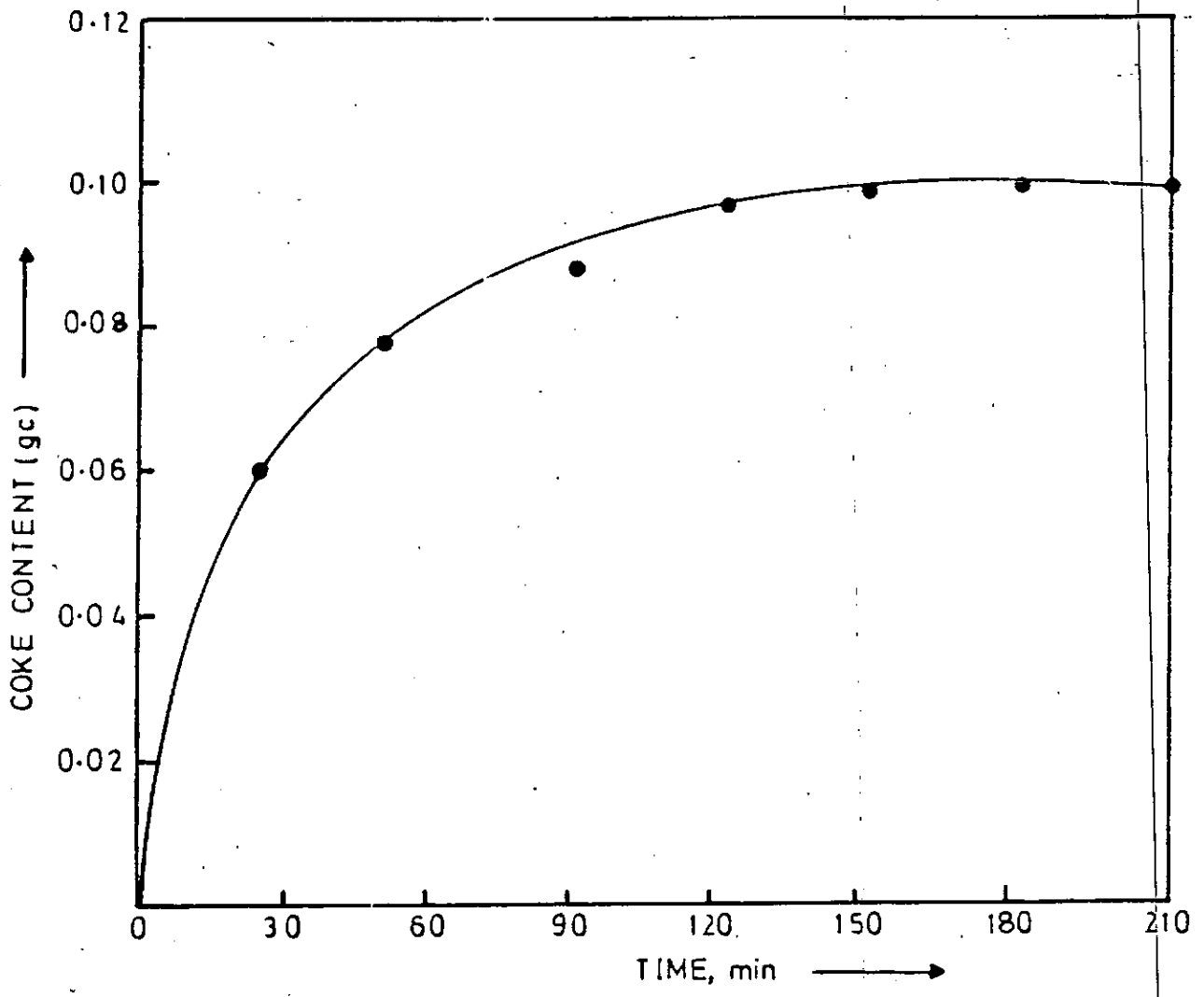

Fig.4.3.1: Rate of coke removal from deactivated Pt-Re/Al_2O_3(DRIED) catalyst during regeneration in air at 420°C

CHAPTER 5

EXPERIMENTAL RESULTS

5.0 Experimental Results

Experimental results on the reactions of n-octane, iso-octane and MCP on constant activity Pt/Al_2O_3 and $Pt-Re/Al_2O_3$ catalysts are presented in section 5.1 while results obtained for the variable activity catalysts for iso-octane and methylcyclopentane (MCP) are presented in section 5.2. The catalyst mortality results are presented in section 5.3.

The results at constant activity were obtained as reported under procedure in Chapter 4 under conditions where coking of the catalyst surface was negligible. Generally, the activity was constant for the duration of a run at given process conditions. The activity of the catalyst was checked after every 30mins with those obtained at the beginning of the run. If there is activity difference, the catalyst is regenerated in air (flow rate 150ml/min) for 20 mins at 420°C and reduced in H_2 (40ml/min) at 500°C for 2 hrs.

The deactivation kinetics experiments were performed at 0.11, 0.33, 0.5 and 0.778 atm H_2 partial pressures and the conversions as functions of time were monitored at different temperatures and reactant partial pressures. Deactivated catalysts were regenerated by passing air at a flowrate of 150m/min and 420°C for 3hrs. This was followed by reduction in H_2 for 2hrs at 500°C.

W/F of 0.1667gmincm^{-3} was used during the mortality experiments. The partial pressures of reactants (n-octane, iso-octane and MCP) were 0.0076, 0.0316 and 0.092 atm respectively while the reactor temperatures were 440°C for n-octane and 430°C for iso-octane and MCP.

5.1 Constant Activity

5.1.1 N - Octane

A. Total Conversion

The products of reaction of n-octane on Pt/Al_2O_3 catalyst were hydrocracked products (C_1-C_5), iso-octane, ethylbenzene, O-, P-, M-xylene and toluene. The variation of the total conversion of n-octane as a function of reciprocal velocity for different partial pressures of n-octane and catalyst temperatures are shown in Figures 5.1.1 - 5.1.4. At partial pressures between 5.7×10^{-3} - 13.7×10^{-3} atm, conversion increased with increasing temperature. However, it is only at the highest pressure investigated (25×10^{-3} atm) that conversion at 460°C was found to be lower than 440°C at reciprocal velocities higher than 0.2gmincm^{-3}. Table 5.1 shows the initial rate of reaction of n-octane at different temperatures and n-octane partial pressures. The table shows that the initial rate decreases with decrease in temperature.

Table 5.1 Initial rates of n-octane conversion on Pt/Al_2O_3 Catalyst at various temperatures and MCP partial pressure

Reactor temp. (°C) / P_{No} (atm)	Initial Rate, $cm^{-3}\ g^{-1}\ min^{-1}$			
	460	440	420	400
0.0057	17.5	10.5	6.25	1.67
0.00763	11.25	7.5	2.5	0.92
0.0137	11.25	8.75	4.375	0.563
0.025	11.25	5	1.875	0.313

The initial rate at 460°C was the same at all the partial pressures except at 5.7×10^{-3} atm P_{No} where the initial rate was 17.5cm^{3}g^{-1} min^{-1}. The initial rate obtained at 420° and 440°C at 13.7×10^{-3} atm P_{No} was higher than those obtained at 7.63×10^{-3}atm. At 400°C the initial rate of reaction decreases with increase in P_{No}. Figures 5.1.1 and 5.1.4 show that although conversion remained high between 5.7×10^{-3} - 13.7×10^{-3} atm it became depressed significantly at 25×10^{-3}atm. However, some of this inhibition is already evident at 440°C for 13.7×10^{-3}atm (see Figure 5.1.3).

B. PRODUCT DISTRIBUTION

The product composition of any component is expressed as the weight fraction of that component in the product stream. At 400°C and partial pressures of n-octane between 7.63×10^{-3} and 13.7×10^{-3} atm, only iso octane and hydrocracked products were formed from n-octane conversion (Figure 5.1.5). At the highest pressure of n-octane investigated (25×10^{-3}atm), only iso-octane was formed as increased pressure completely suppressed the hydrogenolysis property of the Pt/Al_2O_3 catalyst. In the above pressure range, increased pressure decreased product composition. In contrast at the lowest pressure investigated (5.7×10^{-3} atm), dehydrocyclized products were formed (Figure 5.1.6) although iso octane and hydrocracked products are still the major products, in conformity with the results at higher temperatures.

Typical plots of the product composition against W/F are shown in Figures 5.1.7-5.1.10 for 420°C and n-octane partial pressures of 5.7×10^{-3}, 7.63×10^{-3}, 13.7×10^{-3} and

$25x10^{-3}$atm, respectively.

Hydrocracked products were the most predominant at all the conditions investigated. At 420°C and W/F = 0.32 gmincm^{-3} the composition of hydrocracked products was 20%. This percentage was found to decrease with increasing partial pressure of n-octane. The values were 11%, 8% and 4.5% at $7.63x10^{-3}$, $13.7x10^{-3}$ and $25x10^{-3}$ atm respectively. The composition of hydrocracked products increased with increase in W/F at given temperature and P_{No}. The composition of hydrocracked products also decreased with increasing P_{No} although this decrease with increasing partial pressure of n-octane at 440°C was only significant up to $13.7x10^{-3}$atm. The composition of hydrocracked products actually increased at $25x10^{-3}$atm to 21%.The pattern at 440°C was repeated at 460°C. It is important to note that the composition of hydrocracked products was not significantly affected by temperature in the range investigated (400-460°C). Toluene is present only in quantities less than 0.3%.

At 420°C, excepting the hydrocracked products, iso-octane was the predominant product of n-octane conversion. This result is in agreement with our earlier microcatalytic result[1]. However, only at the lowest pressure ($5.7x10^{-3}$atm) did the iso-octane composition go through a maximum. At $5.7x10^{-3}$atm, the order of production of ehylbenzene and the xylene isomers were:

0-xylene ∿ P-xylene > ethylbenzene > m - xylene

This order was not maintained at the higher partial pressures. For example, at $13.7x10^{-3}$atm, the composition of ethylbenzene was larger than those of the xylene isomers. At 440°C, there were significant differences in the product distribution profiles. First, iso-octane is no longer the predominant

product due to its conversion to ethylbenzene (See Figure 5.1.11). Furthermore, the iso octane composition went through a maximum at a higher W/F value compared to the case at 420°C. Secondly, the toluene composition became as high as 1.5% at 7.63×10^{-3} atm (Figure 5.1.13) while at 5.7×10^{-3} atm and 440°C, the decrease in iso-octane concentration was due to its conversion to ethylbenzene. Conversion must have occured more randomly at 460°C to include all the xylene isomers (Figure 5.1.14). Furthermore, the composition of toluene increased significantly to about 5% at W/F = 0.33 gmincm^{-3}.

C. HYDROGEN DEPENDENCE

The variation of the total n-octane conversion as a function of P_{H_2} at 420°C, 440°C and 460°C, are shown in Figure 5.1.15. At the three temperatures, the conversion - P_{H_2} profiles exhibited maxima in agreement with previously reported works on C_6 and C_7 reforming reactions[11,83,84]. Although broad maxima were indicated in these profiles, nevertheless, the optimum P_{H_2} was the least at the lowest temperature of the investigation (420°C). While the optimum P_{H_2} occured at $\sim$ 0.3atm at 420°C, the value was higher ($\sim$ 0.4 atm) at 440° and 460°C. Actually, the optimum P_{H_2} appears slightly lower at 460°C compared to 440°C. Although the experimental observation on the effect of temperature on the optimum P_{H_2} by Paal et al[85] for heptane reforming on Pt- black applies to the individual product profiles, the same explanation should apply to the conversion - P_{H_2} profiles. In that work, as temperature increased, the hydrogen pressure belonging to the maximum rate was shifted toward higher pressures. In view of the above, it is clear that the conversion

P_{H_2} profiles only agreed with the above results at the lower temperatures. Between 440°C and 460°C, the sensitivity of the optimum value P_{H_2} was not pronounced. It will now be useful to consider the product distribution profiles.

Plots of the product distribution against P_{H_2} for 420°, 440° and 460°C are shown in Figures 5.1.16 - 5.1.18, respectively. At 420°C (Figure 5.1.16), iso octane is the predominant product of n-octane conversion with its composition increasing monotonically with P_{H_2}. Significant quantities of hydrocracked products are also formed although it appears to have attained a maximum at very low P_{H_2}. The xylene isomers and ethylbenzene passed through distinct maxima at about $P_{H_2} \sim 0.55$ atm. Toluene is the least product formed and its composition decreased rapidly to zero at 0.5atm. The magnitude of ethylbenzene and the xylene isomers was in the following order:

P - Xylene > 0.-xylene ∿ Ethylbenzene > M-xylene

At 440°C (Figure 5.1.17), the composition of ethylbenzene and the xylene isomers increased significantly while that of iso-octane decreased. It is clear from the profiles that the optimum P_{H_2} for ethylbenzene and m-xylene appears to occur at ∿ 0.52atm while those for 0- and p-xylene occurs at higher P_{H_2} value (∿0.58 atm). The slower increase in iso octane as P_{H_2} is increased must be due in part to its conversion to dehydrocyclization products. However some simultaneous conversion to hydrocracked products cannot be ruled out as their compositions were higher at 440°C. While toluene composition increased threefold initially, the trend at 420°C is retained. The profile of the hydrocracked products showed an optimum P_{H_2} at 0.3 atm and a new feature: a minimum at ∿0.67atm. The

product distribution profiles at 440°C clearly showed that the optimum P_{H_2} for the hydrocracked products is at a lower value compared to ethylbenzene and the xylene isomers (the dehydrocyclization products). The relative magnitude of ethylbenzene and the xylene isomers were generally retained except that the composition of 0-xylene is now greater than ethylbenzene.

At 460°C (Figure 5.1.18), the composition of iso-octane decreased more significantly although the compositions of the dehydrocyclized products were lower compared to their values at 440°C. The composition of hydrocracked products was higher than at 440°C while that of toluene was lower. With regard to the optimum P_{H_2} values, all the products exhibited maxima in the following order:

Toluene, Hydrocracked products, ethylbenzene (0.33atm) < P-xylene (0.45atm) < 0-xylene (0.5atm) ∿ M-xylene (broad max. ∿0.5atm). Again, the relative magnitude of ethylbenzene and the xylene isomers at 440°C was retained at higher temperature of 460°C.

Profiles of product composition against temperature for P_{H_2} = 0.11, 0.33, 0.5, 0.67 and 0.89 atm were used to understand the effect of temperature on the location of the maximum P_{H_2}. These plots complement the product composition - P_{H_2} plots (Figures 5.1.16 - 5.1.18) and show more clearly the direction of temperature dependence of the maximum P_{H_2}.

By the postulate of Paal[85,86], at constant hydrogen pressure, the reaction requiring the least dissociated surface species should have its maximum rate at the lowest temperature. This was actually observed by Sachtler et al[88] on Platinum-

based hydrocarbon - conversion catalysts where they reported that maximum yields of various reactions are not at the same temperature over Pt-black. The work reported here is on bifunctional Pt/Al_2O_3 and it will be useful to check if the above conclusions are applicable on the bifunctional catalyst.

Since iso octane requires the least dissociated surface intermediate, its maximum P_{H_2} should occur at the lowest temperature. This is borne out by the result shown in Figures 5.1.19 and 5.1.20 at P_{H_2} = 0.33 and 0.5atm, respectively. The P_{H_2} maxima of the dehydrocyclized products occur at higher temperatures as expected. The P_{H_2} maxima for ethylbenzene, 0- and P-xylene occur at 440°C irrespective of hydrogen pressure. The behaviour of the P_{H_2} maximum for m-xylene appears to be dependent on hydrogen pressure although at $P_{H_2} \geq 0.5$atm (Figure 5.1.20), the maximum P_{H_2} occurs again at 440°C. Figure 5.1.21 at P_{H_2} = 0.89atm shows that the maximum P_{H_2} for iso octane precedes those of the other products. Again, the order of appearance of the maximum for the hydrocracked products is not in conformity with the Paal scheme as the temperature of its occurence is higher than those for the dehydrocyclized products.

5.1.2 ISO-OCTANE

The product of reaction of iso octane (2,2,4 trimethylpentane) over 0.3% Pt/Al_2O_3 and 0.6%Pt/Al_2O_3 catalyst between 390°C and 430°C was 1,1,3 trimethylpentane. The variation of conversion of iso octane on 0.3%Pt/Al_2O_3 catalyst as a function of reciprocal velocity for different partial pressures of iso octane and catalyst temperatures are shown in Figures 5.1.22 - 5.1.25. At all the partial pressures investigated

(0.0236 to 0.082atm), conversion increased with increasing temperature. However, at 0.082atm iso octane partial pressure, the difference in conversion at the higher temperature became small. For example, at W/F = 0.33gminom^{-3} the conversions of iso octane at 420° and 430°C were 0.60 and 0.62, respectively while at 0.056atm iso octane partial pressure, the difference was ∿0.1 at the same conditions. The conversion obtained at 0.0236atm was generally higher than those obtained at higher iso octane partial pressure. At 430°C and 0.33gminom^{-3} reciprocal velocity, the conversion obtained at 0.0236atm was 0.84 (Figure 5.1.22) while the values were 0.76, 0.77 and 0.76 for 0.0316, 0.056 and 0.082 atm, respectively. The pattern at 430°C was repeated at 420° and 410°C. At 390°C and 400°C, however, this trend was not maintained as the conversion obtained at 0.082atm became higher than those at lower iso octane partial pressures (0.0316 and 0.056 atms). It appears that at high iso octane partial pressures and low temperatures (P_{iso} = 0.056 atm, 390°C; P_{iso} = 0.082atm 390°C and 400°C) the conversion - W/F profiles can be described by linear relationships as opposed to the other profiles where the conversion increased rapidly at lower W/F followed by a slower increase with further increase in W/F.

Plots of conversion of iso octane on 0.6%Pt/Al_2O_3 catalyst as function of reciprocal velocity are shown in Figures 5.1.26-5.1.28. The highest conversion of ∿0.85 was obtained at the lowest iso octane partial pressure investigated (0.0316atm) and highest temperature (430°C). This value was higher than the conversion of 0.76 obtained with 0.3%Pt/Al_2O_3 catalyst at the same set of conditions. The same trend can be obtained

at the other temperatures except at 390°C where the conversion level obtained on 0.3%Pt/Al_2O_3 catalyst was higher than obtained on 0.6%Pt/Al_2O_3. On the other hand, results obtained at 0.056atm and 430°C shows that the conversion on 0.6%Pt/Al_2O_3 catalyst is slightly lower than that obtained on 0.3%Pt/Al_2O_3 catalyst. The pattern at 430°C was repeated at 390°C. At 400°C and 410°C however, the highest conversion obtained were the same on both catalysts while at 420°C the conversion on 0.6%Pt/Al_2O_3 catalyst was higher than on 0.3%Pt/Al_2O_3 catalyst. The conversion - reciprocal velocity profile at 0.082 atm (Figure 5.1.28) shows that at 420° and 430°C, conversions were the same on both the 0.3% and 0.6%Pt/Al_2O_3 catalysts for the same set of conditions. At the other temperatures however, the conversion obtained using 0.3%Pt/Al_2O_3 catalyst was higher.

It appears that increasing the platinum content of the bifunctional Pt/Al_2O_3 reforming catalyst from 0.3%Pt to 0.6% Pt does not have any significant effect on the isomerization of 2,2,4 trimethylpentane. The difference in the conversion levels observed can be attributed to the quality of the experimental data.

5.1.3 Methylcyclopentane

I: Pt/Al_2O_3 Catalyst

A. Total Conversion

The products of reaction of MCP on Pt/Al_2O_3 catalyst were hydrogenolysis products (2 methylpentane, 3 methylpentane and n hexane), cyclohexane and benzene. The reaction was carried out between 370°C and 400°C as there was low conversion

below 370°C and heavy coking above 400°C. The variation of the total conversion of MCP as function of reciprocal velocity is shown in Figures 5.1.29 - 5.1.32. The conversion of MCP increased with increase in temperature at all the MCP partial pressures investigated. The rate of increase in conversion with W/F was higher at low W/F except at MCP partial pressure of 0.058atm and reactor temperature of 380°C (Figure 5.1.29) where the rate of increase is slowest between 0.08 and 0.16 $gmin\,cm^{-3}$.

B. Product Distribution

Figures 5.1.33 - 5.1.40 show the plots of product composition against W/F at various MCP partial pressures. The product composition of cyclohexane was small ~4%, and passed through maxima at all the MCP partial pressures and temperatures except for the product composition obtained at 0.092atm MCP partial pressure where the value rose steeply initially and became constant afterwards.

The composition of hydrogenolysis products increased linearly with increase in reciprocal velocity except at 0.1447 atm MCP partial pressure and 400°C (Figure 5.1.39) where the composition increase with W/F was slow for low W/F and fast at high values of W/F. The composition of hydrogenolysis products increased with temperature throughout the temperature range investigated. The composition became very small (between 0.3% and 4%) except at 0.1447atm where the composition were 6 and 7% respectively.

The predominant product in the reactions of MCP on Pt/Al_2O_3 catalyst is benzene. Its composition increased with increase in temperature. At 0.058atm MCP partial pressure, the benzene composition increased linearly with reciprocal velocity at 370°, 380° and 390°C while at 400°C the benzene composition was almost constant at high values of W/F. The pattern at 0.058atm was repeated at 0.092 and 0.1816atm MCP partial pressures except that at 0.092atm the profile of benzene composition at 390°C was similar to that obtained at 400°C while at 0.1816atm linear relationship was obtained between the product composition of benzene and W/F at 400°C instead of 370°C. The benzene composition obtained was between 0.1 and 0.33 and the composition generally decreased with increase in MCP partial pressure except at 0.1816atm MCP partial pressure and 400°C where the composition was relatively high (see Figures 5.1.37 - 5.1.38).

II. Pt - Re/Al_2O_3 (UNDRIED)

A. Total Conversion

The variation of the total conversion of MCP as functions of reciprocal velocity are shown in Figures 5.1.41 - 5.1.44. Similar to the results obtained with Pt/Al_2O_3 catalyst, the conversion of MCP increased with increase in temperature at all the MCP partial pressures investigated. The conversions obtained at 0.058atm MCP partial pressure at various temperatures are however much higher than the conversions obtained at higher MCP partial pressures. This is definitely not due to

the effect of MCP partial pressure alone. Our results on the effect of the number of regenerations on the catalyst activity (section 5.2.3) shows that undried Pt-Re/Al_2O_3 catalyst loses the beneficial effect of rhenium addition after three or four regeneration and behaves more like Pt/Al_2O_3 catalyst. The conversion - W/F profiles (Figures 5.1.41 - 5.1.44) shows that there was rapid increase in conversion, with increase in W/F at low W/F value and slow increase or constant conversion at high W/F values. The conversions at 0.1447atm MCP partial pressure (Figure 5.1.43) were slighly higher than those obtained at 0.092atm while the least conversions were obtained at the highest MCP partial pressure (Figure 5.1.44). The conversions obtained with this catalyst is slightly higher than those obtained using Pt/Al_2O_3 at the same conditions. For example the conversion of MCP on Undried Pt/Al_2O_3 and Pt-Re/Al_2O_3 (UNDRIED) catalysts at 0.32gmincm^{-3}, 0.092atm MCP partial pressure and 370°, 380°, 390° and 400°C are as follows:

0.17, 0.24, 0.285 and 0.43 respectively for Pt/Al_2O_3 catalyst and 0.2, 0.275, 0.39 and 0.45 respectively for Pt-Re/Al_2O_3 (UNDRIED) catalyst.

B. Product Distribution

The variation of the product compositions with W/F are shown in Figure 5.1.45 - 5.1.52. The cyclohexane composition passed through maxima at MCP partial pressures of 0.058 and 0.092atm except at 400°C and 0.092atm where the cyclohexane composition rose rapidly initially and became constant afterwards except at 0.1447atm and 370°C and 390°C where the

composition passed through maxima. Similar to the results obtained with Pt/Al_2O_3 catalyst, the cyclohexane composition was low at all the conditions investigated.

The composition of hydrogenolysis products showed almost linear relationship with W/F at 0.058 and 0.092atm MCP partial pressures except at 380°C and 0.058atm where the composition of hydrogenolysis products increased at low W/F and remained constant at high W/F values. At 0.1447 and 0.1816atm, the composition of hydrogenolysis products passed through maxima at all the temperatures except at 370°C where the composition increased at low W/F and remained constant at high W/F values for 0.1447 and 0.1816atm.

At 0.058atm MCP partial pressure (Figures 5.1.45 - 5.1.46) high benzene composition were obtained and they passed through maxima at 390°C and 400°C. The composition of benzene were about 0.4 and 0.5, respectively at the maximum values. At 370° and 380°C, the compositions of benzene increased rapidly initially with W/F at low W/F and slowly at high W/F. Compositions of 0.22 and 0.30 were obtained at W/F of 0.32gmincm^{-3} at 370° and 380°C, respectively. The high benzene composition dropped significantly at 0.092atm and it seems that the effect of rhenium addition is no longer pronounced as the highest benzene composition was ∿0.33. This value is comparable to that obtained using 0.3%Pt/Al_2O_3 at the same reaction conditions (figure 5.1.36). Similar results were also obtained at the other temperatures investigated.

III. Pt - Re/Al_2O_3 (DRIED)

A. Total Conversion

The variation of the total conversion of MCP as functions of reciprocal velocity at various MCP partial pressures and temperatures are shown in Figures 5.1.53 - 5.1.56. The figures show that total conversion increases with increase in temperature at all MCP partial pressures investigated in conformity with the results obtained on Pt/Al_2O_3 and $Pt-Re/Al_2O_3$ (UNDRIED). Tables 5.2 - 5.4 show the initial rate of MCP reaction on the three reforming catalysts (Pt/Al_2O_3, $Pt - Re/Al_2O_3$ (UNDRIED) and $Pt-Re/Al_2O_3$ (DRIED) at various temperatures and MCP partial pressures.

Table 5.2: Initial rates of MCP conversion on Pt/Al_2O_3 catalyst at various temperatures and MCP partial pressures.

Temp (°C) / P_{MCP} (atm)	Initial Rate, $cm^{-3}\ g^{-1}\ min^{-1}$			
	370°C	380°C	390°C	400°C
0.058	1.56	2.50	2.50	5.0
0.092	1.46	2.50	3.58	5.38
0.1447	1.44	1.56	1.88	5.0
0.1816	1.04	2.08	2.50	3.33

Table 5.3: Initial rates of MCP conversion on Pt-Re/Al_2O_3 (UNDRIED) catalyst at various temperatures and MCP partial pressures.

Temp. (°C) / P_{MCP} (atm)	Initial Rate, $cm^{-3}\ g^{-1}\ min^{-1}$			
	370	380	390	400
0.058	2.92	4.5	6.25	11.25
0.092	0.94	1.66	3.25	5
0.1447	1,88	1.67	11.11	16.67
0.1816	1.5	2.84	3.5	5.83

Table 5.4 : Initial rates of MCP conversion on Pt-Re/Al_2O_3 (DRIED) catalyst at various temperatures and MCP partial pressures.

Temp. (°C) / P_{MCP} (atm)	Initial Rate, $cm^{3}\ g^{-1}\ min^{-1}$			
	370	380	390	400
0.058	5.63	7.5	10.29	13.33
0.092	2.5	5	6	8.75
0.1447	2.27	3.75	4.58	6
0.1816	1.67	3	4.5	7.5

The initial rates increase with increase in temperature for the three catalysts. The order of reactivity based on the initial rate data is given by:

$Pt\text{-}Re/Al_2O_3$ (DRIED) > $Pt\text{-}Re/Al_2O_3$ (UNDRIED) > Pt/Al_2O_3

Exception to this rule is the initial rate of reaction of MCP for $Pt\text{-}Re/Al_2O_3$ (DRIED) and $Pt\text{-}Re/Al_2O_3$ (UNDRIED) at 0.1447atm and 390° and 400°C temperatures where the order is reversed. It is interesting to note that the conversion is very high at low W/F . There are marked differences in conversion between 370° and 380°C, and 390°C and 400°C than between 380° and 390°C. The conversion obtained on $Pt\text{-}Re/Al_2O_3$ (DRIED) is higher than that obtained on $Pt\text{-}Re/Al_2O_3$ (UNDRIED) at all the temperatures investigated at high W/F. For example, the conversions obtained at 0.092 atm and 400°C are 0.8 and 0.45 at 0.32gmincm^{-3} W/F for the DRIED and UNDRIED $Pt\text{-}Re/Al_2O_3$ catalysts respectively, while at 370°C the values were 0.5 and 0.19 respectively. The conversion-W/F profiles obtained at 0.1447atm and 0.1816atm partial pressures (Figures 5.1.55 - 5.1.56) are similar to that obtained at 0.058atm (Figure 5.1.53) except that the conversion was higher at 0.058atm and also that at 0.1447atm and 370°C there is a linear relationship between conversion and W/F.

B. Product Distribution

Figures 5.1.57 - 5.1.64 shows the variation of product composition with W/F on $Pt\text{-}Re/Al_2O_3$ (DRIED) catalyst at various MCP partial pressures and temperatures. The cyclohexane compositions passed through maxima for most experimental conditions investigated. At 0.058 and 0.092atm and 390°C and

400°C, however, the composition profiles increased rapidly at low W/F and slowly afterwards. The composition of cyclohexane is small(∿4%) and this is similar to the composition obtained using Pt-Re/Al_2O_3 (UNDRIED) catalyst.

The hydrogenolysis product composition profiles are similar to the typical benzene composition profiles. However, the benzene composition profiles passed through maxima at MCP partial profiles of 0.1816atm and reactor temperatures of 380°C and 390°C.

The highest benzene composition was obtained at 400°C and 0.092atm MCP partial pressure where the value reached 0.6 at W/F value of 0.33gmin cm^{-3}. The benzene composition increased with increase in W/F except at 0.058 atm MCP partial pressure and 400°C where it passed through a broad maximum. The rate of increase in benzene composition is generally slower at high W/F values except at 0.1816atm and 380°C where linear relationship exists between benzene composition and W/F . Also, the linear relationship exists at 0.092atm and 370°C where the benzene composition increase with W/F was slowest in the W/F range 0.08 - 0.20 gmin cm^{-3}.

5.2 Variable Activity

Three variables determine the deactivating characteristics of the reforming catalysts (Pt/Al_2O_3, Pt-Re/Al_2O_3) during the isomerization of iso octane and aromatization of MCP at constant temperature. These variables are the partial pressure of iso-octane or MCP, hydrogen partial pressure(in the carrier gas) and time on stream. Catalyst deactivation

was monitored through the decline in the conversion of iso-octane or MCP as coke builds up on the catalyst surface. The regenerated catalyst is then used to perform deactivation studies using different sets of variables.

5.2.1 ISO OCTANE ON 0.3% Pt/Al_2O_3 AND 0.6% Pt/Al_2O_3 CATALYSTS

The variations of the conversion of iso-octane with reaction time at various H_2 partial pressures are shown in Figures 5.2.1 - 5.2.3. Initial conversions lie between 0.25-0.28, 0.31 - 0.36 and and 0.35 - 0.39 for various H_2 partial pressures at 390°, 410° and 430°C respectively. The figures show that at constant temperature, conversion decreases with H_2 partial pressure. There is a rapid decrease of conversion in the first 60 minutes at 390°C and 410°C followed by a very slow drop in conversion with time. At 430°C (Figure 5.2.3), the region of rapid drop in conversion was less than 40 minutes except for the profiles at 0.5 and 0.778atm H_2 partial pressures where the times were about 60 min and 30 min, respectively. Figure 5.2.4 demonstrates the effect of iso octane partial pressure on conversion at 410°C and H_2 partial pressure of 0.5atm. The conversion decreases with increasing reaction time and increasing iso octane partial pressure. The deactivation profiles in Figure 5.2.4 exhibited two characteristic regions similar to those exhibited by changing H_2 partial pressure, namely: a region of fast deactivation followed by a slow deactivation region after 60 mins.

Figure 5.2.5 - 5.2.7 show the plot of conversion of iso-octane with reaction time at different H_2 partial pressures on 0.6%Pt/Al_2O_3 catalyst. The conversion in the absence of coking (at zero time) is higher on the 0.6%Pt/Al_2O_3 catalyst compared to the lower metal 0.3%Pt/Al_2O_3 catalyst. Furthermore, the region of fast deactivation is generally longer on the 0.6%Pt/Al_2O_3 catalyst. In fact, no deactivation was observed at P_{H_2} = 0.778 atm and 390°C on 0.6%Pt/Al_2O_3 (Figure 5.2.5) in contrast to the deactivation observed on the 0.3% Pt/Al_2O_3 catalyst (Figure 5.2.1). At P_{H_2} = 0.11atm, the conversion decreases rapidly initially and slowly afterwards at all the temperatures investigated. This result is in conformity with the results obtained with 0.3%Pt/Al_2O_3 catalyst at the same condition. Figure 5.2.8 illustrates the variation of conversion of iso-octane with reaction time and iso-octane partial pressure on 0.6%Pt/Al_2O_3 catalyst. Similar to the curve obtained using 0.3%Pt/Al_2O_3 (Figure 5.2.4), there were short fast deactivation and long slow deactivation regions.

5.2.2 Methylcyclopentane (MCP)

I. Pt/Al_2O_3 Catalyst

A. Total Conversion

Figure 5.2.9 - 5.2.11 shows the variation of the conversion of MCP with reaction time at different H_2 partial pressures. The conversion at zero time at 390°C varied between 0.24-0.3 while at 400°C and 410°C these values lie between 0.175 - 0.49 and 0.44 - 0.59, respectively. A significant feature of the MCP deactivation profiles is the fact that maxima were exhibited. The conversion - time profiles

at 390°C passed through maximum values within the first 8 min except at P_{H_2} = 0.5atm. This pattern was repeated at 400°C and 0.778atm H_2 partial pressure. This phenomenon was not observed in iso octane. Similar to the results obtained with iso octane, two regions can be distinguished: a region of rapid deactivation between 5 - 20 min after the maxima followed by a slow deactivation region. Experimental results show that the region of fast deactivation obtained with MCP reactant (5-20min) is shorter than that of iso octane which is between 0 - 50 min. This implies that MCP deactivates the catalysts faster than iso octane. This inference is in agreement with deactivation function obtained for these two reactants (See Tables D.1 and D.2

Figure 5.2.24 shows the variation of the total conversion as a function of time at H_2 partial pressure of 0.778atm and various MCP partial pressure. The conversion passed through maxima at about 7 min at 0.092 and 0.1447 atm MCP partial pressure. A comparison of the deactivation functions (See Table D.2 show that deactivation is more rapid at higher MCP partial pressures. It is important to note that at lower MCP or iso-octane partial pressures and high H_2 partial pressure the conversion value at the slow deactivation region (residual conversion) is higher than at higher MCP partial pressures and low H_2 partial pressure.

B. Product Distribution

Figures 5.2.12 - 5.2.23 show the variation of the product composition of MCP conversions on Pt/Al_2O_3 catalyst as functions of time at different temperatures and H_2 partial pressures.

At 390°C (Figures 5.2.12 - 5.2.15), the cyclohexane composition was low at all H_2 partial pressures investigated. The cyclohexane composition decreased slightly as a function of time at 0.11 and 0.33atm H_2 partial pressures (Figures 5.2.12-5.2.13), passed through a maximum at 0.5atm H_2 partial pressure (Figure 5.2.14) and was constant at 0.778atm hydrogen partial pressure (Figure 5.2.15).

The hydrogenolysis product composition first passed through maxima before dropping owing to severe coke deposition on the catalyst surface. The composition profile at P_{H_2} = 0.778atm (Figure 5.2.15) however did not pass through maximum but decreased throughout as function of time.

Similar to the composition profile for the hydrogenolysis products, the benzene composition passed through maxima as functions of time at 390°C except at 0.5atm H_2 partial pressure where the benzene composition was predominant at zero time in agreement with the results obtained in pure hydrogen (See Figure 5.1.33). The highest value of benzene composition of 26% was obtained at P_{H_2} = 0.778atm.

Figures 5.2.16 - 5.2.19 show the variation of product composition as functions of time and P_{H_2} on Pt/Al_2O_3 catalyst at 400°C. The low cyclohexane composition at 390°C was maintained at 400°C. At 0.11atm H_2 partial pressure (Figure 5.2.16), the cyclohexane composition decreased linearly as functions of time while at 0.33atm the composition was constant for the first 5mins and decreased thereafter. The cyclohexane composition at 0.5atm decreased from 2.6% to 2% in the first 35mins and remained constant afterwards while at 0.778atm the cyclohexane composition actually passed through a minimum.

In contrast with the results obtained at 390°C, the composition of hydrogenolysis products did not pass through a maximum with time at 400°C. The composition of hydrogenolysis products was higher than the cyclohexane composition. Its profile decreases fastly initially and slowly afterwards at this temperature.

Similar to the results obtained at 390°C, the benzene composition was predominant at 400°C. It should be noted however that the benzene composition at zero time was lower at P_{H_2} = 0.11atm than at the higher H_2 partial pressure. For example, the benzene composition was 0.12 at zero time at P_{H_2} = 0.11atm while at P_{H_2} = 0.5atm the benzene composition was 36% (See Figures 5.2.16 - 5.2.18). The benzene composition each passed through a maximum with time at P_{H_2} of 0.5atm and 0.778atm.

Figures 5.2.20 - 5.2.23 show the variation of product composition as functions of time at 410°C and various H_2 partial pressure. The cyclohexane composition was also low at this temperature (< 3%). At P_{H_2} = 0.11atm the composition profile passed through a maximum in the first 15 min after which the composition became constant. The cyclohexane composition was lowest at P_{H_2} = 0.33atm. At this partial pressure the highest composition was 1.5% (composition at zero time), and this decreased rapidly to 0.2% in 30min. The composition at P_{H_2} = 0.5atm increased linearly with time while at 0.778atm H_2 partial pressure the composition decreased from 4% (at zero time) to 1.4% in 40 mins and it remained constant at this value for the rest of the time investigated.

The composition of hydrogenolysis products increased remarkably at this temperature. The highest value obtained at 400°C was 11% (at P_{H_2} = 0.778atm) as opposed to 19% obtained at 410°C at P_{H_2} = 0.5atm. The composition of hydrogenolysis products passed through a maximum at P_{H_2} = 0.11atm while at the other partial pressure, the composition of hydrogenolysis products increased rapidly initially and slowly afterwards.

In contrast with the results obtained at lower temperatures, the benzene composition at P_{H_2} = 0.11atm was high (∿44%) at zero time. At this partial pressure, the benzene composition decreased in the first 20 min and slowly afterwards while at 0.33atm H_2 partial pressure the composition was constant for the first 5min and decreased to zero in the first 33min. At H_2 partial pressures of 0.5atm the benzene composition decreased rapidly in the first 30min followed by a slow decrease as function of time. At P_{H_2} = 0.778atm the composition was constant with time after the fast deactivation period.

The relationship between product composition and time at 400°C and at various MCP partial pressure is shown in Figures 5.2.25 - 5.2.27. The cyclohexane compositions were almost constant as functions of time at lower MCP partial pressures while at 0.1816atm MCP partial pressure the profile behaved in the same manner as the hydrogenolysis products profile.

The composition of both cyclohexane and hydrogenolysis products were low ($\leq$ 5%). At 0.092atm MCP partial pressure, the composition of hydrogenolysis products decreased rapidly in the first 45min (Figure 5.2.25) and remained constant

afterwards, while at 0.1447atm MCP partial pressure, the composition of the hydrogenolysis products was almost constant with time. The profile of the hydrogenolysis products composition obtained at 0.092atm MCP partial pressure (Figure 5.2.25) was repeated at 0.1816atm MCP partial pressure except that the fast deactivation region was shorter (∿ 25min).

The benzene composition passed through a maximum with time at MCP partial pressures of 0.092 and 0.1447atm, respectively. The benzene composition was highest at 0.1816atm (∿23% at zero time).

The results of the experiments with MCP on Pt/Al_2O_3 catalyst indicate that the cyclohexane yield was low throughout at all conditions investigated. It appears that the rate of cyclohexane formation from MCP is lower than the rate of cyclohexane dehydrogenation to benzene.

II. Pt - Re/Al_2O_3 (DRIED)

A. Total Conversion

The variations of the total conversion of MCP with reaction time at different H_2 partial pressures on Pt-Re/Al_2O_3 (DRIED) catalyst are shown in Figures 5.2.28 - 5.2.30. At P_{H_2} = 0.778atm, there was only a slight decrease in conversion with time, probably due to the transformation of coke precusors to harmless products in H_2 stream. At the other partial pressures, conversion was constant in the first 5min, decreased rapidly between 5 and 45min and decreased slowly afterwards except at P_{H_2} = 0.33atm and 390°C and 400°C when each profile

passed through a maximum. It can be observed that the fast deactivation region is much longer (∿38min) than that obtained with Pt/Al_2O_3 catalyst (∿20min). Also a comparison of the deactivation functions obtained for these two reforming catalysts (Table D.2) show that $Pt\text{-}Re/Al_2O_3$ (DRIED) catalyst is more resistant to coking than Pt/Al_2O_3 catalyst. The plots of total conversion of MCP at 400°C as functions of time at H_2 partial pressure of 0.5atm and various MCP partial pressures are shown in Figure 5.2.43. Conversion was higher at low MCP partial pressure. The initial conversions were 0.65, 0.6 and 0.25 at MCP partial pressures of 0.058, 0.092 and 0.1447 atm, respectively. The initial conversion decreased from these values to about 0.35, 0.3 and 0.175 in 5min.

B. Product Distribution

Figures 5.2.31 - 5.2.42 show the relationship between product composition and time at different temperatures and H_2 partial pressures. Similar to the results obtained on Pt/Al_2O_3 catalyst, the cyclohexane composition was low at 390°C. The cyclohexane composition was constant for 25min before it started to decrease at P_{H_2} = 0.11atm (Figure 5.2.31) while at 0.33atm H_2 partial pressure (Figure 5.2.32), the cyclohexane composition passed through a broad maximum. The composition at 0.5atm H_2 partial pressure was constant with time after an initial slight increase while at 0.778atm (Figure 5.2.34) the cyclohexane composition increased slightly with time.

The composition of hydrogenolysis products were slightly higher than 10% except at 0.5atm (Figure 5.2.33) where the

composition value at zero time was 15%. The composition profile for the hydrogenolysis products decreases rapidly initially and slowly afterwards. The initial benzene composition were 0.15, 0.14, 0.19 and 0.125 at 0.11, 0.33, 0.5 and 0.778atm H_2 partial pressures. This is comparable to the benzene composition obtained at 390°C with Pt/Al_2O_3 catalyst (See Figures 5.2.12 - 5.2.15), The benzene composition decreases rapidly initially and slowly afterwards except at 0.33atm H_2 partial pressure where it passed through a maximum.

The variations of product composition with time at reactor temperature of 400°C and at various H_2 partial pressure are shown in Figures 5.2.35 - 5.2.38. The cyclohexane composition passed through maxima at all H_2 partial pressures investigated except at 0.33atm H_2 partial pressure where it first increased and later became constant.

The composition of hydrogenolysis products was low (∿15%) and its profiles passed through an early maxima except at P_{H_2} = 0.11atm and 0.778atm where the composition - time profiles decreased initially and slowly thereafter.

The benzene composition obtained at 400°C was higher than that obtained at 390°C and the value at zero time was ∿45% at P_{H_2} = 0.5atm (Figure 5.2.37). At 0.778atm H_2 partial pressure, the benzene composition was constant for over 75min. At the other H_2 partial pressure however, the composition of benzene decreased rapidly initially and slowly thereafter.

Figures 5.2.39 - 5.2.42 show the variation of product compositions of MCP as functions of time at 410°C. The cyclohexane composition was still low at this temperature and its profile passed through a broad maximum at 0.11atm H_2 partial

pressure. At 0.33 and 0.778 atm H_2 partial pressure the cyclohexane composition increased slightly initially and became constant later while at 0.5atm H_2 partial pressure the composition was constant with time.

Similar to the results obtained at lower temperatures the benzene composition was higher than the composition of hydrogenolysis products and cyclohexane. The benzene composition at 0.778atm H_2 partial pressure was trapezoidal in shape and the composition value was ∿40% while the benzene composition at P_{H_2} = 0.33atm passed through a maximum within the first 12min. Apart from these exceptions the hydrogenolysis products and benzene composition profiles were the same as those obtained at 400°C. A comparison of the deactivation functions shows that deactivation is more severe at higher temperatures and lower H_2 partial pressures. For example, the deactivation function at P_{H_2} = 0.33atm and 390°, 400° and 410°C are 0.028, 0.038 and 0.068, respectively while the corresponding values at 0.5atm H_2 partial pressure are 0.011, 0.02 and 0.051, respectively (See Tables D.5 and D.6).

Figure 5.2.44 - 5.2.46 show the relationship between product composition and time at various MCP partial pressure and 410°C. The cyclohexane composition was low (∿3%). Its profiles each passed through a maximum at 0.058atm and 0.092 atm while at 0.1447atm the composition was almost constant with time.

The profiles for hydrogenolysis products show that the composition decreased rapidly in the first 15min followed by a slow decrease with time at 0.058 and 0.092atm MCP partial pressures. The composition of hydrogenolysis products was

low at 0.1447atm MCP partial pressure (∿4%) and its values decreased sharply reaching zero within 28min.

The benzene composition was 32% at 0.058 and 0.092atm MCP partial pressures while at 0.1447atm MCP partial pressure, the composition was ∿15% at zero time. The benzene composition at 0.058atm MCP partial pressure passed through a maximum within the first 10 min. It then decreased sharply followed later by a slow decrease with time. The pattern of benzene composition profile at 0.058atm MCP partial pressure was repeated at 0.092atm MCP partial pressure. The benzene profile at 0.1447atm MCP partial pressure decreased linearly from 18% at zero time to 4% in 40min afterwhich it started decreasing slowly.

The results of the investigation of the deactivation kinetics of Pt/Al_2O_3, and $Pt-Re/Al_2O_3$ (DRIED) using MCP was reactant, show that higher initial conversion was obtained with $Pt-Re/Al_2O_3$ (DRIED) catalyst. In addition, the $Pt-Re/Al_2O_3$ (DRIED) catalyst is more resistant to coking as its deactivation function value was lowest (Table D.5 and D.6).

5.3 Catalyst Mortality

In this section, we present the results obtained during catalyst mortality studies on commercial Pt and Pt-Re on alumina reforming catalysts. The catalysts were subjected to several deactivation - regeneration cycles. This was done with a view to studying the changes in conversion, selectivity, coking level and deactivation kinetic mechanism as the catalysts

progressively approach the mortal state. The mortality experiments were performed using nitrogen as carrier in order to accelerate the aging process.

5.3.1 N-Octane

A. Total Conversion

Seven deactivation - regeneration cycles were investigated on the fresh Pt/Al_2O_3 catalyst using the dehydrocyclization of n-octane as a model reforming reaction. The deactivation reaction was carried out at 440°C, $W/F = 0.11 gmin cm^{-3}$, n-octane partial pressure of 1.37×10^{-2} atm and total system pressure of 1atm. Figure 5.3.1 shows the variation of total conversion of n-octane as function of time for the seven cycles. The conversion at zero time varied between 0.54-0.86. The lowest conversion was obtained at the 1st and 3rd cycles when the conversions were 0.54 and 0.65, respectively. At the other cycles, conversions lay between 0.8 and 0.86. At the 6th cycle the total conversion - time profile passed through a maximum at 20min. The conversion - time profile shows that the conversion decreases slowly for the first 20min for the 4th, 5th and 7th cycles, followed by a rapid drop in conversion between 20 and 60min afterwhich the decrease in conversion with time became very slow. The profile obtained in the 1st and 3rd cycles were similar to those of 4th, 5th and 7th cycles except that the first slow deactivation region (first 20min) was absent.

B. Product Distribution

Figures 5.3.2 - 5.3.8 show the variation of product composition against time for different cycles. At all the cycles investigated, the hydrocracked products were predominant. The hydrocracked products composition decreased slightly in the first 20min and rapidly afterwards for all cycles except the second where the initial drop in conversion was fast. In the first cycle (Figure 5.3.2) ethylbenzene was the predominant aromatic (5.6%), but this quickly dropped to 1% within the first 5min. The drops in conversion of P-xylene, 0-xylene and toluene were not as rapid as their compositions were already higher than that of ethylbenzene after 5min. The iso-octane composition was high at zero time (~10%) and this decreased linearly to 1% in 30min afterwhich it remained constant. The pattern during the 1st cycle was maintained in the 2nd cycle. However, the composition of hydrocracked products in the 2nd cycle at zero time was more than the 1st (45% vs 22%) and the ethylbenzene composition did not decrease as rapidly. In the 3rd cycle (Figure 5.3.4), the P-, 0-xylenes and the hydrocracked products decreased only slightly in the first 20min while the composition of toluene was actually constant over this period. Apart from this, the profile was the same as for the 2nd cycle.

Figures 5.3.5 - 5.3.7 show the composition - time profiles for the 4th, 5th and 6th cycles. The hydrocracked products were still high (50%) and in the 4th cycle, ethylbenzene and m-xylene each passed through two minima at 20 and 40min, respectively. The P-xylene, 0-xylene and toluene compositions

were almost constant for the first 20min and each then passed through a maximum at 40min. Similar to the results obtained in the 3rd cycle, product compositions were very low at about 60min (∿0.2%) except for hydrocracked products (about 8%). At the 5th cycle (Figure 5.3.6), ethylbenzene and m-xylene profiles had no minimum like in the 4th cycle but were about constant for 20min before decreasing rapidly with time between 20-50min and then slow thereafter. The toluene, P-, and O-xylene compositions each passed through a maximum while the profile of iso-octane remained the same as in the 4th cycle. Iso-octane was no longer the predominant product (apart from hydrocracked products) in the 4th and 5th cycles. In the 6th cycle, ethylbenzene, m-xylene, toluene, P- and O-xylene all passed through their respective maximum while the hydrocracked products and iso-octane compositions were about constant for the first 40min after which they decreased rapidly up to 120min. This decrease was then followed by slower decrease. It is important to stress that the composition is still relatively high after 120min as opposed to the 4th and 5th cycles where the compositions became very low after 60min. At the 7th cycle (Figure 5.3.9), the cracked products, O- and P-xylene where constant for about 25 min, decreased rapidly for another 60min and then a slow decrease followed. The profiles of the other product composition were the same as those of the cracked products, O- and P-xylene except that the compositions were not constant in the first 25min.

In Figure 5.3.9, the coke content versus cycle number is shown. The figure shows that the quantity of coke in the 2nd cycle was low (∿0.021gC) while that formed in the 4th cyle was high (0.05gC). The coke content for the other cycles were between 0.03gC and 0.032gC.

5.3.2 ISO-Octane

Twenty four deactivation - regeneration cycles were performed with iso-octane on 0.3%Pt/Al_2O_3 catalyst at reactor temperature of 430°C and 0.0316atm iso octane partial pressure in nitrogen. Figure 5.3.10 shows the variation of conversion with time for the first 7 cycles. The profile of the 6th cycle decreased rapidly in the first 15min followed by a constant conversion with time afterwards. At the other cycles (see Figure 5.3.10), the conversion was constant within the first 5min afterwhich it decreased between 5 and 15min; after 15min the conversion became constant with time. Figure 5.3.11 shows the variation of conversion with time for the 8th - 14th cycles. Similar to the 6th cycle, the conversion - time profiles in the 10th and 11th cycle decreased rapidly in the first 15min followed by a constant conversion. At the 12th cycle, the conversion - time profile passed through slight maximum in the 5th min, decreased rapidly between 5 and 15min and then slowly between 15 and 30min. At the other cycles the conversion was constant within the first 5min afterwhich it decreased rapidly between 5 and 15min. Figure 5.3.12 shows the variation of conversion with time for the 15th - 20th cycles. The conversion was low at the 18th cycle (0.66) while at the 19th cycle the profile passed through a maximum. At the other cycles (Figure 5.3.12), the conversion did not change as function of time for the first 5min. This was followed by rapid decline in conversion between 5 and 20min; after 20min, the conversion changed only slightly with time. Figure 5.3.13 shows the variation of conversion with time for the 21st - 24th cycles. At the 21st cycle the profile

decreased rapidly in the first 15min while at the 24th cycle the profile passed through a maximum at 5min. At the 22nd and 23rd cycles, the conversion was constant for the first 5min followed by a fast decrease as function of time.

Generally, the conversion - time profiles exhibited two regions; a fast deactivation region followed by a slow region. This followed the pattern reported earlier for n-octane. However, there are two significant differences.

(1) In most of the cycles with iso-octane conversion was constant for 5min before the fast deactivation region.

(2) The fast deactivation region is about 10min with iso octane as opposed to about 45min obtained with n-octane.

In Figure 5.3.14, the coke content in (gC) versus cycle number is shown. The coke content varied between 0.021 and 0.03gC. The coke content value showed slight decrease with cycle number.

The results of this investigation show that regeneration of the catalyst (up to 24 regenerations) did not affect the initial conversion. The coke content on the catalyst was lower than that obtained with n-octane.

5.3.3 Methylcyclopentane (MCP)

I. Pt/Al_2O_3

A. Total Conversion

Thirty nine deactivation - regeneration cycles were performed on the Pt/Al_2O_3 catalyst used previously for 24 cycles in iso-octane. The deactivation reaction was MCP reforming at 430°C, W/F of 0.11 gmincm^{-3}, 1atm total pressure and P_{MCP} = 0.092atm. Figure 5.3.15 shows the variation of conversion with time for the first 10cycles. The initial conversion at the 1st cycle was low (∿0.13) while the conversion at the 7th cycle was the highest (0.5). The initial conversion of the other cycles were between 0.275 and 0.41. The conversion - time profiles decreased rapidly reaching a value lower than 0.09 in 15min. At the 10th cycle, however, the conversion passed through a maximum in the 4th min. Figure 5.3.16 shows the variation of conversion with time for the 11th - 20th cycles. The initial conversions at the 17th and 20th cycles were low (0.225 and 0.25) while the conversions at the 16th and 19th cycles were high (0.49 and 0.445). The initial conversions of the other cycles were between 0.3 and 0.4. The conversion - time profiles exhibited constant conversion for the first 5min, rapid decrease between 10-15min and then slow decrease afterwards. However, at cycles 16, 19 and 20 the conversions were not constant for the first 5min but decreased rapidly for 15min followed by the slow decrease with time. Figure 5.3.17 shows the conversion - time profile for the 21st - 30th cycles. The initial

conversions were between 0.29 - 0.44 except at the 30th cycle where the initial conversion was 0.21. At the 30th cycle an almost linear relationship existed between conversion and time for the first 15min while at the 22nd cycle conversion passed through a maximum as a function of time. At the other cycles, changes in conversion for the first 5min were small. This was followed by rapid decrease in conversions between 5 and 15min. After 15min the decrease in conversion as functions of time became small. Figure 5.3.18 shows the conversion - time profile for the 31st - 39th cycles (initial conversions between 0.15 and 0.235) except the 33rd cycle where the initial conversion was 0.28. At the 31st, 37th and 39th cycles conversion decreased only slightly with time while at the 34th cycle there was a slight increase in conversion in the first 5min. At the other cycles, there were slower decreases in conversion throughout the period investigated.

B. Product Distribution

Figures 5.3.19 - 5.3.23 shows the variation of the product compositions as functions of time for some of the 39 deactivation cycles. The cyclohexane composition was low and the highest composition was obtained at the 39th cycle where the value reached 6.8%. At the 2nd, 11th and 20th cycles , the cyclohexane compositions decreased rapidly in the first 5min followed by a slow decrease in conversion after 15min. At the 3rd and 23rd cycles, the cyclohexane composition decreased rapidly initially and became constant afterwards. The composition - time profiles

of cyclohexane passed through maxima at the 15th, 16th, 28th 30th, 31st, 33rd, 24th and 38th cycles while at 10th, 24th and 27th cycles the relationship between composition and time was linear. At the 35th cycle, the cyclohexane composition was constant for 15min. before it decreased while at the 16th cycle the composition was almost constant throughout the period investigated. At the 7th, 14th, 17th, 18th, 19th, 21st, 22nd, 25th, 29th and 34th cycles, the cyclohexane compositions were almost constant for 5min before decreasing rapidly as functions of time. At the other cycles investigated, the cyclohexane compositions decreased rapidly in the first 15min followed by a slow decrease in composition with time.

Similar to cyclohexane, the composition of hydrogenolysis products were low. The highest composition of the hydrogenolysis products was obtained at the 11th cycle where the initial composition was 10.8%. The hydrogenolysis products composition at the other cycles were below 6% except at the 7th, 10th, 12th, 24th and 25th cycles where the compositions were 7.8%, 9%, 7.5% and 7.1%, respectively. The compositions of the hydrogenolysis products passed through maxima in the 5th, 10th 14th, 18th, 21st, 22nd and 26th cycles, while at the 31st cycle linear relationship exists between the hydrogenolysis products composition and time. At the 11th, 12th, 13th, 15th, 17th, 19th, 29th, 32nd and 34th cycles the hydrogenolysis products composition was almost constant for 5min, decreased rapidly between 5 and 15min and then slowly afterwards. At the other cycles investigated, the hydrogenolysis products composition decreased rapidly in the first 15min and slowly

afterwards.

Unlike the cyclohexane and hydrogenolysis product compositions, the benzene composition was high. Its initial compositions in the first 29 cycles were between ∿20% and ∿30% except at the 1st, 6th, 25th and 28th cycles were they were 7.5%, 35%, 34% and 35% respectively. After the 29th cycle, the benzene compositions for the remaining cycles were below 15% except at the 33rd cycle where the benzene composition was 20%. The benzene composition was constant for the first 5min, decreased rapidly between 5 and 15 min. and then slowly afterwards in the 10th, 13th, 20th, 23rd, 27th, 29th, 34th and 39th cycles. The compositions of benzene passed through maxima at the 11th, 17th, 22nd and 24th cycles while at the 37th cycle the relationship between benzene composition and time was linear. At the 32nd cycle, the benzene composition decreased rapidly between zero and 5min, was constant between 5 and 15min and decreased rapidly thereafter.

The coke content (in gC) versus cycle number is shown in Figure 5.3.24. The coke level on the catalyst surface exhibited a sharp rise after the 5th cycle indicative of a transition between one stability state to another. The coke level in this state was between 0.041 and 0.047gC while the coke level in the second state was about 0.09gC. The lifetime of the second state appears to be very long as it continued up to the 39th cycle when the investigation was discontinued.

As has been disclosed earlier, the total conversion of MCP at zero time on Pt/Al_2O_3 catalyst decreased after the 29th cycle. Experimental results show that the conversion at zero time was below 0.3 after the 29th cycle. The benzene

composition also decreased below 15% after the 29th cycle. It is important to note that the cyclohexane composition did not decrease much as a function of time after the 32nd cycle.

A comparison of the coke levels obtained with MCP on Pt/Al_2O_3 catalyst at the 1st stability state with the coke levels obtained with n-octane and iso octane on Pt/Al_2O_3 catalyst (Figure 5.3.9 and Figure 5.3.14) shows that the coke content obtained with MCP is higher than the coke content obtained with n-octane or iso-octane. The coke level of MCP iso-octane and n-octane are ∿0.04gC, 0.03gC and ∿0.03gC respectively. The conversion - time profiles of MCP (5.3.15-5.3.19) shows that the fast deactivation region is about 10min. This is exactly the same as that obtained using iso-octane. The conversion level obtained with MCP in the first 5min was constant for some cycles in agreement with the results obtained using iso-octane. However one can infer from the relative coke contents that MCP deactivates the catalyst faster than iso octane or n-octane.

Omoleye [52], however reported that the primary coke is not responsible for the mortality of the catalyst. They believed that secondary coke (more resistant coke) is responsible for the catalyst mortality as they are much more difficult to remove during the regeneration of the catalyst.

In conclusion it is important to point out that the profiles of MCP conversion on Pt/Al_2O_3 catalyst are similar to those obtained with iso-octane on Pt/Al_2O_3 catalyst in the following ways: (1) Their conversions for 5min for most of the cycles on Pt/Al_2O_3 for both iso-octane and MCP were constant. (2) The conversion decreased from about 0.8 to below 0.1 for iso

octane and from about 0.4 to below 0.1 for MCP within the first 15min. (in the fast deactivation region). (3) During the slow deactivation region the conversion was either constant or decreased very slowly as function of time. For example in the 1st deactivation cycle with iso-octane conversion decreased by 0.6 in the fast deactivation region (first 15min) while in the slow deactivation region (between 15-30min) the drop in conversion was only 0.03. For practical purposes, the catalyst can be regarded as dead after the fast deactivation region.

II. Pt - Re/Al_2O_3 (UNDRIED)

A. Total Conversion

The variation of the total conversion of MCP with reaction time for 12 deactivation - regeneration cycles on Pt-Re/Al_2O_3 (UNDRIED) catalyst is shown in Figure 5.3.25. The conversion in the absence of coking (at zero time) varied between 0.34 and 0.54. This is higher than the conversion with MCP on Pt/Al_2O_3 catalyst where the conversion at zero time varied between 0.275 and 0.41 during the first 12 cycles except the 1st, 7th and 11th cycles where the conversion (at zero time) were 0.127, 0.51 and 0.49, respectively. The total conversion - time profiles show that the conversion decreases slowly with time up to 5min, then rapidly between 5 and 15min followed again by a region of slow decrease with time at the lowest conversion levels.

B. Product Distribution

Figures 5.3.26 - 5.3.30 shows the variation of product compositions on Pt - Re/Al_2O_3 (UNDRIED) catalyst as functions of time for some of the 12 deactivation cycles. The cyclohexane composition was low for all the cycles and its highest value at zero time (1.5%) was obtained at the 5th cycle. The cyclohexane composition were linear and almost insensitive to variation in time during cycles 1, 2, 6 and 9 while at the 3rd and 7th cycles the compositions were constant for about 10min before decreasing slighly. At the 5th, 10th and 11th cycles, the cyclohexane composition each passed through a maximum while at the 8th and 12th cycles, the composition decreased slightly as functions of time. During the 4th cycle, the cyclohexane composition increased slightly up to 8min and became constant with time afterwards.

The composition of hydrogenolysis products obtained on the Pt-Re/Al_2O_3 (UNDRIED) catalyst was high. The composition at zero time were 32% at cycles 7,8 and 9 while in cycle 12 it was 37.5%. This is much higher than the value obtained on Pt/Al_2O_3 catalyst where the highest composition obtained was 10.8% (at the 11th cycle). In all the cycles investigated, the profiles for the hydrogenolysis products decreased rapidly in the first 15min followed by a slow decrease with time afterwards except at the 1st cycle where the period of rapid deactivation was 5min (Figure 5.3.26) and the 5th cycle where the composition of the hydrogenolysis products passed through a maximum.

The benzene compostion (at zero time) in the first two cycles was 10% and rose to 27% in the 3rd and 4th cycles and dropped to 20% in the 5th, 6th, 7th and 8th cycles. These

composition further decreased to below 10% after the 8th cycle. It is important that the benzene composition obtained on Pt/Al_2O_3 catalyst in the first 12 cycles (between 20-30%) is generally higher than the benzene composition obtained on $Pt\text{-}Re/Al_2O_3$ (UNDRIED) catalyst. The conversion was not constant for the first 5min like iso octane on Pt/Al_2O_3 catalyst. This might be an evidence that the deactivating ability of MCP is higher than that of iso - octane. The benzene composition was over 20% up to the 29th cycle on Pt/Al_2O_3 catalyst while with $Pt\text{-}Re/Al_2O_3$ (UNDRIED), the benzene composition dropped to below 10% after the 8th cycle. The benzene composition passed through maxima in the 6th and 9th cycles while at the 1st cycle the profile showed an almost linear decrease with time. At the 5th, 10th, 11th and 12th cycles, the benzene compositions were constant in the first 5min, decreased more slowly after 15min. The profiles of benzene composition versus time at the 7th and 8th cycles were the same as those for the 5th, 10th, 11th and 12th cycles except that these profiles did not show any decline from zero time.

The coke content versus cycle number (Figure 5.3.31) shows that coke contents remained approximately constant for all the cycles investigated and the value is between 0.1gC and 0.117gC. The quantity of coke deposited on the $Pt\text{-}Re/Al_2O_3$ (UNDRIED) catalyst is much higher than that deposited on Pt/Al_2O_3 catalyst ($\sim$0.046gC) under the same conditions.

It is important to note that the deactivation profiles of MCP on $Pt\text{-}Re/Al_2O_3$ (UNDRIED) are similar to those obtained with MCP and iso-octane on Pt/Al_2O_3 catalyst except that with

the MCP on Pt-Re/Al_2O_3 (UNDRIED) catalyst the conversion was not constant for the first 15min.

III Pt-Re/Al_2O_3 (DRIED)

A. Total Conversion

The variation of MCP conversion as functions of time for 12 deactivation - regeneration cycles on Pt-Re/Al_2O_3(DRIED) is shown in Figure 5.3.32. The conversion - time profiles show that the conversion at zero time varies between 0.26 and 0.63. The lowest conversion was obtained at the 12th and 8th cycles when the conversion at zero time were 0.26 and 0.32, respectively. The conversion is about the same as with undried Pt-Re/Al_2O_3 catalyst. However, the Pt-Re/Al_2O_3 (DRIED) catalyst has been regenerated 15times before being used for the mortality study while the Pt-Re/Al_2O_3 (UNDRIED) catalyst was regenerated 2times before it was used for the mortality study. It is not impossible that the conversions of MCP on Pt-Re/Al_2O_3(DRIED) catalyst in earlier regenerated states might have been higher than the conversions on undried Pt-Re/Al_2O_3 regnerated only two times. The conversion - time profiles in Figure 5.3.32 show that conversion was almost constant in the first 5min followed by a rapid decline between 5 and 15min. The conversion then declined slowly as a function of time after 15min.

B. Product Distribution

Figures 5.3.33 - 5.3.37 shows the variation of product composition on Pt-Re/Al_2O_3(DRIED) catalyst as functions of time for some of the 12 deactivation cycles. The cyclohexane composition was low in all the cycles investigated and its highest value,obtained at the 3rd cycle, was 5.5%. The cyclohexane composition passed through maxima at the 1st, 2nd, 8th, 9th and the 10th cycles while the profiles showed almost linear decrease with time at the 4th,5th and 7th cycles. At the 3rd cycle, the cyclohexane composition was constant up to 5min, decreased rapidly between 5 and 15min and then decreased slowly afterwards while at the 6th cycle the cyclohexane composition decreased for the first 15min and became constant afterwards.

The composition of the hydrogenolysis products at zero time was about 22% at cycles 2,4,9 and 11. At the other cycles, the compositions at zero time were between 10 to 16%. These are higher than the value obtained on Pt/Al_2O_3 catalyst where the highest composition obtained was 10.8% (at the 11th cycle), but lower than the hydrogenolysis products composition obtained on Pt-Re/Al_2O_3 (UNDRIED) catalyst where the composition of the hydrogenolysis products were above 30% at cycles 7, 8, 9 and 12. The hydrogenolysis products composition passed through maxima at cycles 3,7 and 10. At the 1st, 6th 11th and 12th cycles, the hydrogenolysis product's composition was constant for the first 5min, followed by a fast decrease with time between 5 and 15min and then constant after 15min. At the other cycles investigated, the hydrogenolysis products composition decreased rapidly in the first 15min followed by

a slow decrease in composition with time except at the 5th and 6th cycles where the composition declined slowly in the first 5min. The benzene composition was about 30% at zero time in most cycles except 1st, 6th, 8th, 9th, 11th and 12th cycles where the compositions were 40, 26, 20, 25, 18 and 15%, respectively. The benzene composition did not change much with regeneration in contrast to the composition obtained when Pt-Re/Al_2O_3(UNDRIED) catalyst was used. With the Pt-Re/Al_2O_3(UNDRIED) catalyst benzene composition decreased to below 10% after the 8th cycle. The benzene composition on Pt-Re/Al_2O_3 (DRIED) catalyst was also higher than the composition on Pt/Al_2O_3 catalyst.

The benzene profiles showed that at cycles 1,3, 4, 5, 6, 7, 11, and 12, the benzene composition remained relatively unchanged in the first 5min. After the 5th min, the benzene composition decreased rapidly between 5 and 15min followed by a slow decrease. At the 2nd, 8th and 10th cycles, the benzene composition decreased almost linearly with time. It is important to note that the benzene composition was constant for 5min in most of the cycles on Pt-Re/Al_2O_3(DRIED) catalyst while it is not so when Pt-Re/Al_2O_3(UNDRIED) catalyst is used. This also implies that Pt-Re/Al_2O_3(UNDRIED) catalyst deactivates faster than the dried Pt-Re/Al_2O_3(DRIED) catalyst.

Figure 5.3.38 shows the plot of coke content against cycle number. The coke content obtained were between 0.083 and 0.098gC. The coke content is about twice as high as that obtained on Pt/Al_2O_3 and lower than the quantity obtained on Pt-Re/Al_2O_3(UNDRIED) catalyst.

Similar to the profile obtained with iso octane and MCP on Pt/Al_2O_3 catalyst the conversion of MCP on $Pt-Re/Al_2O_3$ (DRIED) was constant for 5min followed by a region of fast deactivation between 5 and 15min and then a region of slow deactivation. The drop in conversion in the slow deactivation region is very small compared to the drop in conversion during the fast deactivation region. That the conversion of MCP on $Pt-Re/Al_2O_3$(DRIED) was constant for 5min and not for the Undried catalyst suggests that the $Pt-Re/Al_2O_3$(UNDRIED) deactivates faster than the dried catalyst. The dried catalyst was able to withstand the deactivating environment for 5min.

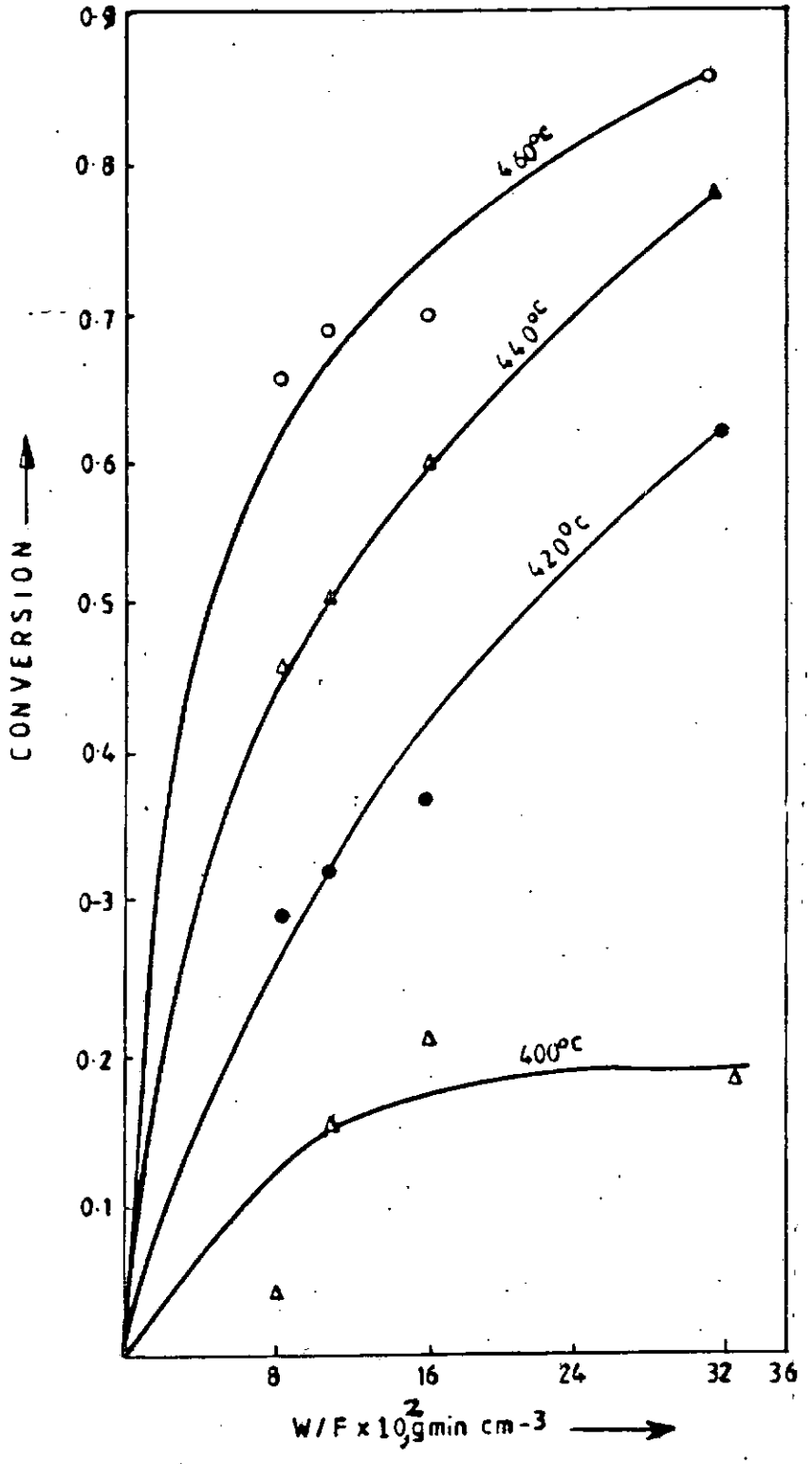

Fig. 5.1.1: N-octane conversion on Pt/Al_2O_3 versus W/F at $P_N = 5.7 \times 10^{-3}$ atm in H_2 and various temperatures.

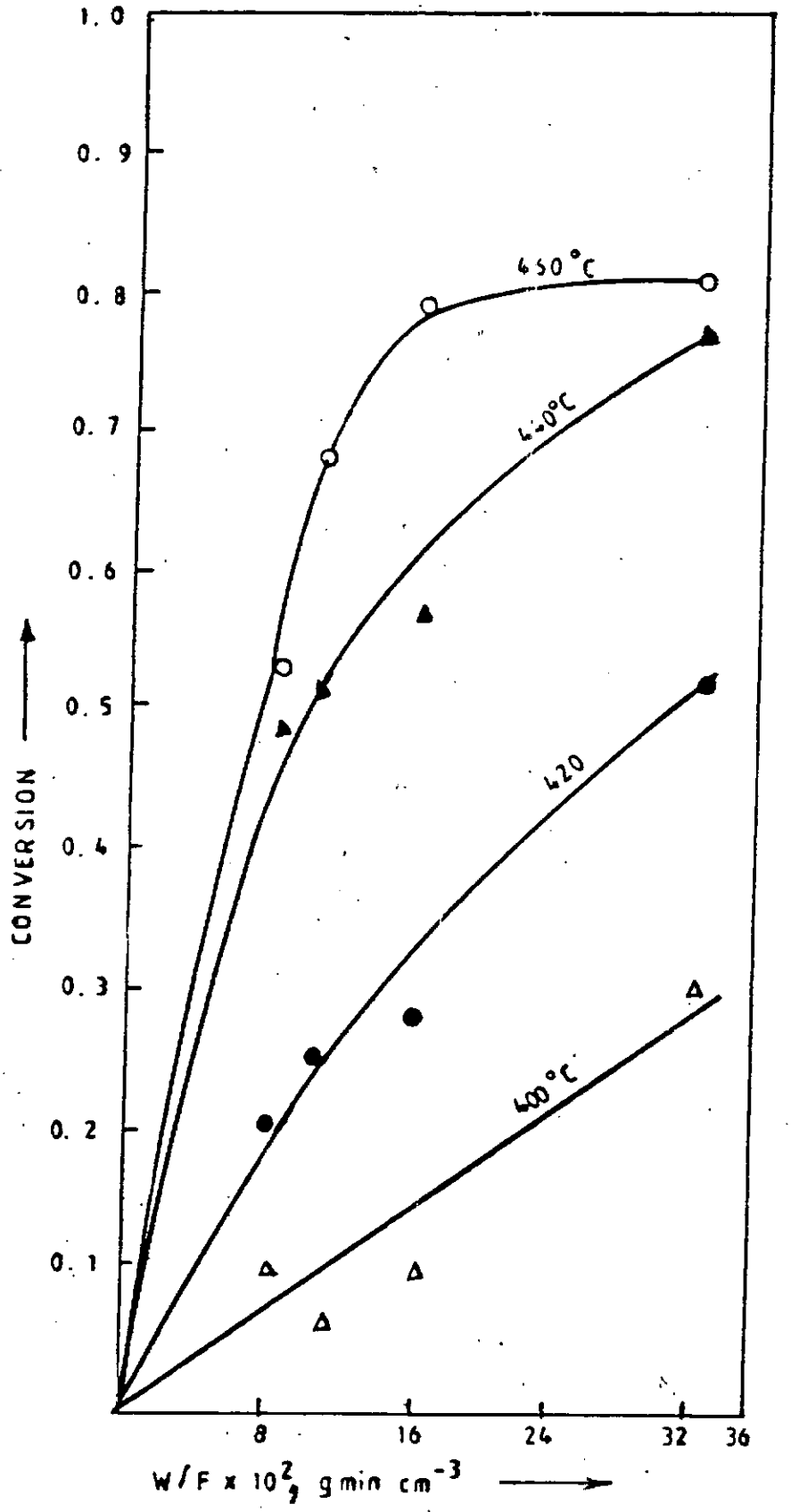

Fig. 5.1.2: N-octane conversion on Pt/Al_2O_3 versus W/F at $P_N = 7.63 \times 10^{-3}$ atm in H_2 and various temperatures.

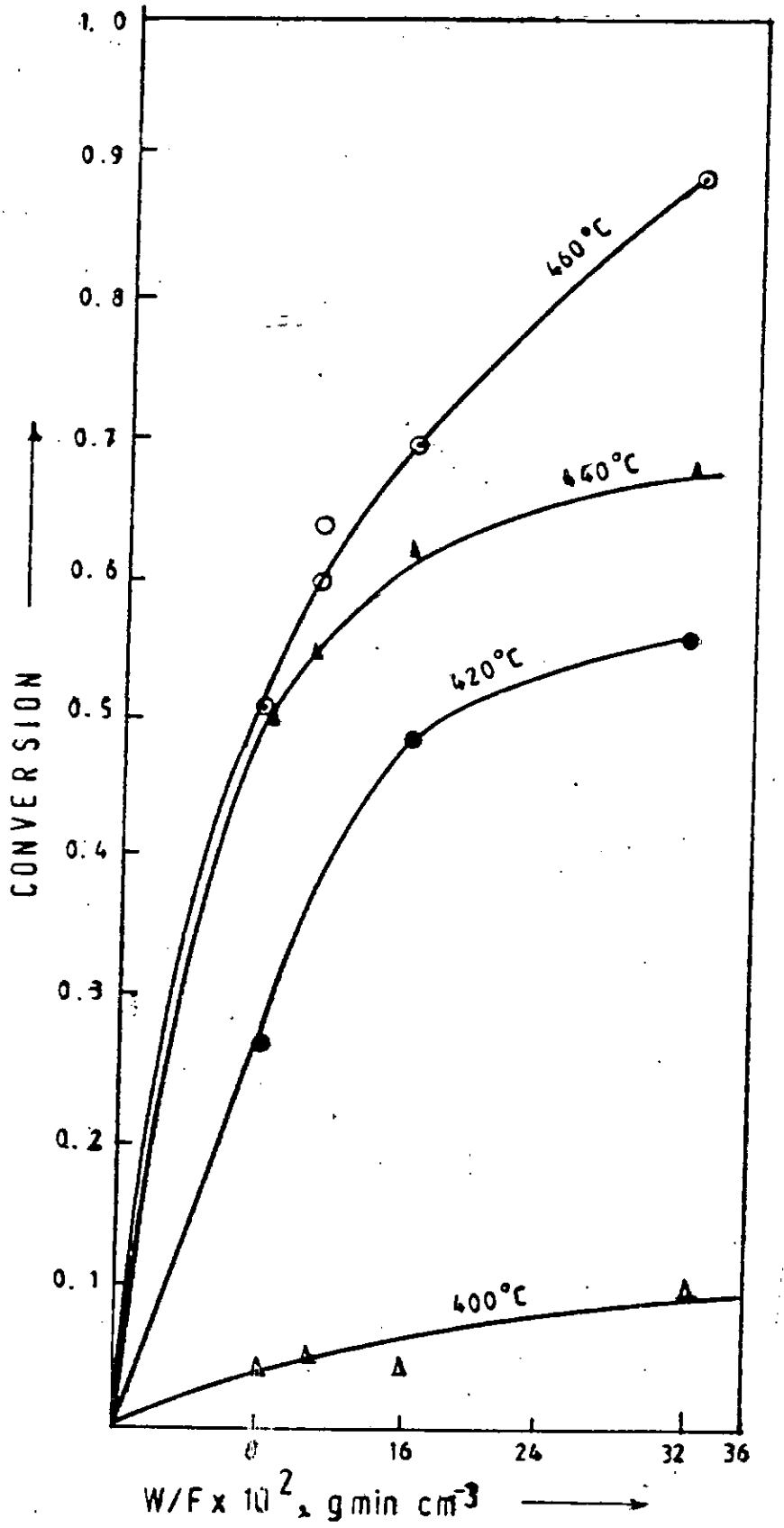

Fig. 5.1.3: N-octane conversion on Pt/Al_2O_3 versus W/F at $P_N = 13.7 \times 10^{-3}$ atm in H_2 and various temperatures.

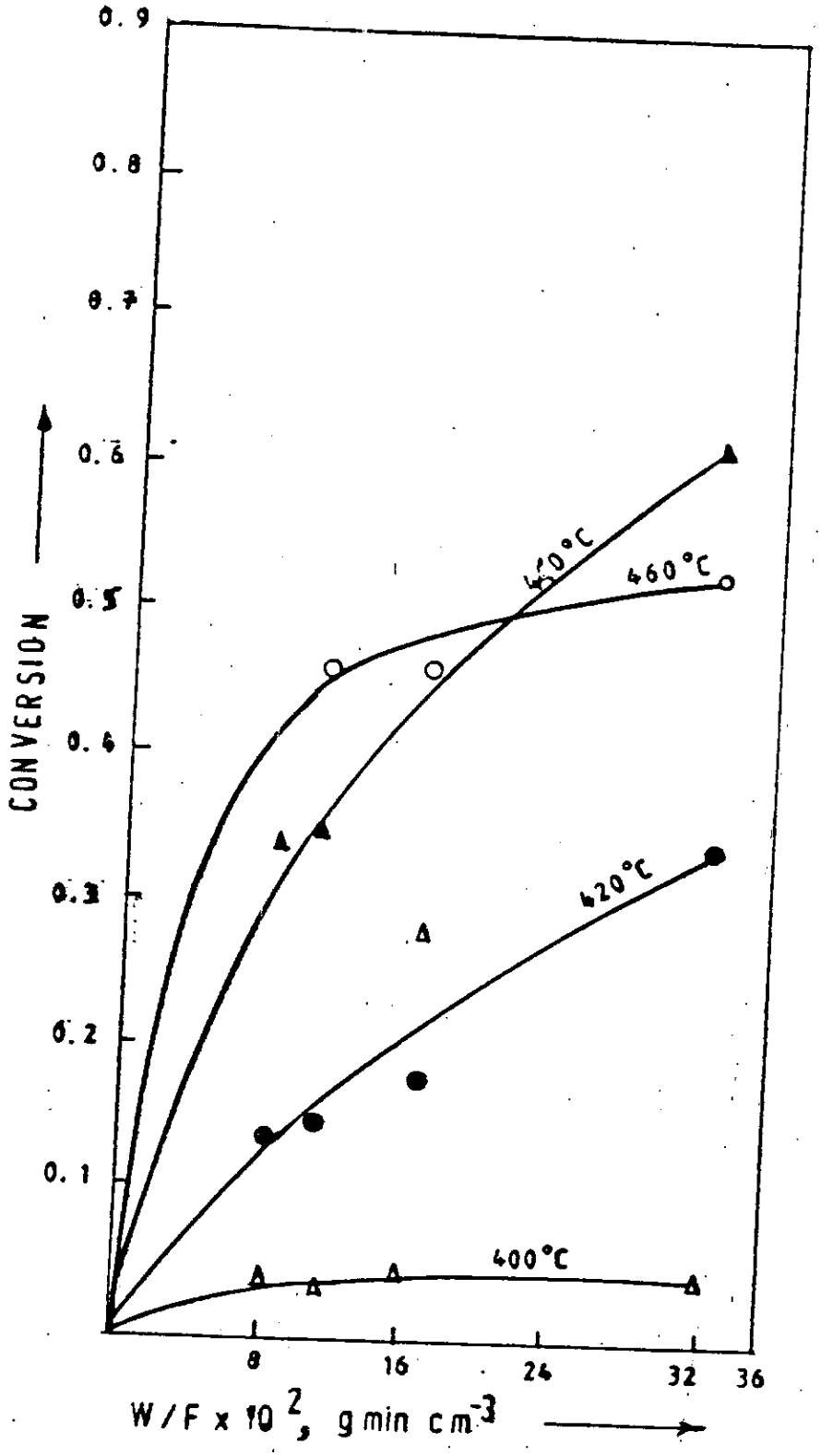

Fig. 5.1.4: N-octane conversion on Pt/Al_2O_3 versus W/F at P_N=25x10^{-3}atm in H_2 and various temperatures.

Products of N-Octane conversion on Pt/Al_2O_3 versus W/F.

Figures 5.1.5 - 5.1.21

LEGEND

1. Iso Octane
2. Hydrocracked Products
3. Ethylbenzene
4. O-xylene
5. P-xylene
6. M-xylene
7. Toluene

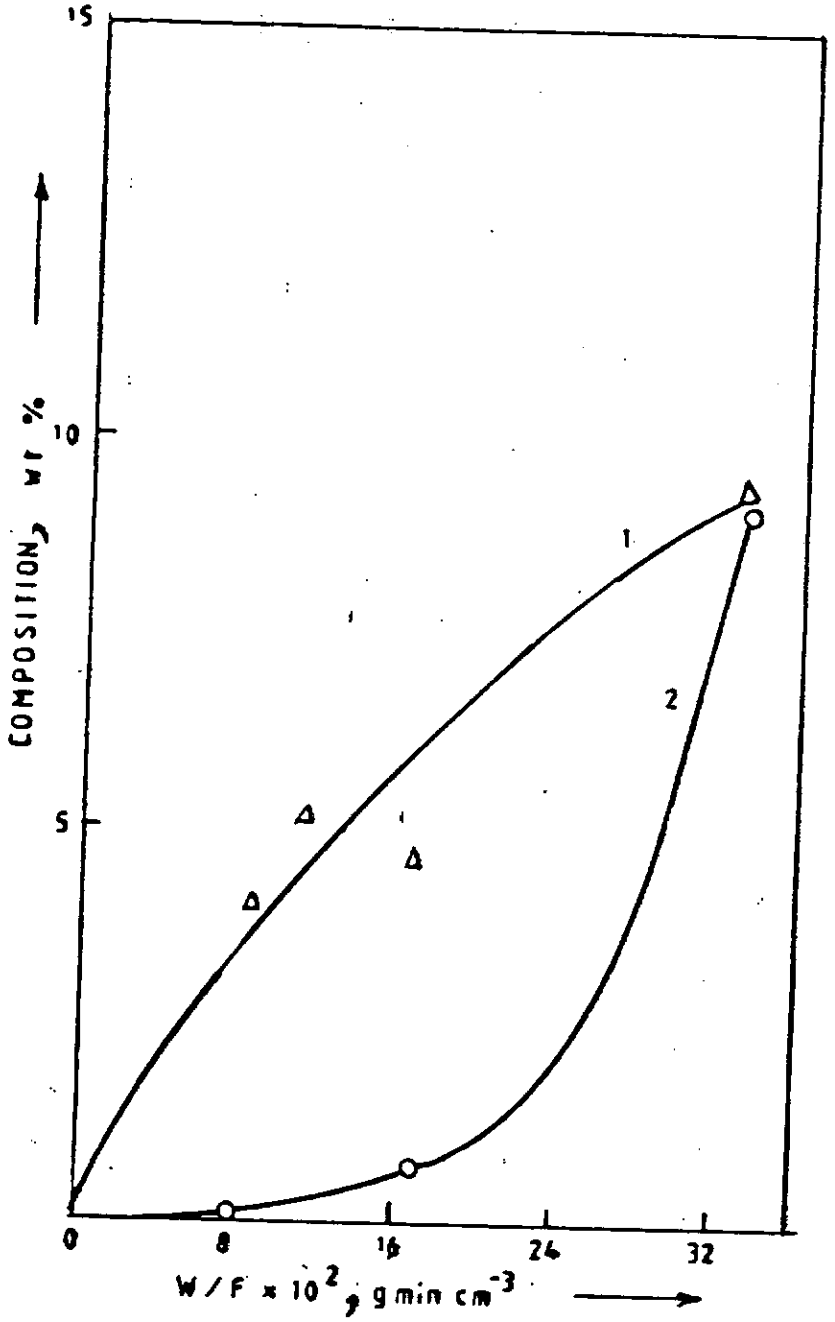

Fig. 5.1.5: Product composition of n-octane conversion on Pt/Al_2O_3 versus W/F at $P_N=13.7\times10^{-3}$atm in H_2 at 400°C .

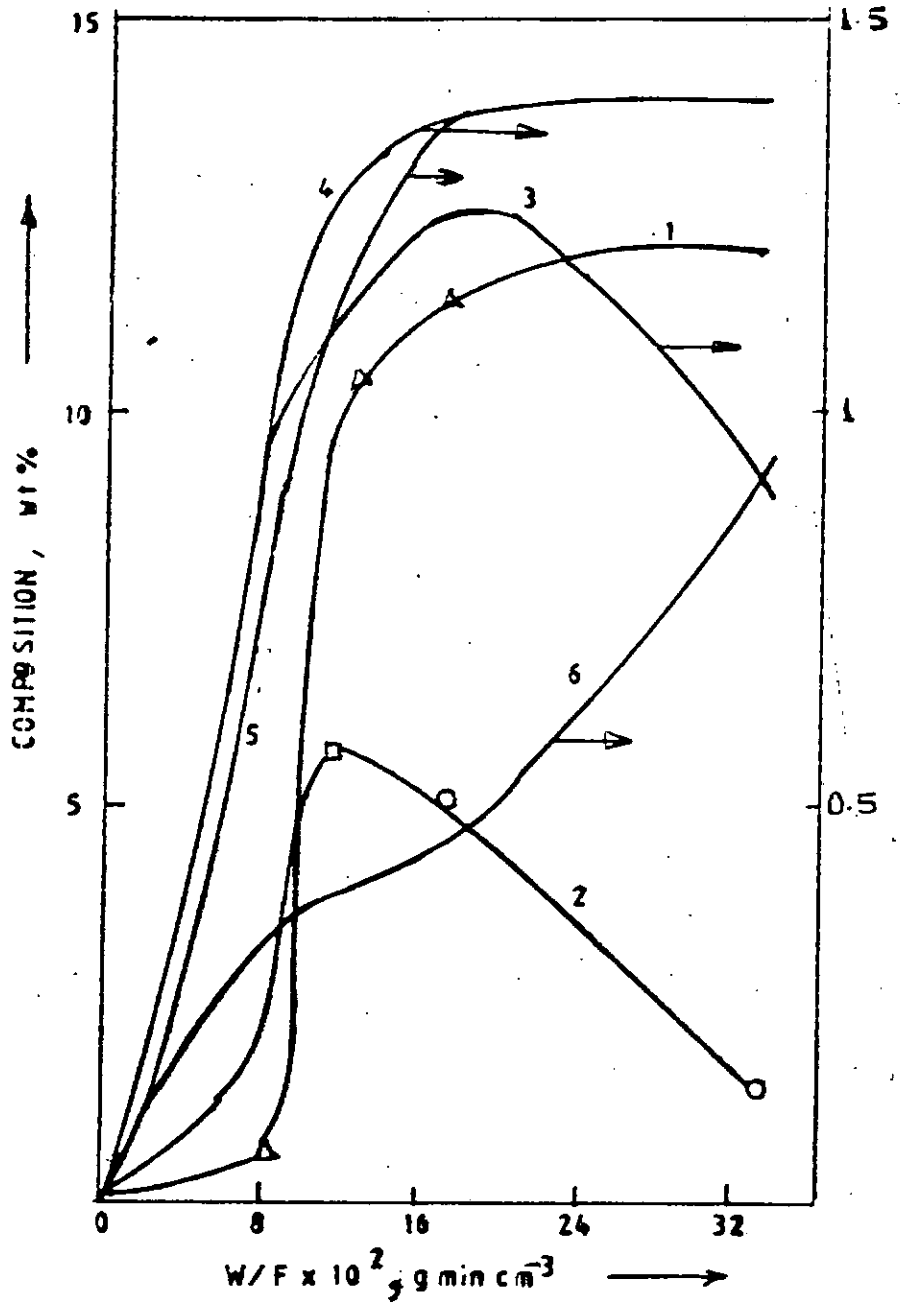

Fig.5.1.6: Product composition of n-octane conversion on Pt/Al_2O_3 versus W/F at $P_N = 5.7 \times 10^{-3}$ atm in H_2 at 400°C

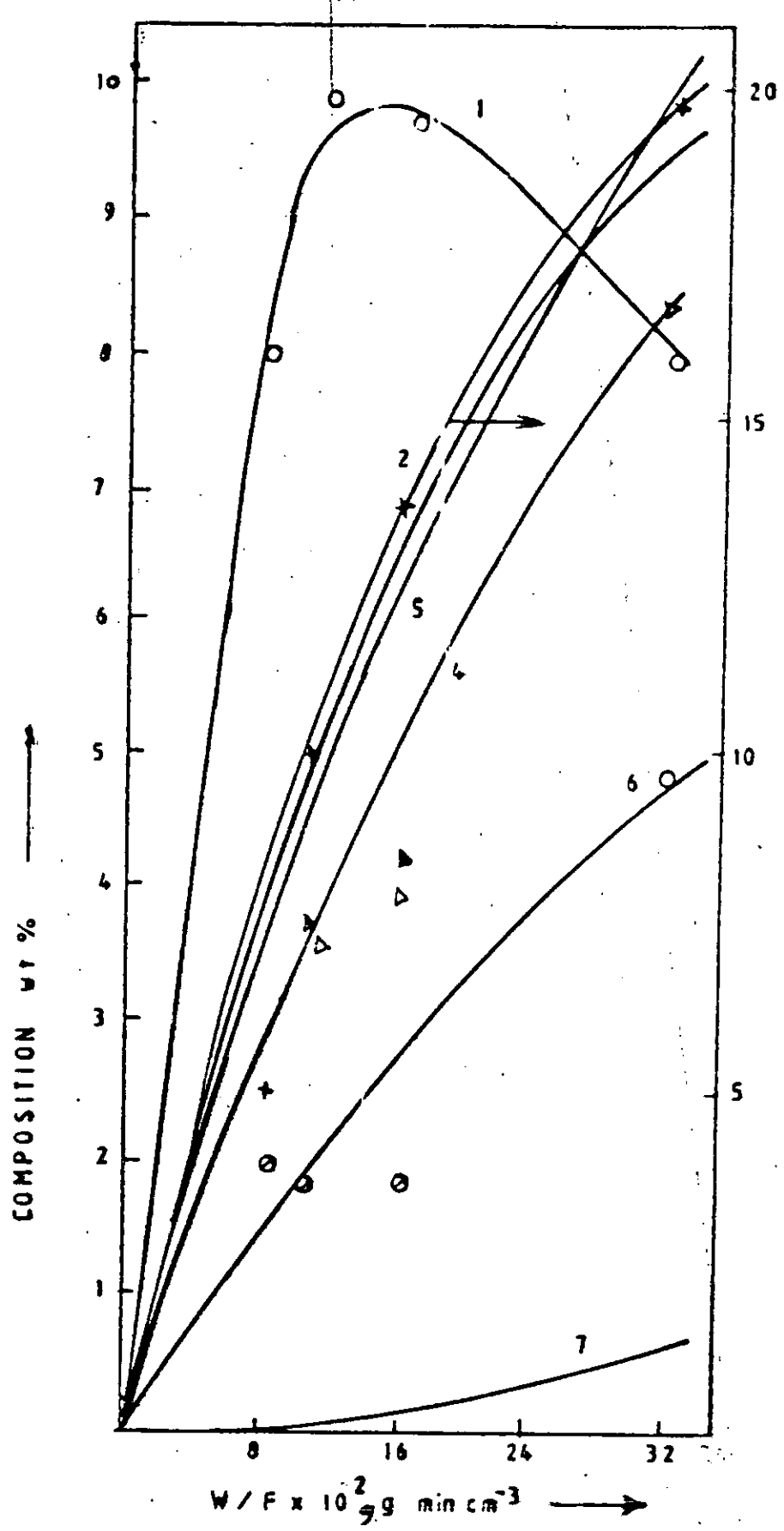

Fig.5.1.7: Product composition of n-octane conversion on Pt/Al_2O_3 versus W/F at $P_N=5.7\times10^{-3}$ atm in H_2 at 420°C

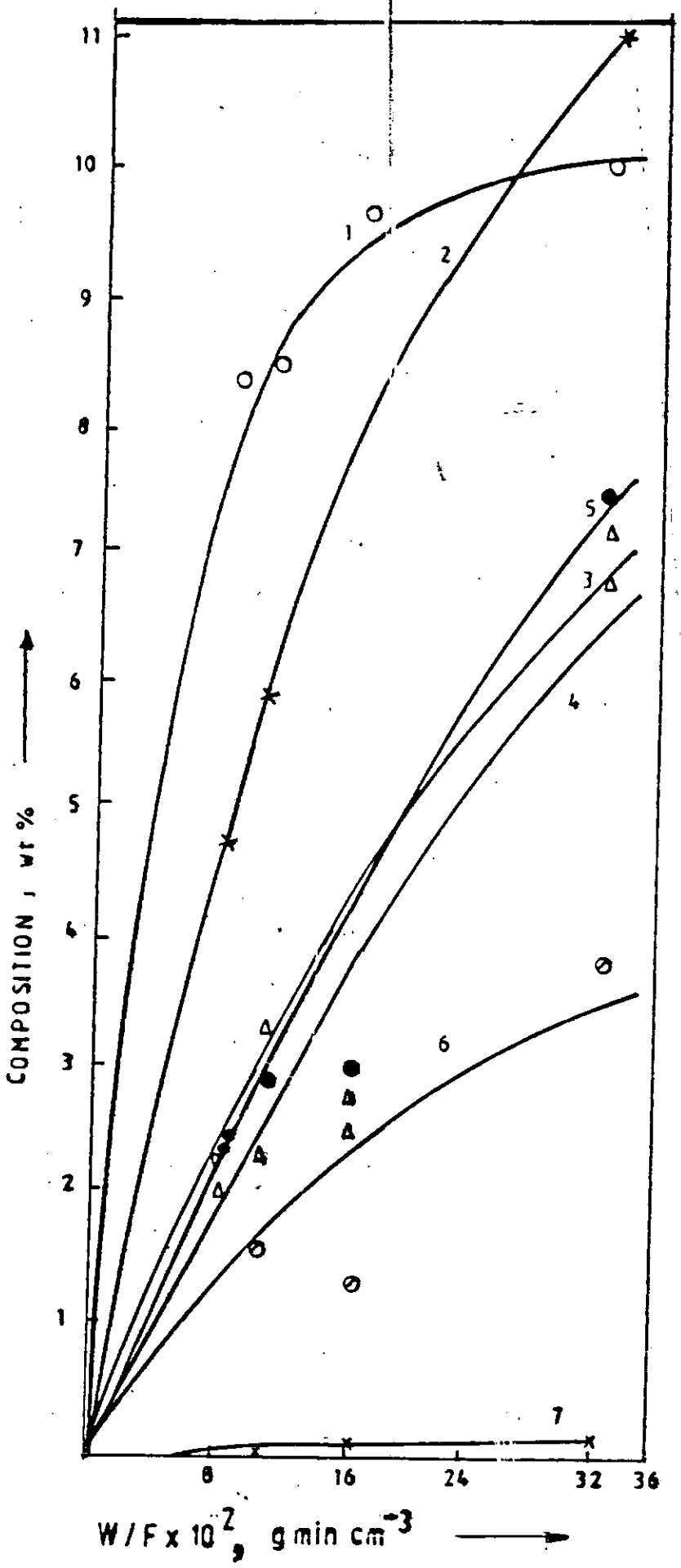

Fig. 5.1.8: Product composition of n-octane conversion on Pt/Al_2O_3 versus W/F at $P_N=7.63\times10^{-3}$ atm in H_2 at 420°C

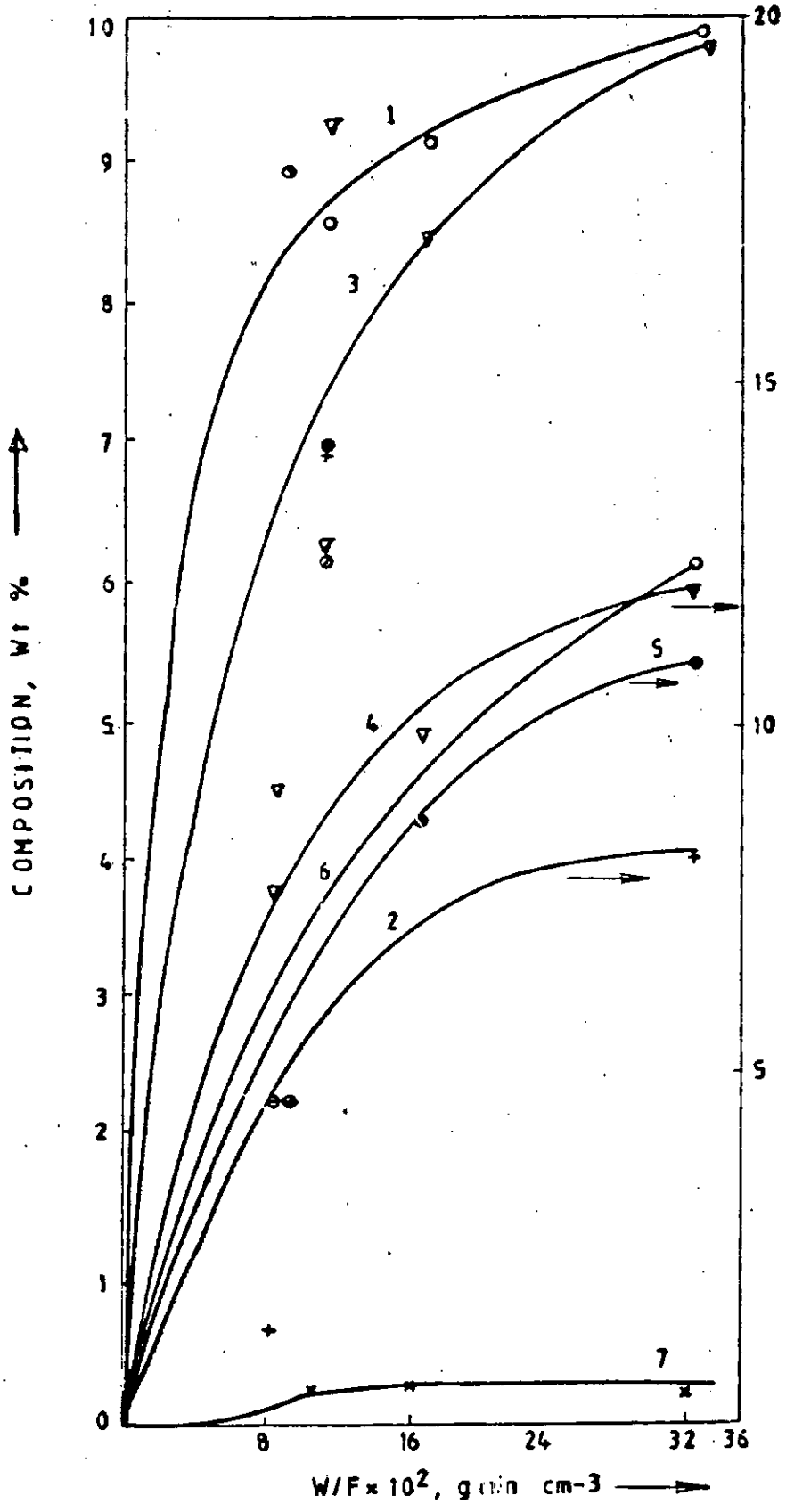

Fig. 5.1.9: Product composition of n-octane conversion on Pt/Al_2O_3 versus W/F at $P_N=13.7\times10^{-3}$ atm in H_2 at 420°C

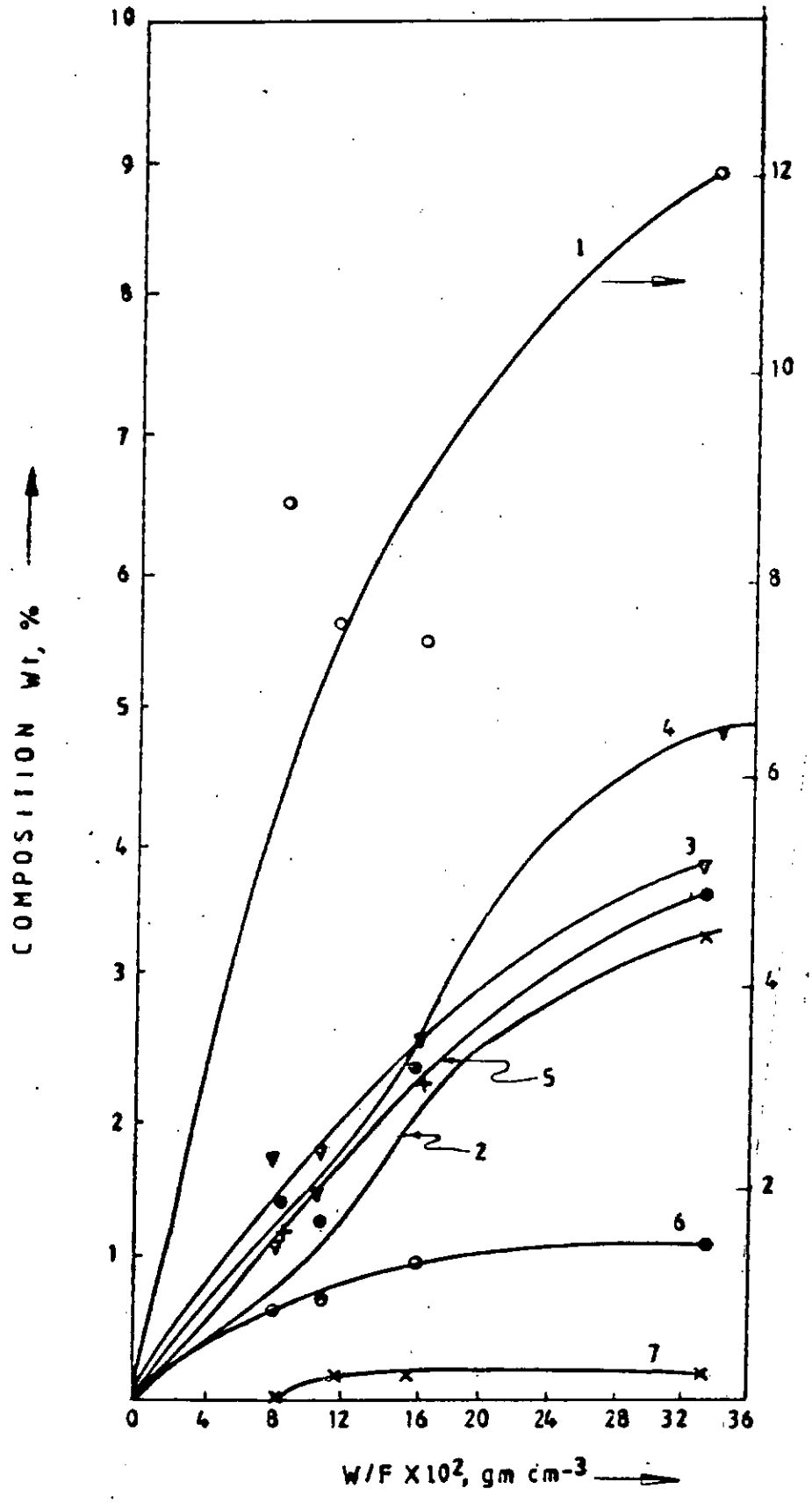

Fig.5.1.10: Product composition of n-octane conversion on Pt/Al_2O_3 versus W/F at $P_N=25.0\times10^{-3}$ atm in H_2 at 420°C

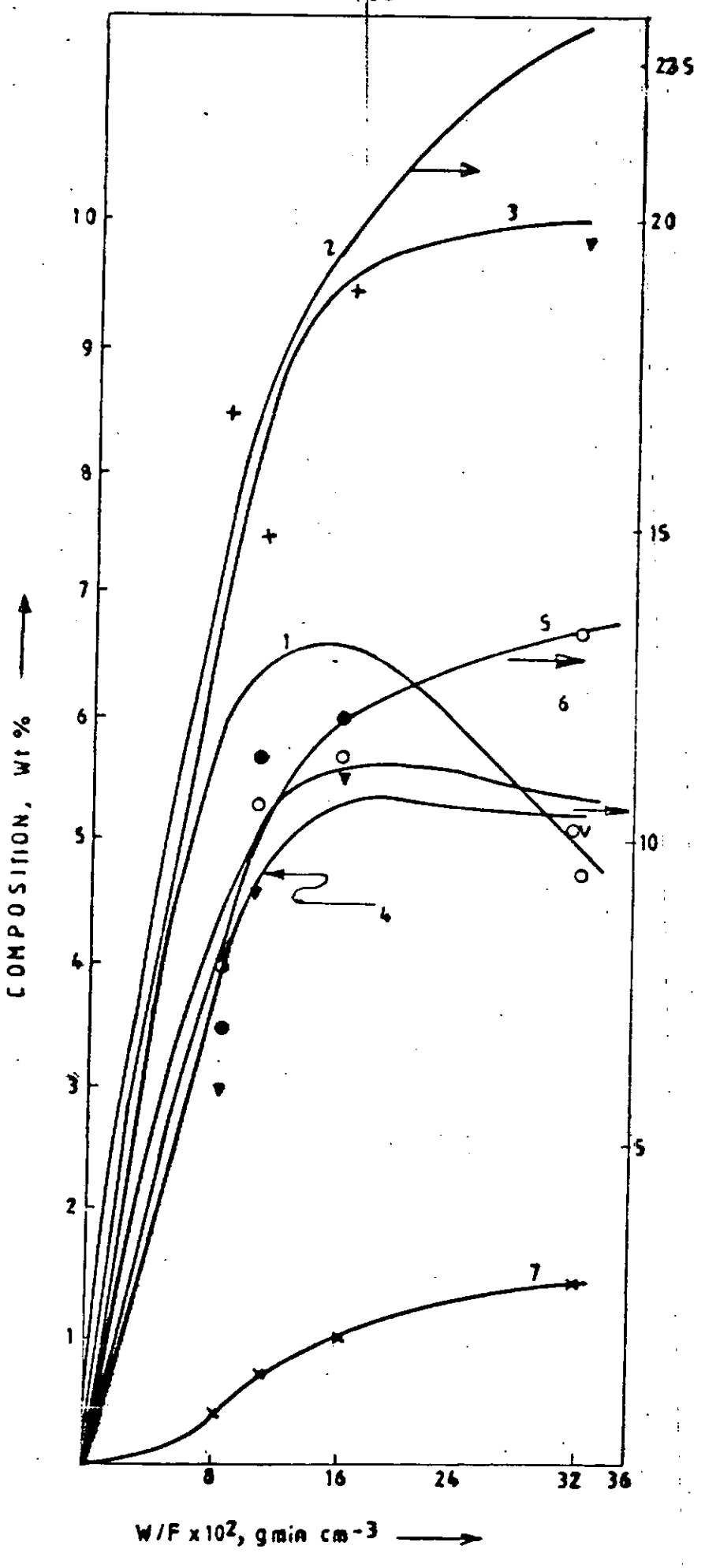

Fig. 5.1.11: Product composition of n-octane conversion on Pt/Al_2O_3 versus W/F at $P_N=25.0\times10^{-3}$ atm in H_2 at 420°C

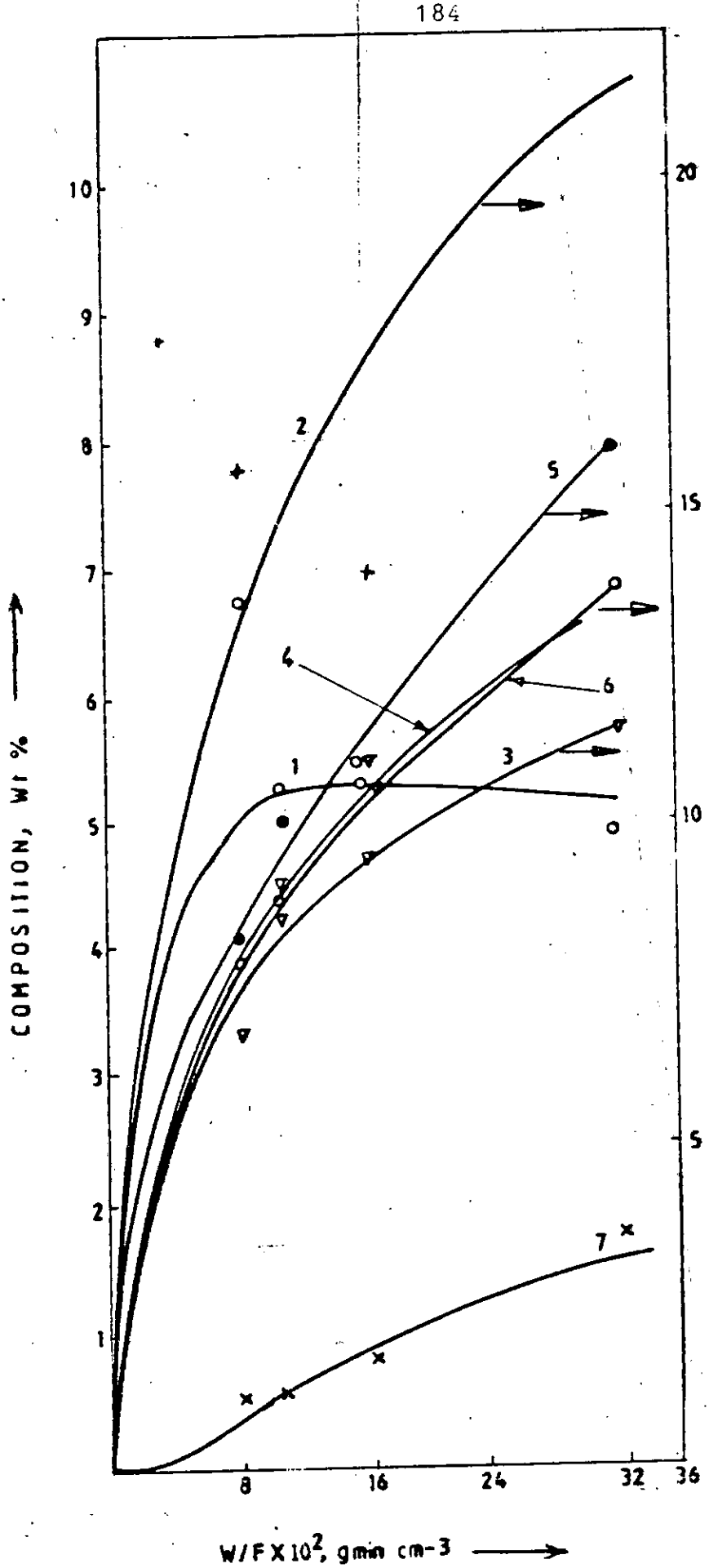

Fig.5.1.12: Product composition of n-octane conversion on Pt/Al_2O_3 versus W/F at $P_N=7.63\times10^{-3}$ atm in H_2 at 440°C

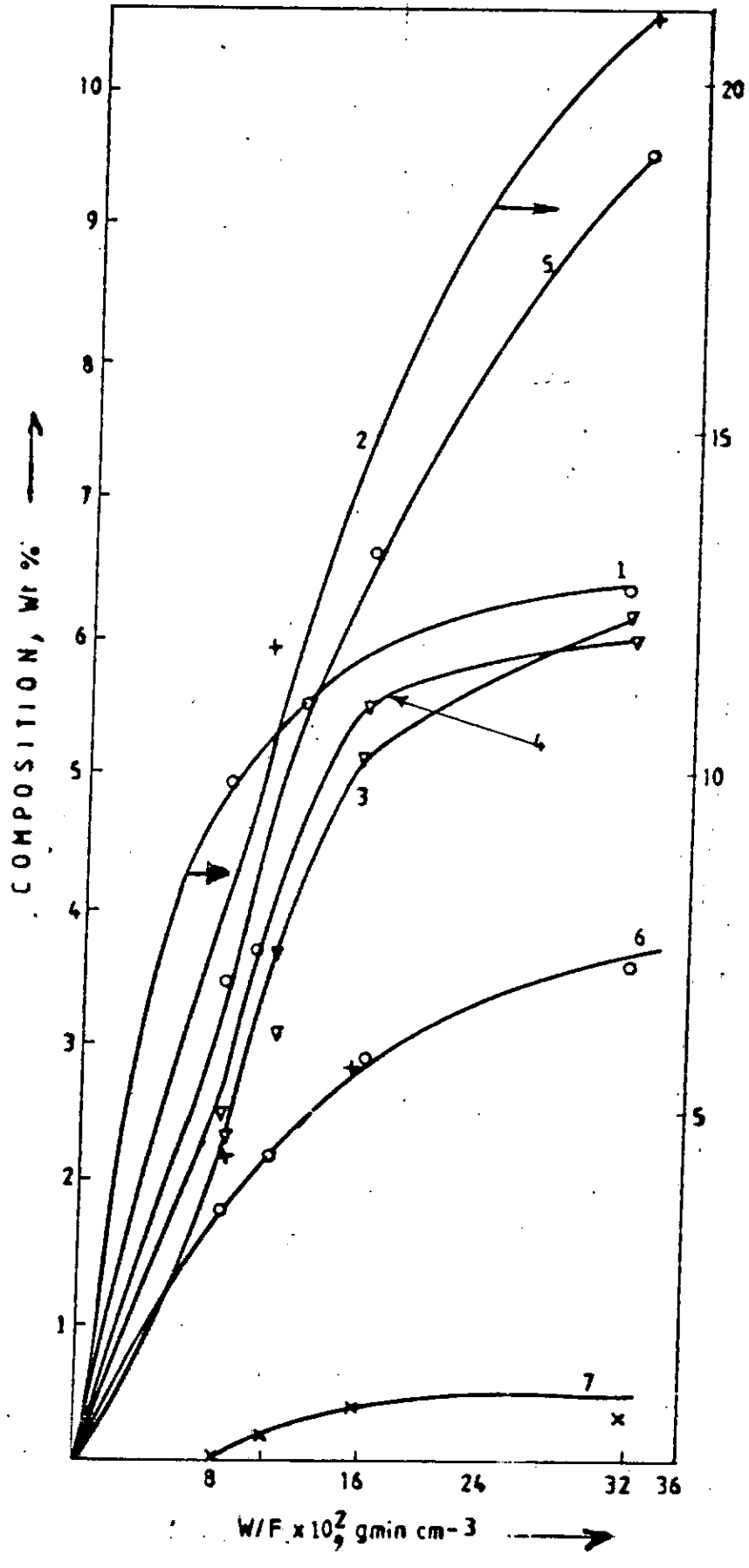

Fig.5.1.13: Product composition of n-octane conversion on Pt/Al_2O_3 versus W/F at $P_N = 25 \times 10^{-3}$ atm in H_2 at 440°C

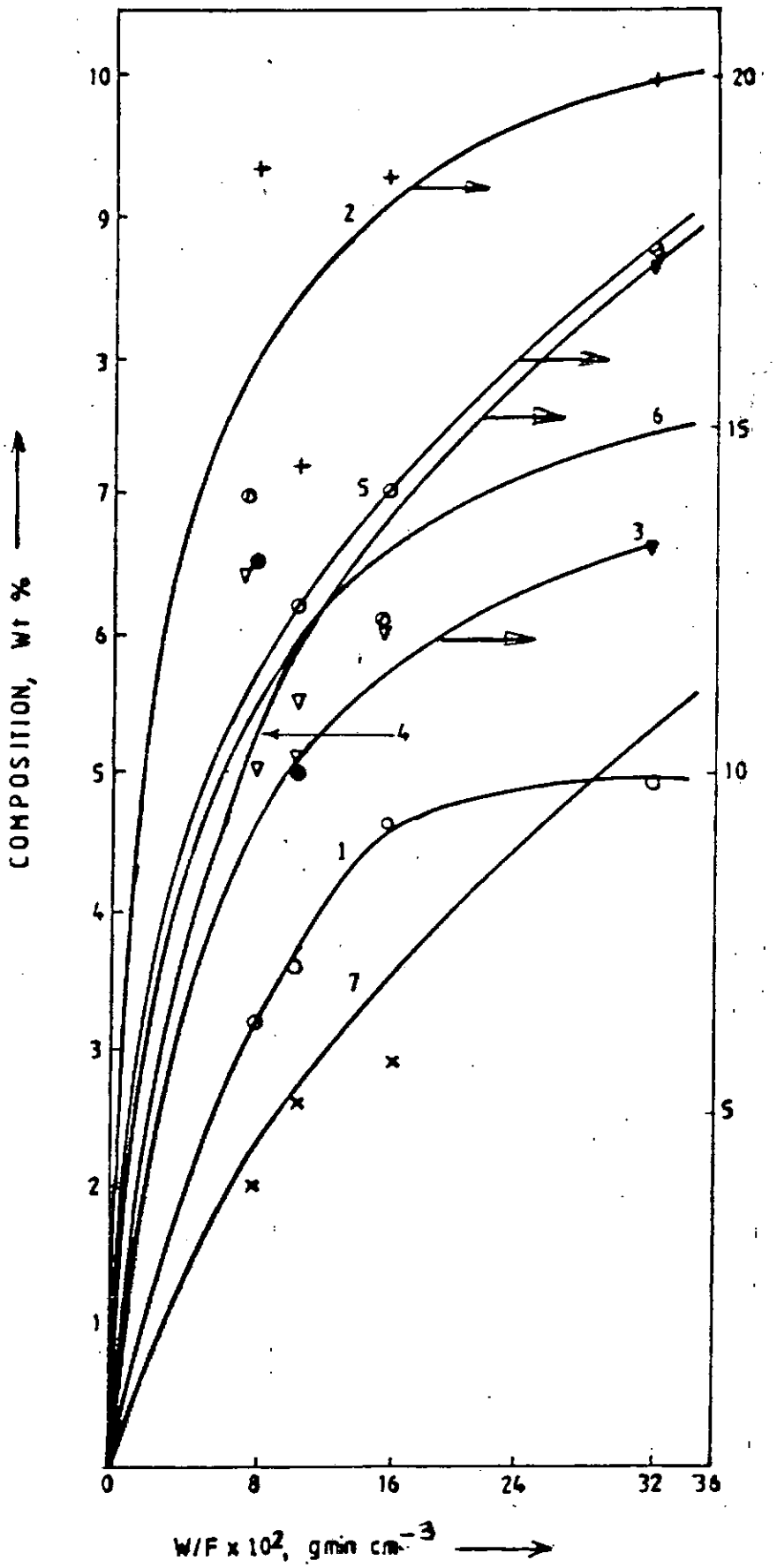

Fig. 5.1.14: Product composition of n-octane conversion on Pt/Al_2O_3 versus W/F at $P_N=5.7\times10^{-3}$ atm in H_2 at 460°C

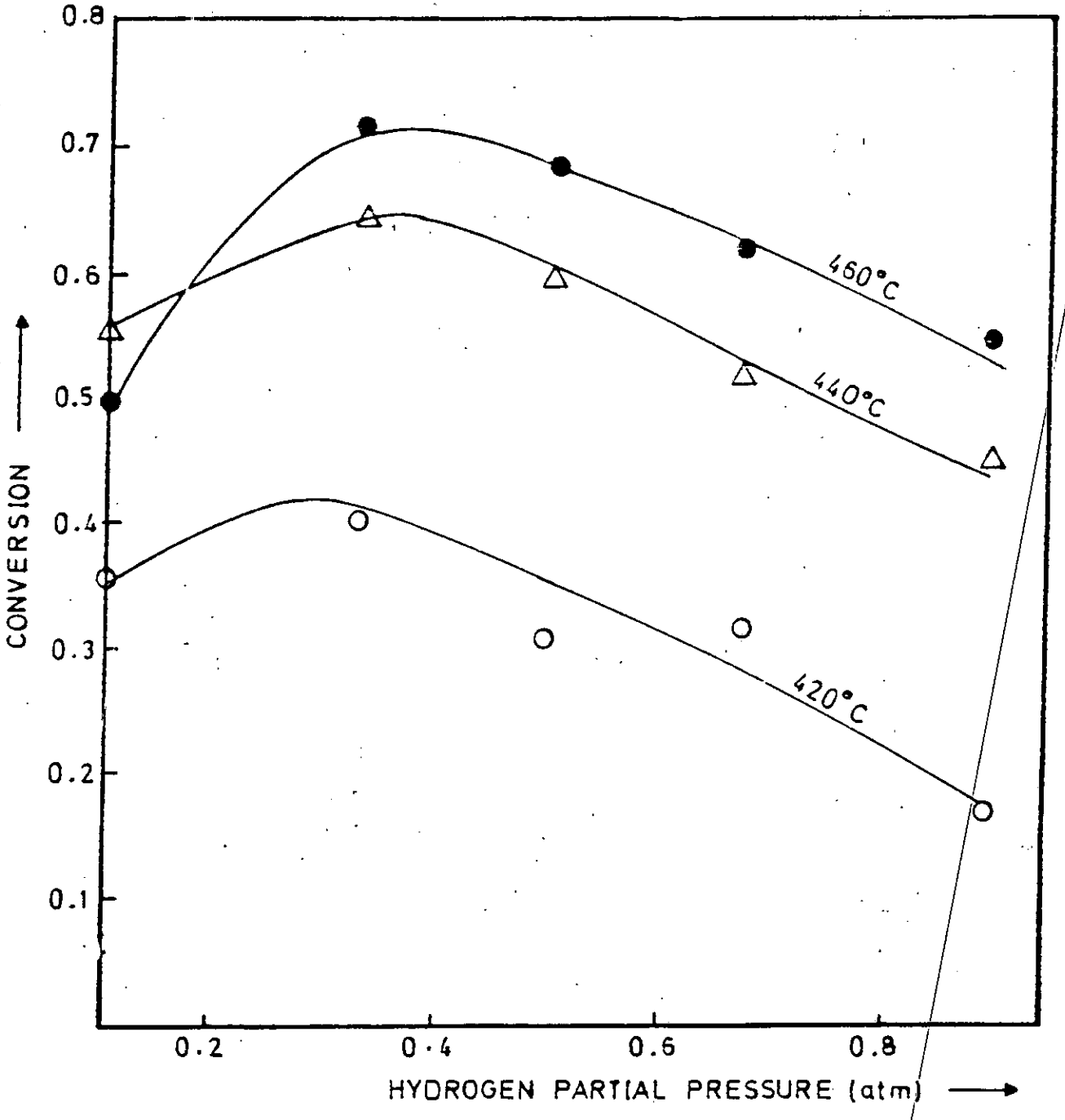

Fig.5.1.15: N-octane conversion on Pt/Al_2O_3 versus P_{H_2} at 420°C, 440° and 460°C at $P_N = 7.63 \times 10^{-3}$ atm
W/F = 0.11gmincm^{-3}

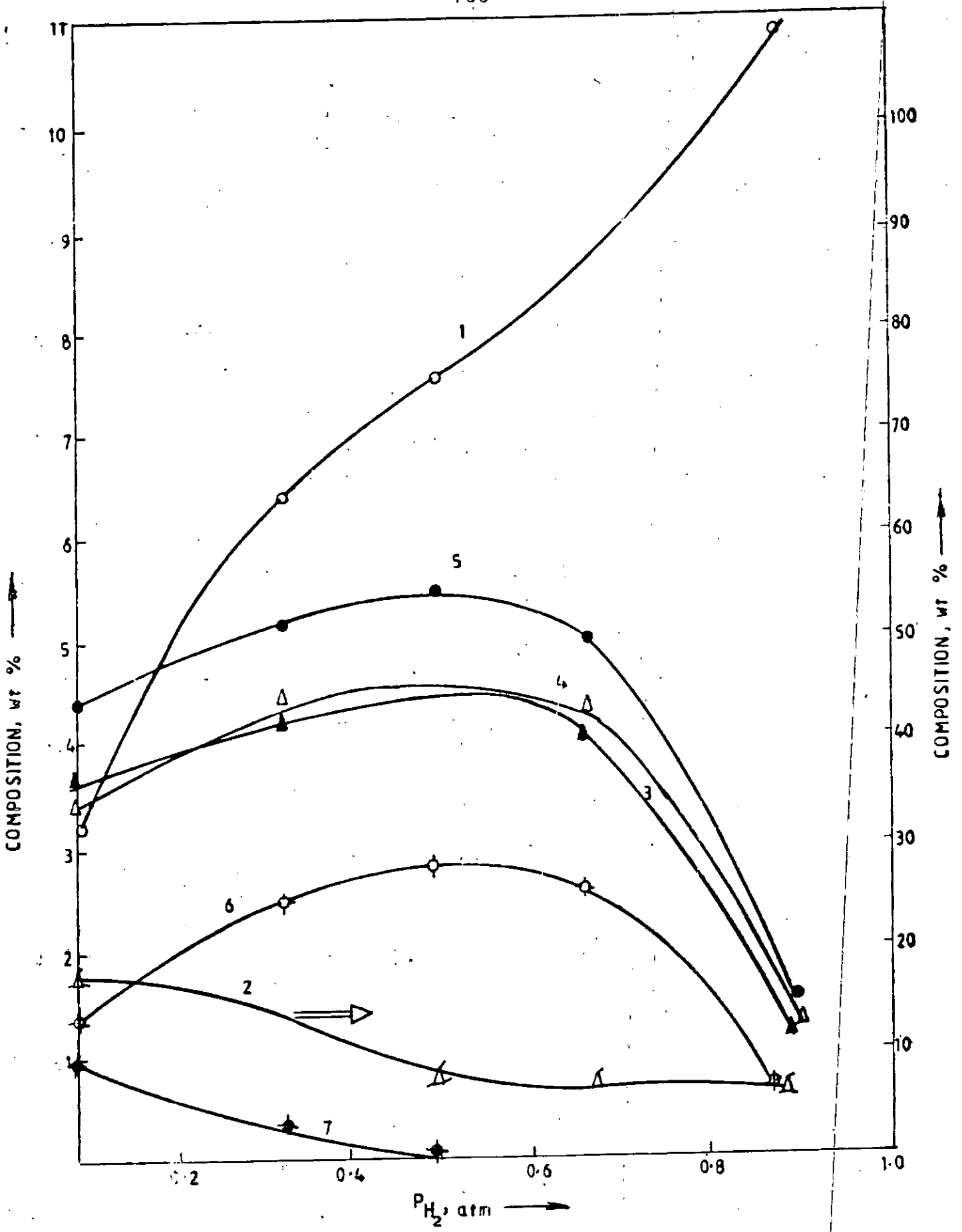

Fig.5.1.16: Product composition of n-octane conversion on Pt/Al_2O_3 versus P_{H_2} at 420°C, $P_N = 7.63 \times 10^{-3}$ atm
$W/F = 0.11 gmin cm^{-3}$

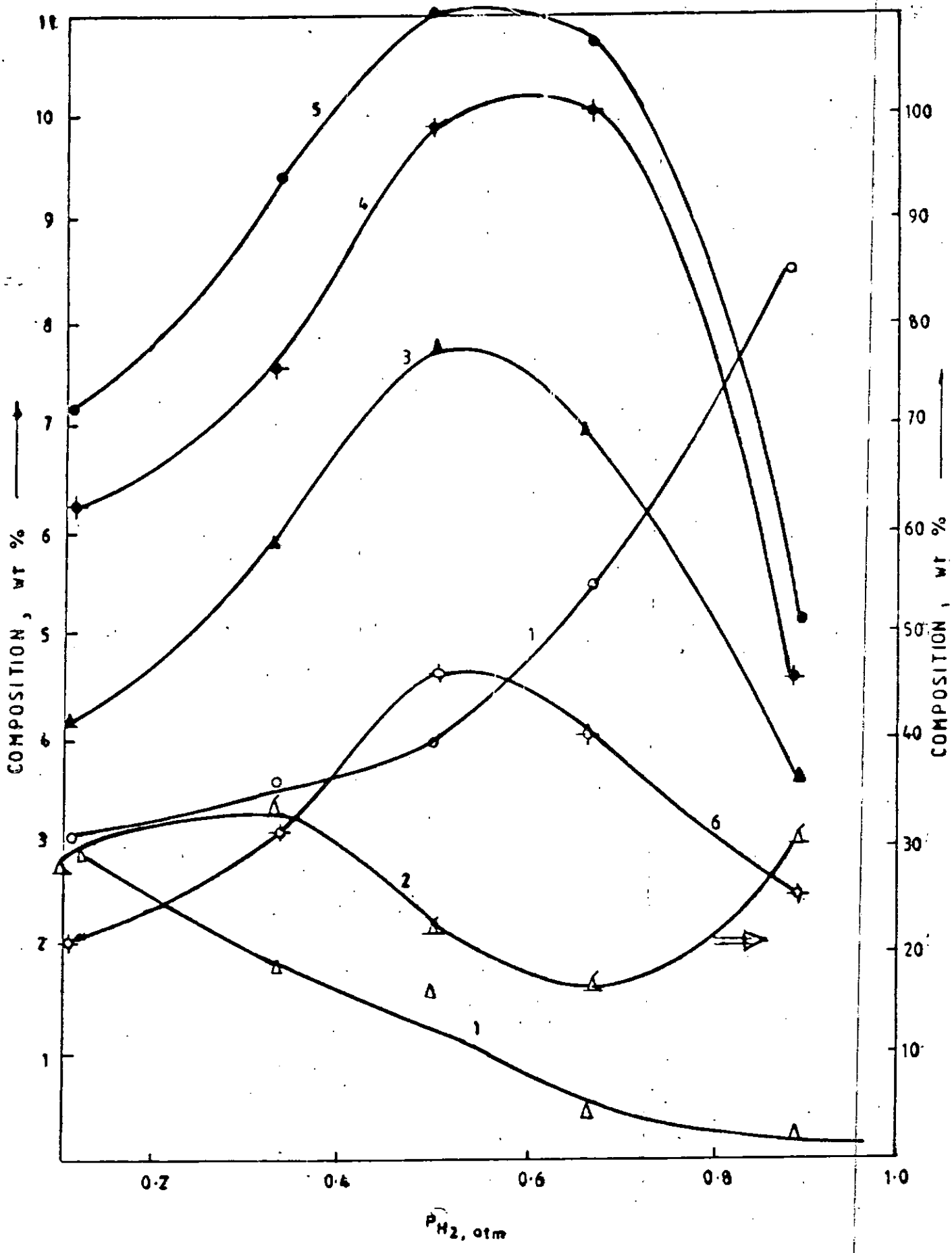

Fig.5.1.17: Product composition of n-octane conversion on Pt/Al_2O_3 versus P_{H_2} at 440°C, $P_N = 7.63 \times 10^{-3}$ atm, $W/F = 0.11 \text{ gmin cm}^{-3}$

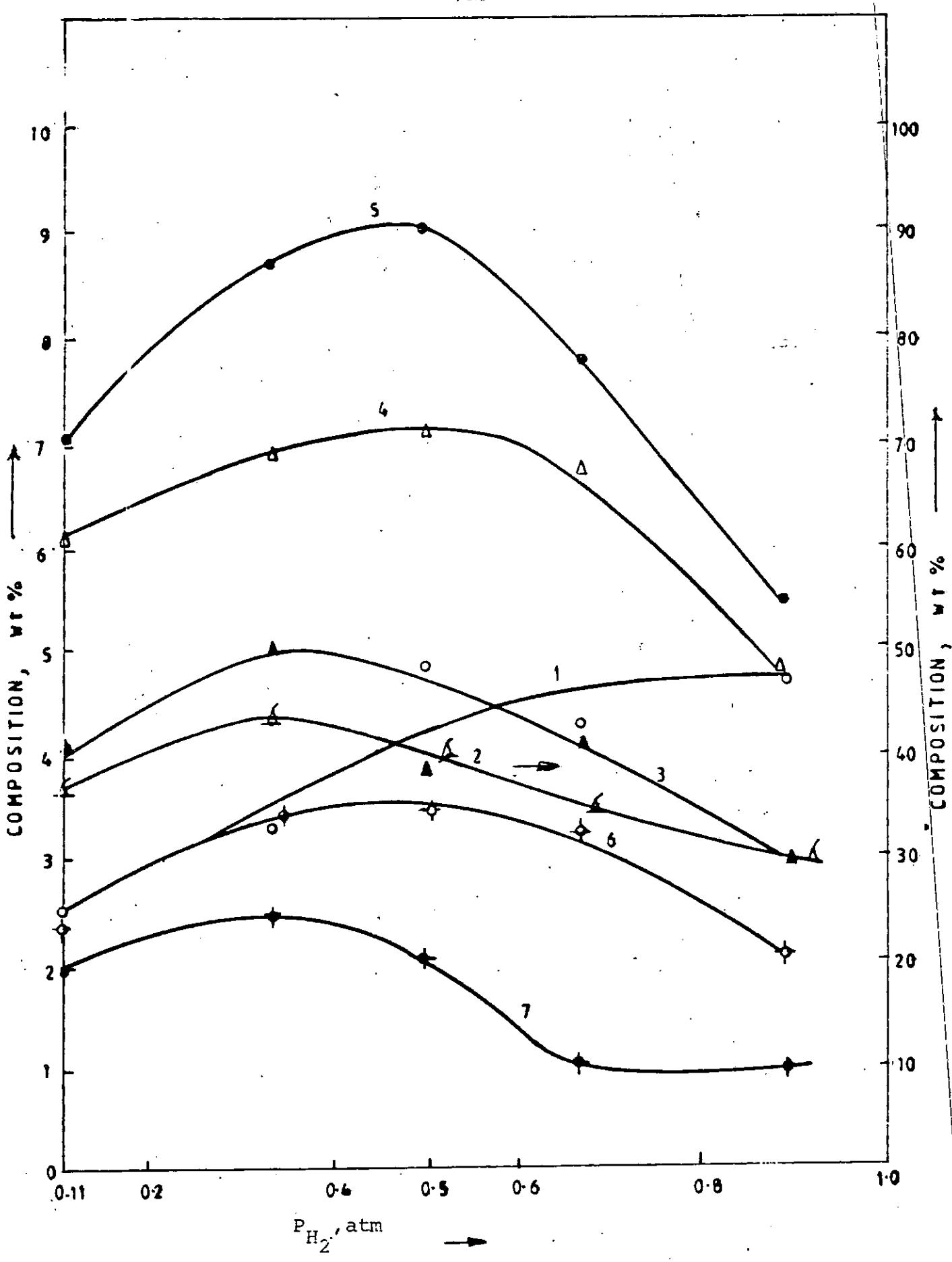

Fig.5.1.18: Product composition of n-octane conversion on Pt/Al_2O_3 versus P_{H_2} at 460°C, $P_N = 7.63 \times 10^{-3}$ atm W/F = 0.11gmincm^{-3}

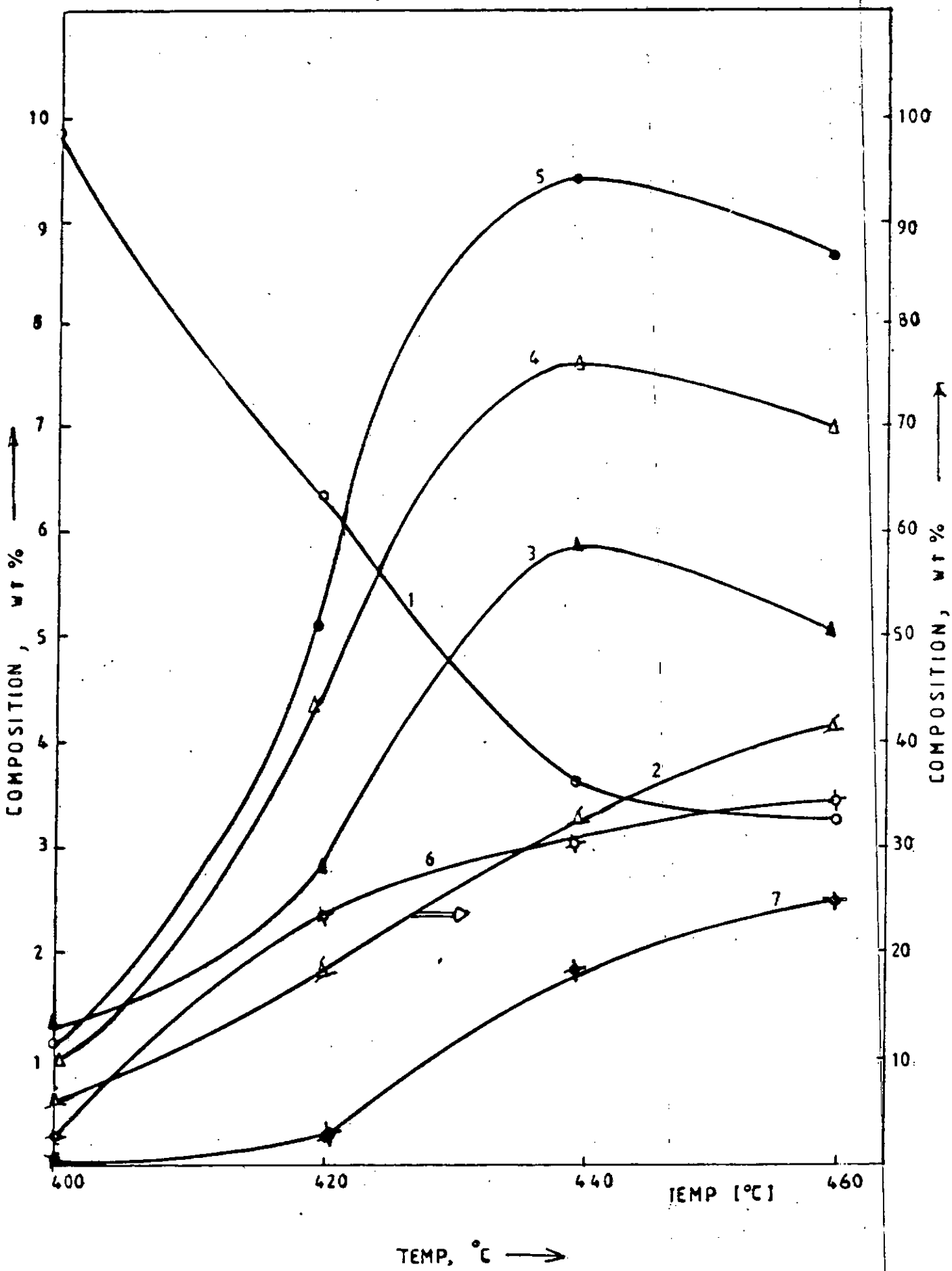

Fig.5.1.19: Product composition of n-octane conversion on Pt/Al_2O_3 versus temperature at P_{H_2} = 0.33atm, P_N= 7.63×10^{-3}atm, W/F = 0.11gmincm^{-3}

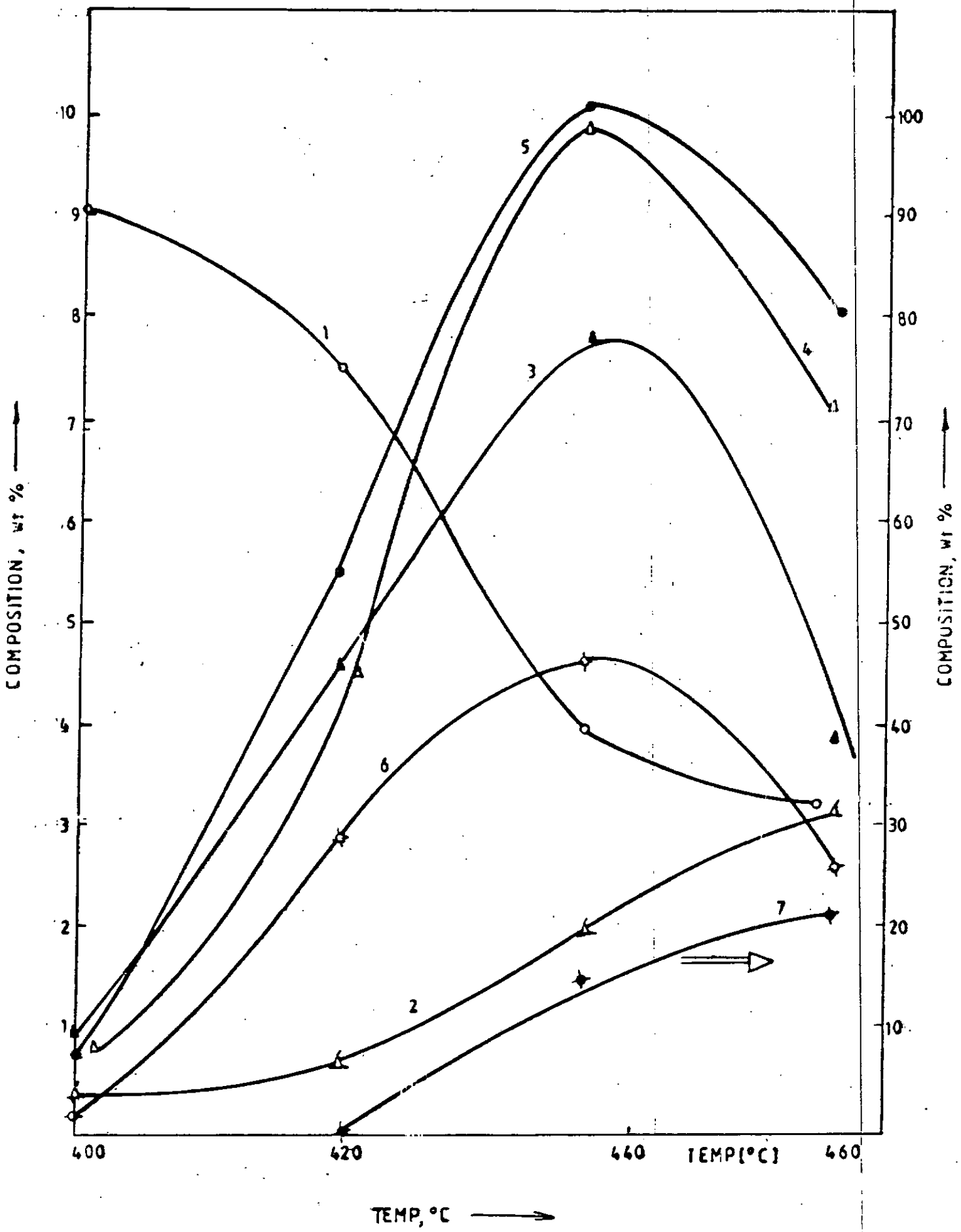

Fig. 5.1.20: Product composition of n-octane conversion on Pt/Al_2O_3 versus temperature at P_{H_2} = 0.5atm, $P_N = 7.63 \times 10^{-3}$ atm, W/F = 0.11gmincm^{-3}

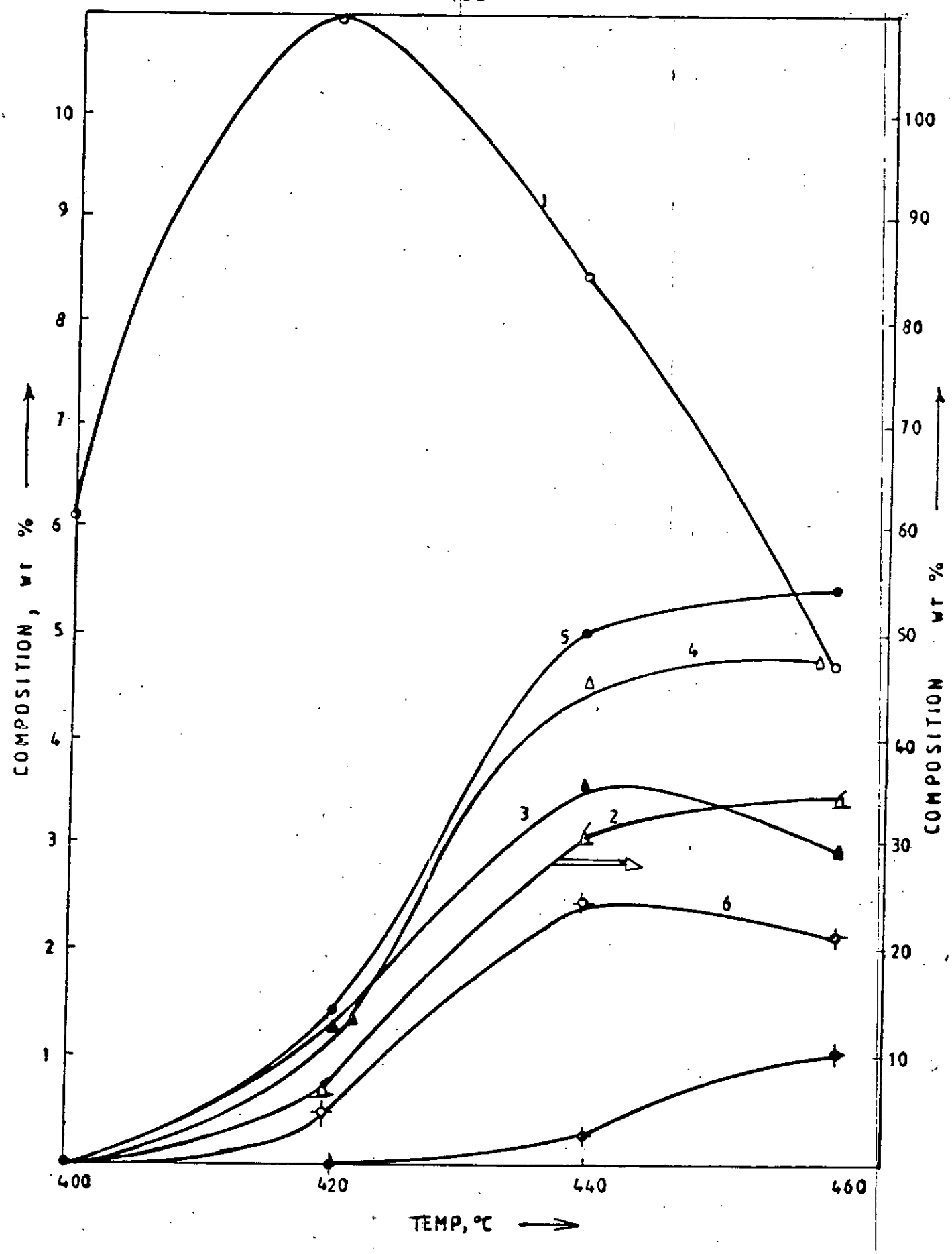

Fig.5.1.21: Product composition of n-octane conversion on Pt/Al_2O_3 versus temperature at P_{H_2} = 0.89atm, $P_N = 7.63 \times 10^{-3}$atm, W/F = 0.11gmincm^{-3}

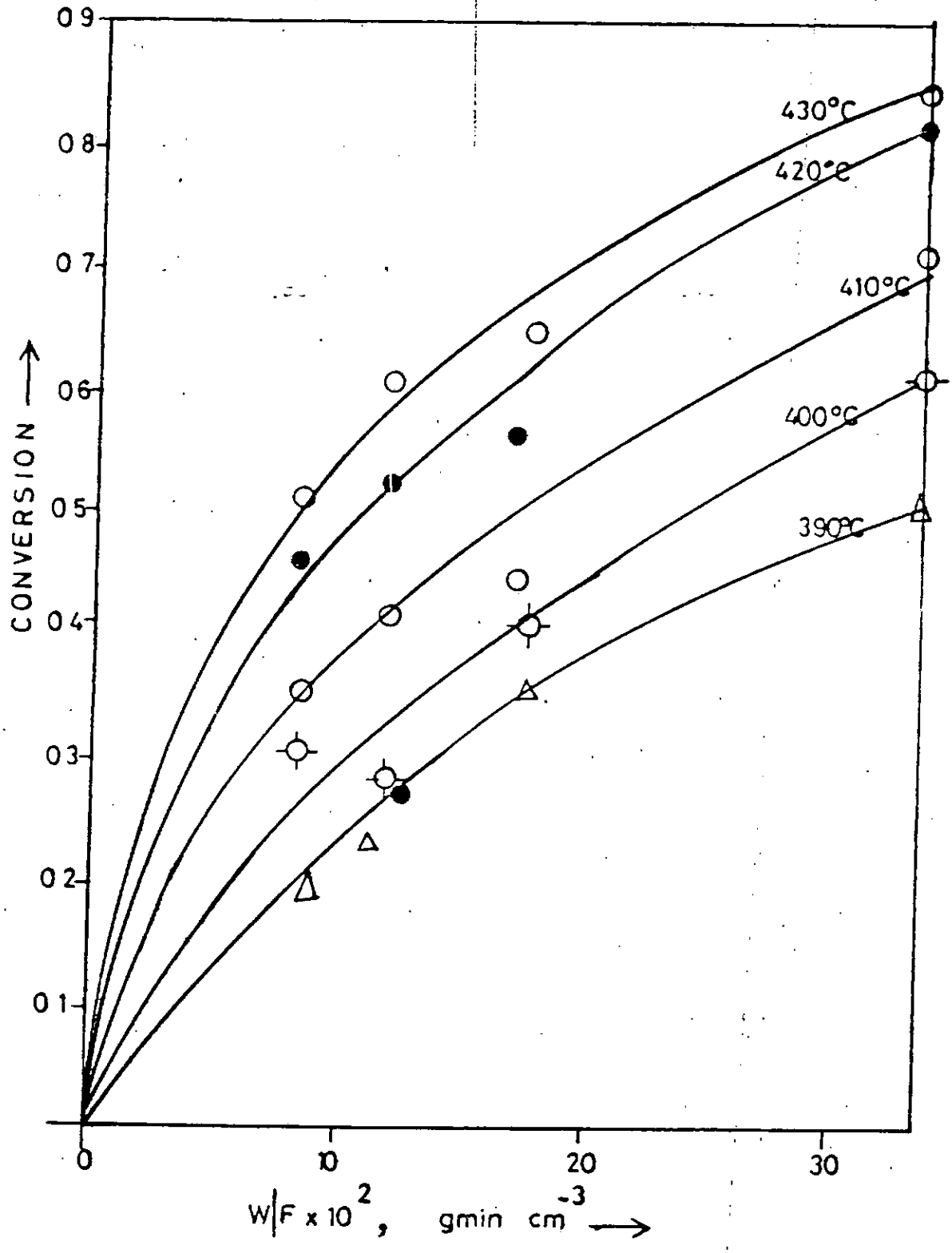

Fig. 5.1.22: Iso-octane conversion on 0.3%Pt/Al_2O_3 versus W/F at P_{iso} = 2.63×10^{-2} atm in H_2 and various temperatures.

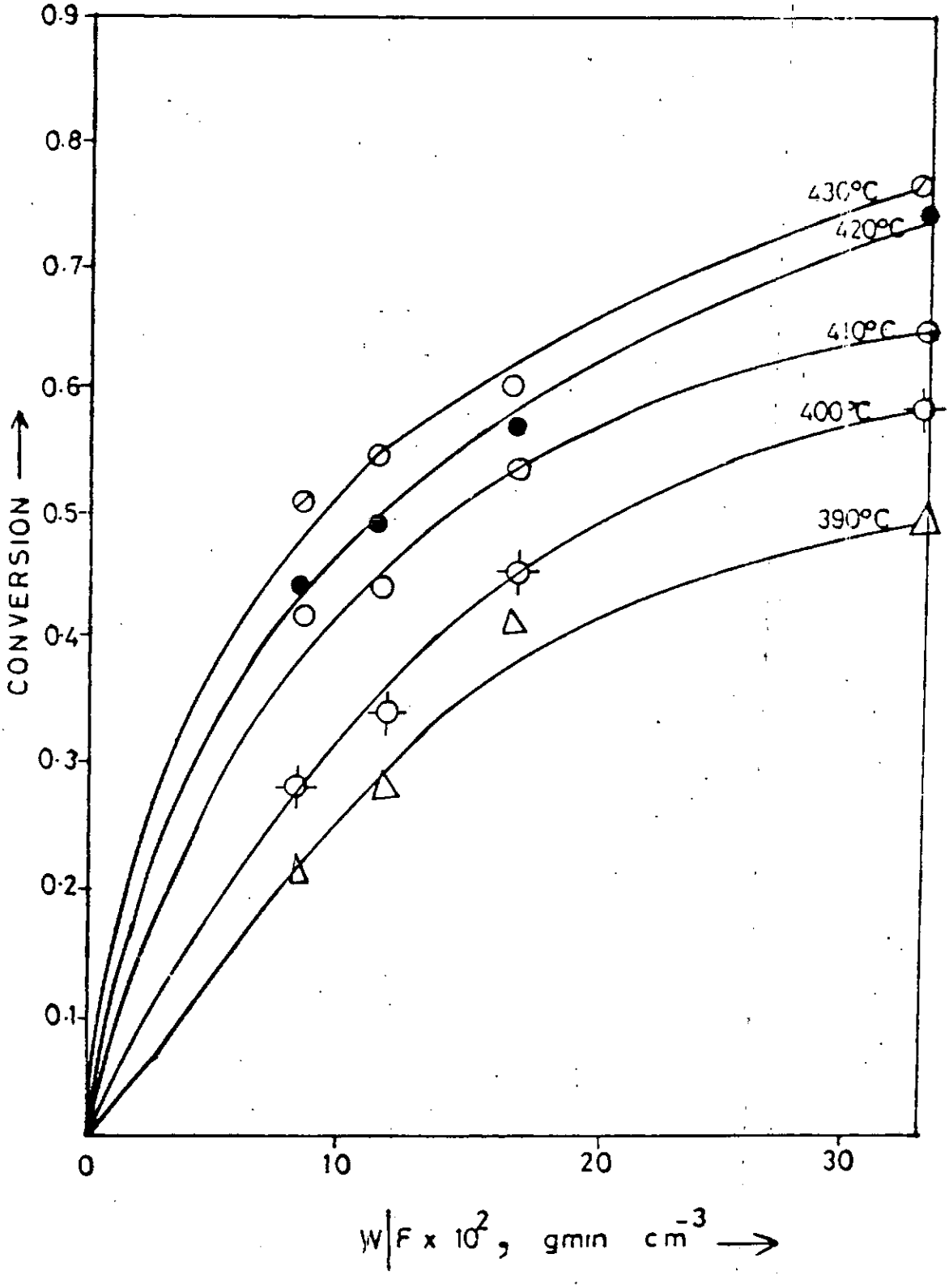

Fig. 5.1.23: Iso-octane conversion on 0.3%Pt/Al_2O_3 versus W/F at P_{iso} = 3.16×10^{-3}atm in H_2 and various temperatures.

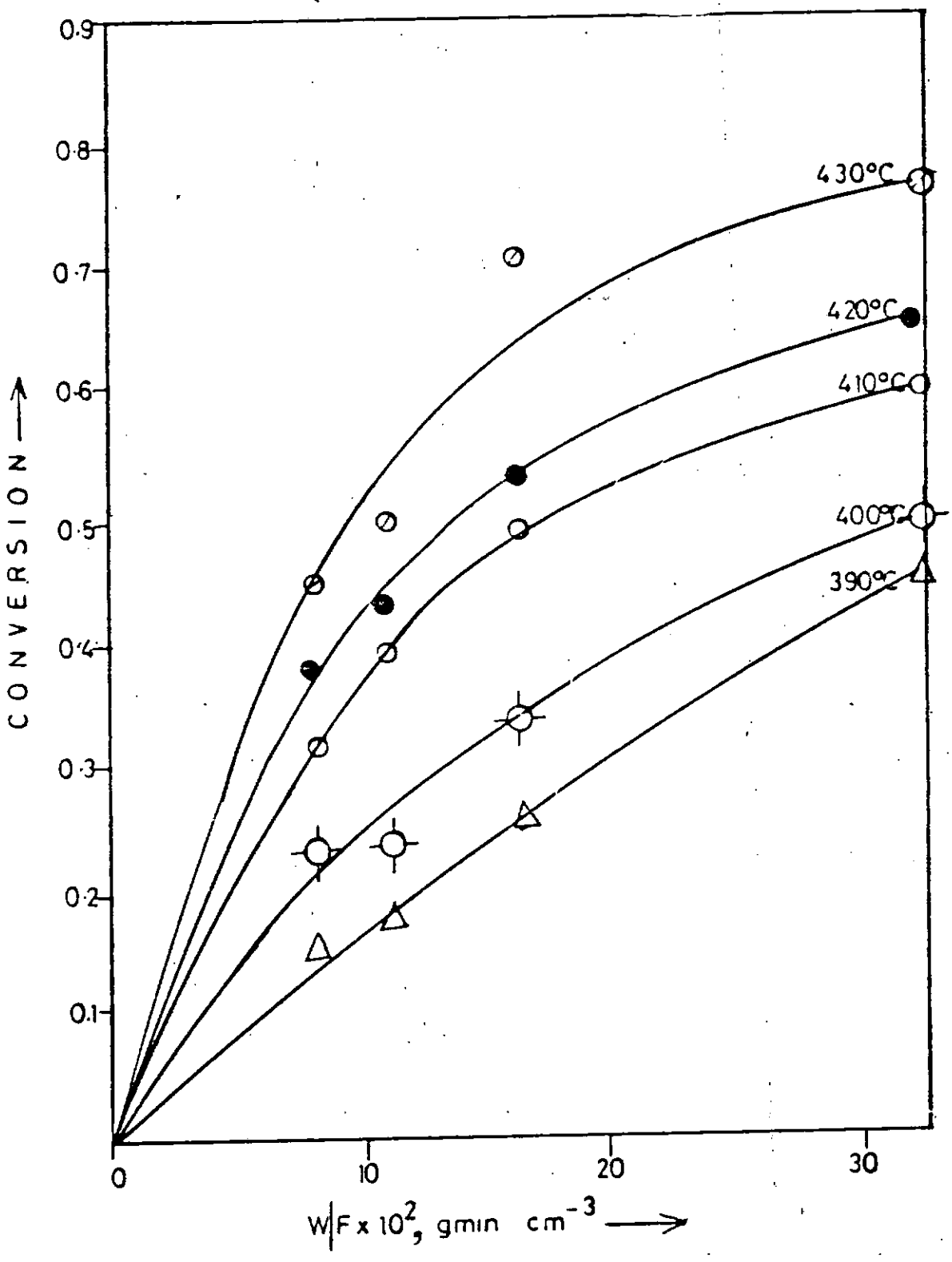

Fig.5.1.24: Iso-octane conversion on 0.3%Pt/Al_2O_3 versus W/F at P_{iso}= $5.6x10^{-2}$atm in H_2 and various temperatures.

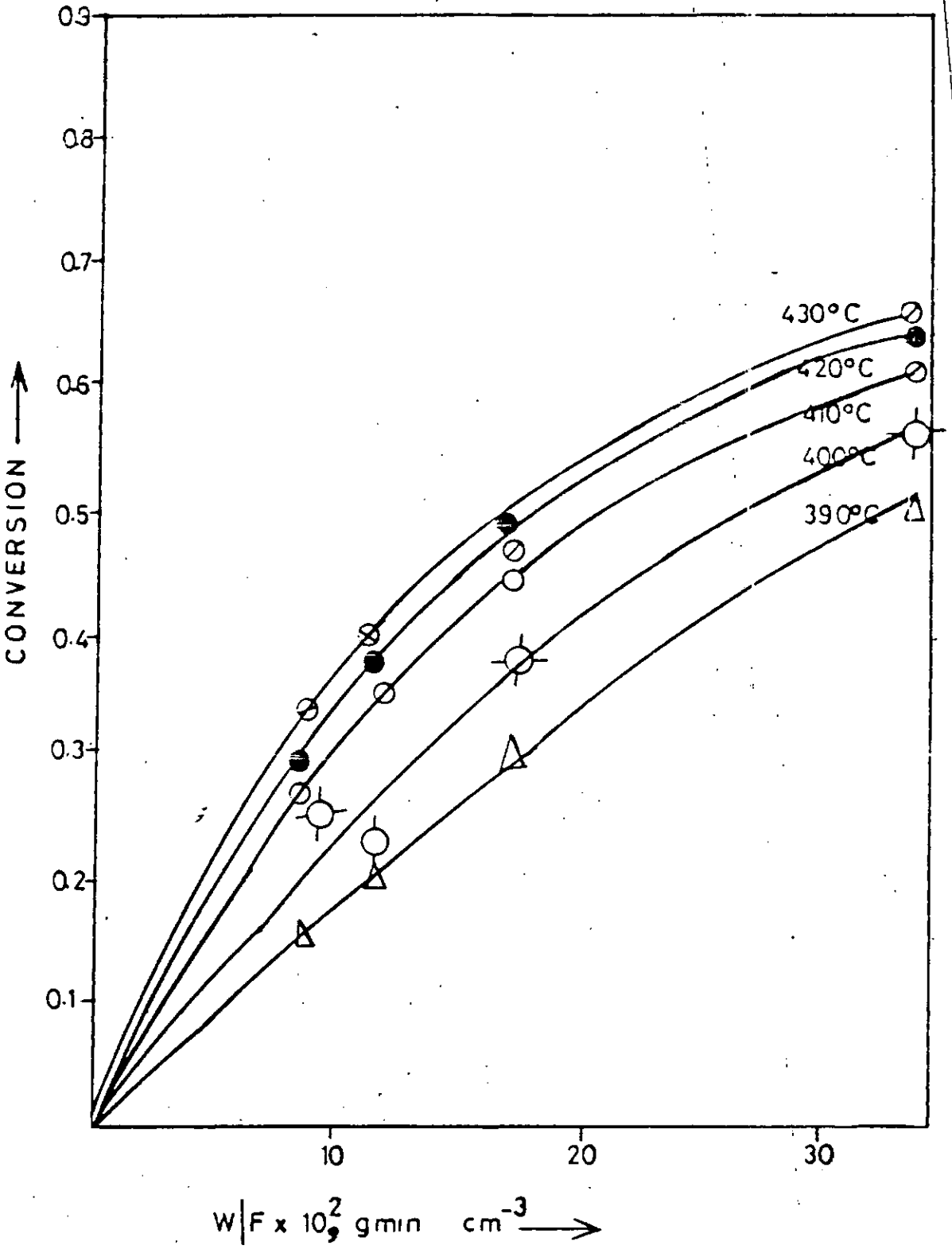

Fig. 5.1.25: Iso-octane conversion on 0.3%Pt/Al_2O_3 versus W/F at P_{iso} = ~~3.16×10^{-2}~~ atm in H_2 and various temperatures.

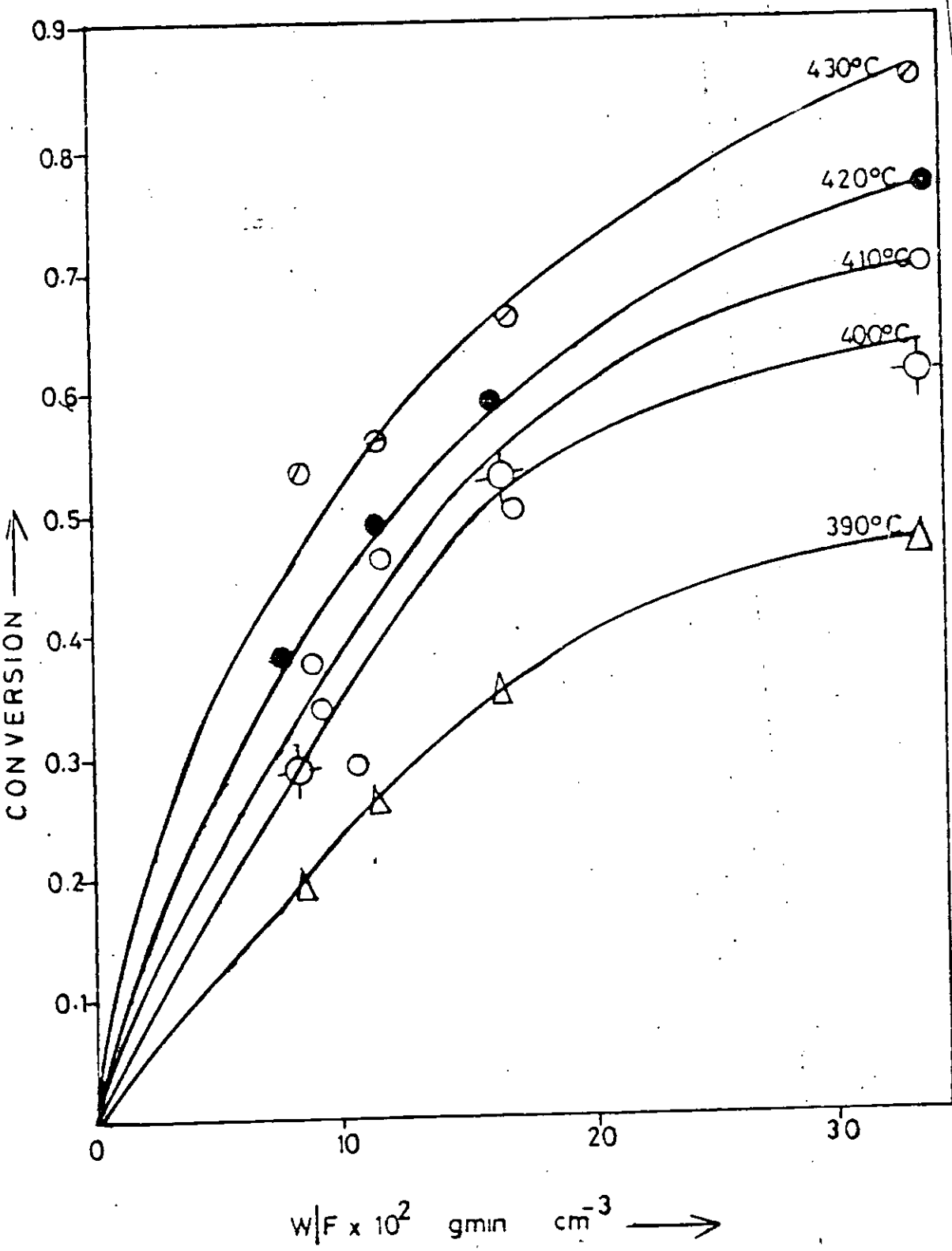

Fig. 5.1.26: Iso-octane conversion on 0.6%Pt/Al_2O_3 versus W/F at P_{iso}= 3.16×10^{-2}atm in H_2 and various temperatures.

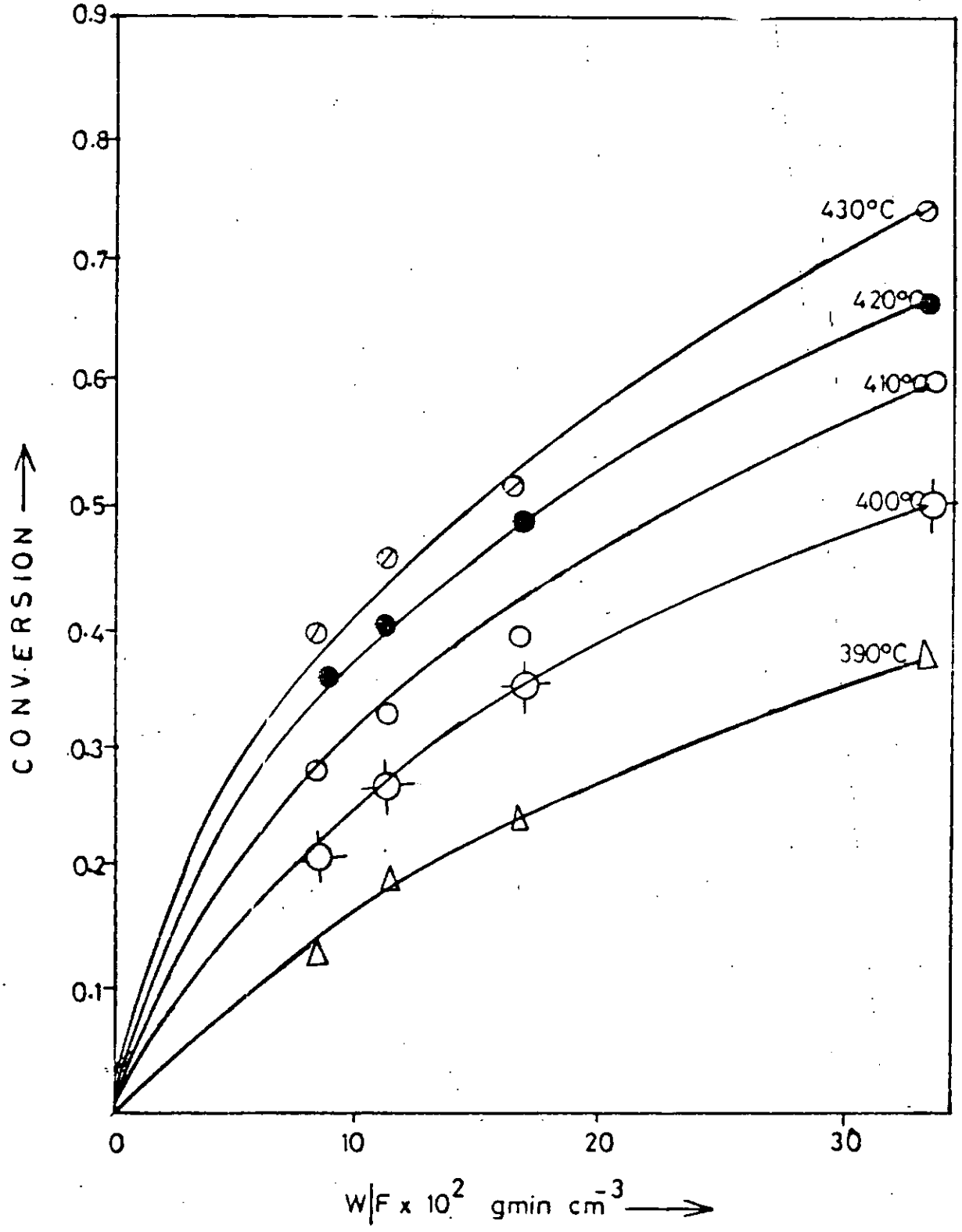

Fig.5.1.27: Iso-octane conversion on 0.6%Pt/Al_2O_3 versus W/F at P_{iso} = 5.6x10^{-2}atm in H_2 and various temperatures.

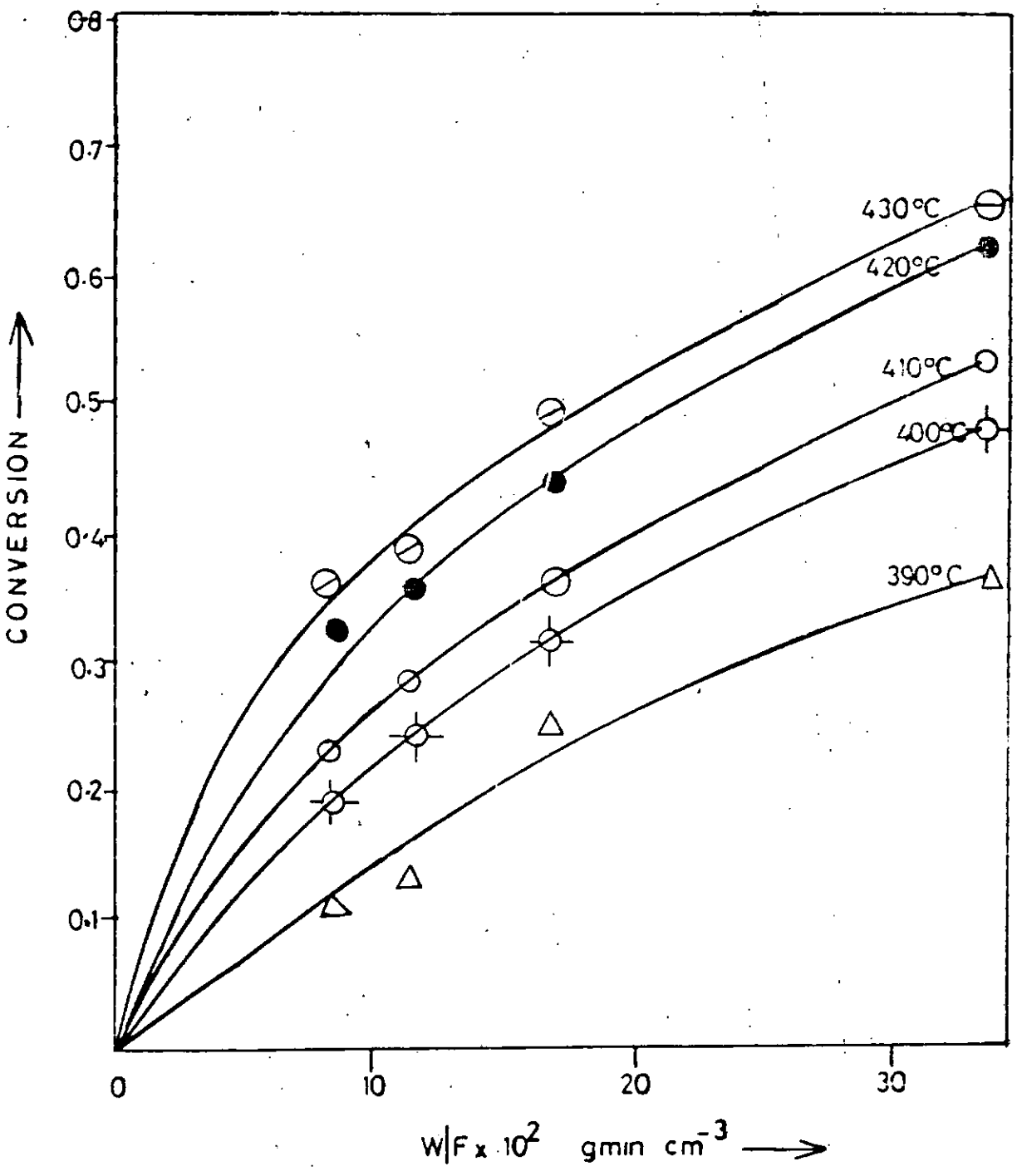

Fig.5.1.28: Iso-octane conversion on 0.6%Pt/Al_2O_3 versus W/F at P_{iso} = 8.2×10^{-2} atm and various temperatures.

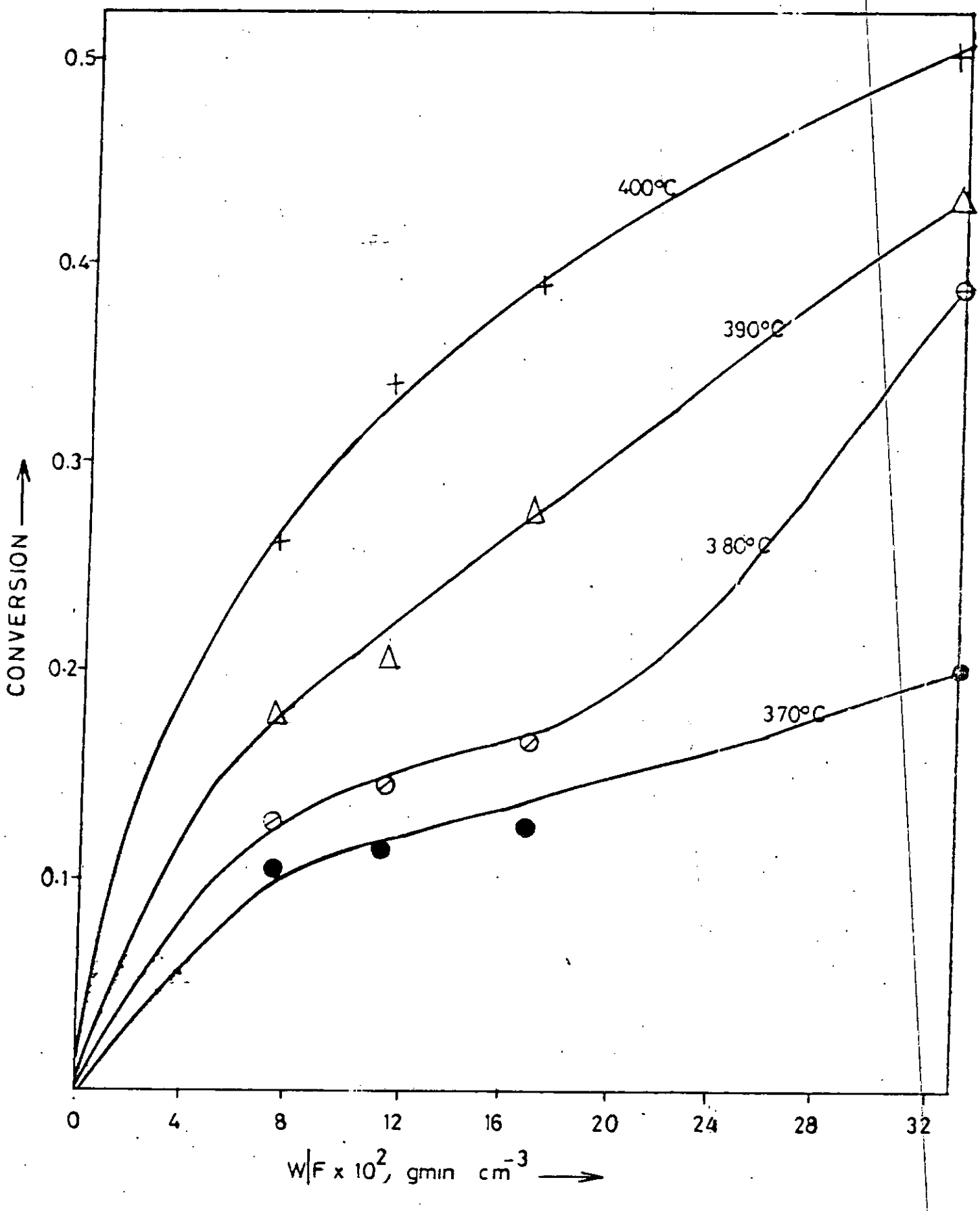

Fig.5.1.29: MCP Conversion on Pt/Al_2O_3 versus W/F at $P_{MCP} = 5.8 \times 10^{-2}$ atm in H_2 and various temperatures.

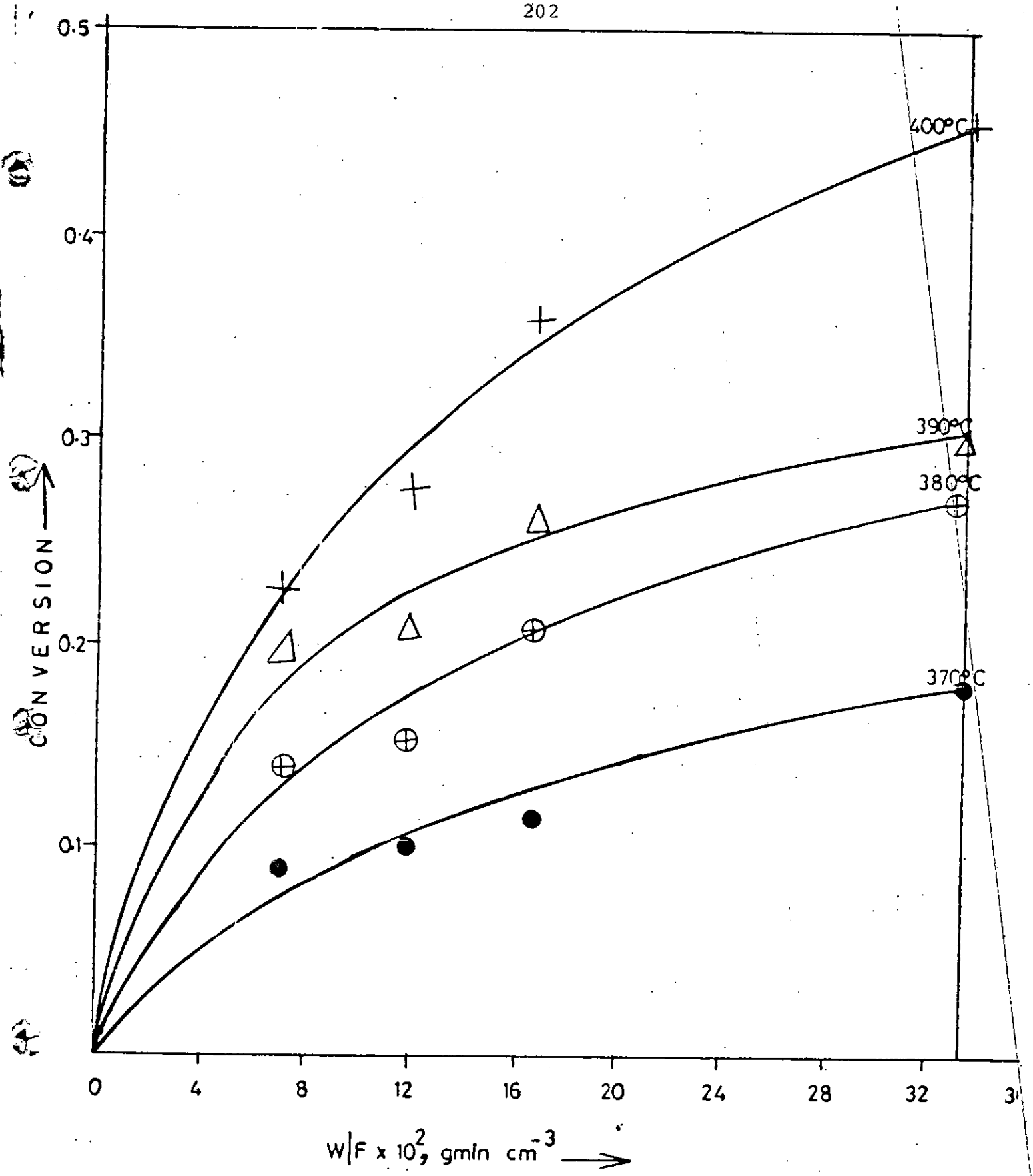

Fig.5.1.30: MCP Conversion on Pt/Al_2O_3 versus W/F at $P_{MCP} = 9.2 \times 10^{-2}$ atm in H_2 and various temperatures.

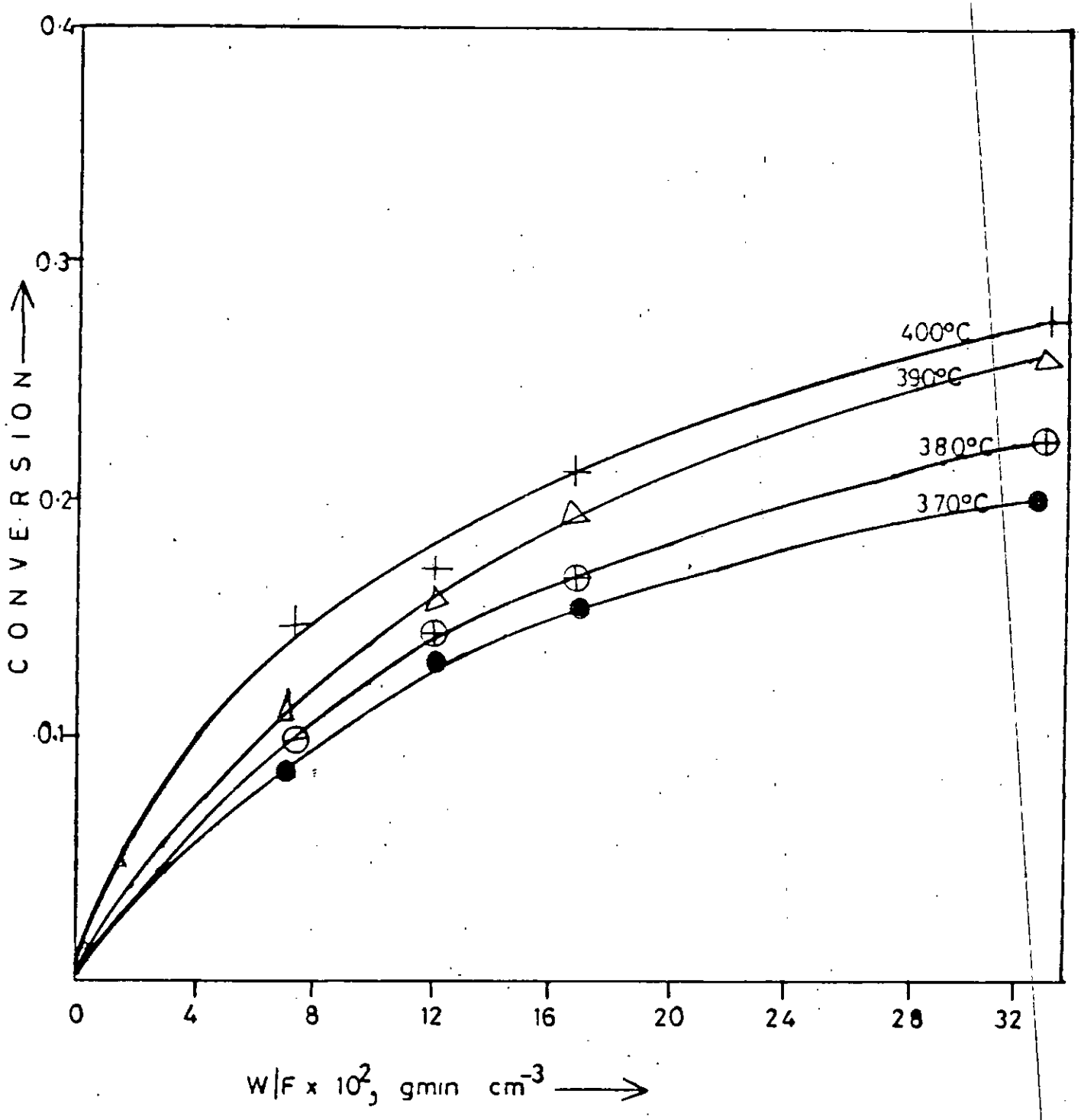

Fig.5.1.31: MCP Conversion on Pt/Al_2O_3 versus W/F at $P_{MCP} = 14.47 \times 10^{-2}$ atm in H_2 and various temperatures.

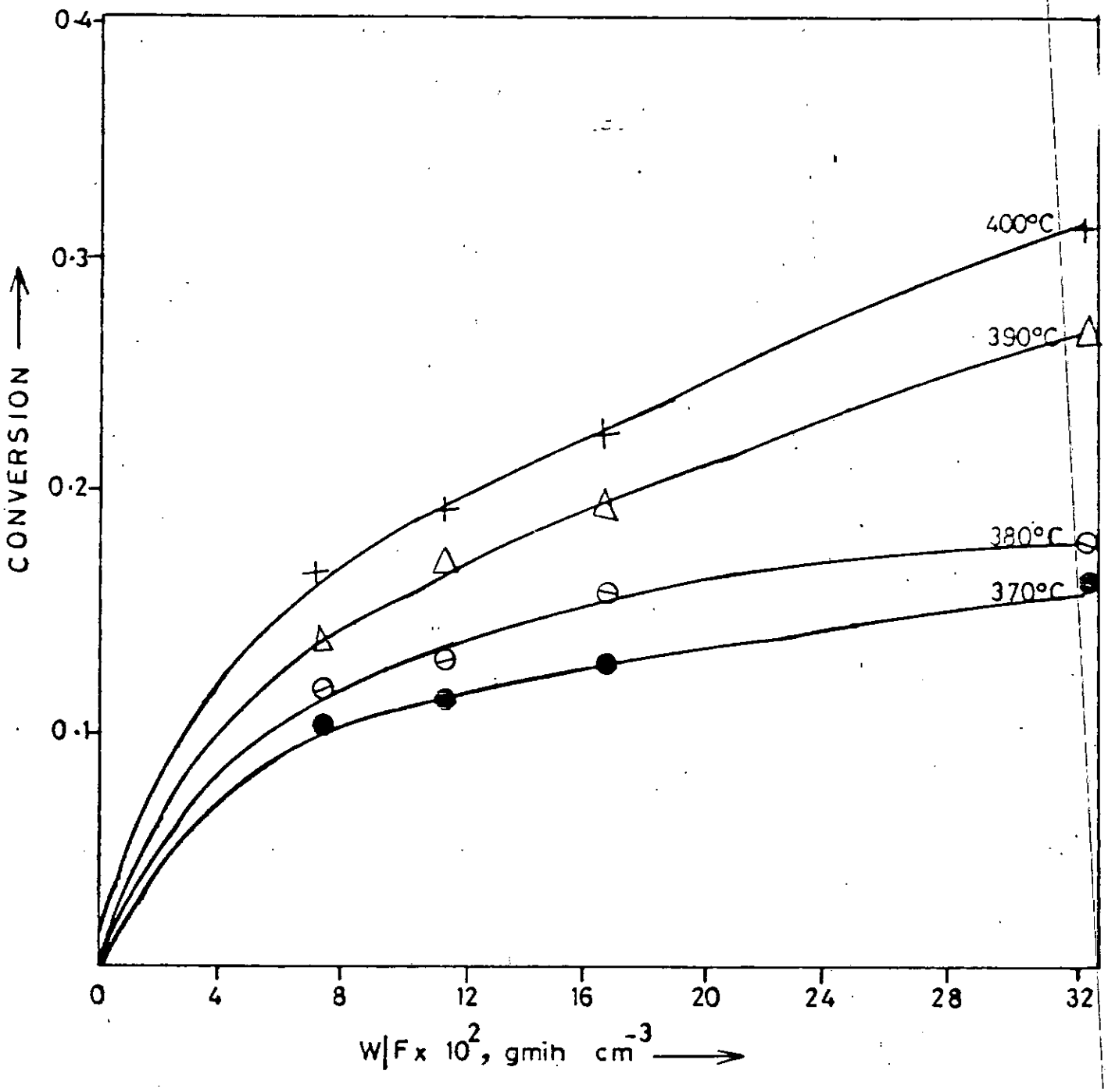

Fig.5.1.32: MCP Conversion on Pt/Al_2O_3 versus W/F at P_{MCP} =18.16x10^{-2}atm in H_2 and various temperatures.

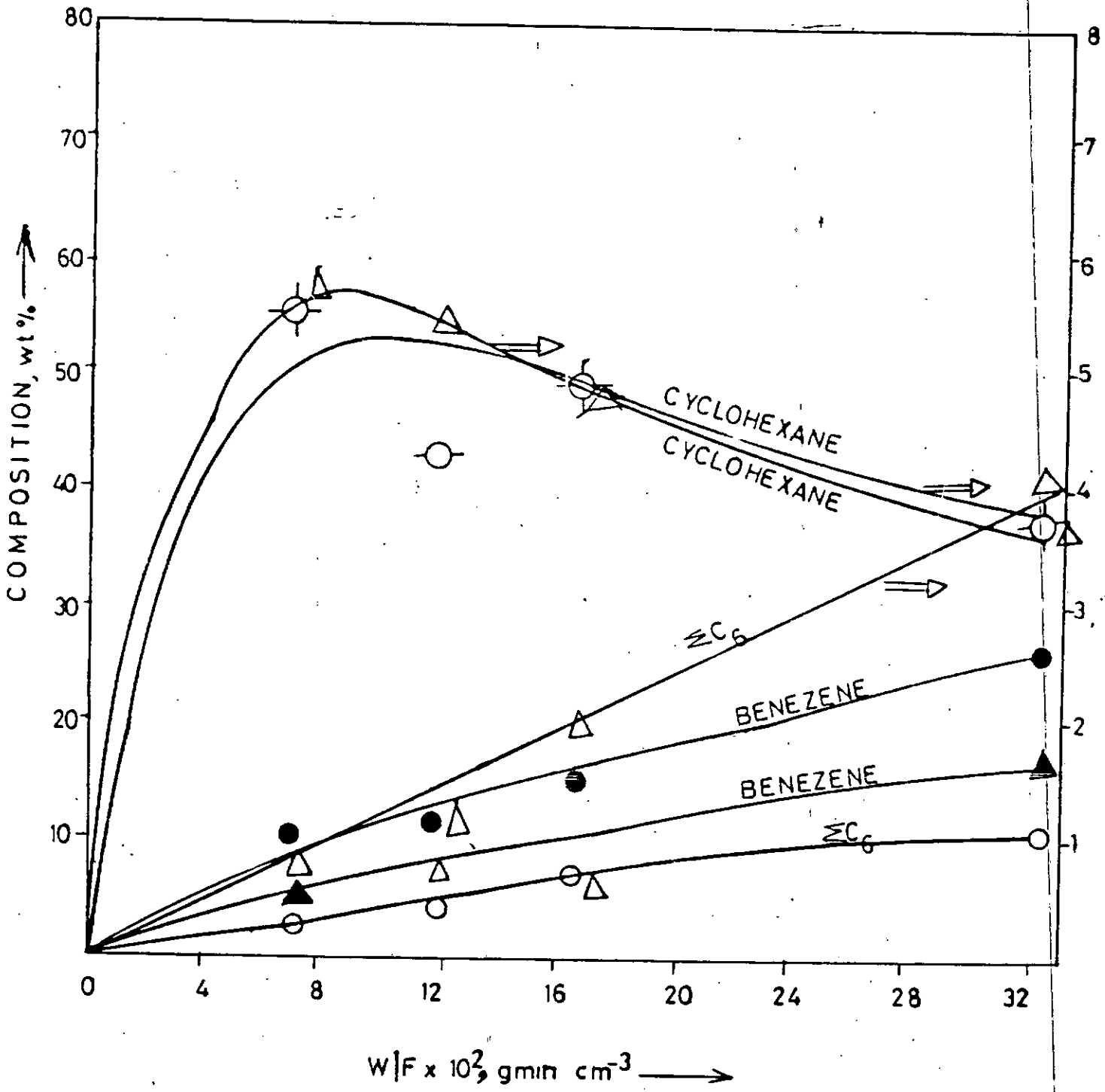

Fig.5.1.33: Product composition of MCP conversion on Pt/Al_2O_3 versus W/F at $P_{MCP} = 5.8 \times 10^{-2}$ atm in H_2 at 370° and 390°C.

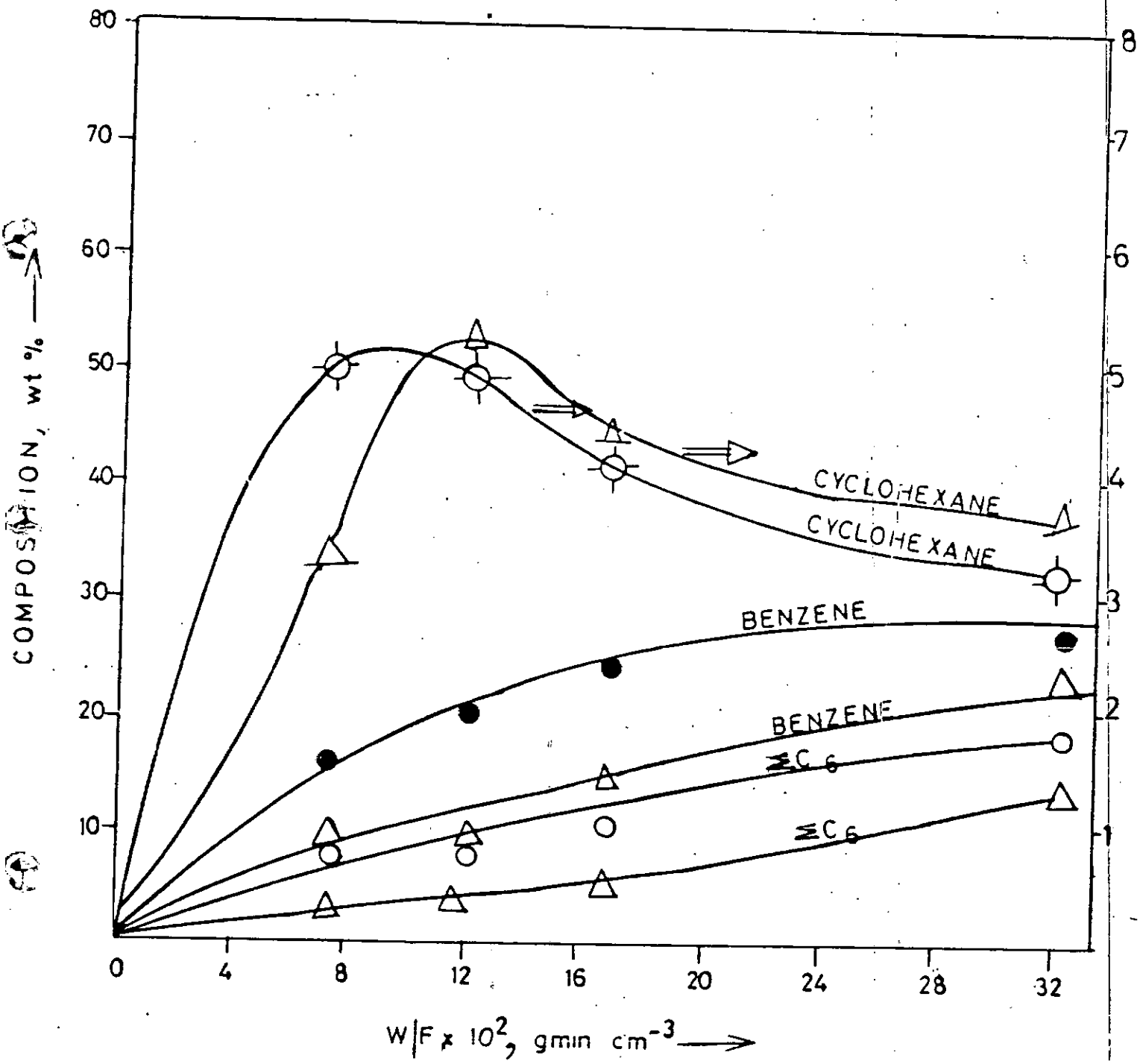

Fig.5.1.34: Product composition of MCP conversion on Pt/Al_2O_3 versus W/F at $P_{MCP} = 5.8 \times 10^{-2}$ atm in H_2 at 380° and 400°C.

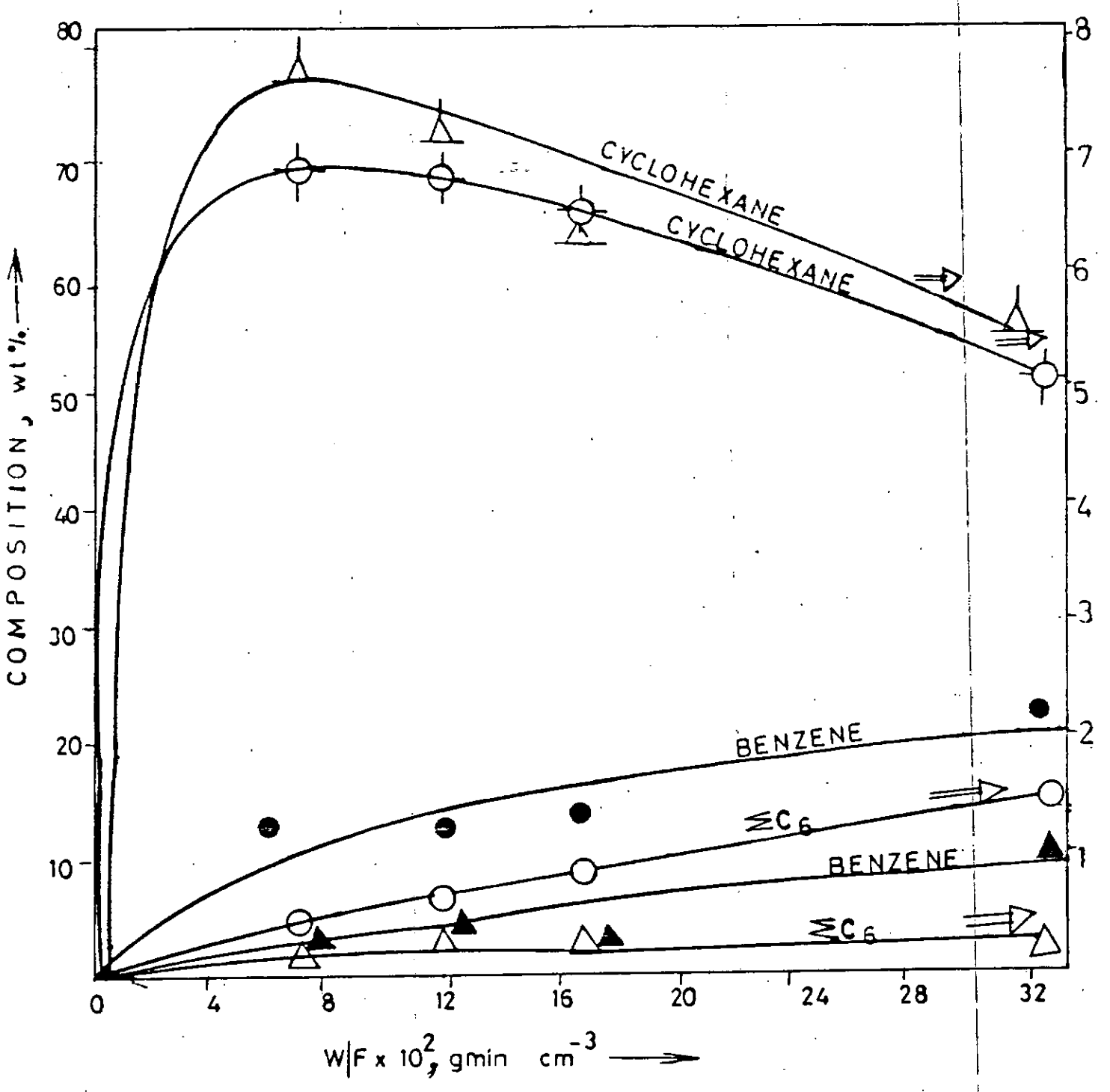

Fig.5.1.35: Product composition of MCP conversion on Pt/Al_2O_3 versus W/F at $P_{MCP} = 9.2 \times 10^{-2}$ atm in H_2 at 370° and 390°C.

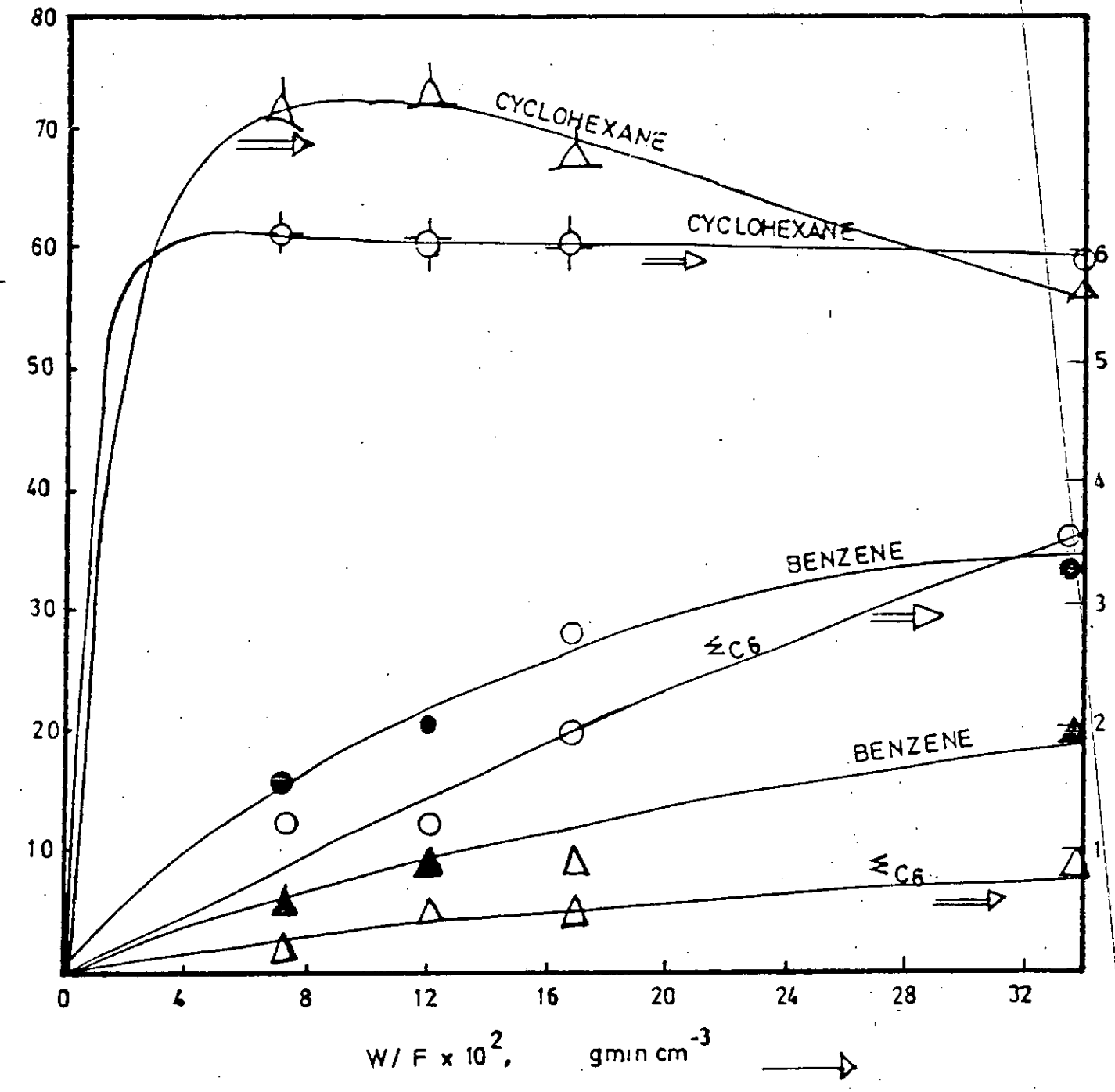

Fig.5.1.36: Product composition on MCP conversion on Pt/Al_2O_3 versus W/F at $P_{MCP} = 9.2 \times 10^{-2}$ atm in H_2 at 380° and 400°C.

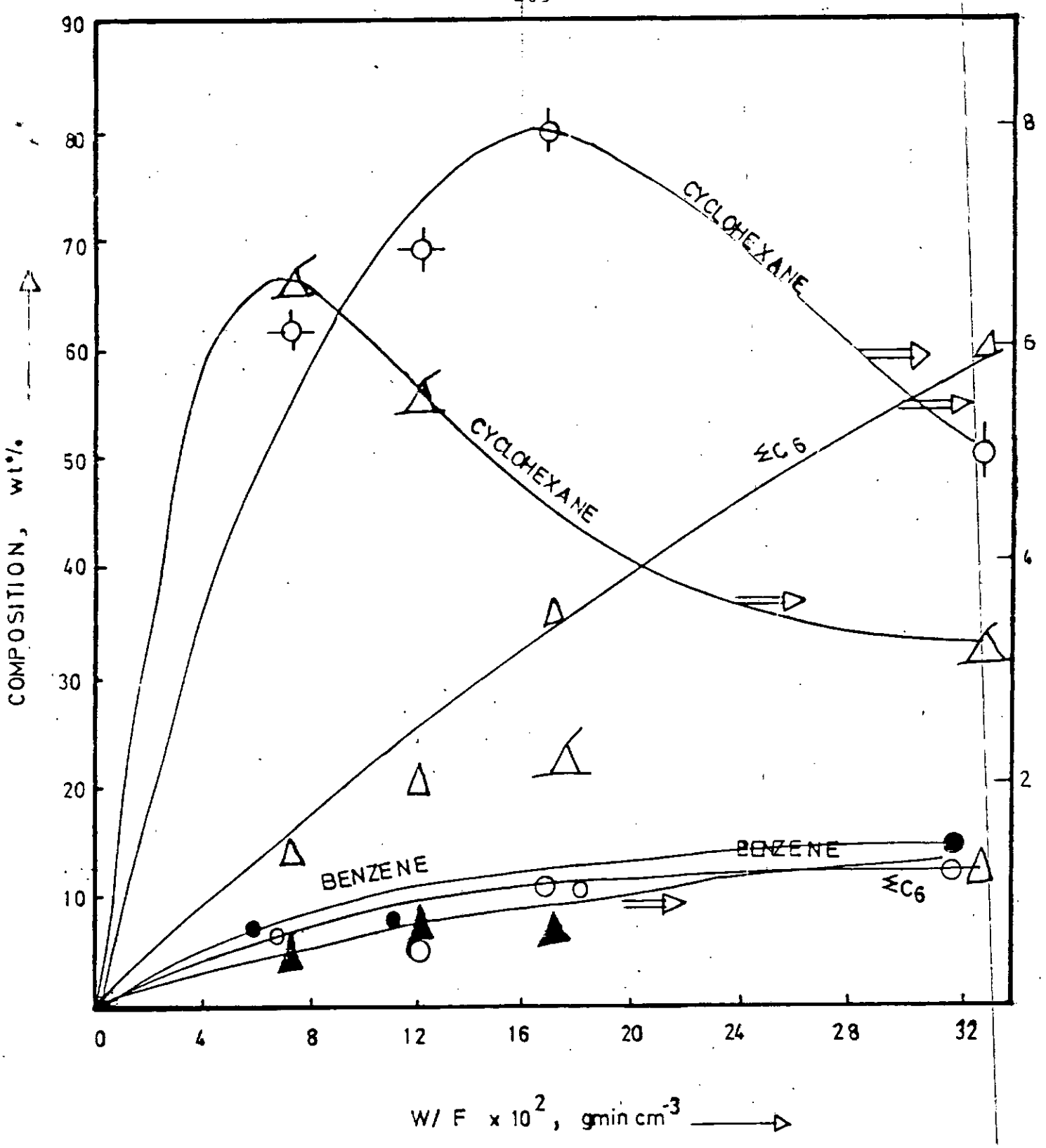

Fig.5.1.37: Product composition of MCP conversion on Pt/Al_2O_3 versus W/F at $P_{MCP}=14.47\times10^{-2}$atm in H_2 at 370° and 390°C.

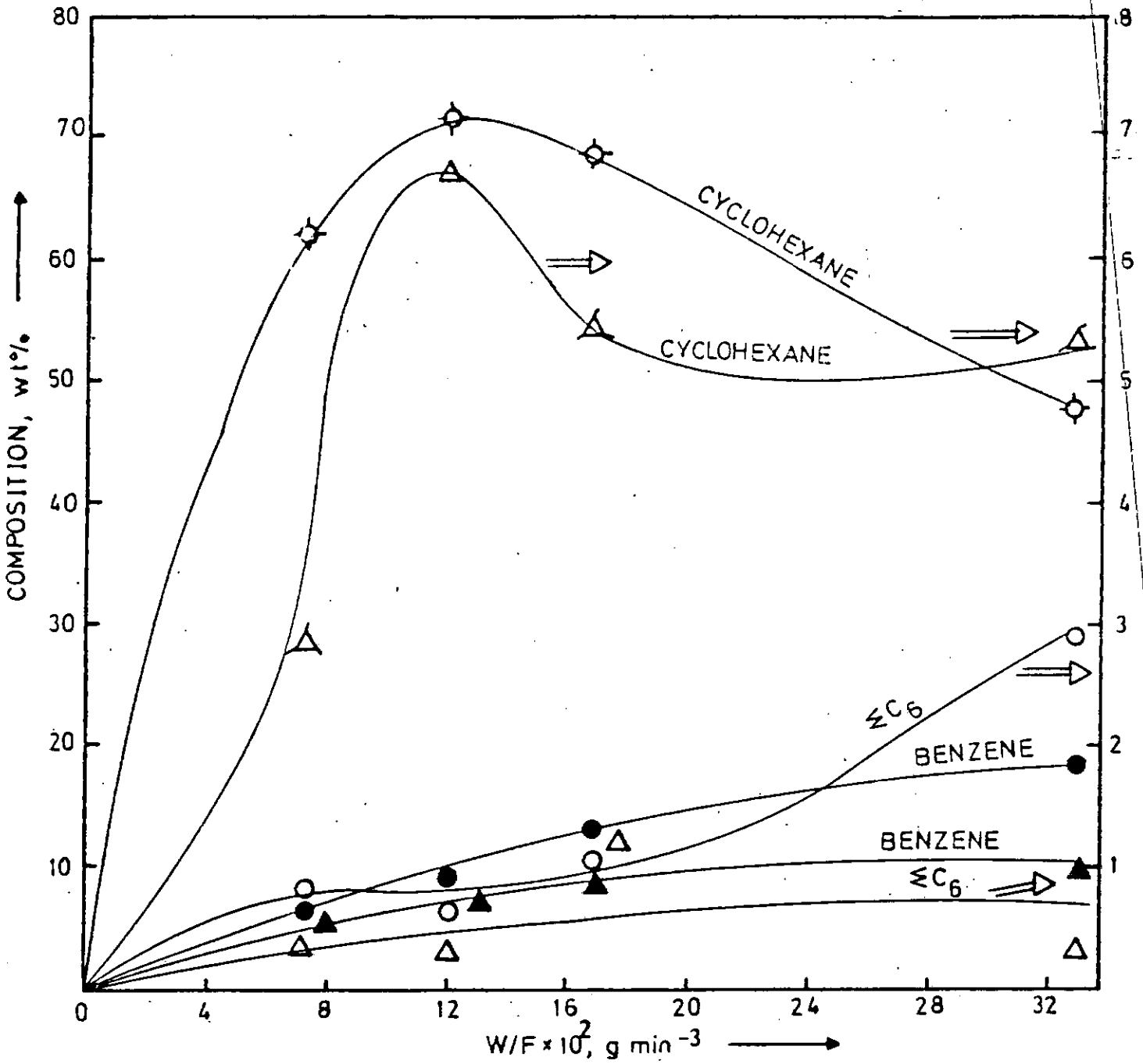

Fig.5.1.38: Product composition of MCP conversion on Pt/Al_2O_3 versus W/F at $P_{MCP} = 14.47 \times 10^{-2}$ atm in H_2 at 380° and 400°C.

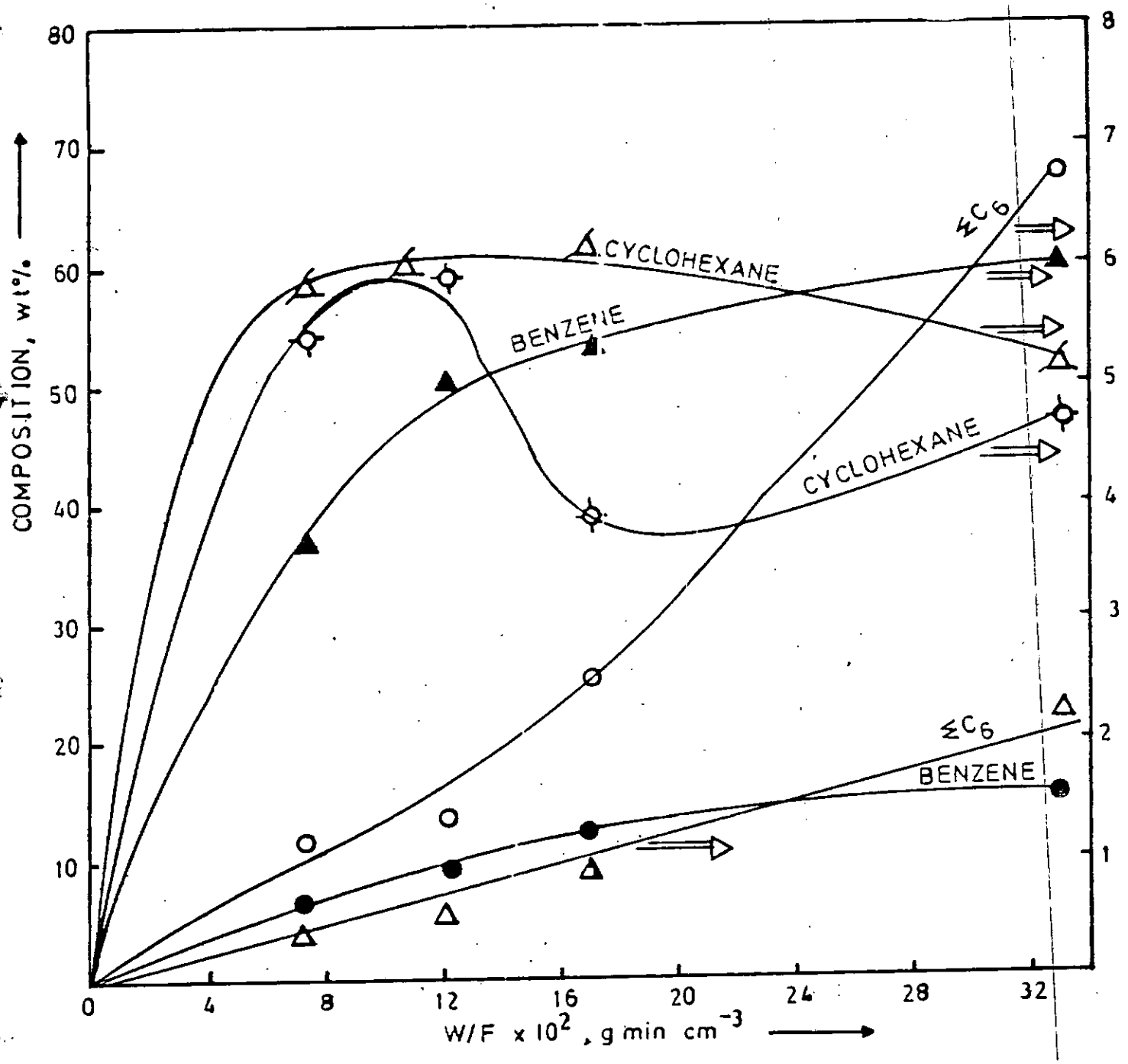

Fig.5.1.39: Product composition of MCP conversion on Pt/Al_2O_3 versus W/F at $P_{MCP} = 18.16 \times 10^{-2}$ atm in H_2 at 370° and 390°C.

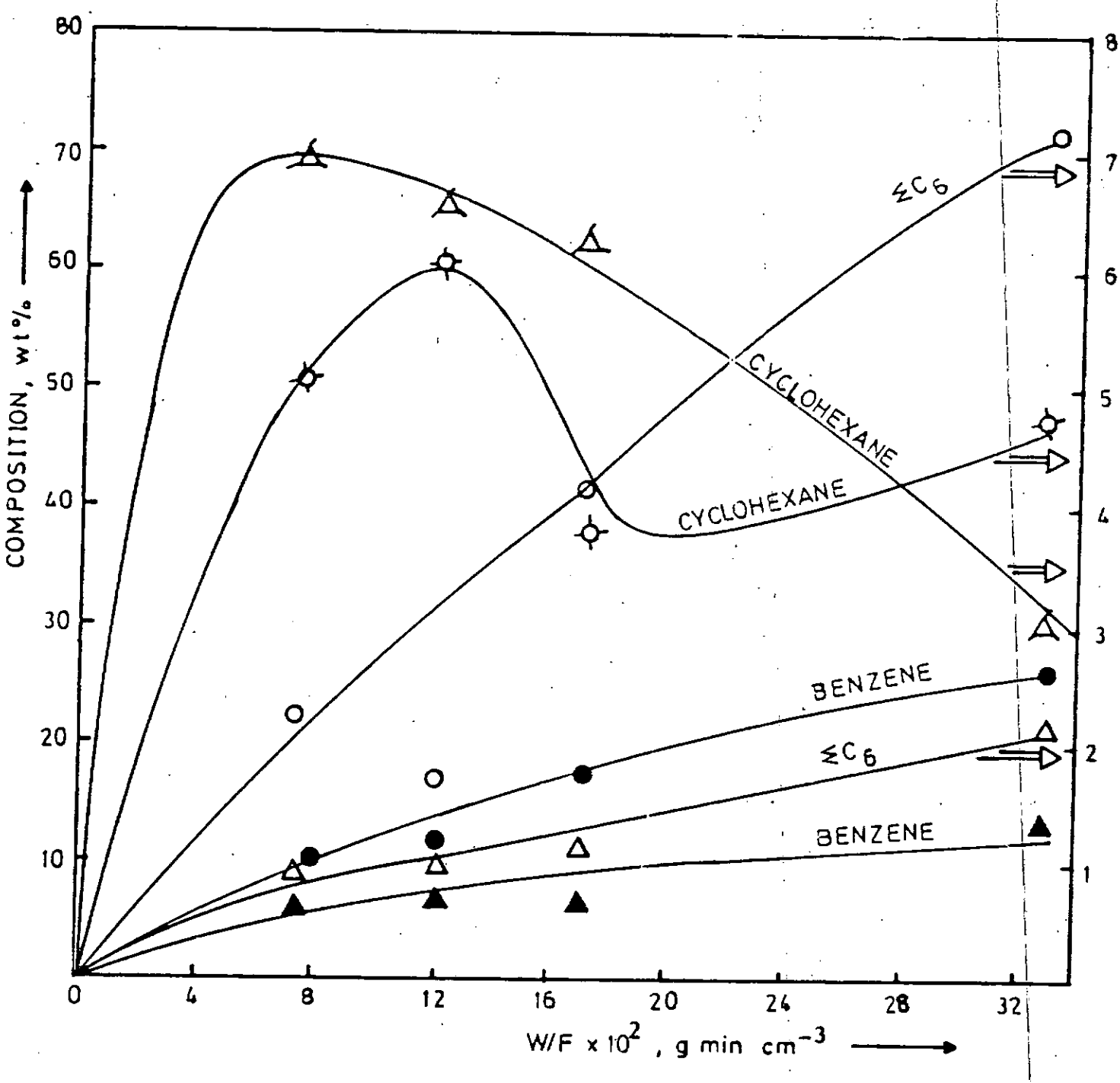

Fig.5.1.40: Product composition of MCP conversion on Pt/Al_2O_3 versus W/F at P_{MCP} = 18.16×10^{-2} atm in H_2 at 380° and 400°C .

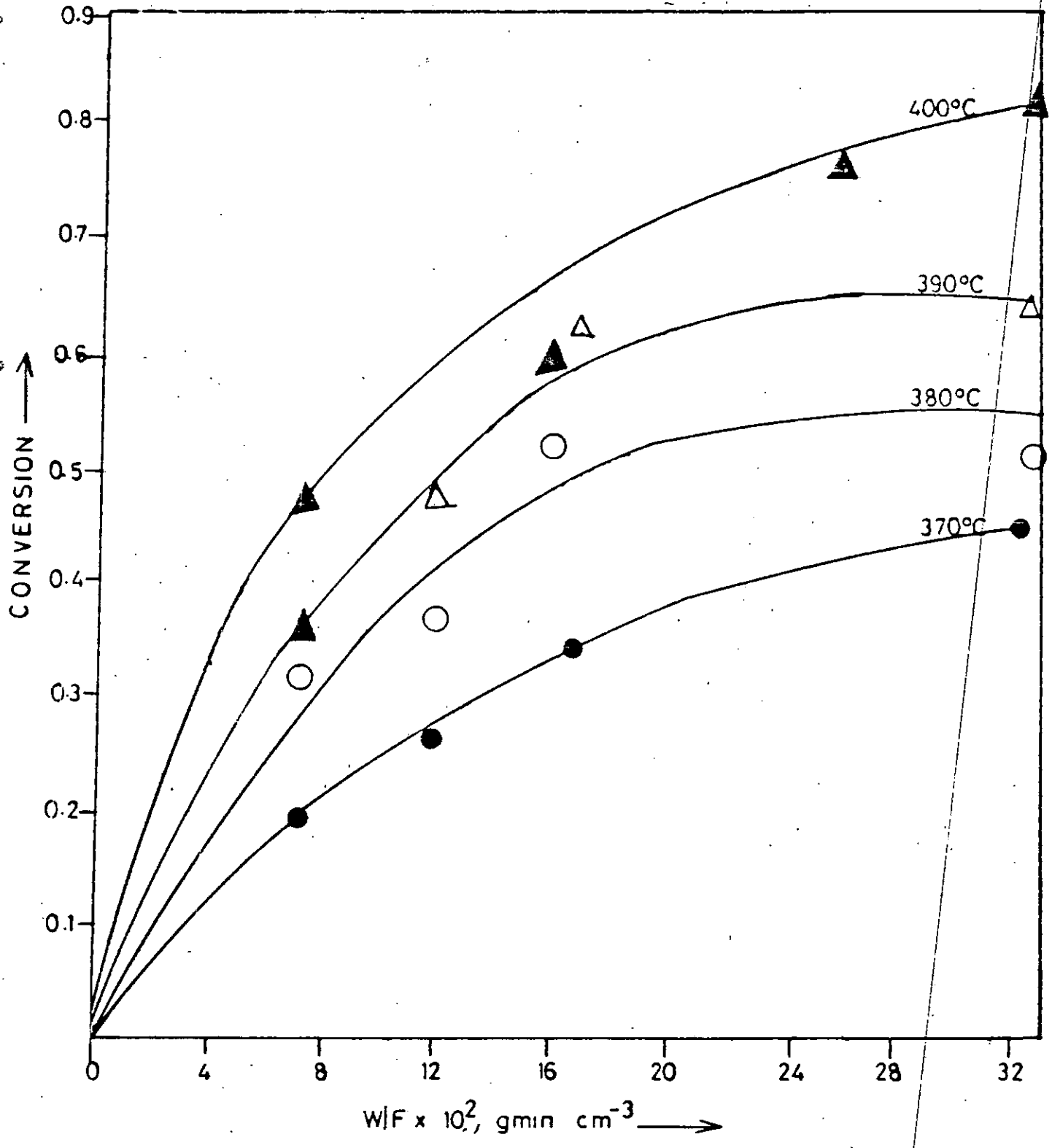

Fig.5.1.41: MCP conversion on Pt-Re/Al_2O_3(UNDRIED) versus W/F at P_{MCP} = 5.8×10^{-2}atm in H_2 at various temperatures.

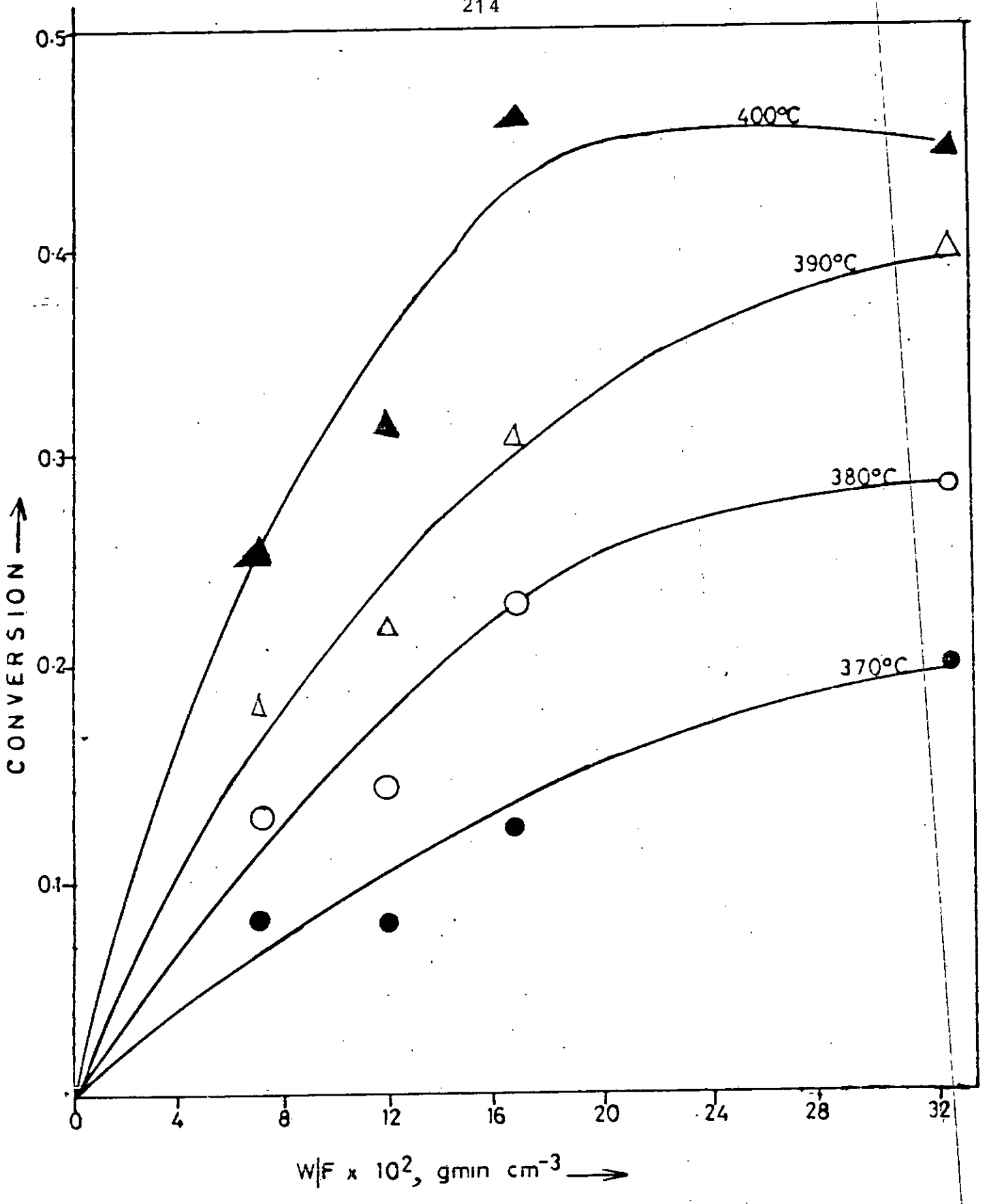

Fig.5.1.42: MCP conversion on Pt-Re/Al_2O_3(UNDRIED) versus W/F at $P_{MCP}=9.2\times10^{-2}$atm in H_2 at various temperatures.

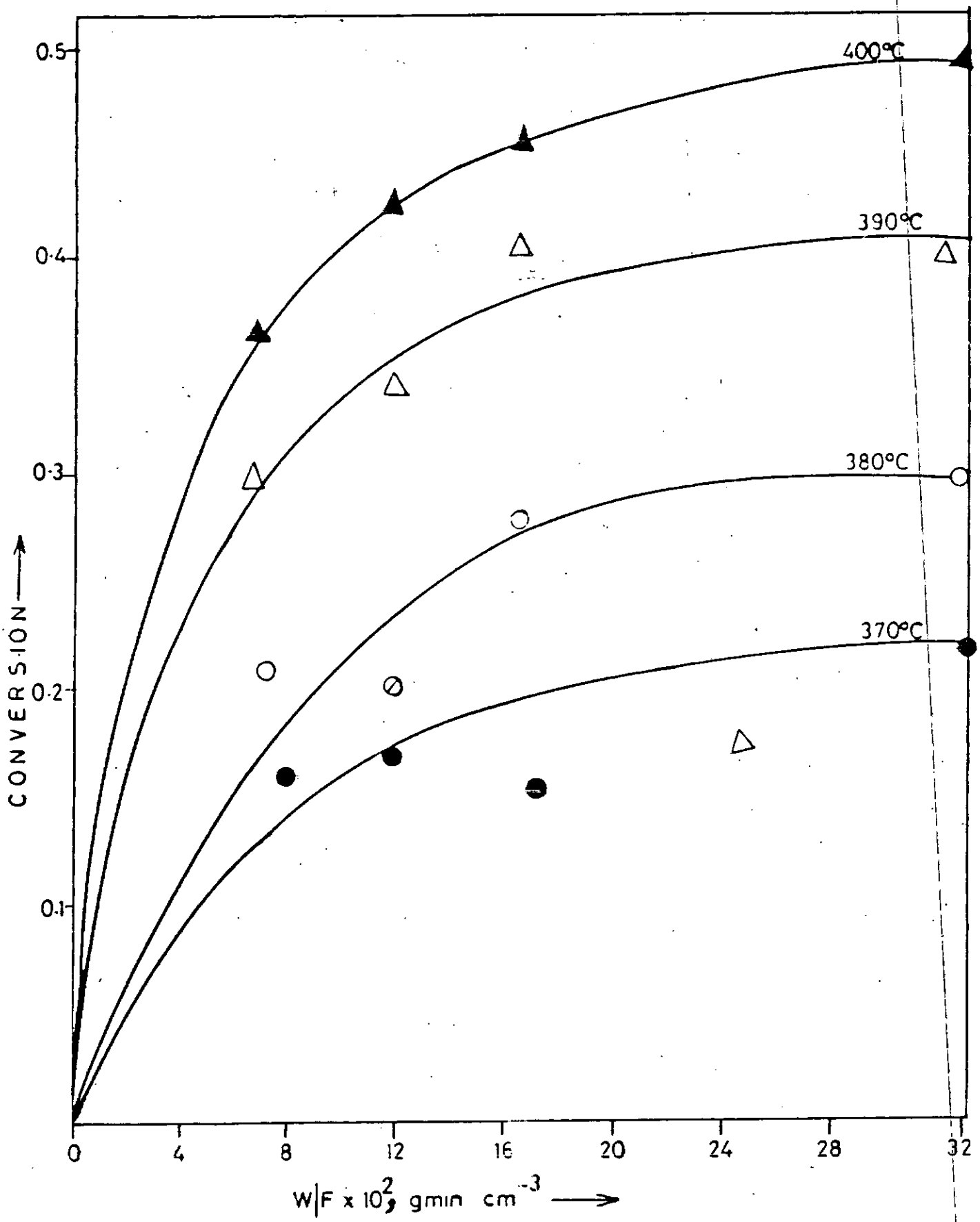

Fig.5.1.43: MCP conversion on Pt-Re/Al_2O_3 (UNDRIED) versus W/F at $P_{MCP}=14.47\times10^{-2}$ atm in H_2 at various temperatures.

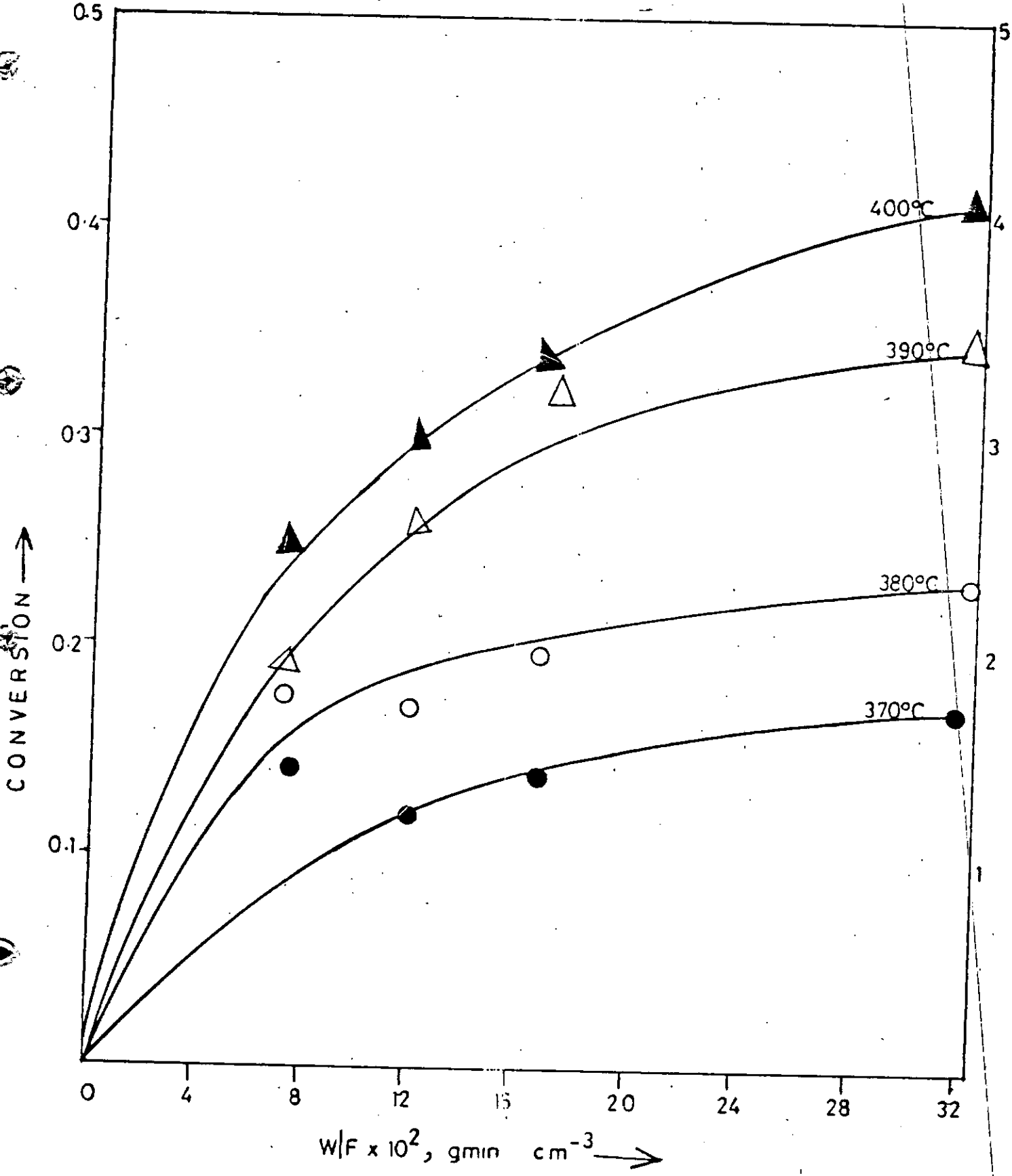

Fig.5.1.44: MCP conversion on Pt-Re/Al_2O_3 (UNDRIED) versus W/F at $P_{MCP} = 18.16 \times 10^{-2}$ atm in H_2 at 370° and 390°C.

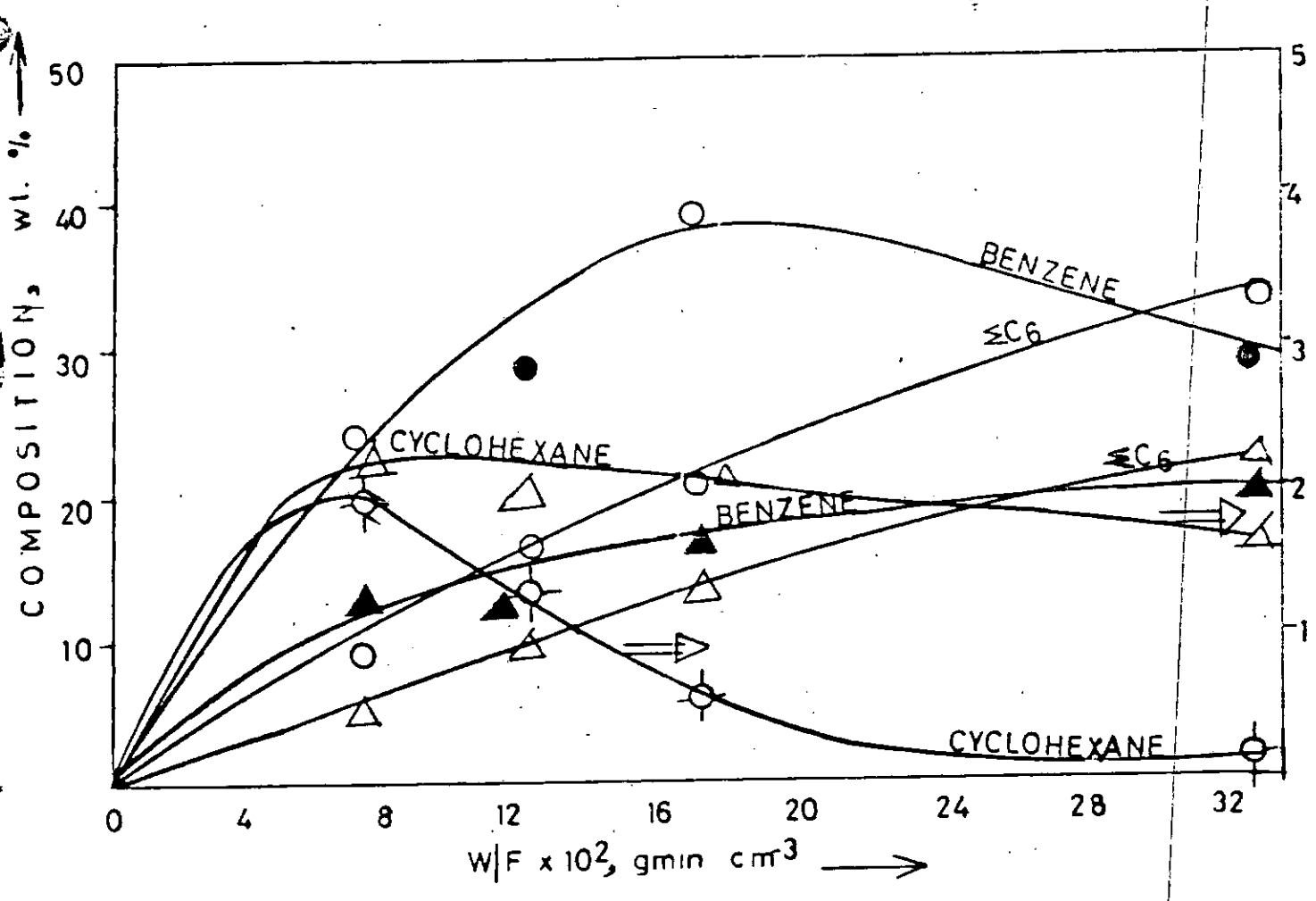

Fig.5.1.45: Product composition of MCP conversion on Pt-Re/Al_2O_3 (UNDRIED) versus W/F at $P_{MCP}=5.8\times10^{-2}$atm in H_2 at 370° and 390°C.

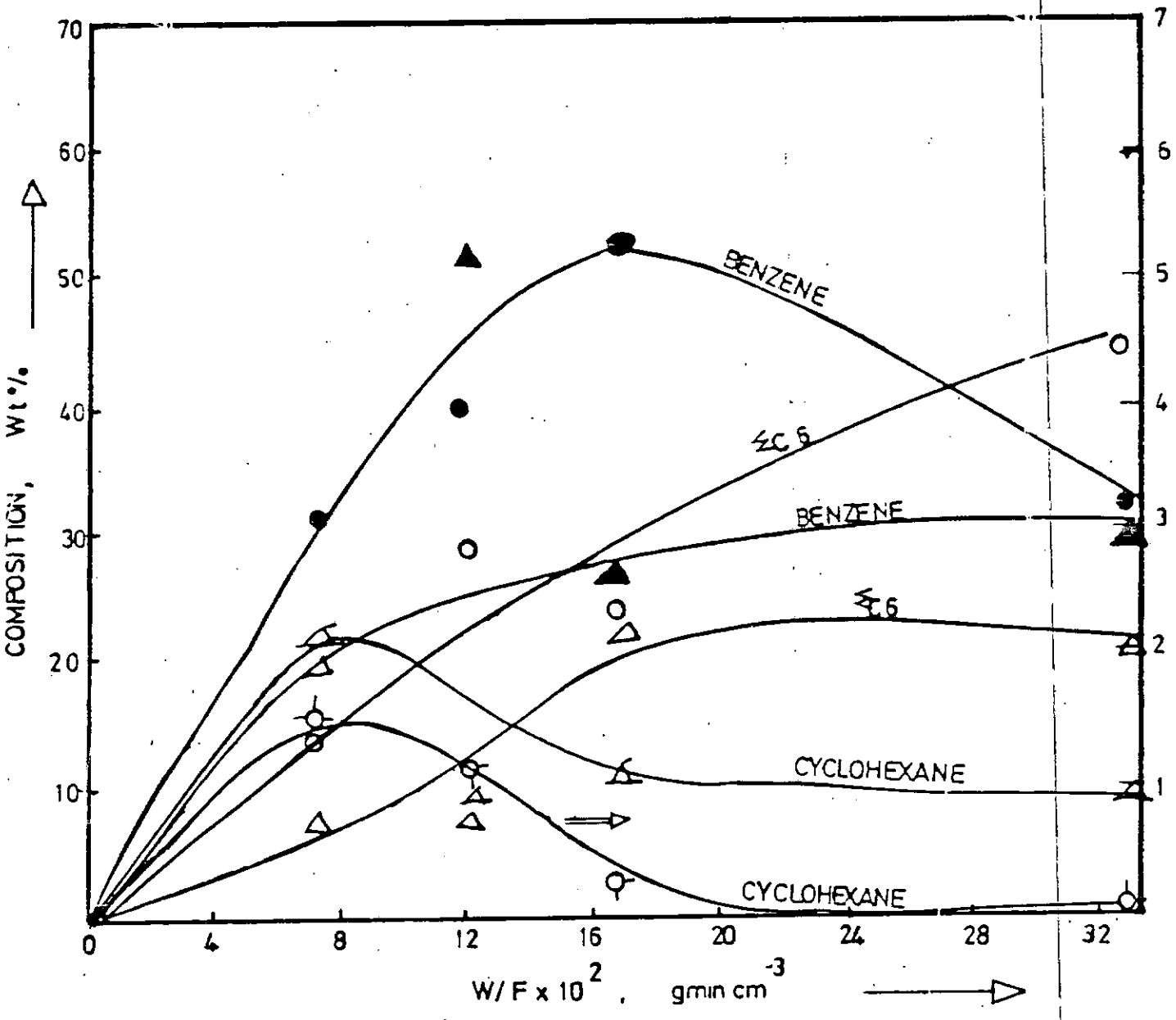

Fig.5.1.46: Product composition of MCP conversion on Pt-Re/Al_2O_3(UNDRIED) versus W/F at $P_{MCP}=5.8\times10^{-2}$ atm in H_2 at 380° and 400°C.

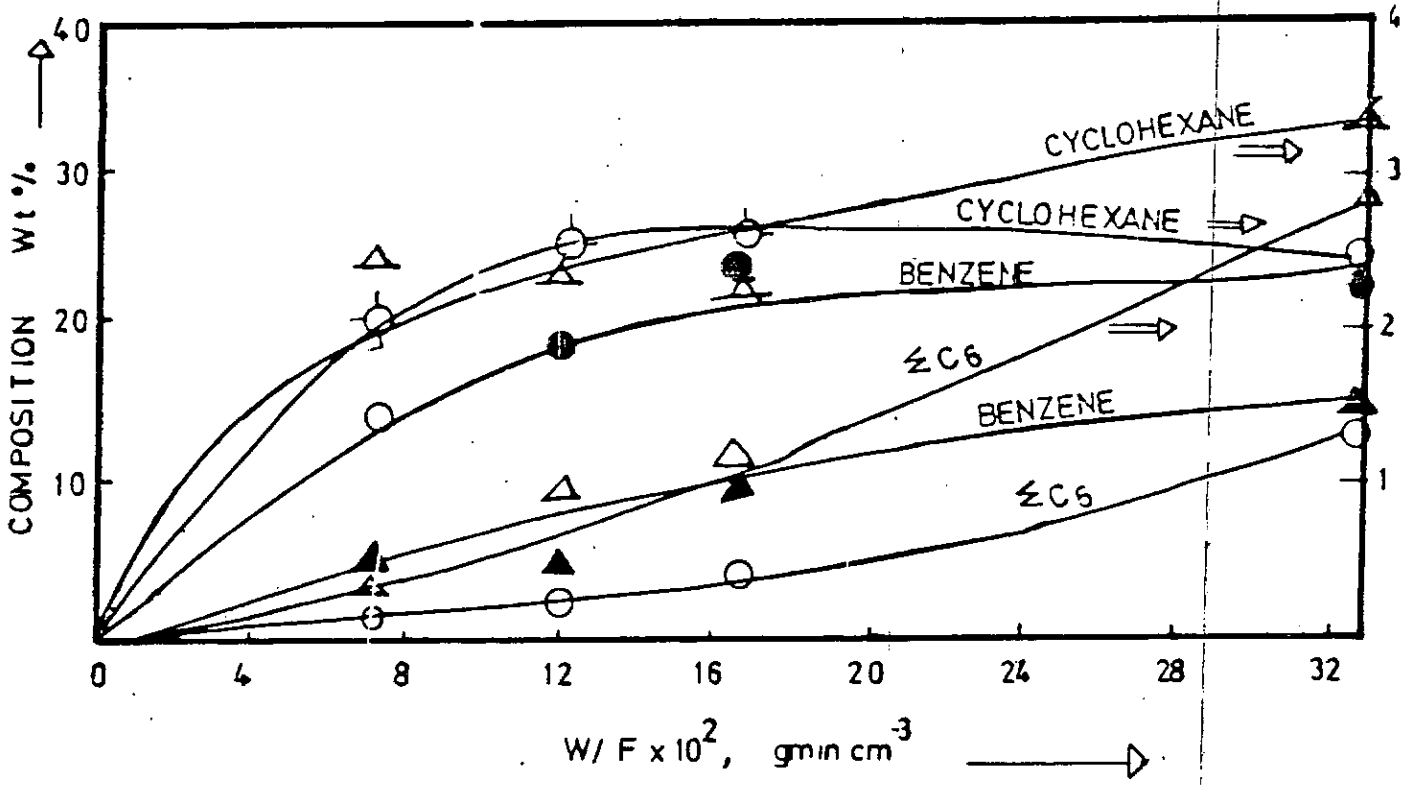

Fig. 5.1.47: Product composition of MCP conversion on $Pt\text{-}Re/Al_2O_3$ (UNDRIED) versus W/F at P_{MCP} = 9.2×10^{-2} atm in H_2 at 370° and 390°C.

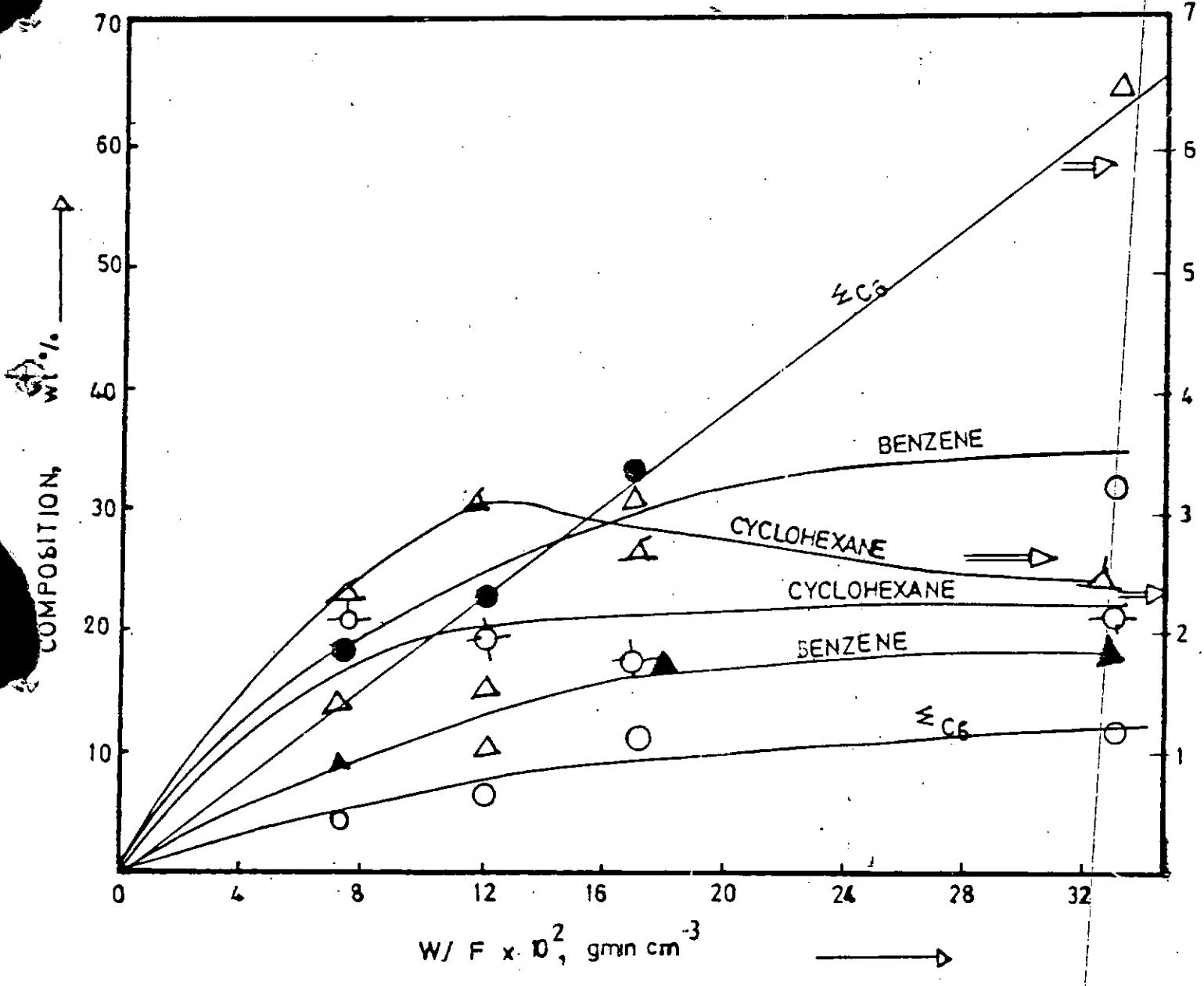

Fig.5.1.48: Product composition of MCP conversion on $Pt-Re/Al_2O_3$ (UNDRIED) versus W/F at P_{MCP} = 9.2×10^{-2} atm in H_2 at 380° and 400°C.

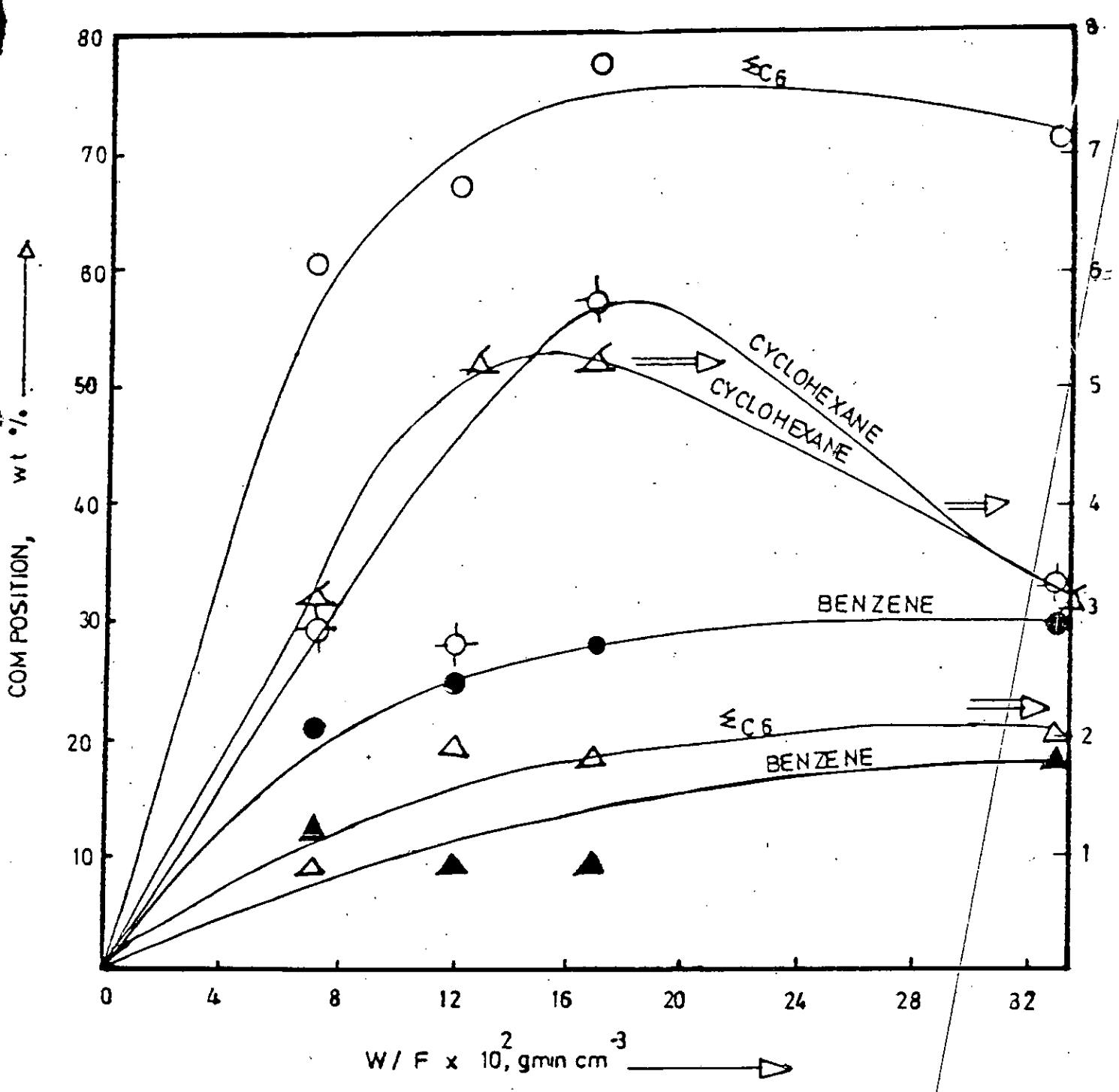

Fig. 5.1.49: Product composition of MCP conversion on Pt-Re/Al_2O_3 (UNDRIED) versus W/F at P_{MCP} = 14.47×10^{-2} atm in H_2 at 370° and 390°C

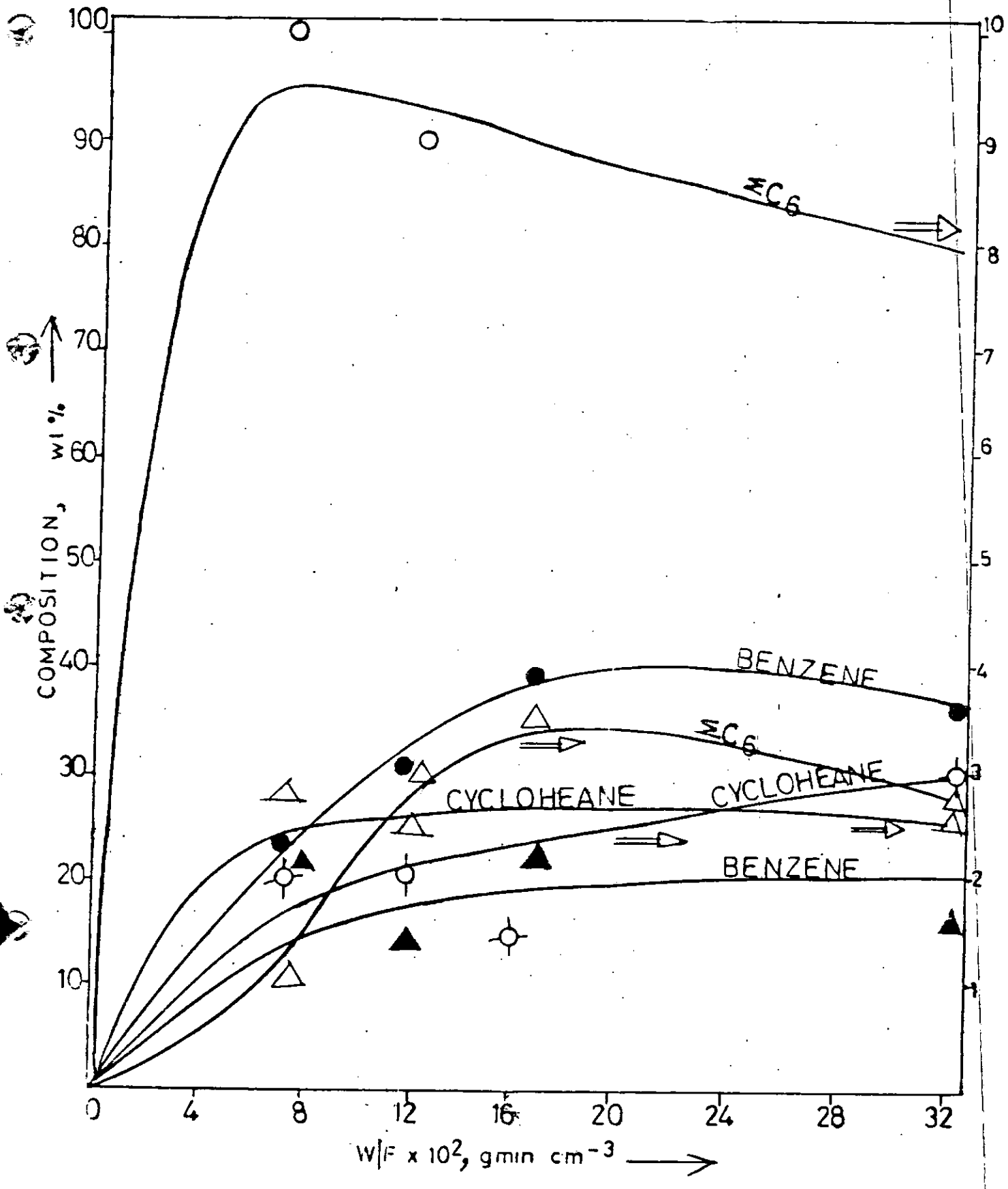

Fig. 5.1.50: Product composition of MCP conversion on Pt-Re/Al_2O_3 (UNDRIED) versus W/F at P_{MCP} = 14.47×10^{-2} atm in H_2 at 380° and 400°C

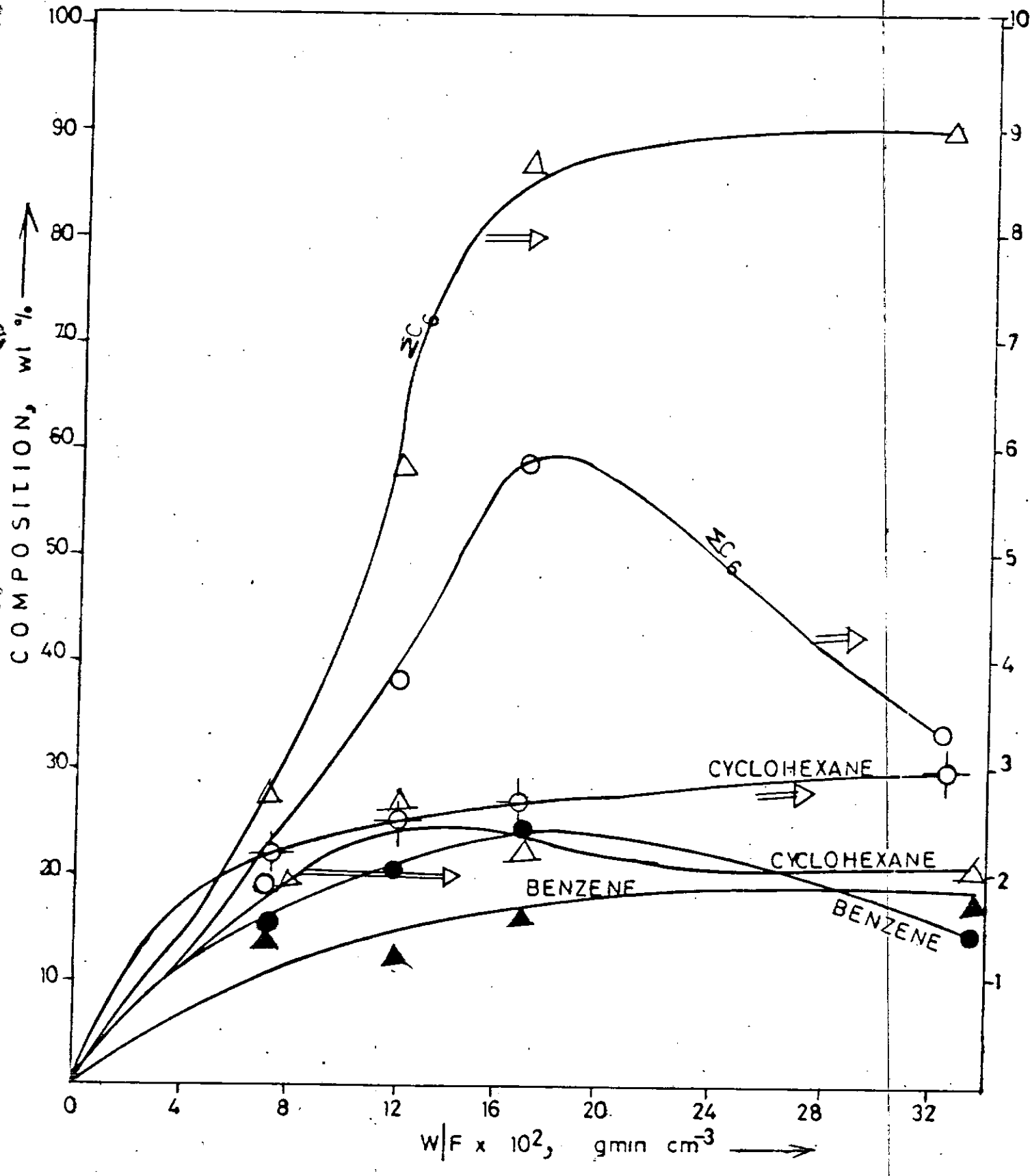

Fig.5.1.51: Product composition of MCP conversion on Pt-Re/Al_2O_3 (UNDRIED) versus W/F at P_{MCP} = 18.16×10^{-2} atm in H_2 at 370° and 390°C.

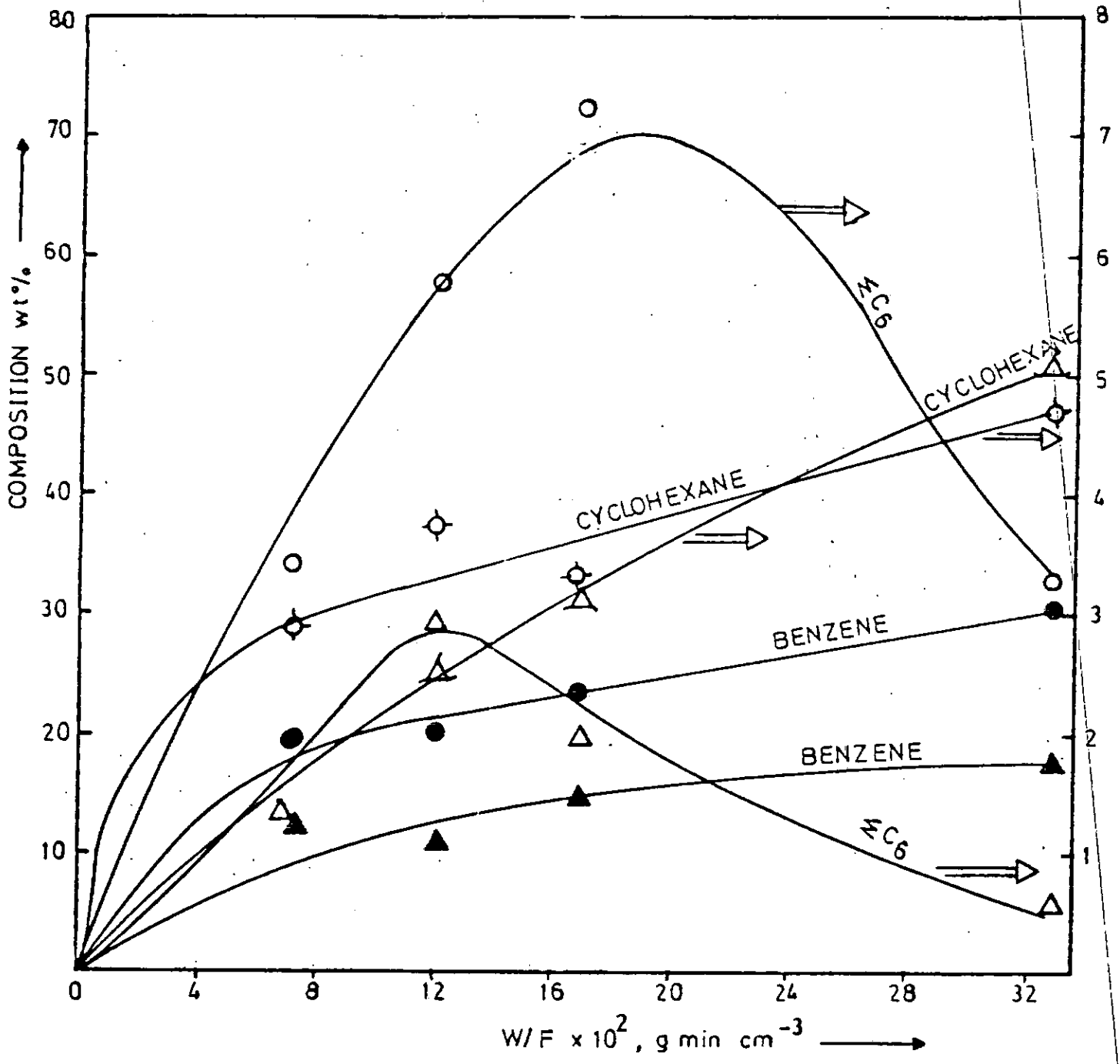

FIG.5.1.52: Product composition of MCP conversion on Pt-Re/Al_2O_3 (UNDRIED) versus W/F at P_{MCP}= 18.16x10^{-2} atm in H_2 at 380° and 400°C.

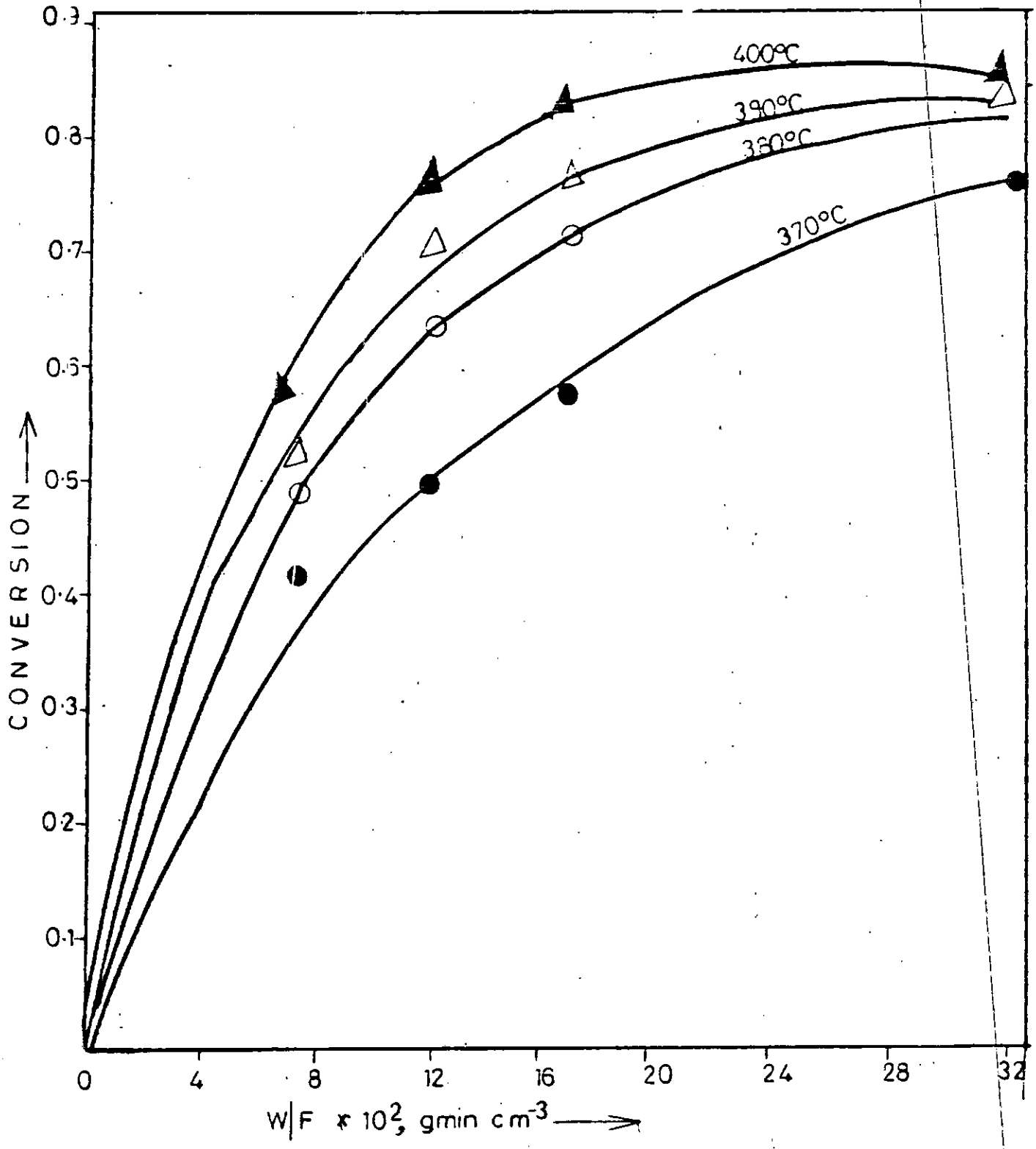

Fig.5.1.53: MCP conversion on Pt-Re/Al_2O_3(DRIED) versus W/F at P_{MCP}= 5.8×10^{-2}atm in H_2 and various temperatures.

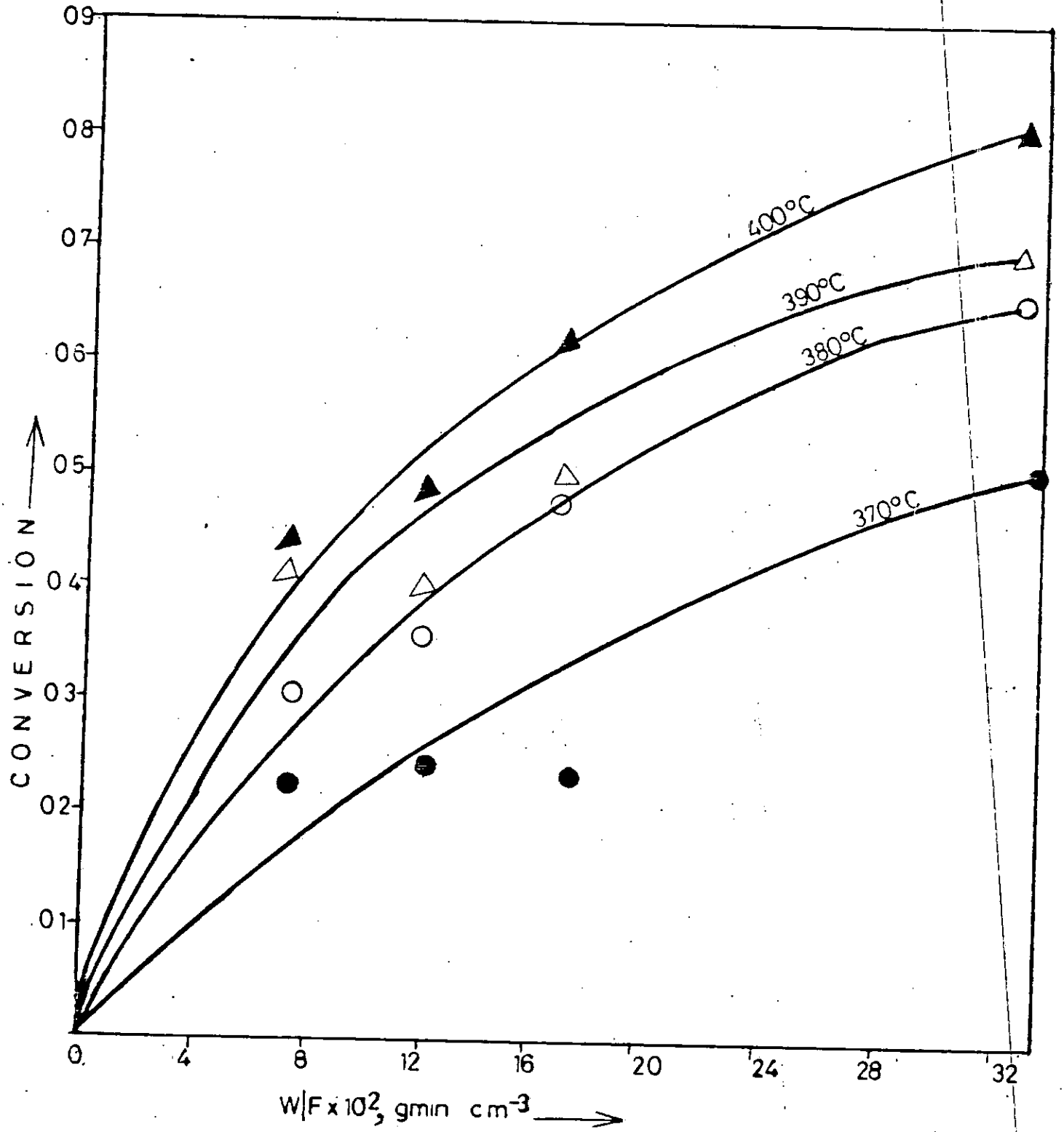

Fig.5.1.54: MCP conversion on Pt-Re/Al_2O_3 (DRIED) versus W/F at P_{MCP} = 9.2×10^{-2} atm in H_2 and various temperatures.

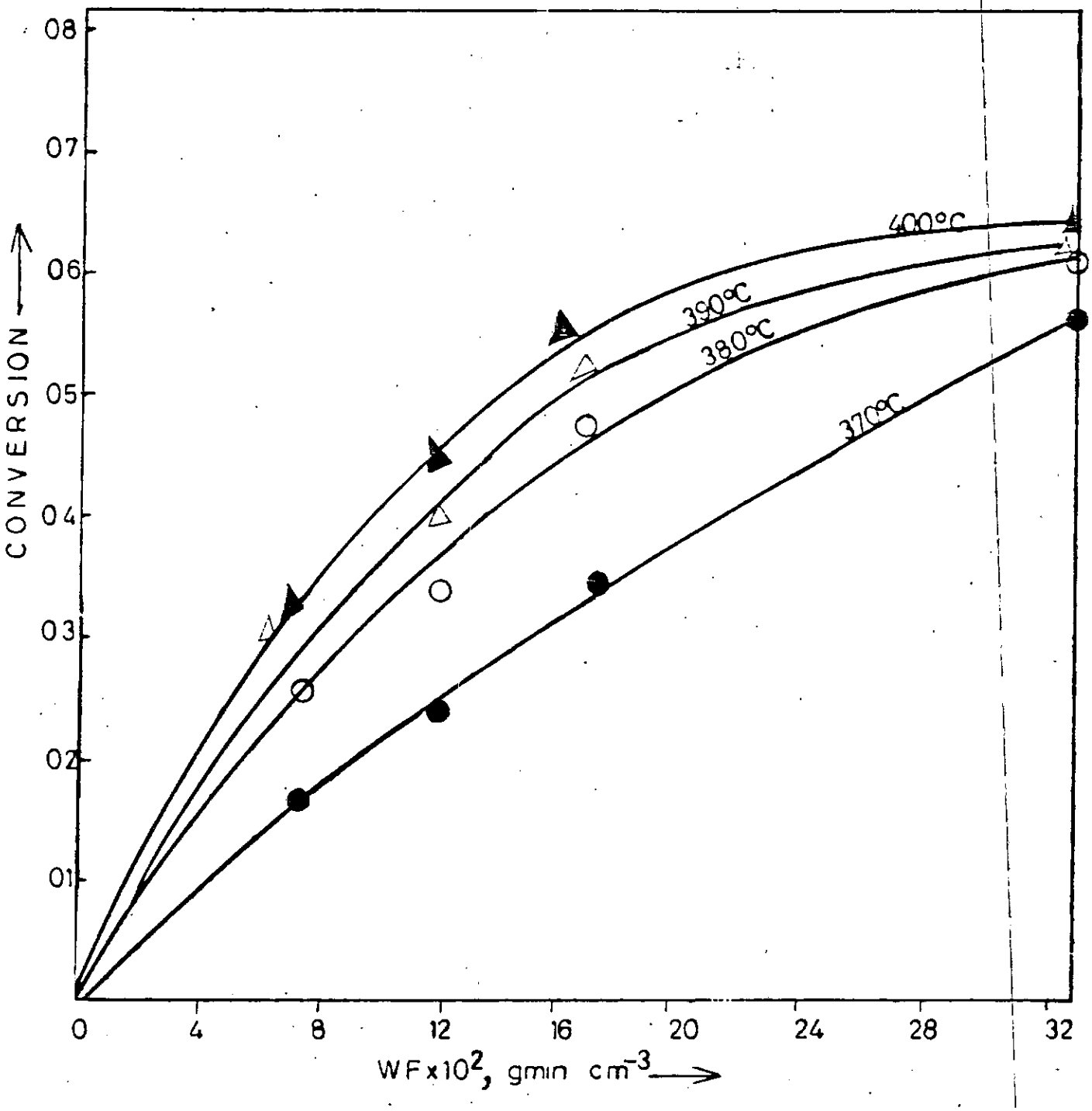

Fig.5.1.55: MCP conversion on Pt-Re/Al_2O_3(DRIED) versus W/F at P_{MCP} = 14.47x10^{-2}atm in H_2 and various temperatures.

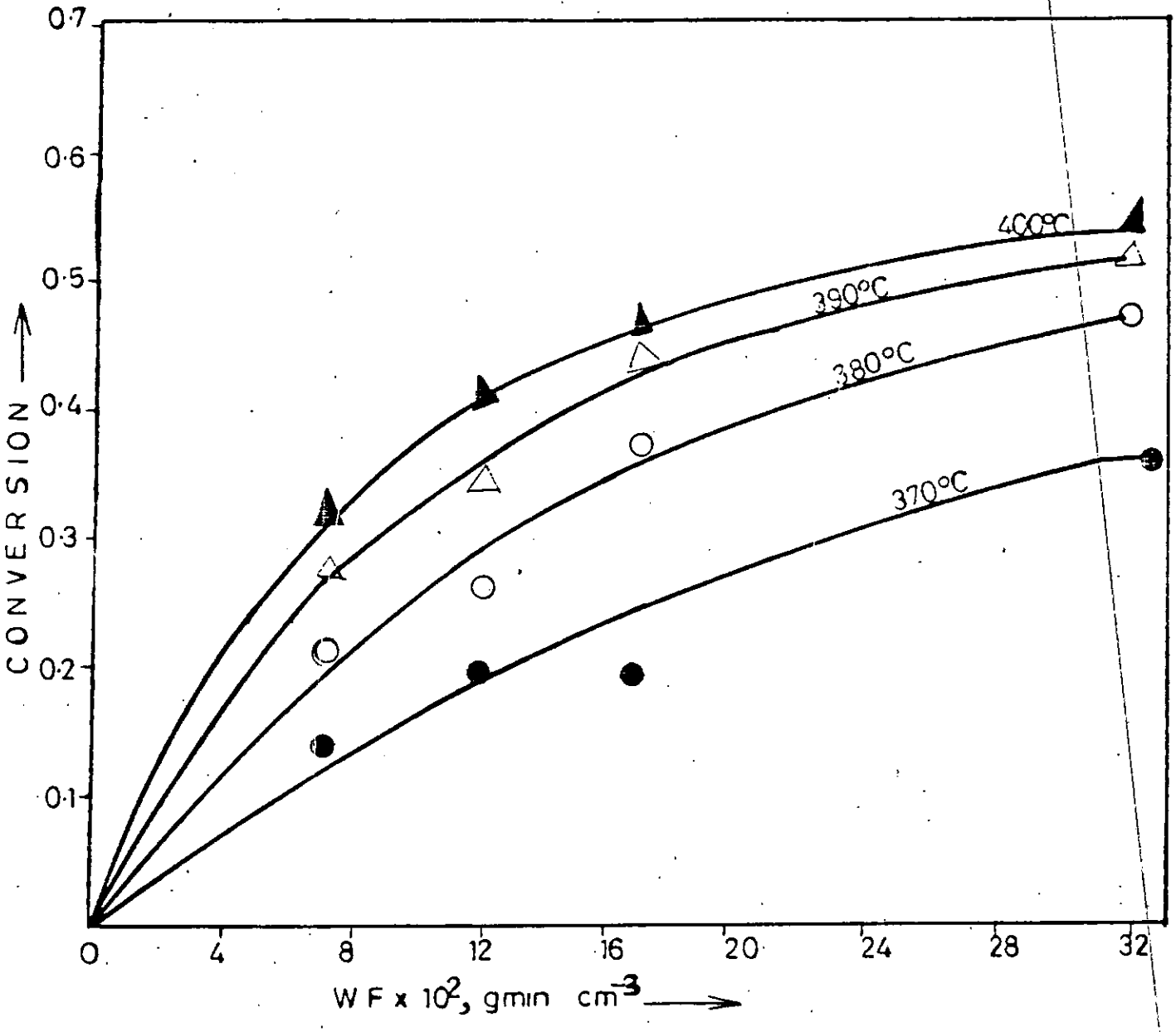

Fig. 5.1.56: MCP conversion on Pt-Re/Al_2O_3 (DRIED) versus W/F at P_{MCP} = 18.16×10^{-2} atm in H_2 and various temperatures.

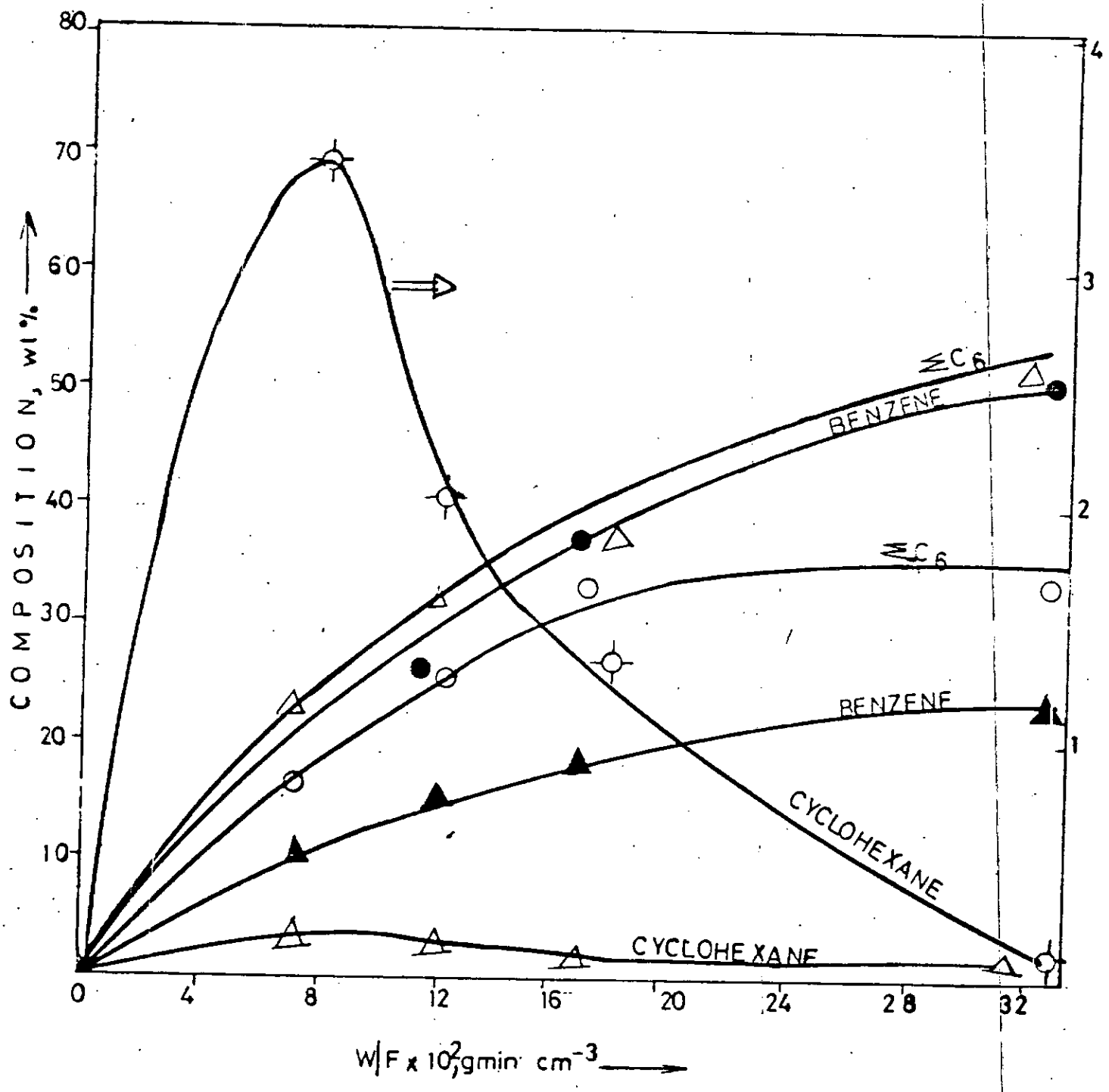

Fig 5.1.57: Product composition of MCP conversion on Pt-Re/Al_2O_3 (DRIED) versus W/F at $P_{MCP} = 5.8 \times 10^{-2}$ atm in H_2 at 370° and 390°C

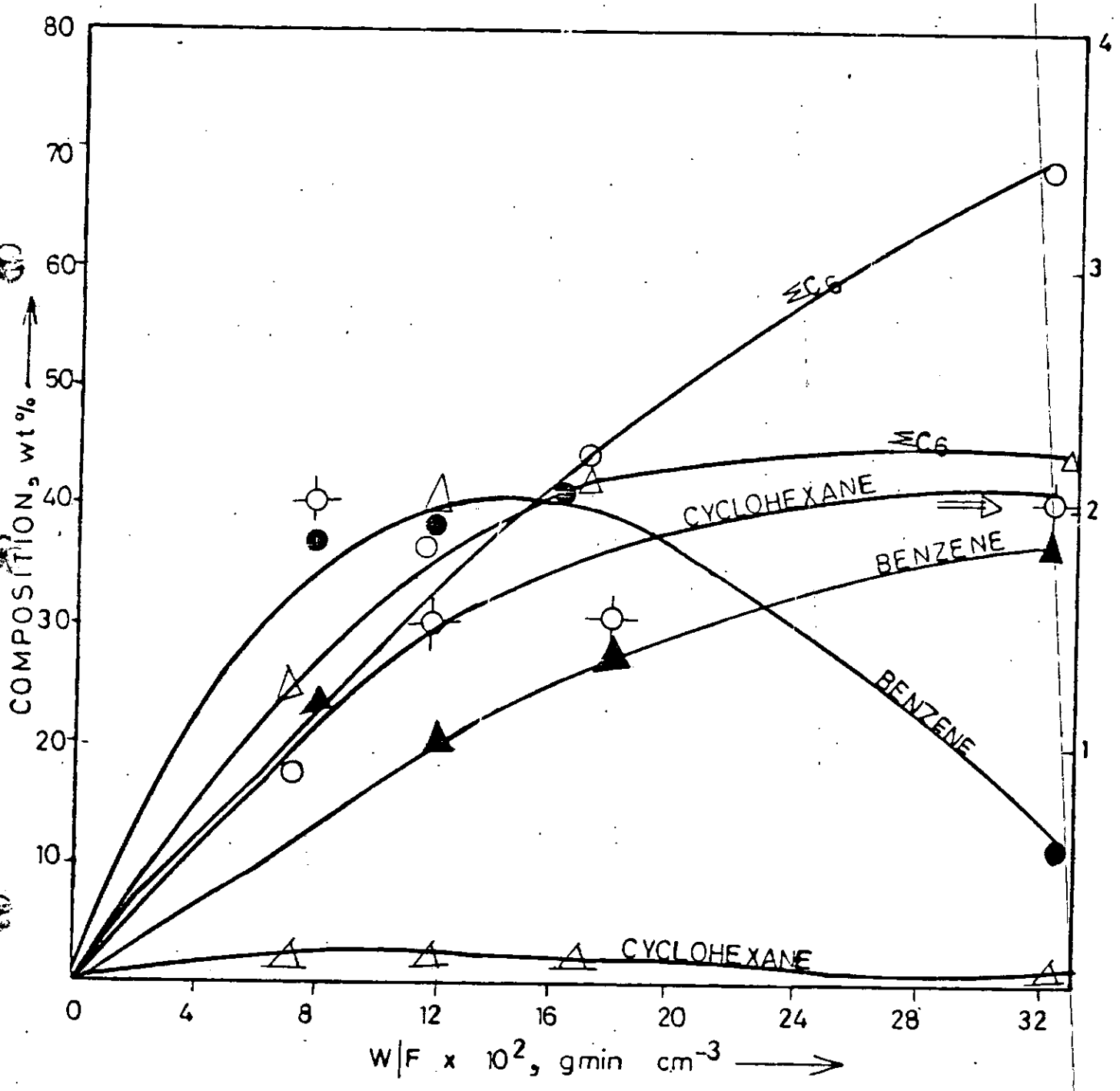

Fig.5.1.58: Product composition of MCP conversion on Pt-Re/Al_2O_3 (DRIED) versus W/F at P_{MCP}= 5.8×10^{-2}atm in H_2 at 380° and 400°C.

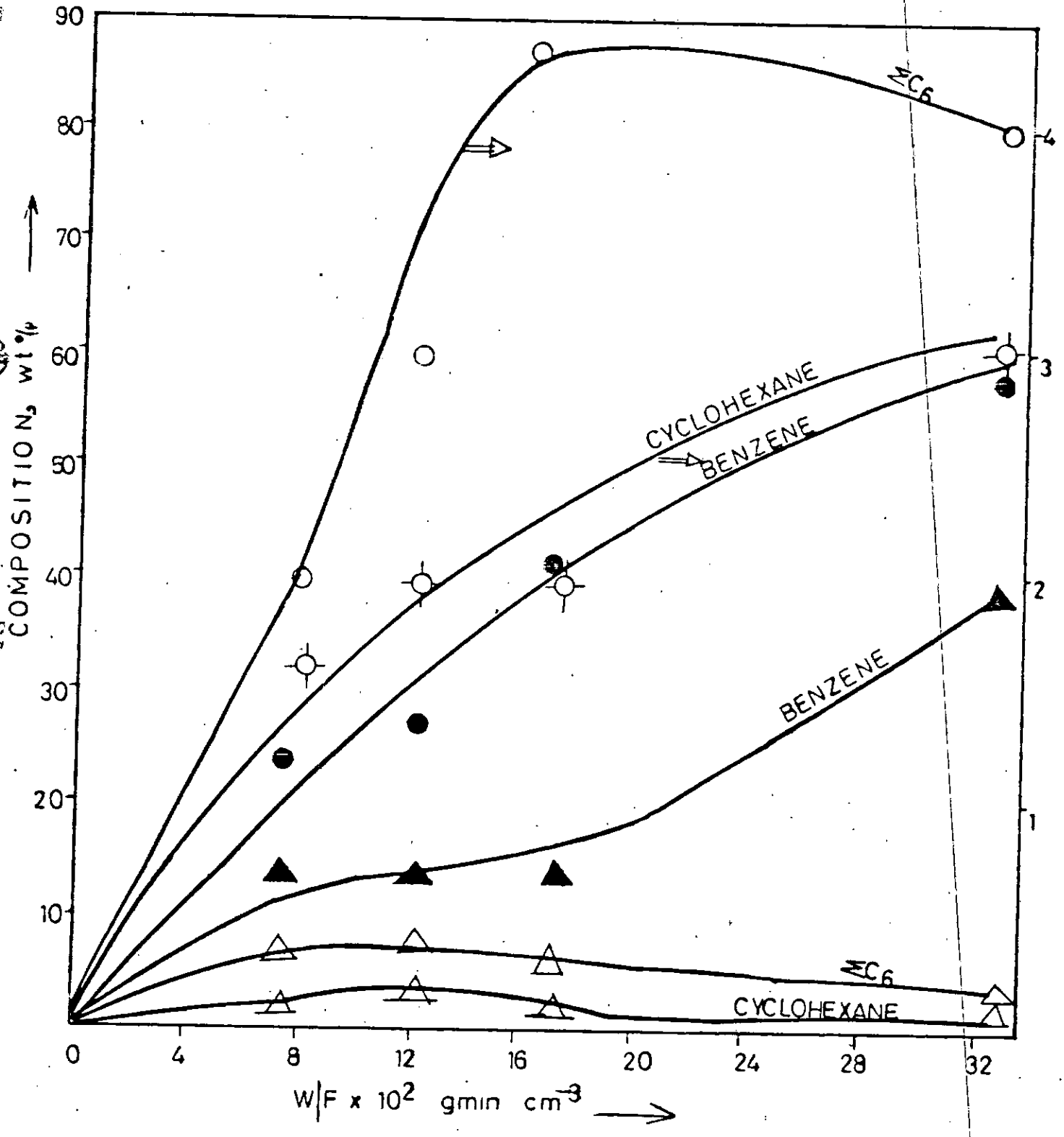

Fig.5.1.59: Product-composition of MCP conversion on Pt-Re/Al_2O_3 (DRIED) versus W/F at P_{MCP}= 9.2×10^{-2}atm in H_2 at 370° and 390°C.

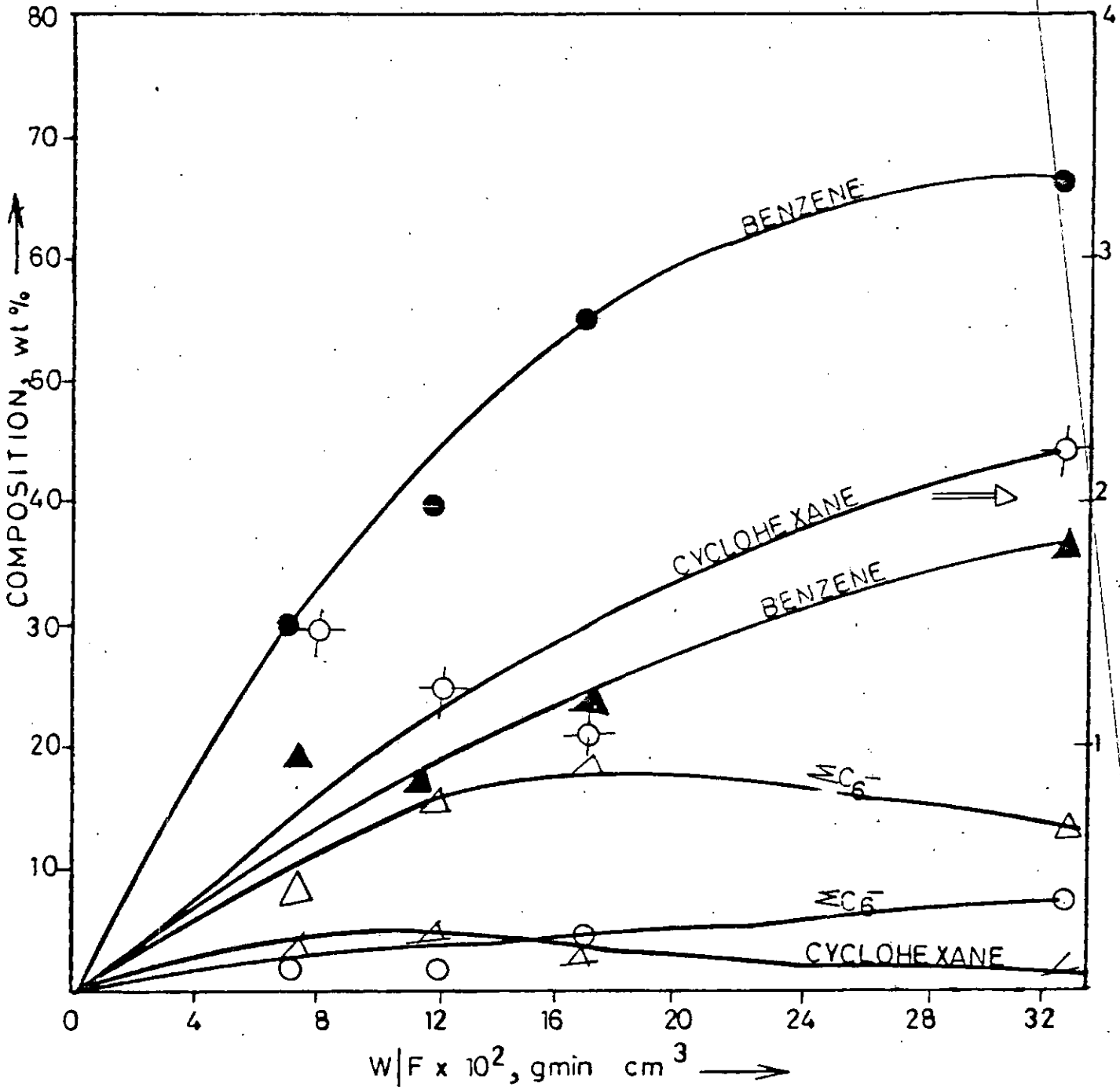

Fig.5.1.60: Product composition of MCP conversion on Pt-Re/Al_2O_3 (DRIED) versus W/F at P_{MCP}= 9.2×10^{-2}atm in H_2 at 380° and 400°C.

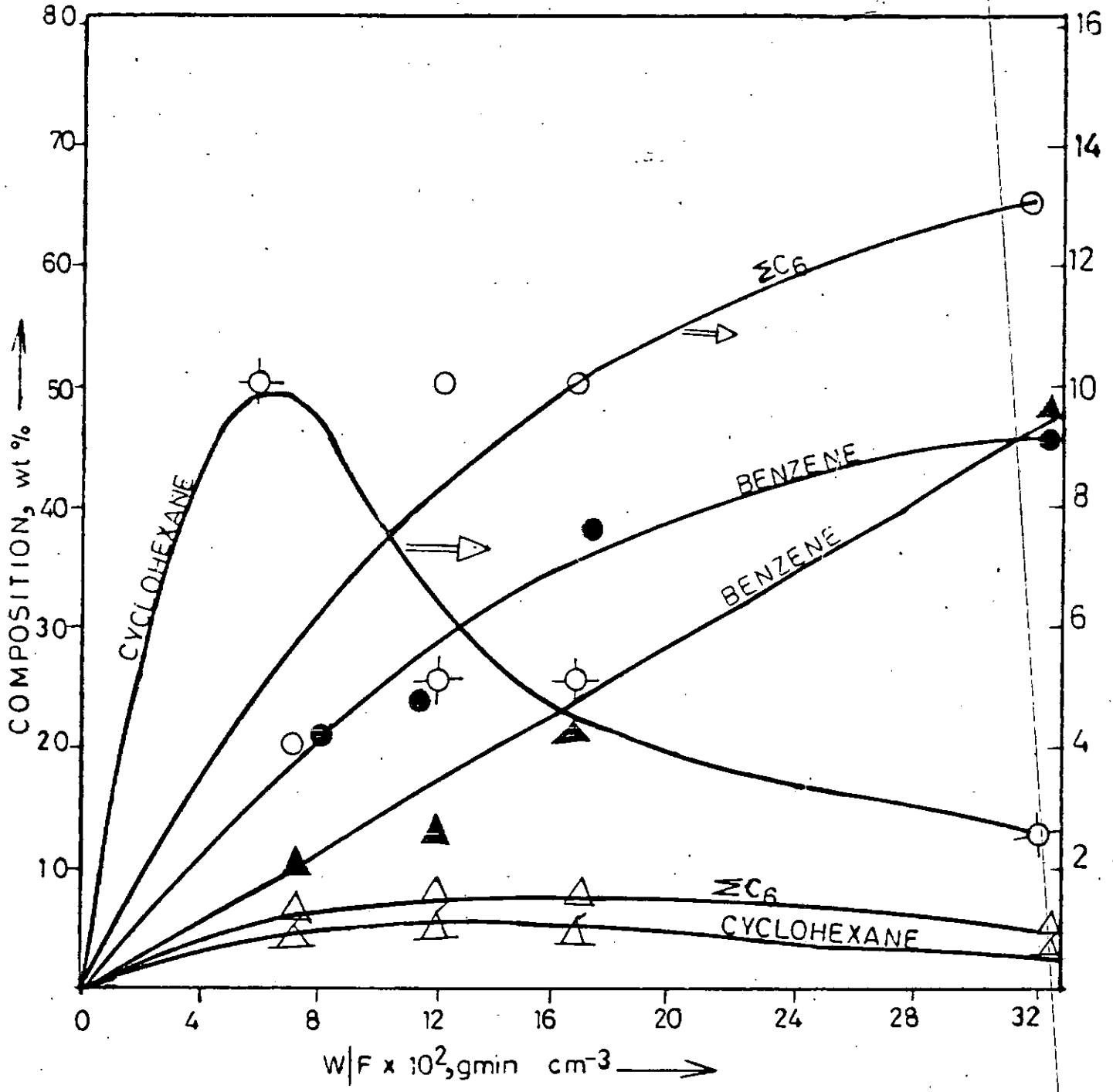

Fig.5.1.61: Product composition of MCP conversion on Pt-Re/Al_2O_3 (DRIED) versus W/F at P_{MCP}=14.47x10^{-2}atm in H_2 at 370° and 390°C.

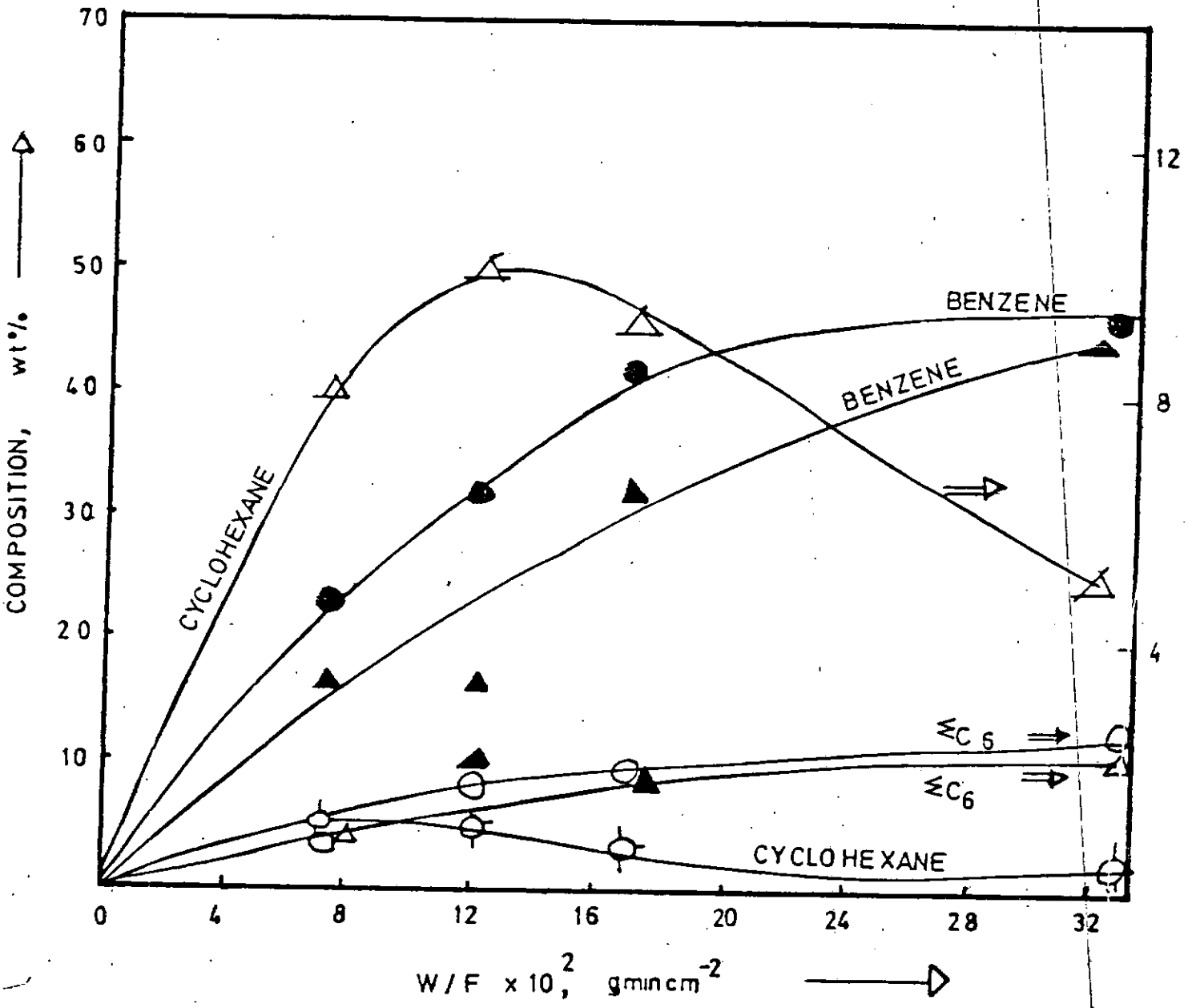

Fig.5.1.62: Product composition of MCP conversion on Pt-Re/Al_2O_3 (DRIED) versus W/F at $P_{MCP}=14.47\times10^{-2}$atm in H_2 at 380° and 400°C.

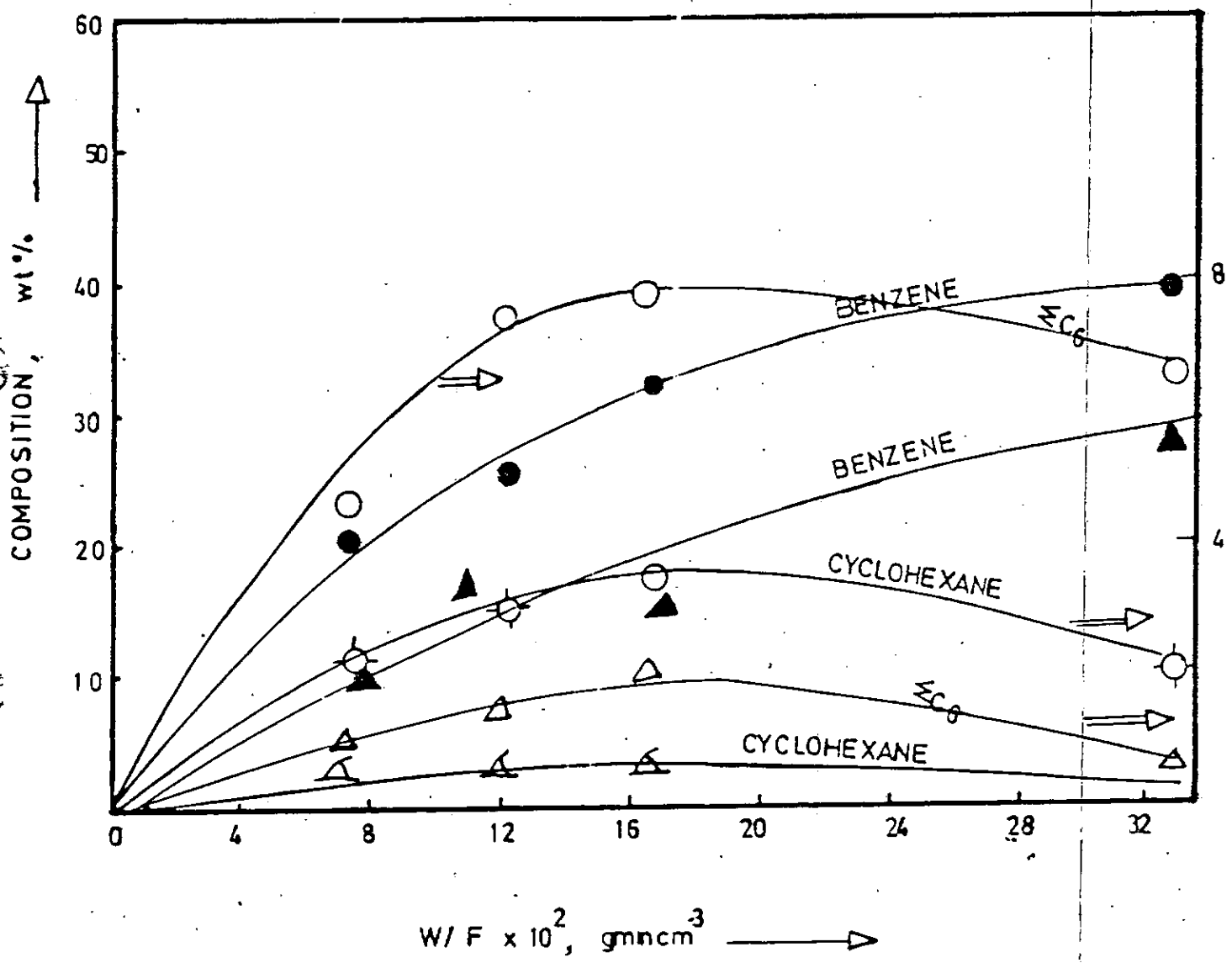

Fig.5.1.63: Product composition of MCP conversion on Pt-Re/Al_2O_3 (DRIED) versus W/F at P_{MCP}= 18.16×10^{-2}atm in H_2 at 370° and 390°C.

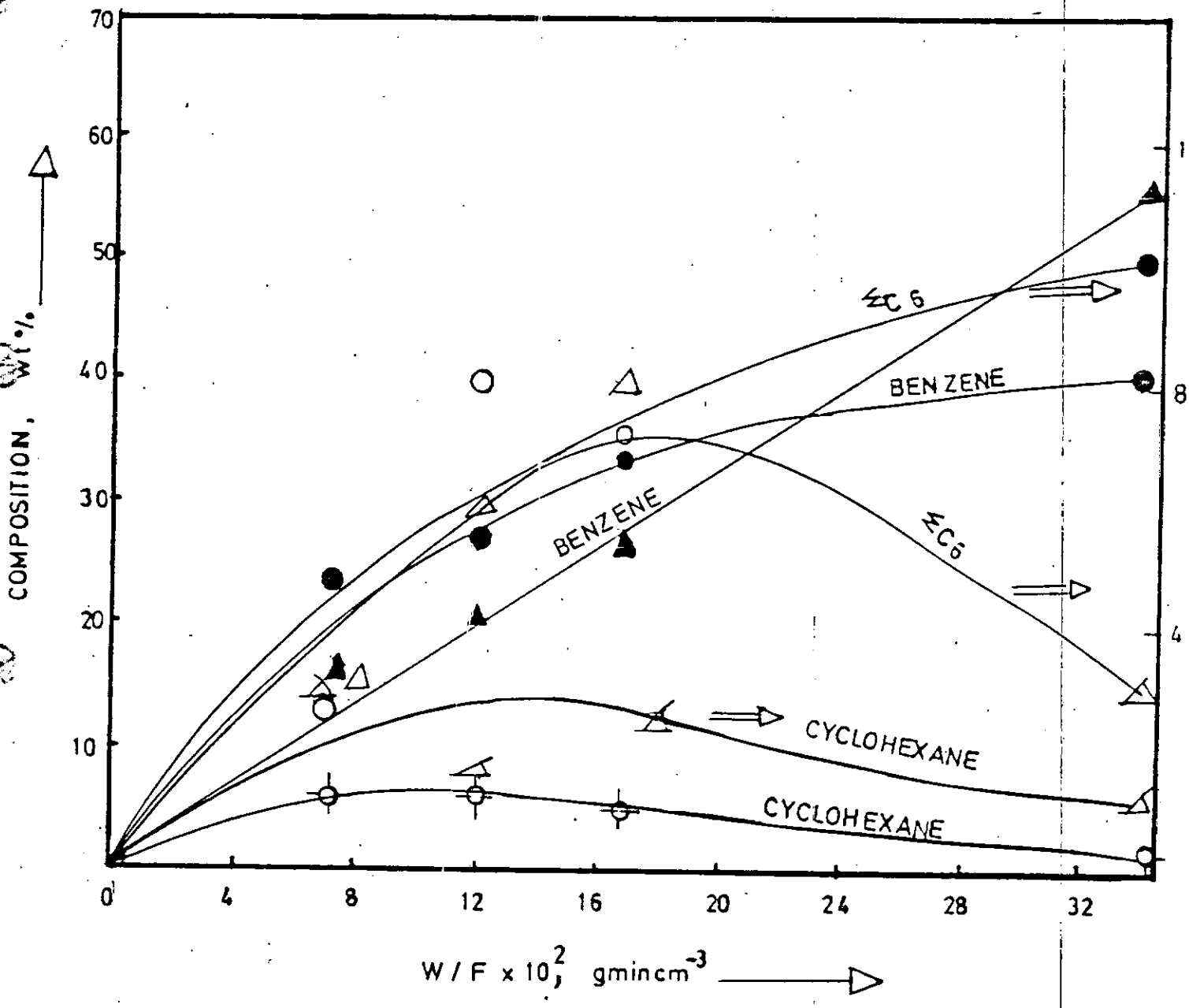

Fig.5.1.64: Product composition of MCP conversion on Pt-Re/Al_2O_3 (DRIED) versus W/F at $P_{MCP}=18.16\times10^{-2}$atm in H_2 at 380° and 400°C.

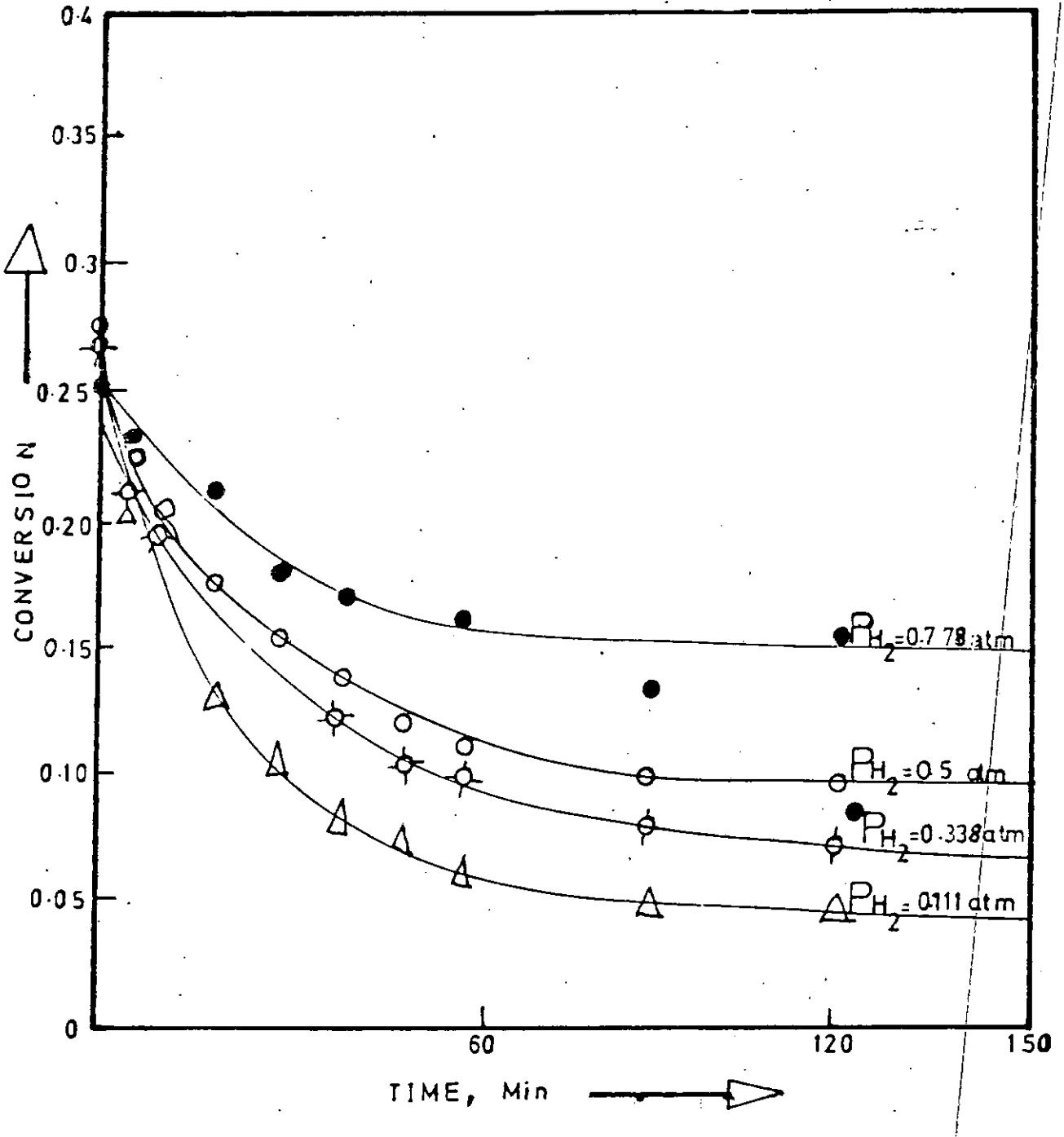

Fig.5.2.1 : Iso-octane conversion on 0.3%Pt/Al_2O_3 versus time at P_{iso}=3.. 6x10^{-2}atm; W/F = 0.11gmincm^{-3}, temperature = 390°C and various P_{H_2} .

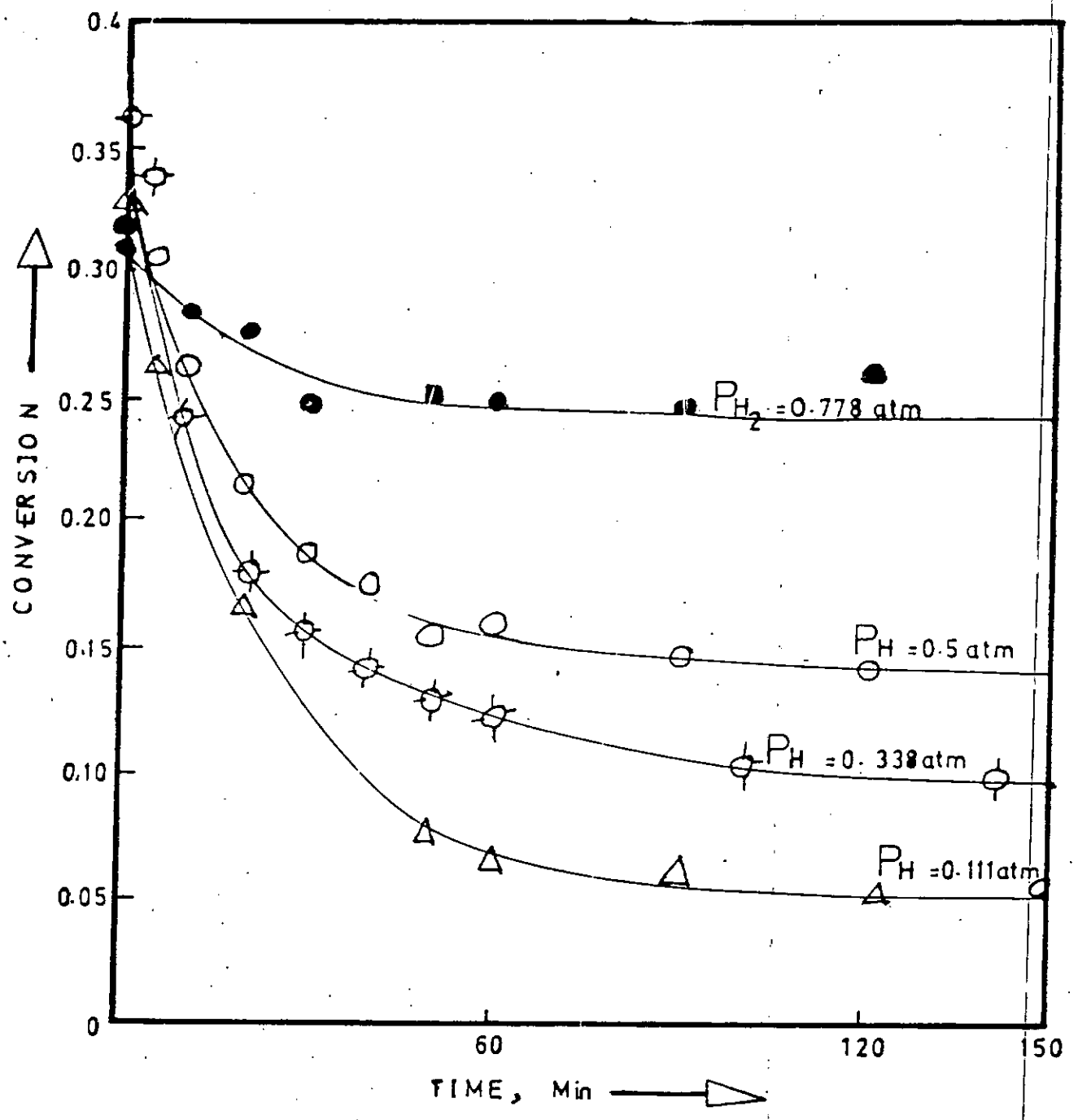

Fig.5.2.2 Iso-octane conversion on 0.3%Pt/Al_2O_3 versus time at $P_{iso}=3.16\times10^{-2}$atm; W/F = 0.11gmincm^{-3}; temperature = 410°C and various P_{H_2}

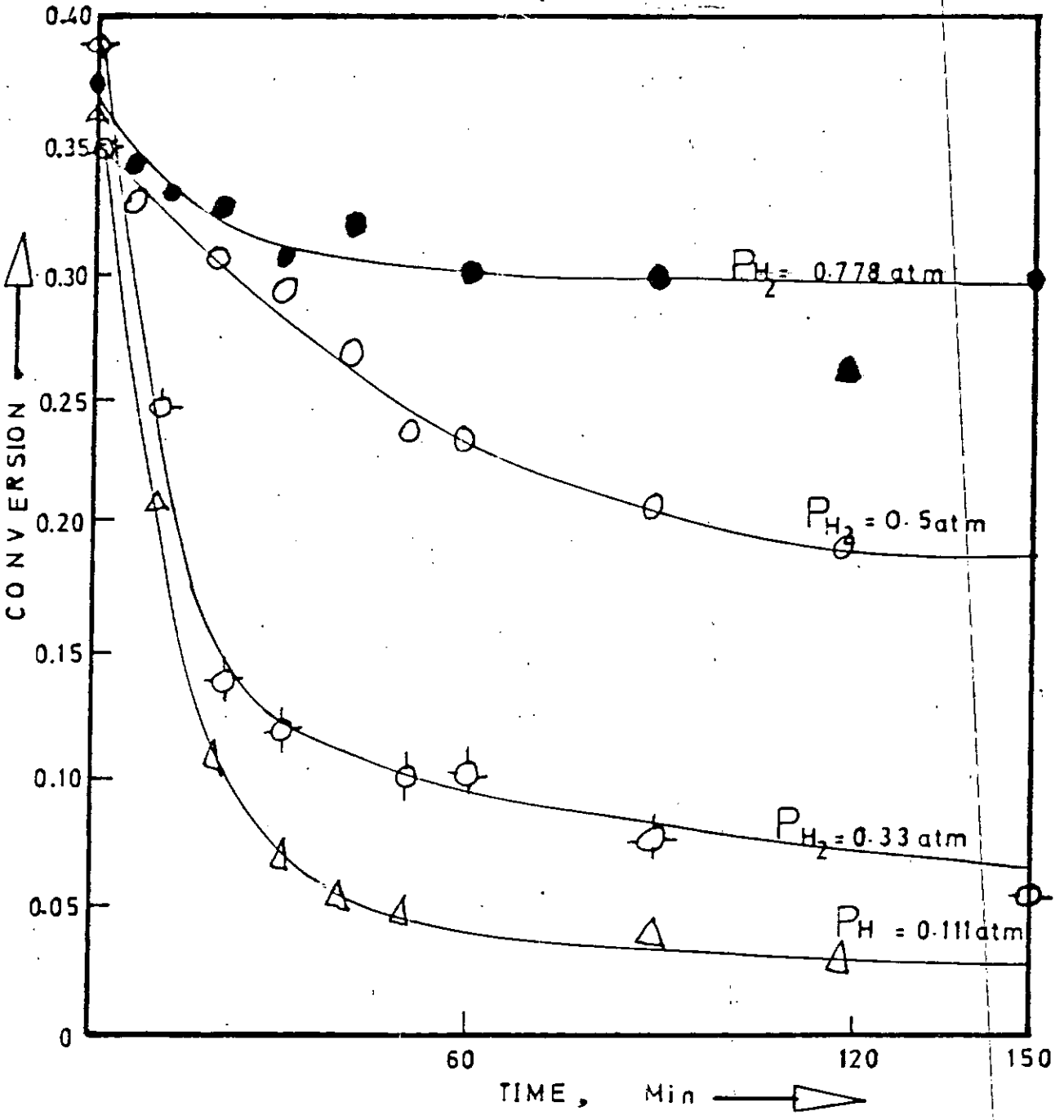

Fig.5.2.3 :Iso-octane conversion on 0.3%Pt/Al_2O_3 versus time at $P_{iso}=3.16\times10^{-2}$atm, W/F = 0.11gmincm^{-3}, temperature = 430°C and various P_{H_2}.

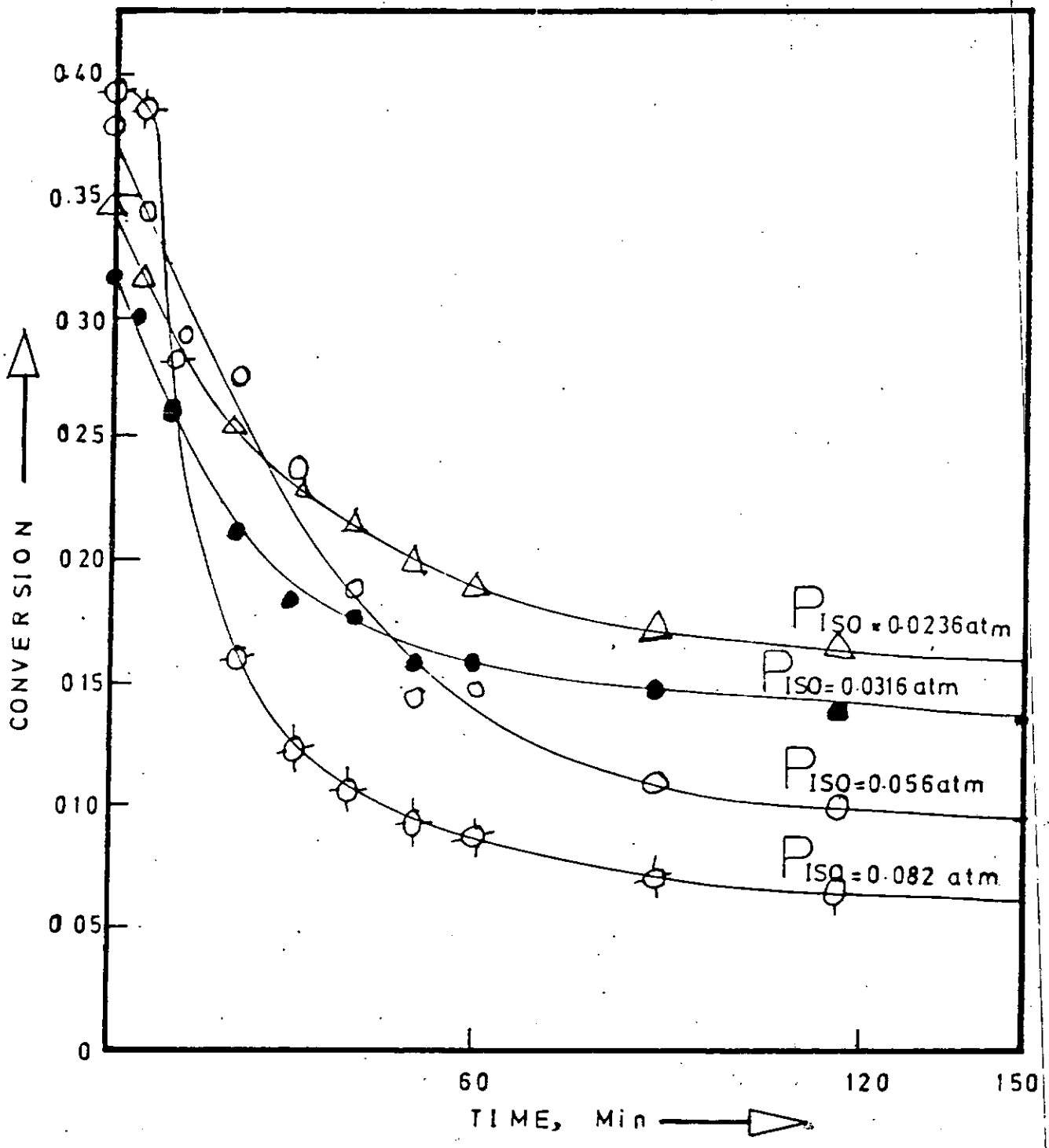

Fig. 5.2.4: Iso-octane conversion on 0.3%Pt/Al_2O_3 versus time at P_{H_2} = 0.5atm; W/F = 0.11gmincm^{-3}; temperature = 410°C and various P_{iso} .

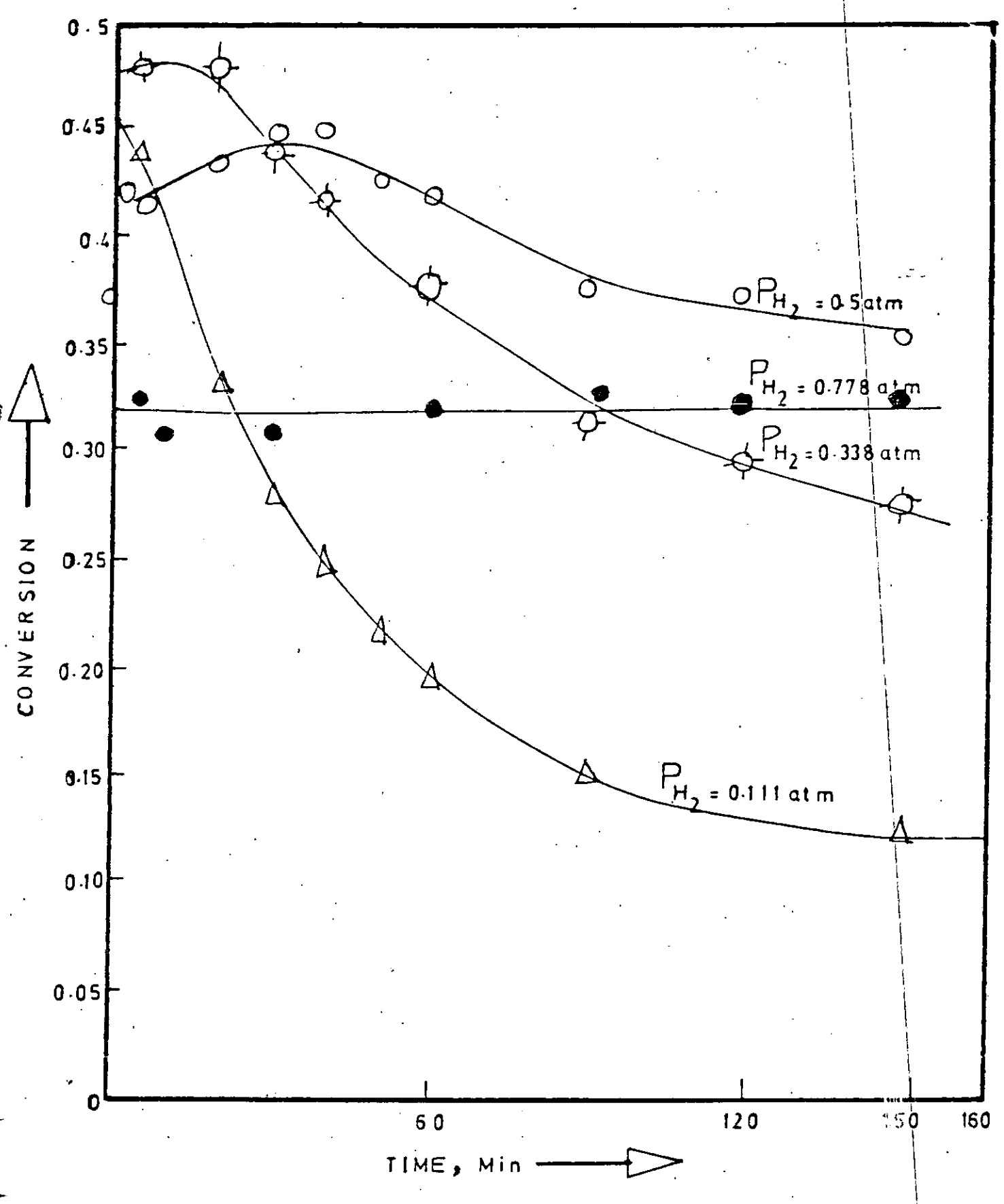

Fig.5.2.5: Iso-octane conversion on 0.6%Pt/Al_2O_3 versus time at P_{iso} = 3.16×10^{-2} atm; W/F = 0.11 gmin cm^{-3}; temperature = 390°C and various P_{H_2}

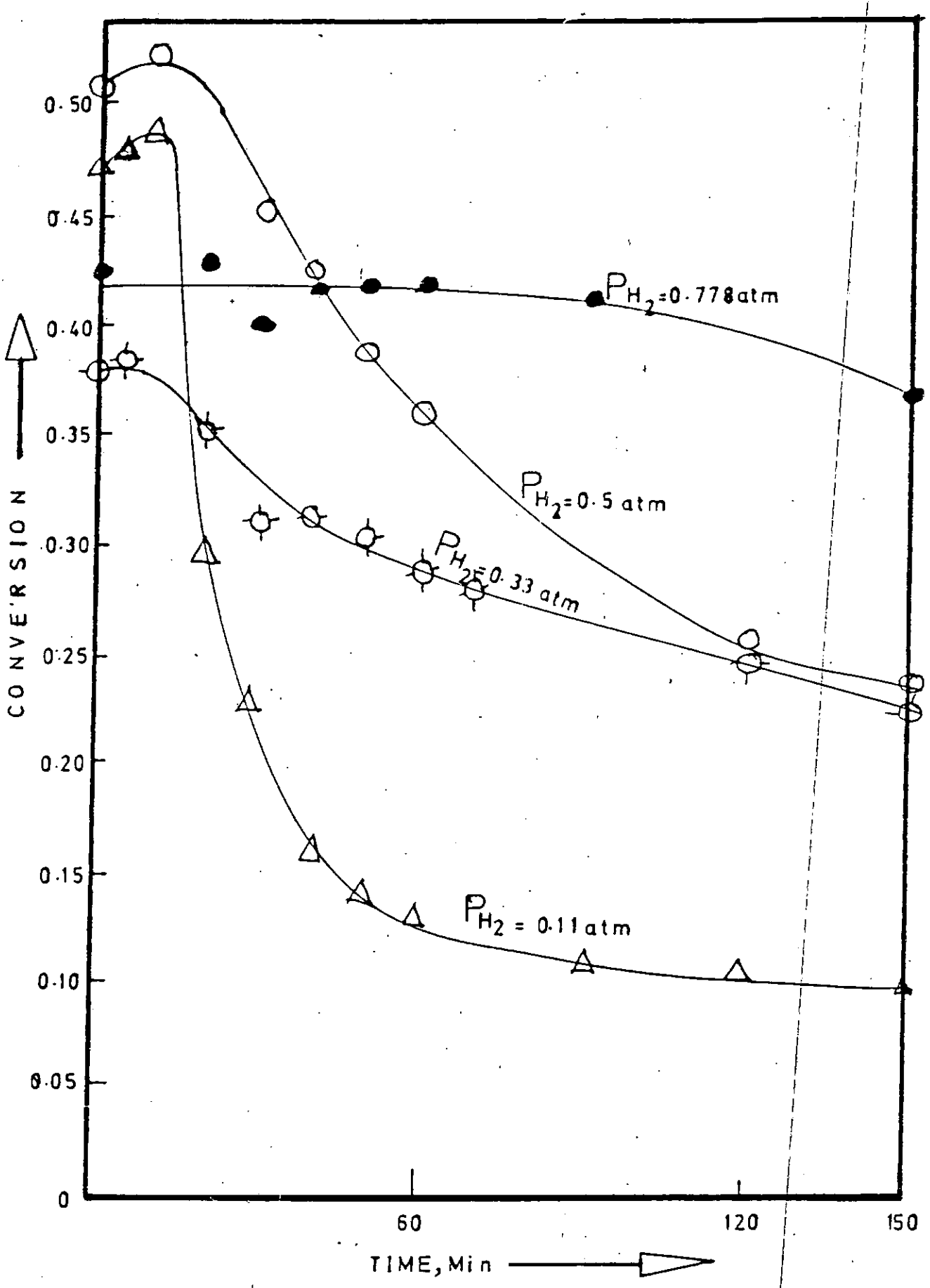

Fig.5.2.6: Iso-octane conversion on 0.6%Pt/Al_2O_3 versus time at P_{iso} = 3.16×10^{-2}atm; W/F = 0.11gmincm^{-2}; temperature = 410°C and various P_{H_2}

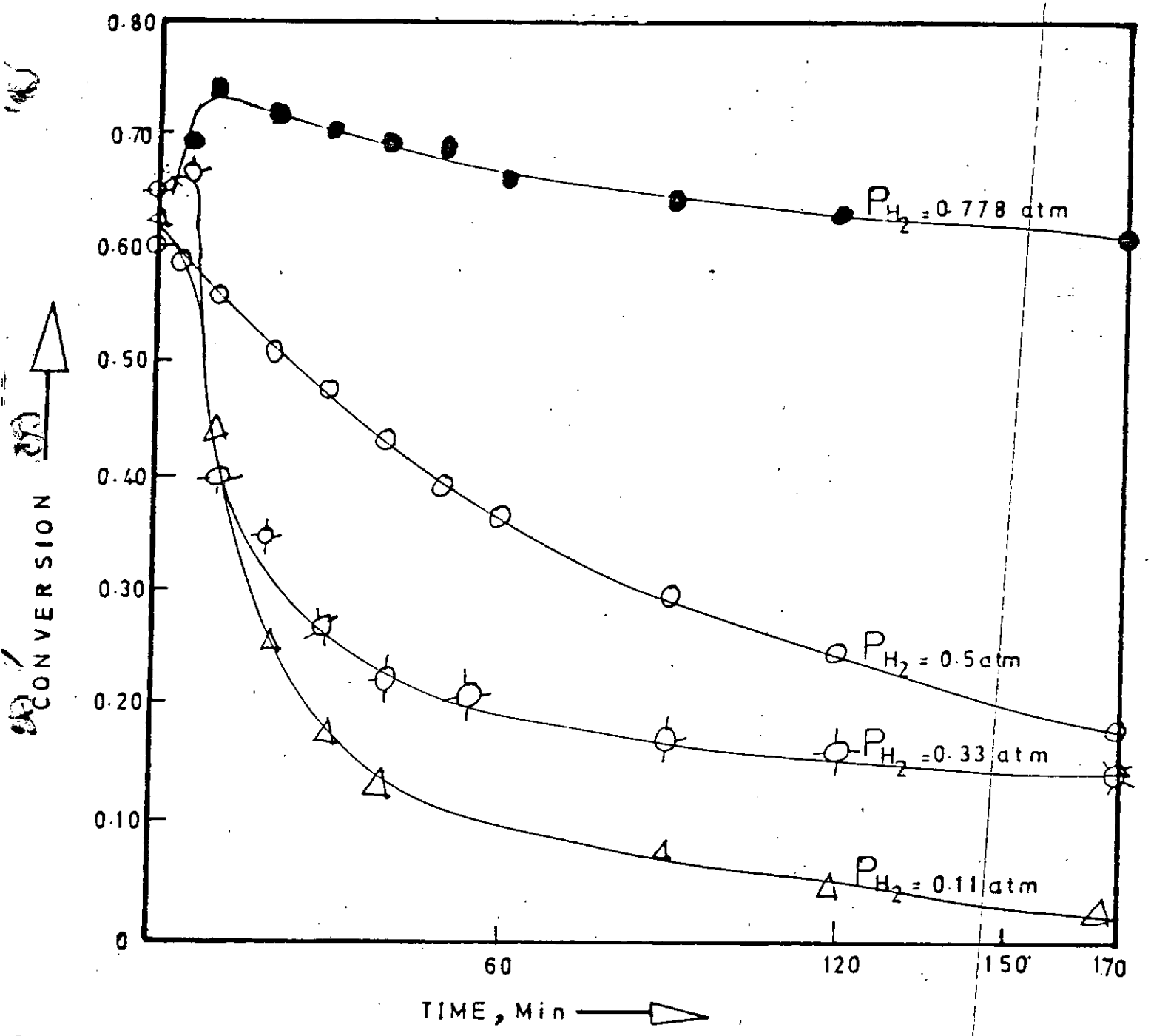

Fig.5.2.7: Iso-octane conversion on 0.6%Pt/Al_2O_3 versus time at P_{iso} = 3.16×10^{-2} atm; W/F = 0.11gmincm^{-3}, temperature = 430°C and various P_{H_2}

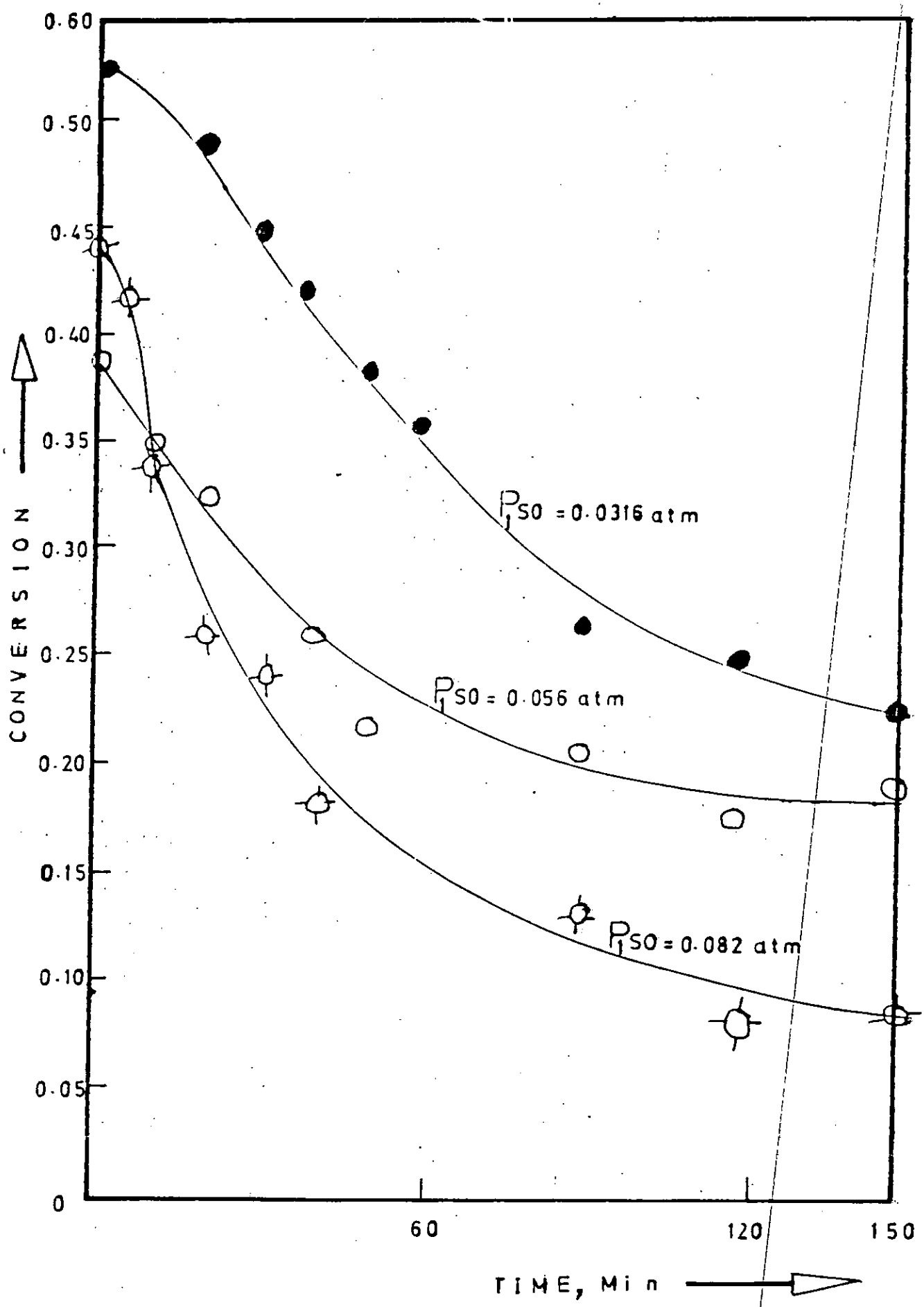

Fig.5.2.8: Iso-octane conversion on 0.3%Pt/Al_2O_3 versus time at P_{H_2} = 0.5atm;W/F= 0.11gmincm^{-3}; temperature = 410°C and various P_{iso}

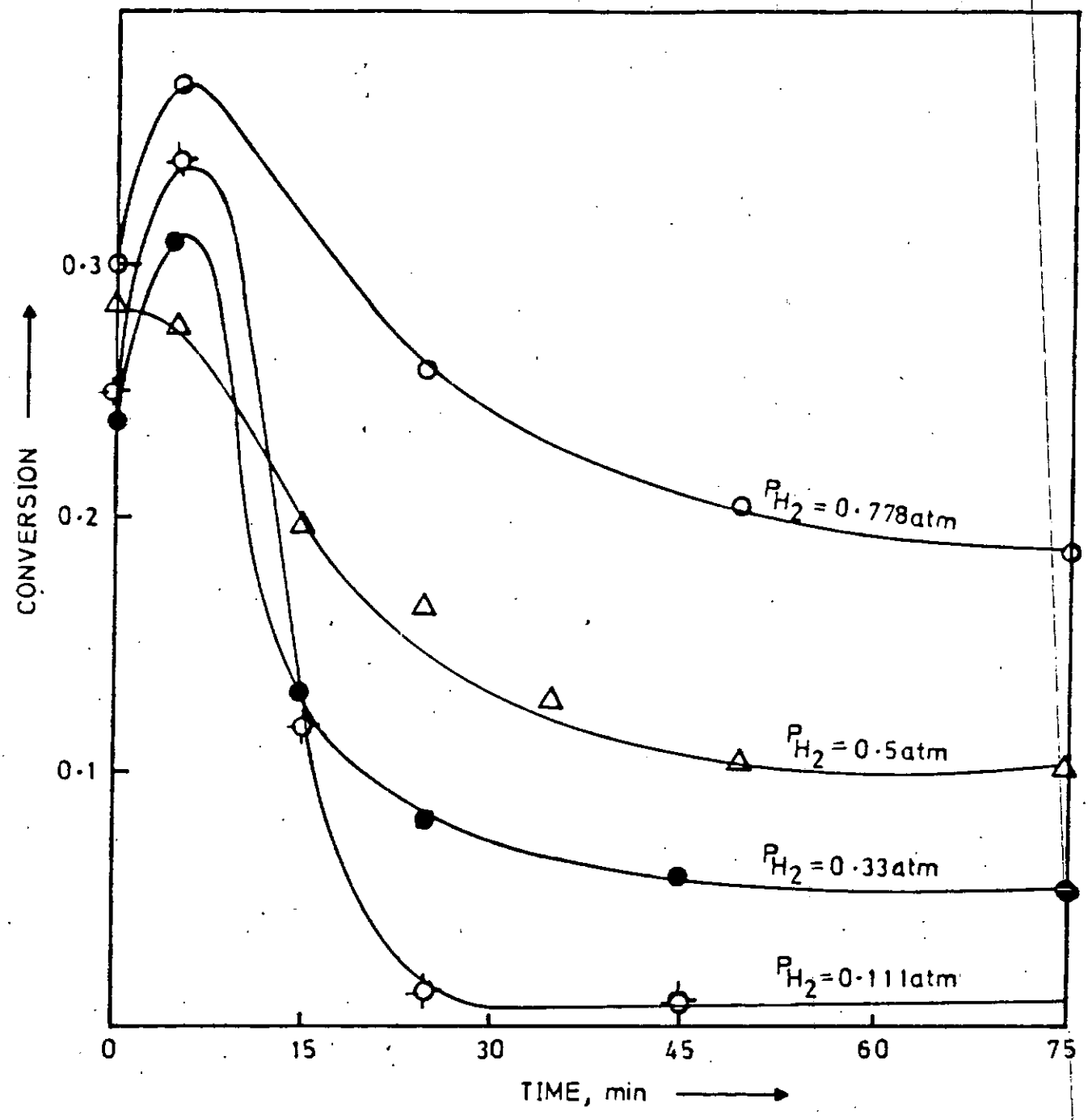

Fig.5.2.9: MCP conversion on Pt/Al_2O_3 versus time at $P_{MCP} = 9.2 \times 10^{-2}$ atm; W/F = 0.11gmincm^{-3}; temperature = 390°C and various P_{H_2}.

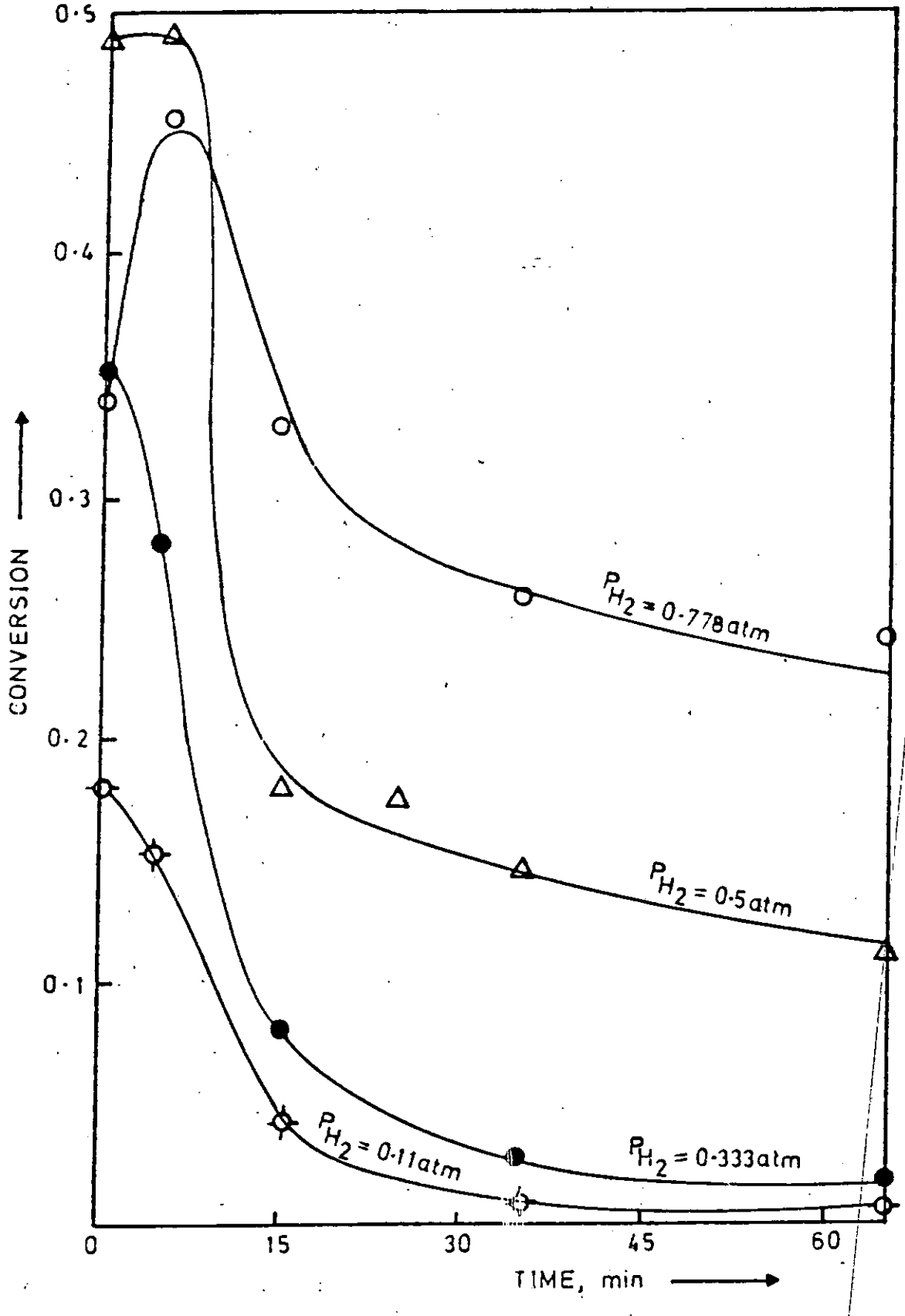

Fig.5.2.10: MCP conversion on Pt/Al_2O_3 versus time at $P_{MCP} = 9.2 \times 10^{-2}$atm, W/F = 0.11gminc$m^{-3}$; temperature = 400°C and various P_{H_2}.

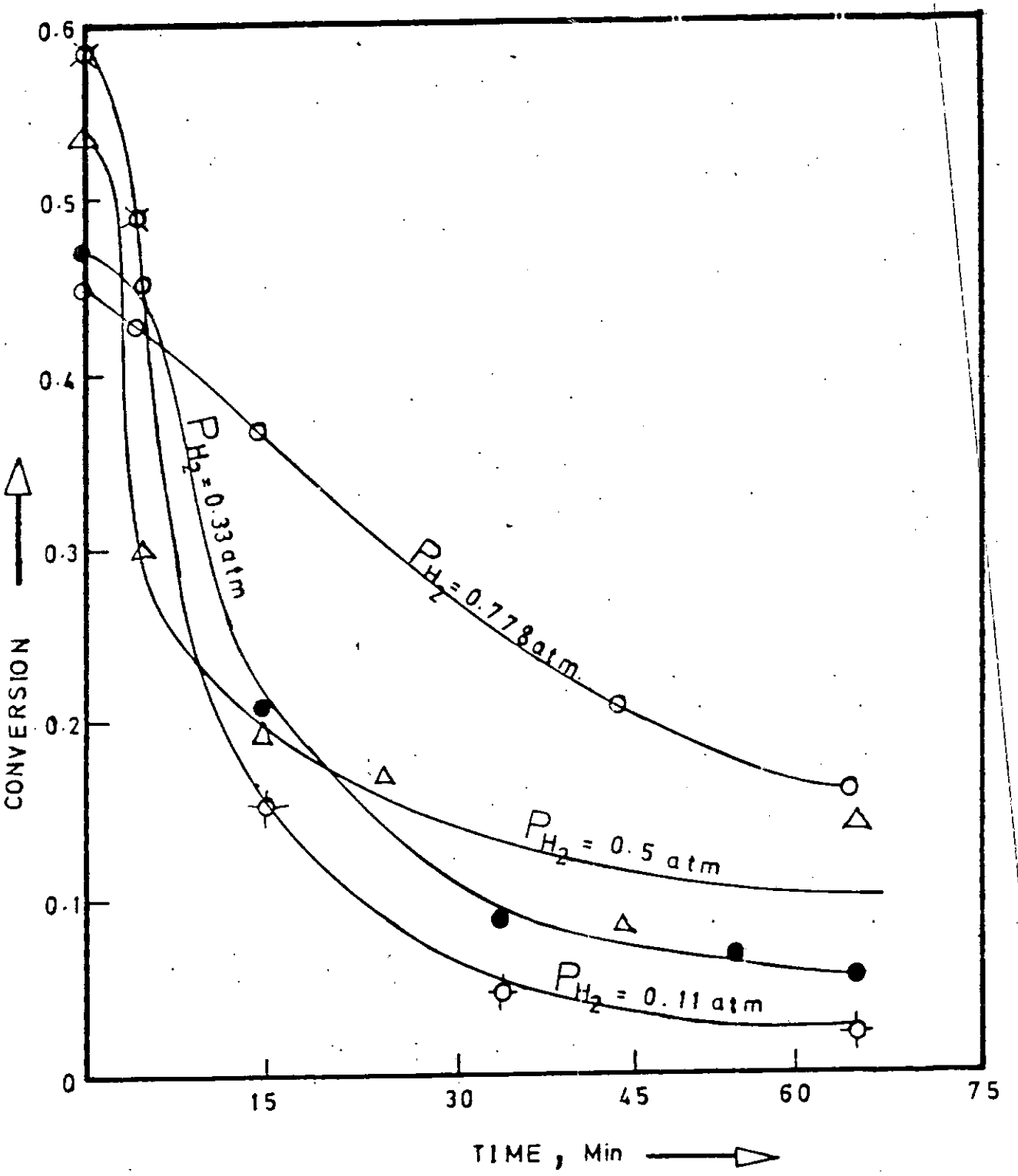

Fig.5.2.11: MCP conversion on Pt/Al_2O_3 versus time at $P_{MCP} = 9.2 \times 10^{-2}$ atm; $W/F = 0.11 g\,min\,cm^{-3}$; temperature = 410°C and various P_{H_2}

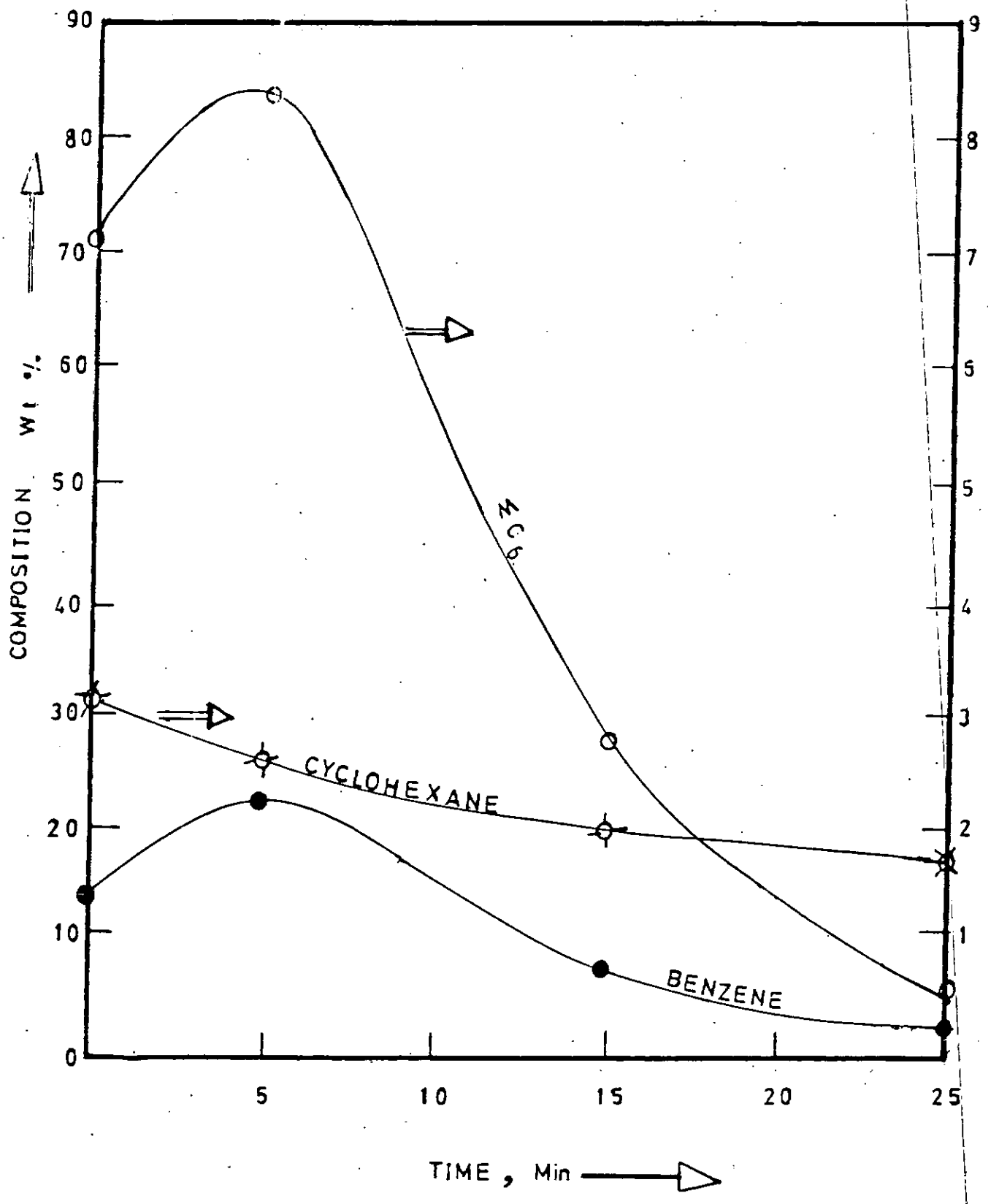

Fig.5.2.12: Product composition of MCP conversion on Pt/Al_2O_3 versus time at $P_{MCP}=9.2\times10^{-2}$atm; W/F = 0.11gmincm^{-3} temperature = 390°C and P_{H_2} = 0.11atm.

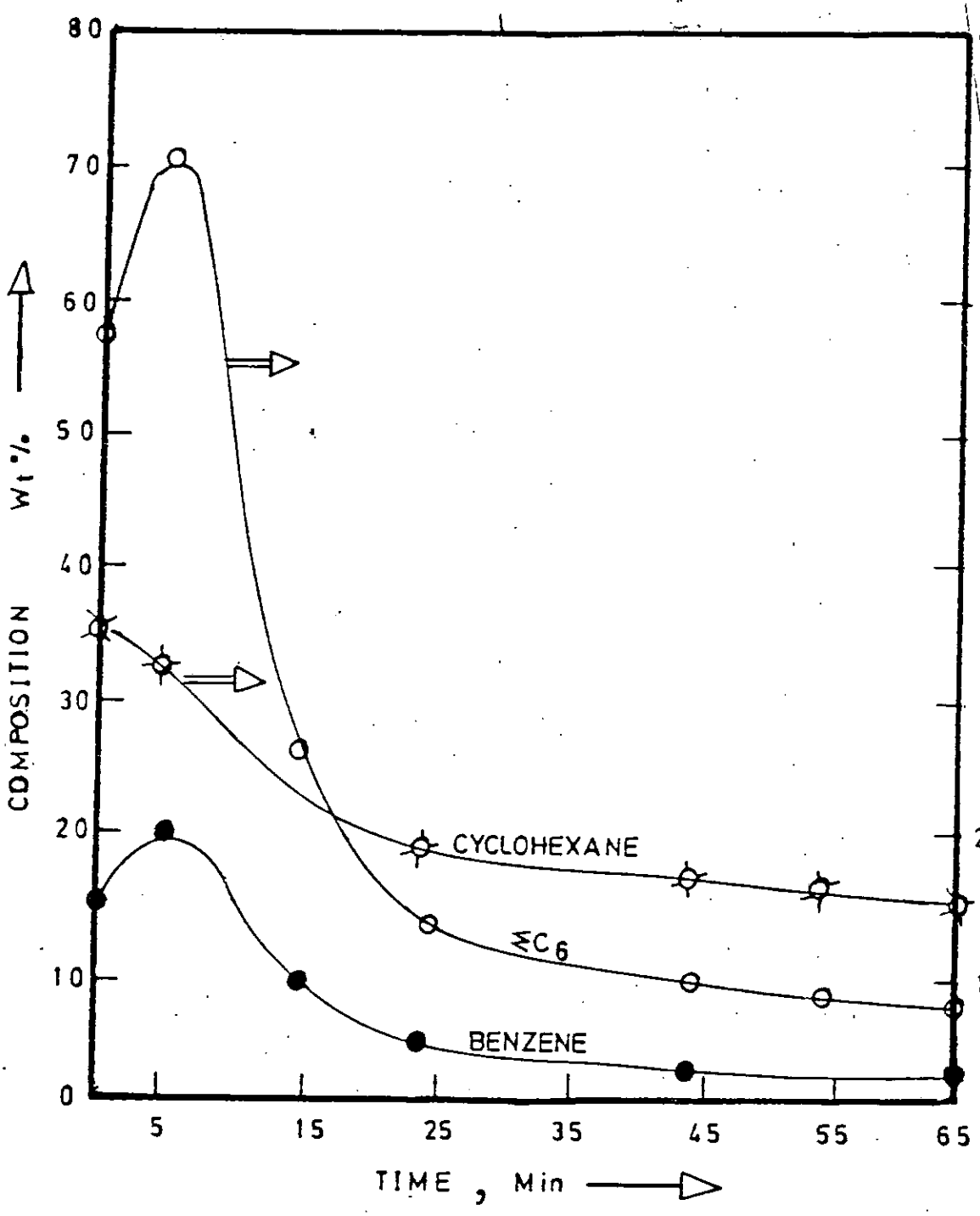

Fig.5.2.13: Product composition of MCP conversion on Pt/Al_2O_3 versus time at P_{MCP} = 9.2×10^{-2} atm; W/F = 0.11 gm.min.cm^{-3} temperature = 390°C and P_{H_2} = 0.33 atm.

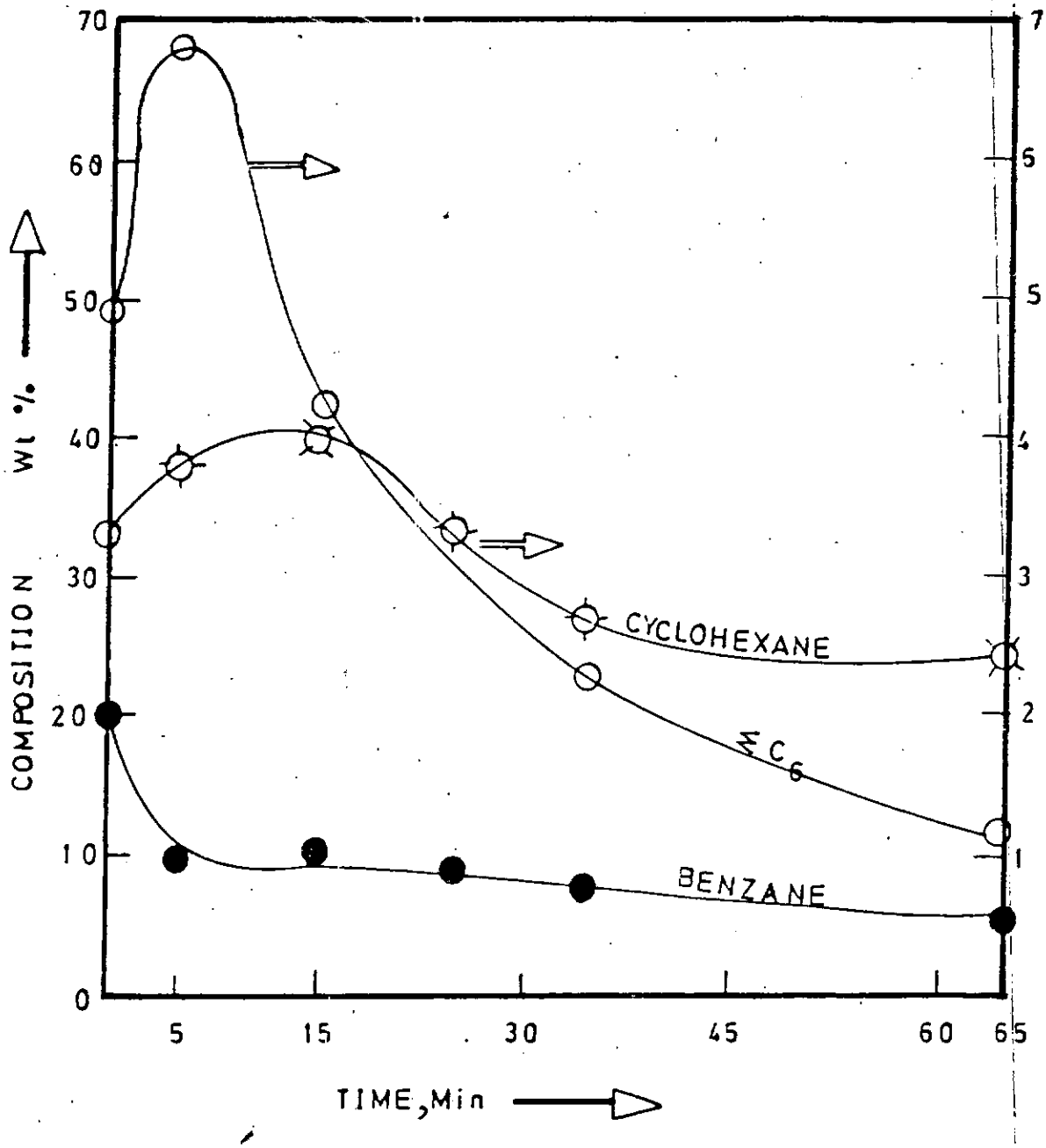

Fig. 5.2.14: Product composition of MCP conversion on Pt/Al_2O_3 versus time at $P_{MCP} = 9.2 \times 10^{-2}$ atm; W/F = 0.11gmincm^{-3} temperature = 390°C and P_{H_2} = 0.5atm.

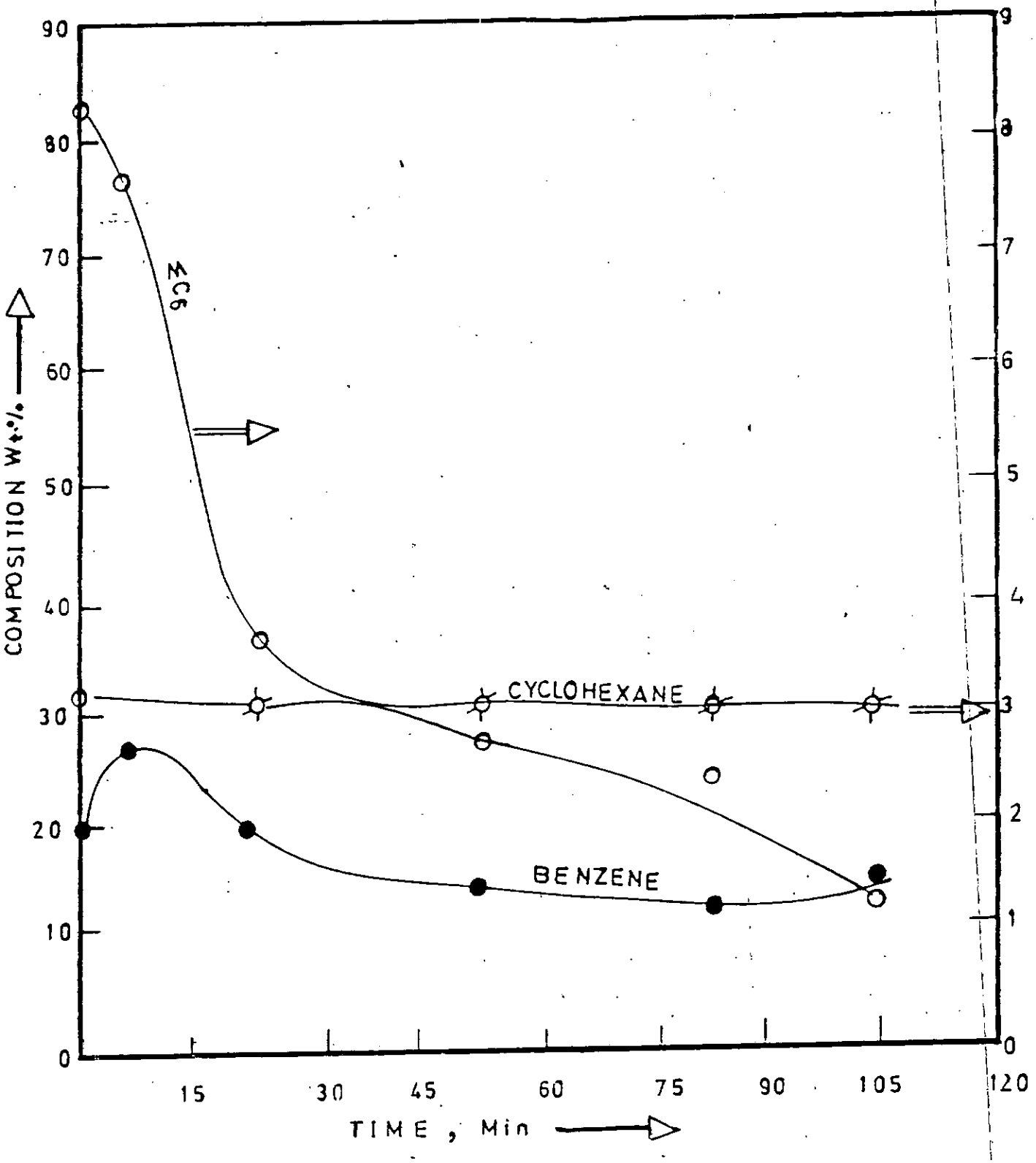

Fig.5.2.15: Product composition of MCP conversion on Pt/Al_2O_3 versus time at P_{MCP} = 9.2×10^{-2} atm; W/F=0.11gmincm^{-3} temperature = 390°C and P_{H_2} = 0.778atm.

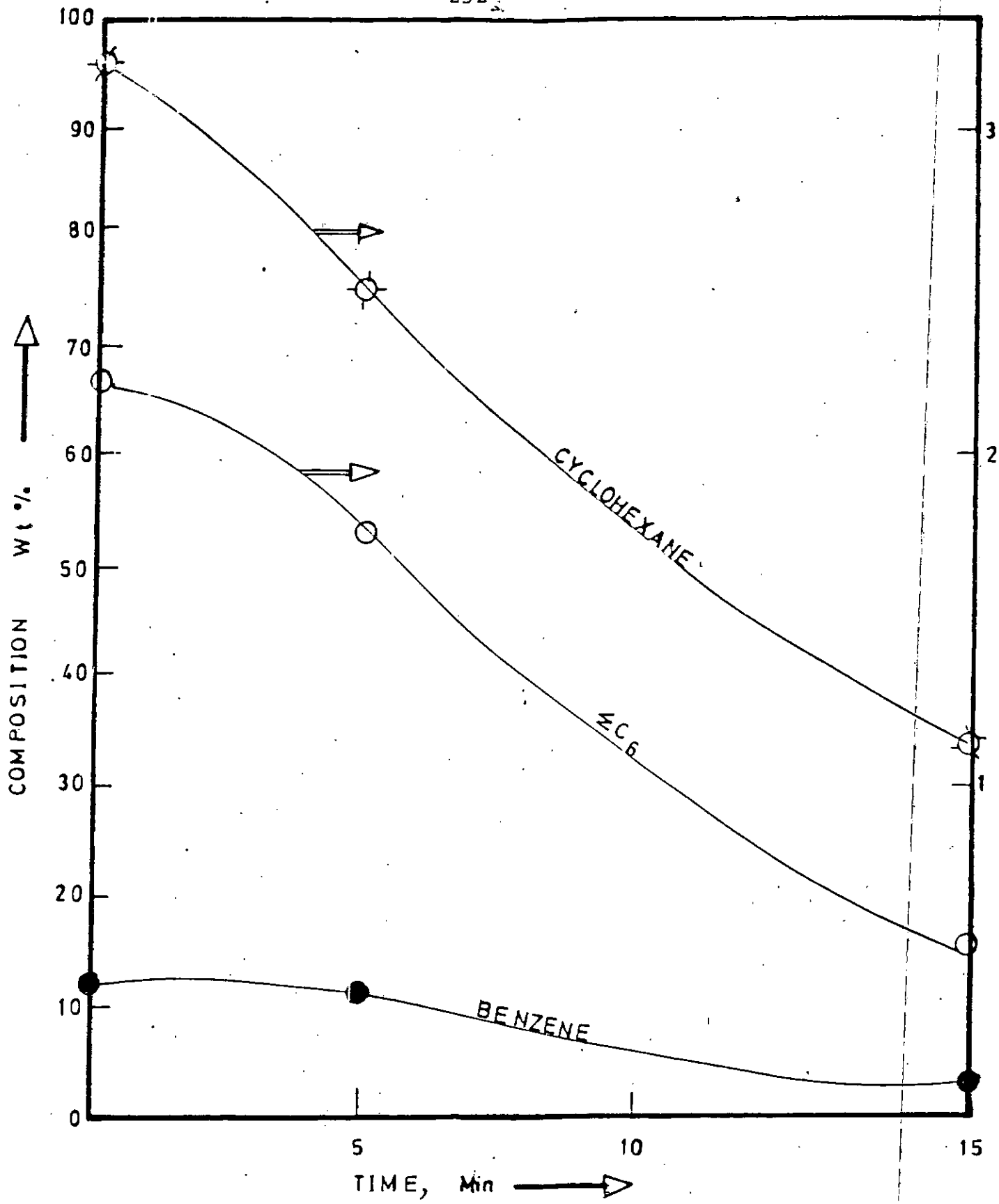

Fig.5.2.16: Product composition of MCP conversion on Pt/Al_2O_3 versus time at $P_{MCP} = 9.2 \times 10^{-2}$ atm; $W/F = 0.11 gmin cm^{-3}$; temperature = 400°C and $P_{H_2} = 0.11$ atm.

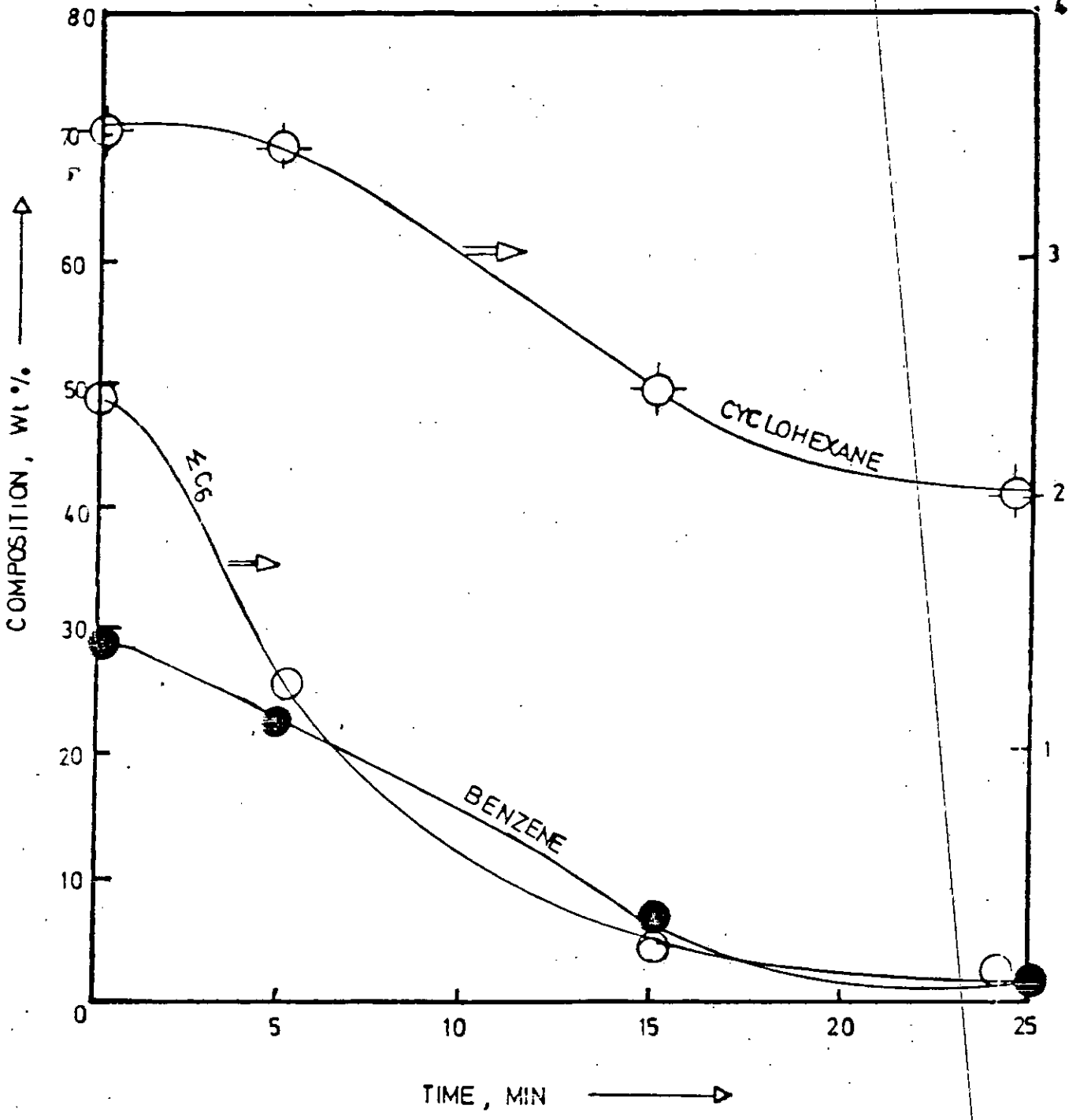

Fig.5.2.17: Product composition of MCP conversion on Pt/Al_2O_3 versus time at $P_{MCP}=9.2\times10^{-2}$atm; W/F = 0.11gmincm^{-3}; temperature = 400°C and P_{H_2} = 0.33atm.

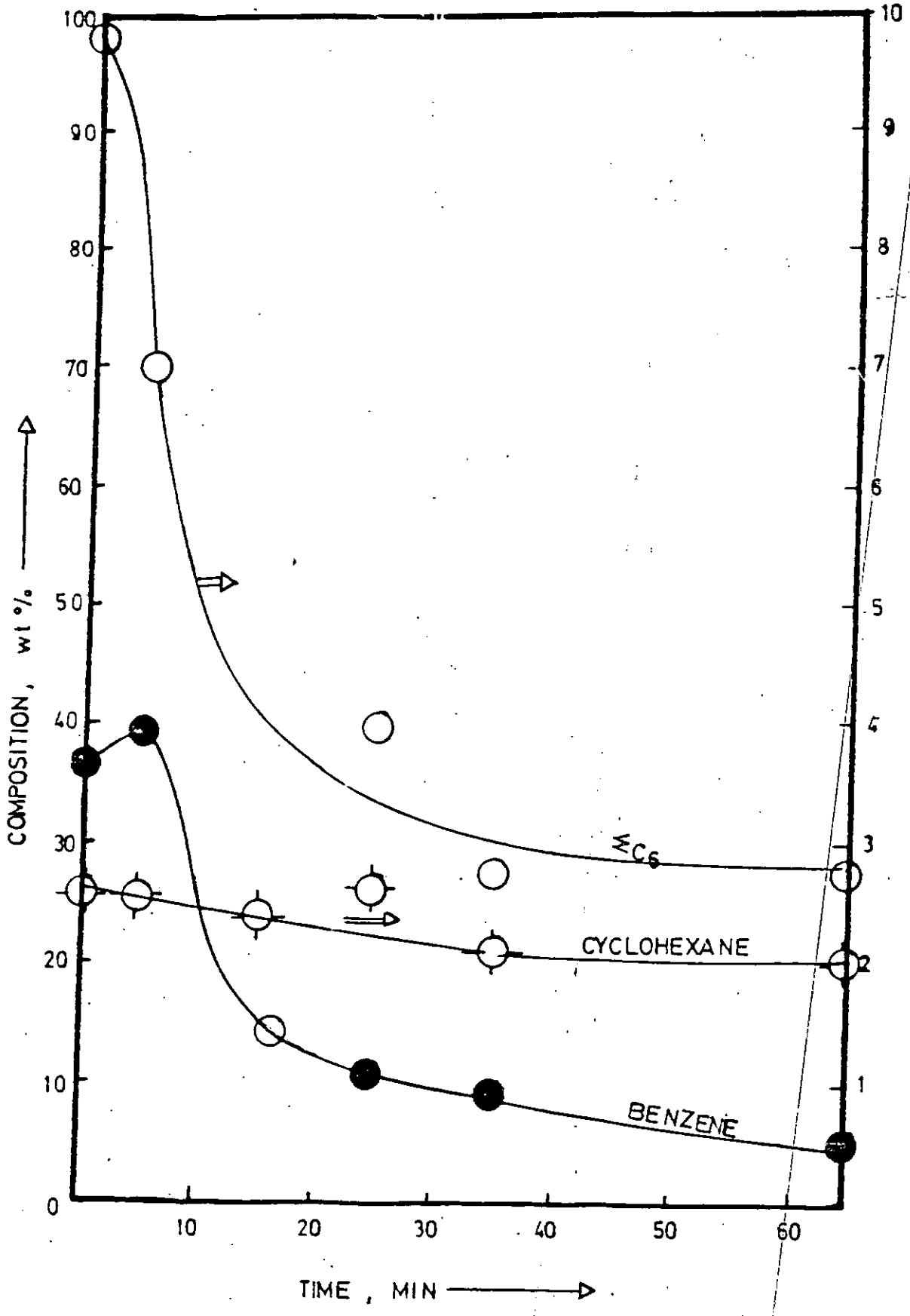

Fig.5.2.18: Product composition of MCP conversion on Pt/Al_2O_3 versus time $P_{MCP} = 9.2 \times 10^{-2}$ atm; $W/F = 0.11 gmin cm^{-3}$; temperature = 400°C and $P_{H_2} = 0.5$ atm.

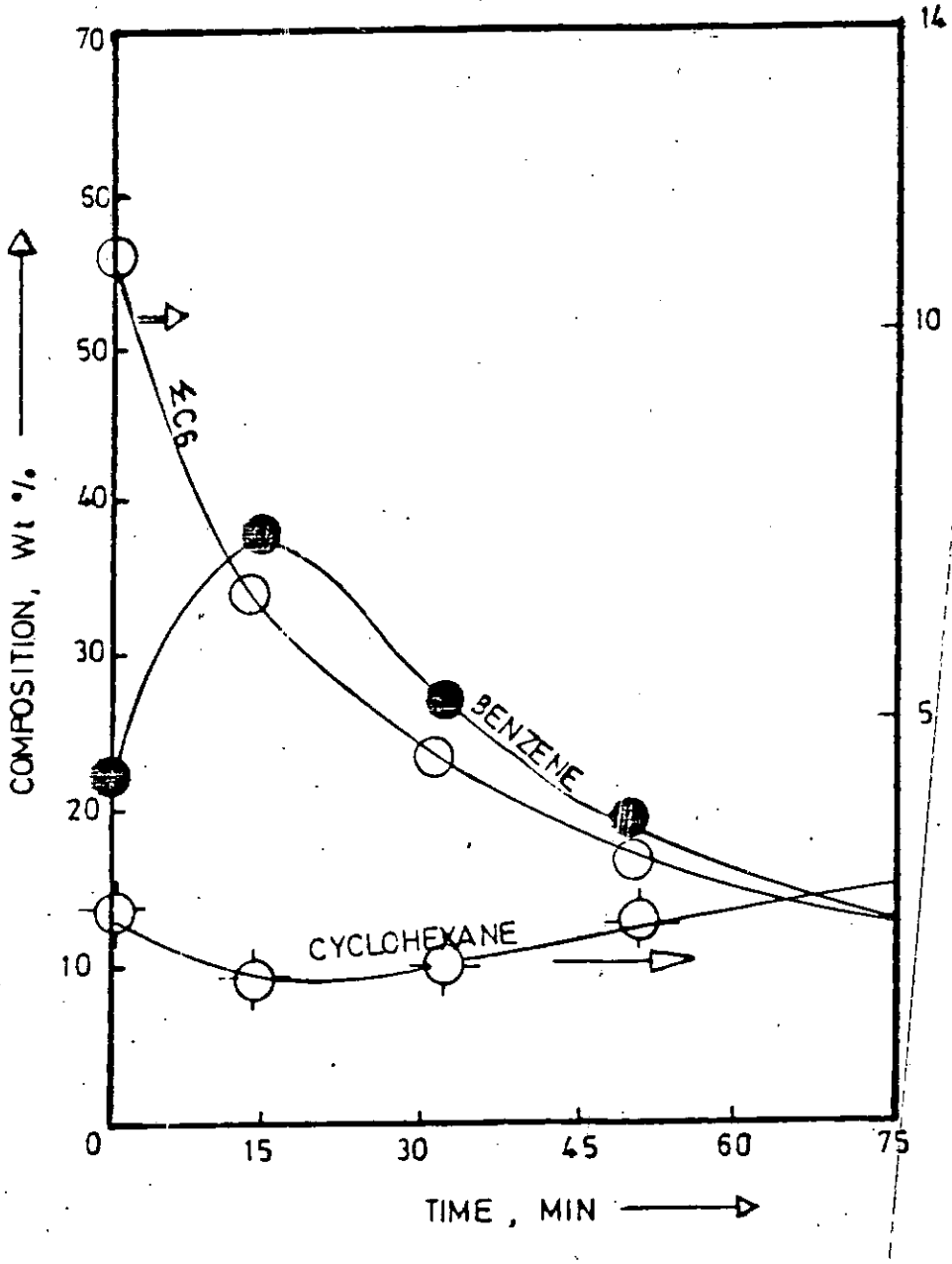

Fig.5.2.19: Product composition of MCP conversion on Pt/Al_2O_3 versus time at P_{MCP} $=9.2\times10^{-2}$atm; W/F = 0.11gmincm^{-3}; temperature = 400°C and P_{H_2} = 0.11atm.

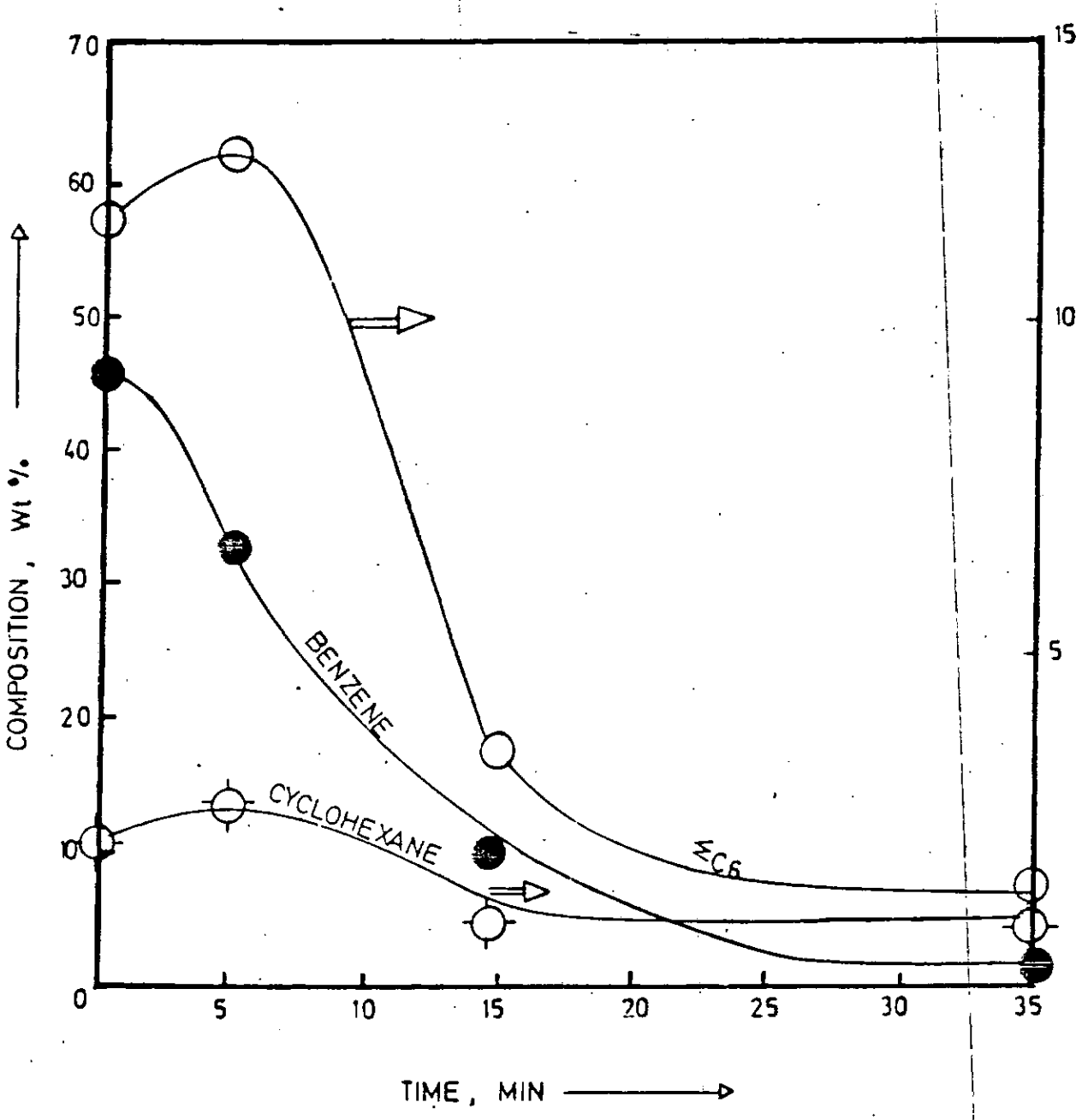

Fig. 5.2.20: Product composition of MCP conversion on Pt/Al_2O_3 versus time at $P_{MCP} = 9.2 \times 10^{-2}$ atm; $W/F = 0.11 g\,min\,cm^{-3}$; temperature = 410°C and $P_{H_2} = 0.11$ atm.

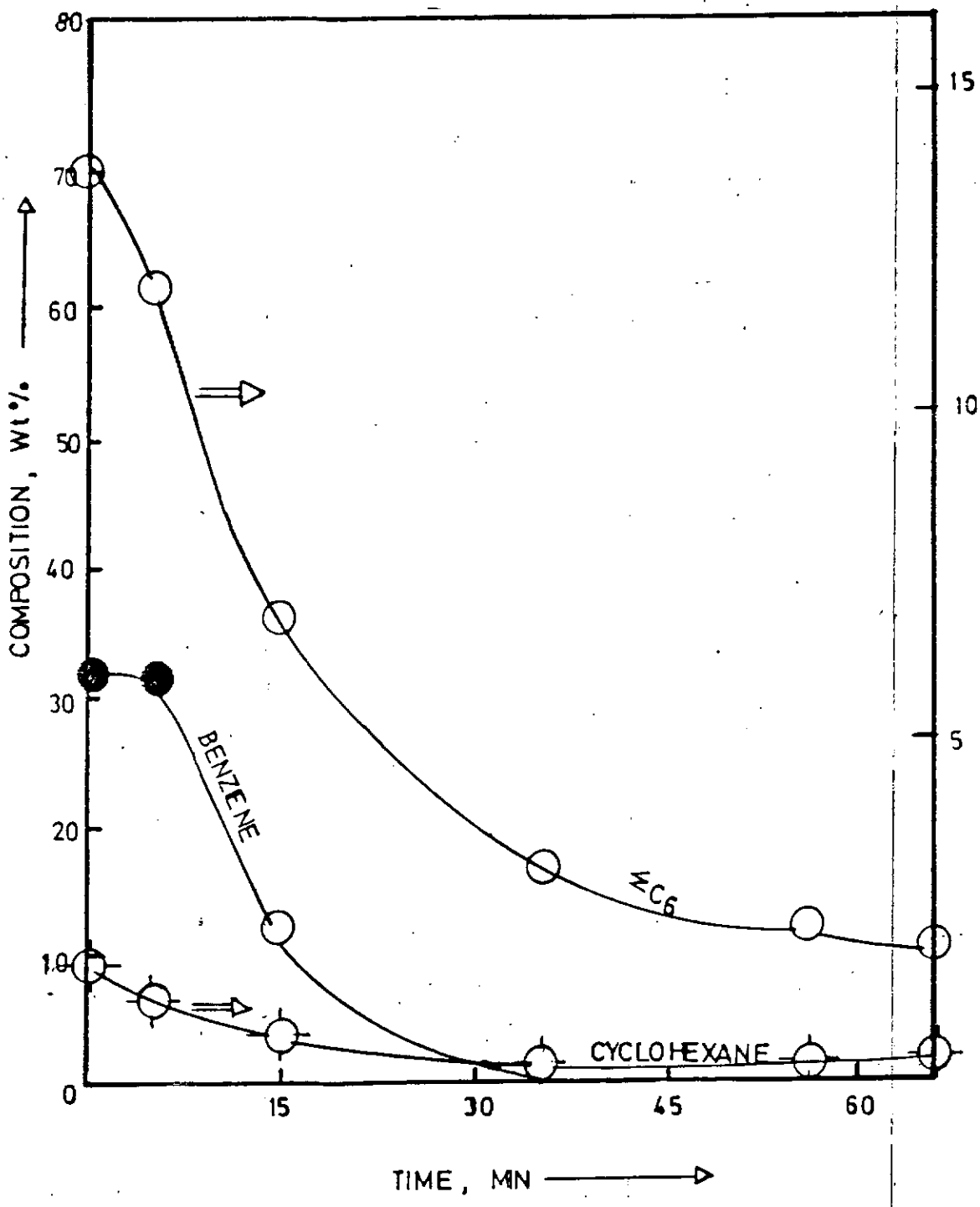

Fig. 5.2.21: Product composition of MCP conversion on Pt/Al_2O_3 versus time at $P_{MCP} = 9.2 \times 10^{-2}$atm; $W/F = 0.11 gmin cm^{-3}$; temperature = 410°C and $P_{H_2} = 0.33$atm.

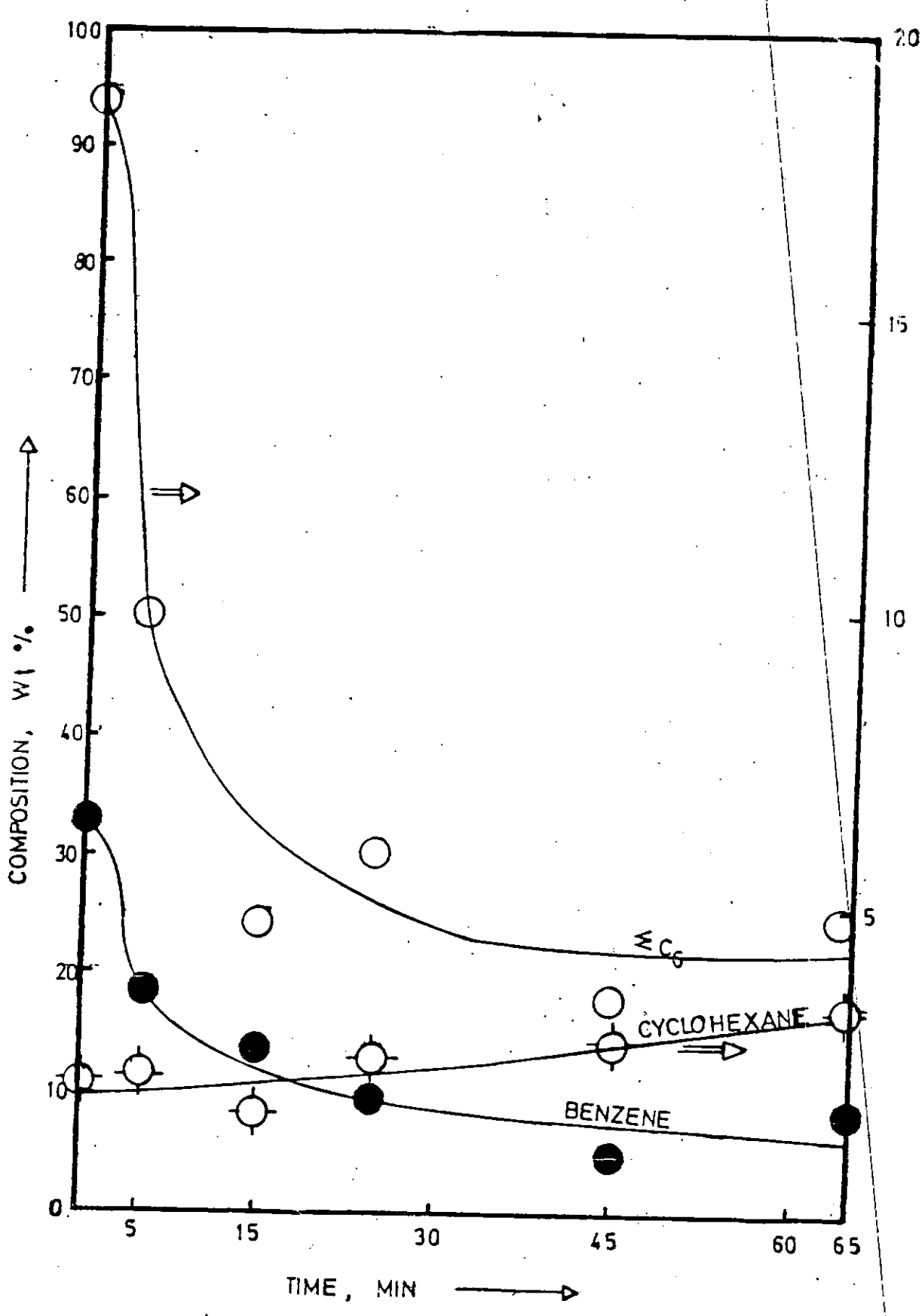

Fig. 5.2.22: Product composition of MCP conversion on Pt/Al_2O_3 versus time at $P_{MCP} = 9.2 \times 10^{-2}$ atm; $W/F = 0.11 g min cm^{-3}$; temperature = 410°C and $P_{H_2} = 0.5$ atm.

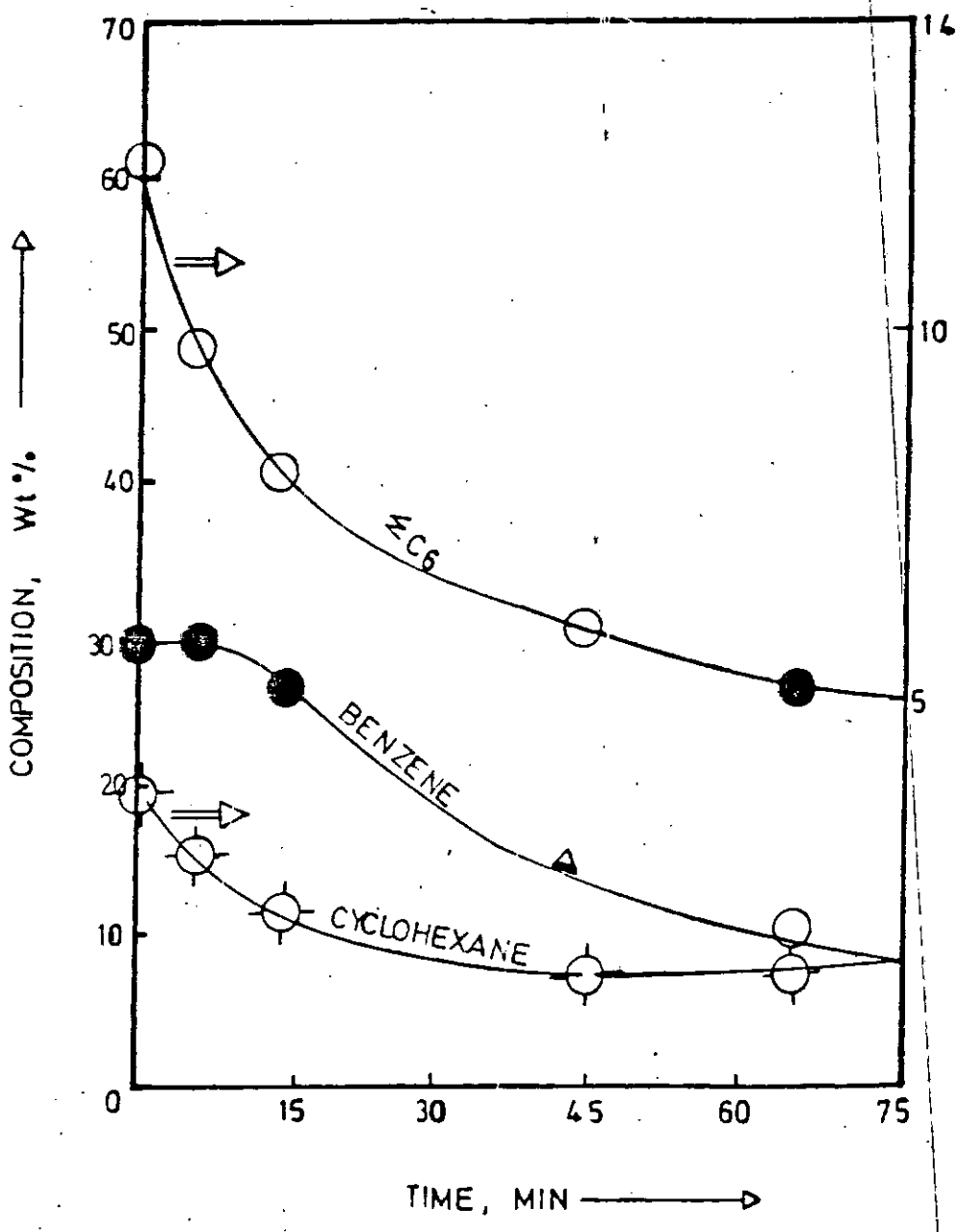

Fig. 5.2.23: Product composition of MCP conversion on Pt/Al_2O_3 versus time at $P_{MCP} = 9.2 \times 10^{-2}$ atm; $W/F = 0.11 gmin cm^{-3}$; temperature = 410°C and $P_{H_2} = 0.778$ atm.

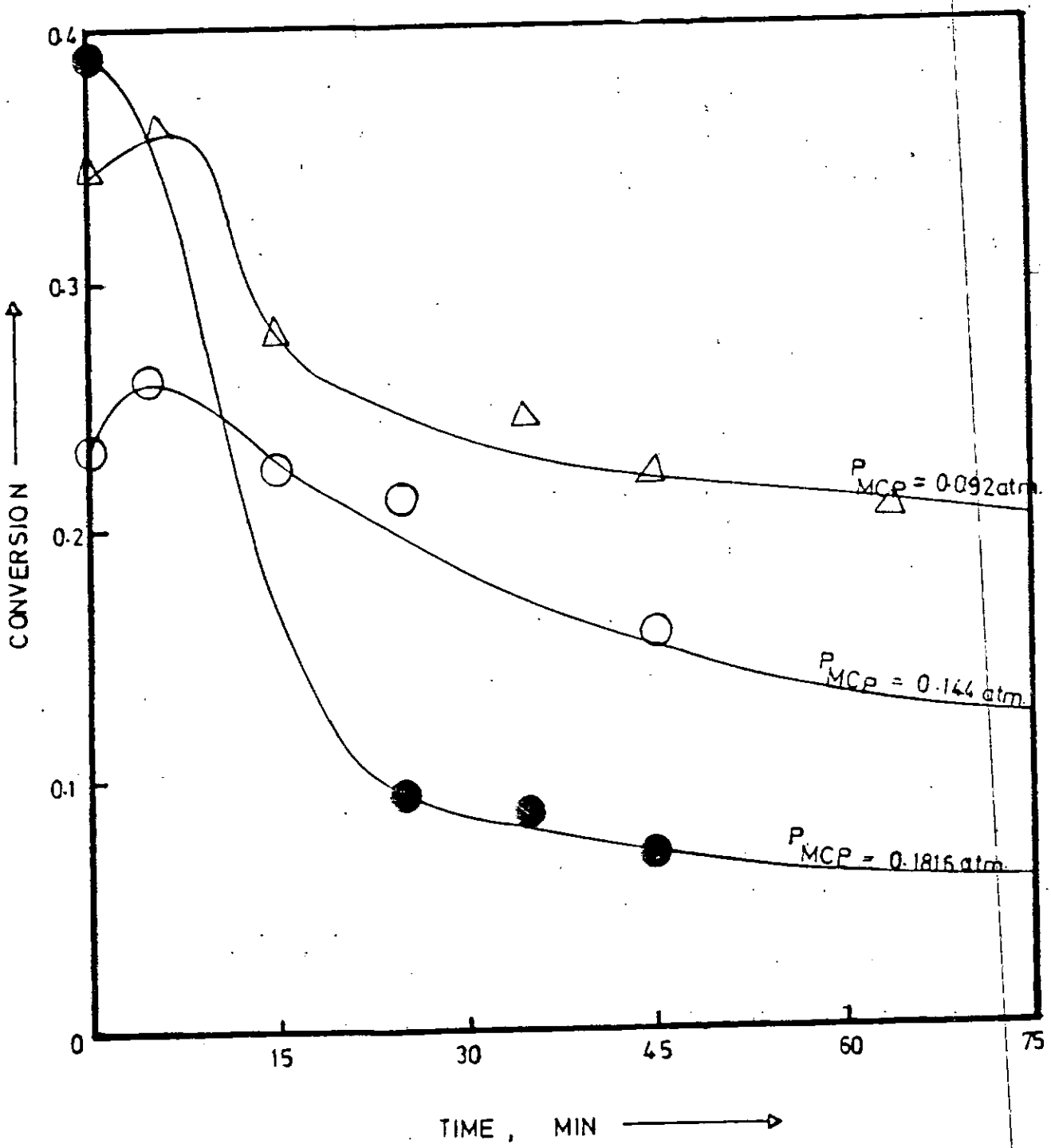

Fig. 5.2.24: Product composition of MCP conversion on Pt/Al_2O_3 versus time at P_{H_2} = 0.778atm; W/F = 0.11gmincm^{-3}; temperature = 400°C and various P_{MCP}

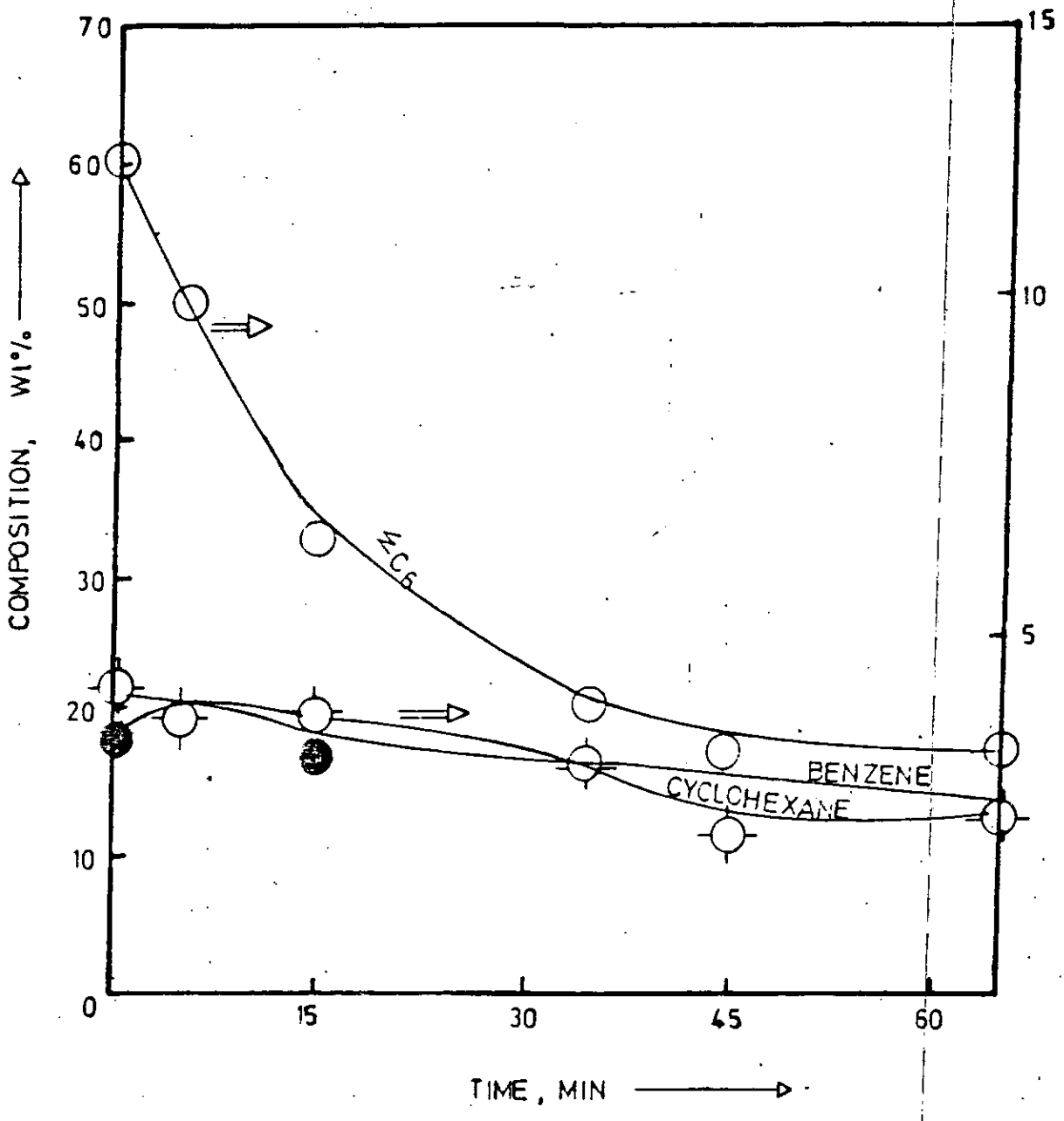

Fig. 5.2.25: Product composition of MCP conversion on Pt/Al_2O_3 versus time at P_{H_2} = 0.778atm; W/F = 0.11gmincm^{-3}; P_{MCP} = 9.2×10^{-2}atm and temperature = 400°C

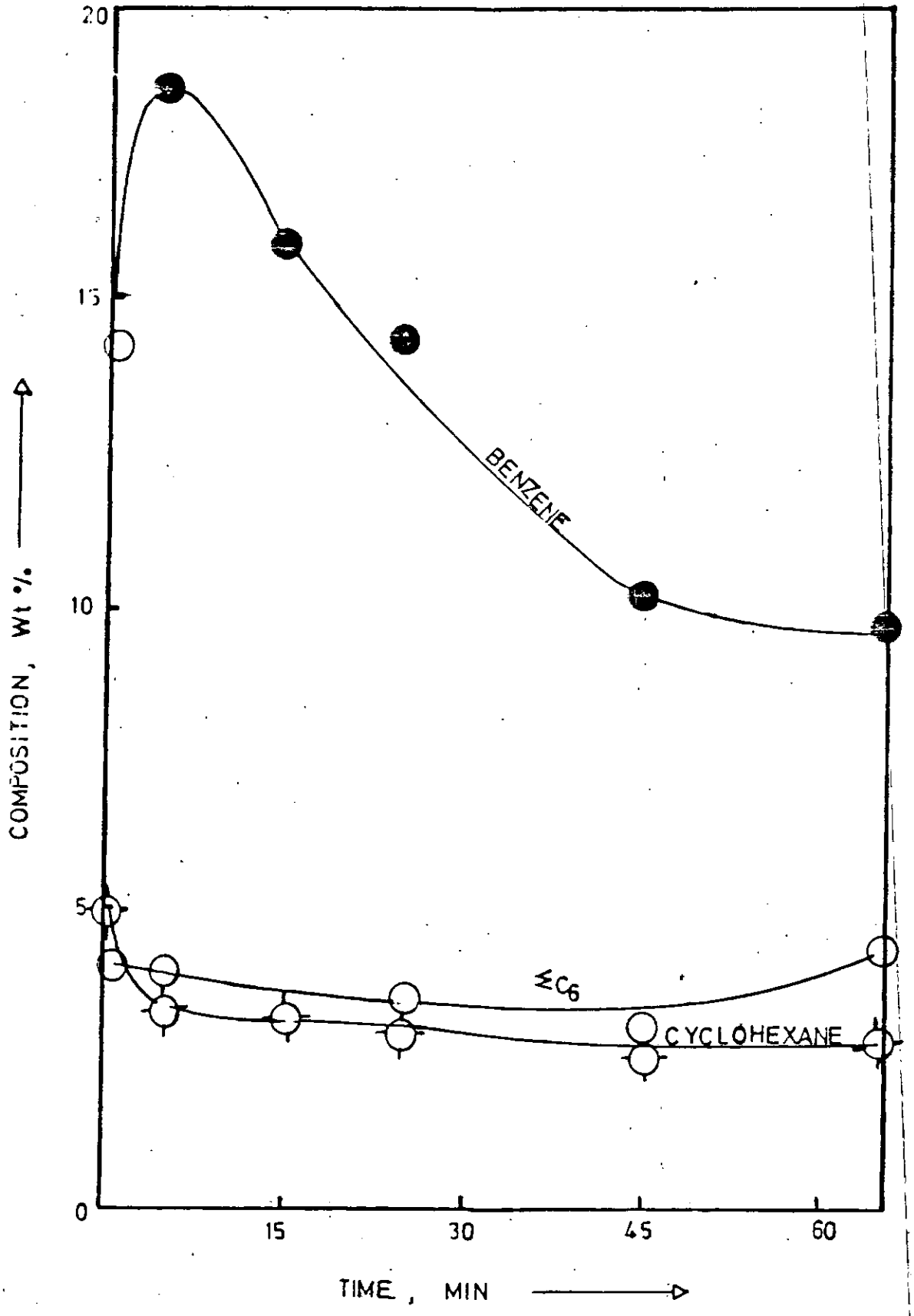

Fig. 5.2.26: Product composition of MCP conversion on Pt/Al_2O_3 versus time at P_{H_2} = 0.778atm; W/F = 0.11gmincm^{-3} P_{MCP} = 14.47×10^{-2} atm and temperature = 400°C .

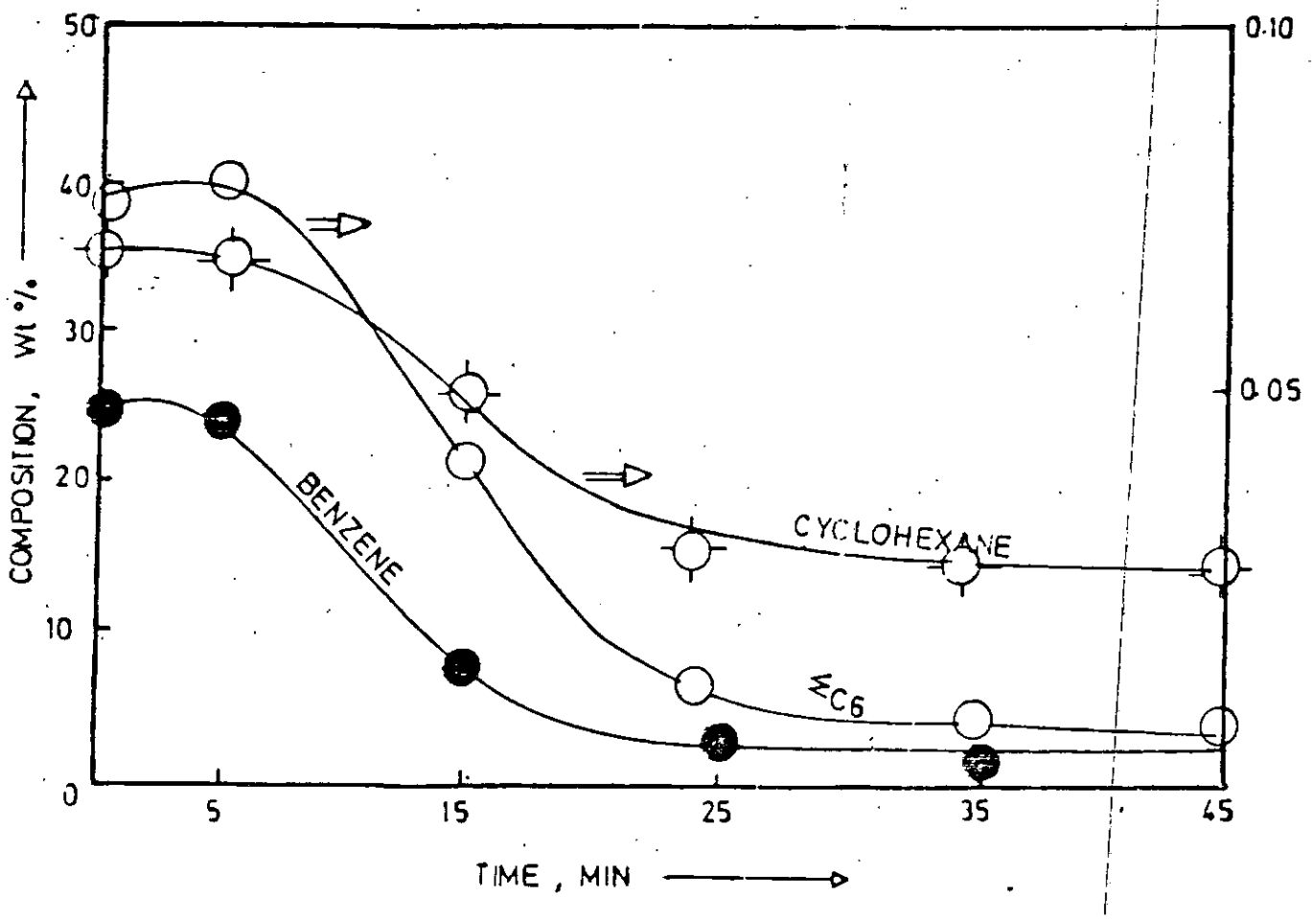

Fig. 5.2.27: Product composition of MCP conversion on Pt/Al_2O_3 versus time at P_{H_2} = 0.778atm; W/F = 0.11gmincm^{-3}; P_{MCP} = 18.16x10^{-2}atm and temperature = 400°C

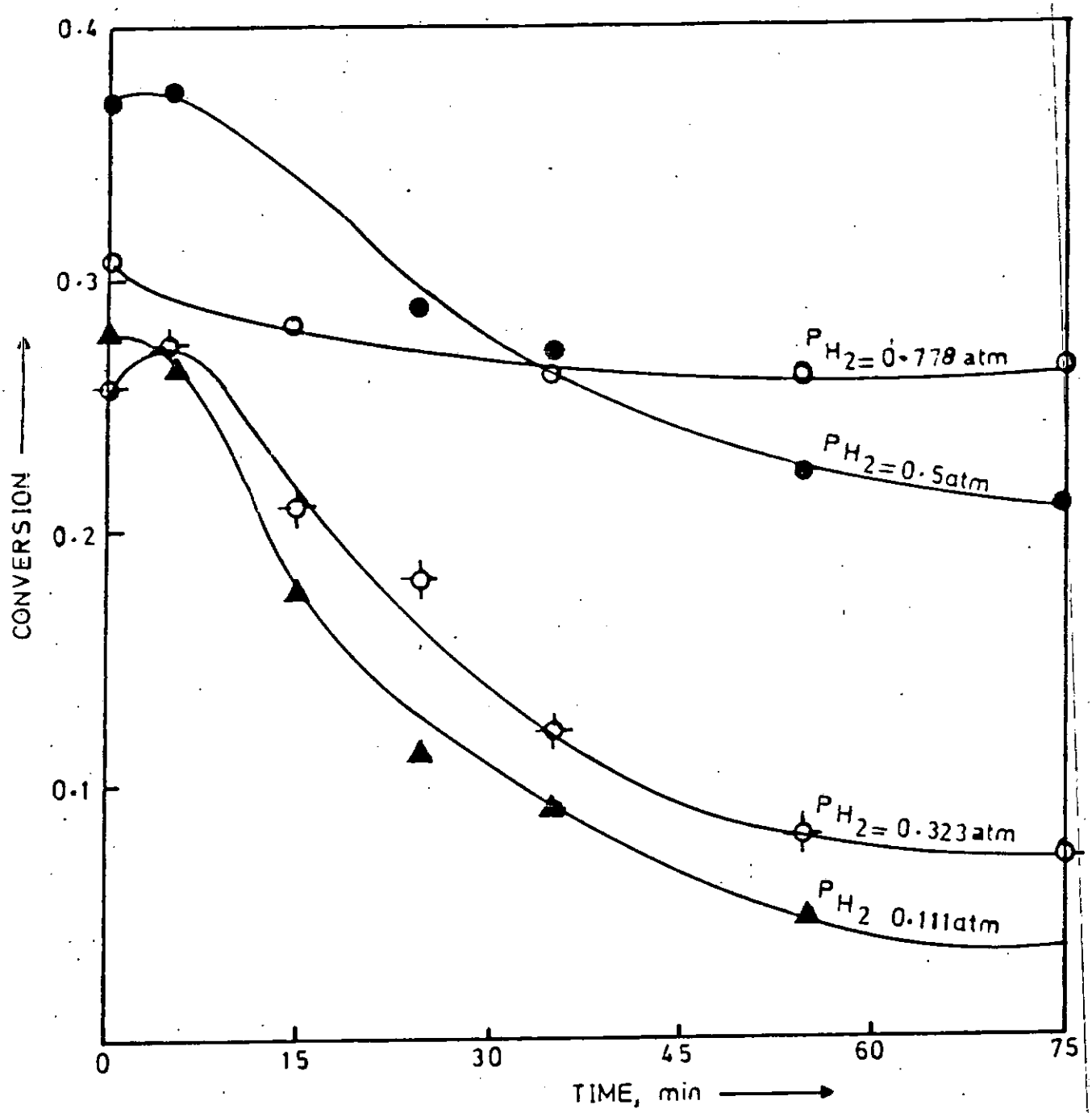

Fig. 5.2.28: MCP conversion on Pt-Re/Al_2O_3(DRIED) versus time at P_{MCP}= 9.2×10^{-2}atm; W/F = 0.11gmincm^{-3}; temperature = 390°C and various P_{H_2}

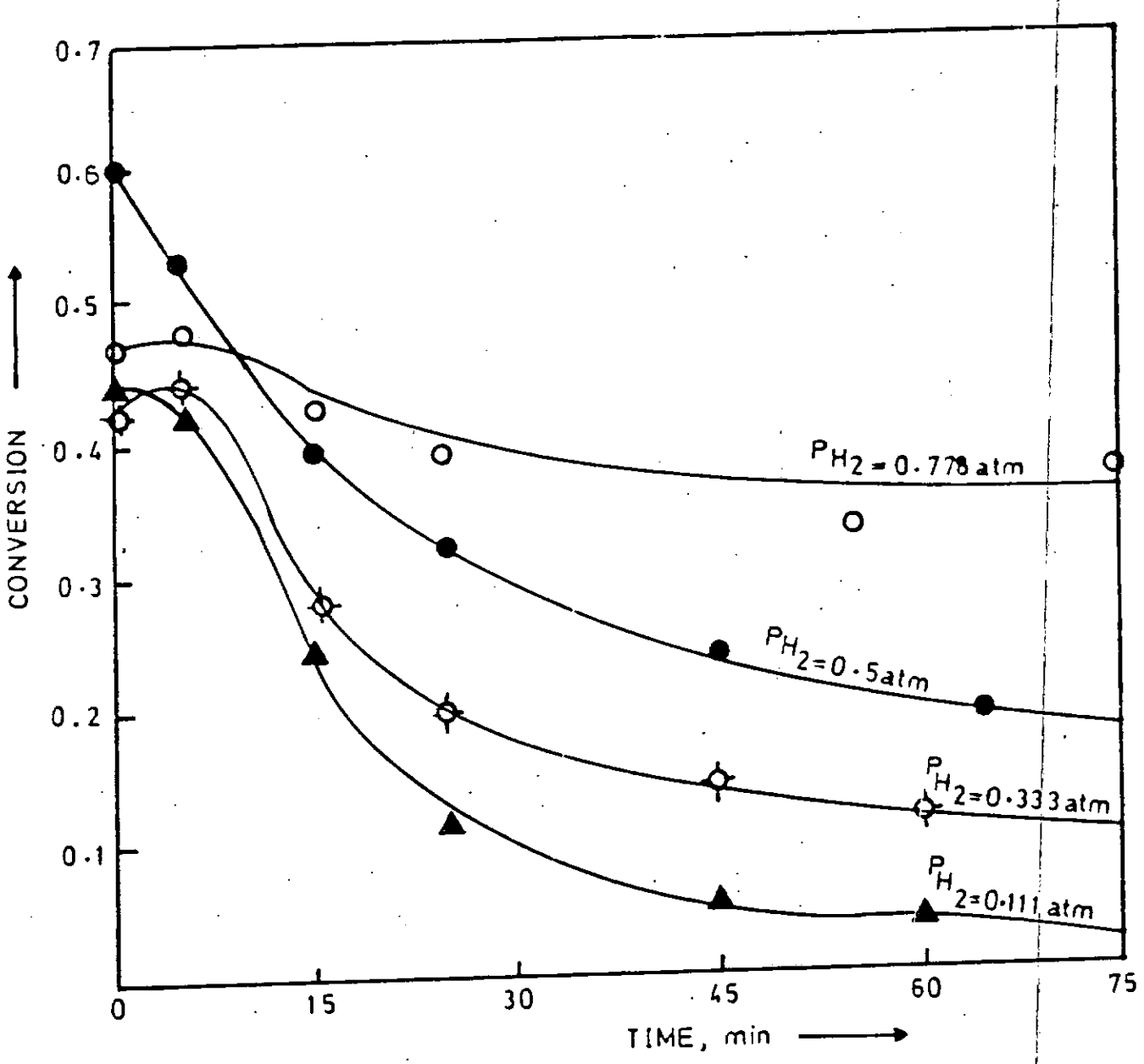

Fig. 5.2.29: MCP conversion on Pt-Re/Al_2O_3(DRIED) versus time at P_{MCP} = 9.2×10^{-2} atm; W/F = 0.11 g min cm^{-3}; temperature = 400°C and various P_{H_2}

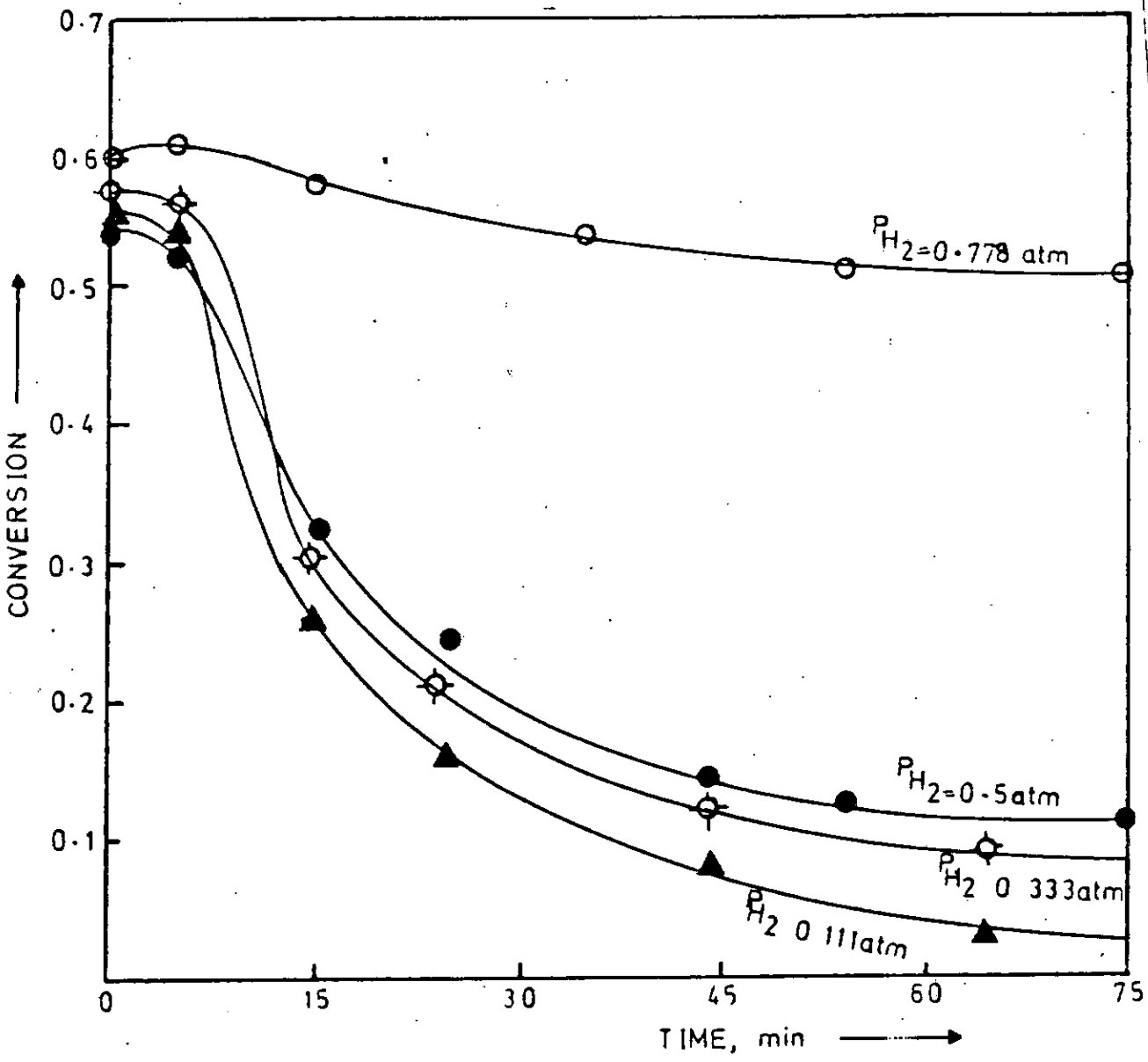

Fig. 5.2.30: MCP conversion on Pt-Re/Al_2O_3(DRIED) versus time at P_{MCP}= 9.2×10^{-2}atm; W/F = 0.11gmincm^{-3} temperature = 410°C and various P_{H_2}.

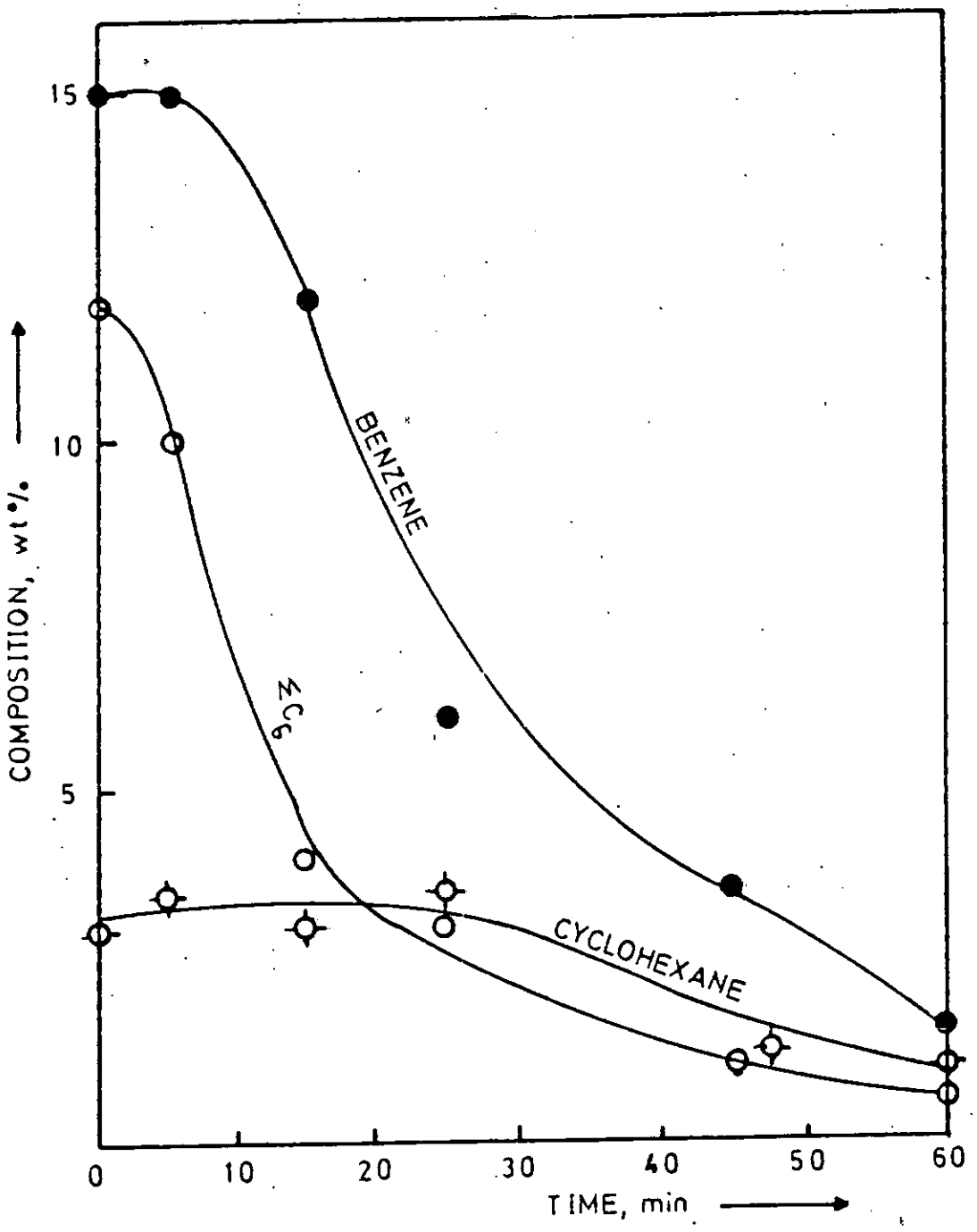

Fig. 5.2.31: Product composition of MCP conversion on Pt-Re/Al_2O_3 (DRIED) versus time at P_{MCP} = 9.2×10^{-2} atm; W/F = 0.11 g min cm^{-3}; temperature = 390°C and P_{H_2} = 0.11 atm.

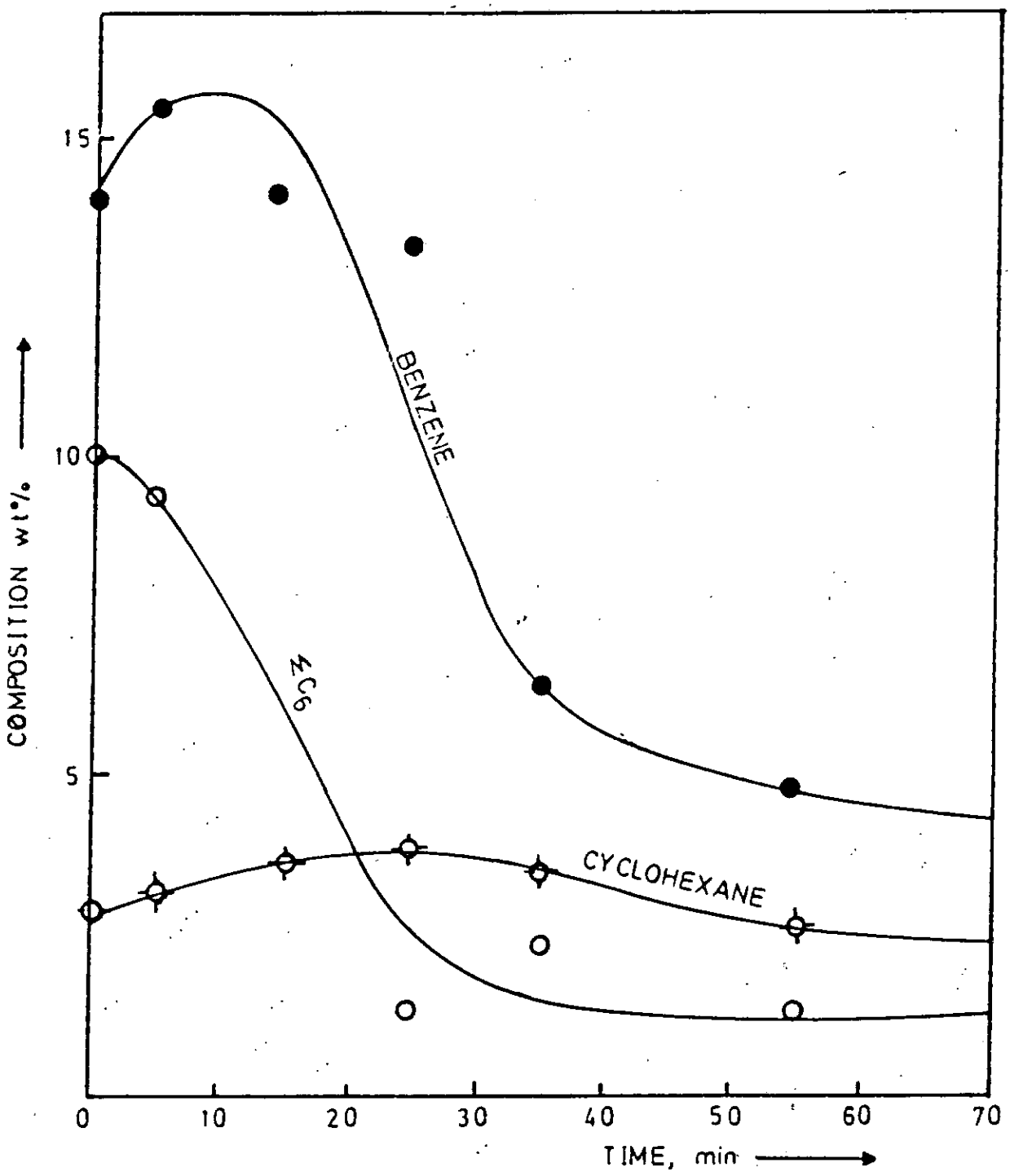

Fig. 5.2.32: Product composition of MCP conversion on $Pt\text{-}Re/Al_2O_3$(DRIED) versus time at $P_{MCP} = 9.2 \times 10^{-2}$atm; $W/F = 0.11 gmin cm^{-3}$; temperature = 390°C and $P_{H_2} = 0.33$atm.

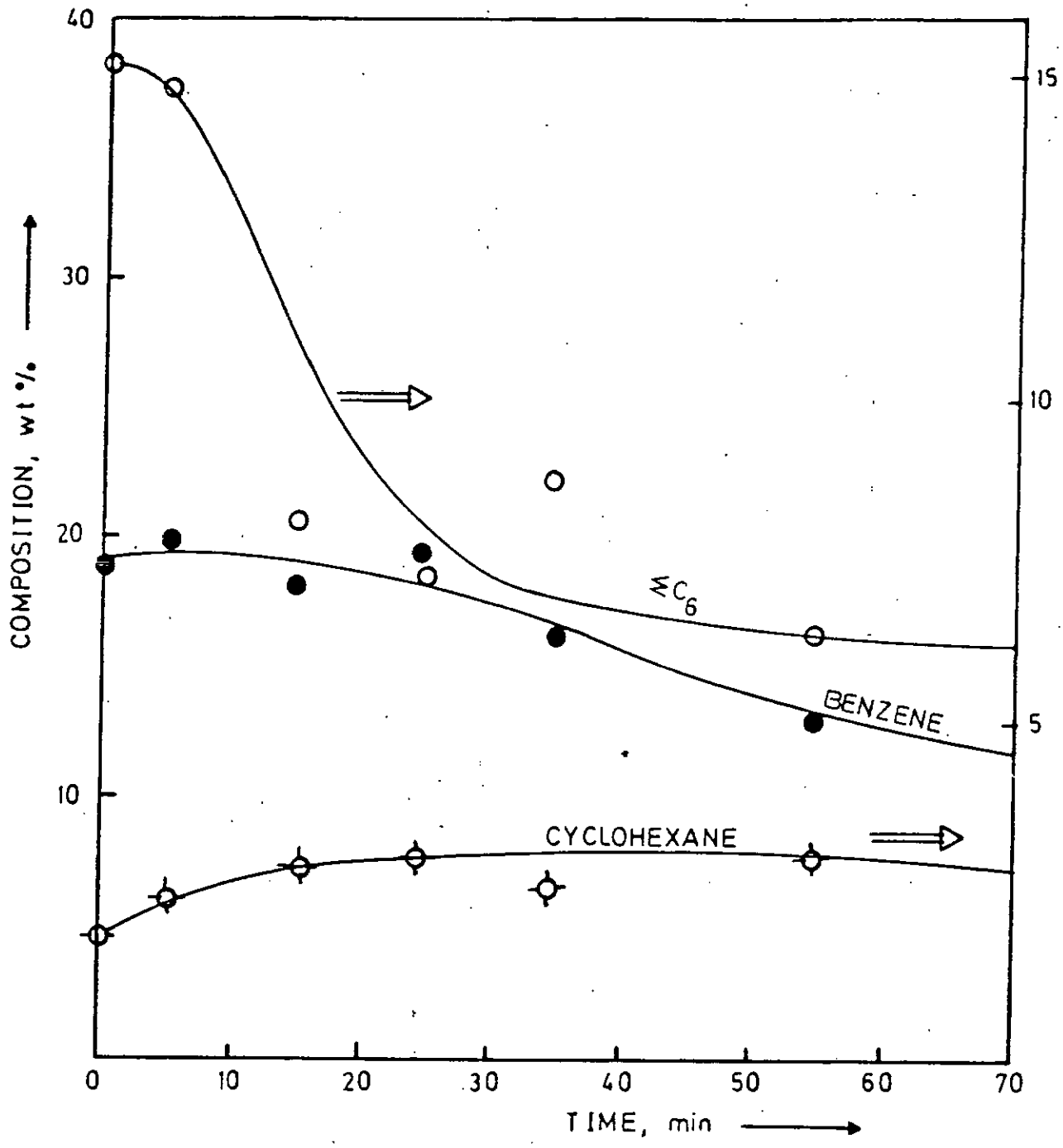

Fig. 5.2.33: Product composition of MCP conversion on Pt-Re/Al_2O_3(DRIED) versus time at P_{MCP}= 9.2×10^{-2}atm; W/F = 0.11gmincm^{-3}; Temperature = 390°C and P_{H_2} = 0.5atm.

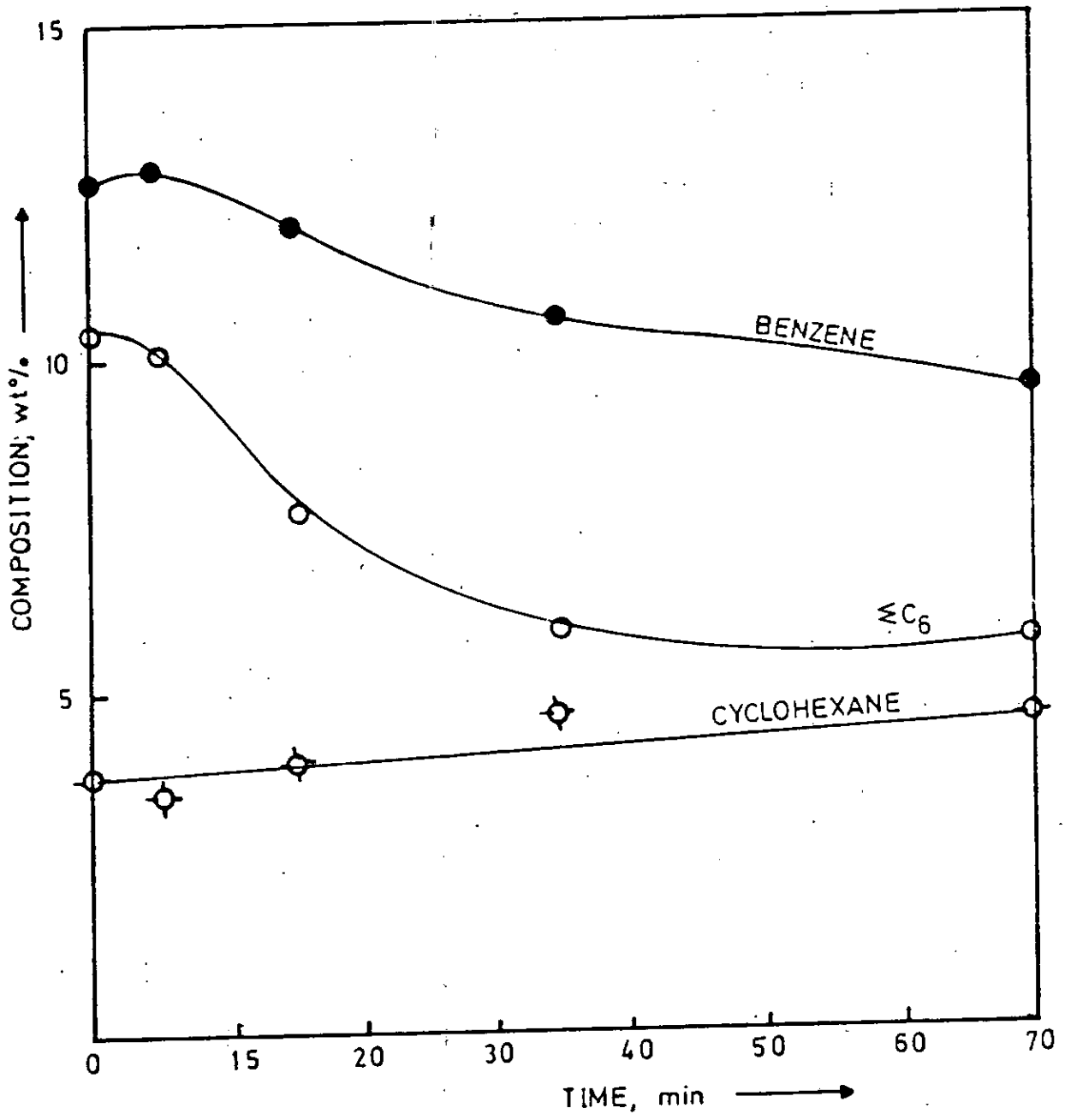

Fig. 5.2.34: Product composition of MCP conversion on Pt-Re/Al_2O_3(DRIED) versus time at P_{MCP}= 9.2×10^{-2}atm; W/F = 0.11gmincm^{-3}; temperature = 390°C and P_{H_2} = 0.778atm.

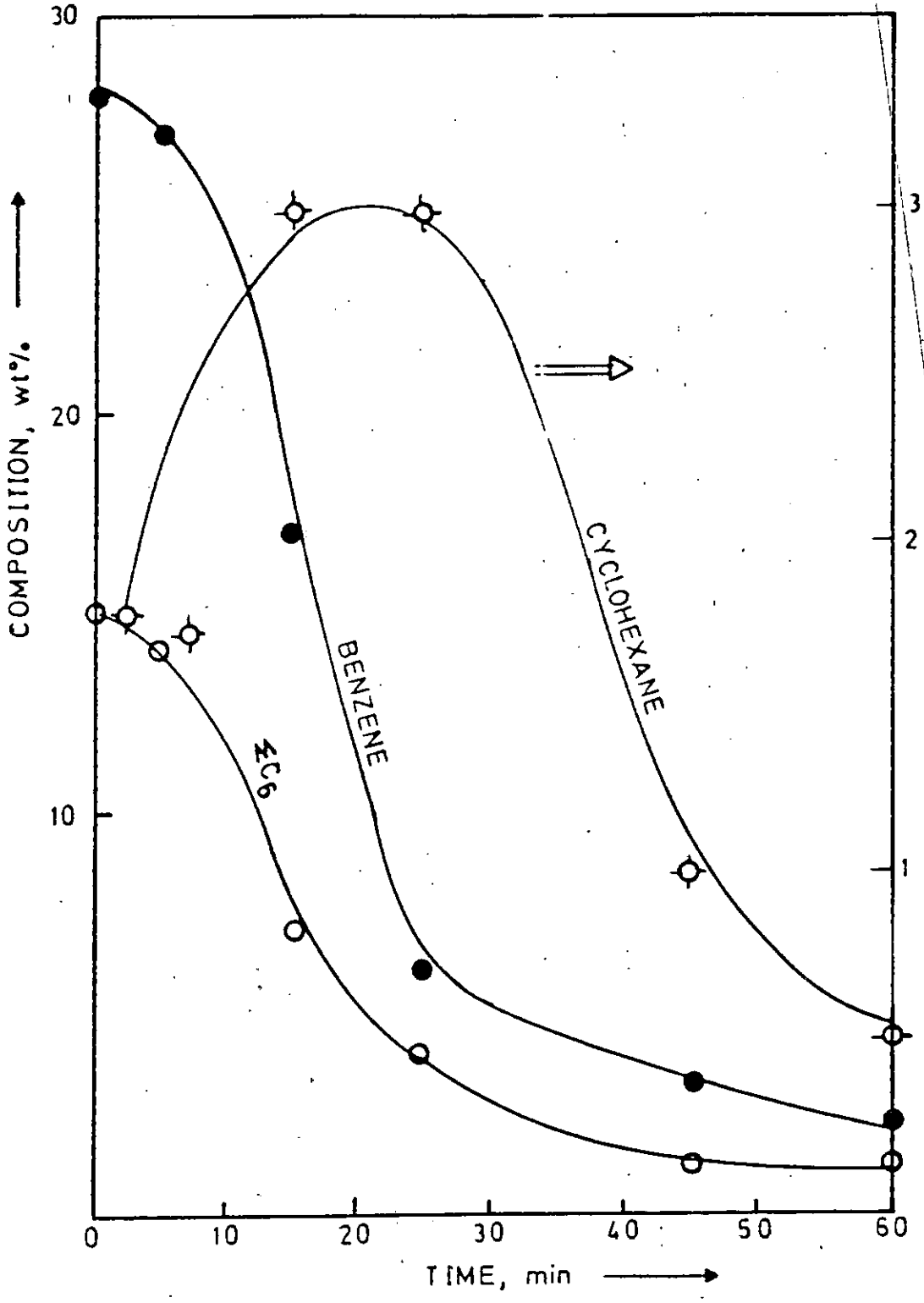

Fig. 5.2.35: Product composition of MCP conversion on Pt-Re/Al_2O_3(DRIED) versus time at $P_{MCP}=9.2\times10^{-2}$atm; $W/F = 0.11 gmin cm^{-3}$; temperature = 400°C and $P_{H_2} = 0.11$atm.

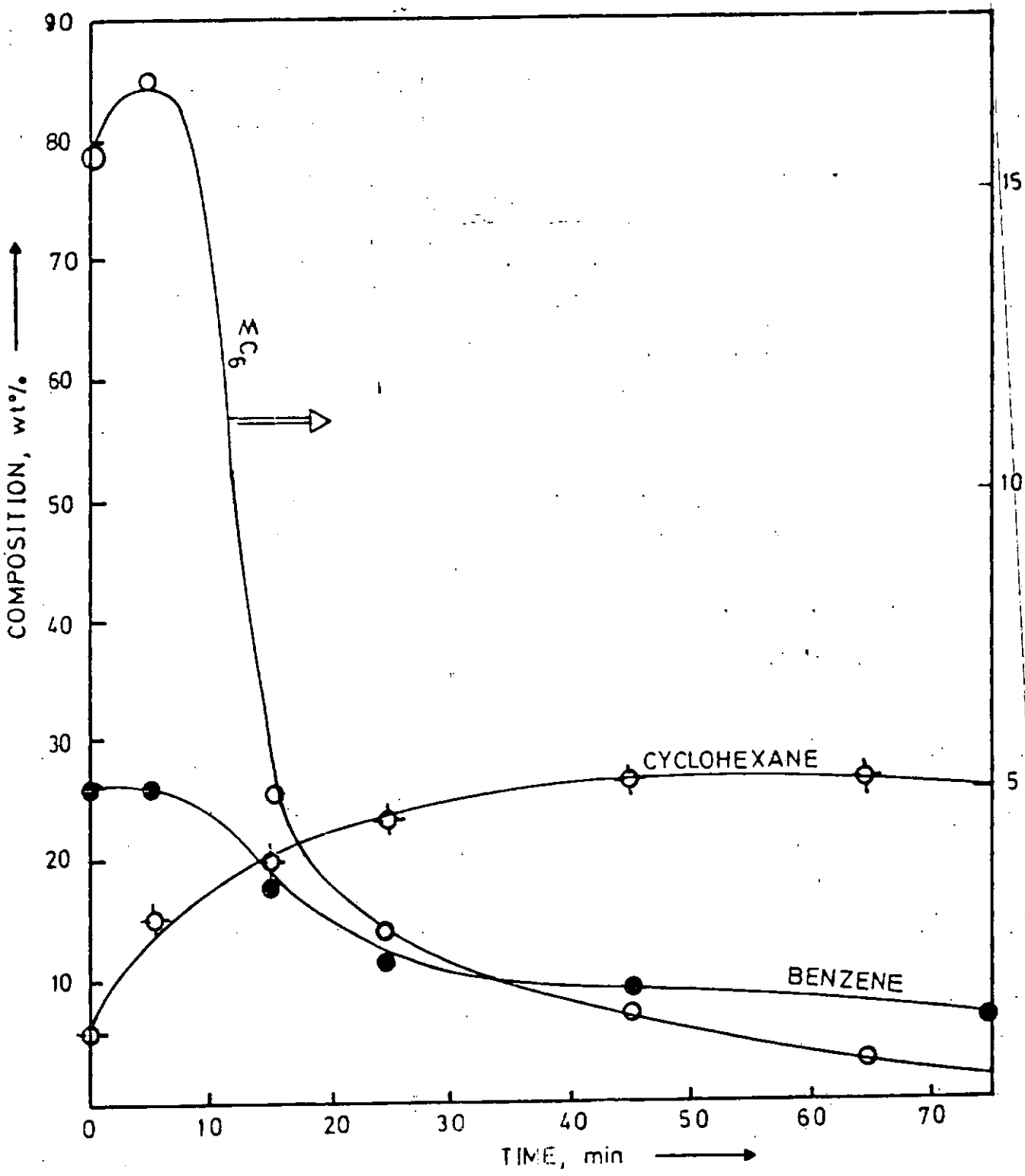

Fig. 5.2.36: Product composition of MCP conversion on $Pt\text{-}Re/Al_2O_3$(DRIED) versus time at P_{MCP}= 9.2×10^{-2}atm; W/F = 0.11gmincm^{-3}; temperature = 400°C and P_{H_2} = 0.33atm.

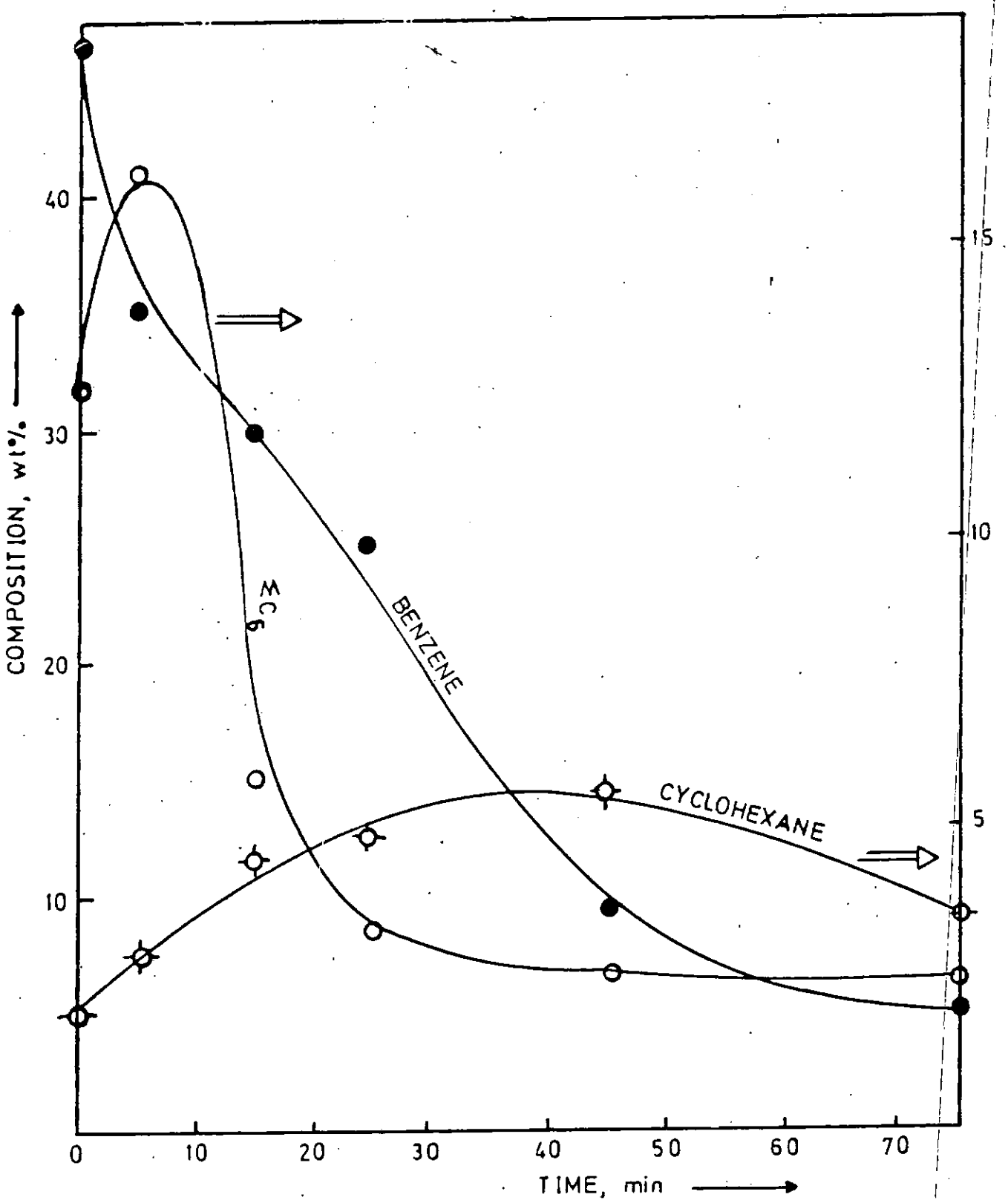

Fig. 5.2.37: Product composition of MCP conversion on Pt-Re/Al_2O_3(DRIED) versus time at $P_{MCP}=9.2\times10^{-2}$atm; W/F = 0.11gmincm^{-3}; temperature = 400°C and P_{H_2} = 0.5atm.

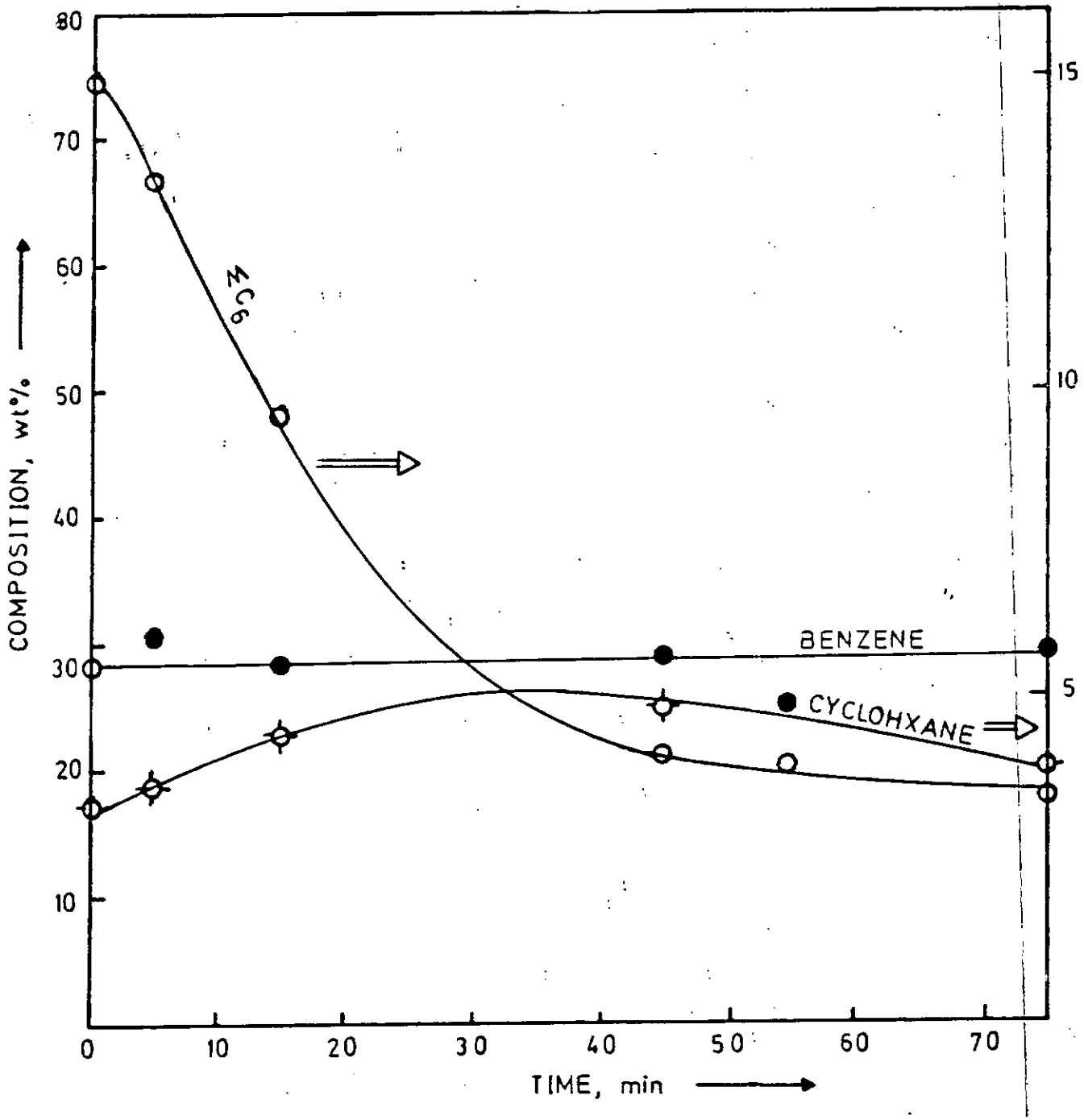

Fig. 5.2.38: Product composition of MCP conversion on Pt-Re/Al_2O_3(DRIED) versus time at P_{MCP}= 9.2×10^{-2}atm; W/F = 0.11gmincm^{-3}; temperature = 400°C and P_{H_2} = 0.778atm.

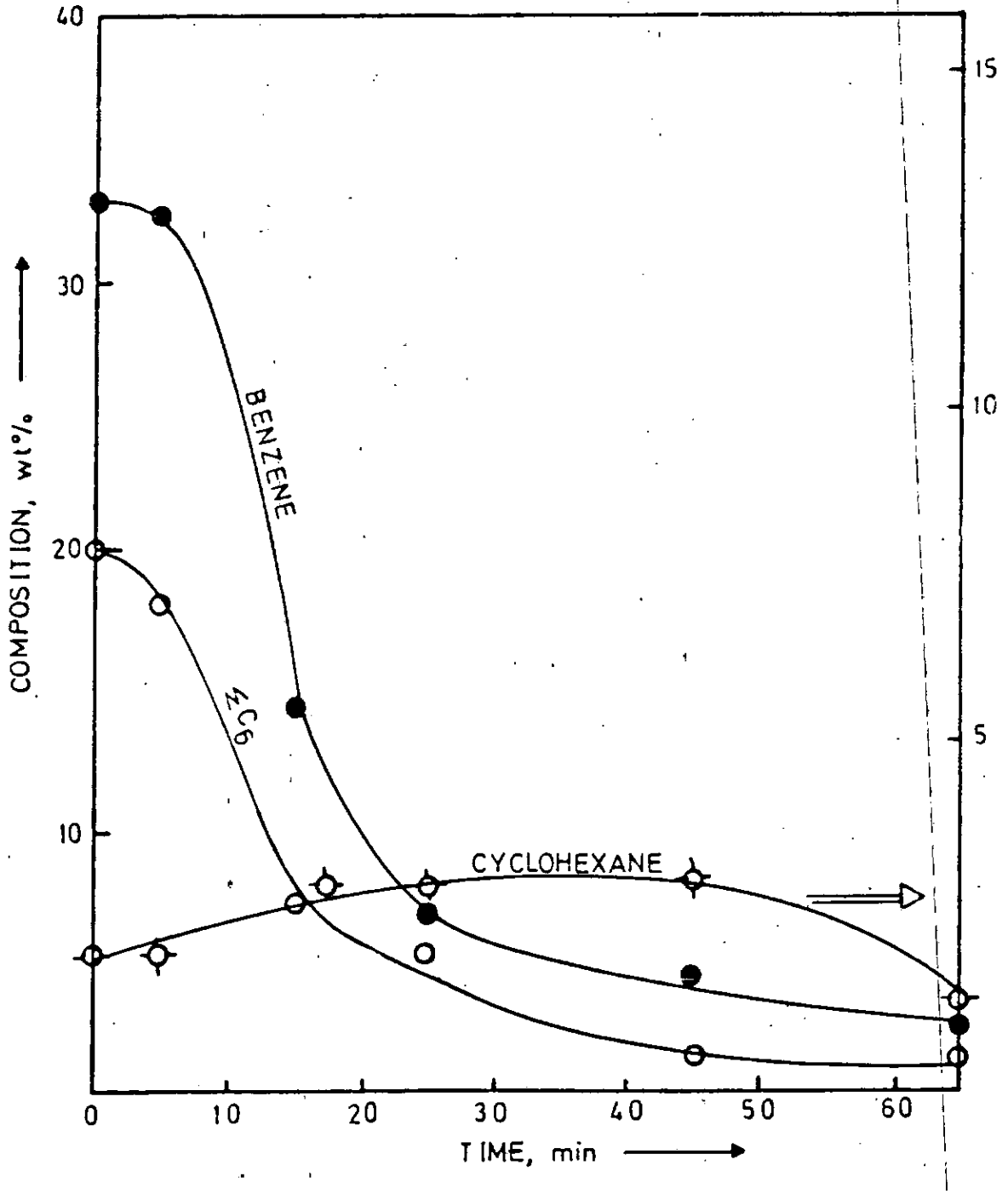

Fig. 5.2.39: Product composition of MCP conversion Pt-Re/Al_2O_3(DRIED) versus time at P_{MCP}= 9.2×10^{-2} atm; W/F = 0.11 gmin cm^{-3}; temperature = 410°C and P_{H_2} = 0.11 atm.

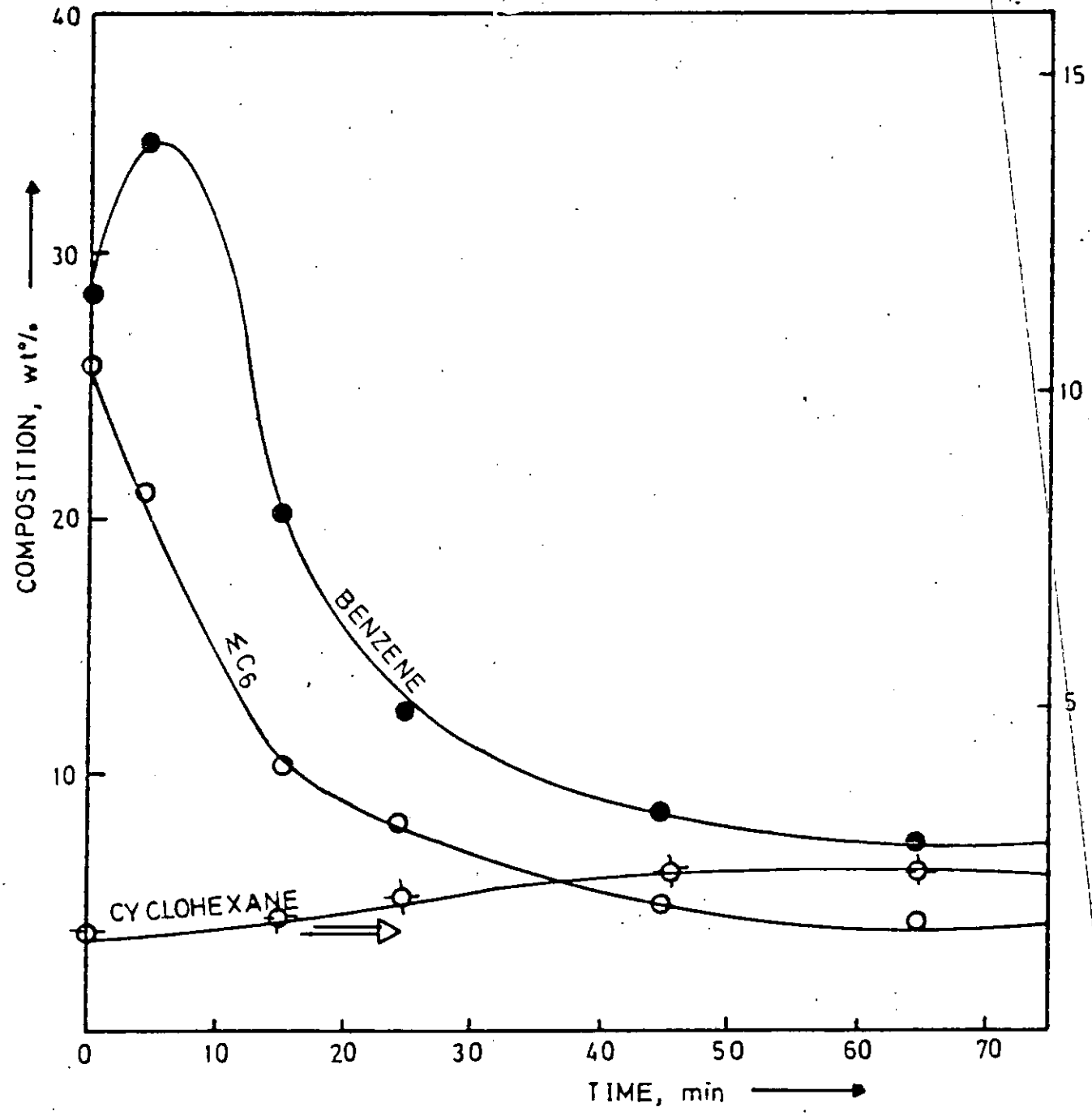

Fig. 5.2.40: Product composition of MCP conversion on $Pt\text{-}Re/Al_2O_3$(DRIED) versus time at $P_{MCP} = 9.2 \times 10^{-2}$atm; $W/F = 0.11 gmin cm^{-3}$; temperature = 410°C and $P_{H_2} = 0.33$atm.

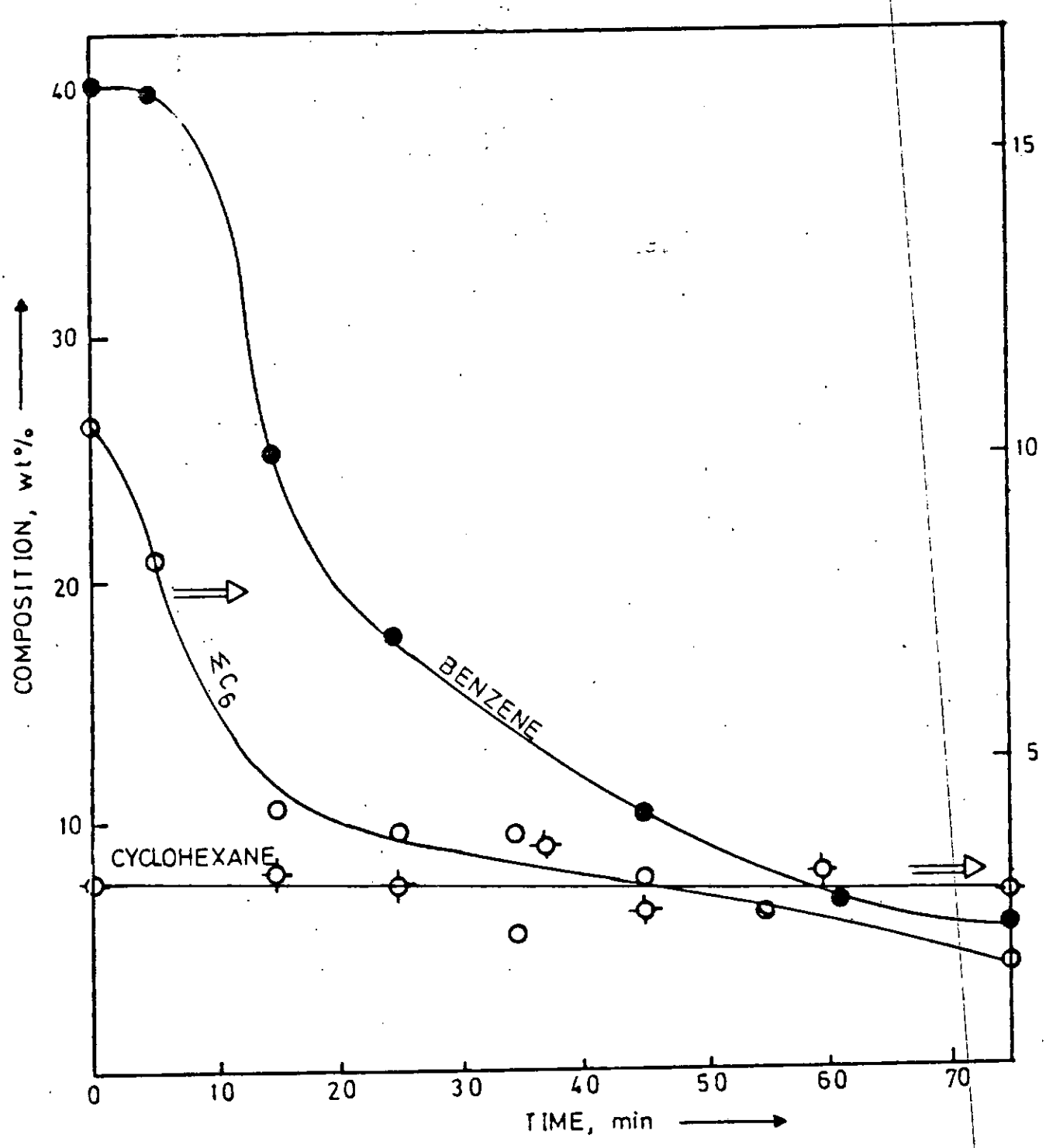

Fig. 5.2.41: Product composition of MCP conversion on Pt-Re/Al_2O_3(DRIED) versus time at P_{MCP}= 9.2×10^{-2}atm; W/F = 0.11gmincm^{-3}; temperature = 410°C and P_{H_2} = 0.5atm.

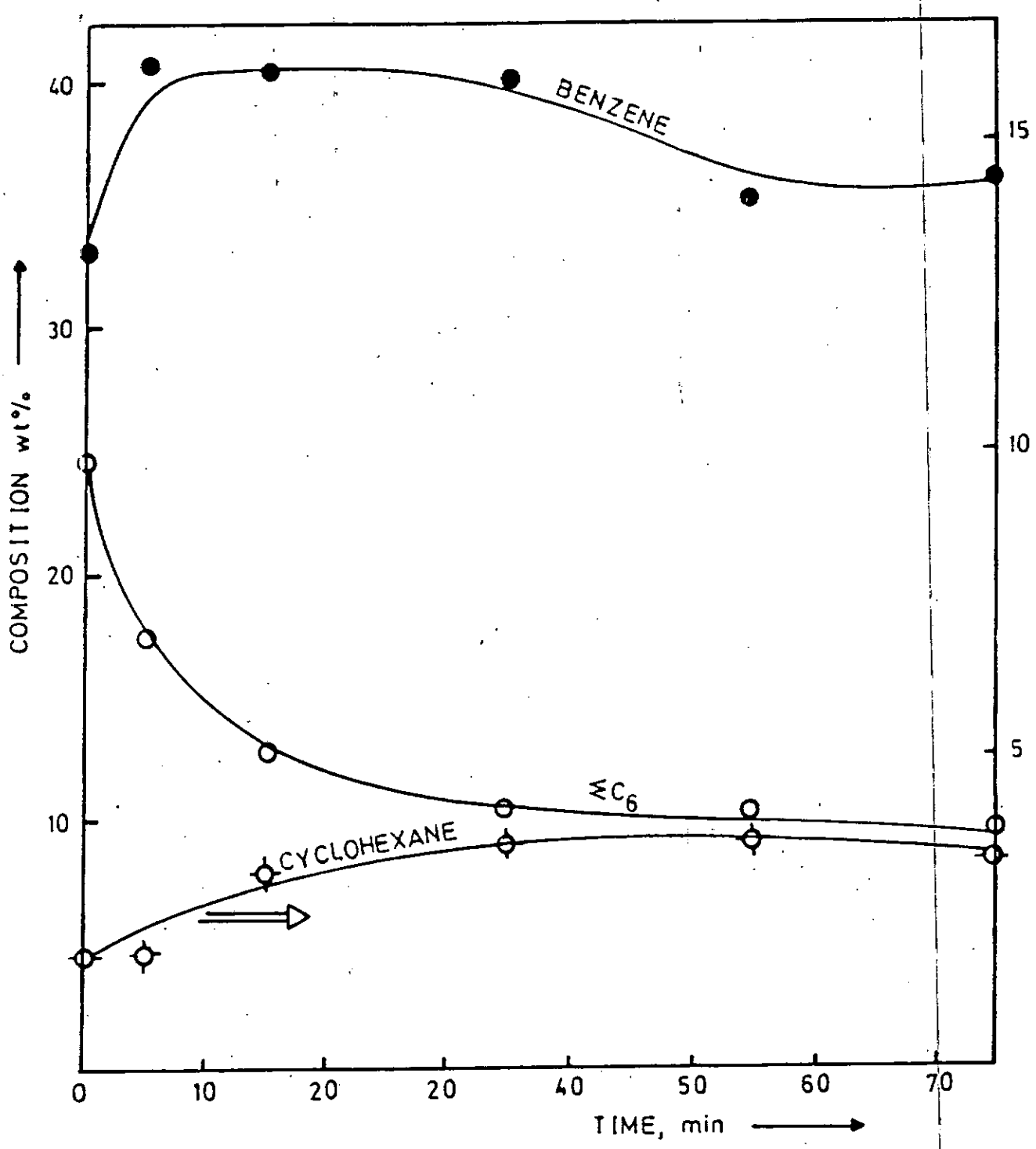

Fig.5.2.42: Product composition of MCP conversion on Pt-Re/Al_2O_3(DRIED) versus time at P_{MCP}=9.2x10^{-2}atm; W/F = 0.11gmincm^{-3}; temperature = 410°C and P_{H_2} = 0.778atm.

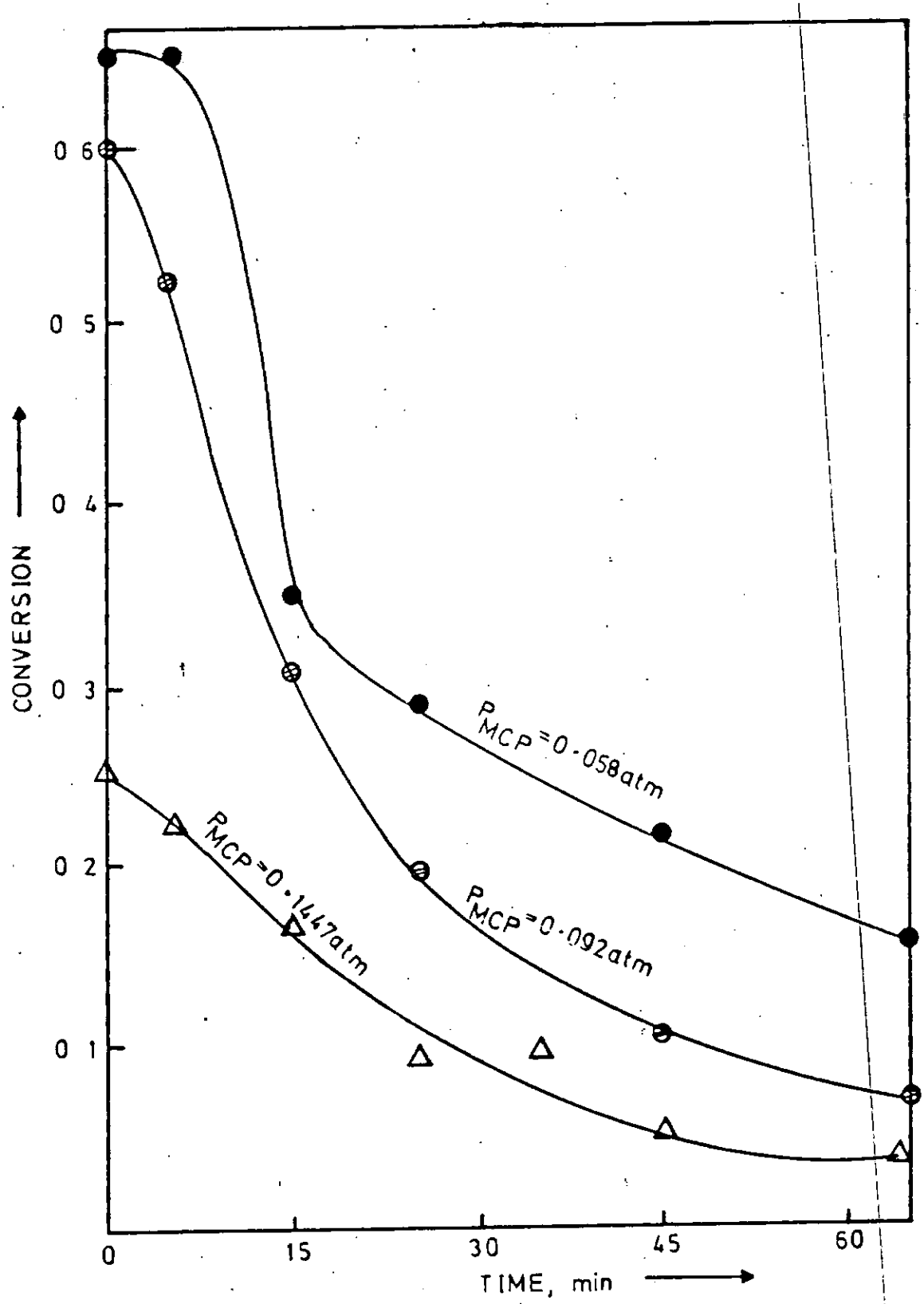

Fig. 5.2.43: MCP conversion on Pt-Re/Al_2O_3(DRIED) versus time at P_{H_2} = 0.5atm; W/F = 0.11gmincm^{-3}; temperature = 410°C and various P_{MCP}

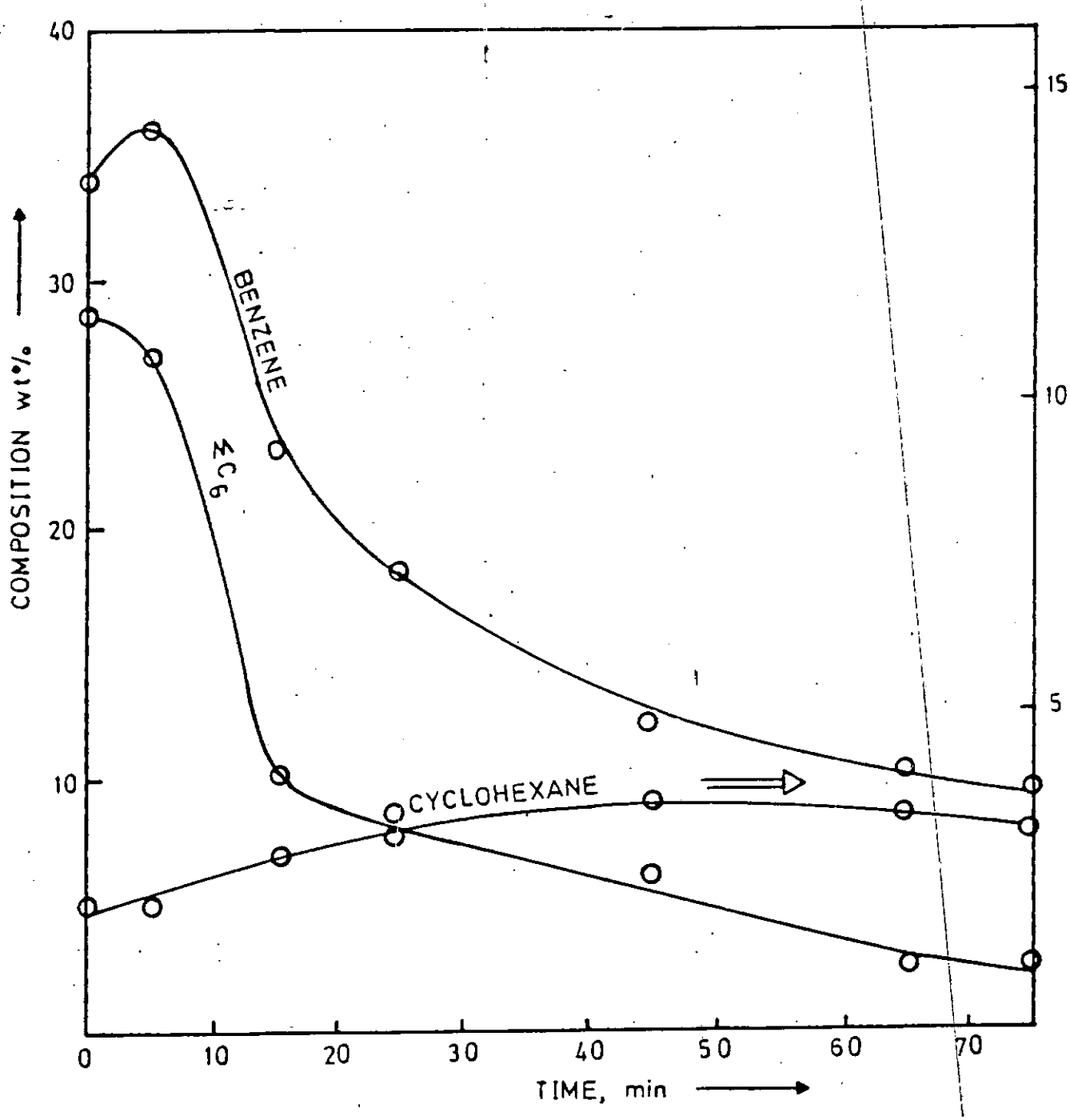

Fig. 5.2.44: Product composition of MCP conversion on Pt-Re/Al_2O_3(DRIED) versus time at P_{H_2} = 0.5atm; W/F = 0.11gmincm^{-3}; temperature = 410°C and P_{MCP}= 5.8x10^{-2}atm.

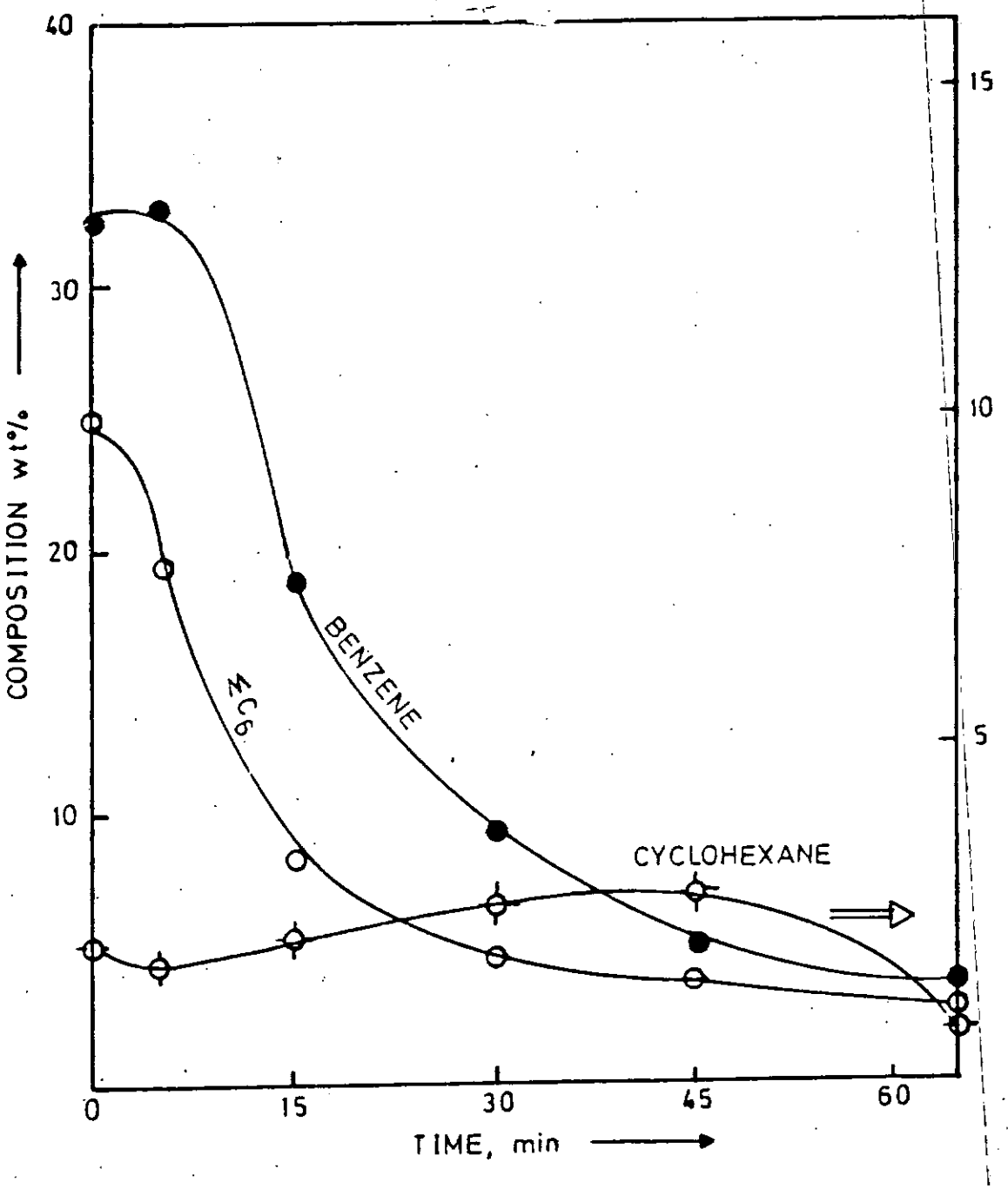

Fig. 5.2.45: Product composition of MCP conversion on Pt-Re/Al_2O_3(DRIED) versus time at P_{H_2} = 0.5atm; W/F = 0.11gmincm^{-3}; temperature = 410°C and P_{MCP}= 9.2x10^{-2}atm.

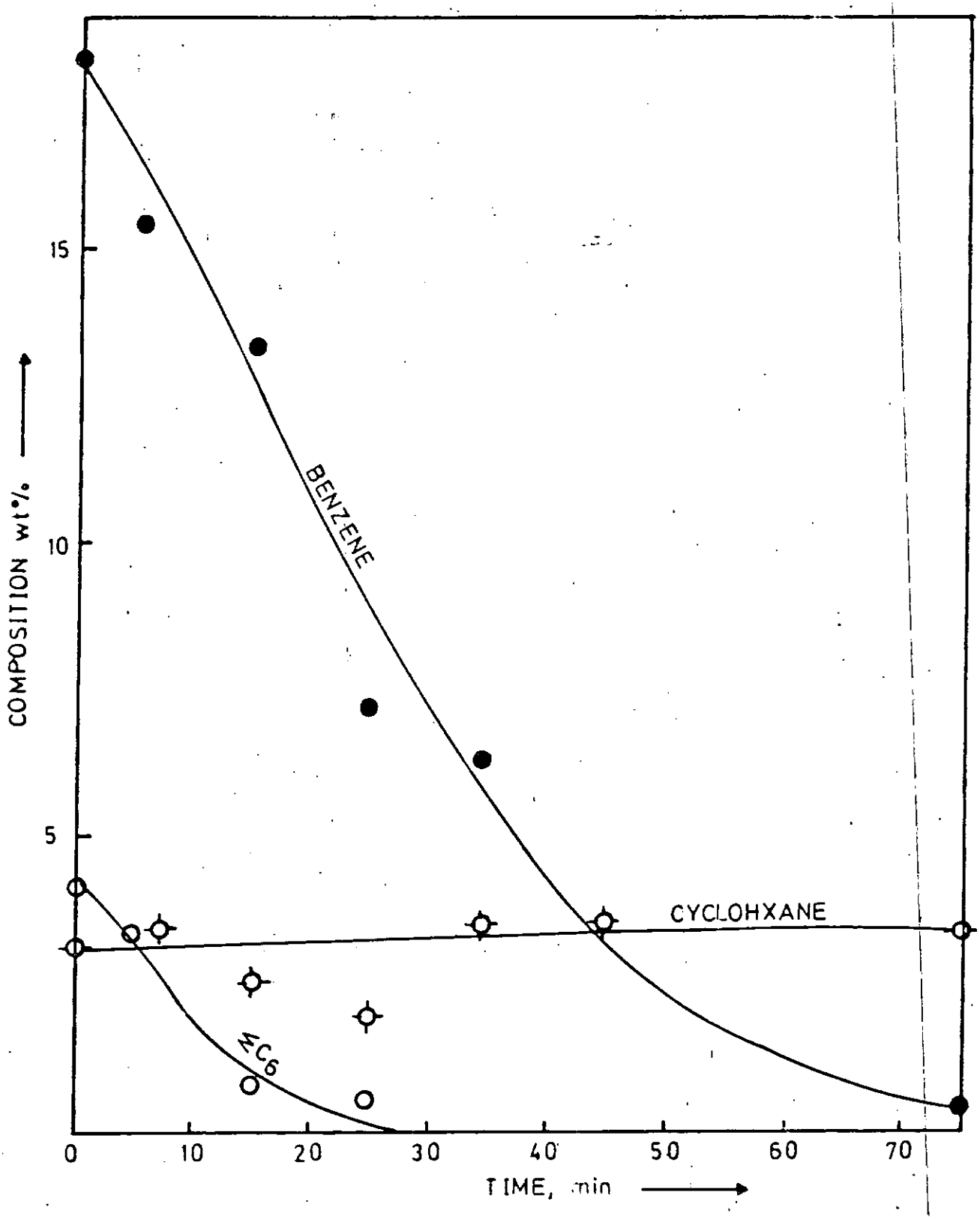

Fig. 5.2.46: Product composition of MCP conversion on Pt-Re/Al_2O_3(DRIED) versus time at P_{H_2} = 0.5atm; W/F = 0.11gmincm^{-3}; temperature = 410°C and P_{MCP}= 14.47x10^{-2}atm.

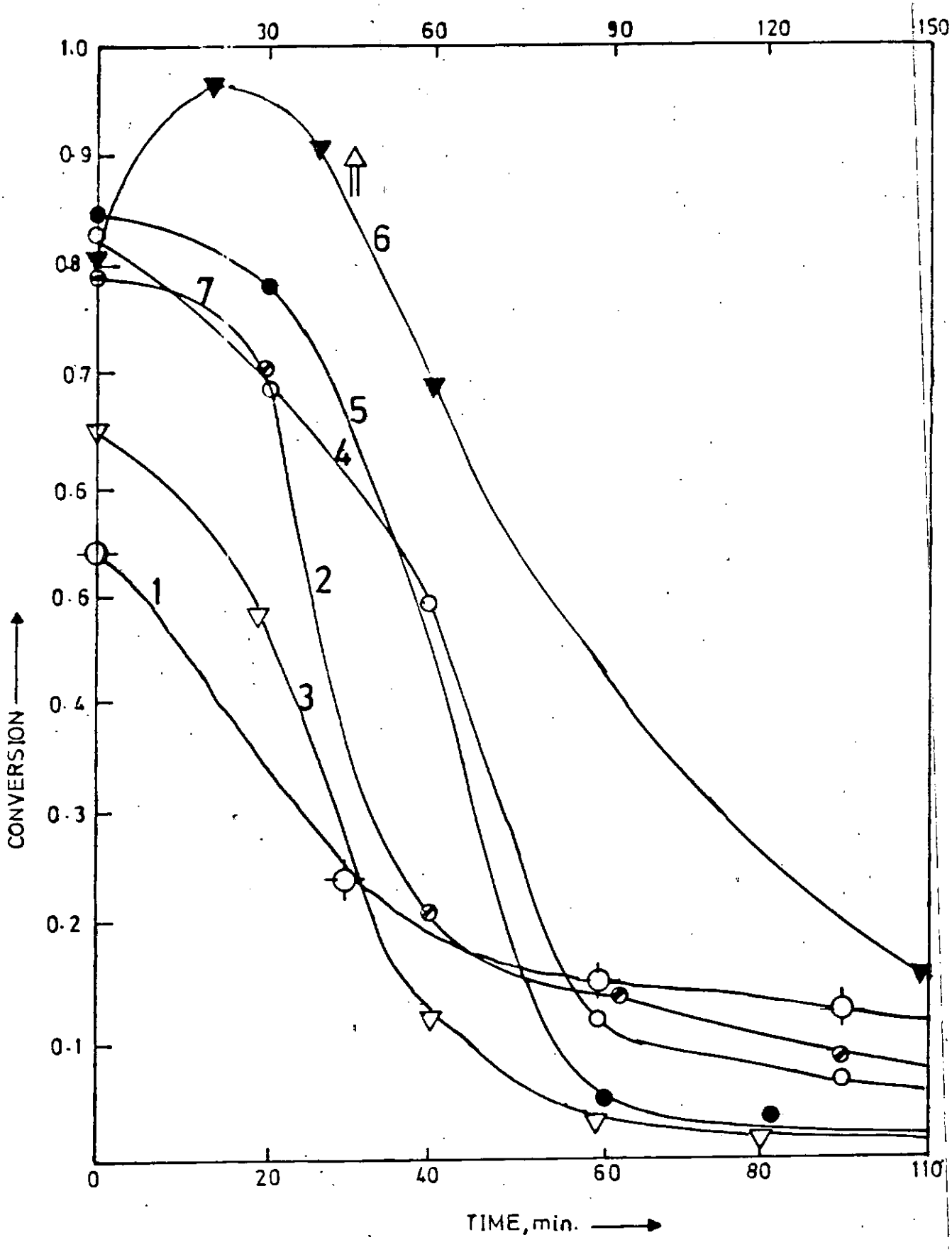

Fig. 5.3.1: N-octane conversion on Pt/Al_2O_3 versus time for 7-deactivation cycles in N_2 at $P_N = 13.7 \times 10^{-3}$ atm; $W/F = 16.67 \times 10^{-2}$ gmincm^{-3} and temperature = 440°C.

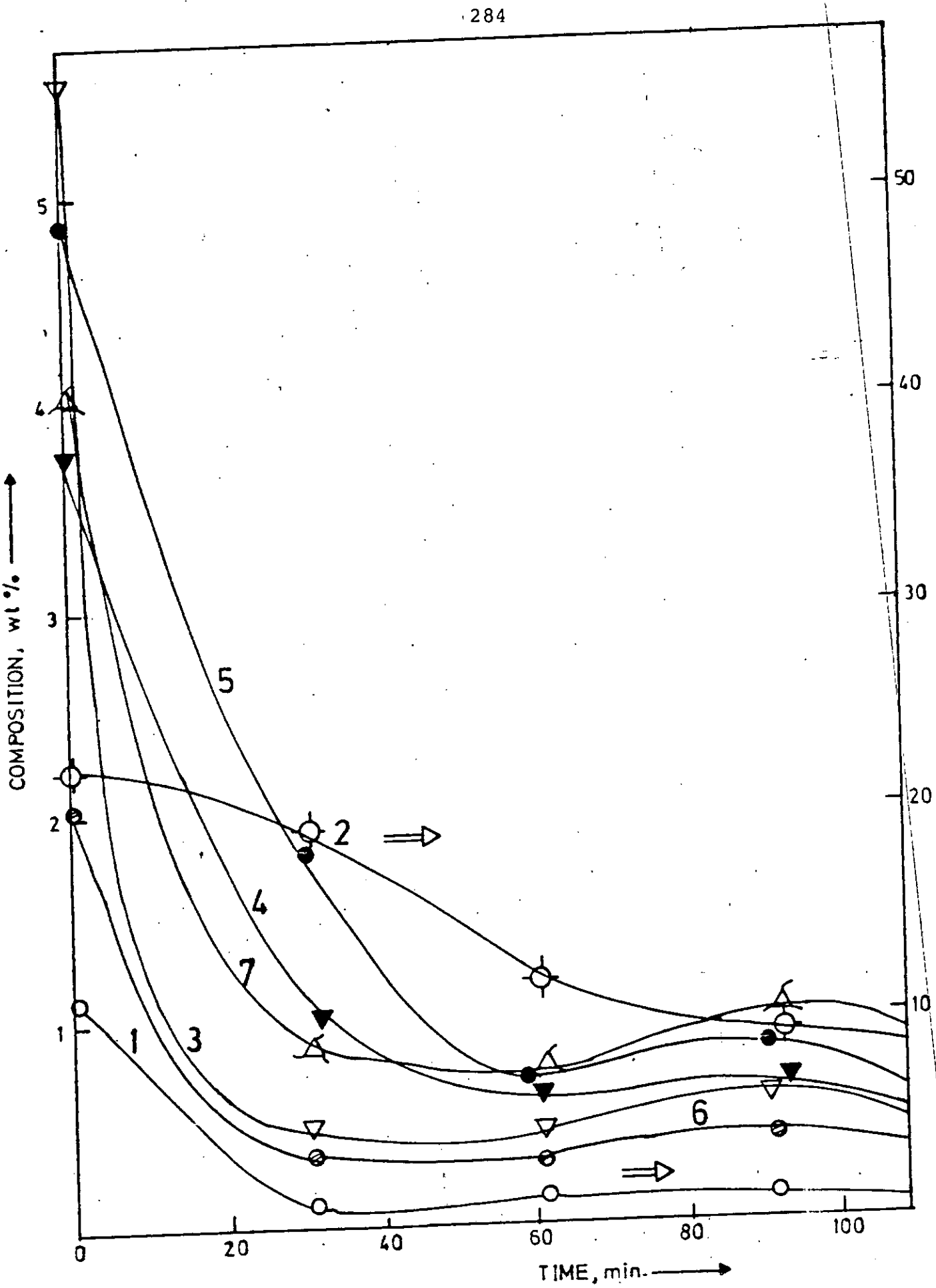

Fig. 5.3.2: Product composition for n-octane conversion on Pt/Al_2O_3 versus time for the first deactivation cycle in N_2 at $P_N = 13.7 \times 10^{-3}$ atm; $W/F = 16.67 \times 10^{-2}$ gmincm^{-3} and temperature = 440°C.

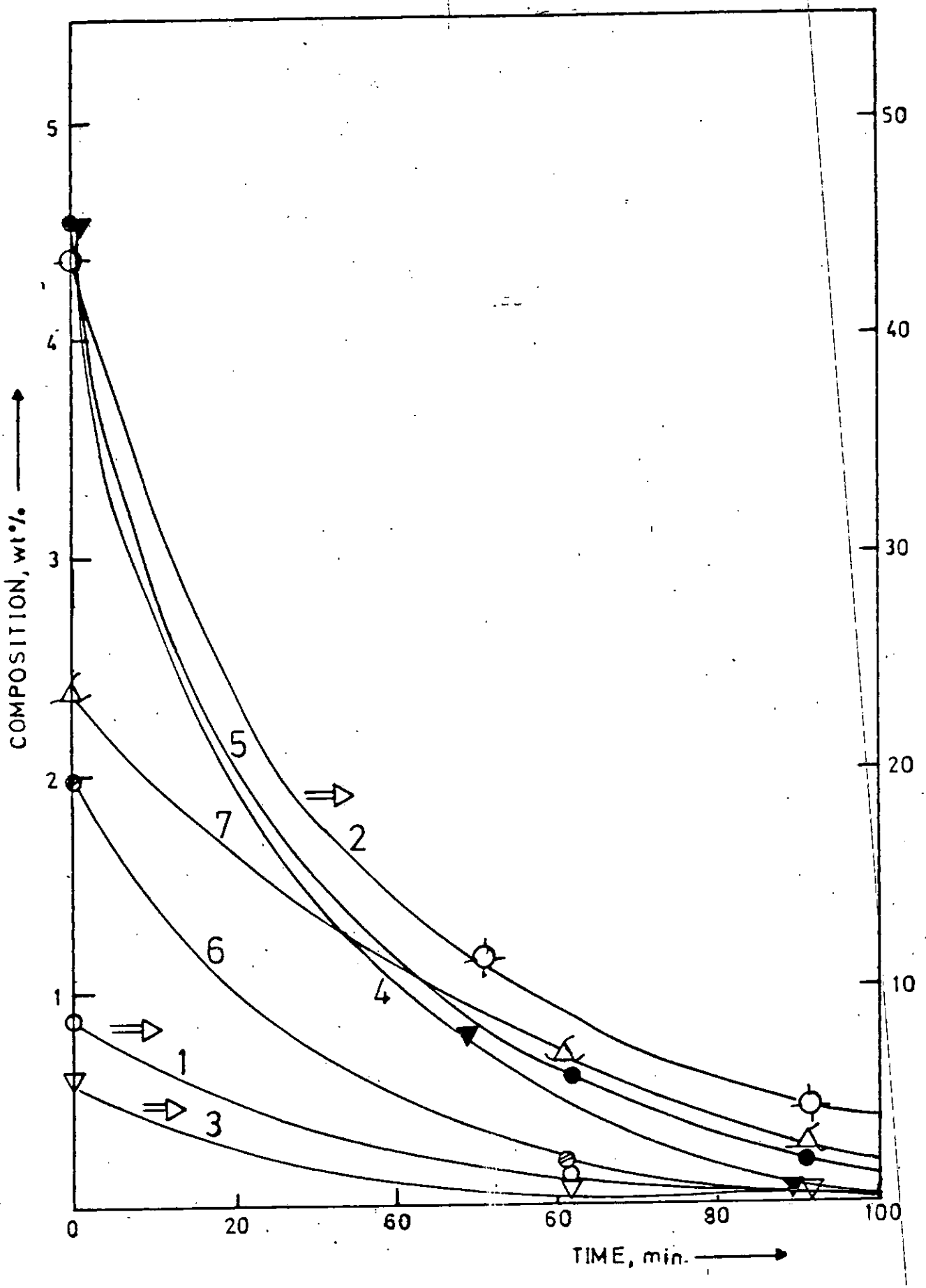

Fig. 5.3.3: Product composition for n-octane conversion on Pt/Al_2O_3 versus time for the second deactivation cycle in N_2 at P_N=13.7x10^{-3}atm; W/F = 16.67x10^{-2} gmincm^{-3} and temperature = 440°C

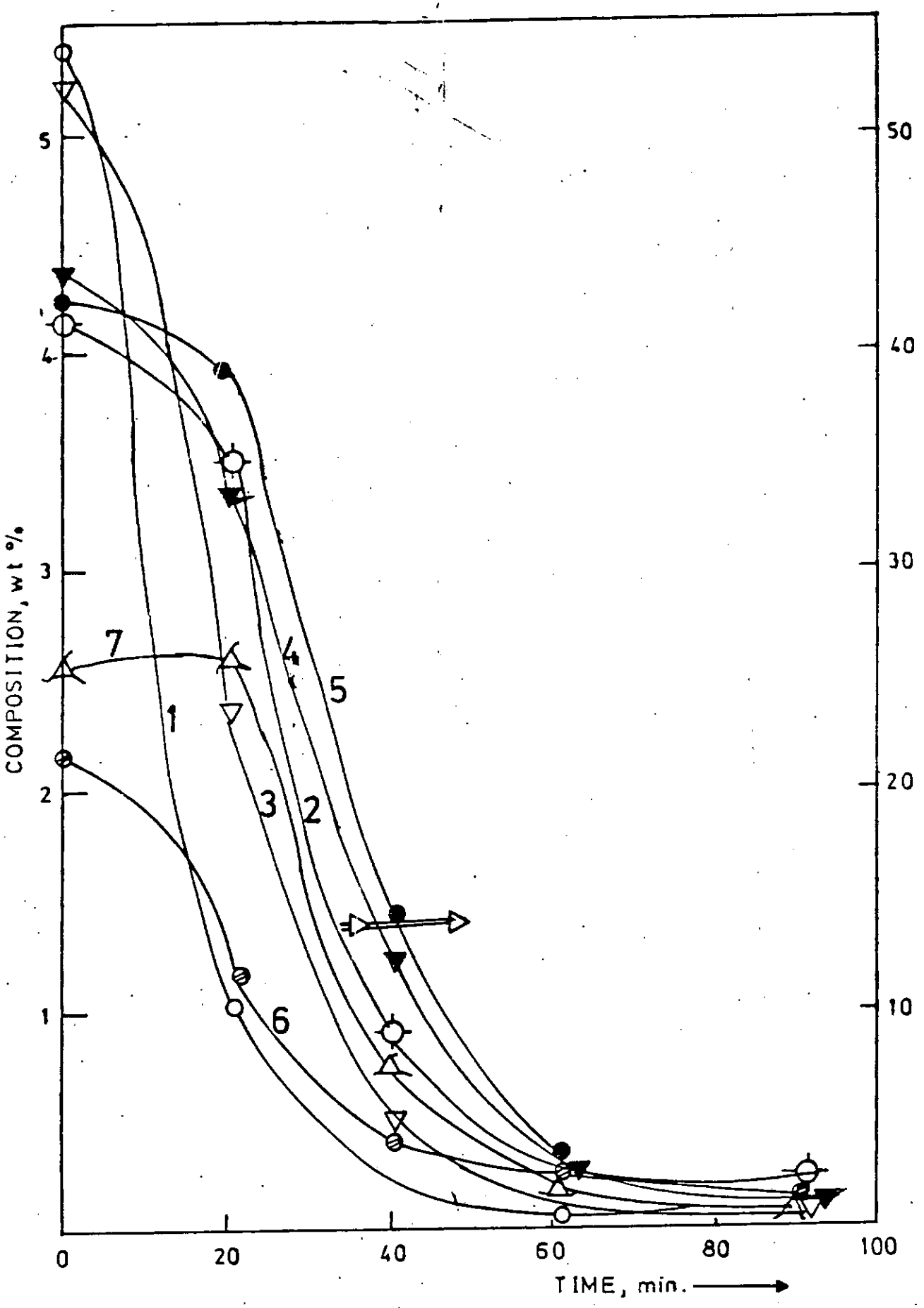

Fig.5.3.4: Product composition for n-octane conversion on Pt/Al_2O_3 versus time for the third deactivation cycle in N_2 at $P_N = 13.7 \times 10^{-3}$ atm; $W/F = 16.67 \times 10^{-2}$ gmincm^{-3} and temperature = 440°C

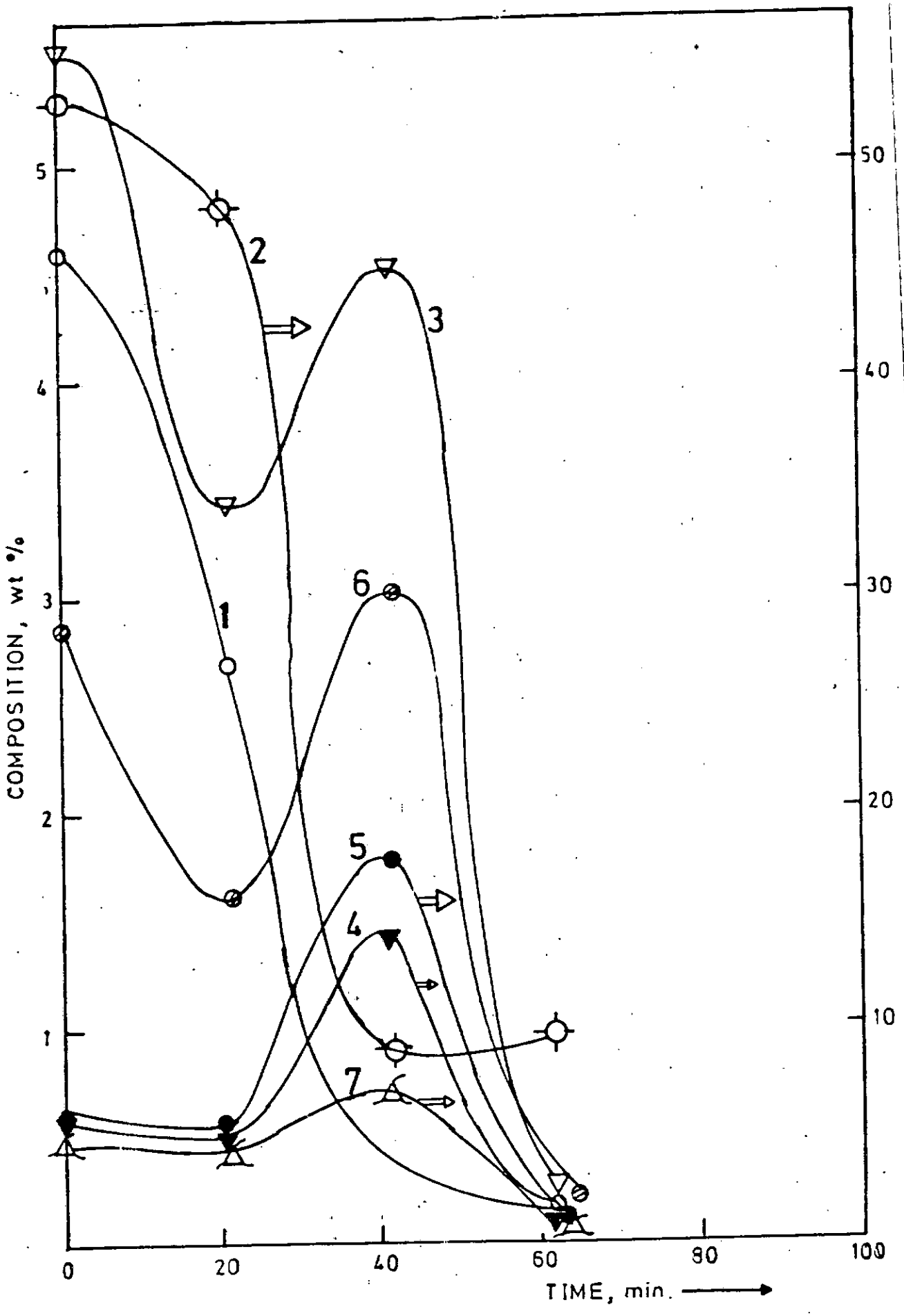

Fig. 5.3.5: Product composition for n-octane conversion on Pt/Al_2O_3 versus time for the fourth deactivation cycle in N_2 at $P_N = 13.7 \times 10^{-3}$ atm; $W/F = 16.67 \times 10^{-2}$ gmincm^{-3} and temperature = 440°C

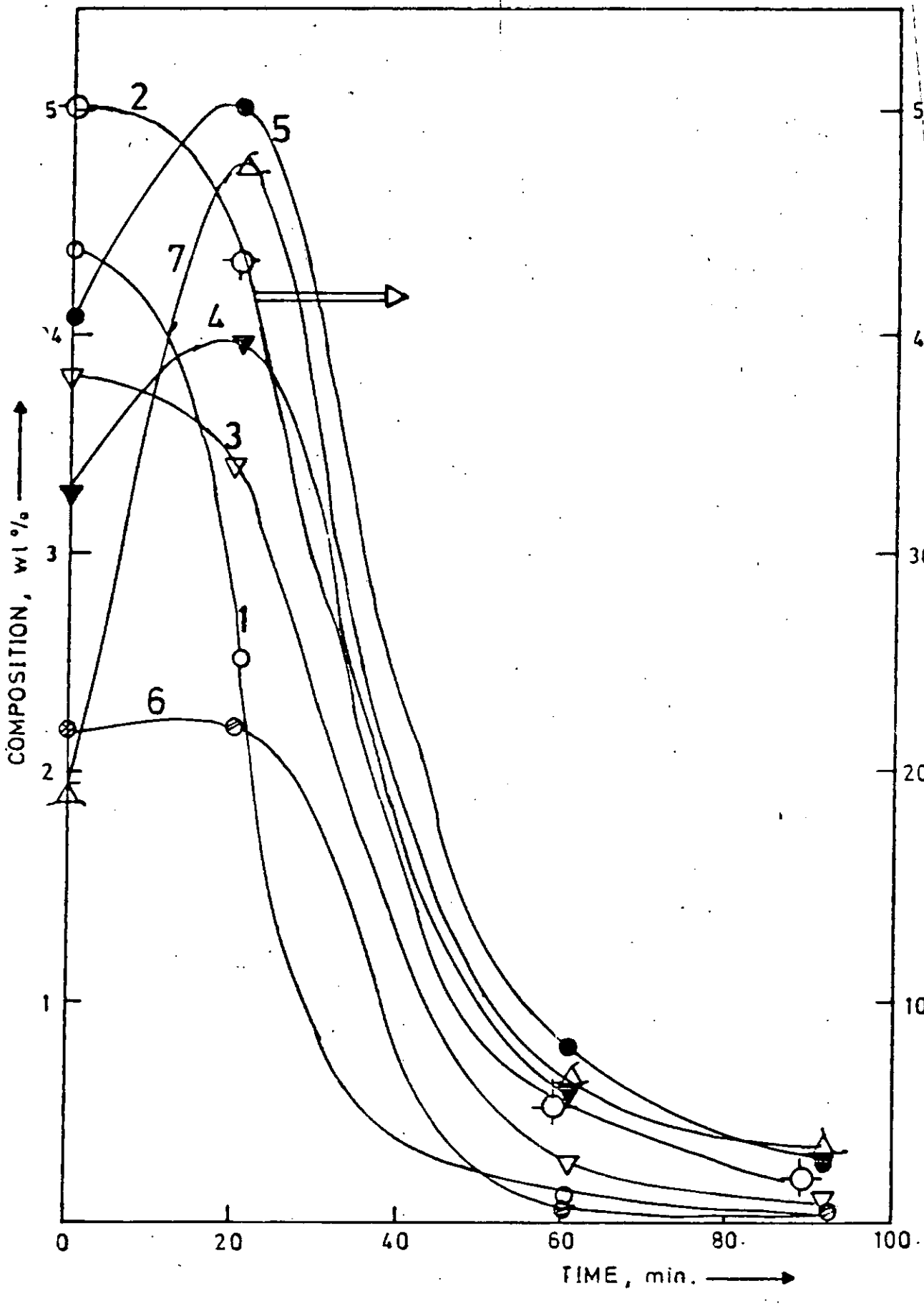

Fig. 5.3.6: Product composition for n-octane conversion on Pt/Al_2O_3 versus time for the fifth deactivation cycle in N_2 at $P_N = 13.7 \times 10^{-3}$ atm; $W/F = 16.67 \times 10^{-2}$ gmincm^{-3} and temperature = 440°C

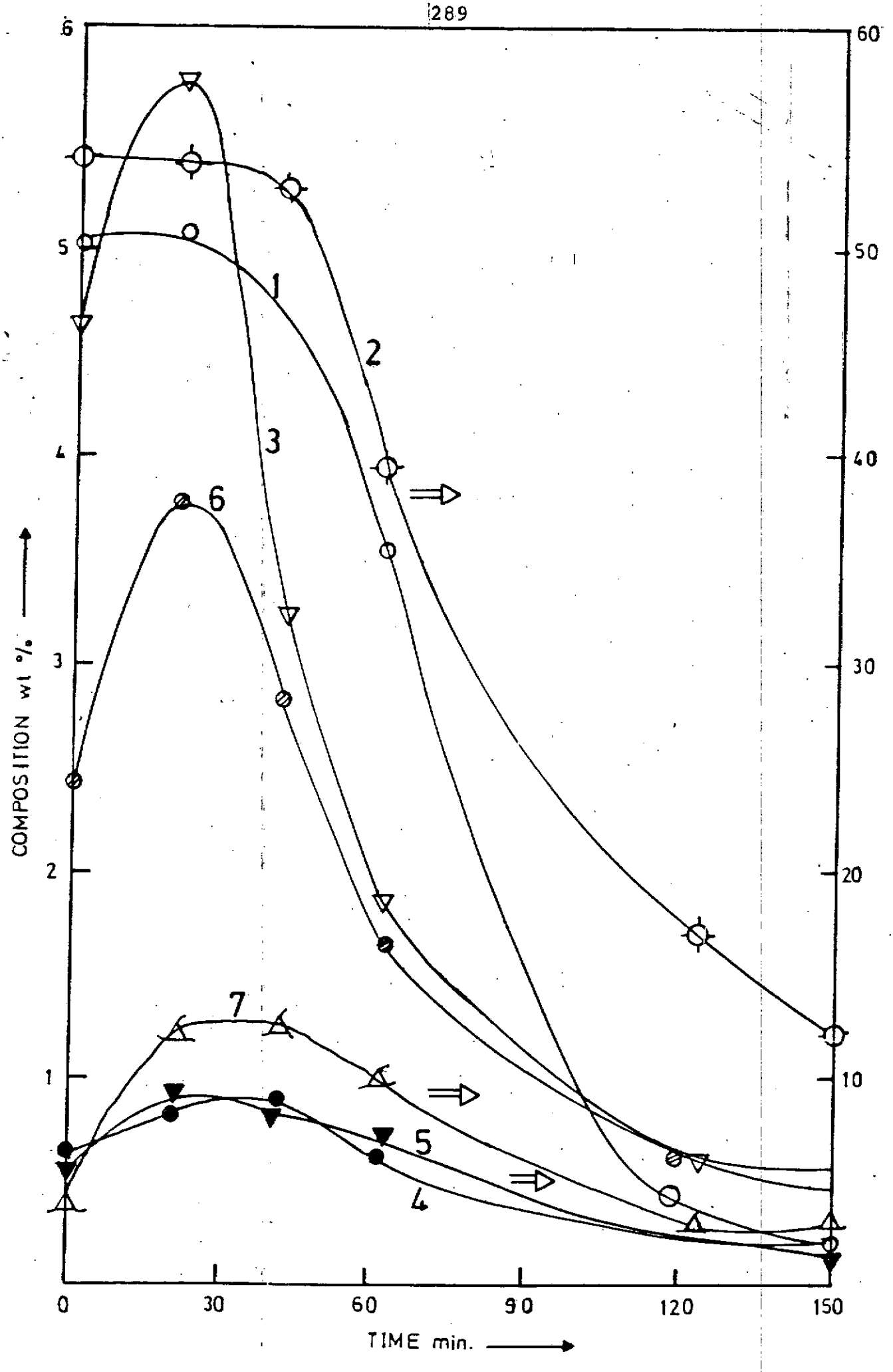

Fig.5.3.7: Product composition for n-octane conversion on Pt/Al_2O_3 versus time for the sixth deactivation cycle in N_2 at $P_N=13.7\times10^{-3}$atm; $W/F = 16.67\times10^{-2}$gmincm^{-3} and temperature = 440°C

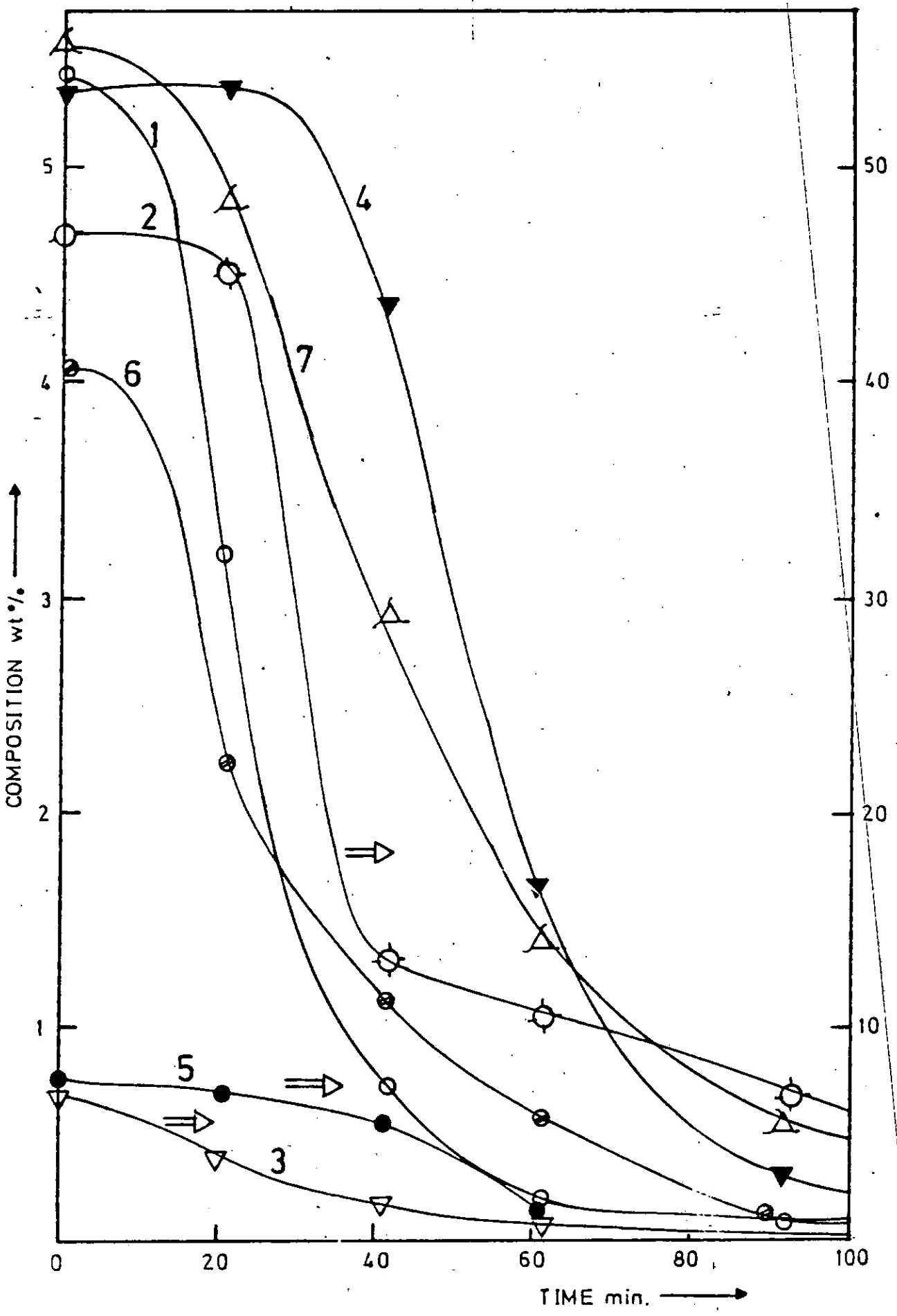

Fig. 5.3.8: Product composition for n-octane conversion on Pt/Al_2O_3 versus time for the seventh deactivation cycle in N_2 at $P_N = 13.7 \times 10^{-3}$ atm; $W/F = 16.67 \times 10^{-2}$ gmincm^{-3} and temperature = 440°C

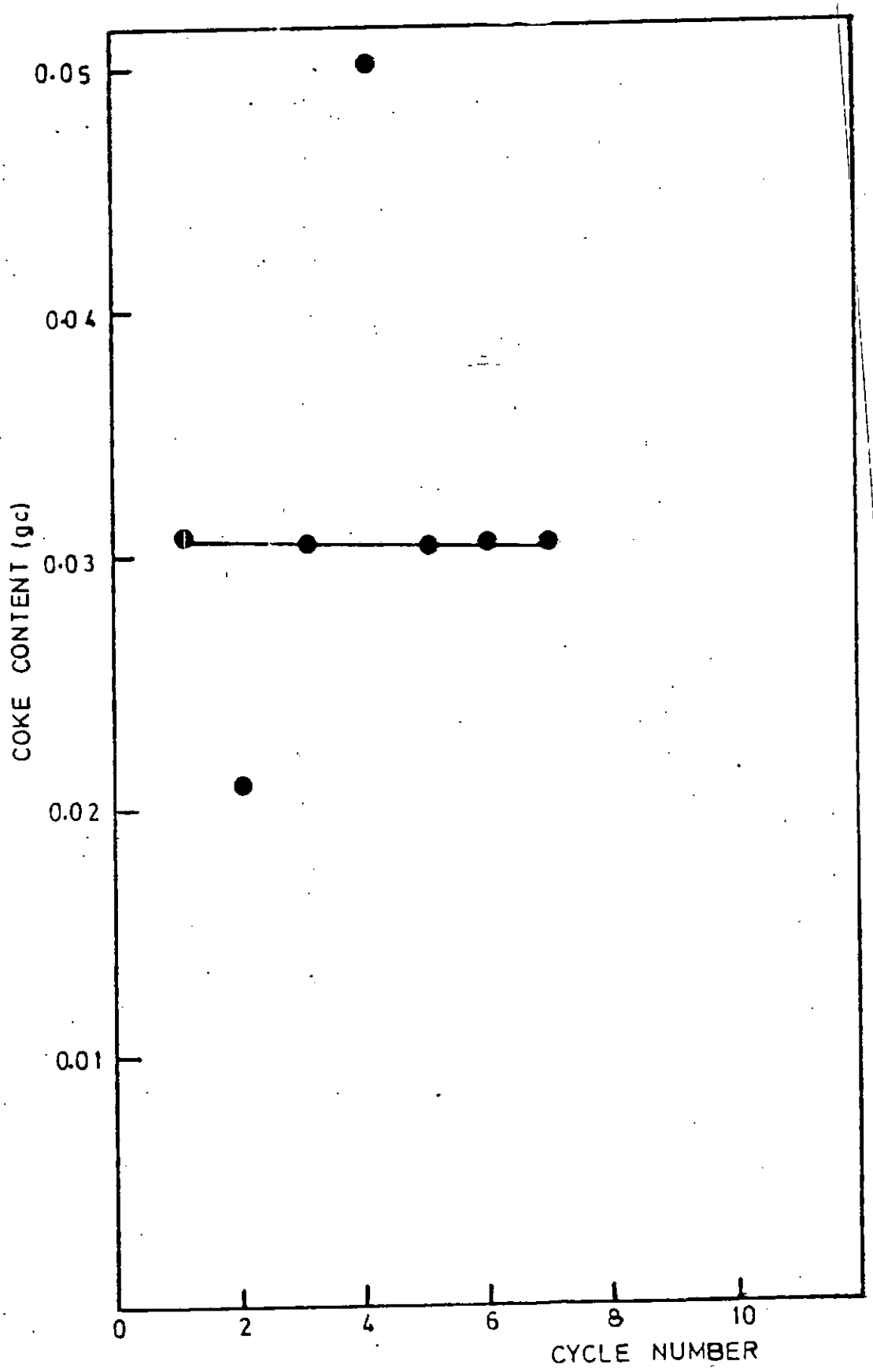

Fig. 5.3.9: Coke content for n-octane conversion on Pt/Al_2O_3 versus cycle number at 430°C.

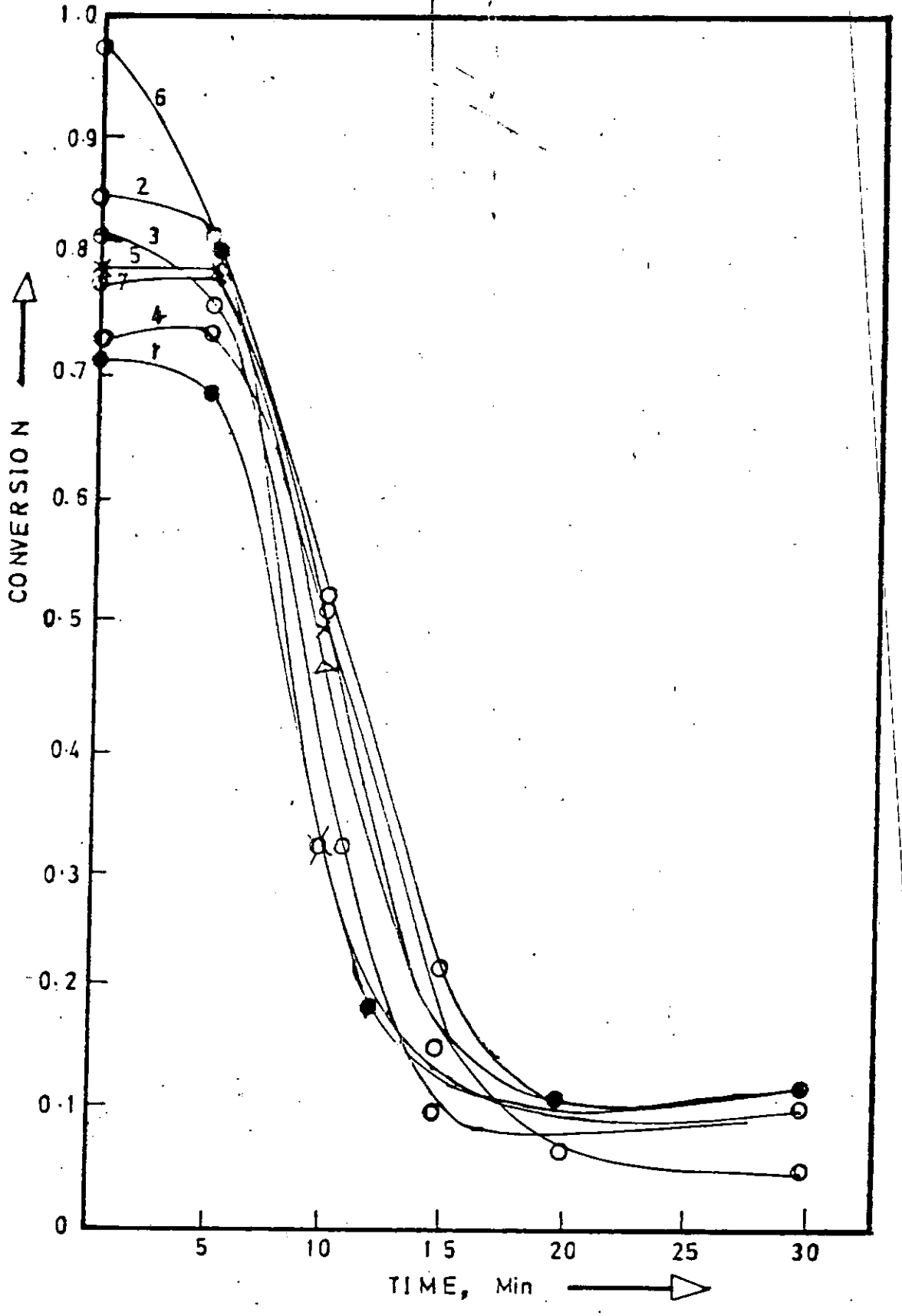

Fig. 5.3.10: Iso-octane conversion on 0.3%Pt/Al_2O_3 versus time for the first 7 deactivation cycles in N_2 at $P_{iso} = 3.16 \times 10^{-2}$atm; $W/F = 0.11 gmin cm^{-3}$ and temperature = 430°C

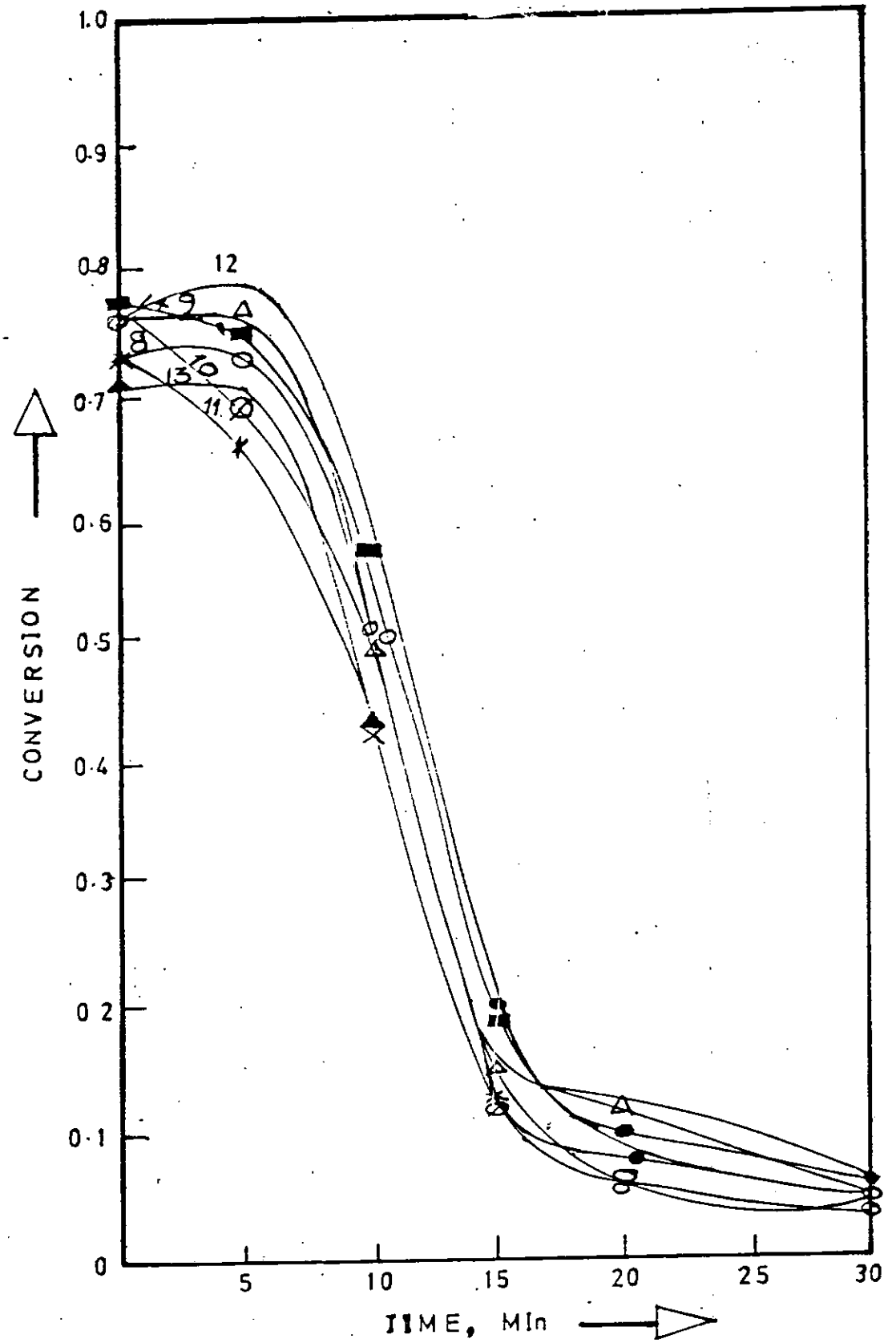

Fig. 5.3.11: Iso-octane conversion on 0.3%Pt/Al_2O_3 versus time for the 8th-14th deactivation cycles in N_2 at P_{iso}= 3.16×10^{-2}atm; W/F = 0.11gmincm^{-3} and temperature = 430°C.

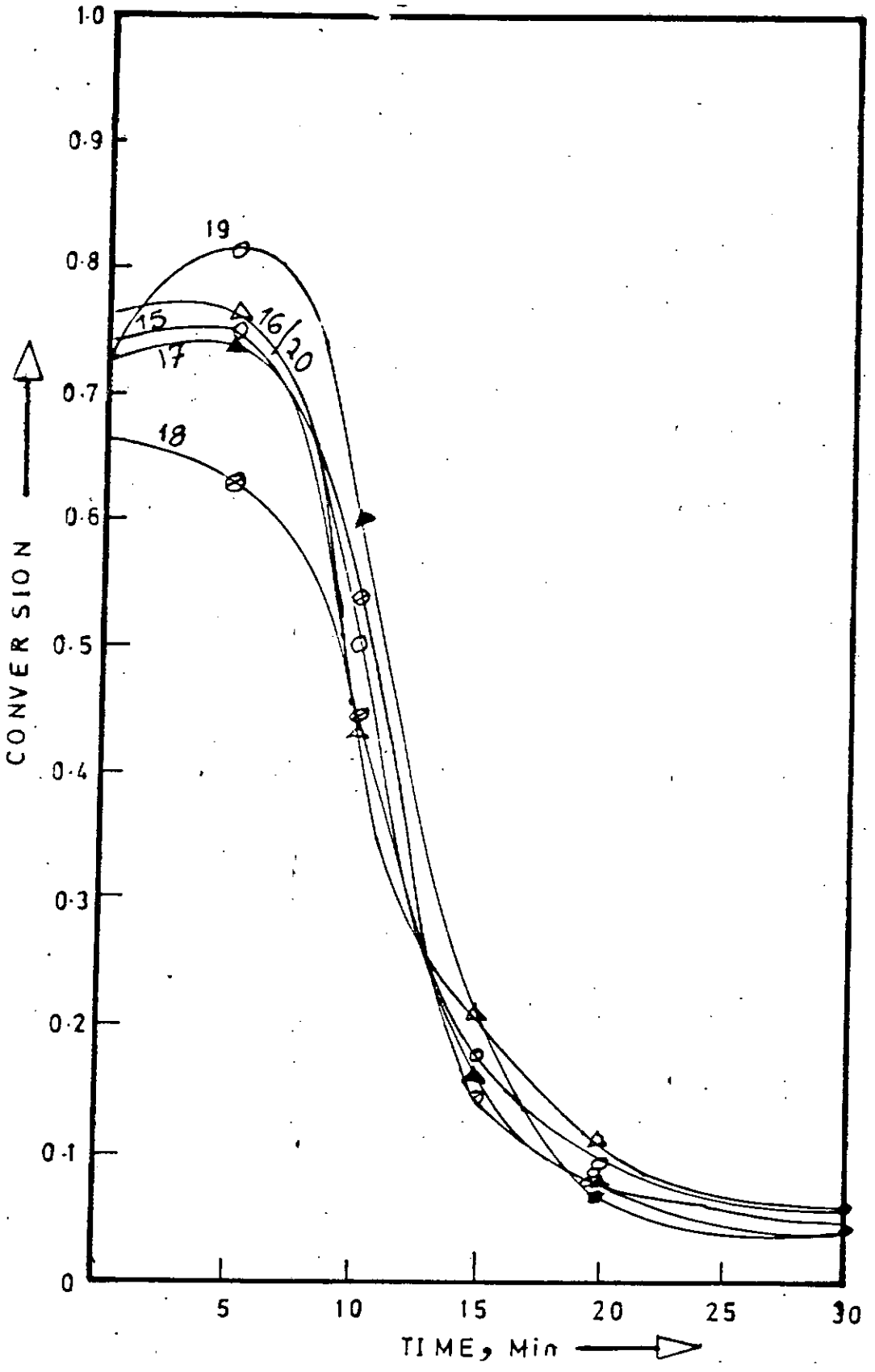

Fig. 5.3.12: Iso-octane conversion on 0.3%Pt/Al_2O_3 versus time for the 15-20th deactivation cycles in N_2 at P_{iso} = 3.16×10^{-2} atm; W/F = 0.11gmincm^{-3} and temperature = 430°C

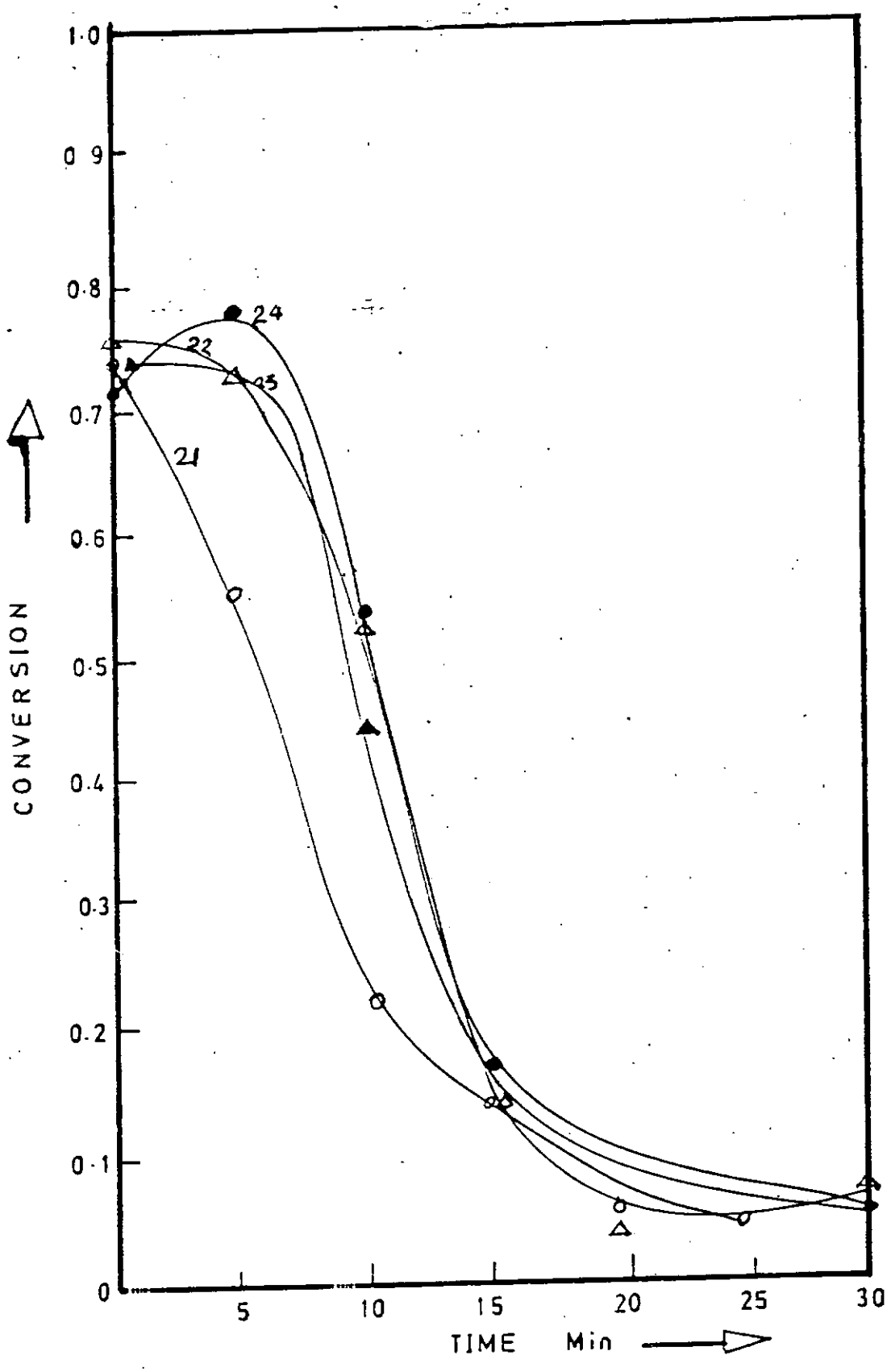

Fig.5.3.13: Iso-octane conversion on 0.3%Pt/Al_2O_3 versus time for the 21st-24th deactivation cycles in N_2 at P_{iso}= 3.16×10^{-2}atm; W/F = 0.11gmincm^{-3} and temperature = 430°C

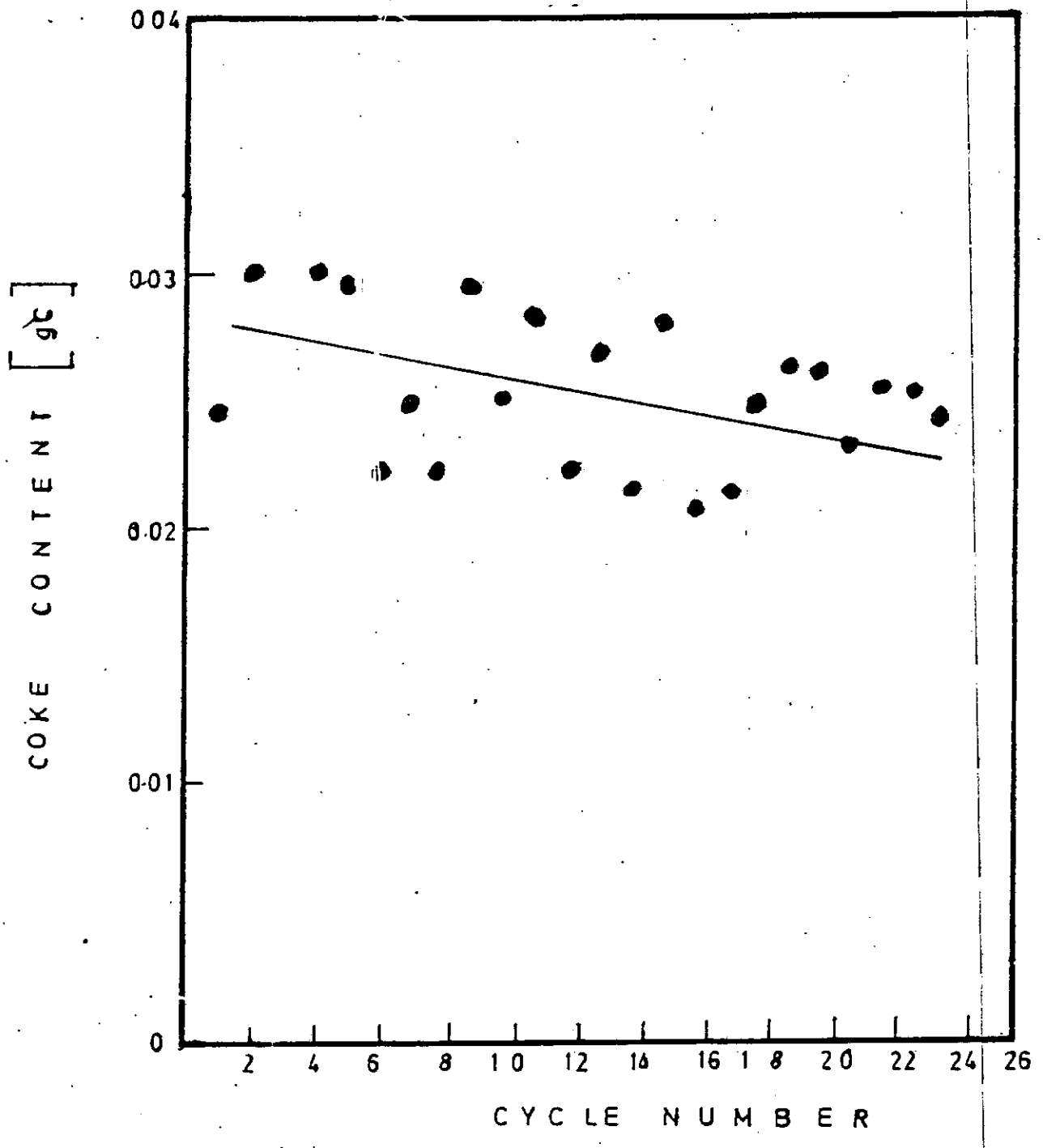

Fig. 5.3.14: Coke content for iso-octane conversion on 0.3%Pt/Al_2O_3 versus cycle number at 430°C

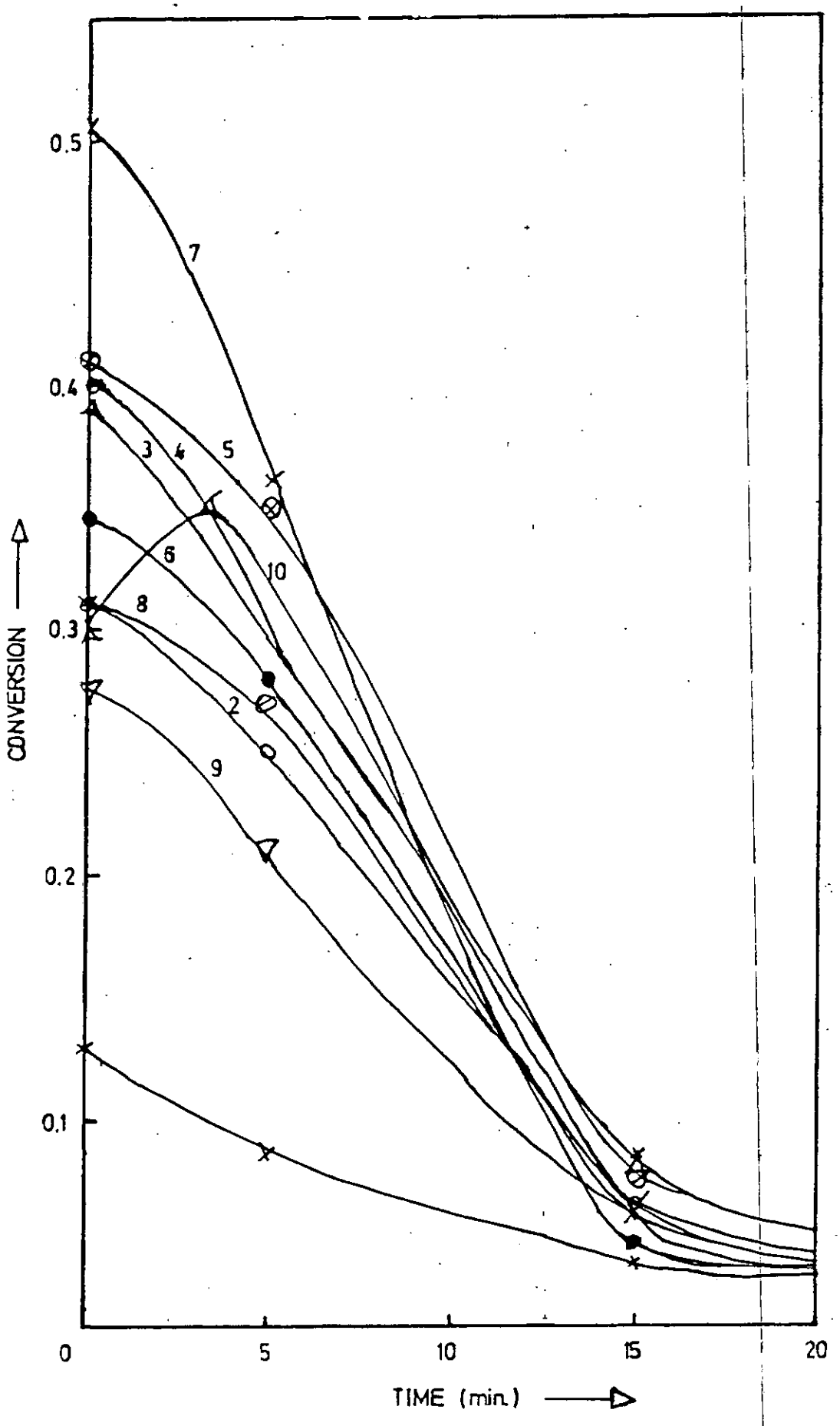

Fig. 5.3.15: MCP conversion on Pt/Al_2O_3 versus time for the first 10 deactivation cycles in N_2 at $P_{MCP} = 9.2 \times 10^{-2}$ atm; $W/F = 0.11 gmincm^{-3}$ and temperature = 430°C

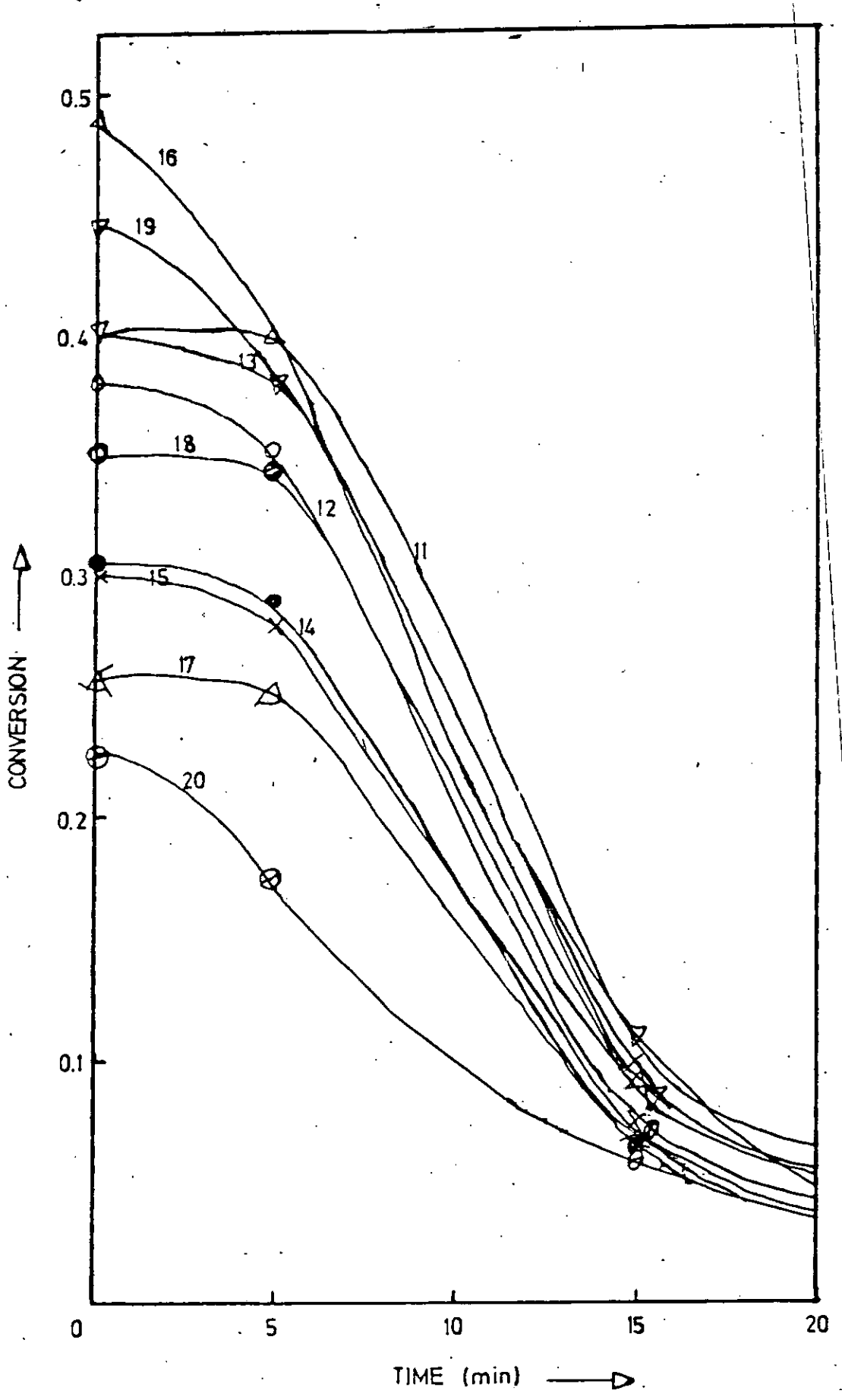

Fig. 5.3.16: MCP conversion on Pt/Al_2O_3 versus time for the 11th - 20th deactivation cycles in N_2 at $P_{MCP} = 9.2 \times 10^{-2}$ atm; W/F = 0.11 gmin cm^{-3} and temperature = 430°C

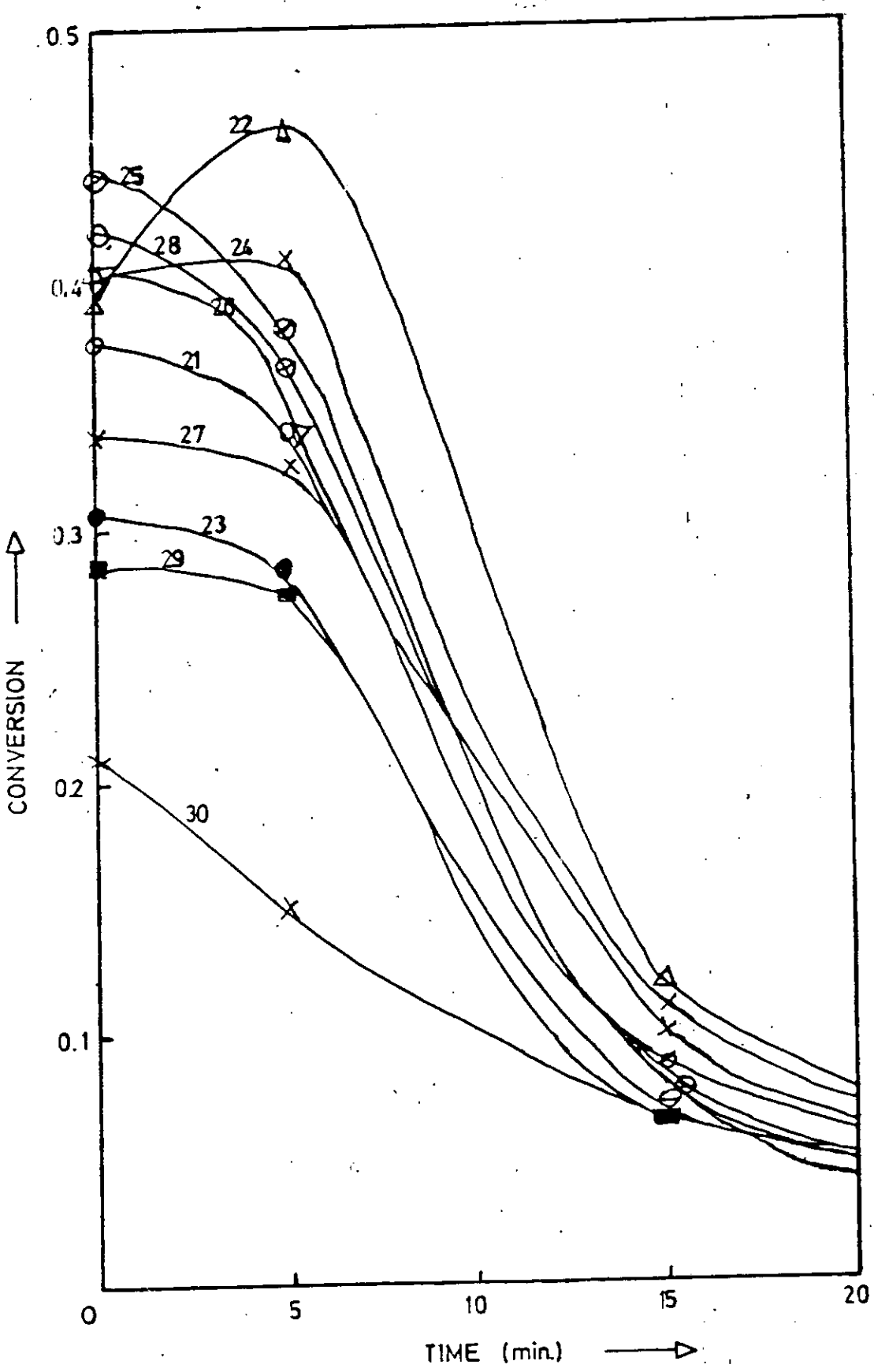

Fig. 5.3.17: MCP conversion on Pt/Al_2O_3 versus time for the 21st-30th deactivation cycles in N_2 at $P_{MCP} = 9.2 \times 10^{-2}$ atm; W/F = 0.11 gmin cm^{-3} and temperature = 430°C

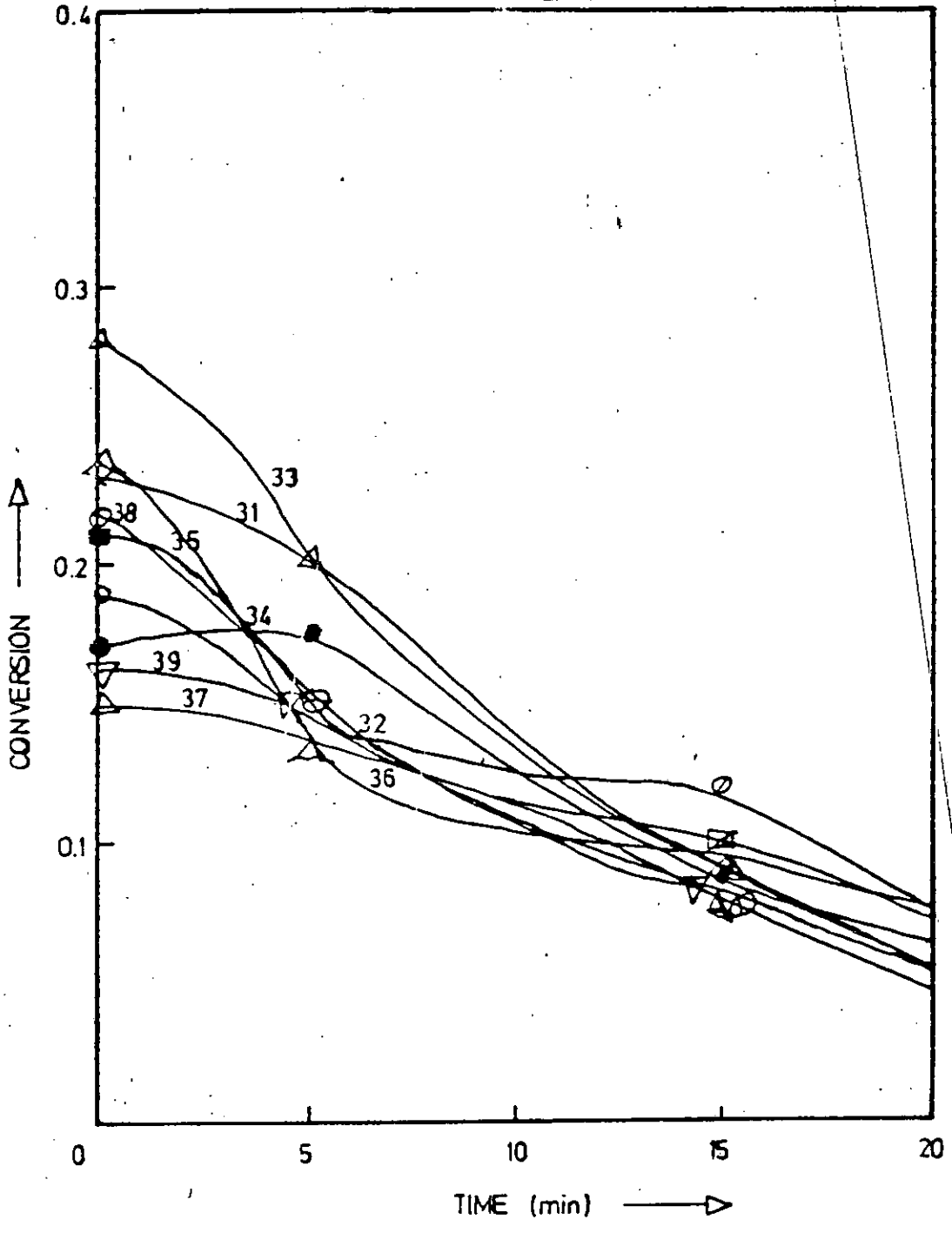

Fig. 5.3.18: MCP conversion on Pt/Al_2O_3 versus time for the 31st-40th deactivation cycles in N_2 at $P_{MCP} = 9.2 \times 10^{-2}$ atm; $W/F = 0.11 \text{ g min cm}^{-3}$ and temperature = 430°C

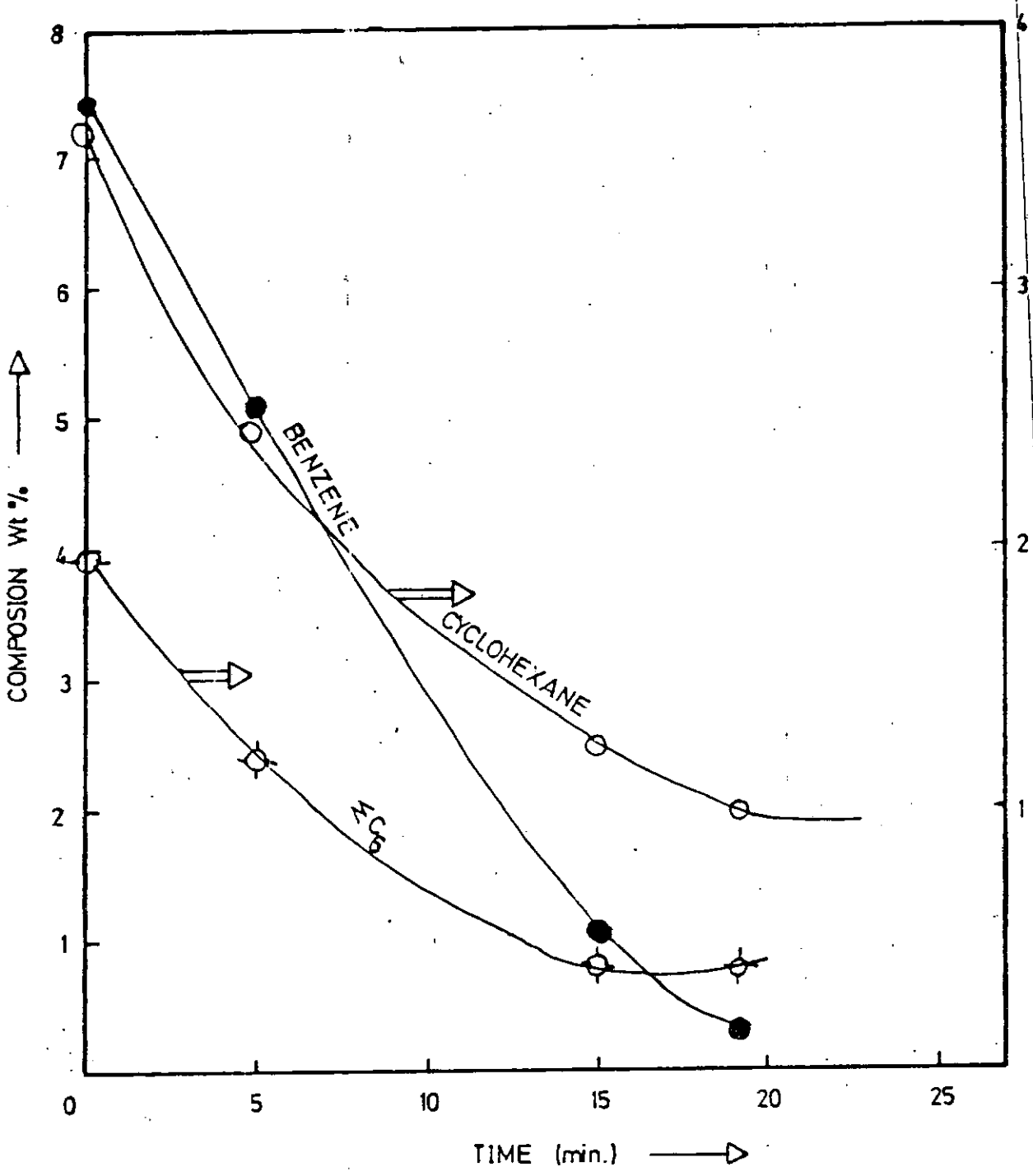

Fig. 5.3.19: Product composition for MCP conversion on Pt/Al_2O_3 versus time for the first deactivation cycle in N_2 at $P_{MCP} = 9.2 \times 10^{-2}$ atm; W/F = 0.11gmincm^{-3} and temperature = 430°C

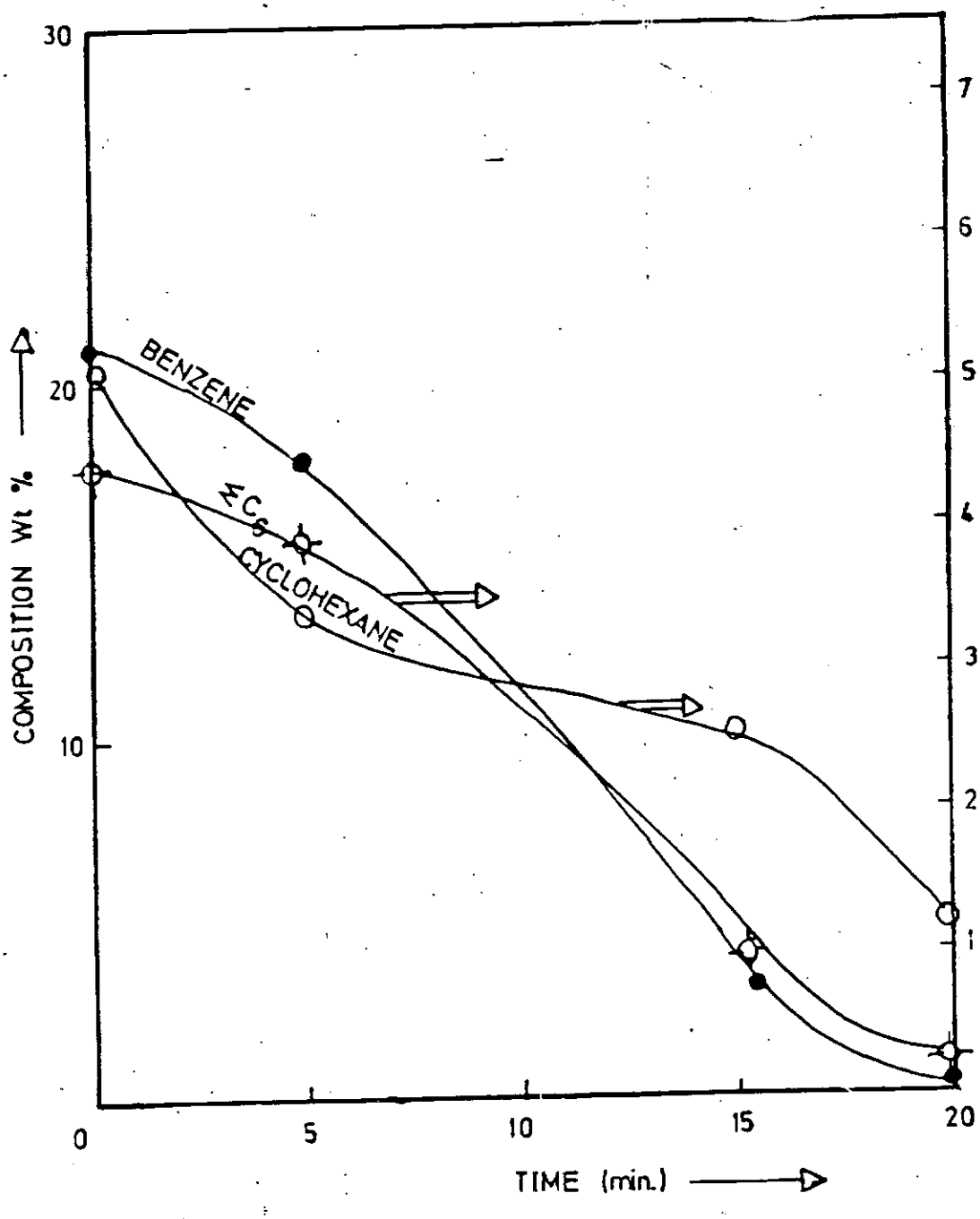

Fig. 5.3.20: Product composition for MCP conversion on Pt/Al_2O_3 versus time for the second deactivation cycle in N_2 at P_{MCP} = 9.2×10^{-2} atm; W/F = 0.11 gmin cm^{-3} and temperature = 430°C

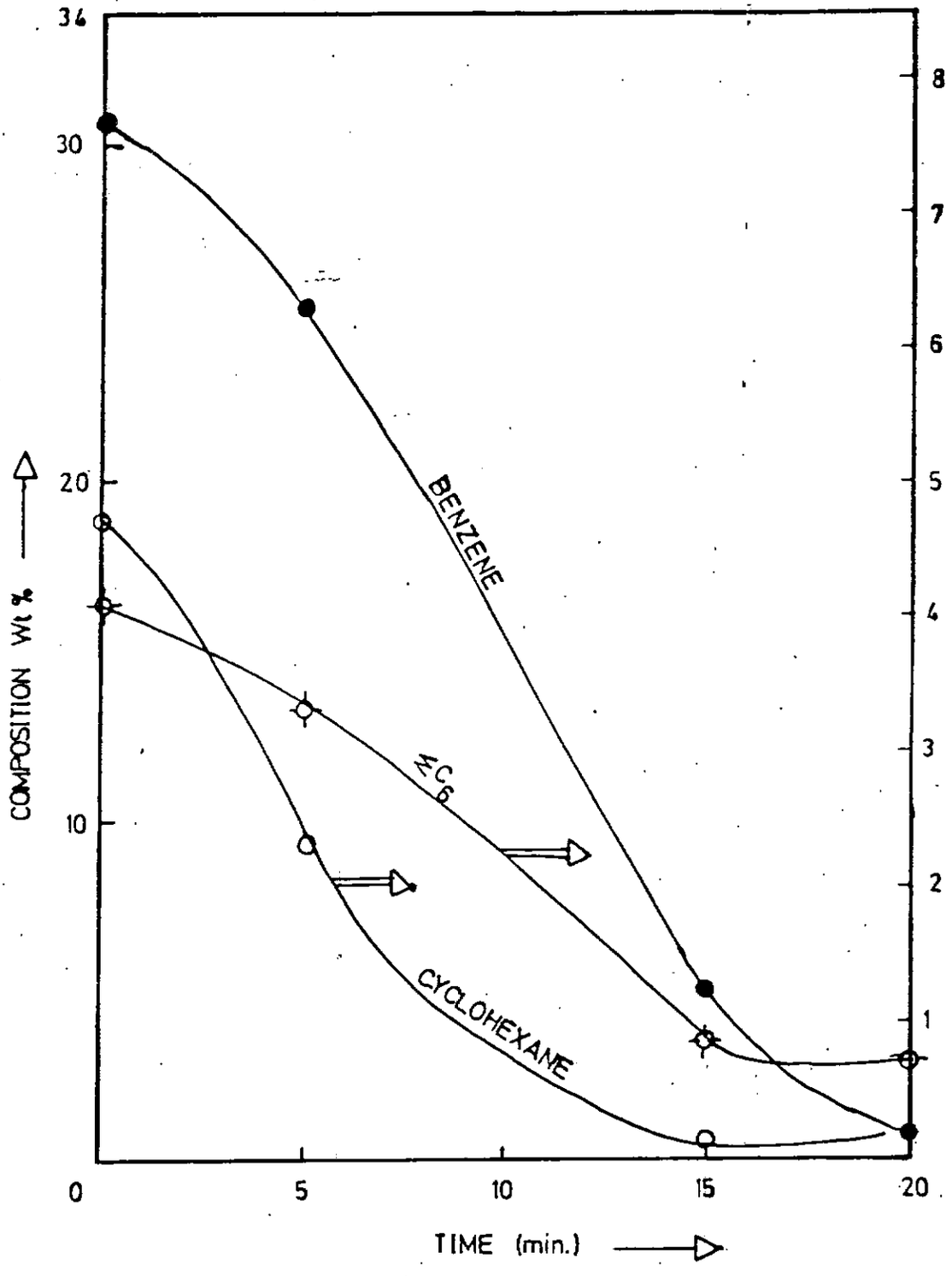

Fig. 5.3.21: Product composition for MCP conversion on Pt/Al_2O_3 versus time for the fourth deactivation cycle in N_2 at $P_{MCP} = 9.2 \times 10^{-2}$ atm; W/F = 0.11 gmincm^{-3} and temperature = 430°C

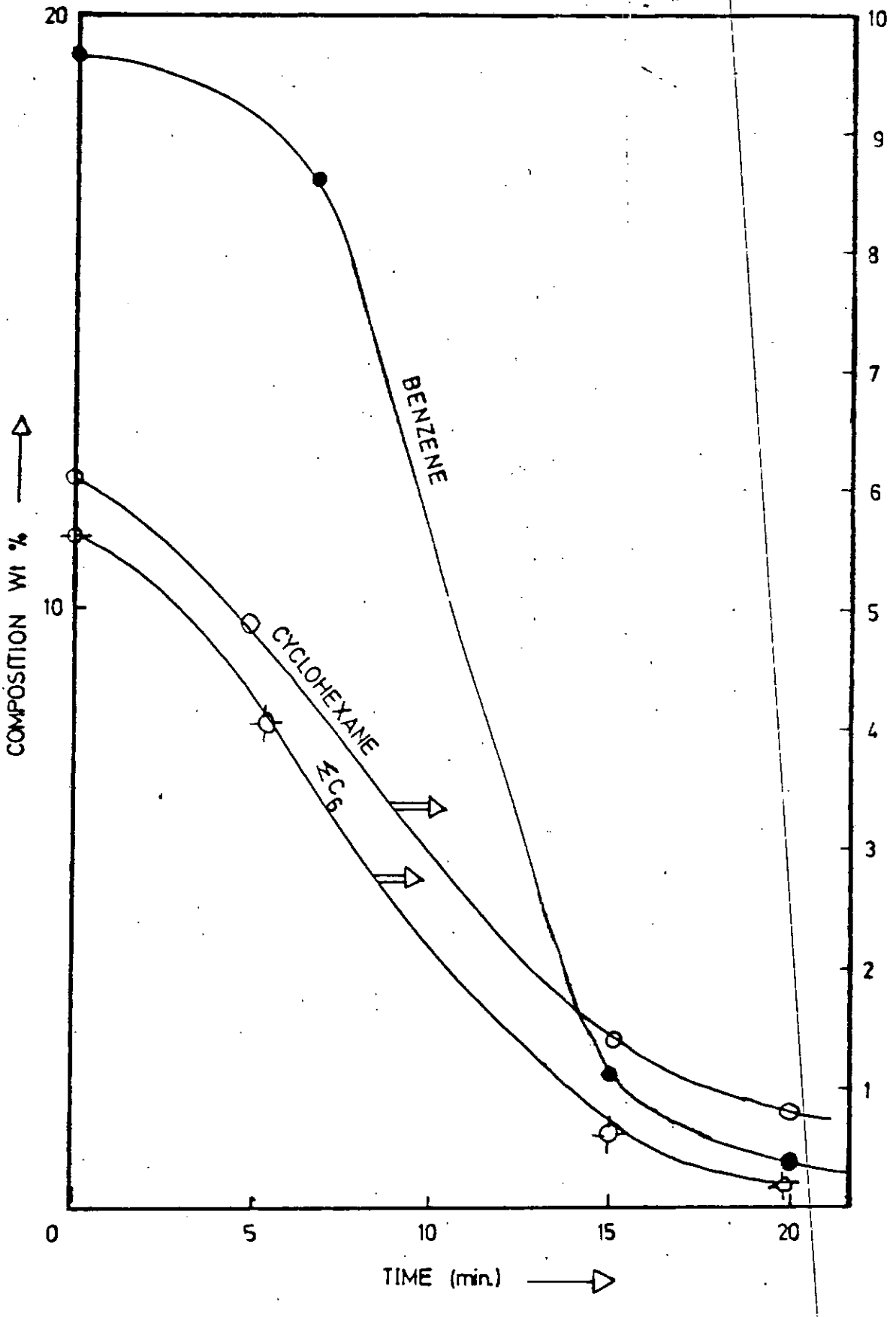

Fig.5.3.22: Product composition for MCP conversion on Pt/Al_2O_3 versus time for the eight deactivation cycle in N_2 at $P_{MCP} = 9.2 \times 10^{-2}$ atm; $W/F = 0.11 gmin cm^{-3}$ and temperature = 430°C.

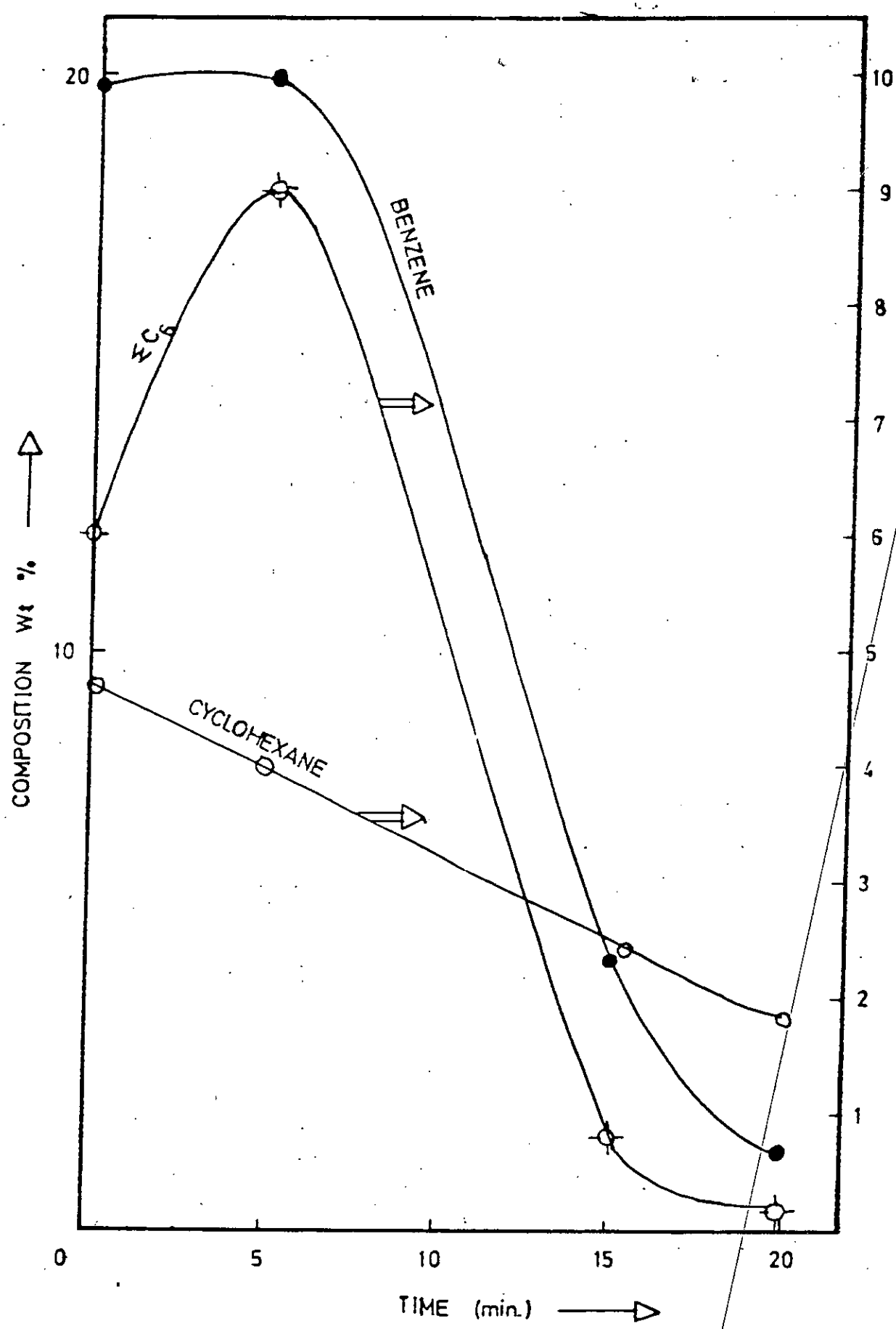

Fig.5.3.23: Product composition for MCP conversion on Pt/Al_2O_3 versus time for the tenth deactivation cycle in N_2 at $P_{MCP} = 9.2 \times 10^{-2}$ atm; $W/F = 0.11 gmin cm^{-3}$ and temperature = 430°C

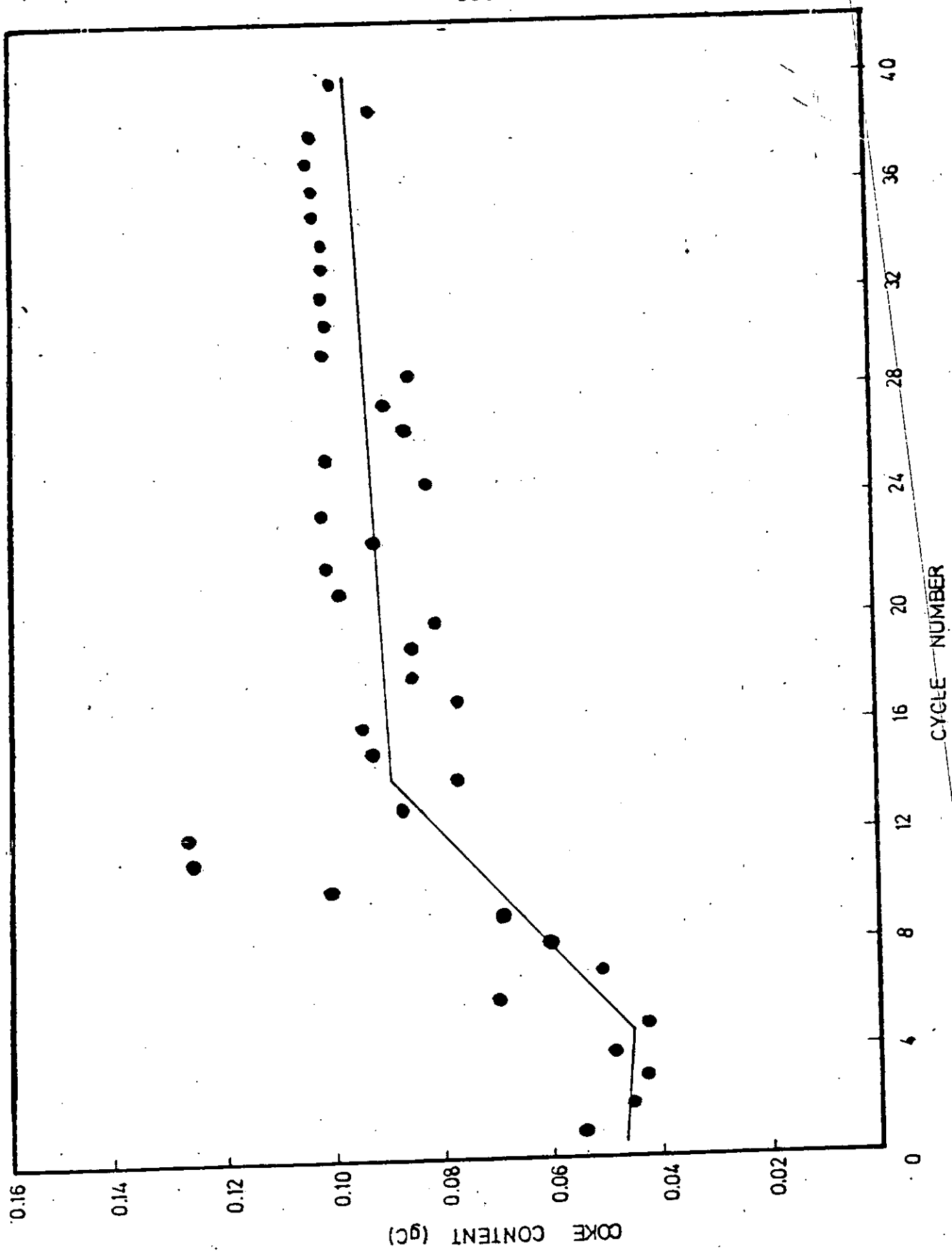

Fig.5.3.24: Coke content for MCP conversion on Pt/Al_2O_3 versus cycle number at 430°C

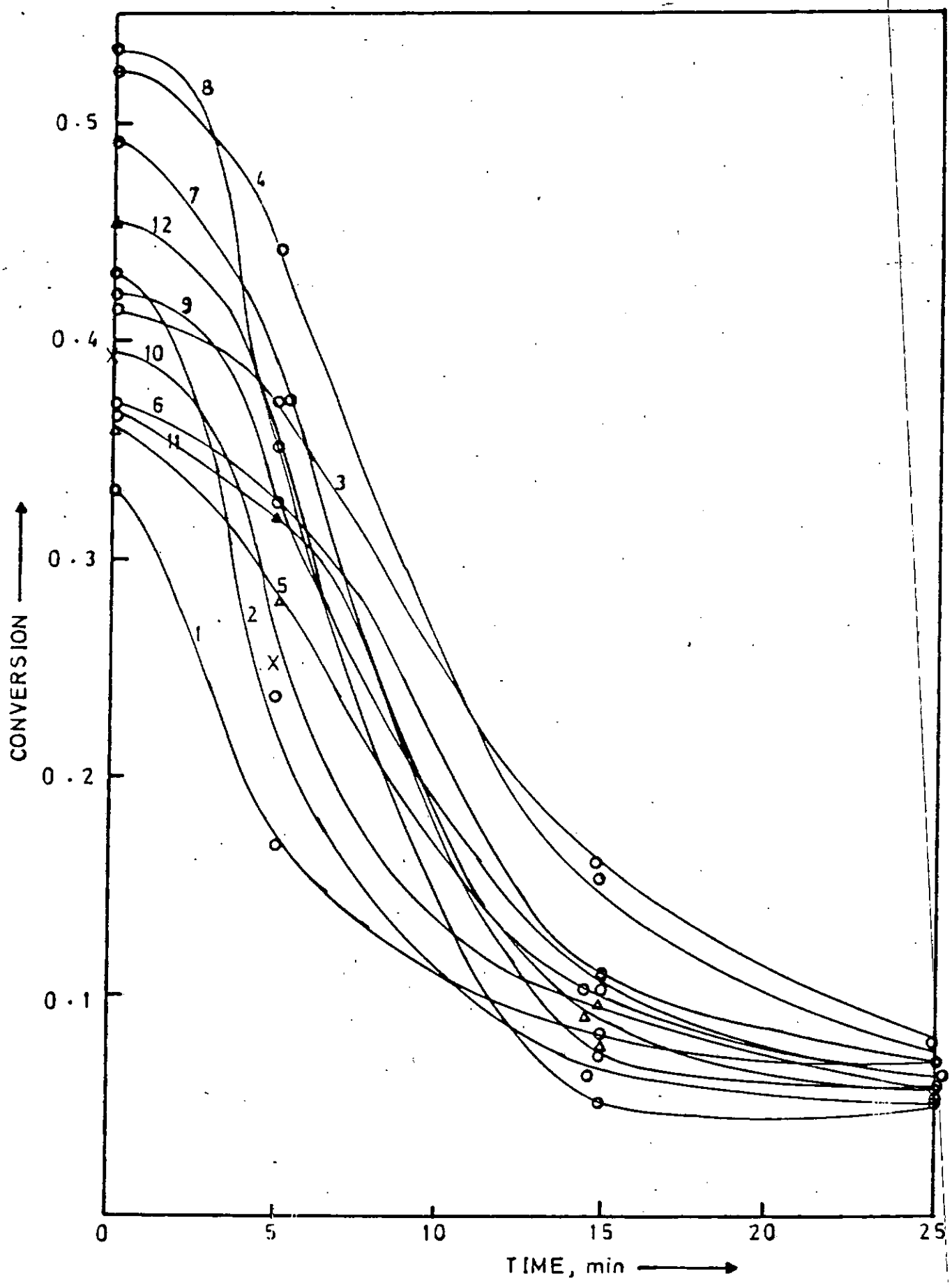

Fig.5.3.25: MCP conversion on Pt-Re/Al_2O_3(UNDRIED) versus time for 12 deactivation cycles in N_2 at P_{MCP}= 9.2×10^{-2}atm; W/F = 0.11gmincm^{-3} and temperature = 430°C.

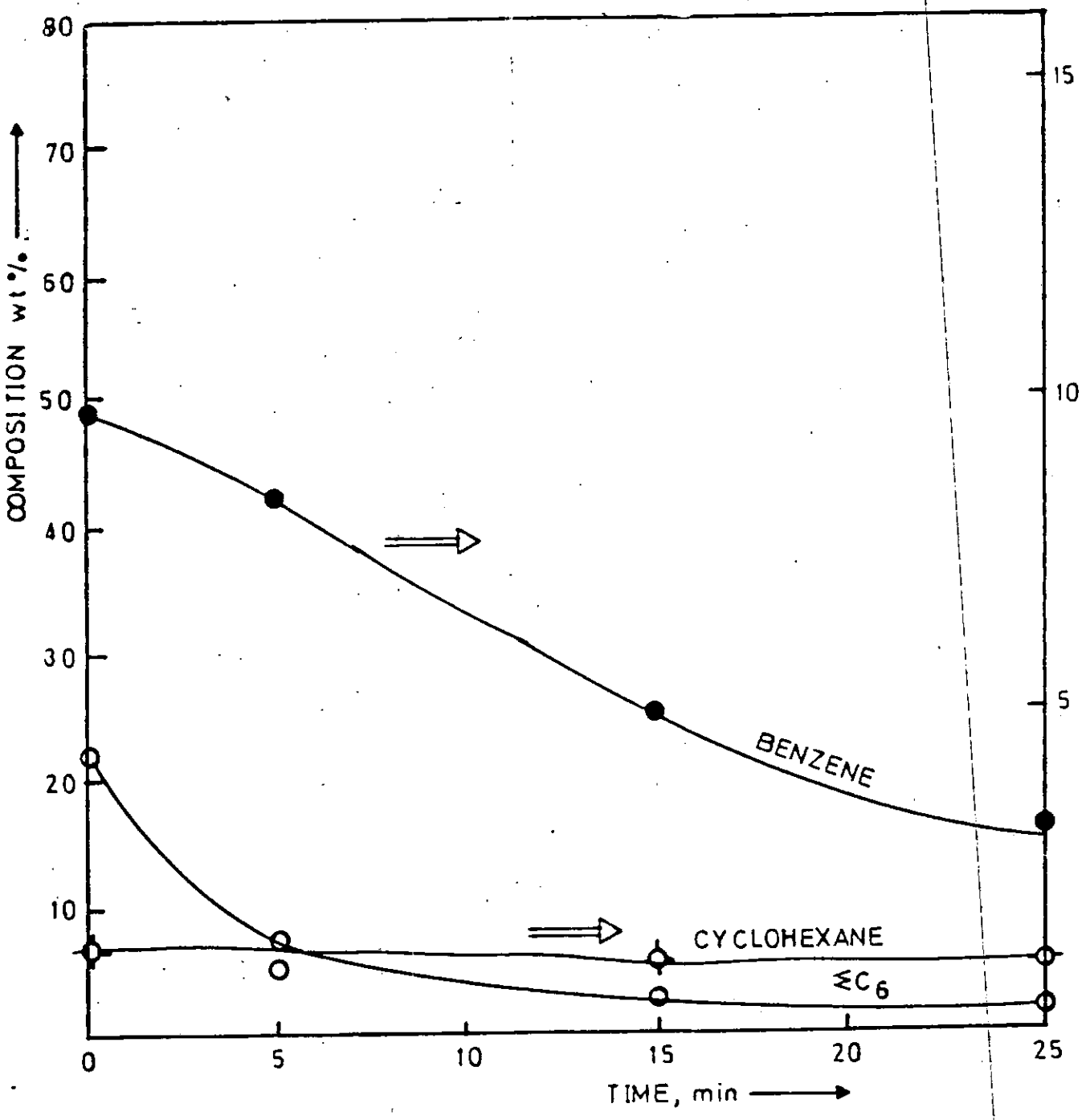

Fig. 5.3.26: Product composition for MCP conversion on Pt-Re/Al_2O_3 (UNDRIED) versus time for the first deactivation cycle in N_2 at P_{MCP} = 9.2×10^{-2}atm;W/F = 0.11gmincm^{-3} and temperature = 430°C.

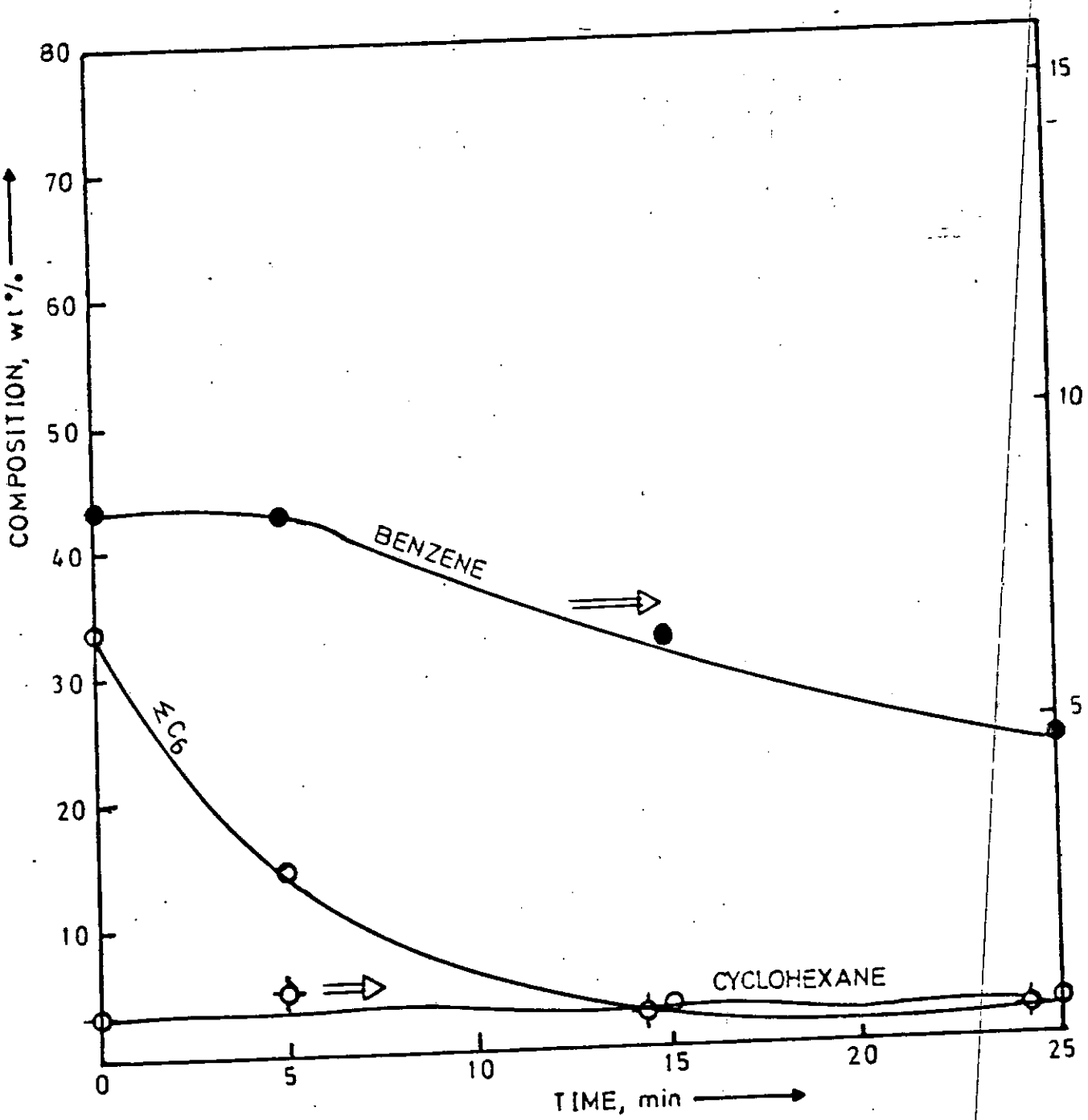

Fig.5.3.27: Product composition for MCP conversion on Pt-Re/Al_2O_3 (UNDRIED) versus time for the second deactivation cycle in N_2 at P_{MCP} = 9.2×10^{-2}atm; W/F = 0.11gmincm^{-3} and temperature = 430°C

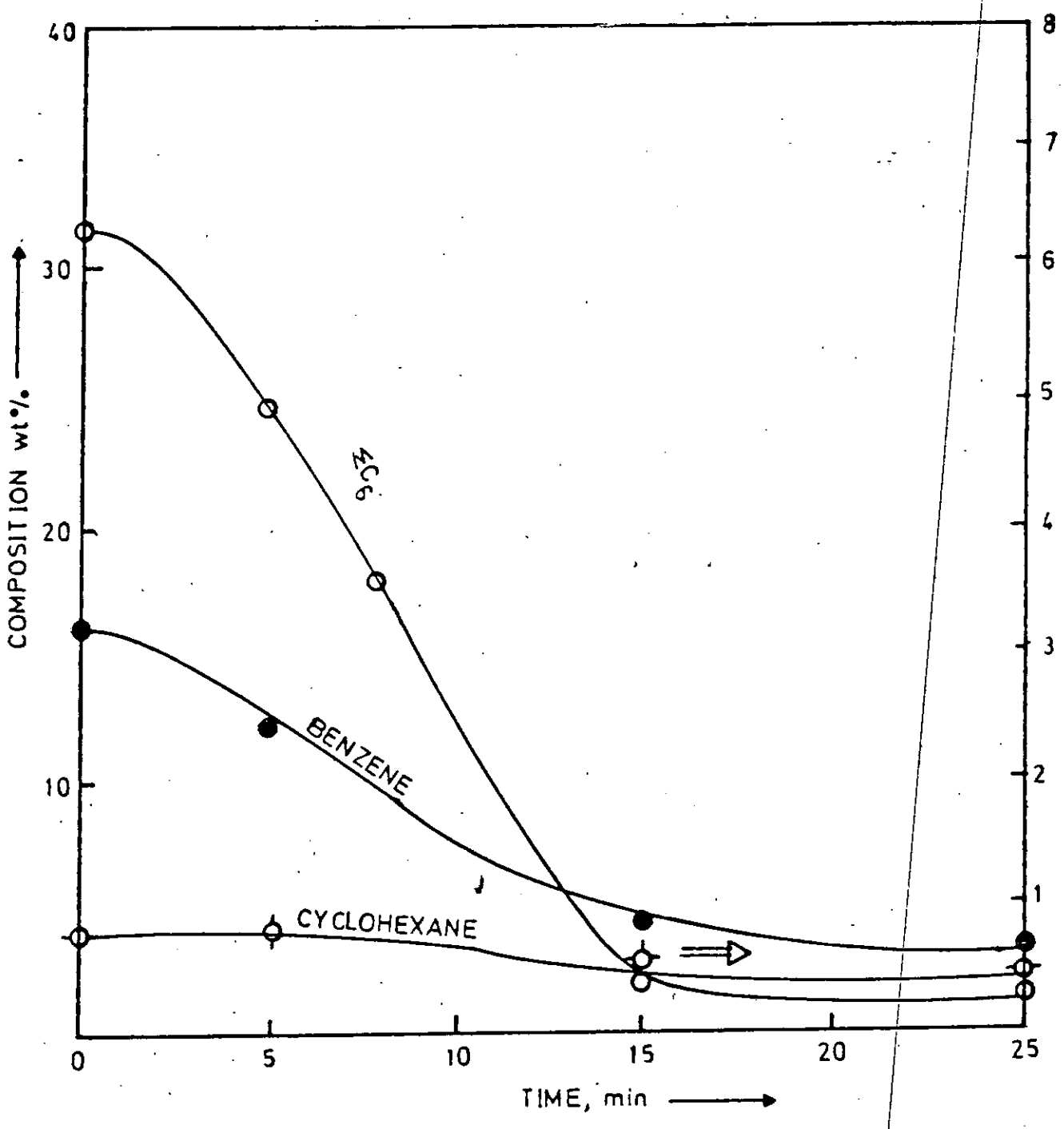

Fig.5.3.28: Product composition for MCP conversion on Pt-Re/Al_2O_3 (UNDRIED) versus time for the seventh deactivation cycle in N_2 at P_{MCP} = 9.2×10^{-2} atm; W/F = 0.11 gmincm^{-3} and temperature = 430°C

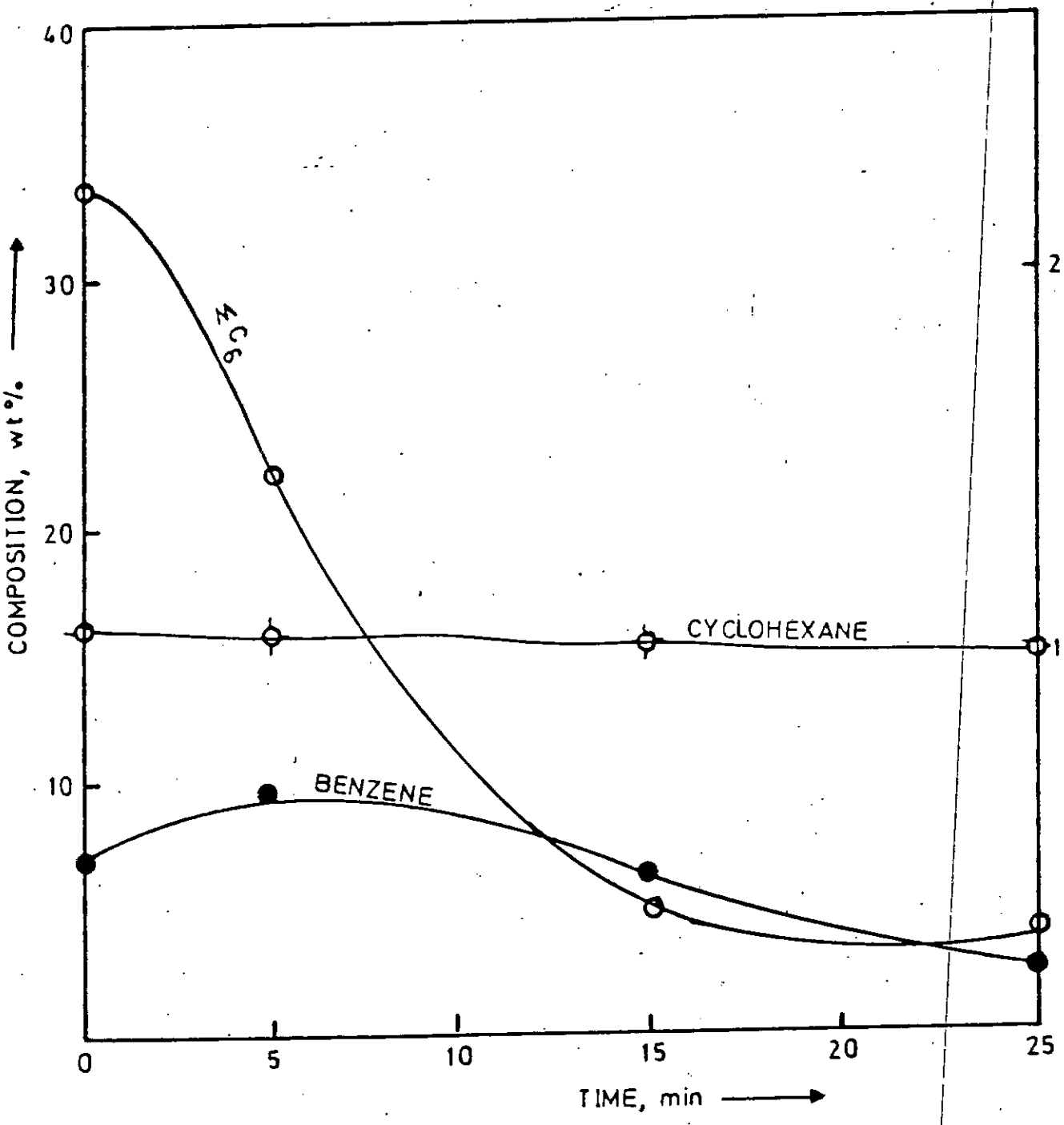

Fig.5.3.29: Product composition for MCP conversion on Pt-Re/Al_2O_3 (UNDRIED) versus time for the ninth deactivation cycle in N_2 at P_{MCP} = 9.2×10^{-2}atm; W/F = 0.11gmincm^{-3} and temperature = 430°C.

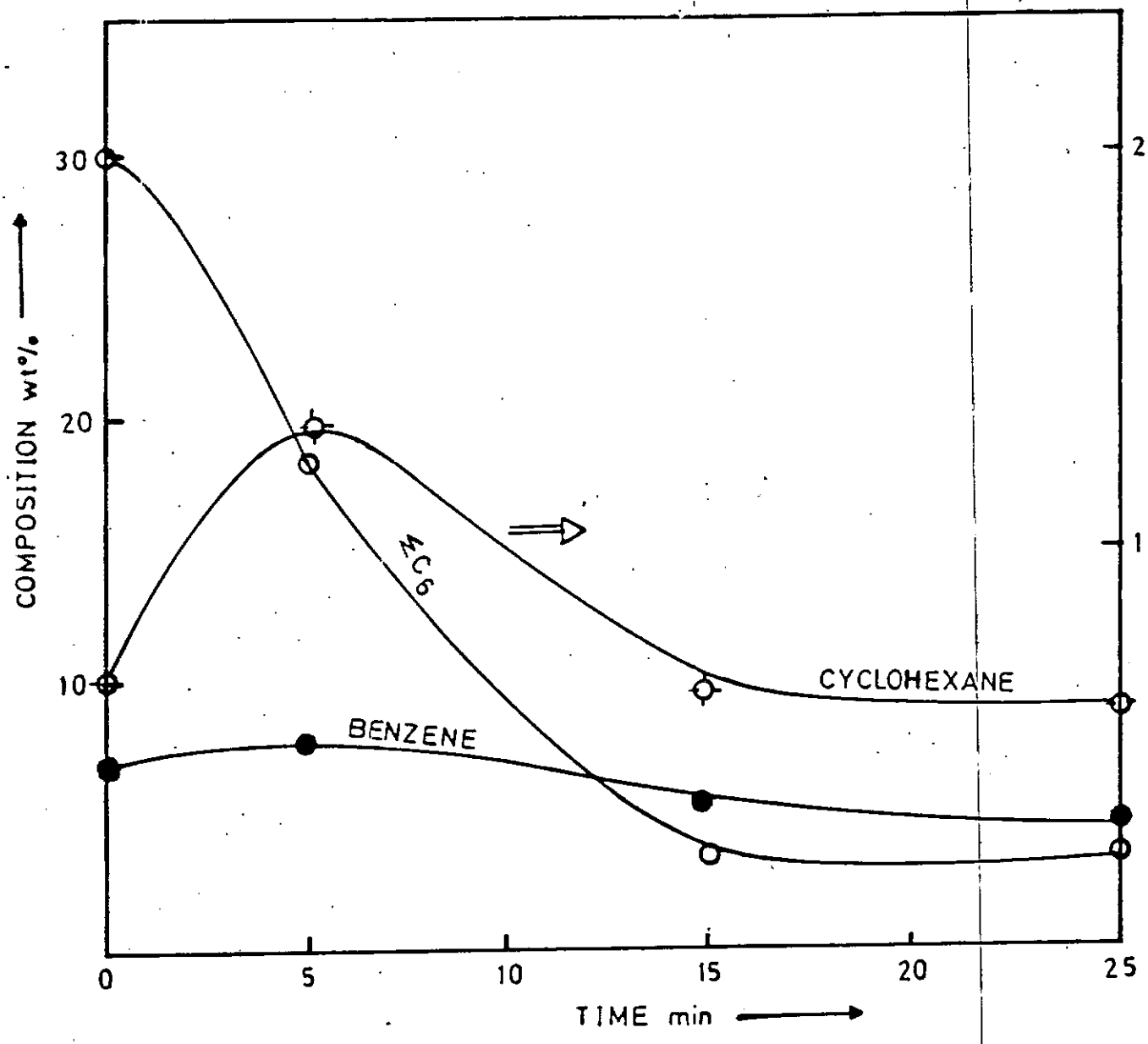

Fig.5.3.30: Product composition for MCP conversion on Pt-Re/Al_2O_3 (UNDRIED) versus time for the eleventh deactivation cycle in N_2 at P_{MCP} = 9.2×10^{-2}atm; W/F = 0.11gmincm^{-3} and temperature = 430°C.

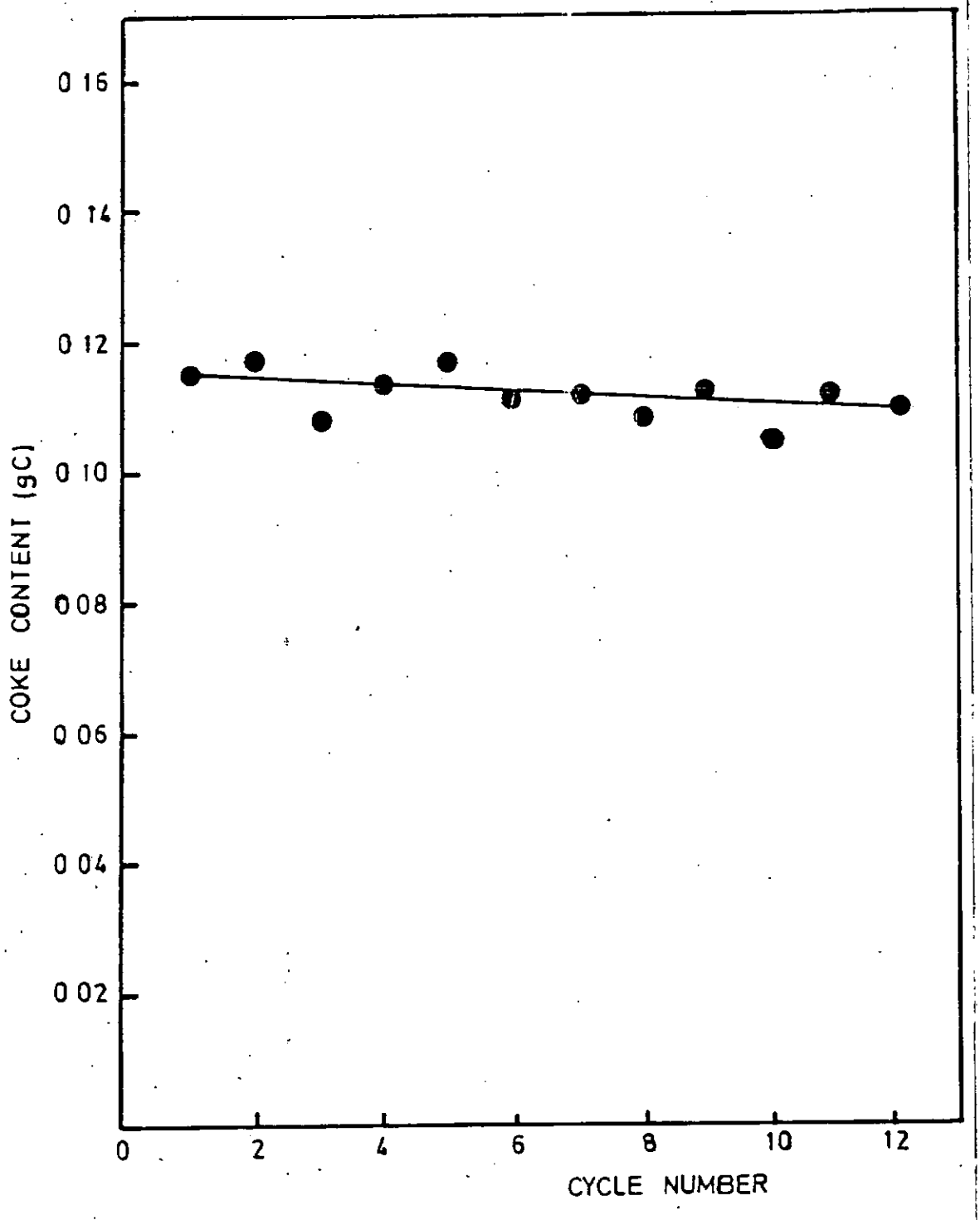

Fig. 5.3.31: Coke content for MCP conversion on Pt-Re/Al_2O_3 (UNDRIED) versus cycle number at 430°C.

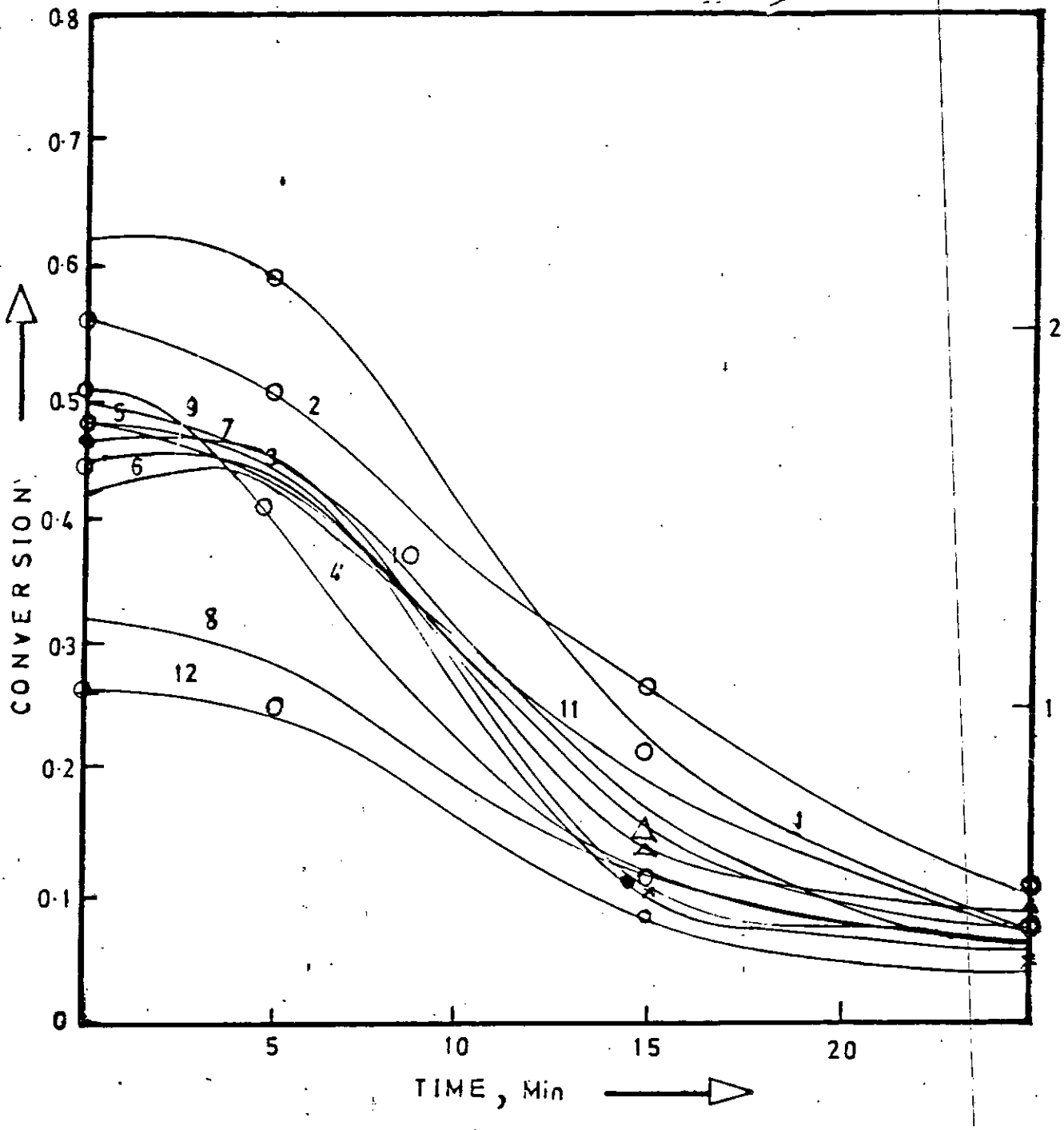

Fig. 5.3.32: MCP conversion on Pt-Re/Al_2O_3 (DRIED) versus time for 12 deactivation cycles in N_2 at P_{MCP} = 9.2×10^{-2} atm; W/F = 0.11gmincm^{-3} and temperature = 430°C.

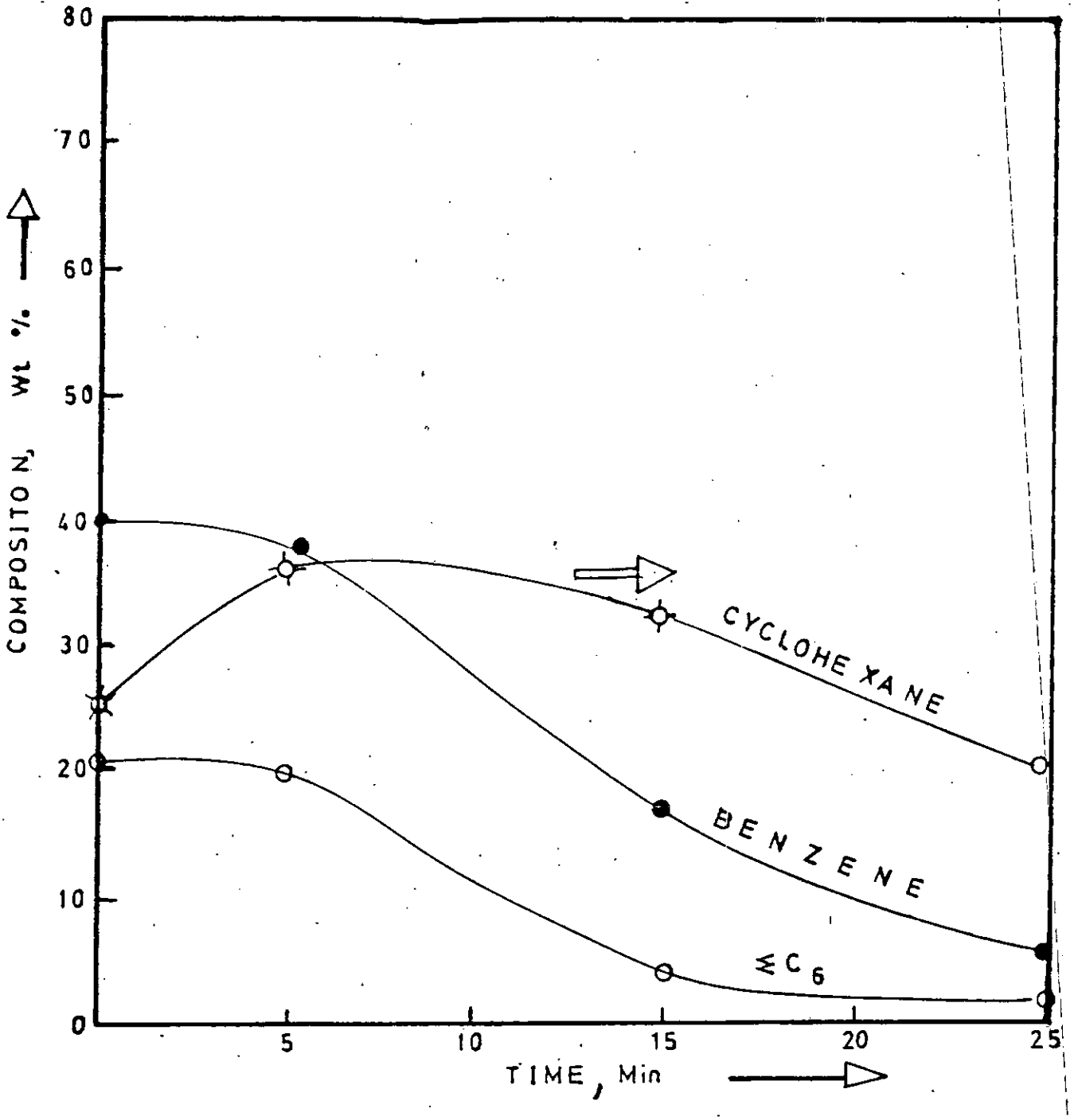

Fig.5.3.33: Product composition for MCP conversion on Pt-Re/Al_2O_3 (DRIED) versus time for the first deactivation cycle in N_2 at P_{MCP} = 9.2×10^{-2}atm; W/F = 0.11gmincm^{-3} and temperature = 430°C.

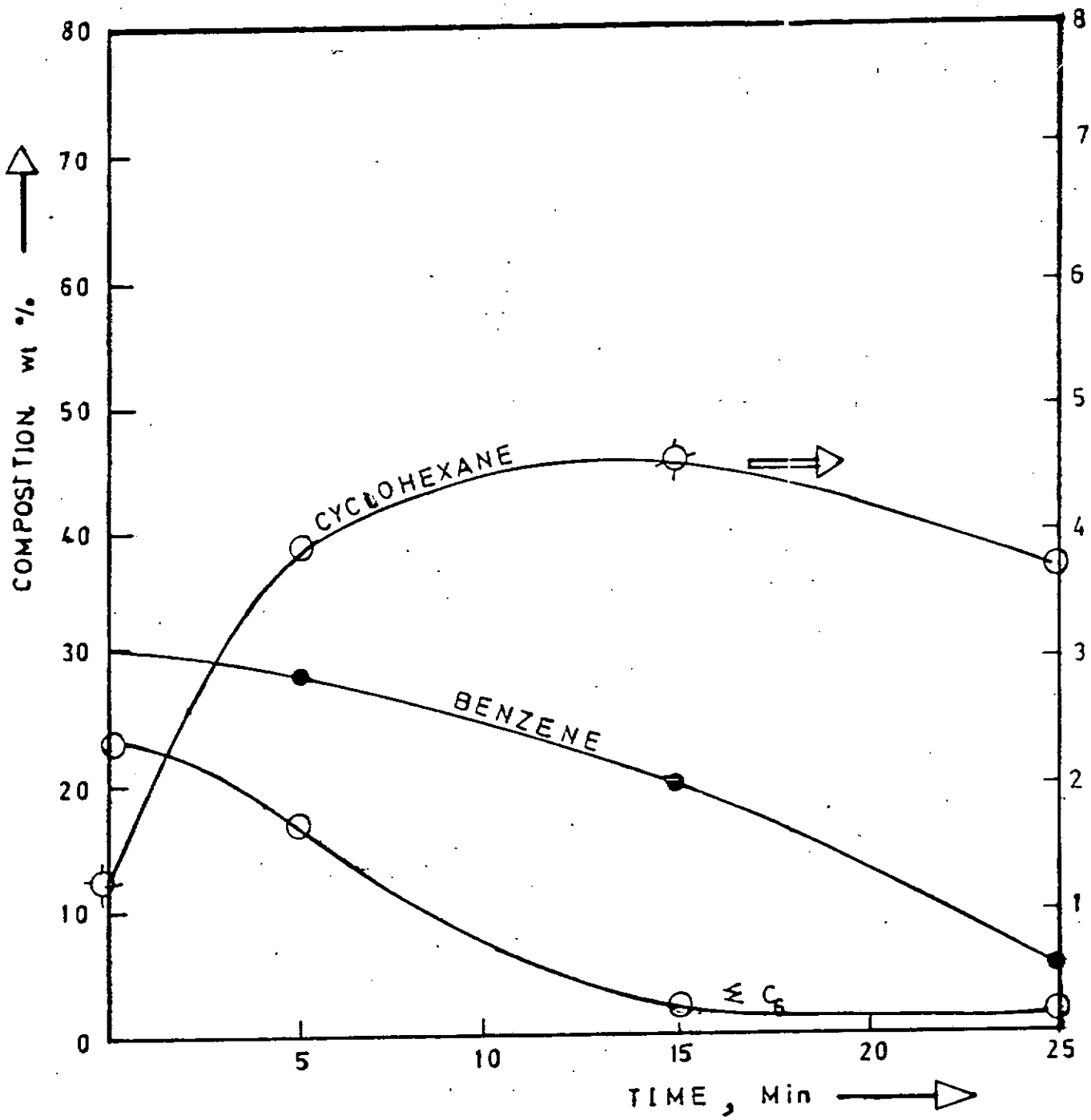

Fig.5.3.34: Product composition for MCP conversion on $Pt\text{-}Re/Al_2O_3$ (DIRED) versus time for the second deactivation cycle in N_2 at $P_{MCP} = 9.2 \times 10^{-2}$ atm; W/F = 0.11gmincm^{-3} and temperature = 430°C .

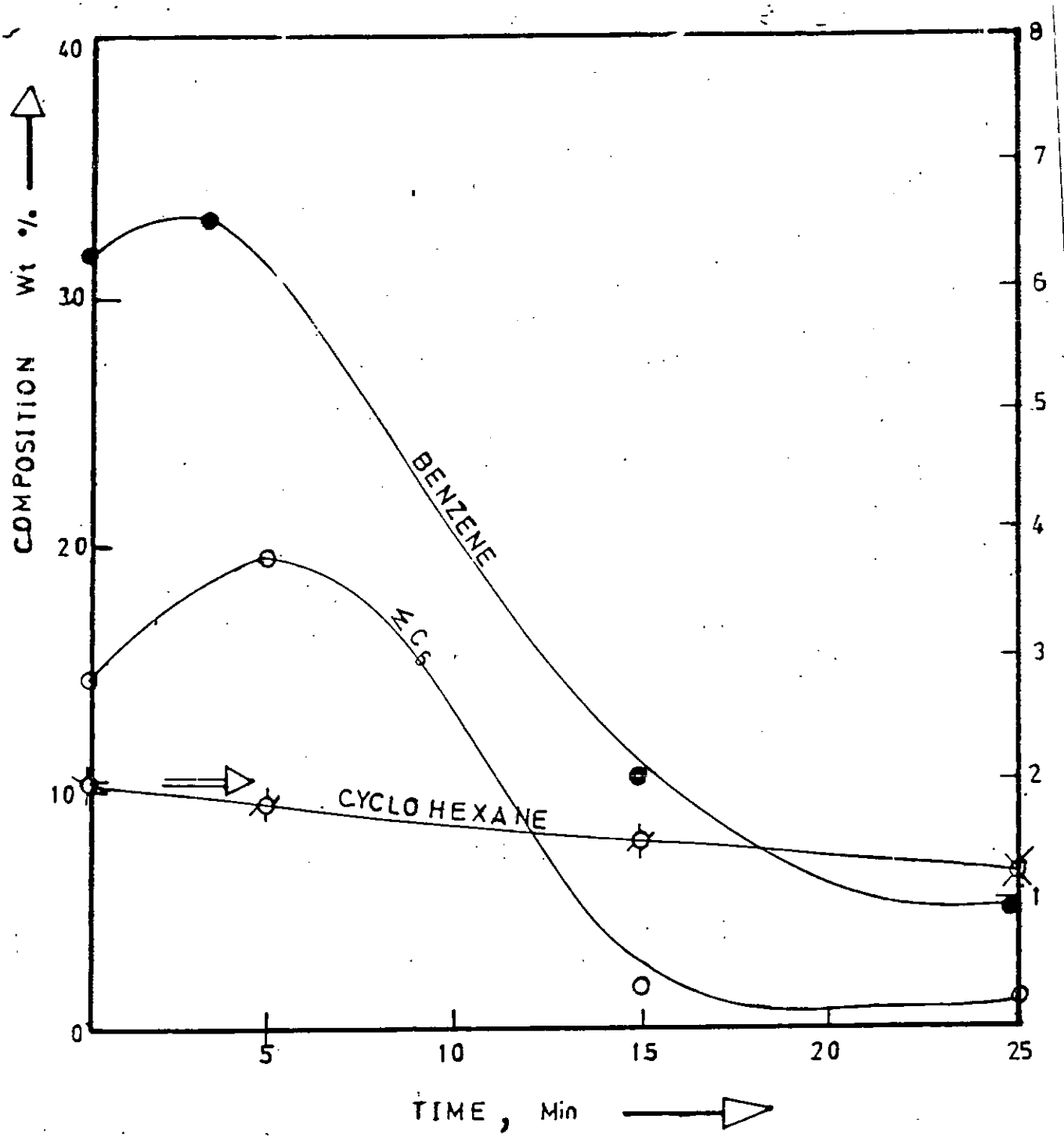

Fig.5.3.35: Product composition for MCP conversion on Pt-Re/Al_2O_3 (DRIED) versus time for the seventh deactivation cycle in N_2 at P_{MCP} = 9.2×10^{-2} atm; W/F = 0.11gmincm^{-3} temperature = 430°C.

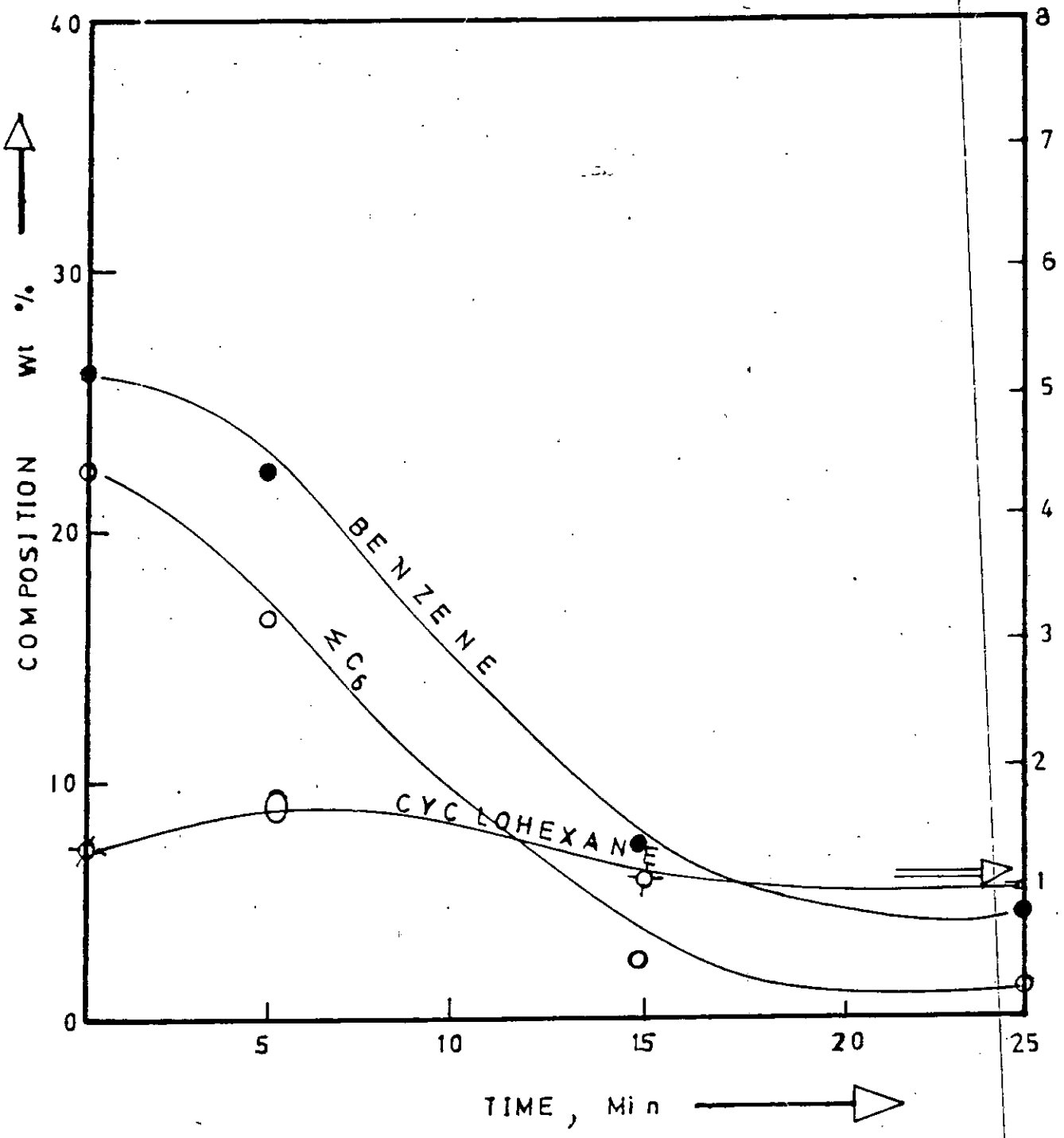

Fig.5.3.36: Product composition for MCP conversion on Pt-Re/Al_2O_3 (DRIED) versus time for the ninth deactivation cycle in N_2 at P_{MCP} = 9.2×10^{-2} atm; W/F = 0.11gmincm^{-3} and temperature = 430°C.

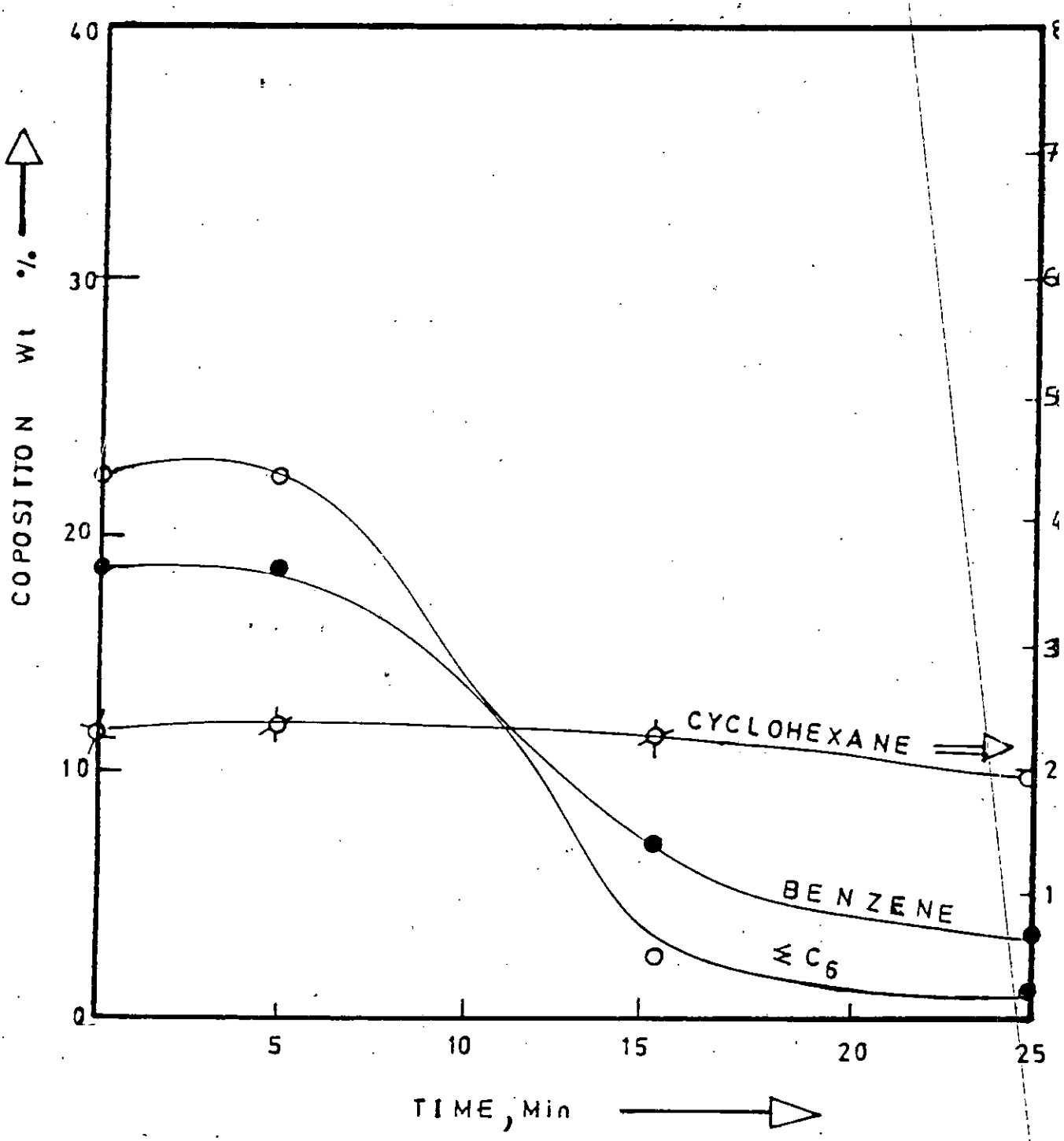

Fig.5.3.37: Product composition for MCP conversion on Pt-Re/Al_2O_3 (DRIED) versus time for the eleventh deactivation cycle in N_2 at P_{MCP} = 9.2×10^{-2} atm; W/F = 0.11 gmin cm^{-3} and temperature = 430°C

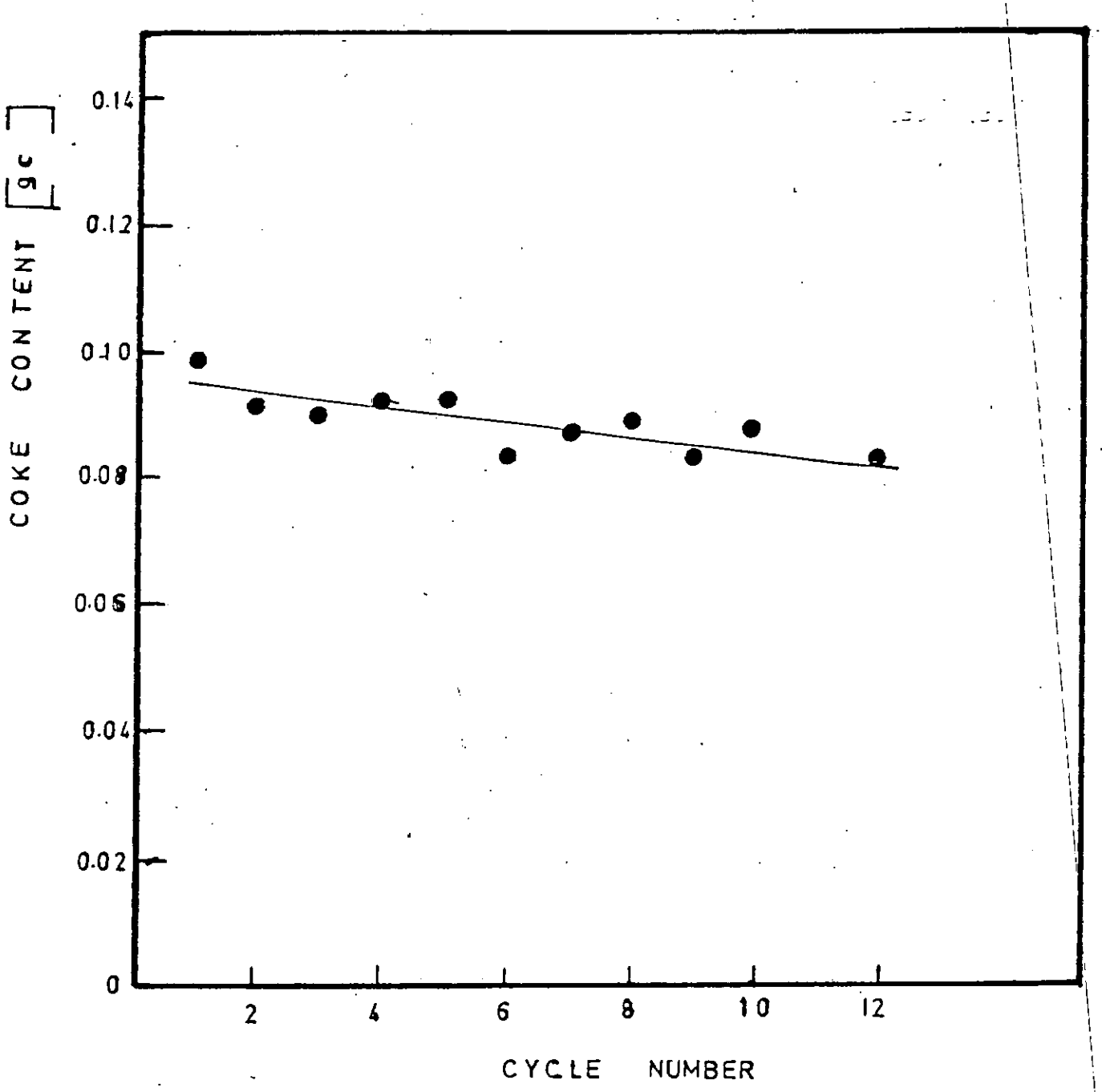

Fig.5.3.38: Coke content for MCP conversion on Pt-Re/Al_2O_3 (DRIED) versus cycle number at 430°C.

CHAPTER 6

MODELLING RESULTS

6.1 Constant Activity Modelling Results

In Chapter 3, mechanistic rate models were derived for the conversions of n-octane, iso-octane and MCP. Parameters of these models (rates and equilibrium constants) were estimated by using the modified simplex algorithm (Search method) of Nelder and Mead[55,56] to minimize the sum of squares of all the errors between the experimental and predicted rates. The numerical technique has been exhaustively discussed under Literature Review (Chapter 2). The optimization routine tried different values for all the constants until it found no other values that produced a smaller error. All the models developed were tried and discrimination among rival models was based on the positiveness of the rate and adsorption equilibrium constants, on the goodness of fit and on the increase of the rate constant of the reaction with increase in temperature.

The experimental yield and conversion values used in the modelling were read off from plots of composition and conversion against space time. Rate expressions for reactions in stirred tank reactors were used to evaluate the experimental rates. From the rate and equilibrium constants obtained at different temperatures the activation and adsorption energies with corresponding pre-exponential factors were evaluated using the least squares technique.

Particular difficulties associated with optimization arises because non-linear systems can have more than one

optimum. The optimization method of Nelder and Mead is capable of finding one or more of the optimum points depending on the initial guesses and stepsizes used. It was observed that at initial guesses and stepsizes larger than 5, very poor prediction of the rate was obtained. At initial guesses of constants and stepsizes less than 1, at least a negative value was obtained for one rate or equilibrium constant in all the models developed.

The rate and adsorption equilibrium constants were evaluated using the departmental Epson QX-10 microcomputer. The time for convergence varies with the model, the temperature, initial guesses of constants and stepsizes used. The time for convergence when n-octane kinetic parameters were evaluated was between 45-75min. With iso-octane convergence time ranged between 25-45min while with MCP kinetic model the time for convergence was between 45-60min.

6,1.1 N-Octane Kinetic Modelling Results

The mechanistic rate equations developed on the basis of the mechanism obtained from a modified reaction network proposed by Ako and Susu[1] (See Chapter 3) were used as models. Nineteen rate equations were derived and the rate equations that best fitted the experimental data (conversion -W/F data) obtained at 0.00763atm n-octane partial pressure are:

1. Rate expression of equation 3.1.5

$$r_4 = \frac{k_7 K_1 C_N - \frac{k_8}{K_5} C_I}{1+K_1 C_N + \frac{C_I}{K_5} + \frac{C_{cP}}{K_3} + \frac{C_{EB}}{K_8} + \frac{C_{ox}}{K_9} + \frac{C_{mx}}{K_{11}} + \frac{C_{Px}}{K_{12}} + \frac{(C_{H_2})^{\frac{1}{2}}}{K_{10}}}$$

This rate model is based on:

(a) Dissociative adsorption of hydrogen and

(b) Conversion of adsorbed n-octane to adsorbed iso-octane as rate limiting step.

2. Rate expression of equation 3.1.6.

$$r_5 = \frac{k_9 K_1 K_4 C_N - k_{10} C_I}{1+(K_1+K_4K_1)C_N + \frac{C_{cP}}{K_3} + \frac{C_{EB}}{K_8} + \frac{C_{ox}}{K_9} + \frac{C_{Mx}}{K_{11}} + \frac{C_{Px}}{K_{12}} + \frac{(C_{H_2})^{\frac{1}{2}}}{K_{10}}}$$

This rate model is based on:

(a) Dissociative adsorption of hydrogen and

(b) Desorption of adsorbed iso-octane.

3. Rate expression of equation 3.1.7.

$$r_6 = \frac{k_{11} K_1 K_4 C_N - \frac{k_{12}}{K_8 K_{10}} C_{EB} C_{H_2}^{\frac{1}{2}}}{(1+ K_1 C_N + \frac{C_I}{K_5} + \frac{C_{cP}}{K_3} + \frac{C_{EB}}{K_8} + \frac{C_{ox}}{K_9} + \frac{C_{Mx}}{K_{11}} + \frac{C_{Px}}{K_{12}} + \frac{C_{H_2}^{\frac{1}{2}}}{K_{10}})^2}$$

This rate model is based on:

(a) Dissociative adsorption of hydrogen and

(b) Conversion of adsorbed iso-octane to adsorbed ethyl benzene as rate limiting step.

4. Rate expression of equation 3.1.8.

$$r_7 = \frac{k_{13}K_4K_1C_N - k_{14}C_{ox}C_{H_2}^{\frac{1}{2}}}{(1+K_1C_N+\frac{C_I}{K_5}+\frac{C_{cP}}{K_3}+\frac{C_{EB}}{K_8}+\frac{C_{ox}}{K_9}+\frac{C_{Mx}}{K_{11}}+\frac{C_{Px}}{K_{12}}+\frac{C_{H_2}^{\frac{1}{2}}}{K_{10}})^2}$$

This rate model is based on:

(a) Dissociative adsorption of hydrogen and

(b) Conversion of adsorbed iso-octane to adsorbed O-xylene as the rate limiting step.

5. Rate expression of equation 3.1.13

$$r_4 = \frac{k_7K_1C_N - \frac{k_8}{K_5}C_I}{1+(\frac{1+K_1K_5}{K_5})C_I+\frac{C_{cP}}{K_3}+\frac{C_{EB}}{K_8}+\frac{C_{ox}}{K_9}+\frac{C_{Mx}}{K_{10}}+\frac{C_{Px}}{K_{11}}}$$

This rate model is based on:

(a) Molecular desorption of hydrogen and

(b) Conversion of adsorbed n-octane to adsorbed iso-octane as rate limiting step.

The rate models of n-octane dehydrocyclization were derived from the following reaction network (See Chapter 3, section 3.1.1)

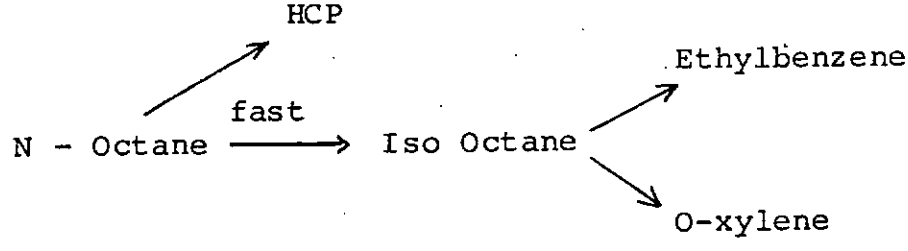

According to the network, n-octane conversion to iso-octane is fast. This implies that the elementary steps involved in the transformation of n-octane to iso-octane are fast and therefore cannot be rate determining. As a consequence, only two model equations (3.1.7 and 3.1.8) out of the five that satisfied the set criteria are likely to be rate determining as the other model equations were derived from the elementary steps where the rate of reaction should be fast.

Predicted rate and adsorption equilibrium constants of n-octane dehydrocyclization on Pt/Al_2O_3 catalyst at various temperatures using the five model equations that satisfied the set criteria are shown in Tables 6.1.1 - 6.1.21. Tables 6.1.1 - 6.1.3 shows the values of the predicted rate and adsorption equilibrium constants using rate equation 3.1.5. The activation energy for the reaction was about 24kcal/gmole at the initial guesses of 5 stepsize 3 and initial guesses of 3 stepsize 3. At initial guesses of 5, stepsize 1, however, the activation energy obtained was 38.87kcal/gmole. It is important to recall that step 1 of the mechanism (Chapter 3, Scheme I) from which the rate model was derived is an adsorption step and as such the adsorption energy should be negative. Steps 3,5,8,9 and 10 of Scheme I are desorption steps and since desorption is endothermic, the desorption energies should be positive. Table 6.1.22 shows the extent to which these thermodynamic criteria were met using rate equation (3.1.5). Tables 6.1.4 - 6.1.8 show the values of the predicted rate and adsorption equilibrium constants using rate equation 3.1.6. The activation energies obtained using different initial guesses and stepsizes ranged between 18-38kcal/gmole.

Table 6.1.23 shows the extent to which the kinetic and thermodynamic criteria were met using rate equation 3.1.6. Tables 6.1.9-6.1.14 show the values of the predicted rate and adsorption equilibrium constants using rate equation (3.1.7). The activation energies varied between 14-24 kcal/gmole. Table 6.1.24 shows the extent to which the kinetic and thermodynamic criteria were met using equation (3.1.7). Tables 6.1.15 - 6.1.19 show the values of the predicted rate and adsorption equilibrium constants using rate equation 3.1.8. The activation energies varied between 20-28kcal/gmole. Table 6.1.25 shows the extent to which the kinetic and thermodynamic criteria were met using rate equation (3.1.8). Tables 6.1.20 and 6.1.21 show the values of the predicted rate and adsorption equilibrium constants using rate equation (3.1.13). Rate equation 3.1.13 was derived using the mechanism presented in Scheme II (see Chapter 3). According to this scheme, step 1 is an adsorption step and steps 3,5,8 and 9 are desorption steps. Since adsorption is exothermic the adsorption energy should be negative. Desorption is endothermic and the desorption energy should be positive. Table 6.1.25 shows the extent to which the kinetic and thermodynamic criteria were met using rate equation (3.1.13).

It can be observed that none of the models satisfied all the thermodynamic criteria. However, the model equation 3.1.13 satisfied all but one criterion at initial guesses of 5 for all constants, stepsize 5 and initial guesses of 3 for all constants, stepsize 1 while with model equations 3.1.6 and 3.1.8 all but one criterion was satisfied at

initial guesses of 5 for all constants, stepsize 3 and initial guesses of 5 for all constants, stepsize 1, respectively.

Figures 6.1.1 and 6.1.2 show the experimental and predicted conversion versus W/F profiles. Rate model equation (3.1.7) was used in predicting conversion at initial guesses of 5 for all constants, stepsize 3 in Figure 6.1.1 while in Figure 6.1.2 rate equation 3.1.8 was used at initial guesses of 3 for all constants, stepsize 1. The Figures show that the best fit was obtained at 420°C. The fit at the higher temperatures were not as good. Even at the higher temperatures, the fit was good at lower W/F values where the production of secondary products are minimized due to the higher flow rates.

The rate equations (3.1.7), (3.1.8) were then used to predict the conversion - hydrogen partial pressure profiles that exhibited maximum conversions as hydrogen partial pressure was increased. The rate equations were found to predict well the maximum in the conversion - P_{H_2} data as shown in Figure 6.1.3 for rate equation 3.1.7 at initial guesses of 5, stepsize 5. The kinetic and adsorption parameters for the two equations are shown in Table 6.1.27 and 6.1.28. Table 6.1.29 shows that the parameters did not satisfy most of the kinetic and thermodynamic criteria.

Table 6.1.1

Model Parameters for N-Octane Conversion

Rate Equation (3.1.5); Catalyst = Pt/Al_2O_3

Initial guesses : 5

Stepsize: 3

	420°C	440°C	460°C	A	ΔE,ΔH(Kcal/gmol)
k_7 $\frac{gmol}{gCat.h}$	2.1086	4.2173	5.3183	1.516×10^{8a}	23.6
k_8 $\frac{g\ mole}{gcat.h}$	2.465	1.0660	1.9293	4.08×10^{-3a}	-9.96
K_1	0.9934	2.2227	2.1360	1.62×10^{6}	19.64
K_3	5.9452	3.9231	5.3799	0.7453	-2.71
K_5	5.9265	6.5542	2.722	5.38×10^{-6}	-19.5
K_8	5.8833	5.2922	4.1285	9.43×10^{-3}	-8.95
K_9	8.3100	7.7292	5.4856	4.52×10^{-3}	-10.48
K_{10}	5.5244	6.8035	10.2493	4.25×10^{-5}	15.64
K_{11}	6.1674	5.6160	2.6260	1.25×10^{-6}	-21.52
K_{12}	4.6510	4.7566	6.7581	3.93×10^{3}	9.416

(a) Unit of A is given by $\frac{gmol}{g\ Cat.h}$

Table 6.1.2

Model Parameters for N-Octane Conversion

Rate Eqn.(3.1.5) ; Catalyst = Pt/Al_2O_3

Initial guesses : 5

Stepsize : 1

	420°C	440°C	460°C	A	ΔE,ΔH(Kcal/gmol)
k_7 $\frac{gmol}{gCat.h}$	1.1123	3.255	5.1095	5.0×10^{12a}	38.87
k_8 $\frac{gmol}{gCat.h}$	1.6805	1.8191	2.899	8.72×10^{4a}	13.76
K_1	4.2519	3.1151	2.1494	1.63×10^{-5}	17.3
K_3	5.3981	6.6368	2.7424	3.2×10^{-5}	-16.93
K_5	5.1993	4.6131	5.9091	47.465	3.045
K_8	6.0683	4.8914	2.8726	7.56×10^{-6}	-18.9
K_9	6.0758	5.6772	1.9216	5.95×10^{-9}	28.98
K_{10}	4.7938	2.7566	5.3222	21.628	2.26
K_{11}	6.1546	3.2482	3.3565	7.38×10^{-5}	-15.55
K_{12}	5.8322	7.9080	5.8142	6.7395	0.062

Table 6.1.3

Model Parameters for N-Octane Conversion

Rate Eqn. (3.1.5); Catalyst = Pt/Al_2O_3

Initial guesses : 3

Stepsize : 3

	420°C	440°C	460°C	A	ΔE,ΔH(Kcal/gmol)
k_7 $\frac{gmol}{gCat.h}$	1.3827	3.0028	3.599	1.86×10^{8a}	24.44
k_8 $\frac{gmol}{gCat.h}$	2.1568	0.621	0.4523	1.61×10^{-12a}	-39.88
K_1	2.6349	3.9689	6.7693	8.09×10^{7}	23.92
K_3	0.4294	3.2635	1.0801	2.66×10^{7}	24.17
K_5	1.4301	6.6147	0.5297	6.87×10^{-8}	-24.23
K_8	4.4426	0.8067	4.6778	3.377	0.474
K_9	3.9255	2.9179	3.1534	0.063	-5.65
K_{10}	4.6260	5.0541	5.0398	21.264	2.14
K_{11}	5.1694	0.4560	0.5518	3.45×10^{-18}	-57.43
K_{12}	3.0066	1.3498	3.7889	113.41	5.446

Table 6.1.4

Model Parameters for N-Octane Conversion

Rate Eqn. (3.1.6); Catalyst = Pt/Al_2O_3

Initial guesses : 5

Stepsize: 5

	420°C	440°C	460°C	A	ΔE,ΔH(Kcal/gmol)
k_9 $\frac{gmol}{gCat.h}$	0.3296	0.5204	0.9505	2.27×10^{8a}	26.87
k_{10} $\frac{gmol}{gCat.h}$	3.4631	2.992	2.3168	6.16×10^{-3a}	-10.18
K_1	5.8321	4.8969	2.7335	6.28×10^{-6}	-19.14
K_3	7.0927	6.4388	7.6937	28.50	1.99
K_4	3.0199	4.6734	5.0614	4.38×10^{4}	13.2
K_5	7.6173	8.1612	8.6051	71.5216	3.10
K_8	6.6089	6.7087	0.4986	4.45×10^{-20}	-64.97
K_9	7.0065	6.2838	18.049	1.59×10^{8}	23.74
K_{10}	5.6292	6.4131	5.5196	4.2888	0.44
K_{11}	7.3429	7.1493	3.2565	3.17×10^{-6}	-20.484
K_{12}	4.6121	4.1493	7.1475	1.13×10^{4}	10.86

Table 6.1.5

Model Parameters for N-Octane Conversion

Rate Eqn. (3.1.6); Catalyst = Pt/Al_2O_3

Initial guesses : 5

Stepsize: 3

	420°C	440°C	460°C	A	ΔE,ΔH(Kcal/gmol)
k_9 $\frac{g\ mol}{gCat.h}$	0.2492	0.689	1.1163	6.74×10^{11a}	38.19
k_{10} $\frac{gmol}{gCat.h}$	2.5218	2.5856	3.1199	3.18×10^{2a}	5.364
K_1	5.3746	4.5908	4.1624	0.0487	-7.508
K_3	7.1022	6.6289	6.8123	36.27	2.432
K_4	3.8014	3.8787	3.5854	1,3580	-1.488
K_5	6.1953	6.7646	6.8123	36.27	2.432
K_8	5.7804	6.1474	6.9204	153.24	4.556
K_9	6.0483	5.8879	6.4879	20.905	1.748
K_{10}	6.1268	6.2218	3.6121	4.59×10^{-4}	-13.296
K_{11}	6.4625	6.5465	7.1778	43.034	2.646
K_{12}	6.6781	5.6442	6.1429	1.3218	-2.188

Table 6.1.6

Model Parameters for N-Octane Conversion

Rate Eqn. (3.1.6); Catalyst = Pt/Al_2O_3

Initial guesses : 5

Stepsize: 1

	420°C	440°C	460°C	A	ΔE,ΔH(Kcal/gmol)
$k_9 \frac{gmol}{gCat.h}$	0.2334	0.6084	0.8779	$2.66x10^{10a}$	33.788
$k_{10} \frac{gmol}{gCat.h}$	2.3588	2.3415	2.4157	9.699^a	0.59
K_1	5.2084	5.4650	5.0026	2.614	0.986
K_3	5.3855	5.7851	5.3562	5.073	-0.11
K_4	4.5436	4.5649	4.1499	0.7882	-2.286
K_5	6.2912	4.9650	5.1731	0.1593	-5.03
K_8	5.4654	5.6600	5.6690	10.88	0.94
K_9	5.7286	5.6444	5.5454	3.1614	-0.824
K_{10}	5.6169	4.7561	5.2696	1.5888	-1.69
K_{11}	5.6306	5.8463	5.8976	13.3298	1.188
K_{12}	5.4922	5.5422	5.3393	0.0316	-7.132

Table 6.1.7

Model Parameters for N-Octane Conversion

Rate Eqn. (3.1.6); Catalyst = Pt/Al_2O_3

Initial guesses : 3

Stepsize: 3

	420°C	440°C	460°C	A	ΔE,ΔH(Kcal/gmol)
$k_9 \frac{gmol}{gCat.h}$	0.5772	1.4311	1.5312	$1.18x10^{8a}$	24.96
$k_{10} \frac{gmol}{gCat.h}$	1.7368	1.6217	2.087	45.422^a	3.154
K_1	3.3049	1.6370	3.9157	43.7284	3.934
K_3	3.8524	3.0731	0.9547	$4.26x10^{-11}$	-35.18
K_4	2.2316	3.8935	3.7118	$3.04x10^{4}$	13.05
K_5	3.6994	3.6347	3.4032	0.732	-2.182
K_8	4.6940	3.4549	0.1723	$5.95x10^{-26}$	-83.274
K_9	4.6940	5.8057	6.6335	$2.71x10^{3}$	8.798
K_{10}	3.5186	2.0174	2.3115	$1.27x10^{-3}$	-10.832
K_{11}	4.6940	4.5100	8.3992	$1.66x10^{5}$	14.67
K_{12}	2.1869	3.0558	0.2425	$1.84x10^{-17}$	-55.15

Table 6.1.8

Model Parameters for N-Octane Conversion

Rate Eqn. (3.1.6); Catalyst = Pt/Al_2O_3

Initial guesses : 3

Stepsize : 1

	420°C	440°C	460°C	A	ΔE, ΔH (Kcal/gmol)
k_9 $\frac{gmol}{gCat.h}$	0.9846	1.1912	2.0045	1.07×10^{6a}	17.966
k_{10} $\frac{gmol}{gCat.h}$	1.577	1.4485	1.0205	618.93^{a}	-10.98
K_1	2.9074	2.6945	0.9893	1.05×10^{-8}	-27.154
K_3	3.4414	0.7198	3.1806	0.2897	-2.748
K_4	1.4238	3.3714	5.3334	5.25×10^{10}	33.64
K_5	3.2922	4.9519	3.1439	1.863	-9.84
K_8	3.6744	3.4239	3.0110	0.0996	-5.014
K_9	3.7650	3.3620	1.1524	2.20×10^{-9}	-29.68
K_{10}	3.1158	2.4511	2.9716	1.1388	-1.29
K_{11}	3.8415	3.2871	4.2707	23.2429	2.49
K_{12}	3.5677	3.3975	3.5178	2.6832	-0.376

Table 6.1.9

Model Parameters for N-Octane Conversion

Rate Eqn. (3.1.7); Catalyst = Pt/Al_2O_3

Initial guesses : 5

Stepsize: 5

	420°C	440°C	460°C	A	ΔE,ΔH(Kcal/gmol)
k_{11} $\frac{gmol}{gCat.h}$	1.0476	2.52	2.658	$9.53x10^{7a}$	23.84
k_{12} $\frac{gmol}{gCat.h}$	2.274	2.34	0.59	$1.93x10^{-10a}$	-33.85
K_1	5.762	0.7174	0.6507	$1.315x10^{-17}$	-55,87
K_3	6.6148	1.3123	6.9651	5.63	0.5
K_4	4.7079	5.6664	7.5970	$3.04x10^{4}$	12.186
K_5	7.1797	4.9377	7.1239	4.84	-0.38
K_8	6.0611	4.4555	5.4603	0.754	-2.77
K_9	6.1179	9.8898	6.0785	7.57	0.076
K_{10}	6.6176	5.3505	4.2926	$2.4x10^{-3}$	-10.99
K_{11}	9.6195	7.0092	15.3376	$3.38x10^{4}$	11.666
K_{12}	6.6347	12.2251	6.0907	2.16	-1.848

Table 6.1.10

Model Parameters for N-Octane Conversion

Rate Eqn. (3.1.7); Catalyst = Pt/Al_2O_3

Initial guesses : 5

Stepsize : 3

	420°C	440°C	460°C	A	ΔE,ΔH(Kcal/gmol)
k_{11} $\frac{gmol}{gCat.h}$	1.104	2.172	2.55	$1.6x10^{7a}$	21.366
k_{12} $\frac{gmol}{gCat.h}$	2.604	2.466	2.4	1.614^{a}	-2.038
K_1	7.0558	0.6117	0.8064	$1.57x10^{-17}$	-55.74
K_3	5.8805	3.2092	4.7079	0.0714	-5,89
K_4	4.7630	6.4122	6.8232	$3.72x10^{3}$	9.18
K_5	5.4142	6.9974	10.0104	$3.8x10^{5}$	15.49
K_8	5.6668	4.4203	4.3614	0.0426	6.724
K_9	6.2143	7.2070	4.3608	0.0118	-8.838
K_{10}	5.1158	6.7703	5.5485	26.735	2.186
K_{11}	4.5488	5.1041	5.8936	517.5	6.57
K_{12}	6.0613	7.5195	4.8337	0.1205	-5.58

Table 6.1.11
Model Parameters for N-Octane Conversion
Rate Eqn. (3.1.7); Catalyst = Pt/Al_2O_3
Initial guesses : 5
Stepsize: 1

	420°C	440°C	460°C	A	ΔE,ΔH(Kcal/gmol)
k_{11} $\frac{gmol}{gCat.h}$	1.1562	1.998	1.98	$8.26x10^{4a}$	13.98
k_{12} $\frac{gmol}{gCat.h}$	2.124	2.2278	2.1	5.181^{a}	-0.168
K_1	5.8593	1.0069	1.3723	$8.3x10^{-12}$	37.36
K_3	5.3826	5.0159	5.2604	3.394	-0.612
K_4	4.5771	5.5553	5.7278	294.12	5.736
K_5	5.3240	6.2263	6.8734	589.9	6.514
K_8	5.4959	4.3610	5.1375	1.395	-1.812
K_9	5.2106	5.2731	5.4532	12.013	-1.164
K_{10}	5.2869	5.3419	5.0463	2.328	-1.152
K_{11}	5.4011	6.3781	5.6373	12.95	1.148
K_{12}	5.9732	5.4050	5.6133	1.822	-1.616

Table 6.1.12
Model Parameters for N-Octane Conversion
Rate Eqn. (3.1.7); Catalyst = Pt/Al_2O_3
Initial guesses : 3
Stepsize : 5

	420°C	440°C	460°C	A	ΔE, ΔH(Kcal/gmol)
k_{11} $\frac{gmol}{gCat.h}$	1.2516	2.2764	2.388	$5.61x10^{5a}$	16.534
k_{12} $\frac{gmol}{gCat.h}$	2.0604	2.0676	3.024	$5.67x10^{3a}$	9.684
K_1	1.0077	1.5167	1.4502	927.9	9.32
K_3	4.7180	6.6648	3.5168	0.031	-7.184
K_4	3.7055	5.1980	6.9407	$3.66x10^{5}$	15.932
K_5	5.7493	0.9362	3.2821	$7,1x10^{-5}$	-14.98
K_8	1.4538	5.6735	2.1178	$3.14x10^{3}$	10.12
K_9	5.1388	0.9036	3.6157	$2.86x10^{-3}$	-9.69
K_{10}	3.555	5.7836	3.1053	0.4326	-3.068
K_{11}	4.2216	0.3095	4.5895	3.28	0.842
K_{12}	5.1214	5.2538	3.6754	0.0134	-8.33

Table 6.1.13
Model Parameters for N-Octane Conversion
Rate Eqn. (3.1.7); Catalyst = Pt/Al_2O_3
Initial guesses : 3
Stepsize: 3

	420°C	440°C	460°C	A	ΔE, ΔH(Kcal/gmol)
k_{11} $\frac{gmol}{gCat.h}$	1.2342	2.742	2.9085	2.67×10^{7a}	21.86
k_{12} $\frac{gmol}{gCat.h}$	2.1354	0.6324	0.2694	1.75×10^{-16a}	-52.65
K_1	0.9375	0.6167	0.7940	0.036	-4.366
K_3	2.2157	1.5847	2.0655	0.497	-1.938
K_4	4.0658	6.4566	7.4735	3.12×10^{5}	15,526
K_5	3.3916	2.6311	1.9473	1.32×10^{-4}	-14.088
K_8	2.0769	5.8901	1.4967	0.0118	-7.7
K_9	4.3148	3.9155	1.8230	7.52×10^{-7}	-21.726
K_{10}	3.1355	6.9823	6.5523	3.05×10^{6}	18.924
K_{11}	5.3903	1.9622	6.2038	33.784	3.03
K_{12}	3.8265	0.9205	3.9365	2.42	0.01

Table 6.1.14
Model Parameters for N-Octane Conversion
Rate Eqn. (3.1.7); Catalyst = Pt/Al_2O_3
Initial guesses : 3
Stepsize : 1

	420°C	440°C	460°C	A	ΔE, ΔH (Kcal/gmol)
k_{11} $\frac{gmol}{gCat.h}$	1.38	2.4	2.5152	2.47×10^{5a}	15.27
k_{12} $\frac{gmol}{gCat.h}$	1.1619	1.2756	0.7608	1.67×10^{-3a}	-10.592
K_1	0.7147	0.9075	1.9561	6.12×10^{7}	25.44
K_3	3.8148	0.7605	1.2143	1.48×10^{-9}	-29.6
K_4	3.75	7.8180	5.6748	1.13×10^{4}	10.868
K_5	4.0986	2.4208	3.2028	0.0345	-6.44
K_8	2.3942	4.7185	2.2109	0.897	-1.684
K_9	2.6005	1.8717	1.9536	0.0113	-6.454
K_{10}	4.0640	4.9041	4.4046	19.65	2.12
K_{11}	3.4805	0.9346	5.1632	1.725×10^{3}	9.28
K_{12}	3.1048	3.2037	2.5022	0.0655	-5.4

Table 6.1.15
Model Parameters for N-Octane Conversion
Rate Eqn. (3.1.8); Catalyst = Pt/Al_2O_3
Initial guesses : 5
Stepsize : 3

	420°C	440°C	460°C	A	ΔE, ΔH(Kcal/gmol
k_{13} $\frac{gmol}{gCat.h}$	1.31136	1.9728	2.8798	$6.5x10^{6a}$	19.984
k_{14} $\frac{gmol}{gCat.h}$	2.5128	3.1764	2.532	9.17^{a}	0.31
K_1	7.0098	1.2507	0.7441	$6.78x10^{-18}$	-57.23
K_3	5.7140	4.4357	4.2006	0.019	-7.868
K_4	4.3271	5.9836	7.2883	$6.29x10^{4}$	13.26
K_5	5.4149	7.2366	12.9629	$4.31x10^{7}$	22.096
K_8	5.3971	6.4689	3.3922	$1.40x10^{-3}$	-11.63
K_9	5.7587	2.3962	2.9517	$1.92x10^{-5}$	-17.24
K_{10}	5.2698	4.8753	5.3506	6.547	0.34
K_{11}	6.0616	5.7044	5.4233	0.82	-2.77
K_{12}	5.8991	7.0729	3.6676	$1.30x10^{-3}$	-11.858

Table 6.1.16
Model Parameters for N-Octane Conversion
Rate Eqn. (3.1.8); Catalyst = Pt/Al_2O_3
Initial guesses : 5
Stepsize: 1

	420°C	440°C	460°C	A	ΔE, ΔH(Kcal/gmol)
k_{13} $\frac{gmol}{gCat.h}$	1.06875	2.1102	3.2034	$1.65x10^{9a}$	27.918
k_{14} $\frac{gmol}{gCat.h}$	2.178	2.3658	1.71	0.08^{a}	-6.046
K_1	5.9474	0.6921	0.5902	$1,28x10^{-18}$	-59.14
K_3	5.6017	4.3894	5.7068	6.67	0.358
K_4	4.6079	7.7565	6.7057	$5.5x10^{3}$	9.684
K_5	5.3110	6.1670	6.3478	144.6	4.554
K_8	5.6045	4.9933	5.8140	9.99	0.86
K_9	5.3445	4.3830	4.9381	1.13	-2.084
K_{10}	5.2350	3.1808	5.6174	13.316	1.534
K_{11}	5.5361	7.1861	5.8688	18.95	1.6
K_{12}	5.4606	5.6027	3.4551	$1.48x10^{-3}$	-11.5

Table 6.1.17

Model Parameters for N-Octane Conversion

Rate Eqn. (3.1.8); Catalyst = Pt/Al_2O_3

Initial guesses : 3

Stepsize : 5

	420°C	440°C	460°C	A	ΔE, ΔH(Kcal/gmol)
k_{13} $\frac{gmol}{gCat.h}$	1.30398	2.0916	3	1.6×10^{7a}	21.2
k_{14} $\frac{gmol}{gCat.h}$	1.7892	2.094	3.14904	1.4×10^{5a}	14.29
K_1	1.4197	0.8748	0.9607	9.2×10^{-4}	-10.044
K_3	1.0639	6.8964	1.8014	4.8×10^{4}	14.152
K_4	3.7434	5.9865	7.5771	1.6×10^{6}	17.958
K_5	6.5741	1.5382	2.4901	1.5×10^{7}	-25.11
K_8	7.3432	1.6567	3.9235	3.4×10^{-5}	-16.49
K_9	0.4636	6.2786	1.7042	3.9×10^{10}	34.00
K_{10}	3.9466	7.6332	3.2792	0.22	-4.33
K_{11}	3.9880	0.7935	6.009	2.1×10^{3}	9.532
K_{12}	7.2415	7.6932	3.2758	4.9×10^{-6}	-19.9

Table 6.1.18

Model Parameters for N-Octane Conversion

Rate Eqn. (3.1.8); Catalyst = Pt/Al_2O_3

Initial guesses : 3

Stepsize: 3

	420°C	440°C	460°C	A	ΔE, ΔH(Kcal/gmol)
k_{13} $\frac{gmol}{gCat.h}$	1.08	2.4132	2.9232	2.9×10^{8a}	25.388
k_{14} $\frac{gmol}{gCat.h}$	1.9344	0.9996	0.5244	2.18×10^{-10a}	-33.12
K_1	1.1372	0.9279	0.6642	6.18×10^{-5}	-12.644
K_3	3.0617	2.5963	1.000	5.02×10^{-9}	-28.22
K_4	4.326	6.3821	8.2624	6.33×10^{5}	16.46
K_5	3.5908	2.6993	1.9482	6.18×10^{-5}	-12.644
K_8	4.4173	5.1772	1.3483	2.68×10^{-9}	29.76
K_9	2.4364	4.68	2.7114	25.89	3.08
K_{10}	2.8982	5.0949	6.1640	1.19×10^{7}	21.04
K_{11}	4.7379	2.8697	5.1605	15.85	1.92
K_{12}	4.0385	1.2925	3.8712	0.88	-1.61

Table 6.1.19

Model Parameters for N-Octane Conversion
Rate Eqn. (3.1.37); Catalyst = Pt/Al_2O_3
Initial guesses : 3
Stepsize : 1

	420°C	440°C	460°C	A	ΔE, ΔH(Kcal/gmol)
k_{13} $\frac{gmol}{gCat.h}$	1.2987	2.4	3.0516	2.5×10^{7a}	21.786
k_{14} $\frac{gmol}{gCat.h}$	1.2834	1.2756	0.56052	1.17×10^{-6a}	-20.844
K_1	1.1295	0.9075	1.1115	0.731	-0.508
K_3	3.7848	0.7605	0.5742	2.45×10^{-15}	-48.18
K_4	3.3472	7.8180	7.2075	3.87×10^{6}	19.138
K_5	3.8387	2.4208	4.1404	11.02	1.688
K_8	3.7981	1.8717	2.1529	8.74×10^{-5}	-14.6
K_9	3.0641	4.7182	0.7139	1.73×10^{-11}	-36.4
K_{10}	3.6777	4.9041	5.1692	2.05×10^{3}	8.7
K_{11}	3.0118	0.9346	6.1776	5.52×10^{5}	17.488
K_{12}	2.8122	3.2037	2.1280	0.02	-6.954

Table 6.1.20

Model Parameters for N-Octane Conversion

Rate Eqn.(3.1.13); Catalyst = Pt/Al_2O_3

Initial guesses : 5

Stepsize : 5

	420°C	440°C	460°C	A	ΔE,ΔH(Kcal/gmol)
k_7 $\frac{gmol}{gCat.h}$	2.3389	2.5715	5.4482	2.72×10^{7a}	21.3
k_8 $\frac{gmol}{gCat.h}$	4.9258	3.1529	1.0697	8.55×10^{10a}	-38.63
K_1	0.8754	5.9502	1.9828	7.69×10^{6}	21.49
K_3	4.3102	0.5821	11.8496	8.80×10^{7}	24.46
K_5	2.8355	0.1081	0.8326	8.48×10^{-11}	32.4
K_8	6.9082	5.6757	0.5463	9.297×10^{-20}	63.8
K_9	9.2114	5.6877	9.2838	7.7214	-0.024
K_{10}	6.0133	7.0682	10.6480	1.94×10^{5}	14.448
K_{11}	3.8213	5.7226	11.0507	9.77×10^{8}	26.9

Table 6.1.21

Model Parameters for N-Octane Conversion

Rate Eqn. (3.1.13): Catalyst = Pt/Al_2O_3

Initial guesses : 3

Stepsize : 1

	420°C	440°C	460°C	A	ΔE,ΔH(Kcal/gmol)
k_7 $\frac{gmol}{gCat.h}$	1.5139	4.2157	4.1298	5.59×10^{8a}	25.73
k_8 $\frac{gmol}{gCat.h}$	1.8730	1.4114	0.9564	2.35×10^{-5a}	-17.04
K_1	6.1226	2.5421	3.9011	1.02×10^{-3}	-11.76
K_3	2.9420	3.4642	0.2301	4.186×10^{-20}	-64
K_5	0.1162	0.3185	3.8215	4.27×10^{26}	88.32
K_8	0.1410	0.6141	4.0939	7.6×10^{25}	85.428
K_9	0.1089	4.0660	5.2704	2.42×10^{30}	99.3
K_{10}	0.8744	0.6082	2.6607	3.34×10^{8}	27.8
K_{11}	2.6908	0.3195	8.6859	1.157×10^{3}	9.456

Table 6.1.22
Parameters that satisfy thermodynamic criteria using rate eqn. (3.1.5)

(N-Octane, Pt/Al_2O_3)

Model Equation	Initial guesses and Stepsize	Activation Energy	Adsorption Energy	Desorption Energy for desorption steps				
				3	5	8	9	10
3.1.5	5^a_b 3^b	+	-	-	-	-	-	+
	3 3	+	-	+	-	+	-	+
	3 1	+	-	-	+	-	+	+

+ Parameter satisfies Kinetic and equilibrium criteria

- Parameter violates kinetic and equilibrium criteria

(a) Initial guesses (b) Stepsize

Table 6.1.23 (N-Octane; Pt/Al_2O_3)
Parameters that satisfy thermodynamic criteria using rate eqn. (3.1.6); (N-Octane; Pt/Al_2O_3)

Model Equation	Initial guesses and Stepsize	Activation Energy	Adsorption Energy	Desorption Energy for desorption Steps				
				3	5	8	9	10
3.1.6	5 5	+	+	+	+	-	+	-
	5 3	+	+	+	+	+	+	-
	5 1	+	-	-	-	+	-	-
	3 3	+	-	-	-	-	+	-
	3 1	+	+	-	-	-	-	-

Table 6.1.24
Parameters that satisfy thermodynamic criteria using rate eqn. (3.1.7). (N-Octane; Pt/Al_2O3)

Model Equation	Initial guesses and Stepsize	Activation Energy	Adsorption Energy	Desorption Energy for desorption Steps				
				3	5	8	9	10
3.1.7	5 5	+	+	+	-	-	+	-
	5 3	+	+	-	+	+	-	+
	5 1	+	-	-	+	-	-	-
	3 5	+	-	-	-	+	-	-
	3 3	+	+	-	-	-	-	+
	3 1	+	-	-	-	-	-	+

Table 6.1.25 (N-Octane ; Pt/Al_2O_3)
Parameters that satisfy thermodynamic criteria using rate equation (3.1.8)
(N-Octane ; Pt/Al_2O_3)

Model Equation	Initial guesses and Stepsize	Activation Energy	Adsorption Energy	Desorption Energy for desorption Steps				
				3	5	8	9	10
3.1.8	5 3	+	+	-	+	-	-	+
	5 1	+	+	+	+	+	-	+
	3 5	+	+	+	-	-	+	-
	3 3	+	+	-	-	+	+	+
	3 1	+	+	-	+	-	-	+

Table 6.1.26
Parameters that satisfy thermodynamic criteria using rate equation (3.1.13)
(N-Octane ; Pt/Al_2O_3)

Model Equation	Initial guesses and Stepsize	Activation Energy	Adsorption Energy	Desorption Energy for desorption Steps				
				3	5	8	9	10
3.1.13	5 5	+	-	+	+	+	+	
	3 1	+	+	-	+	+	+	

Table 6.1.27

Model Parameters for H_2 Dependence Using Eqn. (3.1.7)

Initial guesses of constants: 5

Stepsize: 5

	420°C	440°C	460°C	A	ΔE,ΔH(Kcal/gmol)
K_{11} $\frac{gmol}{gCat.h}$	1.3421	2.1284	2.8212	3.15×10^{6a}	18.92
K_{12} $\frac{gmol}{gCat.h}$	2.7558	2.4391	1.9566	0.0145^{a}	-8.676
K_1	8.3834	9.2012	14.856	2.61×10^{5}	14.432
K_3	3.2711	7.9507	7.2533	9.83×10^{6}	20.456
K_4	6.858	5.979	6.1504	0.8825	-2.804
K_5	5.3742	5.7187	3.6872	6.41×10^{-3}	-9.444
K_8	6.0552	3.2404	7.2533	5.11×10^{-12}	-38.866
K_9	6.7960	3.8121	1.3068	2.26×10^{-12}	-39.928
K_{10}	4.0582	7.5544	1.4043	7.61×10^{6}	19.92
K_{11}	7.0028	6.7196	8.8541	2.21	-1.586
K_{12}	6.3033	3.6064	2.9248	4.37×10^{-6}	-19.58

Table 6.1.28

Model Parameters for H_2 Dependence Using Eqn.(3.1.8)

Initial guesses: 3

Stepsize : 5

	420°C	440°C	460°C	A	ΔE,ΔH(kcal/gmol)
K_{13} $\frac{gmol}{gCat.h}$	1.3182	2.599	2.529	6.95×10^{5}	16.73
K_{14} $\frac{gmol}{gCat.h}$	2.763	2.112	2.396	0.4785	-3.72
K_1	8.5948	14.0745	13.8010	6.01×10^{4}	12.156
K_3	4.1376	5.1615	9.1225	7.2×10^{6}	20.0
K_4	7.1304	6.549	7.2402	8.846	0.34
K_5	5.0704	7.418	4.291	0.3266	-4.01
K_8	6.7424	2.4344	4.8368	8.57×10^{-3}	-8.86
K_9	5.3439	5.926	3.9026	0.02	-7.86
K_{10}	3.9274	6.2627	10.3357	1.43×10^{8}	24.35
K_{11}	7.0055	5.441	4.4407	1.62×10^{-3}	-11.5
K_{12}	6.1513	1.3235	1.19	3.19×10^{-13}	-42.1

Table 6.1.29
Parameters that satisfy thermodynamic criteria
using rate eqn. (3.1.5)
(N-Octane; Pt/Al_2O_3

Model Equation	Initial guesses and Stepsize	Activation Energy	Adsorption Energy	Desorption Energy for desorption Steps				
				3	5	8	9	10
3.1.7	5 5	+	-	+	-	-	-	+
3.1.8	3 5	+	-	+	-	-	-	+

6.1.2 Iso - Octane Kinetic Modelling Results

The rate equations used were derived on the basis of the generally accepted mechanism for skeletal isomerization (see Chapter 3, Section 3.1.2). The rate equations that best fitted the experimental data (conversion - W/F data) obtained at 0.092 atm iso-octane partial pressure are:

1. Rate expression of equation 3.1.25

$$r_6 = \frac{\frac{k_{11} K_5 K_d [A]}{[H_2]} - \frac{k_{12}[B]}{K_h K_7 [H_2]}}{1 + \frac{K_5 K_d [A]}{[H_2]} + \frac{[B]}{K_7 K_h [H_2]}}$$

This rate model is based on the isomerization of adsorbed iso-octene on the acidic site as the rate limiting step.

2. Rate expression of equation 3.1.27

$$r_7 = \frac{\frac{k_{13} K_{15} K_d K_A [A]}{[H_2]} - \frac{k_{14}[B]}{K_h [H_2]}}{1 + \frac{K_5 K_d [A]}{[H_2]} + \frac{K_6 K_5 K_d [A]}{[H_2]}}$$

This rate model is based on the desorption of iso octene (that which forms product) from the acidic site as the rate limiting step.

Predicted rate of the isomerization of iso-octane on 0.3% Pt/Al_2O_3 at various temperatures using the two models

that satisfied the set criteria are shown in Tables 6.1.30 - 6.1.36 while the predicted rate parameters on 0.6%Pt/Al_2O_3 are shown in Tables 6.1.37 - 6.1.44. The activation energy obtained with 0.3%Pt/Al_2O_3 using model Eqn.(3.1.25) was higher than those obtained when model Eqn.(3.1.27) was used. The activation energies obtained using model Eqn.(3.1.27) was ∿ 26 Kcal/gmol found comparable to those obtained for n-octane dehydrocyclization on the same type of catalyst. On 0.6%Pt/Al_2O_3 catalyst, however, lower value of activation energies were obtained with model equation 3.1.25 than those obtained using model equation 3.1.27. The rate equation predicted well the conversion - W/F profiles at all the temperatures investigated. Selected predicted conversions, plotted alongside experimental conversions at different temperatures and various initial guesses and stepsizes are shown in Figures 6.1.4 - 6.1.7.

Table 6.1.30

Model Parameters for Iso-Octane Conversion

Rate Eqn. (3.1.25); Catalyst = 0.3% Pt/Al_2O_3

Initial guesses : 5

Stepsize: 5

	390°C	400°C	410°C	420°C	430°C	A	ΔE,ΔH(Kcal/gmol
k_{11} $\frac{gmol}{gCat.h}$	1.055	1.654	2.6152	5.774	5.743	3.76×10^{14a}	43.07
k_{12} $\frac{gmol}{gCat.h}$	3.914	4.468	3.954	4.645	0.3944	1.78×10^{-3a}	-11.170
K_d	3.6697	2.03	2.0954	0.5411	1.676	4.55×10^{-9}	-26.95
K_h	6.9556	10.97	3.3799	8.2805	1.94	2.49×10^{-8}	-26.18
K_5	4.52	4.17	5.3999	6.4653	1.3291	5.62×10^{-6}	-18.36
K_7	10.2099	10.75	10.0072	1.234	15.5194	7.85×10^{-4}	-12.48

Table 6.1.31

Model Parameters for Iso-Octane Conversion

Rate eqn. (3.1.25)

Catalyst : 0.3%Pt/Al_2O_3

Initial guesses : 5

Stepsize: 3

	390°C	400°C	410°C	420°C	430°C	A	ΔE,ΔH(Kcal/gmol
k_{11} $\frac{gmol}{gCat.h}$	1.065	1.774	3.906	5.161	8.272	4.19×10^{15a}	46.14
k_{12} $\frac{gmol}{gCat.h}$	3.918	2.85	1.265	13.592	100.3	5.46×10^{24a}	73.69
K_d	3.3177	1.52	1.2526	2.66	0.5809	3.61×10^{-9}	-27.168
K_h	8.0119	8.05	6.4817	13.46	313.487	1.46×10^{24}	72.05
K_5	4.3072	3.47	1.5719	3.262	20.6197	3.27×10^{9}	27.954
K_7	9.495	7.15	4.7297	0.788	9.06	6.14×10^{-7}	-21.644

Table 6.1.32
Model Parameters for Iso-Octane Conversion
Rate Eqn. (3.1.25)
Catalyst: 0.3%Pt/Al_2O_3
Initial guesses 5
Stepsize: 1

	390°C	400°C	410°C	420°C	430°C	A	ΔE,ΔH(Kcal/gmol
k_{11} $\frac{gmol}{gCat.h}$	1.065	1.654	4.257	4.27	11.855	$9.54x10^{17a}$	53.528
k_{12} $\frac{gmol}{gCat.h}$	3.918	4.468	2.097	9.436	3.0623	59.5^{a}	2.296
K_d	3.3177	2.03	0.9425	1.7954	1.4421	$7.54x10^{-6}$	-16.87
K_h	8.0119	10.97	7.3438	3.3568	18.8909	271.78	4.754
K_5	4.3072	4.17	1.9772	4.135	1.54124	$1.85x10^{-6}$	-19.5
K_7	9.4950	10.75	5.7009	0.3414	2.1479	$3.92x10^{-19}$	-59.53

Table 6.1.33
Model Parameters for Iso-Octane Conversion
Rate Eqn. (3.1.25)
Catalyst : 0.3%Pt/Al_2O_3
Initial guesses : 3
Stepsize: 3

	390°C	400°C	410°C	420°C	A	ΔE,ΔH(Kcal/gmol)
k_{11} $\frac{gmol}{gCat.h}$	1.0827	1.468	3.646	5.167	$1.93x10^{17a}$	51.44
k_{12} $\frac{gmol}{gCat.h}$	1.811	0.0122	0.282	4.362	$2.35x10^{16a}$	50.95
K_d	4.0555	0.972	1.572	2.93	0.048	-5.112
K_h	4.873	0.0013	14.034	14.133	$1.25x10^{36}$	102.6
K_5	2.0688	3.9944	4.33	3.03	$1.63x10^{4}$	11.56
K_7	4.8558	6.077	1.1826	0.79	$3.68x10^{-21}$	-64.9

Table 6.1.34

Model Parameters for Iso-Octane Conversion

Rate Eqn. (3.1.25)

Catalyst : 0.3% Pt/Al_2O_3

Initial guesses : 3

Stepsize: 1

	390°C	400°C	410°C	420°C	A	ΔE,ΔH(Kcal/gmol)
k_{11} $\frac{gmol}{gCat.h}$	1.129	1.679	3.328	3.761	2.8×10^{13a}	39.534
k_{12} $\frac{gmol}{gCat.h}$	1.362	1.999	0.9228	8.72×10^{-4}	2.394×10^{-67a}	-207.25
K_d	2.0962	2.43	0.897	1.189	1.676×10^{-8}	-24.85
K_h	3.2871	3.61	0.3865	0.0013	2.0×10^{-76}	-234.6
K_5	3.201	2.38	3.515	3.37	1.27×10^{21}	63.62
K_7	3.7418	1.26	1.5196	6.78	8.81×10^{48}	149.8

Table 6.1.35

Model Parameters for Iso-Octane Conversion

Rate Eqn.(3.1.27)

Catalyst: 0.3%Pt/Al_2O_3

Initial guesses : 3

Stepsize: 5

	390°C	400°C	410°C	420°C	430°C	A	ΔE,ΔH(Kcal/gmol
k_{13} $\frac{gmol}{gCat.h}$	1.044	2.266	2.504	2.563	3.97	1.19×10^{9a}	26.032
k_{14} $\frac{gmol}{gCat.h}$	2.2557	1.7	9.396	1.672	4.246	4.74×10^{4a}	11.8
K_d	5.05	1.188	0.5271	3.1	4.1768	59.74	4.578
K_h	5.5665	0.689	0.0315	0.07	0.0279	1.0×10^{-39}	-60.32
K_5	1.0919	1.067	37.259	1.39	6.1416	4.87×10^{11}	35.13
K_7	4.1756	2.865	14.351	8.55	4.895	1.06×10^{5}	13.38

Table 6.1.36
Model Parameters for Iso-Octane
Rate Eqn. (3.1.27)
Catalyst :0.3%Pt/Al_2O_3

Initial guesses : 3
Stepsize : 1

	390°C	400°C	410°C	420°C	430°C	A	ΔE,ΔH(Kcal/gmol)
k_{13} $\frac{gmol}{gCat.h}$	1.554	2.1265	3.126	5.091	3.887	8.38×10^{8a}	25.22
k_{14} $\frac{gmol}{gCat.h}$	3.91	1.558	3.303	0.1883	0.998	1.37×10^{-14a}	-45.3
K_d	0.6957	0.613	0.7433	1.9	0.5573	90	6.45
K_h	1.7046	0.295	0.2177	6.06	0.0594	6.24×10^{-12}	-34.21
K_5	2.4753	3.5	3.7383	0.07	2.3784	2.34×10^{-12}	-37.02
K_7	2.8436	3.163	4.268	7.74	11.0476	2.099	33.39

Table 6.1.37

Model Parameters for Iso-Octane Conversion

Rate Eqn. (3.1.25)

Catalyst : 0.6%Pt/Al_2O_3

Initial guesses : 5

Stepsize: 5

	390°C	400°C	410°C	420°C	A	ΔE,ΔH(Kcal/gmol)
k_1 $\frac{gmol}{gCat.h}$	0.934	1.477	1.9691	2.783	$1.38x10^{11a}$	32.716
k_2 $\frac{gmol}{gCat.h}$	3.1978	9.1294	2.690	3.1627	$2.59x10^{-3a}$	-11.314
K_d	5.0598	12.0776	2.0034	1.7739	$8.43x10^{-17}$	-50.88
K_h	8.0785	28.81	5.5974	6.8005	$5.336x10^{-6}$	-19.54
K_5	4.6793	30.5734	6.2763	3.9666	$9.36x10^{-6}$	-18.47
K_7	8.832	66.645	7.6442	1.219	$4.84x10^{-25}$	-79.75

Table 6.1.38

Model Parameters for Iso-Octane Conversion

Rate Eqn. (3.1.25)

Catalyst: 0.6%Pt/Al_2O_3

Initial guesses : 5

Stepsize: 1

	390°C	400°C	410°C	420°C	430°C	A	ΔE,ΔH(Kcal/gmol)
k_1 $\frac{gmol}{gCat.h}$	0.942	1.601	1.9893	2.598	4.3533	$1.62x10^{11a}$	32.904
k_2 $\frac{gmol}{gCat.h}$	2.377	1.773	2.514	2.008	0.2113	$6.29x10^{-14a}$	-43.3
K_d	6.2587	3.8301	3.7344	1.925	1.5021	$1.096x10^{-10}$	-32.83
K_h	6.0054	3.9552	6.4961	8.5187	12.5416	$2.52x10^{7}$	20.62
K_5	2.2821	3.595	2.9131	3.5127	3.574	$1.235x10^{3}$	8.164
K_7	6.375	11.5199	6.6654	5.1767	1.1577	$2.49x10^{-12}$	-38.664

Table 6.1.39
Model Parameters for Iso-Octane Conversion
Rate Eqn. (3.1.25)
Catalyst: 0.6%Pt/Al_2O_3
Initial guesses : 3
Stepsize : 5

	390°C	400°C	410°C	420°C	430°C	A	ΔEΔH(Kcal/gmol)
k_1 $\frac{gmol}{gCat.h}$	1.062	1.577	2.049	2.819	4.0286	2.18×10^{10a}	30.126
k_2 $\frac{gmol}{gCat.h}$	2.395	4.619	3.607	0.6955	3.068	5.34×10^{-4a}	-12.886
K_d	2.922	3.8866	6.5424	2.2481	3.3342	0.606	-2.41
K_h	6.589	10.8994	8.4451	9.6414	6.6146	4.216	-0.92
K_5	3.839	4.6259	4.9834	3.447	6.8341	1.56×10^{3}	7.95
K_7	6.589	5.6891	0.2115	0.8489	0.228	2.84×10^{-26}	-80.44

Table 6.1.40
Model Parameters for Iso-Octane Conversion
Rate Eqn. (3.1.25)
Catalyst: 0.6%Pt/Al_2O_3
Initial guesses : 3
Stepsize: 1

	390°C	400°C	410°C	420°C	A	ΔE,ΔH(Kcal/gmol)
k_1 $\frac{gmol}{gCat.h}$	1.096	1.828	2.247	2.769	3.05×10^{9a}	27.378
k_2 $\frac{gmol}{gCat.h}$	1.611	0.706	0.894	0.201	4.756×10^{-18a}	-54.9
K_d	2.455	4.0072	2.1407	2.8419	0.797	-1.694
K_h	3.050	1.2559	5.0695	2.6276	1.65×10^{3}	8.714
K_5	2.3633	1.1968	2.6567	3.4059	7.06×10^{5}	17.16
K_7	4.499	4.3649	1.8189	0.6475	5.707×10^{-20}	-61.13

Table 6.1.41
Model Parameters for Iso-Octane Conversion
Rate Eqn. (3.1.27)
Catalyst: 0.6%Pt/Al_2O_3

Initial guesses : 5
Stepsize : 5

	390°C	400°C	410°C	420°C	A	ΔE, ΔH(Kcal/gmol)
k_1 $\frac{gmol}{gCat.h}$	1.221	2.132	2.843	5.4	6.18×10^{14a}	43.54
k_2 $\frac{gmol}{gCat.h}$	3.124	1.647	1.615	9.826	5.5×10^{10a}	30.664
K_d	1.4157	0.1683	4.8142	0.6857	3.054×10^{3}	10.96
K_h	4.7713	17.2076	1.8429	32.6045	1.29×10^{11}	31.8
K_5	0.0958	2.9149	0.0408	0.1389	1.44×10^{-10}	-28.53
K_7	21.5592	2.3788	11.8435	9.4566	0.017	-8.45

Table 6.1.42
Model Parameters for Iso-Octane Conversion
Rate Eqn. (3.1.27)
Catalyst: 0.6%Pt/Al_2O_3

Initial guesses : 3
Stepsize: 3

	390°C	400°C	410°C	420°C	A	ΔE,ΔH(Kcal/gmol
k_1 $\frac{gmol}{gCat.h}$	1.586	1.794	2.396	3.606	4.07×10^{14a}	42.93
k_2 $\frac{gmol}{gCat.h}$	3.532	7.155	1.564	4.737	0.115^{a}	-6.08
K_d	0.4270	13.4974	0.6034	3.5104	6.58×10^{9}	29.8
K_h	1.4249	0.4801	0.4240	1.1243	1.68×10^{-3}	-8.28
K_5	3.5209	0.4115	2.2787	1.3900	7.51×10^{-4}	-10.268
K_7	2.6967	5.5961	5.3525	1.4628	1.53×10^{-5}	-16.646

Table 6.1.43
Model Parameters for Iso-Octane Conversion
Rate Eqn. (3.1.27)
Catalyst: 0.6%Pt/Al_2O_3
Initial guesses : 3
Stepsize : 1

	390°C	400°C	410°C	420°C	A	ΔE,ΔH(Kcal/gmol)
k_1 $\frac{gmol}{gCat.h}$	1.357	1.804	2.734	4.115	$6.3x10^{11a}$	34.34
k_2 $\frac{gmol}{gCat.h}$	1.052	0.175	1.136	1.847	$4.15x10^{10a}$	32.1
K_d	2.3213	1.5606	0.5039	0.6557	$1.57x10^{-11}$	-33.93
K_h	7.2931	5.4896	0.2721	0.9094	$7.33x10^{-28}$	-85.47
K_5	0.6274	0.1714	5.4167	2.6364	$3.32x10^{17}$	55.12
K_7	2.3672	3.527	2.6481	1.7912	$1.47x10^{-3}$	-10.043

Table 6.1.44
Model Parameters for Iso-Octane Conversion
Rate Eqn. (3.1.27)
Catalyst: 0.6%Pt/Al_2O_3
Initial guesses : 1
Stepsize: 3

	390°C	400°C	410°C	A	ΔE, ΔH(Kcal/gmol)
k_1 $\frac{gmol}{gCat.h}$	1.393	2.682	3.494	$1.69x10^{14a}$	40.79
k_2 $\frac{gmol}{gCat.h}$	0.314	0.8083	0.528	$6.35x10^{7}$	23.72
K_d	0.4785	0.6427	0.1669	$1.14x10^{-14}$	-47.25
K_h	0.1574	1.4362	1.2508	$1.38x10^{30}$	93.9
K_5	0.3611	0.7751	0.8681	$5.75x10^{16}$	52.4
K_7	0.28364	3.6820	9.6520	$6.32x10^{51}$	159.49

6.1.3 MCP Kinetic Modelling Results

The mechanism used to obtain the rate equations were derived on the basis of the reaction network proposed below by this author.

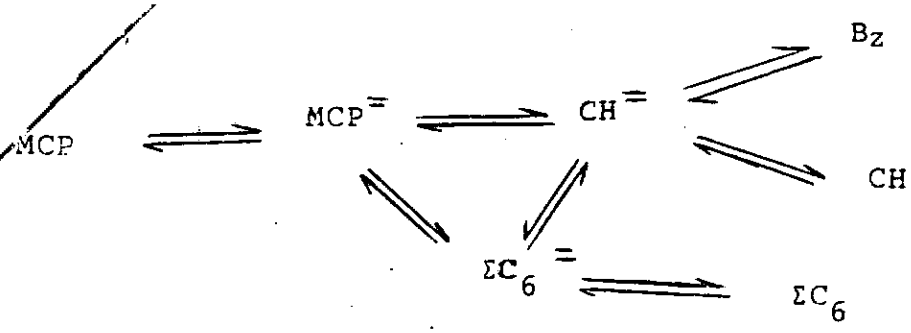

This network is similar to that proposed by Dartigues et al[34], except that here the formation of hydrogenolysis products was taken into account.

Eleven rate models were developed and tested. Six out of the eleven models satisfied the set criteria when Pt/Al_2O_3 catalyst was used in the conversion of MCP. The six rate equations that fitted the experimental data (conversion - W/F data) obtained at 0.092 atm MCP partial pressure are:

1 Rate equation (3.1.44)

$$r_2 = \frac{k_3K_1[MCP] - \frac{k_4[CH][H_2]}{K_8K_7K_3}}{1 + K_1[MCP] + \frac{[\Sigma C_6]}{K_{11}K_6K_4} + \frac{[CH]}{K_8K_7[H_2]} + \frac{[CH]}{K_8} + \frac{[Bz]}{K_{10}} + \frac{[\Sigma C_6]}{K_{11}K_6[H_2]} + \frac{[\Sigma C_6]}{K_{11}}}$$

The rate model is based on the dehydrogenation of adsorbed methylcyclopentane as the rate determining step.

2. Rate equation 3.1.46

$$r_4 = \frac{\frac{k_7 K_2 K_1 [MCP]}{[H_2]} - \frac{k_8 [\Sigma C_6]}{K_{11} K_6 (H_2)}}{1 + K_1 [MCP] + \frac{K_2 K_1 [MCP]}{[H_2]} + \frac{[CH]}{K_8 K_7 [H_2]} + \frac{[CH]}{K_8} + \frac{[Bz]}{K_{10}} + \frac{[\Sigma C_6]}{K_{11} K_6 [H_2]} + \frac{[\Sigma C_6]}{K_{11}}} \quad 3.1.46$$

The rate model is based on the conversion of adsorbed methylcyclopentene to adsorbed olefinic hydrogenolysis products as the rate determining step.

3. Rate equation 3.1.48

$$r_6 = \frac{k_{11} K_4 K_2 K_1 [MCP] - \frac{k_{12} [\Sigma C_6]}{K_{11}}}{1 + K_1 [MCP] + \frac{K_2 K_1 [MCP]}{[H_2]} + \frac{[CH]}{K_8 K_7 [H_2]} + \frac{[CH]}{K_8} + \frac{[Bz]}{K_{10}} + \frac{K_4 K_2 K_1 [MCP]}{[H_2]} + \frac{[\Sigma C_6]}{K_{11}}} \quad 3.1.48$$

The rate model is based on the hydrogenation of adsorbed olefinic hydrogenolysis products to adsorbed hydrogenolysis products as the rate - determining step.

4. Rate Equation 3.1.49

$$r_7 = \frac{k_{13}K_3K_2K_1[MCP] - \frac{k_{14}[CH]}{K_8}}{1 + K_1[MCP] + \frac{K_2K_1[MCP]}{[H_2]} + \frac{K_5[\Sigma C_6]}{K_{11}K_6[H_2]} + \frac{[CH]}{K_8} + \frac{[Bz]}{K_{10}} + \frac{[\Sigma C_6]}{K_{11}K_6[H_2]} + \frac{[\Sigma C_6]}{K_{11}}} \quad 3.1.49$$

The rate model is based on the hydrogenation of adsorbed cyclohexene to adsorbed cyclohexane as the rate - determining step.

5. Rate equation 3.1.50.

$$r_8 = \frac{k_{15}K_7K_3K_2K_1[MCP] - K_{16}[CH]}{1 + K_1[MCP] + \frac{K_2K_1[MCP]}{[H_2]} + \frac{K_5[\Sigma C_6]}{K_{11}K_6} + \frac{K_7K_5[\Sigma C_6]}{K_{11}K_6} + \frac{[Bz]}{K_{10}} + \frac{[\Sigma C_6]}{K_{11}K_6[H_2]} + \frac{[\Sigma C_6]}{K_{11}}} \quad 3.1.50$$

The rate model is based on the desorption of hydrogenolysis products as the rate - determining step.

The predicted rate and adsorption equilibrium constants of MCP conversion on Pt/Al_2O_3 catalyst at various temperatures using the six model equations that satisfied the set criteria are shown in Tables 6.1.45 - 6.1.68. Tables 6.1.45 - 6.1.50 show the values of the predicted rate and adsorption equilibrium constants using rate equation (3.1.44). The computed activation energy for the forward reaction varied between 10-28 Kcal/gmole for different initial guesses and stepsizes. According to the mechanism for the aromatization of MCP proposed in Chapter 3 section 3.1.2 (Scheme IV), the first step is adsorption while steps 8, 10 and 11 are desorption steps. Since adsorption is exothermic and desorption endothermic the adsorption and desorption energies are negative and positive respectively. Table 6.1.69 shows the extent to which these kinetic and thermodynamic criteria were met using equation (3.1.44). Table 6.1.51 - 6.1.54 show the values of the predicted rate and adsorption equilibrium constants using rate equation (3.1.46). The activation energies obtained using different initial guesses and stepsizes ranged between 17-36 kcal/gmole except at initial guesses of constants 5, stepsize 5 (Table 6.1.51) where the activation energy was 50Kcal/gmole. Table 6.1.70 shows the extent to which the kinetic and thermodynamic criteria were met using rate equation (3.1.46). Tables 6.1.55 - 6.1.59 show the values of the predicted rate and adsorption equilibrium constants using rate equation (3.1.48). The activation energies varied between 15-41 Kcal/gmole. Table 6.1.71 shows the extent to which the kinetic and thermodynamic criteria were met when rate equation (3.1.48) was used to evaluate the model parameters. Tables 6.1.59 -

6.1.64 show the values of the predicted rate and adsorption equilibrium constants at various initial guesses and stepsizes using rate equation (3.1.49). The activation energies obtained with the different initial guesses and stepsizes varied between 16 - 35Kcal/gmole. Table 6.1.72 shows the extent to which the kinetic and thermodynamic criteria were met using rate equation (3.1.49) for model parameters evaluation. Tables 6.1.65 - 6.1.68 show the values of the predicted rate and adsorption equilibrium constants at various initial guesses and stepsizes using rate equation (3.1.50). The activation energies obtained with the different initial guesses and stepsizes ranged between 14-29Kcal/gmole except at initial guesses of constants 1, stepsize 3 where a value of 1.7Kcal/gmole was determined as the activation energy. Table 6.1.73 shows the extent to which the kinetic and thermodynamic criteria were met using equation (3.1.50) to evaluate the model parameters. It can be observed from Tables 6.1.69 - 6.1.73 that all the kinetic and thermodynamic criteria were met only when rate equation (3.1.50) was used to evaluate the kinetic parameters at initial guesses of constants 5, stepsize 1.

Figures 6.1.8 and 6.1.9 show the experimental and predicted conversion versus W/F profiles. Rate equation (3.1.44) was used in predicting conversion at initial guesses of constants 5, stepsize 5 in Figure 6.1.8 while in Figure 6.1.9 rate equation (3.1.46) was used at initial guesses of constant 5, stepsize 5. The figures show that there are reasonably good fit between the experimental and predicted values.

Using Pt-Re/Al_2O_3 (Dried) catalyst, only two out of the eleven models satisfied the set criteria and they are:

1 Rate expression of equation (3.1.48)

$$r_6 = \frac{k_{11}K_4K_2K_1[MCP] - \frac{k_{12}[\Sigma C_6]}{[H_2]}}{1 + K_1[MCP] + \frac{K_2K_1[MCP]}{[H_2]} + \frac{[CH]}{K_8K_7[H_2]} + \frac{[CH]}{K_8} + \frac{[Bz]}{K_{10}} + \frac{K_4K_2K_1[MCP]}{[H_2]} + \frac{[\Sigma C_6]}{K_{11}}}$$

The rate model is based on the hydrogenation of adsorbed olefinic hydrogenolysis products to adsorbed hydrogenolysis products as the rate - determining step.

2 Rate expression of equation (3.1.49)

$$r_7 = \frac{k_{13}K_3K_2K_1[MCP] - \frac{k_{14}[CH]}{K_8}}{1 + K_1[MCP] + \frac{K_2K_1[MCP]}{[H_2]} + \frac{K_5[\Sigma C_6]}{K_{11}K_6[H_2]} + \frac{[CH]}{K_8} + \frac{[Bz]}{K_{10}} + \frac{[\Sigma C_6]}{K_{11}K_6[H_2]} + \frac{[\Sigma C_6]}{K_{11}}}$$

The rate model is based on the hydrogenation of adsorbed cyclohexene to cyclohexane as the rate determining step.

It is important to note that both eqns.(3.1.48) and (3.1.49) are among the five rate equations that were shown

to predict MCP conversion on Pt/Al_2O_3. Since the constant activity kinetic behaviour of the bimetallic $Pt-Re/Al_2O_3$ catalyst is not expected to deviate from that of the monometallic Pt/Al_2O_3, it becomes very significant that rate equation (3.1.49) is the only one of the five rate equations that satisfied all kinetic and thermodynamic criteria. It will thus be interesting to see if the same rate equation attains the same status for $Pt/Re/Al_2O_3$.

The predicted rate and adsorption equilibrium constants on $Pt-Re/Al_2O_3$ (DRIED) catalysts are shown in Tables 6.1.74 and 6.1.75 for rate equation (3.1.48) and Tables 6.1.76 and 6.1.77 for rate equation (3.1.49). The computed activation energy obtained using rate equation (3.1.48) is 21.8Kcal/gmole using initial guesses of constants 5, stepsize 5 and 23.1Kcal/gmole using initial guesses of constants 3, stepsize 3. Table 6.1.78 shows the extent to which the kinetic and thermodynamic criteria were met using rate equation (3.1.48). The computed activation energy obtained using rate equation (3.1.49) is 43.7Kcal/gmole using initial guesses of constants 3, stepsize 3 to evaluate the kinetic parameters. Table 6.1.79 show the extent to which the kinetic and thermodynamic creteria were met. It can be seen from Table 6.1.78 and 6.1.79 that not all the thermodynamic criteria were met when the rate equations 3.1.48 and 3.1.49 were used to evaluate the kinetic parameters of the reaction of MCP on $Pt-Re/Al_2O_3$ (DRIED) catalyst. This contrasted with the case for the Pt/Al_2O_3 catalyst where all the criteria were met for the rate equation (3.1.49).

Figures 6.1.10 and 6.1.11 show the plots of experimental and predicted conversions versus W/F profiles obtained using each of the rate equations. The prediction of the conversion on this catalyst is not as good as the prediction obtained for the conversion of MCP on Pt/Al_2O_3 catalyst (See Figures 6.1.8 - 6.1.9).

Table 6.1.45

Model Parameters for MCP Conversion

Rate Eqn. (3.1.44)

Catalyst: 0.3%Pt/Al_2O_3

Initial guesses : 5

Stepsize: 5

	370°C	380°C	400°C	A	ΔE;ΔH(Kcal/gmol)
k_3 $\frac{gmol}{gCat.h}$	1.032	1.036	1.946	7.46×10^{6a}	19.62
k_4 $\frac{gmol}{gCat.h}$	3.918	3.759	4.893	7.389^a	0.04
K_1	4.2454	4.1988	3.6751	0.1353	-4.44
K_3	7.6696	7.3166	7.5392	6.166	-0.24
K_4	7.2008	7.9304	6.9838	2.347	-1.5
K_6	7.5094	8.3867	8.0787	27.605	1.62
K_7	7.7411	7.7106	7.7929	9.189	0.224
K_8	5.4224	5.9074	4.9260	0.39	-3.448
K_{10}	6.6212	5.8074	5.5148	0.142	-4.9
K_{11}	6.1232	4.8027	5.5654	1.655	-1.56

Table 6.1.46

Model Parameters for MCP Conversion

Rate Eqn. (3.1.44)

Catalyst: 0.3%Pt/Al_2O_3

Initial guesses : 5

Stepsize: 3

	370°C	380°C	400°C	A	ΔE,ΔH(Kcal/gmol)
k_3 $\frac{gmol}{gCat.h}$	0.723	0.91	1.869	4.01×10^{9a}	28.1
k_4 $\frac{gmol}{gCat.h}$	3.477	3.529	3.32	2.024^a	-1.52
K_1	4.7394	4.4814	3.7058	0.016	-7.29
K_3	6.7590	6.8330	7.4295	54.598	2.69
K_4	6.2382	6.0179	6.6251	30.508	2.07
K_6	6.2743	6.3405	6.2753	6.031	-0.056
K_7	6.8169	7.02	7.684	105.95	3.52
K_8	5.711	5.06	4.2317	140.752	-8.6
K_{10}	5.8857	5.1663	5.4093	1.315	-1.87
K_{11}	6.2215	7.6636	5.6326	1.217	-2.0

Table 6.1.47

Model Parameters for MCP Conversion

Rate Eqn. (3.1.44)

Catalyst: 0.3%Pt/Al_2O_3

Initial guesses : 5

Stepsize: 1

	370°C	380°C	400°C	A	ΔE,ΔH(Kcal/gmol)
k_3 $\frac{gmol}{gCat.h}$	0.641	0.902	1.08	8.196×10^{4a}	14.23
k_4 $\frac{gmol}{gCat.H}$	3.345	3.437	3.265	3.171^a	-0.894
K_1	4.6808	4.1847	4.6634	6.706	0.522
K_3	5.1868	5.4856	5.2427	5.366	0.014
K_4	2.75	6.029	6.1824	3.07×10^7	20.6
K_6	5.9618	6.2187	5.5043	0.748	-2.7
K_7	6.9427	6.2042	5.9472	0.267	-5.16
K_8	5.0421	4.0477	5.2650	34.124	2.586
K_{10}	5.6356	5.8049	5.5019	2.818	-0.91
K_{11}	5.3578	5.6275	5.3748	4.735	-0.184

Table 6.1.48

Model Parameters for MCP Conversion

Rate Eqn. (3.1.44)

Catalyst: 0.3%Pt/Al_2O_3

Initial guesses : 3

Stepsize: 3

	370°C	380°C	400°C	A	ΔE,ΔH(Kcal/gmol)
k_3 $\frac{gmol}{gCat.h}$	1.06	1.413	1.565	1.789×10^{7a}	10.4
k_4 $\frac{gmol}{gCat.h}$	2.487	2.315	2.313	1.095^a	-1.83
K_1	2.1709	1.9792	3.898	3.78×10^6	18.644
K_3	4.5097	4.5266	5.3109	222.739	5.046
K_4	4.1159	4.1476	4.5101	35.588	2.79
K_6	4.4748	4.8962	4.6365	7.294	0.586
K_7	4.6874	4.7591	4.3085	0.587	-2.698
K_8	3.1418	2.8368	1.6113	5.425×10^{-7}	-20.1
K_{10}	3.5892	3.247	2.5082	1.01×10^{-3}	-10.528
K_{11}	3.3674	3.5150	3.4186	4.047	0.216

Table 6.1.49
Model Parameters for MCP Conversion
Rate Eqn. (3.1.44)
Catalyst: 0.3%Pt/Al_2O_3
Initial guesses : 3
Stepsize: 1

	370°C	380°C	400°C	A	ΔE,ΔH(Kcal/gmol)
k_3 $\frac{gmol}{gCat.h}$	0.624	1.981	2.074	1.978×10^{12a}	36.362
k_4 $\frac{gmol}{gCat.h}$	1.981	2.011	2.176	33.515^a	2.84
K_1	2.5608	2.7280	2.2335	0.077	-4.566
K_3	3.1365	3.0659	4.6454	4.16×10^{4}	12.3
K_4	3.6241	3.5752	2.3719	1.376×10^{-4}	-13.16
K_6	3.6124	3.6889	3.6125	3.32	-0.12
K_7	4.0538	4.1316	4.5262	52.72	3.1
K_8	3.1328	3.0919	2.2125	7.99×10^{-4}	-10.7
K_{10}	3.4082	3.2661	2.7604	0.026	-6.28
K_{11}	3.5161	3.4036	2.1206	2.239	15.46

Table 6.1.50
Model Parameters for MCP Conversion
Rate Eqn. (3.1.44)
Catalyst: 0.3%Pt/Al_2O_3
Initial guesses : 1
Stepsize : 5

	370°C	380°C	400°C	A	ΔE,ΔH(Kcal/gmol)
k_3 $\frac{gmol}{gCat.h}$	0.974	1.073	1.454	1.78×10^{4a}	11.838
k_4 $\frac{gmol}{gCat.h}$	1.224	2.048	0.047	3.23×10^{-35a}	104.1
K_1	1.1205	2.0501	2.7430	1.998×10^{8}	24.28
K_3	2.3416	1.8901	2.0586	0.253	-2.77
K_4	2.3416	2.7584	1.6633	3.368×10^{-4}	-11.53
K_6	2.3416	2.4750	3.4354	1.796	11.55
K_7	2.3416	3.4946	3.8590	7.218×10^{4}	13.17
K_8	2.2371	1.7319	3.4243	1.673×10^{5}	14.65
K_{10}	2.3416	1.1733	1.7586	0.0395	- 4.93
K_{11}	2.3416	0.4657	0.2152	2.164×10^{-22}	-64.84

Table 6.1.51

Model Parameters for MCP Conversion

Rate Eqn. (3.1.46)

Catalyst: 0.3%Pt/Al_2O_3

Initial guesses : 5

Stepsize: 5

	370°C	380°C	400°C	A	ΔE,ΔH(Kcal/gmol)
k_7 $\frac{gmol}{gCat.h}$	0.836	1.026	4.401	1.262×10^{17a}	50.27
k_8 $\frac{gmol}{gCat.h}$	4.443	4.34	11.1	2.98×10^{10a}	28.47
K_1	5.829	5.437	14.9	4.247×10^{10}	29.424
K_2	4.2445	4.605	2.9	3.36×10^{-4}	-12.26
K_6	8.56	8.409	5.44	1.799×10^{-4}	-13.92
K_7	5.185	5.895	0.367	9.77×10^{-28}	-82.676
K_8	9.177	8.5	7.79	0.247	-4.63
K_{10}	4.824	6.97	0.0038	5.78×10^{-75}	-223.4
K_{11}	6.13	5.87	11.01	8.93×10^{6}	18.38

Table 6.1.52

Model Parameters for MCP Conversion

Rate Eqn. (3.1.46)

Catalyst: 0.3%Pt/Al_2O_3

Initial guesses : 5

Stepsize : 3

	370°C	380°C	400°C	A	ΔE,ΔH (Kcal/gmol)
k_7 $\frac{gmol}{gCat.h}$	0.818	1.223	2.836	2.55×10^{12a}	36.2
k_8 $\frac{gmol}{gCat.h}$	3.664	4.165	3.001	0.034^{a}	-6.9
K_1	5.5438	1.83	4.52	3.625	0.016
K_2	4.7566	3.147	1.245	2.914×10^{-13}	-39.15
K_6	6.577	5.36	1.25	8.166×10^{-17}	-50.27
K_7	5.488	5.32	6.14	91.56	3.658
K_8	7.477	10.15	5.7	3.28×10^{-3}	- 10.16
K_{10}	6.126	6.28	6.154	6.19	0
K_{11}	6.31	7.4	12.27	2.73×10^{7}	19.69

Table 6.1.53
Model Parameters for MCP Conversion
Rate Eqn. (3.1.46)
Catalyst: 0.3%Pt/Al_2O_3
Initial guesses : 3
Stepsize : 3

	370°C	380°C	400°C	A	ΔE,ΔH(Kcal/gmol)
k_7 $\frac{gmol}{gCat.h}$	1.356	1.842	2.499	1.67×10^{6a}	17.17
k_8 $\frac{gmol}{gCat.h}$	1.602	2.526	0.935	1.205×10^{-6a}	-19.2
K_1	2.4	2.23	1.68	8.144×10^{-4}	-10.3
K_2	1.43	1.35	5.77	5.62×10^{14}	-43.5
K_6	6.34	5.21	9.32	1.4×10^{5}	13.04
K_7	3.183	2.947	9.246	5.23×10^{11}	33.44
K_8	6.21	5.3476	1.342	1.35×10^{-15}	-46.5
K_{10}	3.67	3.5343	3.6125	2.936	-0.27
K_{11}	4.08	4.0147	0.0658	5.68×10^{-43}	-127.68

Table 6.1.54
Model Parameters for MCP Conversion
Rate Eqn. (3.1.46)
Catalyst: 0.3%Pt/Al_2O_3
Initial guesses : 1
Stepsize : 5

	370°C	380°C	400°C	A	ΔE,ΔH(Kcal/gmol)
k_7 $\frac{gmol}{gCat.h}$	1.068	1.243	2.382	2.35×10^{8a}	23.97
k_8 $\frac{gmol}{gCat.h}$	1.458	0.761	0.902	4.168×10^{-4a}	-11.036
K_1	1.437	1.528	2.50	6.34×10^{5}	16.788
K_2	3.745	4.098	2.53	2.147×10^{-4}	-12.68
K_6	2.1471	0.832	1.49	0.016	-5.89
K_7	4.08	2.9266	2.47	9.37×10^{-5}	-13.65
K_8	0.291	0.1061	1.254	2.5×10^{16}	50.97
K_{10}	0.029	1.8879	2.49	2.88×10^{37}	104.06
K_{11}	3.321	2.696	2.45	5.3×10^{-3}	-8.226

Table 6.1.55
Model Parameters for MCP Conversion
Rate Eqn. (3.1.48)
Catalyst: 0.3%Pt/Al_2O_3
Initial guesses : 5
Stepsize : 5

	370°C	380°C	400°C	A	ΔE,ΔH(Kcal/gmol)
k_{11} $\frac{gmol}{gCat.h}$	0.815	1.034	2.543	3.91×10^{11a}	33.87
k_{12} $\frac{gmol}{gCat.h}$	4.677	4.424	5.736	1.45×10^{3a}	6.636
K_1	6.1523	5.6262	4.3134	1.795×10^{-3}	-10.488
K_2	5.4588	5.8861	4.2722	0.011	-8.018
K_4	4.4158	4.3444	1.5455	5.78×10^{-11}	-32.42
K_7	3.1976	4.4661	5.4798	3.32×10^{5}	14.778
K_8	8.8243	8.6930	10.1483	265.87	4.4
K_{10}	7.7134	6.7398	6.8269	0.7153	-3.0
K_{11}	7.5935	7.5446	5.4960	3.396×10^{-3}	-9.97

Table 6.1.56
Model Parameters for MCP Conversion
Rate Eqn. (3.1.48)
Catalyst: 0.3%Pt/Al_2O_3
Initial guesses : 5
Stepsize : 3

	370°C	380°C	400°C	A	ΔE,ΔH(Kcal/gmol)
k_{11} $\frac{gmol}{gCat.h}$	0.744	1.102	2.976	7.3×10^{13a}	40.68
k_{12} $\frac{gmol}{gCat.h}$	3.477	3.702	3.429	3.387^{a}	-0.77
K_1	5.5744	5.0321	2.0286	2.616×10^{-10}	-30.72
K_2	5.9554	5.5138	3.0557	9.42×10^{-7}	-20.224
K_4	5.1404	4.3602	1.3176	7.95×10^{-14}	-41.06
K_7	6.1746	5.7853	6.9359	131.76	3.99
K_8	7.2227	7.5316	7.8881	50.09	2.486
K_{10}	6.1103	6.1952	18.716	1.142×10^{9}	55.07
K_{11}	6.3450	6.5686	1.0719	6.83×10^{12}	40.65

Table 6.1.57
Model Parameters for MCP Conversion
Rate Eqn. (3.1.48)
Catalyst: 0.3%Pt/Al_2O_3
Initial guesses : 5
Stepsize : 1

	370°C	380°C	400°C	A	ΔE,ΔH(Kcal/gmol)
k_{11} $\frac{gmol}{gCat.h}$	0.831	0.973	1.729	3.215×10^{7a}	21.7
k_{12} $\frac{gmol}{gCat.h}$	2.819	3.261	3.102	28.933^a	2.13
K_1	5.2785	5.3594	5.1196	1.861	-1.348
K_2	5.3484	5.3425	5.4199	21.585	1.83
K_4	5.0543	4.8892	5.0466	105.00	4.064
K_7	4.3276	6.5533	5.2858	0.049	-6.3
K_8	6.4305	5.9477	5.8189	0.719	-2.8
K_{10}	5.5983	5.0541	5.4457	4.397	-0.26
K_{11}	6.0173	5.4774	5.5273	1.153	-2.09

Table 6.1.58
Model Parameters for MCP Conversion
Rate Eqn. (3.1.48)
Catalyst: 0.3%Pt/Al_2O_3
Initial guesses : 3
Stepsize : 3

	370°	380°C	400°C	A	ΔE,ΔH(Kcal/gmol)
k_{11} $\frac{gmol}{gCat.h}$	1.134	1.842	2.008	2.63×10^{5a}	14.93
k_{12} $\frac{gmol}{gCat.h}$	2.665	2.78	3.087	140.19^a	4.29
K_1	3.7672	2.9470	0.63	2.24×10^6	17.23
K_2	3.0311	2.2292	2.59	0.242	3.01
K_4	1.8624	1.3520	5.1	1.981	33.02
K_7	3.4816	3.5343	14.17	1.274×10^{15}	43.38
K_8	5.4233	5.3476	0.79	5.4×10^{-20}	-59.6
K_{10}	3.8971	4.0147	0.446	1.03×10^{-22}	-67.288
K_{11}	4.2263	4.4079	2.66	5.457×10^{-5}	-14.58

Table 6.1.59

Model Parameters for MCP Conversion

Rate Eqn. (3.1.48)

Catalyst: 0.3%Pt/Al_2O_3

Initial guesses : 3

Stepsize : 1

	370°C	380°C	400°C	A	ΔE,ΔH(Kcal/gmol)
k_{11} $\frac{gmol}{gCat.h}$	0.946	1.231	3.022	7.182×10^{11a}	34.46
k_{12} $\frac{gmol}{gCat.h}$	1.920	1.989	1.607	0.044^a	-5.704
K_1	3.1233	3.1785	0.28	2.481×10^{-25}	-74.79
K_2	3.5403	3.0889	2.97	0.092	-4.65
K_4	2.8861	2.8751	2.77	1.093	-1.25
K_7	3.2851	2.9263	6.162	1.806×10^{7}	20.13
K_8	3.7286	3.7578	3.77	4.702	0.296
K_{10}	3.4132	3.4330	1.39	1.52×10^{-9}	-27.86
K_{11}	3.5001	3.4685	2.32	1.926×10^{-4}	-12.688

Table 6.1.60

Model Parameters for MCP Conversion

Rate Eqn. (3.1.49)

Catalyst: 0.3%Pt/Al_2O_3

Initial guesses : 5

Stepsize : 3

	370°C	380°C	400°C	A	ΔE,ΔH(Kcal/gmol)
k_{13} $\frac{gmol}{gCat.h}$	0.203	0.261	0.470	7.199×10^{7a}	24.53
k_{14} $\frac{gmol}{gCat.h}$	3.575	3.594	4.038	120.42^a	3.73
K_1	6.9117	6.98	5.2354	8.643×10^{-3}	-8.664
K_2	5.8124	5.79	6.1983	27.495	2.014
K_3	3.8210	3.94	3.5733	0.68	-2.25
K_5	7.0489	7.08	6.4846	11.787	0.66
	7.6121	7.48	7.2081	2.203	-1.59
	6.0633	6.20	7.2166	1.32×10^{3}	6.93
	6.2560	5.72	7.8152	1.77×10^{-4}	-13.4
	5.5806	5.75	3.6381	4.5×10^{-6}	-15.6

Table 6.1.61
Model Parameters for MCP Conversion
Rate Eqn. (3.1.49)
Catalyst: 0.3%Pt/Al_2O_3
Initial guesses : 5
Stepsize : 1

	370°C	380°C	400°C	A	ΔE,ΔH(Kcal/gmol)
k_{13} $\frac{gmol}{gCat.h}$	0.184	0.230	0.569	7.816×10^{10a}	33.72
k_{14} $\frac{gmol}{gCat.h}$	3.077	3.086	3.765	713.37^{a}	6.23
K_1	5.4492	5.46	0.1904	7.38×10^{-35}	-103.4
K_2	5.0114	5.09	8.8993	4.386×10^{6}	17.69
K_3	4.6152	4.47	5.9993	2.79×10^{3}	8.3
K_5	6.7974	6.73	7.1299	22.109	1.5
K_6	5.9334	5.8	7.1843	632.70	6.054
K_8	5.7410	5.896	5.6291	3.232	-0.65
K_{10}	5.8455	5.93	4.7471	0.038	-6.53
K_{11}	5.8218	5.75	3.0729	1.4×10^{-6}	-19.7

Table 6.1.62
Model Parameters for MCP Conversion
Rate Eqn. (3.1.49)
Catalyst: 0.3%Pt/Al_2O_3
Initial guesses : 3
Stepsize : 5

	370°C	380°C	400°C	A	ΔE,ΔH(Kcal/gmol)
k_{13} $\frac{gmol}{gCat.h}$	0.474	0.527	0.885	1.819×10^{6a}	18.75
k_{12} $\frac{gmol}{gCat.h}$	2.679	2.455	2.887	37.94^{a}	2.65
K_1	4.0985	4.1719	3.8221	0.726	-2.248
K_2	3.1559	3.3158	2.996	0.759	-1.87
K_3	1.9624	2.1141	2.4450	1.237×10^{4}	11.44
K_5	5.0823	5.1194	6.0462	314.82	5.236
K_6	5.5857	5.8398	6.1192	41.43	2.57
K_8	6.5345	4.5382	4.7152	0.0115	-8.026
K_{10}	4.0524	5.5277	4.6337	28.76	2.37
K_{11}	4.4184	4.3984	4.3599	3.235	-0.402

Table 6.1.63
Model Parameters for MCP Conversion
Rate Eqn. (3.1.49)
Catalyst: 0.3%Pt/Al_2O_3
Initial guesses : 3
Stepsize : 1

	370°	380°C	400°C	A	ΔE,ΔH(Kcal/gmol)
k_{13} $\frac{gmol}{gCat.h}$	0.353	0.675	0.954	1.057×10^{9a}	27.09
k_{14} $\frac{gmol}{gCat.h}$	2.202	2.728	2.856	884.48^{a}	6.838
K_1	3.4023	3.6450	1.3402	5.34×10^{-10}	-29.25
K_2	3.1823	3.8162	2.1878	1.97×10^{-4}	-12.64
K_3	2.5945	1.7144	2.8638	144.89	5.418
K_5	3.7131	5.3423	1.9898	2.82×10^{-7}	-21.39
K_6	3.3821	4.9339	3.0380	0.057	-5.48
K_8	3.5004	4.1558	5.0015	9.045×10^{3}	10.08
K_{10}	3.9409	0.3907	5.6524	2.364×10^{8}	24.356
K_{11}	3.4143	4.432	0.6741	1.64×10^{-17}	-51.73

Table 6.1.64
Model Parameters for MCP Conversion
Rate Eqn. (3.1.49)
Catalyst: 0.3%Pt/Al_2O_3
Initial guesses : 1
Stepsize : 3

	370°C	380°C	400°C	A	ΔE,ΔH(Kcal/gmol)
k_{13} $\frac{gmol}{gCat.h}$	0.863	1.112	1.501	3.29×10^{5a}	15.69
k_{14} $\frac{gmol}{gCat.h}$	1.017	0.685	0.224	1.66×10^{-15a}	-44.668
K_1	1.1535	0.2146	1.6538	5.47×10^{6}	20.754
K_2	2.1357	3.4953	1.8804	0.014	-6.752
K_3	1.8235	2.1545	2.8203	3.24×10^{4}	12.57
K_5	1.7814	0.6964	1.0936	6.48×10^{-4}	-9.76
K_6	2.7101	3.2411	0.8027	3.983×10^{-7}	-19.338
K_8	0.4737	1.8066	2.2402	3.106×10^{13}	40.486
K_{10}	0.0302	1.7802	0.1092	5.36×10^{4}	16.538
K_{11}	3.0295	1.400	1.4260	9.91×10^{-7}	-18.93

Table 6.1.65

Model Parameters for MCP Conversion

Rate Eqn. (3.1.50)

Catalyst: 0.3%Pt/Al_2O_3

Initial guesses : 5

Stepsize : 3

	370°C	380°C	400°C	A	ΔE,ΔH(Kcal/gmol)
k_{15} $\frac{gmol}{gCat.h}$	0.045	0.046	0.116	7.017×10^{8a}	29.556
k_{16} $\frac{gmol}{gCat.h}$	4.032	4.176	4.26	24.071^{a}	1.48
K_1	6.4289	6.0873	6.24	3.908	-0.616
K_2	5.7246	6.0071	5.61	2.801	-0.95
K_3	3.8037	3.6316	3.29	0.143	-4.226
K_5	5.3303	5.2805	4.97	1.026	-2.126
K_6	8.4057	8.5049	8.5	10.444	0.274
K_7	4.3354	4.1569	4.1	1.318	-1.518
K_{10}	6.8356	6.8945	6.96	10.155	0.504
K_{11}	6.8808	6.8825	7.3	28.247	1.824

Table 6.1.66

Model Parameters for MCP Conversion

Rate Eqn. (3.1.50)

Catalyst: 0.3%Pt/Al_2O_3

Initial guesses : 5

Stepsize : 1

	370°C	380°C	400°C	A	ΔE,ΔH(Kcal/gmol)
k_{15} $\frac{gmol}{gCat.h}$	0.047	0.0474	0.074	4.372×10^{3a}	13.99
k_{16} $\frac{gmol}{gCat.h}$	3.50	3.492	3.508	7.015^{a}	0.088
K_1	5.8704	5.8638	5.82	22.646	-0.264
K_2	5.6091	5.6509	5.6	5.265	-0.084
K_3	4.3037	4.3619	4.28	3.923	-0.114
K_5	5.5165	5.4704	5.54	6.322	0.18
K_6	7.4440	7.4978	7.34	5.936	-0.29
K_7	4.8699	4.8183	4.9	5.894	0.252
K_{10}	5.9651	5.9252	5.96	5.898	0.008
K_{11}	6.4747	6.5237	6.52	7.389	0.17

Table 6.1.67
Model Parameters for MCP Conversion
Rate Eqn. (3.1.50)
Catalyst: 0.3%Pt/Al_2O_3
Initial guesses : 3
Stepsize : 1

	370°C	380°C	400°C	A	Δ EΔH(Kcal/gmol)
k_{15} $\frac{gmol}{gCat.h}$	0.152	0.154	0.261	1.036×10^{5}[a]	16.56
k_{16} $\frac{gmol}{gCat.h}$	1.712	1.733	1.864	23.5[a]	2.57
K_1	3.8702	3.7115	3.55	0.58	-2.434
K_2	3.4442	3.415	3.26	0.963	-1.646
K_3	2.3551	2.5469	2.61	19.945	2.724
K_5	4.4246	4.2481	4.22	1.684	-1.23
K_6	3.9618	3.9151	3.8	1.531	-1.224
K_7	2.5656	2.7832	2.93	44.434	3.648
K_{10}	3.7898	3.9634	3.73	2.164	-0.748
K_{11}	3.6580	3.648	3.61	2.716	-0.384

Table 6.1.68
Model Parameters for MCP Conversion
Rate Eqn. (3.1.50)
Catalyst: 0.3%Pt/Al_2O_3
Initial guesses : 1
Stepsize : 3

	370°C	380°C	400°C	A	ΔE,ΔH(Kcal/gmol)
k_{15} $\frac{gmol}{gCat.h}$	0.805	0.853	0.860	5.818[a]	1.7
k_{16} $\frac{gmol}{gCat,h}$	0.977	0.993	0.854	0.07[a]	-4.23
K_1	1.8292	1.2566	0.877	1.89×10^{-7}	-20.624
K_2	1,7679	1.2241	1.25	1.99×10^{-3}	-8.6
K_3	1.5666	1.5695	1.94	263.22	6.63
K_5	1.8292	1.8591	1.65	0.143	-3.11
K_6	1.8292	1.8591	1.56	0.0382	-5.01
K_7	0.8815	1.7253	3.0	3.22×10^{11}	34.1
K_{10}	1.8292	1.8591	1.637	0.082	-3.52
K_{11}	1.8292	1.8591	1.49	0.121	-6.43

Table 6.1.69

Parameters that satisfy kinetic and thermodynamic criteria using rate equation (3.1.44) for MCP on Pt/Al_2O_3 catalyst.

Model Equation	Initial Guesses and Stepsize	Activation Energy	Adsorption Energy	Desorption energy for desorption steps		
				8	10	11
3.1.44	5[a] 5[b]	+	+	+	-	-
	5 3	+	+	-	-	+
	5 1	+	-	+	-	-
	3 3	+	-	-	-	+
	3 1	+	+	-	-	-
	1 5	+	-	+	-	-

\+ Parameter satisfies criteria

\- Parameter violates criteria

a Initial guesses of constants; b Stepsize

Table 6.1.70

Parameters that satisfy kinetic and thermodynamic criteria using rate equation 3.1.46 for MCP on Pt/Al_2O_3 Catalyst

Model Equation	Initial guesses and Stepsize	Activation Energy	Adsorption Energy	Desorption energy for desorption Steps		
				8	10	11
3.1.46	5 5	+	-	-	-	-
	5 3	+	-	-	+	+
	3 3	+	+	-	-	-
	1 5	+	-	+	+	-

Table 6.1.71

Parameters that satisfy kinetic and thermodynamic criteria using rate equation 3.1.48 for MCP on Pt/Al_2O_3 catalyst.

Model Equation	Initial guesses and Stepsize	Activation Energy	Adsorption Energy	Desorption energy for desorption steps		
				8	10	11
3.1.48	5 5	+	+	-	-	-
	5 3	+	-	-	-	-
	5 1	+	+	+	-	-
	3 3	+	+	+	-	-
	3 1	+	+	+	-	-

Table 6.1.72

Parameters that satisfy kinetic and thermodynamic criteria using rate equation (3.1.49) for MCP on Pt/Al_2O_3 catalyst

Model Equation	Initial guesses and Stepsize	Activation Energy	Adsorption Energy	Desorption energy for desorption steps		
				8	10	11
3.1.49	5 3	+	+	+	-	-
	5 1	+	+	-	-	-
	3 5	+	+	-	+	-
	3 1	+	+	+	+	-
	1 3	+	-	+	+	-

Table 6.1.73

Parameters that satisfy kinetic and thermodynamic criteria using rate equation 3.1.50 for MCP on Pt/Al_2O_3

Model Equation	Initial guesses and Stepsize	Activation Energy	Adsorption Energy	Desorption energy for desorption steps		
				8	10	11
3.1.50	5 3	+	+	-	+	+
	5 1	+	+	+	+	+
	3 1	+	+	+	-	-
	1 3	+	+	+	-	-

Table 6.1.74

Model Parameters for MCP Conversion

Rate Eqn. (3.1.48)

Catalyst: Pt-Re/Al_2O_3 (DRIED)

Initial guesses : 5

Stepsize : 5

	370°	380°C	400°C	A	ΔE,ΔH(Kcal/gmol)
k_{11} $\frac{gmol}{gCat.h}$	1.173	2.258	2.691	8.57×10^{7a}	21.846
k_{12} $\frac{gmol}{gCat.h}$	1.977	3.714	2.684	5.61×10^{2a}	5.736
K_1	4.8464	0.148	7.4125	2.66×10^{11}	33.796
K_2	1.6187	5.4477	5.4259	3.572×10^{10}	30.196
K_4	0.6222	10.1894	3.9486	8.469×10^{13}	40.676
K_7	5.7607	8.0176	7.679	1.405×10^{3}	6.944
K_8	8.8167	5.775	8.301	12.219	0.64
K_{10}	18.1056	10.8449	0.0446	4.7×10^{-61}	-182.96
K_{11}	8.0224	0.6646	6.9471	8.433×10^{3}	10.282

Table 6.1.75

Model Parameters for MCP Conversion

Rate Eqn. (3.1.48)

Catalyst = Pt-Re/Al_2O_3 (DRIED)

Initial guesses : 3

Stepsize : 3

	370°C	380°C	400°C	A	ΔE,ΔH(Kcal/gmol)
k_{11} $\frac{gmol}{gCat.h}$	1.191	1.4877	2.621	1.947×10^{8a}	23.10
k_{12} $\frac{gmol}{gCat.h}$	1.733	4.699	4.456	4.592×10^{8a}	23.334
K_1	0.6306	1.0113	0.859	142.74	6.774
K_2	4.0454	2.976	3.3401	0.1488	-4.116
K_4	3.2694	4.5384	1.8704	1.31×10^{-6}	-19.232
K_7	4.1599	2.7195	3.1938	0.044	-5.666
K_8	4.4061	16.9644	2.5623	3.676×10^{-8}	-24.762
K_{10}	4.2885	0.0727	1.8149	0.123	-2.50
K_{11}	4.4366	0.9351	0.4893	3.61×10^{-20}	-59.06

Table 6.1.76

Model Parameters for MCP Conversion

Rate Eqn. (3.1.49)

Catalyst = Pt-Re/Al_2O_3 (DRIED)

Initial guesses of constants: 5

Stepsize : 1

	370°C	380°C	400°C	A	ΔE,ΔH(Kcal/gmol)
k_1 $\frac{gmol}{gCat.h}$	0.346	0.6316	1.5899	$5.306x10^{14a}$	43.688
k_2 $\frac{gmol}{gCat.h}$	2.2134	1.909	1.7782	0.0573^a	-5.9
K_1	5.1876	5.004	1.042	$1.254x10^{-16}$	-49.5
K_2	6.9368	7.0585	4.3622	$9.756x10^{-5}$	-14.464
K_3	4.6722	3.8092	2.061	$3.406x10^{-8}$	-24.14
K_5	4.7634	6.5733	9.041	$5.694x10^{6}$	17.94
K_6	6.5905	5.8044	9.6946	$1.15x10^{5}$	12.704
K_8	5.492	6.0344	6.1023	46.155	2.706
K_{10}	6.2381	5.5029	5.054	0.0684	-5.776
K_{11}	6.1352	5.2967	4.0312	$4.95x10^{-4}$	-12.132

Table 6.1.77

Model Parameters for MCP Conversion

Rate Eqn. (3.1.49)

Catalyst = Pt-Re/Al_2O_3 (DRIED)

Initial guesses : 3

Stepsize : 3

	370°C	380°C	400°C	A	ΔE,ΔH(Kcal/gmol)
k_{13} $\frac{gmol}{gCat.h}$	0.543	1.4696	1.694	$1.492x10^{10a}$	29.342
k_{14} $\frac{gmol}{gCat.h}$	1.84	0.3594	0.137	$4.3x10^{-24a}$	-70.82
K_1	3.3776	1.3647	1.4704	$3.377x10^{-7}$	-20.392
K_2	4.8337	4.8152	4.0549	0.0733	-5.412
K_3	2.2127	1.7425	1.6748	$7.665x10^{-3}$	-7.208
K_5	4.8337	5.407	8.179	$8.945x10^{5}$	15.636
K_6	4.8337	6.825	7.3423	$2.56x10^{4}$	10.918
K_8	2.2881	4.7098	4.756	$4.47x10^{5}$	18.372
K_{10}	3.4336	3.6587	3.0815	0.1979	-3.726
K_{11}	3.6203	3.009	2.4816	$9.331x10^{-4}$	10.598

Table 6.1.78

Parameters that satisfy kinetic and thermodynamic criteria using rate equation 4.1.48 for MCP on Pt-Re/Al_2O_3 (DRIED) Catalyst

Model Equation	Initial guesses and Stepsize	Activation Energy	Adsorption Energy	Desorption energy for desorption steps		
				8	10	11
3.1.48	5 5	+	-	+	-	+
	3 3	+	-	-	-	-

Table 6.1.79

Parameters that satisfy kinetic and thermodynamic criteria using rate equation 3.1.49 for MCP on Pt-Re/Al_2O_3 (DRIED) Catalyst.

Model Equation	Initial guesses and Stepsize	Activation Energy	Adsorption Energy	Desorption energy for desorption steps		
				8	10	11
3.1.49	5 1	+	+	+	-	-
	3 3	+	+	+	-	+

6.2 Variable Activity Modelling Results

Rates of catalyst deactivation dictate the temperature and hydrogen pressure at which catalytic reformers operate. Catalysts which are more resistant to coke are desirable in order to permit longer periods between regenerations or to operate for the same time on stream at higher temperatures to give greater conversion, or to operate at lower pressures, thereby favouring the dehydrogenation equilibrium. Thus, catalyst performance is limited in a direct way by the deactivating characteristics of the catalyst.

6.2.1 Deactivation Kinetic Parameters From Variable Reactant Partial Pressure.

Deactivation kinetic equations of the mechanistic type similar to those of Corella and Asua[50,68] were derived in Chapter 3, Section 3.2. for the deactivation of reforming catalysts by the formation of coke. Two deactivation models were derived based on the mechanism that the reactant is adsorbed in the same manner in the coking reaction as well as in the main reaction. The first model was based on the adsorption or the catalyst surface of the substance that produces the deactivation as the rate-limiting step (equation 3.2.11):

$$\frac{P_m^{n+1}}{\psi_{01}(P_i, T)} = \frac{1}{k_d K_A} + \frac{K_A}{k_d K_m} P_A$$

The second model was based on coke precusor formation as the rate-limiting step (equation 3.2.19)

$$\frac{P_m^{n+1}}{\psi_{o1}(P_i, T)} = \frac{1}{k_d K'_m} + \frac{K_A}{k_d K'_m} P_A + \frac{K''_m}{k_d K'_m} P_m^{n+1}$$

It will be recalled that n is the number of gas molecules reacting with the adsorbed molecule to form coke precusor. The deactivation functions were evaluated from the relationship:

$$\ell na = -\psi_{o1}(P_i, T)t.$$

The plots of ℓna versus time for the reactions studied are shown in Appendix (C), Figures C.1 - C.15. Tables D.1 D.7 show the values of the deactivation functions $\psi_{o1}(P_i, T)$ obtained from those plots.

The constants of deactivation were evaluated at n=o, 1 and 2 using the least squares technique (See Appendix E) Table 6.2.1 shows the constants of deactivation for iso-octane at 410°C and P_{H_2} of 0.5atm and the constants of deactivation for MCP at 400°C for Pt/Al_2O_3 and 410°C for $Pt\text{-}Re/Al_2O_3$ P_{H_2} of 0.778 atm using the first model. These constants are positive for iso-octane and MCP at n=o for the catalysts investigated except for 0.6%Pt/Al_2O_3 catalyst which gave negative values for iso-octane alone. When n=1, positive values were obtained only for 0.6% Pt/Al_2O_3 with iso-octane. Thus, n=1 explains the deactivation behaviour for iso-octane on 0.6% Pt/Al_2O_3 catalyst. All the deactivation constants obtained when n=2, contain negative values for all the catalysts and reactants investigated. Therefore the following can be concluded from the first model:

(i) n = 0 predicts the deactivation behavior of iso-octane and MCP on 0.3%Pt/Al_2O_3 catalyst at temperatures between 400° - 410°C.

(ii) n = 0 predicts also the deactivation behavior on $Pt-Re/Al_2O_3$ catalyst. In comparison with the 0.3% Pt/Al_2O_3 the constant k_dK_A is about seven times higher on $Pt-Re/Al_2O_3$ although the constant K_A/k_dK_m was about the same on both catalysts.

The constant of deactivation (k_dK_A) for iso-octane (on 0.3% Pt/Al_2O_3) was about two and half times the value for MCP while the constant K_A/k_dK_m is about twice higher for iso octane on 0.3%Pt/Al_2O_3 catalyst.

Table 6.2.2 shows the constants of deactivation for iso-octane at 410°C and P_{H_2} of 0.5atm and the constants of deactivation for MCP at 400°C for Pt/Al_2O_3 and 410°C for $Pt-Re/Al_2O_3$ at P_{H_2} of 0.778atm using the second model. Similar to the results obtained with the first model, the constants are positive for iso-octane and MCP at n=o for the catalysts investigated except for 0.6%Pt/Al_2O_3 catalyst which gave negative values for iso-octane alone. When n=1, positive constants were obtained with iso-octane and MCP only on 0.3% Pt/Al_2O_3 catalyst while at n=2 only MCP on 0.3%Pt/Al_2O_3 catalyst gave positive deactivation constants. It is important to note that none of the n values considered gave positive constants of deactivation for iso-octane on 0.6%Pt/Al_2O_3 catalyst. The values of k_dK_m' obtained with the second model at n=o is very similar to k_dK_A obtained with the first model at n=o. The value of the constants obtained at n=1 using

the second model is much more than the values of the constants obtained using MCP.

Table 6.2.1

Deactivation Parameters from Variable Reactant Partial Pressure (First Model, Eqn. 3.2.11)

n	Constants	410°C Iso Octane P_{H_2} = 0.5atm 0.6%Pt/Al_2O_3	410°C Iso Octane P_{H_2} = 0.5atm 0.3%Pt/Al_2O_3	400°C MCP P_{H_2} = 0.778atm Pt/Al_2O_3	410°C MCP P_{H_2} = 0.778atm Pt-Re/Al_2O_3
0	$k_d K_A$	0.1544	0.44	0.1575	1.102
	$\frac{K_A}{k_d K_m}$	-25.256	19.18	9.6525	8.9766
1	$k_d K_m$	10.988	-21.739	-5.91	-12.66
	$\frac{K_A}{k_d K_m}$	3.242	4.382	9.009	2.7174
2	$k_d K_m$	-83.32	-100.014	-6.452	-40.24
	$\frac{K_A}{k_d K_m}$	0.496	4.2194	2.2831	0.481

Table 6.2.2

Deactivation Parameters from Variable Reactant Partial Pressure (Second Model, Eqn.3.2.19)

n	Constants	410°C Iso Octane P_{H_2} = 0.5atm 0.6%Pt/Al_2O_3	410°C Iso Octane P_{H_2} =0.5atm 0.3%Pt/Al_2O_3	400°C MCP P_{H_2} =0.778atm 0.3%Pt/Al_2O_3	410°C MCP P_{H_2} = 0.778atm 0.3%Pt-0.3%Re/Al_2O_3
0	$k_d K_m'$	0.1543	0.4407	0.1576	1.1013
	$K_A + K_m''$	-3.9	8.454	1.52	9.89
1	$k_d K_m'$	-4.127	166.8	6.97	-4.127
	K_A	-69.02	322.69	27.988	-69.026
	K_m''	488.6	3861.88	128.1525	488.64
2	$k_d K_m'$	-42.034	-711.54	38.73	-42.034
	K_A	-36.037	-72.648	27.767	-36.037
	K_m''	1464.38	-24836.63	1062.05	1464.38

constants. Therefore, it can be concluded from the results obtained with the first and second models that:

(i) n = 0 does not predict the deactivation behavior of iso-octane on 0.3%Pt/Al_2O_3 catalyst at temperatures between 390°C - 430°C using the first model.

(ii) n=1 predicts the deactivation behavior of iso-octane on 0.3%Pt/Al_2O_3 catalyst at lower temperature (390°-410°C) using the first model.

(iii) n=2 predicts the deactivation behavior of iso-octane on 0.3%Pt/Al_2O_3 catalyst at higher temperature (430°C) using the first model.

(iv) n=0 also predicts the deactivation behavior of iso octane on 0.3%Pt/Al_2O_3 catalyst at 430°C using the second model.

(v) The constants of deactivation was highest at the lowest temperature.

Using iso - octane on 0.6%Pt/Al_2O_3 catalyst (Table 6.2.5) the first model gave positive values for the deactivation parameters at n=2 between 410° and 430°C. No positive value was obtained at 390°C for any value of n. Similar to the results obtained with iso-octane on 0.3%Pt/Al_2O_3, positive deactivation parameters were obtained with the second model only at n=0 and 430°C (Table 6.2.6). It can be concluded that:

(i) The models did not predict the deactivation behavior of iso-octane on 0.6%Pt/Al_2O_3 catalyst at 390°C.

(ii) At n=0 and n=1, the first model did not predict the deactivation behavior of iso-octane on 0.6% Pt/Al_2O_3 catalyst at temperatures between 390° and 430°C

(iii) At n=2, the first model predicted the deactivation behavior of iso-octane on 0.6%Pt/Al_2O_3 at temperatures between 410°C and 430°C. The constants of deactivation obtained at 430°C were higher than those obtained at 410°C.

(iv) At n=1 and 2, the second model did not predict the deactivation behavior of iso-octane on 0.6%Pt/Al_2O_3 at temperatures between 390°C and 430°C.

(v) At n=0 the second model predicted the deactivation behavior of iso-octane on 0.6%Pt/Al_2O_3 only at 430°C.

Tables 6.2.7 and 6.2.8 show the deactivation parameters of MCP from variable H_2 partial pressure using Pt/Al_2O_3 catalyst. Table 6.2.7 show that the deactivation parameters evaluated using the first model were positive at 390°C and 400°C for n=1 and also at 390°C for n=2. With the second model (Table 6.2.8), however positive deactivation parameters were obtained only at 400°C when n=1. Therefore, the following can be concluded from the results:

(i) The models did not predict the deactivation behavior of MCP on Pt/Al_2O_3 catalyst at n=0.

(ii) At n=1, the first model predicted the deactivation behavior of MCP on Pt/Al_2O_3 at temperatures between 390°C and 400°C. The values of the constants of deactivation were higher at 400°C. The k_dK_A value was about 8 times greater at 400°C while the K_A/k_dK_m value was about 6 times greater at 400°C.

(iii) At n=2, the first model predicted the deactivation behavior at 390°C only.

(iv) At n=0 and n=2, the second model did not predict the deactivation behavior of MCP on Pt/Al_2O_3 at temperatures between 390° - 400°C.

(v) At n=1, the second model predicted the deactivation behavior of MCP on Pt/Al_2O_3 catalyst only at 400°C.

Tables 6.2.9 and 6.2.10 show the deactivation parameters of MCP from variable H_2 partial pressure using $Pt-Re/Al_2O_3$ (DRIED) catalyst. Table 6.2.9 show that the deactivation parameters were positive at 390°C and 400°C for n=1 and positive at 400°C for n=2. With the second model (Table 6.2.10), however, positive deactivation parameters were obtained only at 410°C and 390°C for n=2. Therefore the following can be concluded from the results obtained with the first and second models:

(i) At n=0, the first model did not predict the deactivation behavior of MCP from variable H_2 partial pressure on Pt-Re/Al_2O_3 at temperatures between 390°C and 410°C

(ii) At n=1, the first model predicted the deactivation behavior of MCP from variable H_2 partial pressure on Pt-Re/Al_2O_3(DRIED) at temperatures between 390°C and 400°C . The value of the constant of deactivation k_dK_A is about twice at 400°C while the constant K_A/k_dK_A is about the same value at both temperatures.

(iii) At n=2, the first model predicted the deactivation behavior of MCP on Pt-Re/Al_2O_3(DRIED) only at 400°C

(iv) The first model did not predict the deactivation behavior of MCP from variable H_2 partial pressure at 410°C.

(v) At n=0, the second model predicted the deactivation behavior of MCP on Pt-Re/Al_2O_3 (DRIED) at 410°C

(vi) At n=2, the second model predicted the deactivation behavior of MCP on Pt-Re/Al_2O_3 (DRIED) at 390°C.

Table 6.2.3

Deactivation Parameters of Iso Octane From Variable H_2 Partial Pressure (First Model, Eqn 3.2.11)

P_{iso} = 0.0316 atm

Catalyst = 0.3%Pt/Al_2O_3

W/F = 0.111gmin cm^{-3}

n	Constants	390°C	410°C	430°C
0	k_dK_A	0.0376	0.021	0.0145
	$\frac{K_A}{k_dK_m}$	-5	-45.45	-58.82
1	k_dK_A	0.7884	0.1376	0.054
	$\frac{K_A}{k_dK_m}$	29.76	8.1967	-3.125
2	k_dK_A	-0.176	-1.198	0.268
	$\frac{K_A}{k_dK_m}$	31.25	13.46	9.891

Table 6.2.4

Deactivation Parameters From Variable H_2 Partial Pressure

(Second Model, Eqn. 3.2.19)

P_{iso} = 0.0316atm

Catalyst = 0.3%Pt/Al_2O_3;

W/F = 0.11gmin cm^{-3}

n	Constants	390°C	410°C	430°C
0	$k_d K_m'$	0.03768	0.0207	0.01448
	$K_A + K_m''$	-0.18764	-0.942	0.8516
1	$k_d K_m'$	-0.0732	-0.588	-0.1064
	K_A	-7.1157	-35.04	-13.085
	K_m''	4.475	34.896	12.17
2	$k_d K_m'$	-0.1477	-0.306	0.297
	K_A	-5.178	-7.34	-10.20
	K_m''	5.4649	5.1806	7.148

Table 6.2.5

Deactivation Parameters of Iso-Octane From Variable H_2 Partial Pressure (First Model, Eqn.3.2.11)

P_{iso} = 0.0316 ; W/F = 0.111 gmin cm^{-3} ;

Catalyst = 0.6%Pt/Al_2O_3

n	Constants	390°C	410°C	430°C
0	$k_d K_A$	0.0018	-0.0079	0.00547
	$\frac{K_A}{k_d K_m}$	-578.03	-81.40	-207.47
1	$k_d K_A$	0.00399	-0.0153	0.0354
	$\frac{K_A}{k_d K_m}$	-231.86	-29.155	-0.972
2	$k_d K_A$	-0.0311	0.0383	0.1483
	$\frac{K_A}{k_d K_m}$	97.56	5.999	9.542

Table 6.2.6

Deactivation Parameters of Iso-Octane From Variable H_2 Partial Pressure (Second Model, Eqn 3.2.19)

P_{iso}= 0.0316atm; Catalyst = 0.6%Pt/Al_2O_3 ; W/F = 0.111gmincm^{-3}

Second Model

n	Constants	390°C	410°C	430°C
0	k_dK_m'	0.00181	0.0079	0.00547
	$K_A + K_m''$	-1.0487	-0.645	1.1346
1	k_dK_m'	0.00158	-0.001574	0.02213
	K_A	-0.0219	-3.283	-1.0655
	K_m''	0.2432	2.38	0.3825
2	k_dK_m'	0.00497	-0.0033	0.15652
	K_A	-1.4649	-2.51	0.1685
	K_m''	0.765	1.656	-0.1878

Table 6.2.7

Deactivation Parameters of MCP From Variable H_2 Partial Pressure (First Model, Eqn. 3.2.11)

P_{MCP} = 0.092atm; W/F = 0.11gmin cm^{-3}; Catalyst = 0.3%Pt/Al_2O_3

n	Constants	390°C	400°C
0	k_dK_A	0.0578	0.1144
	$\frac{K_A}{k_dK_m}$	-13.572	-3.7411
1	k_dK_A	0.242	1.9616
	$\frac{K_A}{k_dK_m}$	0.903	5.618
2	k_dK_A	2.1095	-1.1402
	$\frac{K_A}{k_dK_m}$	3.9093	5.4171

Table 6.2.8

Deactivation Parameters of MCP From Variable H_2 Partial Pressure (Second Model, Eqn 3.2.19)

P_{MCP} = 0.092atm; W/F = 0.111gmin cm^{-3};

Catalyst = 0.3%Pt/Al_2O_3

n	Constants	390°C	400°C
0	$k_d K_m'$	0.0578	0.1145
	$K_A + K_m''$	-0.7842	-0.4282
1	$k_d K_m'$	-0.415	1.51
	K_A	-12.635	6.75
	K_m''	-11.116	1.465
2	$k_d K_m'$	-0.7074	-3.984
	K_A	-7.371	-10.78
	K_m''	4.527	-17.318

Table 6.2.9

Deactivation Parameters of MCP From Variable H_2 Partial Pressure (First Model, Eqn 3.2.11)

P_{MCP} = 0.092atm; W/F=0.111gmincm^{-3}; Catalyst=Pt-Re/Al_2O_3 (DRIED)

n	Constants	390°C	400°C	410°C
0	k_dK_A	0.01217	0.02769	0.0155
	$\frac{K_A}{k_dK_m}$	-72.568	-25.641	-77.88
1	k_dK_A	0.0669	0.158	0.09083
	$\frac{K_A}{k_dK_m}$	7.072	7.675	-3.413
2	k_dK_A			
	$\frac{K_A}{k_dK_m}$	22.472	13.514	10.142

Table 6.2.10

Deactivation Parameters of MCP From Variable H_2 Partial Pressure (Second Model, Eqn 3.2.19)

P_{MCP} = 0.092atm; Catalyst = Pt-Re/Al_2O_3(DRIED)

W/F = 0.111gmin cm^{-3}

n	Constants	390°C	400°C	410°C
0	$k_d K_m'$	0.01212	0.0277	0.0155
	$K_A + K_m''$	-0.8834	-0.71	1.2015
1	$k_d K_m'$	0.0719	-0.0765	0.0372
	K_A	0.8457	-5.416	-2.785
	K_m''	-0.3065	4.0366	2.4263
2	$k_d K_m'$	1.634	-0.451	0.20012
	K_A	24.4	-7.8514	-1.965
	K_m''	12.1347	1.716	3.927

6.3 Catalyst Mortality Modelling Results

In Chapter 5 Section 3, the conversions, product compositions and coking level obtained during catalyst mortality studies on commercial Pt and Pt-Re on alumina reforming catalysts were presented. In this section we present the modelling results of the mortality studies. The model used to evaluate the deactivation parameters is the same as that developed by Omoleye[52]. The model equation is

$$a = \frac{\alpha(h-n+1)k}{C_t^{n-h-1}} \int_o^t \left(\frac{K_j^h C_j^{n+h} - (K')^h (\pi C_i)^{n+h}}{(1 + \Sigma K_j C_j)^h} dt \right)^{\frac{m}{n-h-1}} + 1 \qquad (6.3.1)$$

The above equation implies that a plot of

$$\frac{n-h-1}{m} \quad \text{versus} \quad \int_o^t \frac{K_j^h C_j^{n+h} - (K')^h (\pi C_i)^{n+h}}{(1 + \Sigma K_j C_j)^h} dt \qquad (6.3.2)$$

should yield a straight line with an intercept of unity for the right values of n, m and h. The concentrations were those obtained during the mortality studies. The rate and adsorption equilibrium constants used for modelling of the mortality of n-octane were those obtained using rate equation 3.1.7 at 440°C when the initial guesses of constants 5, Stepsize 5 were used. The rate model is:

$$r_6 = \frac{k_{11}K_4K_1C_N - \frac{k_{12}C_{EB}(C_{H_2})^{\frac{1}{2}}}{K_8 K_{10}}}{\left(1 + K_1C_N + \frac{C_I}{K_5} + \frac{C_{cP}}{K_3} + \frac{C_{Ex}}{K_8} + \frac{C_{cx}}{K_9} + \frac{(C_{H_2})^{\frac{1}{2}}}{K_{10}} + \frac{C_{Mx}}{K_{11}} + \frac{C_{Px}}{K_{12}}\right)^2}$$

and the values of the constants are

k_{11} = 2.52 gmol/gcat.h, k_{12}= 2.34gmol/gCat.h

K_1 = 0.7174, K_3 = 1.3123, K_4 = 5·6664, K_5 = 4.9377

K_8 = 4.4555, K_9 = 9.8898, K_{10} = 5.3505,

K_{11} = 7.0092, K_{12} = 12.2251.

For the modelling of the mortality of iso-octane, rate equation (3.1.25) was used at 430°C and initial guesses of constants 5, stepsize 3. The rate equation is:

$$r_6 = \frac{\frac{k_{11}K_5K_d[A]}{[H_2]} - \frac{K_{12}[B]}{K_hK_7[H_2]}}{1 + \frac{K_5K_d[A]}{[H_2]} + \frac{[B]}{K_7K_h[H_2]}}$$

and the value obtained for the constants were

k_{11} = 8.272gmol/gcat.h, k_{12} = 100.3gmol/gcat.h,

K_d = 0.5809, K_h = 313.487, K_5 = 20.6197,

K_7 = 9.06.

The parameter selection involves the use of various combinations of n, m and h within the following bounds: $0 \leq n \leq 2$; $1 \leq m \leq 6$; and $1 \leq h \leq 3$. The percentage linearity and intercept are used as criteria for selecting the n, m and h combinations that fit the model. The combination of parameters that give the closest linearity to 100% and intercept to unity are shown in Tables 6.3.1 and 6.3.2. These tables show that a number of n, m and h satisfied the criteria spelt out for n-octane and iso-octane. The final selection of parameters n,m and h was based on the following criteria for n-octane are:

(i) The least standard deviation in predicting activity.

(ii) Linearity better than 99%

(iii) Nearness of intercept to unity

For iso-octane the following criteria was used for the final selection of parameters:

(i) The least standard deviation in predicting activity

(ii) Linearity better than 97%

(iii) Nearness of intercept to unity

Table 6.3.3 shows the final n, m and h combinations that gave the best fit for n-octane while Table 6.3.4 shows the final n,m and h combinations that gave the best fit for iso-octane.

Figure 6.3.1 - 6.3.7 show the corresponding experimental and predicted profiles of activity decay. The figures show that the predicted values are generally in good agreement with the experimentally determined ones. With iso-octane on 0.3%Pt/Al_2O_3 catalyst, however no set of parameters met the criteria set for iso-octane in cycles 2 and 5 while cycles 7 - 10 gave relatively poor prediction.

The following can thus be concluded for n-octane:

(i) n values lie between 0 and 1. The value of n for the first two cycles was 0. This implies that there are no unadsorbed gas molecules reacting with the coke precusor in the proposed deactivation scheme (see Chapter 3 section 3.2). After the 2nd cycle the value of n became 1 implying that one gas molecule reacted with the coke precusor in the proposed deactivation scheme.

(ii) The value of m is 3 and 4 for cycles 1 and 2, respectively. The value of m is 6 for cycles 3 to 5 and 1 for cycle 6

(iii) The value of h lies between 1 and 3

(iv) Good prediction of the catalyst activity was obtained, using the model, for all the cycles investigated.

For iso-octane mortality studies the following can also be concluded:

(i) The model did not predict the deactivation behavior in cycles 2 and 5

(ii) The values of n parameters varied between 1 and 2

(iii) The value of m varied between 2 and 6

(iv) The value of h is 3 except at the 6th cycle where the value is 1

(v) There were poor predictions of the deactivation behavior at cycles 7 - 10.

Table 6.3.1 : Deactivation Parameters for N-Octane on Pt/Al_2O_3 Catalyst

Cycle Number	n	m	h	Criteria % Linearity	Satisfied Intercept
1	0 , 0, 0	3 , 3 , 3	1 , 2 , 3	99	0.97 - 0.995
2	0 , 0, 0	4 , 5 , 6	3 , 2 , 2	99.18-99.4	0.973- 1.03
3	1 , 1, 1, 1	4 , 5, 6, 6	1 , 1 , 1, 2	99.66-99.76	0.953- 0.999
4	1 , 1, 1, 1, 1, 1	4, 4, 5,5, 6, 6	2, 3, 2, 3, 2, 3	99.83-99.95	1.02 - 1.08
5	1, 1, 1, 1, 1, 1	4, 5, 5, 5,6, 6	2, 1, 2, 3, 1, 2	99.81-99.94	0.98 - 1.06
6	0, 0, 0, 1	4, 5, 6, 1	1, 1, 1, 1	99.8 -99.87	0.941- 1.05

Table 6.3.2 : Deactivation Parameters for Iso-Octane on Pt/Al_2O_3 Catalyst

Cycle Number	n	m	h	Criteria % Linearity	Satisfied Intercept
1	1, 1, 1	4 , 5 , 6	2 , 3, 3	97.21-97.54	0.95 - 0.99
3	1, 1	3, 3	2 , 3	97.28-97.5	0.95 - 1.07
4	2, 2 , 2	2, 3, 4	2, 3, 3	99.5 -99.7	0.936 -0.996
6	1, 1, 1, 1, 1	2, 3, 4, 5, 6	1, 1, 1, 1, 1	99.51-99.7	1.02 - 1.07
7	1,1,1,1,1,1,1,1	6,6,6,3,4,5,5,5	1,2,3,1,1,1,2,3	98 - 98.5	0.936- 1.0
8	2, 2, 2	2 , 3 , 4	2, 3, 3	99.69-99.75	0.95 - 1.01
9	1 , 1 , 1	5, 6, 6	1 , 1 , 3	97.27-97.5	0.97 - 0.98
10	2	2	3	99.436	0.998

Table 6.3.3: Selected Deactivation Parameters for N-Octane on Pt/Al_2O_3 Catalyst

Cycle	1	2	3	4	5	6
n	0	0	1	1	1	1
m	3	4	6	6	6	1
h	3	3	2	2	2	1
% Linearity	99.05	99.4	99.66	99.95	99.94	99.87
Intercept	0.995	1.03	0.999	1.02	1.02	1.05
Standard Deviation	0.432	0.151	0.23	0.069	0.133	0.121
Mechanism	Double site	Double site	Double site	Double site	Double site	Single site

Table 6.3.4: Selected Deactivation Parameters for Iso-Octane on Pt/Al_2O_3 Catalyst

Cycle	1	2	3	4	5	6	7	8	9	10
n	1		1	2		1	1	2	1	2
m	6		3	4		2	6	4	6	2
h	3		3	3		1	3	3	3	3
% Linearity	97.24		97.544	99.5		99.7	98	99.7	97.5	99.436
Intercept	0.9930		1.07	0.996		1.02	1.0	1.01	0.98	0.998
Standard Deviation	0.494		0.3996	0.283		0.1588	0.327	0.13	0.416	0.233
Mechanism	Double Site		Double site	Double site		Single site	Double site	Double site	Double site	Double site

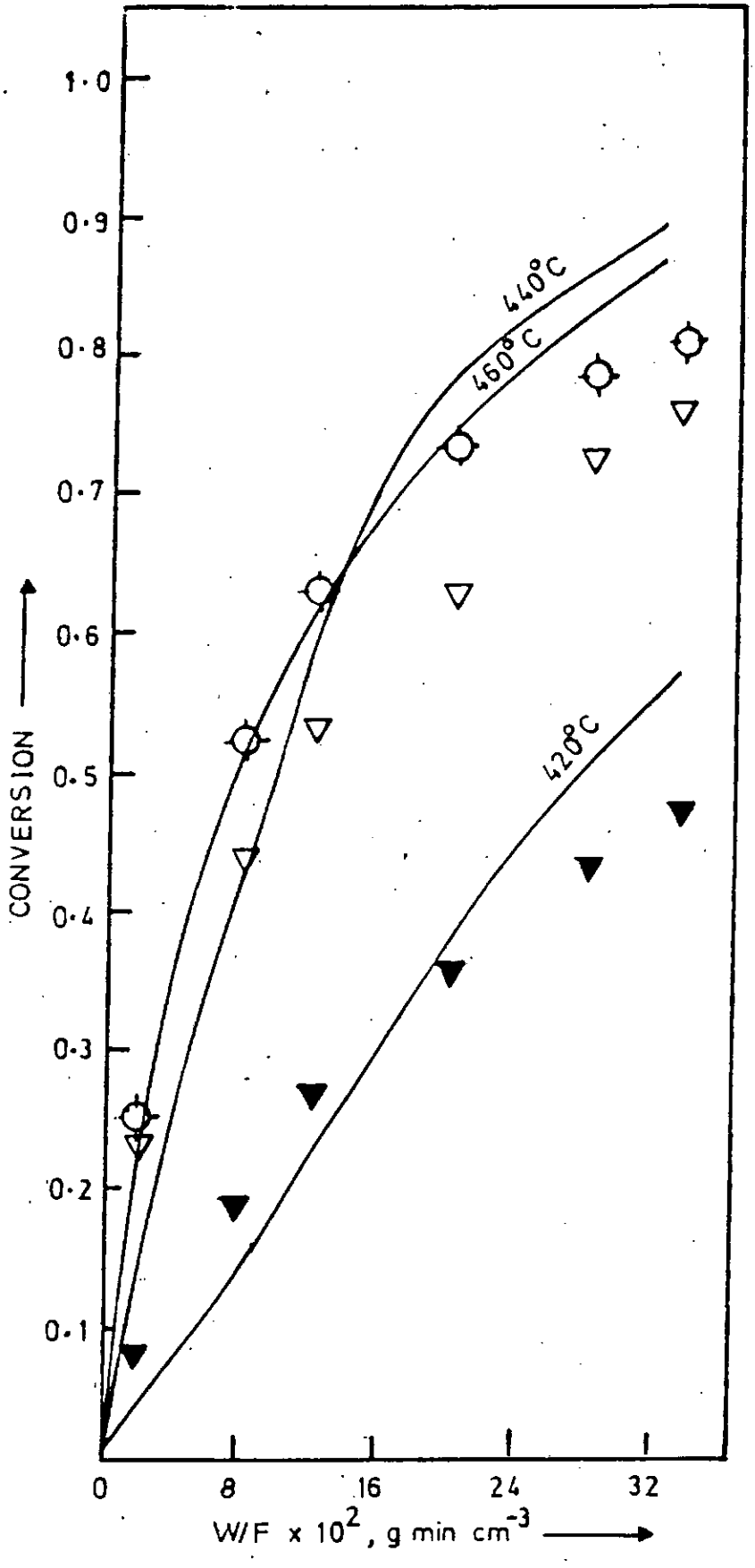

Fig.6.1.1: Prediction of n-octane conversion versus W/F on Pt/Al_2O_3 catalyst at $P_N = 7.63 \times 10^{-3}$ atm; Experimental: ▼420°C; ▽440°C; ⊖460°C. Predicted eqn(3.1.7); ——; Initial guesses = 5; Stepsize = 3; δ(420°C)=0.0198; δ(440°C) = 0.0188; δ(460°C) = 0.0016.

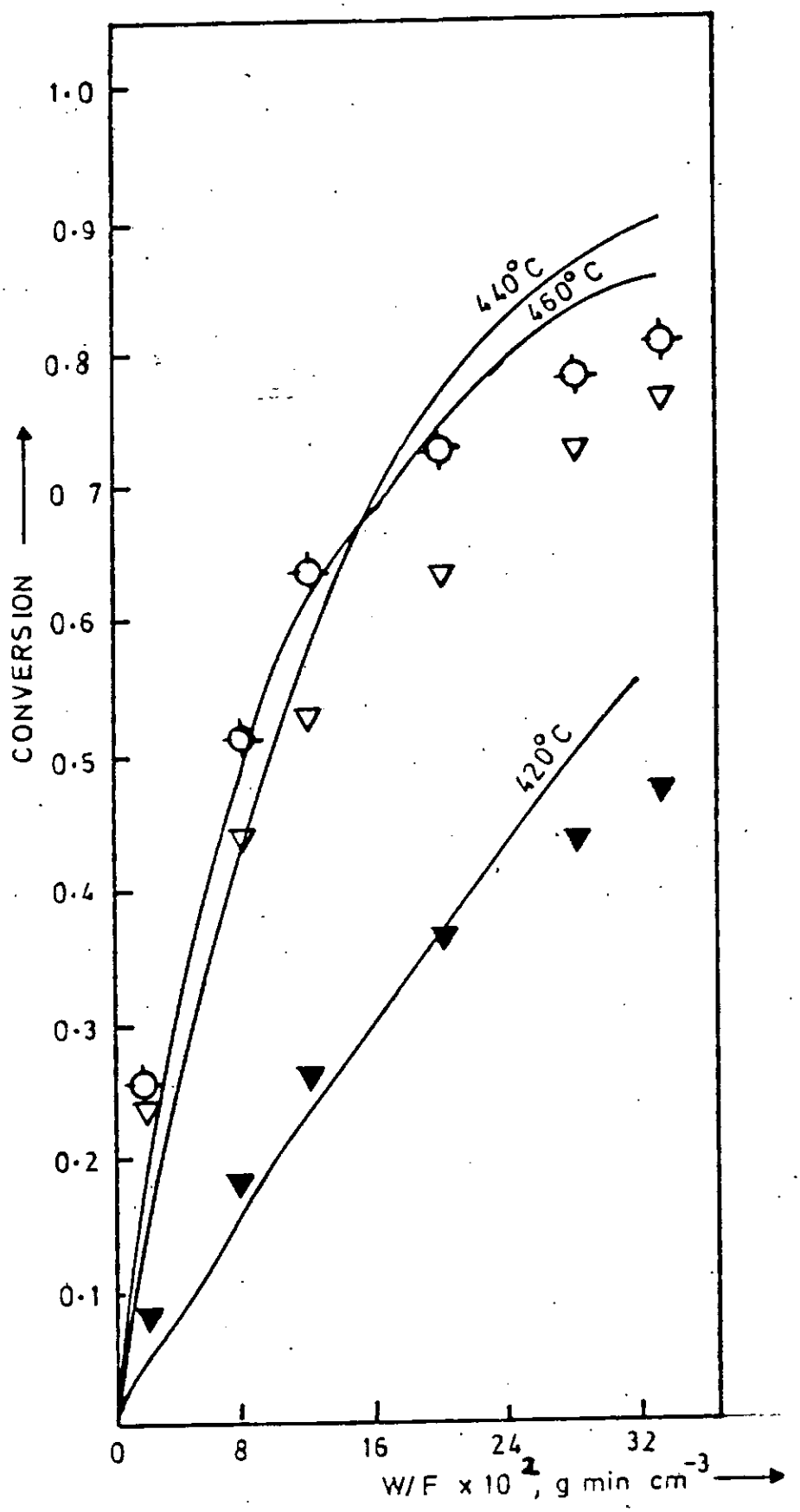

Fig.6.1.2 Prediction of n-octane conversion versus W/F on Pt/Al_2O_3 catalyst at $P_N = 7.63 \times 10^{-3}$ atm; Experimental: ▼420°C; ▽440°C; ⊹460°C. Predicted eqn(3.1.8):——— Initial guesses 3; Stepsize 1; δ(420°C) = 0.0033; δ(440°C) = 0.0125; δ(460°C) = 0.0069.

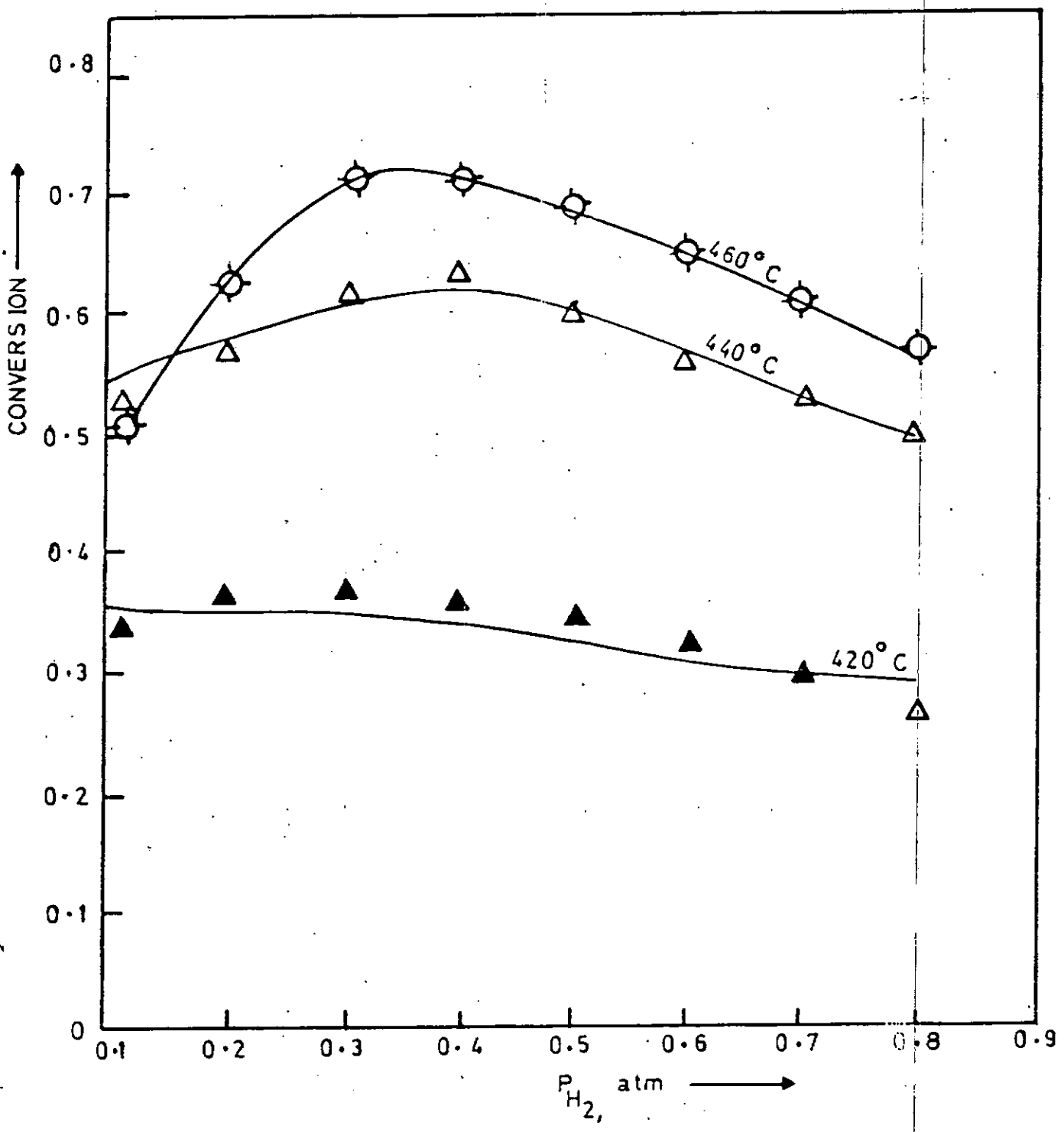

Fig.6.1.3: Prediction of n-octane conversion versus P_{H_2} for 420°C, 440°C and 460°C on Pt/Al_2O_3 catalyst at P_N = 7.63×10^{-3} atm, Experimental: ▼420°C; ▽440°C; ⊹ 460°C. Predicted eqn. (3.1.7) ——; Initial guesses = 5; Stepsize = 5

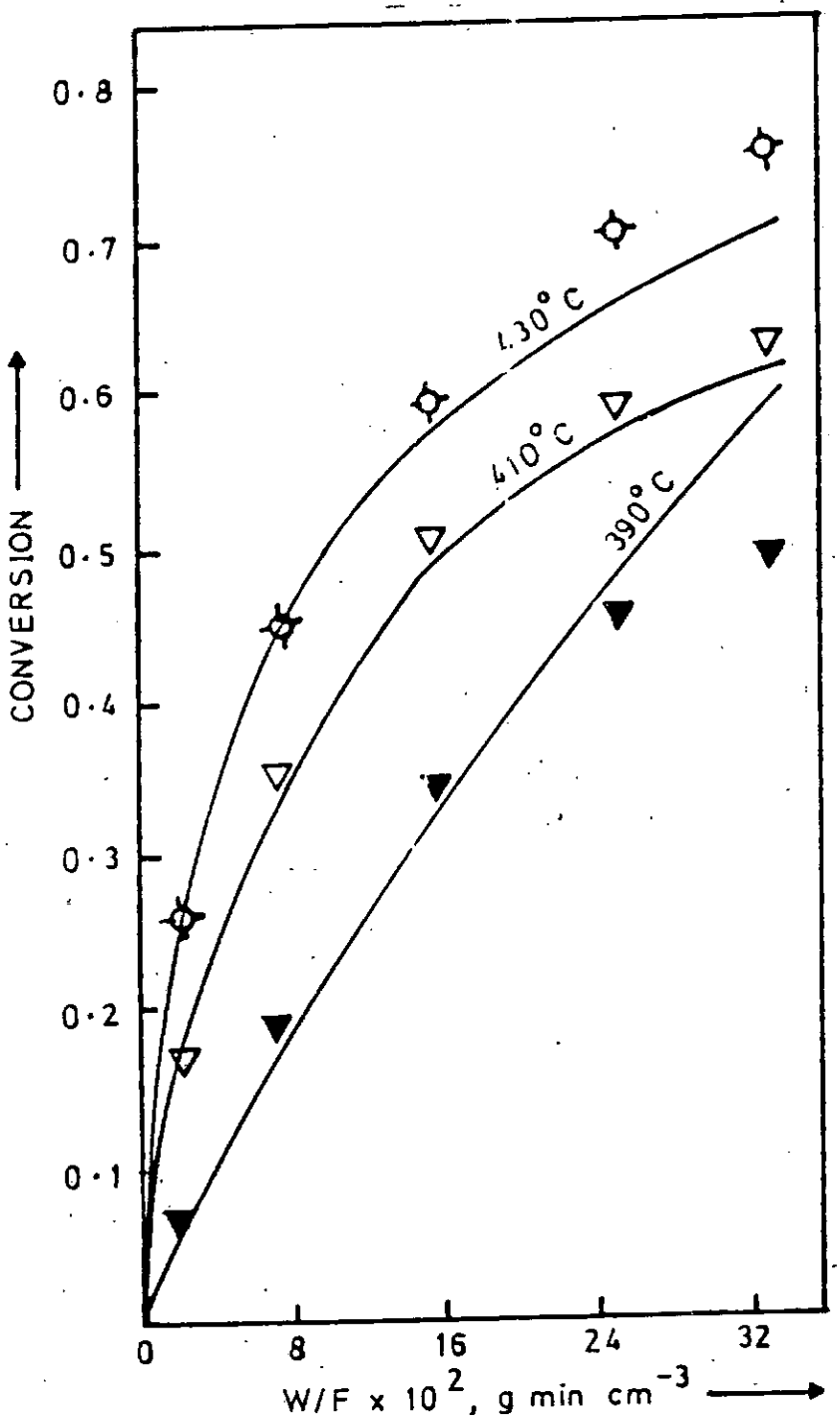

Fig.6.1.4: Prediction of iso-octane conversion versus W/F on 0.3%Pt/Al_2O_3 catalyst at P_N =3.16x10^{-2}atm; Experimental: ▼390°C; ▽410°C; ⊹ 430°C. Predicted eqn(3.1.25) ——; Initial guesses = 3; Stepsize 1; δ(390°C) = 0.0023; δ(410°C) = 0.00026; δ(430°C) = 0.00097.

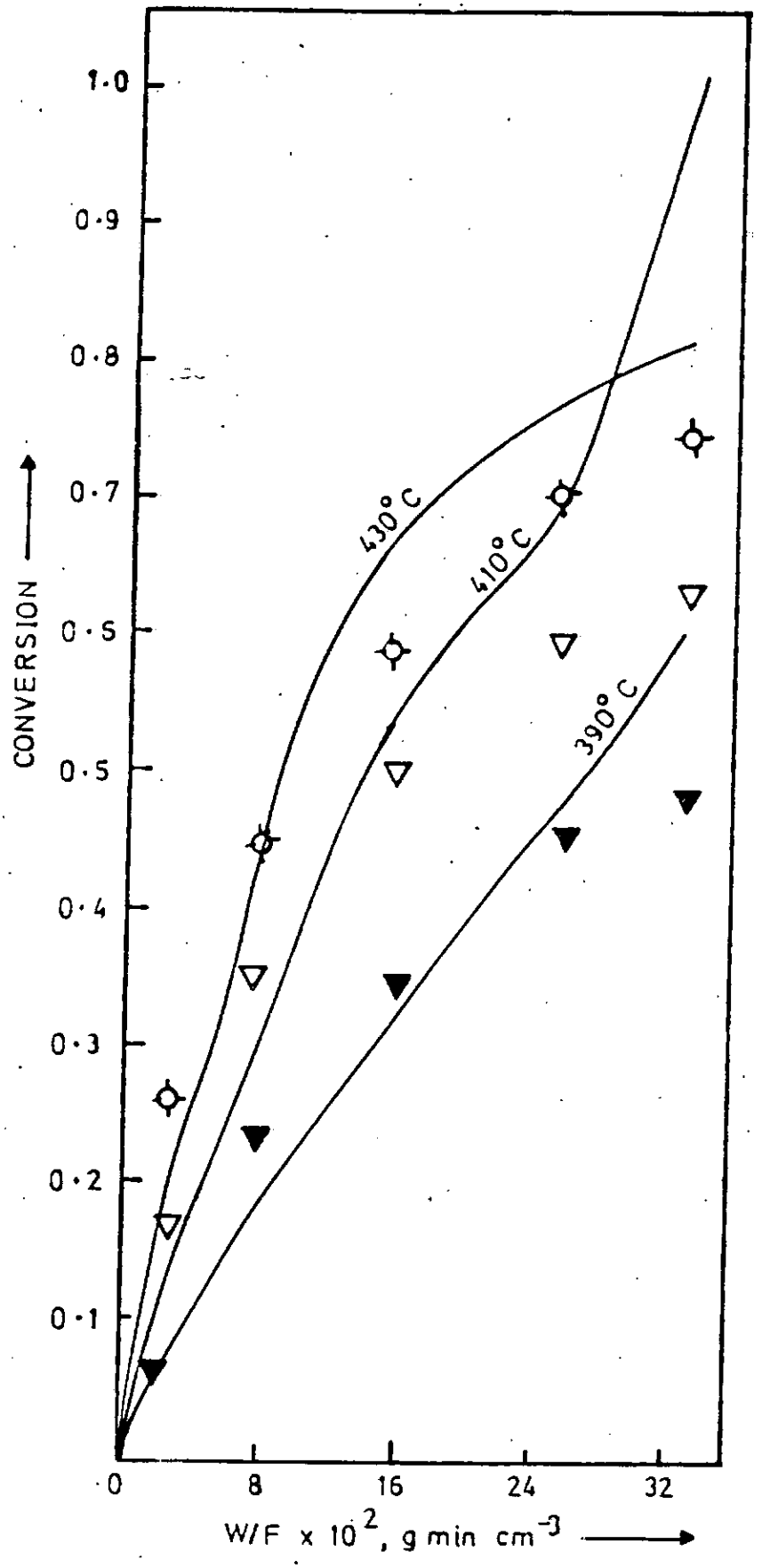

Fig.6.1.5: Prediction of iso-octane conversion versus W/F on 0.3%Pt/Al_2O_3 catalyst at P_N = 3.16x10^{-2}atm. Experimental: ▼390°C; ▽410°C; ⊹430°C; Predicted eqn(3.1.27)——; Initial guesses = 5; Stepsize = 3; δ(390°C) =0.0096; δ(410°C) = 0.031; δ(430°C) = 0.0074

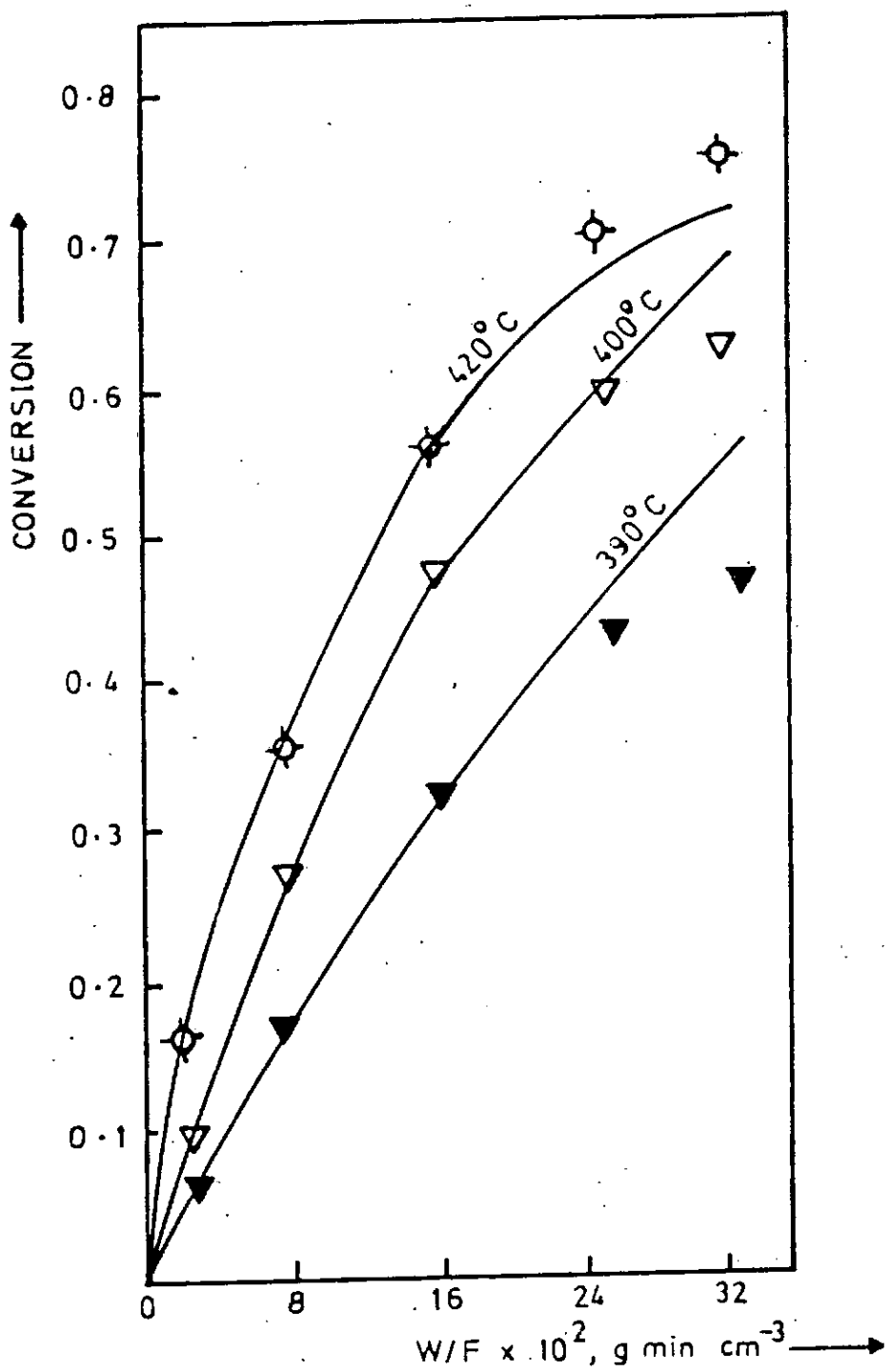

Fig.6.1.6: Prediction of iso-octane conversion versus W/F on 0.6%Pt/Al_2O_3 catalyst at P_{iso} = 3.16×10^{-2} atm; Experimental: ▼390°C; ▽400°C; ⊹ 420°C; Predicted eqn(3.25) —— ; Initial guesses = 5; Stepsize = 5; δ(390°C) = 0.000287; δ(400°C) = 0.0006; δ(420°C) = 0.000425.

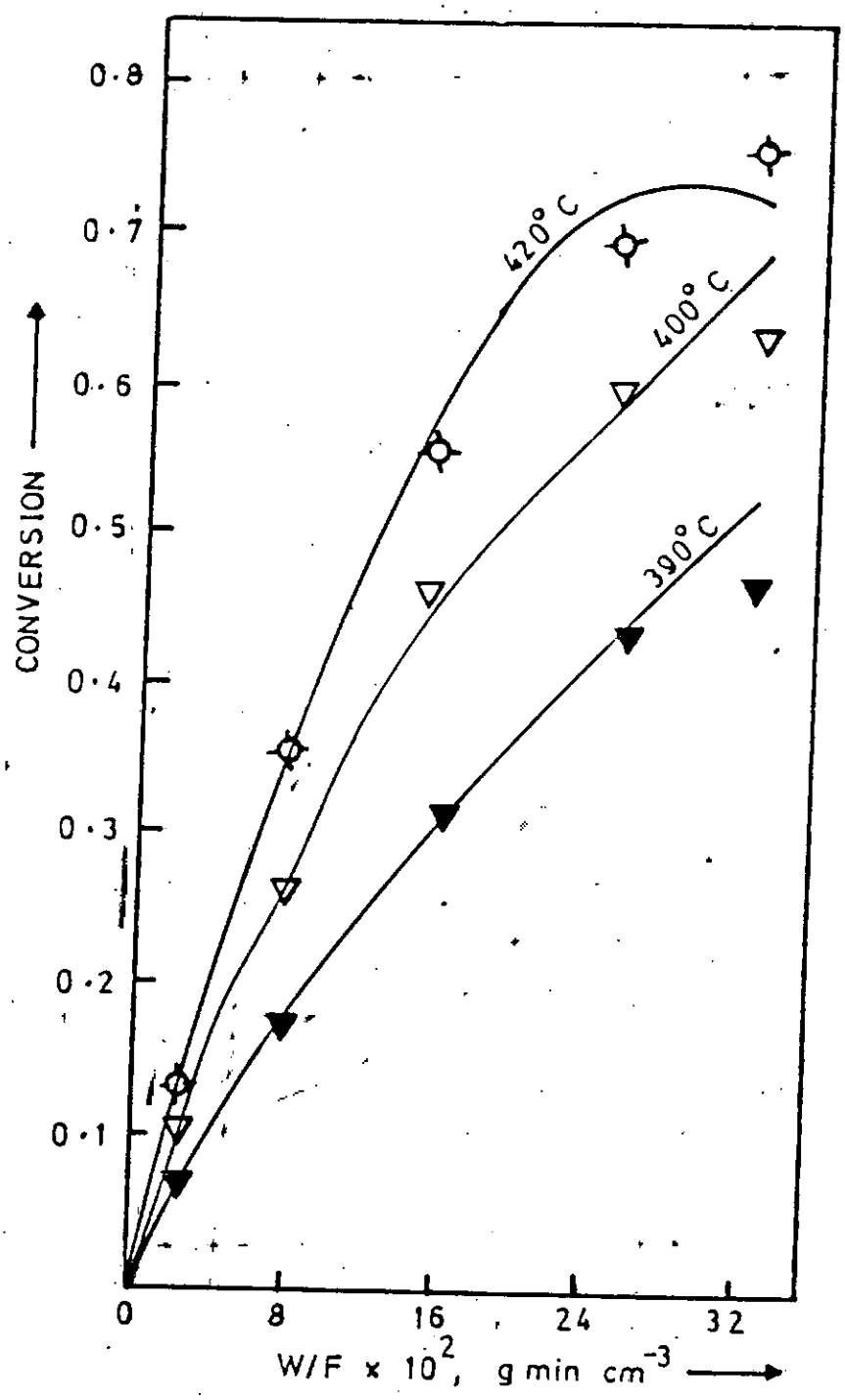

Fig.6.1.7 : Prediction of iso-octane conversion versus W/F on 0.6%Pt/Al_2O_3 catalyst at P_{iso} = 3.16×10^{-2} atm. Experimental: ▼390°C; ▽400°C; ⊹ 420°C. Predicted eqn(3.1.27) ——; Initial guesses = 3; Stepsize =3; δ(390°C) = 0.0006; δ(400°C) = 0.00073; δ(420°C) = 0.00055.

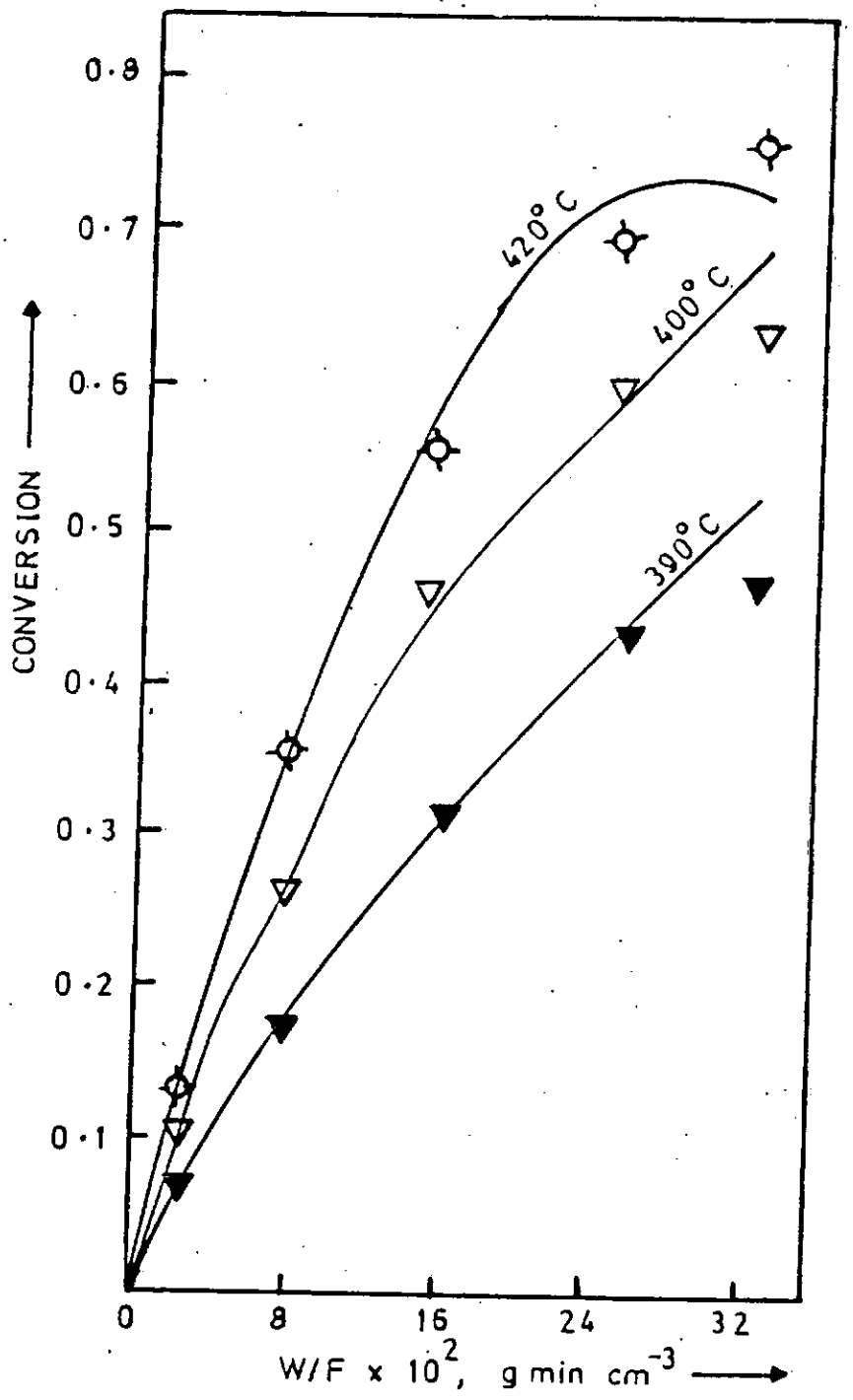

Fig.6.1.7 Prediction of iso-octane conversion versus W/F on 0.6%Pt/Al_2O_3 catalyst at P_{iso} = 3.16×10^{-2}atm. Experimental: ▼390°C; ▽400°C; ⊹ 420°C. Predicted eqn(3.1.27) ——; Initial guesses = 3; Stepsize =3; δ(390°C) = 0.0006; δ(400°C) = 0.00073; δ(420°C) = 0.00055.

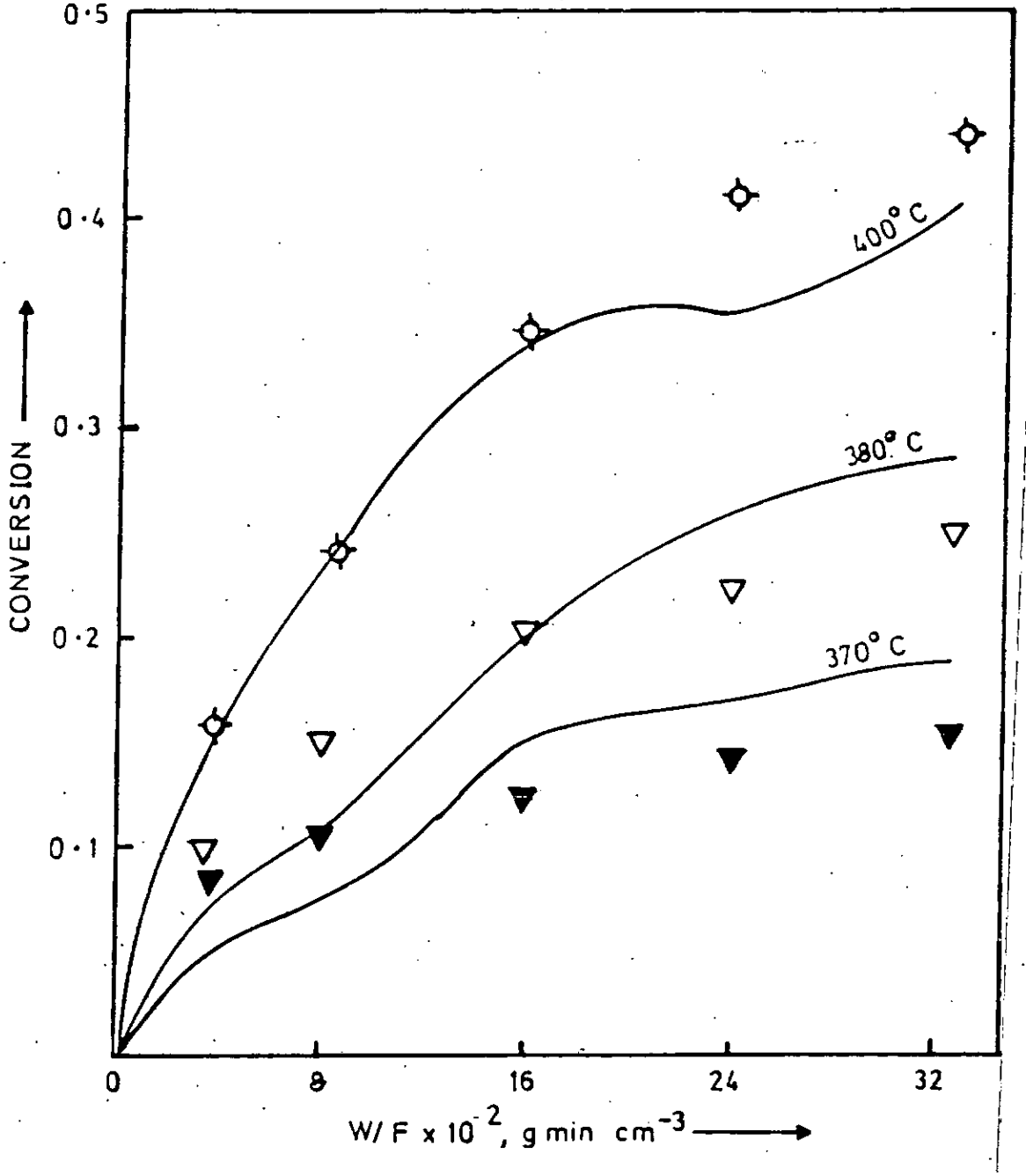

Fig.6.1.8: Prediction of MCP conversion versus W/F on Pt/Al_2O_3 catalyst at P_{MCP} = 9.2×10^{-2}atm. Experimental: ▼370°C; ▽380°C; ☼ 400°C. Predicted eqn(3.1.44) ——; Initial guesses = 5; Stepsize = 5; δ(370°C) = 0.00198; δ(380°C) = 0.00123; δ(400°C) = 0.00067.

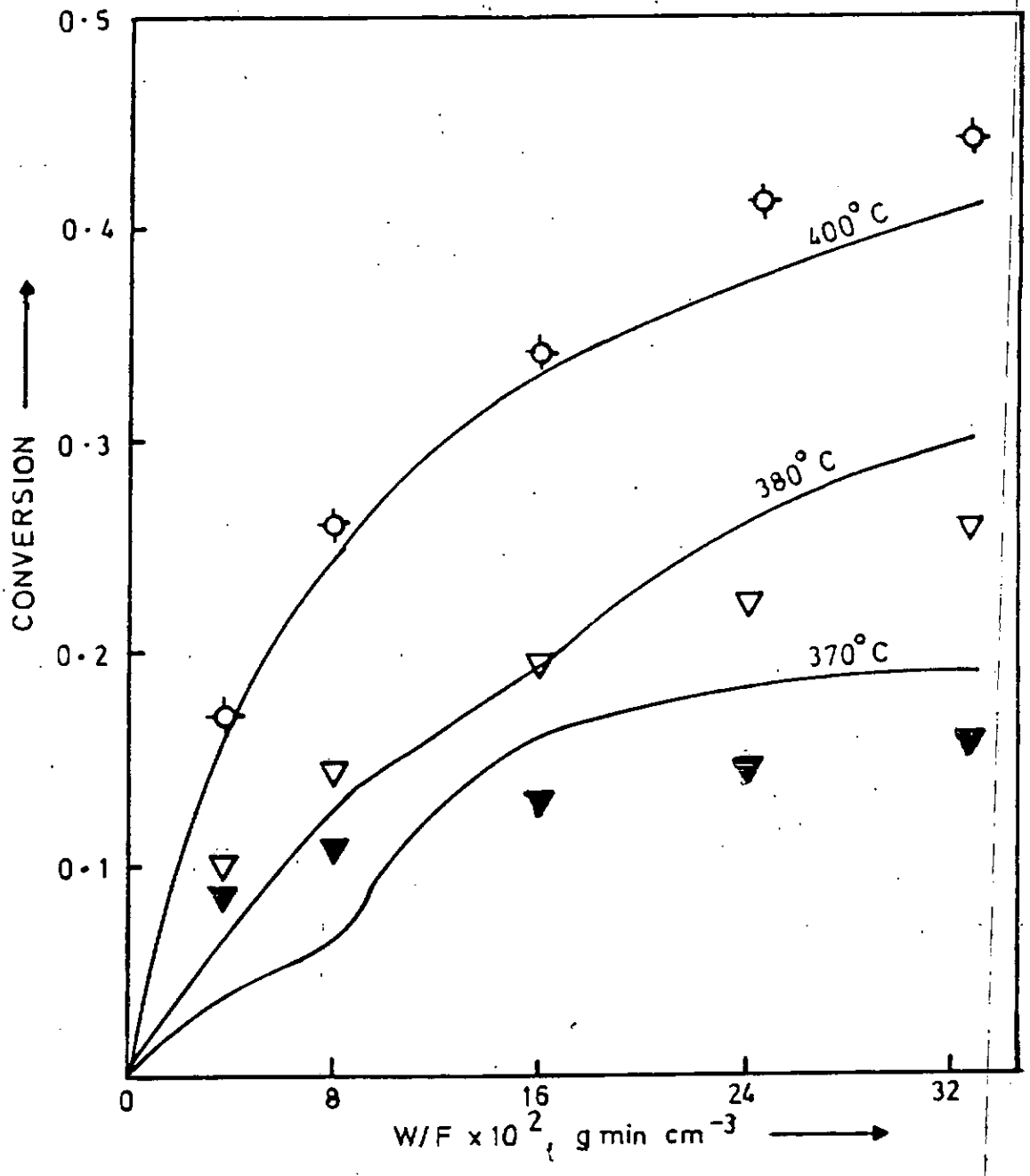

Fig.6.1.9: Prediction of MCP conversion versus W/F on Pt/Al_2O_3 catalyst at $P_{MCP} = 9.2 \times 10^{-2}$ atm. Experimental: ▼370°C; ▽380°C; ⊖ 400°C. Predicted eqn(3.1.46) —
Initial guesses = 5; Stepsize = 5; δ(370°C) = 0.00106; δ(380°C) = 0.003255; δ(400°C) = 0.00069.

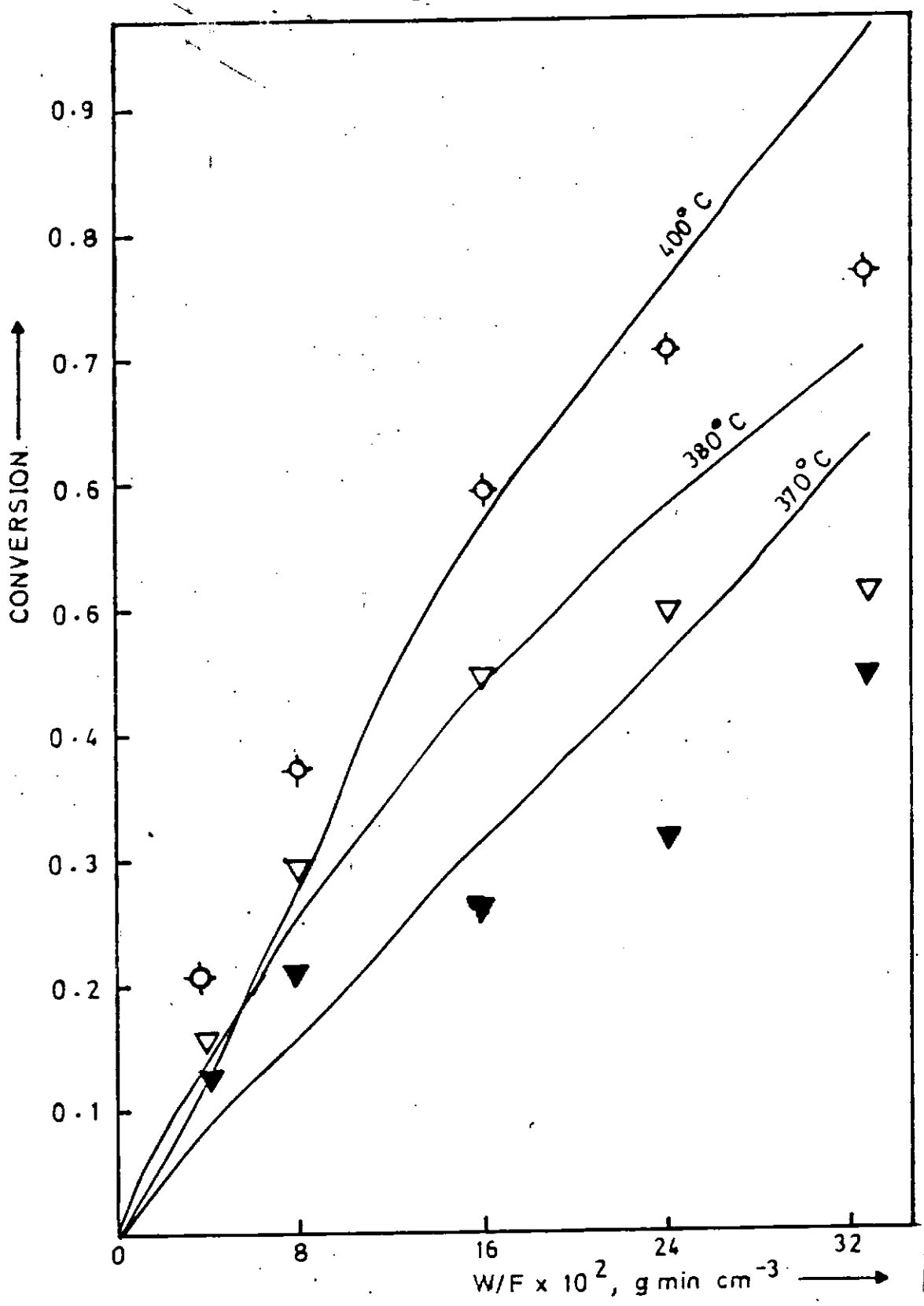

Fig.6.1.10: Prediction of MCP conversion versus W/F on Pt-Re/Al_2O_3 (DRIED) catalyst at P_{MCP} = 9.2×10^{-2}atm. Experimental ▼370°C; ▽380°C; ⊹ 400°C. Predicted eqn(3.1.48) —— Initial guesses = 3; Stepsize = 3; δ(370°C) = 0.0158; δ(380°C) = 0.01226; δ(400°C) = 0.01268.

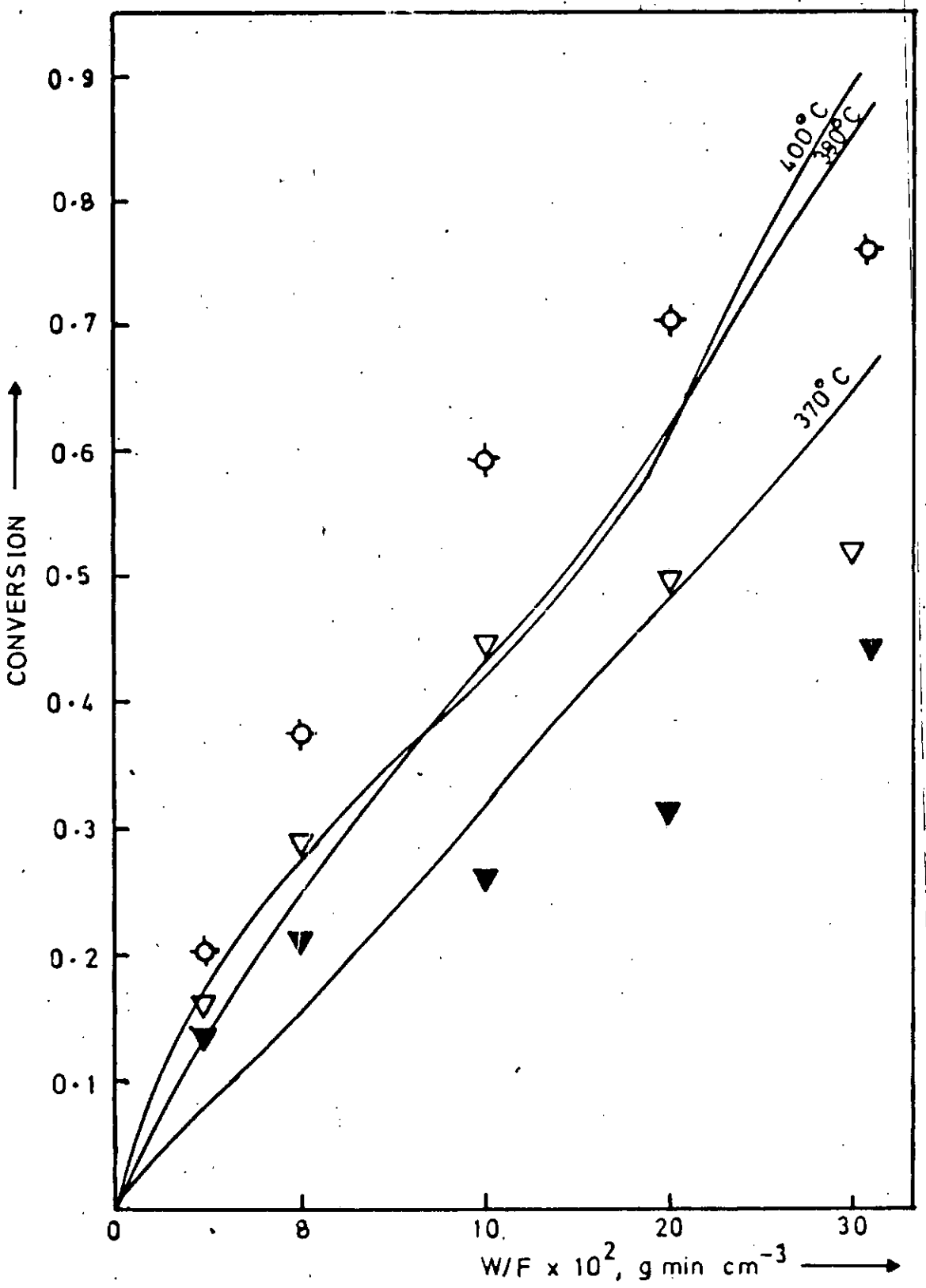

Fig.6.1.11: Prediction of MCP conversion versus W/F on Pt-Re/Al_2O_3 (DRIED) catalyst at P_{MCP} = 9.2×10^{-2} atm. Experimental: ▼370°C; ▽380°C; ⊖ 400°C; Predicted eqn(3.1.48) ——; Initial guesses = 3; Stepsize = 3; δ(370°C)= 0.0204; ∇(380°C) = 0.0355; δ(400°C) = 0.0159.

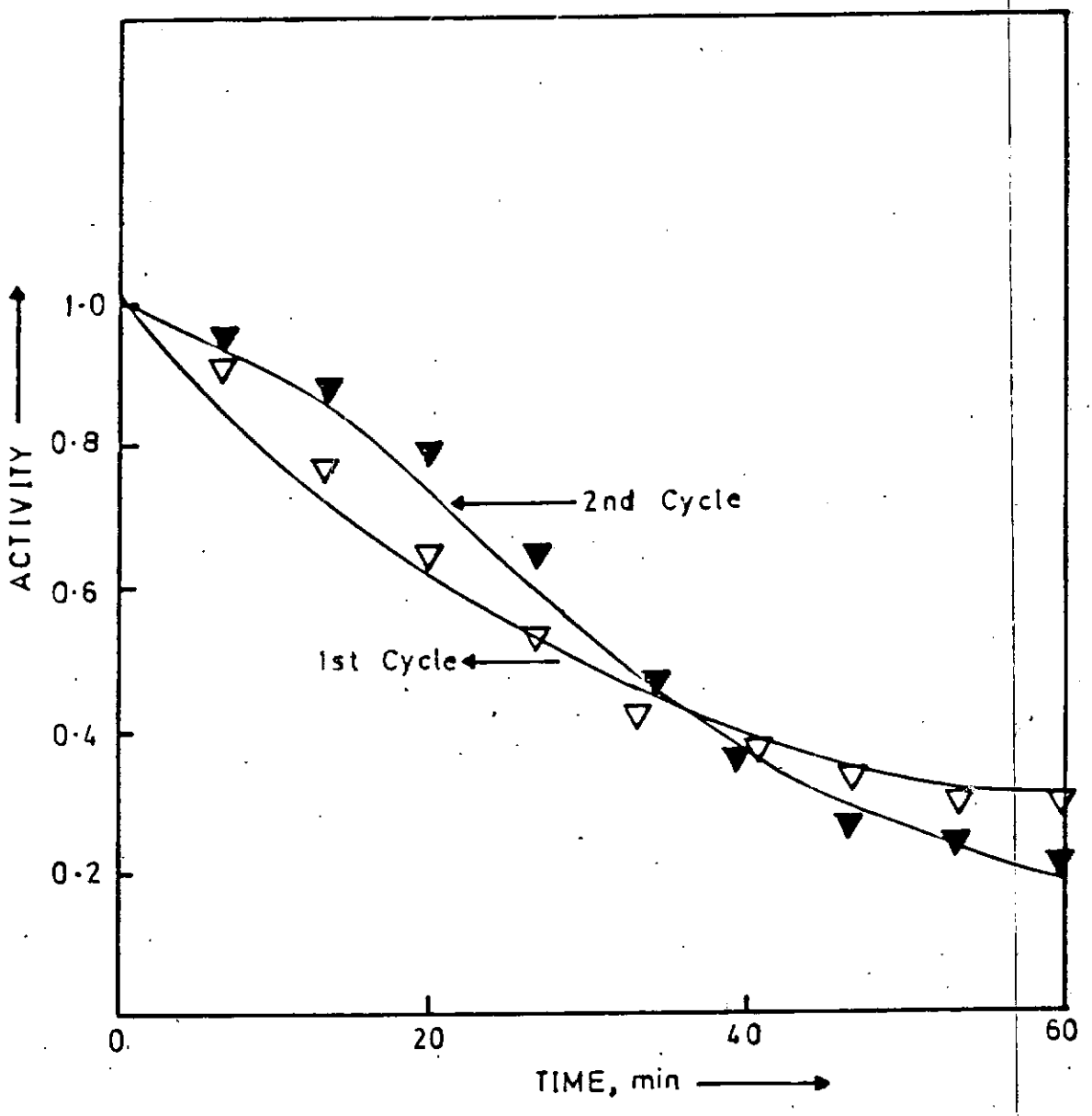

Fig.6.3.1: Prediction of deactivation profiles for n-octane on Pt/Al_2O_3 catalyst; Experimental: ▽ 1st cycle; ▼ 2nd cycle; Predicted eqn(6.3.1) ——; δ (1st cycle) = 0.1868; δ (2nd cycle) = 0.0227.

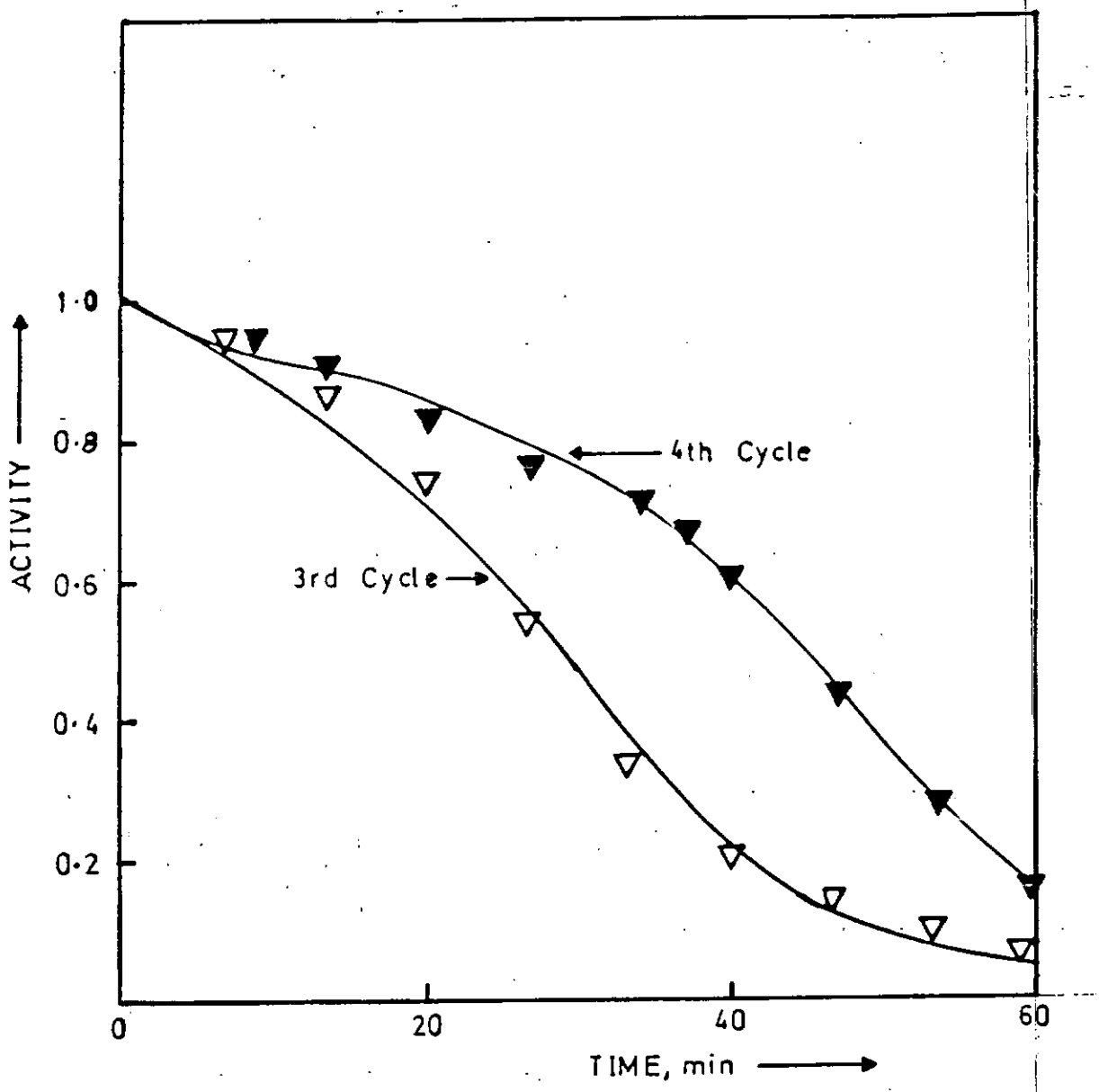

Fig.6.3.2: Prediction of deactivation profiles for n-octane on Pt/Al_2O_3 catalyst; Experimental; ▽ 3rd cycle ; ▼ 4th cycle; Predicted eqn(6.3.1)—— ;δ(3rd cycle)= 0.0528; δ(4th cycle) = 0.0047.

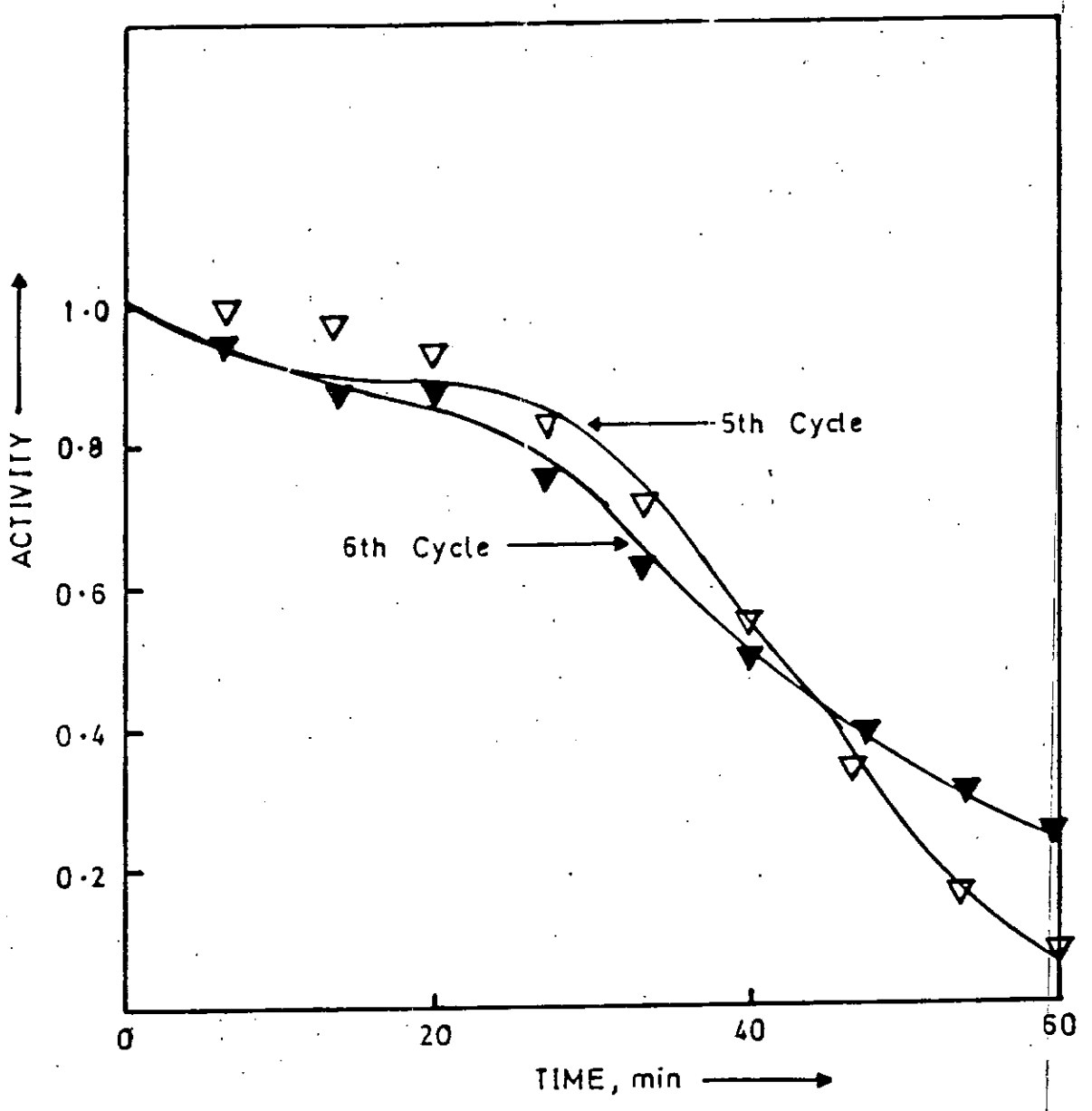

Fig.6.3.3: Prediction of deactivation profiles for n-octane on Pt/Al_2O_3 catalyst; Experimental: ▽ 5th cycle; ▼ 6th cycle; Predicted eqn(6.3.1)——; δ(5th cycle) = 0.0176; δ(6th cycle) = 0.0146.

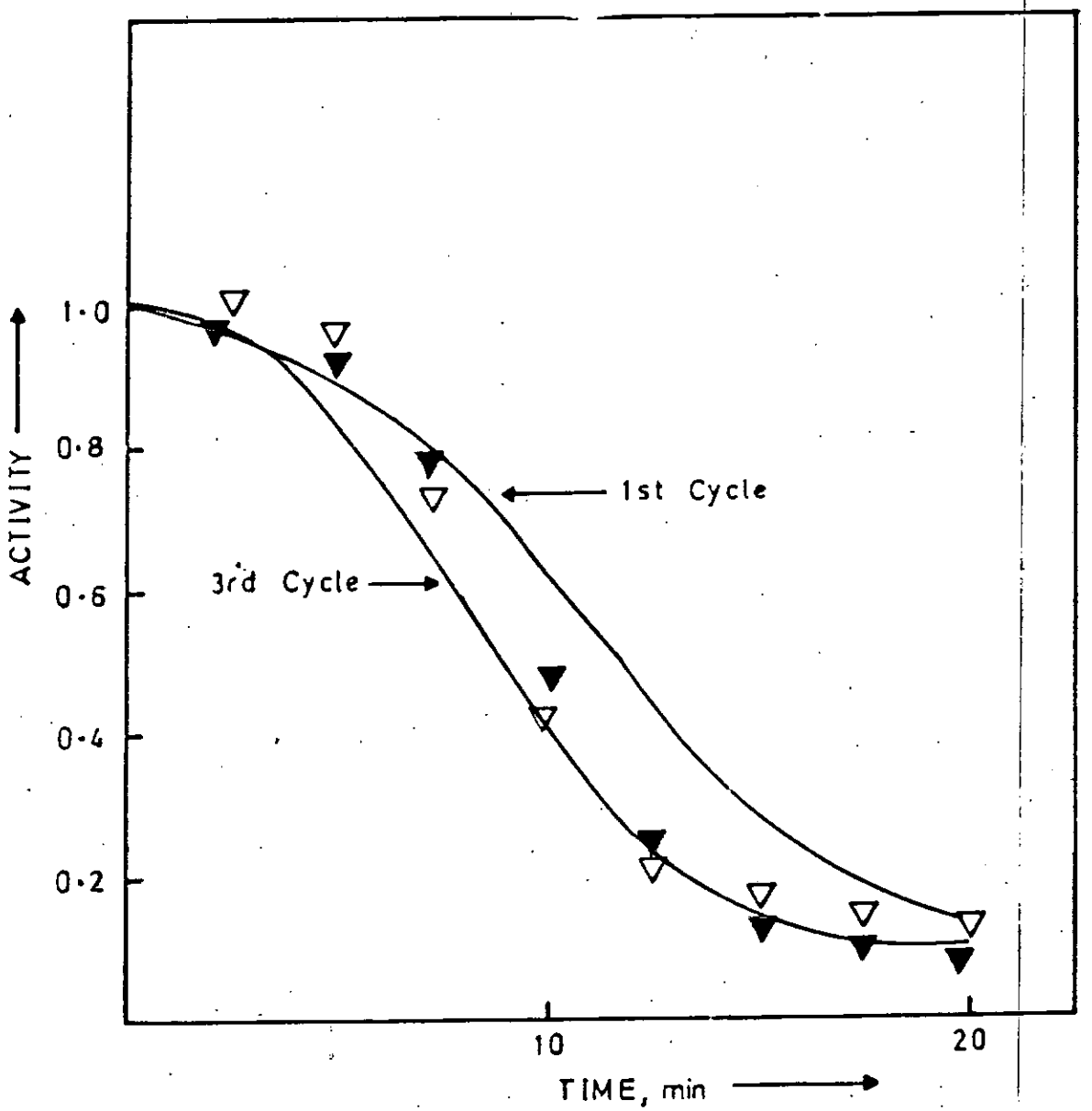

Fig.6.3.4: Prediction of deactivation profiles for iso-octane on 0.3%Pt/Al_2O_3 catalyst; Experimental: ▽ 1st cycle; ▼ 3rd cycle; Predicted eqn(6.3.1)——; δ(1st cycle) = 0.244; δ(3rd cycle) = 0.1597.

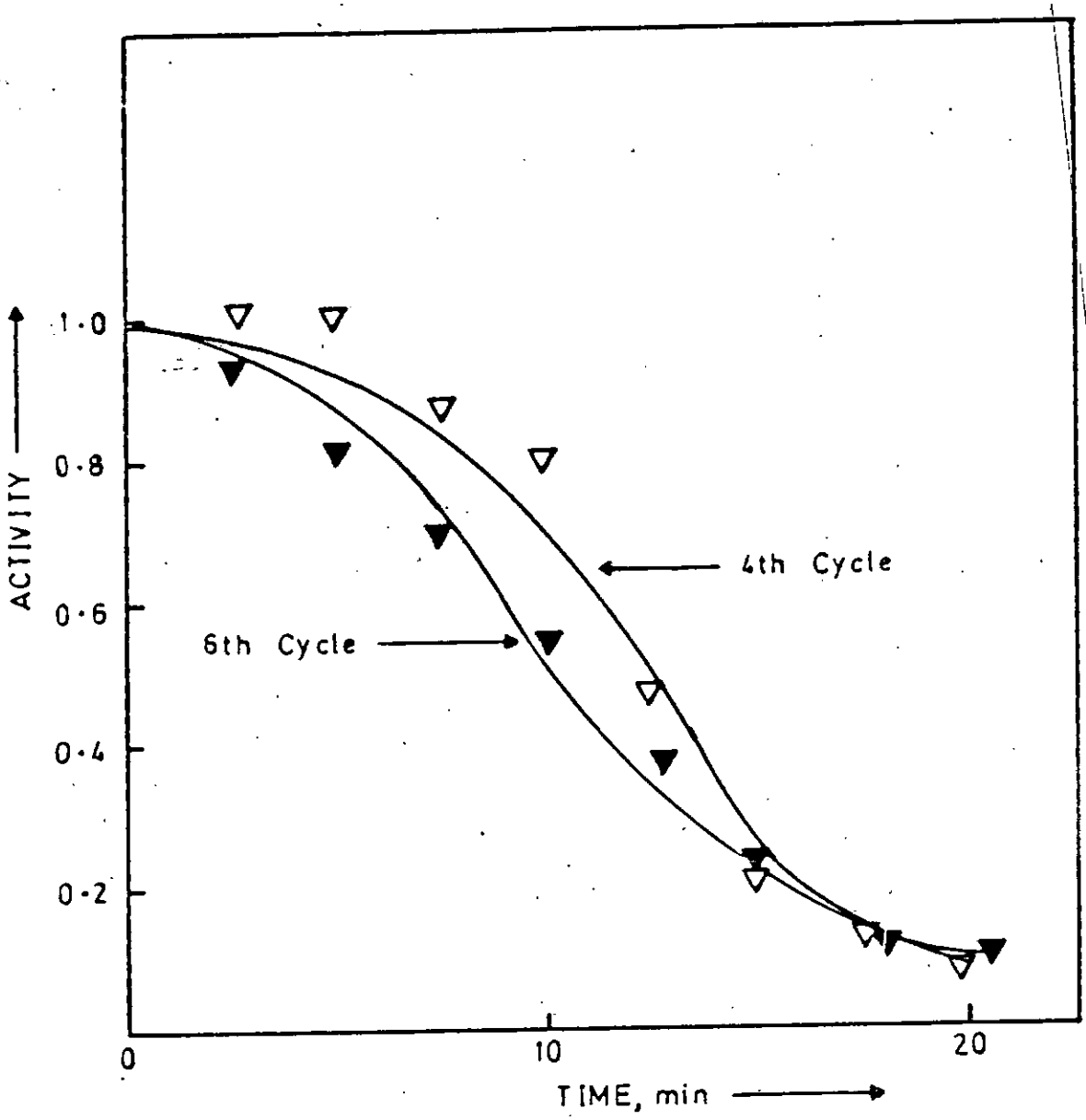

Fig.6.3.5: Prediction of deactivation profiles for iso-octane on 0.3%Pt/Al_2O_3 catalyst; Experimental ▽ 4th cycle; ▼ 6th cycle; Predicted eqn(6.3.1) —; δ(4th cycle)= 0.08; δ(6th cycle) = 0.0252

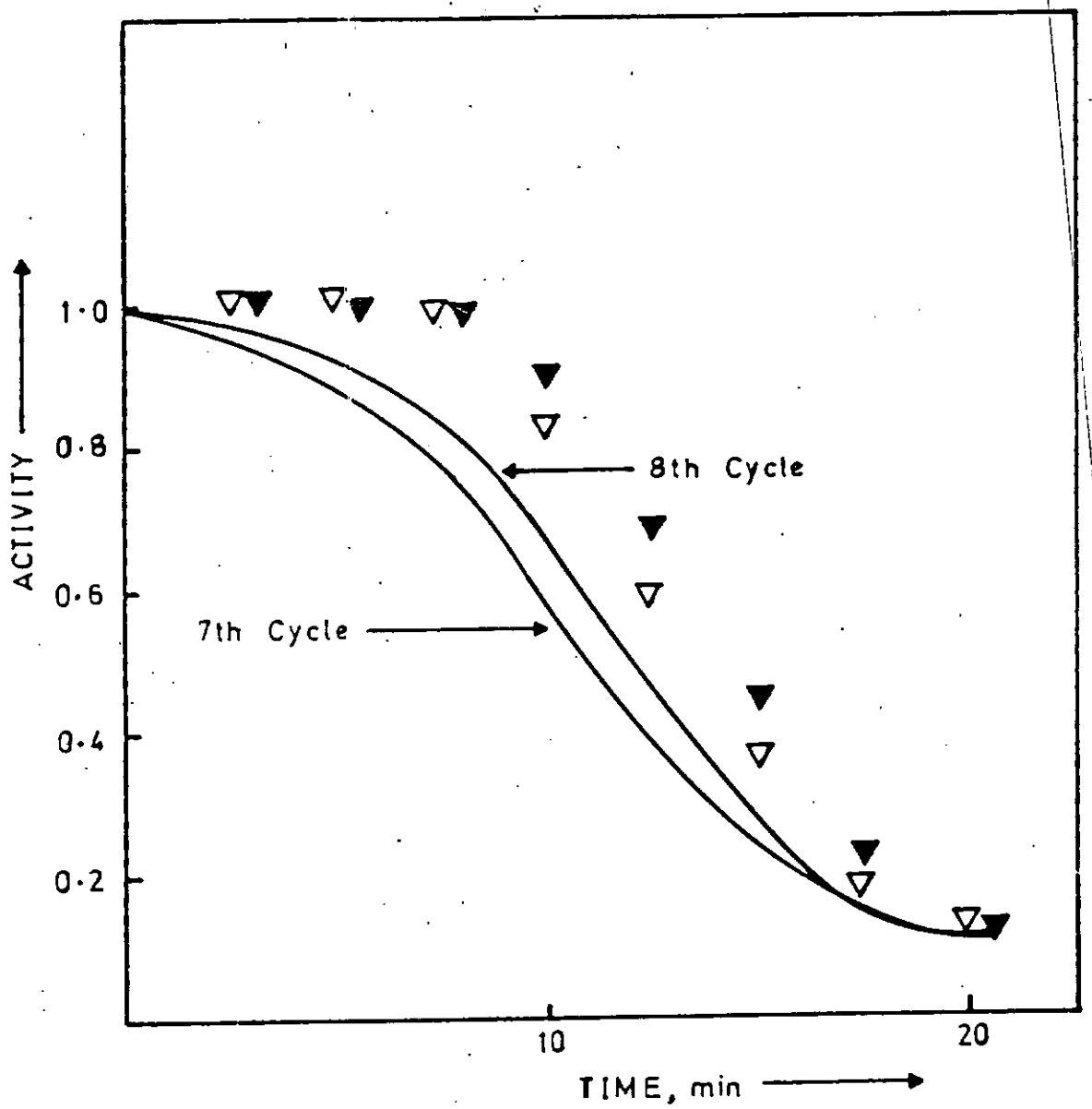

Fig.6.3.6: Prediction of deactivation profiles for iso-octane on 0.3%Pt/Al_2O_3 catalyst; Experimental: ▽ 7th cycle; ▼ 8th cycle; Predicted eqn(6.3.1) ——; δ(7th cycle)= 0.107; δ(8th cycle) = 0.0169.

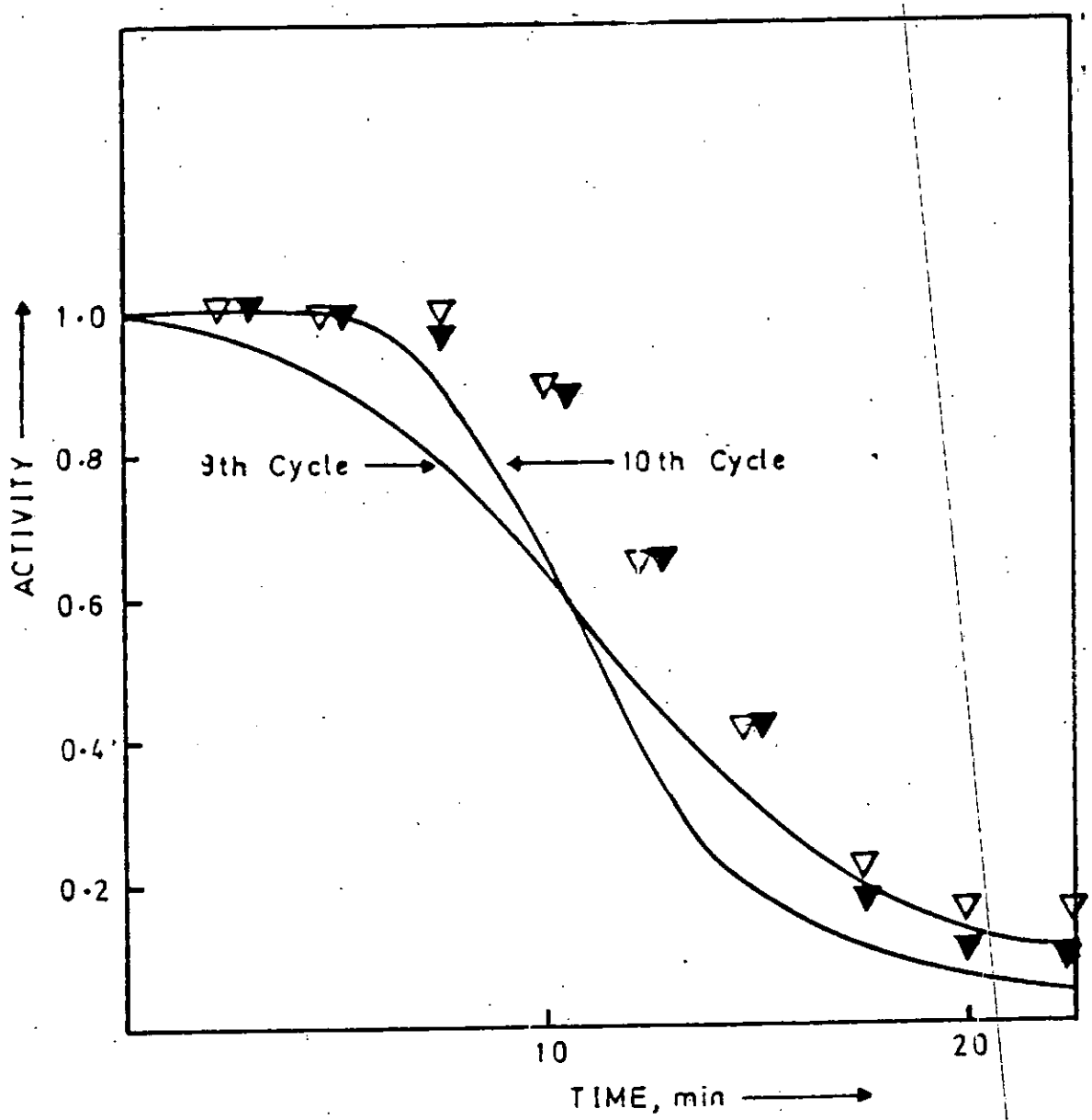

Fig.6.3.7: Prediction of deactivation profiles for iso-octane on 0.3%Pt/Al_2O_3 catalyst; Experimental: ▽ 9th cycle; ▼ 10th cycle; Predicted eqn(6.3.1)——; δ(9th cycle) = 0.173; δ(10th cycle) = 0.0542.

CHAPTER 7

7.o DISCUSSION OF RESULTS

The presentation of the experimental results in Chapter 5 and modelling results in Chapter 6 has been followed side by side by cursory discussion of these results. In this chapter, a global discussion of the experimental and modelling results is presented.

7.1 Constant Activity (Product Distributions).

A. N-Octane and Iso-Octane.

In the reactions of n-octane over Pt/Al_2O_3 catalyst there were significant production of hydrocracked products between 400° and 460°C. This result is at variance with the results of the microcatalytic reactor investigation on bifunctional Pt/Al_2O_3 catalyst by Ako and Susu[1] where no hydrocracked products were formed between 330° and 380°C. It is important to note, however that the temperature range used in our investigation is higher than that used by Ako and Susu[1]. While Ako and Susu obtained appreciable conversion using the pulse technique at 330°C, no appreciable conversion was obtained using the CSTR below 400°C in our investigation. The higher temperature of operation and the lower hydrogen pressure employed in our investigation is probably responsible for the presence of hydrocracked products. This arguement is buttressed by the fact that between 420° and 460°C, the hydrocracked products are the predominant product while at 400°C iso-octane (and not hydrocracked products) was the predominant product.

The presence of low yields of toluene in our investigation can also be explained by the high operating temperature employed. Toluene is formed probably from the dealkylation of the xylenes produced during the dehydrocyclization reaction. No toluene was detected at 400°C. The quantity of toluene in the effluent was found to increase with increase in temperature. The works of Christoffel and Paal[11], Ako and Susu[1] and Davis[6,9] did not report the presence of toluene. Their results are in agreement with ours as they did not work above 400°C.

Christoffel and Paal[11] have shown by using pulse technique, that on a dual-functional Pt/Al_2O_3 in H_2 carrier at 400°C, n-octane was converted to ethylbenzene and 0-xylene. Also C_5-ring naphthenes were also formed as these were not converted further to C_6 ring naphthenes under their experimental conditions. In the present work, no C_5-ring naphthenes were detected. Neither the results of Ako and Susu nor those of Davis show the presence of C_5 ring naphthenes.

Ako and Susu[1] identified the following sequence of reactions as occuring on bifunctional Pt/Al_2O_3 catalyst:

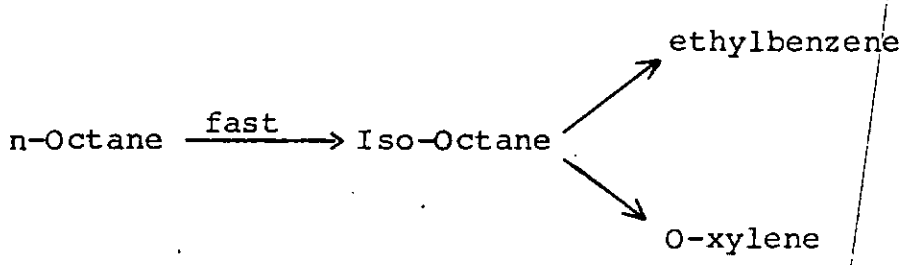

They suggested that P- and m- xylene were formed from the isomerization of ethylbenzene and 0-xylene. According to the network, iso-octane is produced from n-octane and this is turn aromatizes to give ethylbenzene and 0-xylene. Ako[27]

reported the production of ethylbenzene and o-xylene from 2,2,4 trimethylpentane (iso-octane). On the other hand Lester[25] did not detect ethylbenzene or 0-xylene in the aromatization of 2,2,4 trimethylpentane on k_2O-Cr_2O_3 - Al_2O_3 and non-acidic Pt/Al_2O_3 at temperatures between 400° - 500°C. The effluent composition when 2,2,4 trimethylpentane was passed over 0.44g of k_2O-Cr_2O_3-Al_2O_3 100cc (STP)/min at 500°C is shown in Table 7.1

Table 7.1: Composition of Effluents From Reactions of 2,2,4 trimethylpentane over k_2O-Cr_2O_3-Al_2O_3 catalyst at 500°C[25]

Feed	Composition of Effluent (Wt%)
C_1 - C_7	6.6
2,2,4 TMP	74.8
1,1,3 TMP	0.0
C_8 H_{16} (Total)	16.1
C_7 H_8	0.4
P-xylene	2.1
m-xylene	0.0
O-xylene	0.0

It can be seen that P-xylene is the only C_8 aromatic produced by the paraffin.

On non-acidic Pt/Al_2O_3, the effluent composition when 2,2,4 TMP was passed through nonacidic Pt/Al_2O_3 in H_2 at 425°C and 480°C are shown in Table 7.2.

Table 7.2. Composition of Effluents From Reactions of 2,2,4 TMP over Nonacidic Pt/Al_2O_3 Catalyst[25]

Temp°C	425°C	480°C
	Components in Effluents	(Wt%)
$C_1 - C_7$	21.0	52.3
2,2,4 TMP	37.4	14.9
1,1,3 TMP	32.4	2.4
C_7H_8	1.3	12.9
P-xylene	3.2	7.0
m-xylene	4.7	10.5
O-xylene	0.0	0.0

The results show that iso-octane cracked more extensively at 482°C (52.3%) than at 425°C. Furthermore, P- and m-xylene were produced at 480°C while isomerization to 1,1,3 TMP predominated at lower temperature (425°C). The results obtained by this author on the reaction of 2,2,4 trimethylpentane between 370°C and 430°C show that only one product 1,1,3 trimethylpentane (iso-Octane) was formed. This result is not in agreement with the work of Ako[27]. It is in some agreement with the result of Lester[25] as isomerization to 1,1,3 TMP is the predominant reaction in his work.

The variation of total conversion and product composition as functions of hydrogen partial pressure showed that both the conversion and aromatic composition each passed through a maximum. Two basic kinetic arguments are now available based on the explanations of Sinfelt[84] and Paal[85].

The argument of Sinfelt[84] is based on the competing need to keep the catalyst surface free of coke during the ascending part of the activity profile. For example, the isomerization of alkanes and isomerization - dehydroisomerization of alkylcyclopentanes are not observed in the complete absence of hydrogen. However the rates of reaction pass through maxima with increasing hydrogen pressure. In the low hydrogen pressure region, the reaction rates are limited by the rate of formation of intermediate olefins. The extent of coverage of the surface by such residues decreases with increasing hydrogen pressure. However, at sufficiently high hydrogen pressures, coverage of Pt sites by surface residues ceases to be a limiting factor and the formation of intermediate olefins ceases to be rate limiting. The overall reaction then becomes limited by the isomerization of olefins on the acidic sites of the catalyst. The decrease in the rate of isomerization with further increase in H_2 pressure is attributed to the effect of H_2 pressure in limiting the concentration of olefin intermediates attainable at equilibrium. Rohrer,et al[10] also observed the same phenomenon in their study of the kinetics of n-heptane dehydrocyclization on a platinum on alumina catalyst and offered the same explanation for the occurence since dehydrocyclization involves a preliminary dehydrogenation step on the metal prior to ring closure.

In the reforming process, all the reactions discussed above occur simultaneously and it is necessary to know the order in which the maximum hydrogen pressure occures for all these reactions. Paal and Co-workers[21,83,87] have investigated

this problem most extensively and were able to offer suggestion for the order of the optimum hydrogen dependence for several reactions. These studies all suggest that the optimum hydrogen pressure for the various reactions does not correspond to the stoichiometric hydrogen balance of the reaction. They then associated the order of maxima for the various reactions to the degree of dissociation of the surface intermediate for the given reaction and suggested the following order for optimum hydrogen pressure.

Bond-shift dehydroisomerization < C_6 - Dehydrocyclization <Hydrogenolysis < Bond-shift isomerization < C_5 cyclic reactions.

It was also observed that as temperature increases, the hydrogen pressure belonging to the maximum rate is shifted toward higher pressure.

In order to compare the results of this work with the general prediction scheme for optimum P_{H_2} by Paal[85], we first summarize our results for n-Octane conversion

1. Since iso-octane composition increased with increasing P_{H_2}, it has the highest optimum P_{H_2} value. In the terminology of Paal, the isomerization of n-octane to iso-octane must correspond to a surface intermediate with the least degree of dissociation. This is of course true as the dual functional isomerization mechanism for iso-octane production involves dehydrogenation/hydrogenation steps and methyl shifts. In agreement with the Paal Scheme, bond shift isomerization with dual functional catalysis retains the order of the optimum P_{H_2} since the maximum occurs at a higher P_{H_2} than dehydrocyclization reactions.

2. As stated above, the optimum P_{H_2} values for the dehydrocyclization reactions are less than for the isomerization reaction. However, the relative appearance of the various maxima for ethylbenzene and the xylene isomers appear to be temperature dependent. At 420°C, the maxima of the xylene isomers and ethylbenzene occur at about the same P_{H_2} (0.55atm). At 440°C, the optimum P_{H_2} for ethylbenzene and m-xylene was slightly less than those for O- and P- xylene. The optimum P_{H_2} for hydrocracked products was less than for the dehydrocyclized products. This contradicts the order recommended by the Paal scheme. At 460°C where all the products exhibited maxima, the optimum P_{H_2} values were no longer as distinctly delineated between the hydrocracked and dehydrocyclized products as the maxima of m-xylene and hydrocracked products occured at the same P_{H_2} values.

The above results show that the suggested order of optimum P_{H_2} for several reactions on a given catalyst as suggested by Paal[85,86] may not be totally applicable to reforming reactions on bifunctional catalysis. This is not unexpected as several of the reactions occur on both the metal and the support and the effect of spillover hydrogen from the metal to the support is very significant on the bifunctional catalyst.

Profiles of product composition against temperature for P_{H_2} = 0.33, 0.5 and 0.89 atm (Figures 5.1.19 - 5.1.21) were used to understand the effect of temperature on the location of the maximum P_{H_2}. These plots complement the product composition - P_{H_2} plots (Figures 5.1.16 - 5.1.18) and show more clearly the direction of temperature dependence of the maximum P_{H_2}.

By the postulate of Paal[85,86] at constant hydrogen pressure, the reaction requiring the least dissociated surface species should have its maximum rate at the lowest temperature. This was actually observed by Sachtler et al[88] on Pt-black during the reaction of platinum based hydrocarbon - conversion catalyst where they reported that maximum yields of various reactions were not at the same temperature over Pt-black. The work reported here is on bifunctional Pt/Al_2O_3 and it will be useful to check if the above conclusions are applicable on the bifunctional catalyst.

Since iso-octane requires the least dissociated surface intermediate, its maximum P_{H_2} should occur at the lowest temperature. This is borne out by the results of Figures 5.1.19 and 5.1.20 at P_{H_2} = 0.33 and 0.5atm, respectively. The P_{H_2} maxima of the dehydrocyclized products occur at higher temperatures as expected. The P_{H_2} maxima for ethylbenzene, 0- and P- xylene occur at 440°C irrespective of hydrogen pressure. The behavior of the P_{H_2} maximum for m-xylene appears to be dependent on hydrogen pressure although at $P_{H_2} \geq 0.5$atm (Figure 5.1.20), the maximum P_{H_2} occurs again at 440°C. Figure 5.1.21 at P_{H_2} = 0.89atm clearly shows that the maximum P_{H_2} for iso-octane precedes those of the other products. Again, the order of appearance of the maximum for the hydrocracked products is not in conformity with the Paal Scheme as the temperature of its occurence is higher than those for the dehydrocyclized products.

B. Methylcyclopentane (MCP)

The present study investigated the reactions of MCP on bifunctional Pt/Al_2O_3 and bimetallic $Pt-Re/Al_2O_3$ catalysts. The hydrogenolysis products measured in this work is a lumped parameter representing n-hexanes, 2-methylpentane and 3-methylpentane. Following the works of Isaacs and Petersen[79] the $Pt-Re/Al_2O_3$ (DRIED) was first dried in nitrogen at 100°C for 2h before reduction. Reduction of the $Pt-Re/Al_2O_3$ catalyst dried at 100°C, which contains no unalloyed Re, is complete after 1h of 500°C H_2 reduction. The Pt/Al_2O_3 catalyst was reduced at 500°C in H_2 for 2h without drying. In addition to the reactivity studies on $Pt-Re/Al_2O_3$ (DRIED) catalyst, reactivity studies were also performed on the $Pt-Re/Al_2O_3$ (UNDRIED) catalyst that was only presented in the same manner as Pt/Al_2O_3.

Brandenberger et al[89] found that the ring opening of MCP yields selectively n-hexane, 2-methylpentane and 3-methylpentane in a ratio of 2:2:1 on small platinum crystallites. The results obtained in this work could not be compared with the above because of the lumping of these products for the convenience of our analysis.

Bragin et al[46] showed that the main influence on product distribution of MCP hydrogenolysis comes from the structure of the catalysts i.e. from the size of the Pt particles as well as from the nature of the support. The most important parameter determining the selectivity of the reaction is the size of the platinum particles. On small Pt particles, the MCP hydrogenolysis occurs nonselectively leading to about 40% n-hexane, 40% 2-methylpentane and 20% 3-methylpentane which

corresponds to statistical ring opening. On the contrary, on very large Pt particles, the branched hexanes 2MP and 3MP are formed almost selectively.

The dependence of the product distribution of MCP hydrogenolysis on the particle size of platinum is generally attributed to two different reaction pathways called the selective and non-selective mechanisms. It is assumed that four adjacent edge atoms existing only on particles larger than 2.5nm, are necessary for the reaction mechanism[92]. On highly dispersed platinum, low coordinated surface atoms predominated[93]. At these sites, the intermediate C_5 ring is assumed to be bound to one single surface atom forming an $\alpha\beta - \pi$ - adsorbed on an $\alpha\alpha - \beta$ triadsorbed species, respectively. Hence the tertiary carbon atom is not excluded from the reaction intermediate and statistical ring opening may occur.

Other explanations for the non selective mechanism are based on the properties of very small crystallites.

(i) The lattice type of very small particles can be different from that of the bulk i.e. the hcp lattice becomes more stable when the particle size is smaller than 1.5nm[94].

(ii) The lattice constant of small Pt particles is contracted due to the surface stress and the different geometry. This lattice contraction may be responsible for different catalystic behavior[95].

(iii) The crystallographic orientation of the exposed faces may change when the particle size is changed[96].

The benzene yield obtained in the present investigation with Pt-Re/Al_2O_3 (DRIED) was ∿1.6 times greater than that

obtained with Pt/Al_2O_3 showing the beneficial effect of Re addition. The benzene yields obtained on Pt/Al_2O_3 were about the same value as that obtained on $Pt-Re/Al_2O_3$ (UNDRIED). This result is in agreement with the work of Omoleye[52] who found no appreciable difference in the conversion of cyclohexane to benzene on Pt/Al_2O_3 and $Pt-Re/Al_2O_3$ (UNDRIED). For a particular catalyst, the benzene yield generally increases with increase in temperature. The yield of hydrogenolysis products was generally greater at low MCP partial pressure and also at higher temperature for a given catalyst. The cyclohexane yield was low throughout probably due to the fact that a high percentage of adsorbed cyclohexene formed gets converted to benzene.

Christoffel et al[11] investigated the conversions of a number of C_6-C_8 alkanes, naphthenes and aromatics on bifunctional platinum carrier catalysts, on platinum black, and on acid carriers of the bifunctional catalysts in the temperature range 300-500°C. The product distribution from MCP conversion using the pulse microcatalystic reactor on a fresh catalyst showed that the primary ring opening products (n-hexane, 2-methylpentane and 3-methylpentane) are formed nearly in the ratio 2:2:1 whereas over a partially deactivated catalyst and the Al_2O_3 carrier, n-hexane is the main product. Thus, over the fresh catalyst platinum reactions mainly contribute to the measured ring opening products, while on partially deactivated catalysts the acidic sites of the carrier mainly catalyzed the opening reactions. On platinum black with rather large crystallites mainly selective ring opening occurs.

It has been suggested that the dehydroisomerization of MCP to benzene utilizes both metallic and acidic sites of a bifunctional reforming catalyst and proceeds through a methylcyclopentene intermediate[36,39].

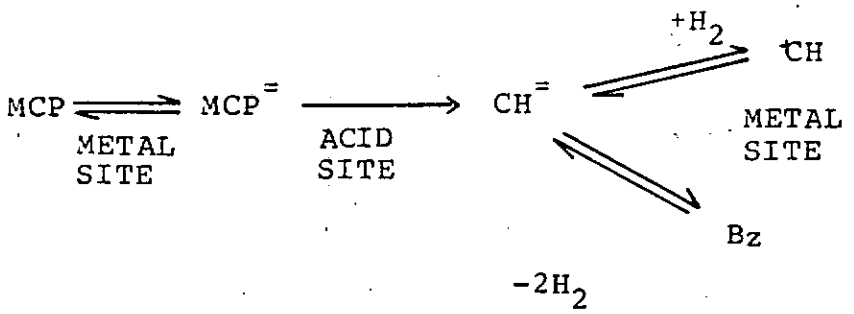

Ring enlargement from methylcyclopentene $MCP^{=}$ to cyclohexene, $CH^{=}$, on an acidic site is thought to be controlling step in this sequential reaction[36,42].

Jossens and Petersen[33] used methylcyclopentane reaction as a model reaction to probe the acidic site contribution on a Pt and Pt-Re catalyst at 475°C and 70torr MCP. Both sulfided and unsulfided catalysts were studied. The conversion of MCP to benzene was found to be less than 20%. MCP dehydroisomerization reaction rates exhibit slightly negative MCP kinetics. For example, under nominal reaction conditions, 0.007 mole of benzene per hour per gram of catalyst was produced. Reducing MCP concentration to one-fourth its nominal value results in an increase in reaction rate to 0.0091 mole per hour per gram of catalyst. The observed rates were in agreement with those published by Sinfelt and Rohrer[25].

Though these catalysts equally catalyze the dehydroisomerization of MCP, the ring opening activity of sulfided

Pt-Re catalyst is less than half that of an unsulfided or sulfided Pt catalyst. There result agrees with the observation of Menon and Prasad[21].

Dartigues et al[34], in their investigation of the structure sensitivity for the ring opening of MCP, found an equal probability of breaking all five cyclic carbon-carbon bonds for a highly dispersed Pt-on alumina catalyst. Similarly De Jougste et al[35] found that a copper rich Pt-Cu catalyst supported on silica also gave non-selective ring opening of MCP. Ring opening of MCP catalyzed by γ (gamma) alumina yields predominantly n-hexane[36]. This suggests that the highly dispersed metal function of Pt or Pt-Re catalyst is responsible for the ring opening activity of these catalysts.

7.2 Constant Activity (Kinetics)

I. N-Octane

A modified version of the suggested reaction pathway of dehydrocyclization of n-octane on bifunctional Pt/Al_2O_3 catalyst by Ako and Susu[1] was used to develop mechanistic rate equations for n-octane dehydrocyclization reaction. The modified reaction pathway is as follows:

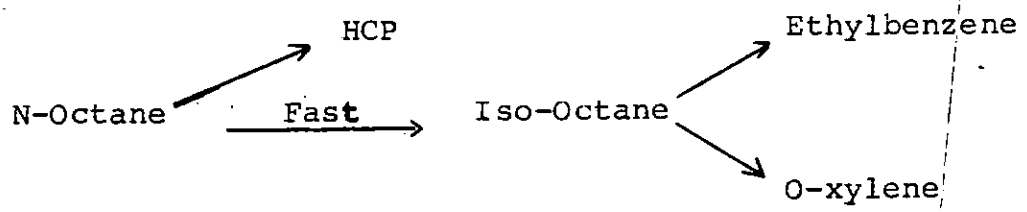

Nineteen rate models were developed based on the modified

reaction network with two different mechanisms. The first mechanisms assumes dissociative adsorption of hydrogen while the second model assumes molecular adsorption of hydrogen. The mechanism and the derived rate models are in Chapter 3.

Since the experimental results were gathered in a Berty CSTR, the rate values can easily be evaluated from the conversion versus W/F data. As many rate values as needed can be evaluated from plots of X_A versus W/F curve. The number of rate values needed is normally greater than the number of kinetic parameters contained in the rate equation. The composition of the products of reaction are also evaluated at the W/F points where the rates were determined. This is necessary as some composition of the products appear in the rate expression. The optimization method employed to minimize the sum of squares of all the errors between experimental and predicted results for all the representative experiments was the simplex method of Nelder and Mead (See Chapter 2).

The optimization routine tried different values for all the constants based on different initial guesses and stepsizes, until it found no other values that produced a smaller error. Nine initial guesses and stepsizes were selected for use after the preliminary work of selecting suitable initial guesses and stepsizes. These are the initial guesses of constants 5, stepsizes of 5,3,1; initial guesses of constants 3, stepsizes of 5,3,1 and initial guesses of constants 1, stepsizes of 5,3 and 1.

For a given model to be accepted, the rate and adsorption equilibrium constants must be positive at all the

temperatures investigated, the rate constants for the rate-determining step must increase with increase in temperature and the predicted conversion has to be near that obtained during experiment. The rate equations that satisfied these conditions were those of equations (3.1.5),(3.1.6),(3.1.7), (3.1.8) and (3.1.13).

From the network used to derive the rate expression, the isomerization of n-octane to iso-octane is fast and it implies that its elementary reactions are also fast. As a consequence, they cannot be rate-limiting steps.

The least squares method was used to evaluate the activation energies, adsorption equilibrium constants and preexponential factors. The activation energies for the forward reaction using model equation (3.1.5) were 23.6, 38.87 and 24.4 kcal/gmole, respectively for initial guesses of constants 3, stepsize 3. The model equation (3.1.6) shows that the activation energy obtained with different stepsizes are between 18-39Kcal/gmole. The activation energies obtained using model equation (3.1.7) for initial guesses of constants 5, stepsizes 5 and 3 and initial guesses of constants 3 and stepsize 3 were between 21-24kcal/gmole while values below 16Kcal/gmole were obtained for other initial guesses and stepsizes. The values obtained with model equation (3.1.8) at all initial guesses and stepsizes were between 20-30Kcal/gmole.

Profiles of experimental conversion as functions of W/F (Figs.6.1.1 and 6.1.2) are compared with predicted values using model equations (3.1.7) and (3.1.8) at initial guesses

of constants 5 stepsize 3 and initial guesses of constants 3 stepsize 1, respectively.

The model equations of (3.1.7) and (3.1.8) were then used to predict the conversion curve obtained by varying the hydrogen partial pressure at constant temperature. The activation energies obtained were 16.7Kcal/gmole and 18.9Kcal/gmole respectively for the two model equations. Figure (6.1.3) shows that very good prediction of the conversion was obtained at all the temperatures investigated.

A study of the kinetics of methylcyclohexane dehydrogenation to toluene in the temperature range 315° to 372°C was reported by Sinfelt and associates[83] for a 0.3%Pt on alumina catalyst. Over the range of methylcyclohexane and hydrogen partial pressures investigated, 0.07 to 2.2atm and 1.1 to 4.1 atm; respectively, the reaction was found to be zero order with respect to hydrogen and nearly zero order with respect to methylcyclohexane. The kinetic data were found to obey a rate law of the form

$$r = \frac{k' \, bP_m}{1 + b \, P_m}$$

where k' and b are parameters which are functions of temperature. From the temperature dependence of k', an activation energy of 33Kcal/gmole was determined.

The kinetics of dehydrogenation of cyclohexane on Pt/Al_2O_3 and $Pt\text{-}Re/Al_2O_3$ catalysts has been investigated by various researchers. Below is a Table of the activation energies obtained under various conditions by various workers.

Despite the diversity, there exists few similarities in the results.

Table 7.3

Kinetic Constants for the dehydrogenation of Cyclohexane on Pt/Al_2O_3 Catalyst.

References	Reaction System	Order	Carrier gas	Temp. range	ΔH kJ/Kmole	ΔE kJ/Kmole
Martman et al[38]	Continuous	0th	N_2	403-423	-	54.4-96.2
Usov et al[90]	Pulse	1st	H_e	573-633		46 - 75
Usov et al[90]	Pulse	1st	H_2	573-633		96 - 134
Omoleye[52]	Continuous	Langmiur	N_2/O_2	573-665	-45	78.5
Omoleye[52]	Continuous	1st	N_2/O_2	573-665	-	41.6

Table 7.4

Kinetic Constants for the dehydrogenation of cyclohexane on $Pt-Re/Al_2O_3$ Catalyst[91]

References	Reaction System	Order	Carrier gas	Temp. range	ΔH kJ/Kmole	ΔE kJ/Kmole
Susu et al[91]	Pulse	1st	N_2	423-503	-	38.1
-11-	Pulse	1st	A_r	429-483	-	50.2
-11-	Pulse	1st	H_e	442-474	-	54
-11-	Pulse	1st	H_2	517-553	-	89
-11-	Pulse	1st	H_2	553-573	-	121.3
-11-	Continuous	1st	H_2	553-623	-	97.9
-11-	Continuous	1st	H_e	543-583	-	37.7

Tables 7.3 and 7.4 show that one of the main causes of the diversities in the values of the kinetic constants by different workers is the type of carrier gas used. Broadly, the type of carrier gas can be classified into two groups: the active and the inert gases. The active gases in Table 7.3 and 7.4 are hydrogen and N_2/O_2 gas mixture, while the inert gases are: helium, nitrogen and argon. Most of the activation energies reported on both Pt/Al_2O_3 and $Pt-Re/Al_2O_3$ catalysts are much higher with active carrier gas than with inert carrier gas. While the activation energies on Pt/Al_2O_3 are mostly between 78 and 134kJ/mole with the active carrier gases, they are between 46 and 96 kJ/mole with inert carrier gases. On $Pt-Re/Al_2O_3$, while the activation energies with active carrier gas are between 89 and 122kJ/mole, they are between 37 and 54 kJ/mole with inert carrier gases. This clearly demonstrates that no uniform value of kinetic constant can be achieved using different types of carrier gas.

The relative values of the activation energies on Pt/Al_2O_3 and $Pt-Re/Al_2O_3$ catalysts show that the presence of rhenium in the bimetallic catalyst has no influence on the kinetic constants of the fresh catalysts.

II Iso - Octane

The modelling results obtained from the rate models developed for the isomerization of iso-octane show that the model equations (3.1.25) and (3.1.27) satisfied the set criteria on both $0.3\%Pt/Al_2O_3$ and $0.6\%Pt/Al_2O_3$ catalyst. The activation energies obtained for iso-octane isomerization

with model equation (3.1.25) for the different initial guesses and stepsizes ranges from 43-53.5 Kcal/gmole while with model equation (3.1.27), the activation energies ranged between 25 and 26 Kcal/gmole on 0.3%Pt/Al_2O_3 catalyst.

On the other hand, lower values of activation energies (27-33kcal/gmole) were obtained with 0.6%Pt/Al_2O_3 compared to 0.3%Pt/Al_2O_3 when rate equation (3.1.25) was used. Rate equation (3.1.27), however, gave activation energies that were higher than those obtained when 0.3%Pt/Al_2O_3 catalyst was used. From the above discussion, it can be inferred that the activation energy does not depend on the Pt loading of the catalyst.

Figures 6.2.1 - 6.24 show that there are good predictions between experimental and predicted conversions when the rate equations 3.1.25 and 3.1.27 were used.

III Methylcyclopentane (MCP)

Mechanistic rate equations for the reactions of MCP on Pt-containing catalysts were developed from the following reaction pathway.

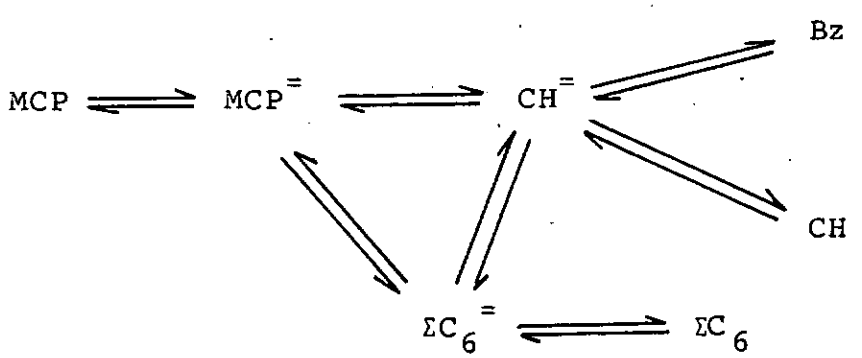

Eleven rate equations were developed and the rate constants evaluated using the method of Nelder and Mead[55]. Five out of the eleven equations gave reasonably good prediction of conversions obtained over Pt/Al_2O_3 catalysts. The rate and adsorption equilibrium constants plus the activation energies and preexponential factors obtained using equation (3.1.44) are presented in Tables 6.1.43 - 6.1.48. The activation energies obtained for the different initial guesses of constants and stepsizes ranged between 10-28kcal/gmole. When rate equation (3.1.46) was used, the activation energies obtained for the different initial guesses of constants and stepsizes ranged between 17-50kcal/gmole. (See Tables 6.1.49 - 6.1.52). With rate equation (3.1.48), the activation energies varied between 15-41kcal/gmole. (Tables 6.1.53 - 6.1.57). With rate equation (3.1.49), the activation energies varied between 16 and 34kcal/gmole, depending on the initial guesses of constants and stepsize used (Tables 6.1.58-6.1.62). When rate equation (3.1.50) was used, the activation energies for the different initial guesses and stepsizes ranged from 14 to 30 kcal/gmole except at initial guesses of constants 1, stepsize 5 where the activation energy obtained was 1.7kcal/gmole (See Tables 6.1.63- 6.1.66). Obviously, this is unacceptable as true activation energies are of the order of bond strenghts.

On $Pt-Re/Al_2O_3$ (DRIED) catalyst, however, only two out of the eleven rate equations predicted the conversion reasonably well with positive rate and adsorption equilibrium constants. One of the rate equations that satisfied the set criteria is the rate equation (3.1.48) at initial guesses of constants 5, stepsize 5 and initial guesses of constants 3, stepsize 3. The rate constants, activation energies and preexponential factors are shown in Table 6.1.72 for initial

guesses of constants 5, stepsize 5 and Table 6.1.73 for initial guesses of constants 3, stepsize 3. The rate constants, activation energies and preexponential factors obtained when equation (3.1.49) was used are shown in Table 6.1.74 and 6.1.75 for initial guesses 5, stepsize 1 and initial guesses 3 stepsize 1 respectively. The activation energy obtained for the rate limiting step, for the different initial guesses and stepsizes were 21.8 and 23.1 kcal/gmole, respectively for rate equation (3.1.48) while for rate equation (3.1.49) the activation energy for the rate determining step was 43.7 and 29.3kcal/gmole for initial guesses of constants 5, stepsize 1 and initial guesses of constants 3, stepsize 3.

It can be concluded from the values of the activation energies of the Pt/Al_2O_3 and $Pt\text{-}Re/Al_2O_3$ that the addition of rhenium to platinum did not affect the activation energy. Figures 6.1.8 and 6.1.9 show the predicted conversions obtained with Pt/Al_2O_3 using rate equations 3.1.44 and 3.1.46 respectively at initial guesses 5, stepsize 5. The figures show that the prediction of experimental conversion obtained using $Pt\text{-}Re/Al_2O_3$ (DRIED) [Figures 6.1.10 - 6.1.11] were not as good.

It can be observed that there are variations in the value of the rate constants, activation energies, adsorption equilibrium constants and preexponential factors obtained at different initial guesses and stepsizes using the same rate equation. This discrepancy might be inherent in the type of problem at hand. The problem we solved is a non-linear equation

capable of having many solutions. There exist in addition to the global minimum, localized minima. If a particular initial guess of constants and stepsize did not converge near the global minimum for all the activation energies and the heat of adsorption calculated therefrom, it is not unexpected that the located minimum might be far away from those obtained using the same equation but with different starting conditions.

7.3 Variable Activity Kinetics

In Chapter 6 Section 6.2, the variable activity modelling results were presented. Deactivation kinetic equations of the mechanistic type were developed (see Chapter 3 section 3.2) and used to evaluate the constants of deactivation. The first model used was based on the mechanism that the reactant is adsorbed in the same manner in the coking reaction as in the main reaction. In addition the adsorption on the catalyst surface of the substance that produces the deactivation is taken as the rate - limiting step (equation (3.2.17)).

$$\frac{P_m^{n+1}}{\Psi_{o1}(P_i,T)} = \frac{1}{k_d K_A} + \frac{K_A}{k_d K_m} P_A$$

The second model is based on the mechanism that the reactant is adsorbed in the same manner in the coking reaction as in the main reaction. In addition, the coke precusor formation is taken as the rate-limiting step (equation(3.2.26))

$$\frac{P_m^{n+1}}{\psi_{o1}(P_i,T)} = \frac{1}{k_d K_m'} + \frac{K_A}{k_d K_m'} + \frac{K_m''}{k_d K_m'} P_m^{n+1}$$

Linear and non linear least squares techniques were used to evaluate the deactivation parameters and discrimination among rival models was based on the positiveness of the values of the constants. The kinetic parameters obtained from variable reactant partial pressure show that the first model predicted the deactivation behavior of iso-octane and MCP on 0.3%Pt/Al_2O_3 catalyst between 400°C - 410°C for n=o. For n=0, the first model also predicted the deactivation behavior on Pt-Re/Al_2O_3 (DRIED) catalyst. The implication of n=0 is that some of the reactants are either very strongly adsorbed (poisons) or block the smaller pores of the catalyst. With 0.6%Pt/Al_2O_3 catalyst, however, the deactivation behavior was predicted only at n=1. At n=0, the second model could not be used to predict the deactivation of iso-octane on 0.3%Pt/Al_2O_3 at 410°C, the deactivation of MCP on Pt/Al_2O_3 at 400°C and the deactivation of Pt-Re/Al_2O_3 (DRIED) at 410°C. However, at n=1, the second model predicted the deactivation of iso-octane on 0.3%Pt/Al_2O_3 at 410°C and the deactivation of MCP on Pt/Al_2O_3 at 400°C. In this case, the adsorbed reactant interacted with a gas-phase molecule to form the coke precusor. Only MCP deactivation on Pt/Al_2O_3 at 400°C was predicted by the second model at n=2.

In contrast with the results obtained from variable iso-octane partial pressure, the deactivation kinetic parameters of iso-octane obtained from variable H_2 partial pressure

show that the first model did not predict the deactivation behavior of iso-octane at n=0. It can also be observed that generally the second model did not predict the deactivation behavior of iso-octane and MCP on the reforming catalysts investigated. The first model predicted the deactivation behavior of iso-octane on 0.3%Pt/Al_2O_3 catalyst between 390°C and 410°C at n=1 while the deactivation behavior at 430°C is predicted at n=2. Over 0.6%Pt/Al_2O_3 catalyst, however, the first model predicted the deactivation behavior only between 410°C - 430°C when n=2. The deactivation parameter obtained at 410°C were higher on 0.3%Pt/Al_2O_3. It can be inferred from the above result that deactivation is faster on 0.3% Pt/Al_2O_3 catalyst than on 0.6%Pt/Al_2O_3 catalyst. The deactivation parameters of MCP from variable H_2 partial pressure obtained on Pt/Al_2O_3 and $Pt-Re/Al_2O_3$ catalysts at n=1 show that the deactivation parameter k_dK_A is higher for Pt/Al_2O_3 catalyst. This result also suggested that $Pt-Re/Al_2O_3$ (DRIED) catalyst is more resistant to coking than the Pt/Al_2O_3 catalyst.

The following, therefore can be concluded:

(i) The deactivation behavior for variable iso-octane partial pressure on Pt/Al_2O_3 catalyst can be described by the two models developed when n=0.

(ii) The deactivation behavior for variable MCP partial pressure on Pt/Al_2O_3 and $Pt-Re/Al_2O_3$(DRIED) can be described by the two models at n=0.

(iii) The deactivation behavior of iso-octane for variable H_2 partial pressure on 0.3%Pt/Al_2O_3 can be described only by the first model at n=1.

(iv) The deactivation behavior of iso-octane for variable H_2 partial pressure on 0.6%Pt/Al_2O_3 catalyst can be described (between 410°C and 430°C)only by the first model at n=2.

(v) The 0.6%Pt/Al_2O_3 catalyst is more resistant to coking by iso-octane than the 0.3%Pt/Al_2O_3 catalyst.

(vi) Only the first model predicted the deactivation behavior of MCP on Pt/Al_2O_3 and Pt-Re/Al_2O_3(DRIED) catalysts.

(vii) The Pt-Re/Al_2O_3(DRIED) catalyst is more resistant to coking than the Pt/Al_2O_3 catalyst.

The results obtained from variable activity experiments show that Pt-Re/Al_2O_3(DRIED) catalyst is preferred to Pt/Al_2O_3 catalyst because of higher aromatic (benzene) yield and because it resists deactivation by coking better. These observation is in agreement with the work of Bertolacini et al[81]. Several theories have been proposed to explain the promotional effect of rhenium. The first theory assumes that a high melting point platinum - rhenium alloy is formed. The alloy is supposed to resist sintering or agglomeration of the active platinum sites and thus deactivation is lessened. Along similar lines a second theory proposed that rhenium in some way

modifies the alumina support so as to maximize the platinum surface area or to resist harmful coke laydown[97]. A third theory suggests that rhenium removes coke precusors or molecules that would eventually foul or block the active surface[97]. The fourth theory suggests that certain components in the feed are converted to coke precusors over the platinum catalyst. The precusors can further react over platinum to form coke and cause deactivation. However, with the addition of rhenium, the coke precusors are converted to harmless products. The coke precusor concentration is lowered and the rate of coke laydown on the platinum is reduced.

7.4 Catalyst Mortality Results

The results of catalyst mortality experiments show that the coking levels of the catalyst depends on the feed. The results obtained by this author shows that on 0.3%Pt/Al_2O_3 catalyst the coking levels of the reactants investigated are in the following order:

Iso - octane ∿ N-octane < MCP

Omoleye and Susu[97] studied the coking levels on fresh and spent Pt/Al_2O_3 reforming catalysts. They found out that the accelerated deactivation they used for the deactivation of the catalyst resulted in a state of Pt/Al_2O_3 catalyst mortality that is comparable to the spent catalyst that has been used in the reformer at the refinery.

Two stability states have been established with MCP reactant on a catalyst that has been used for iso-octane reactions. Results show that after a total of 64 regeneration cycles (24 cycles with iso-octane and 40 cycles with MCP) the catalyst was still active. Omoleye and Susu[95] stated that three stability states existed on the Pt/Al_2O_3 catalyst when cyclohexane was used as reactant. They inferred that each state leads irreversibly to the next and also irreversibly to the mortality state. The stability states are characterized by different coking levels. Only 26 deactivation - regeneration cycles were needed, however, for the catalyst to reach the mortal state. The time on stream during the deactivation process was different for the two reactants - the cyclohexane being much longer than the MCP. It is easily conceivable that more of the resistant coke (formed from primary coke) will result when the time on stream is longer and the mortal state will therefore be attained faster.

The concept of coke catalyzing the formation of more coke or assisting in the growth of a different type of coke has been shown to explain the coking phenomena during hydrocarbon pyrolysis to obtain olefins[98]. At the high temperatures of pyrolysis reactions, at least three major types of coke have been identified: filamentous, amorphous and graphitic coke[99]. These coke types and other subtypes identified by Albright and Tsai[98] occur between 773-1173k. Graphitic coke was found to be denser than amorphous coke and more slowly oxidised. Several investigators[100-104] have provided evidence that adsorbed carbon is an active reaction intermediate and a precusor to inactive forms of carbon. Mc Carty and Wise[101]

reported three types of carbon adsorbed on Ni surface after exposure to CO. Atomic or α carbon (C_α) was easily removed by H_2 at relatively low temperatures while β-carbon (C_β) which is polymerized or amorphous coke is formed at significantly higher temperature and was about 1/100 as active towards H_2. The third type of coke is the graphitic type and is formed by high temperature conversion of C_β. The slow conversion of C_α - C_β occurs above 600k. McCarty and Wise[104] also reported that C_β is gasified at high rate on nickel at 723k and 1atm.

The deactivation of the reforming catalyst with n-octane, iso-octane and MCP is very fast suggestive of pore mouth blockage. The activity of the catalyst (Pt/Al_2O_3 or $Pt-Re/Al_2O_3$) is very low after 15min. This is in contrast with the work of Omoleye[52] who found the activity of Pt/Al_2O_3 catalyst to be high after 60min with cyclohexane. The mechanism of coking in his work is probably due to site blockage. This probably explains why Omoleye was able to observe the differences in reaction time during deactivation at the different stability states.

The beneficial effect of rhenium addition is apparent during the catalyst mortality experiments with Pt/Al_2O_3 and $Pt-Re/Al_2O_3$(DRIED) catalysts. The total conversion and also benzene yield were higher on $Pt-Re/Al_2O_3$(DRIED). The drop in benzene yield with regeneration cycle was less with $Pt-Re/Al_2O_3$ (DRIED) than with Pt/Al_2O_3.

The Pt-Re/Al_2O_3(DRIED) was better than the Pt-Re/Al_2O_3 (UNDRIED) which behaved more or less like the Pt/Al_2O_3 after the first regeneration. This shows the importance of catalyst pretreatment on the performance of the catalyst. The poor performance of the Pt-Re/Al_2O_3(UNDRIED) catalyst was reported by Omoleye[52] in his work on the mortality of mono - and bimetallic reforming catalysts. He reported that the presence of rhenium in the fresh bimetallic Pt-Re/Al_2O_3 catalyst prolonged the lifetime of the catalyst beyond that of the fresh Pt/Al_2O_3. He also reported that the presence of rhenium has an adverse effect on the stability of regenerated Pt-Re/Al_2O_3 (UNDRIED) in an inert atmosphere. He suggested that the formation of coke is catalyzed by the segregated unreduced oxides of rhenium in the catalyst.

Isaacs and Petersen[79] examined the effect of catalyst pretreatment on reduced Pt-Re/Al_2O_3 catalysts. Their results indicated significant alloy formation in reduced Pt-Re/Al_2O_3 for all drying temperatures of 500°C or less. While the surface amount of alloyed Pt-Re is insensitive to the drying temperature, the surface amount of unalloyed Re varies significantly with the drying temperature. They found that reduction of the Pt-Re/Al_2O_3 catalyst dried at 100°C which contains no unalloyed rhenium is complete after 1h of 500°C reduction. Their results also showed that reduction of the Pt-Re/Al_2O_3 catalyst dried at 500°C, which does contain unalloyed Re, is not complete until after 15h of 500°C H_2 reduction. From the work of Isaacs and Petersen[79] it can be inferred that the undried Pt-Re/Al_2O_3 catalyst do contain much unalloyed rhenium oxide which according to Omoleye[52] catalyses coke formation.

CHAPTER 8

C O N C L U S I O N S

The reactivity of n-octane, iso-octane and MCP was studied on constant and variable activity reforming catalysts. From the results of these studies, the following conclusions can be made:

1. The products of dehydrocyclization reactions of n-octane on bifunctional Pt/Al_2O_3 catalyst are hydrocracked products, iso-octane, ethylbenzene, toluene, m- , p- and 0-xylene.

2. The sole product of iso-octane (2,2,4 trimethyl-pentane) reaction on 0.3%Pt/Al_2O_3 and 0.6%Pt/Al_2O_3 catalyst at temperatures between 390°C and 430°C is another isomer of n-octane (1,1,3 trimethyl-pentane).

3. The products of methylcyclopentane (MCP) reactions on Pt/Al_2O_3 and $Pt-Re/Al_2O_3$ catalyst are: hydro-genolysis products (2-methylpentane, 3methylpentane, n-hexane), cyclohexane and benzene.

4. The production of aromatics generally increases with increase in temperature, W/F and decrease in reactant partial pressure.

5. Five out of the nineteen rate equations developed for the dehydrocyclization of n-octane on bifunc-tional Pt/Al_2O_3 catalyst were found to predict the

experimental conversion and also gave positive values for the rate and equilibrium constants.

6. Two out of the three rival models developed for the isomerization reaction of iso-octane predicted the experimental conversion data with positive values for the rate and equilibrium constants.

7. Five out of eleven rate equations developed for the MCP reaction predicted the experimental conversion data and gave positive values for the rate and equilibrium constants.

8. The order of optimum P_{H_2} for reactions of n-octane on bifunctional Pt/Al_2O_3 catalyst was found to occur as follows:
Iso-octane > Dehydrocyclized products > Hydrocracked products.

9. The 0.6%Pt/Al_2O_3 catalyst is more resistant to coking by iso-octane than the 0.3%Pt/Al_2O_3 catalyst.

10. The Pt-Re/Al_2O_3(DRIED) catalyst is more resistant to coking than the Pt/Al_2O_3 catalyst.

11. The MCP coking level was highest for the reactants investigated. The order of coking on the Pt/Al_2O_3 catalyst was given by Iso-octane ∿ N-octane < MCP.

12. At least two stability states exists in the life time of the monometallic Pt/Al_2O_3 catalyst. The two states were clearly shown in the coking level obtained during the mortality study of Pt/Al_2O_3 catalyst using MCP as model reforming reactant. In the first state (cycles 1 - 5) the coke level was about 0.045g while in the second stability state (cycles 6 - 40) the coke level was about 0.09 gC.

REFERENCES

1. Ako, C.T.; Susu,A.A.: "N-Octane dehydrocyclization on monofunctional and bifunctional Pt/Al_2O_3 catalyst". J.Chem. Tech. Biotechnol.,36, 519 - 526 (1986)

2. Pines,H.; Noguiera,L.: "Aromatization of heptanes, ethylcyclopentane and cycloheptane over "non-acidic" platinum-alumina catalyst. Comparison of the mechanisms of aromatization over chromia - alumina and over platinum-alumina catalysts". J.Catal. 70, 391-403 (1981).

3. Noguiera,L. ;Pines,H.: "Aromatization of [1 - ^{14}C] heptane over 'non-acidic' platinum-alumina catalyst" J.Catal.,70, 404-408 (1981).

4. Davis,B.H.: "Dehydrocyclization of Paraffins Aromatic distribution from paraffins and naphthenes containing a quaternary carbon". J.Catal., 23, 340-354 (1971).

5. Davis,B.H.: "Dehydrocyclization of paraffins: Influence of chlorine on cyclization pathway over Pt-Al_2O_3 catalysts". J. Catal., 23, 355-357 (1971)

6. Paal,Z.; Tetenyi,P. "Investigation of dehydrocyclization on metal catalysts, 11.
Aromatization of hexanes on carrier free nickel and platinum catalysts".
Acta. Chim. Acad. Sci. Hung.,53(2), 193-204 (1967).

7. Paal,Z.; Tetenyi,P.: "Investigation of dehydrocyclization of metal catalysts, III; Dehydrocyclization of n-hexane". Acta. Chim. Acad. Sci. Hung, 54(2), 175-188 (1967).

8. Davis,B.H.: "Carbon-14 tracer study of the dehydrocyclization of n-heptane over Pt on non-acidic alumina". J.Catal., 29, 398-403 (1973).

9. Davis,B.H.; Venuto, P.B.: "Paraffin Dehydrocyclization. Distribution of aromatic products obtained with "non-acidic" supported Pt catalysts".
J.Catal., 15, 363 - 372 (1969).

10. Rohrer,J.C.; Hurwitz,H.; Sinfelt, J.C.: "Kinetics of the catalystic dehydrocyclization of n-heptane".
J.Phys. Chem., 65,1458-1460 (1961).

11. Christoffel,E.G.; Paal,Z.: "Activity and selectivity of bifunctional platinum catalysts in hydrocarbon reactions".
J.Catal.,73, 30-44(1982).

12. Paal,Z.; Tetenyi,P.: "The mechanism of aromatization on platinum - black catalyst. Dehydrocyclization of hexadienes and hexatrienes".
J.Catal. , 30, 350-361 (1973).

13. Pines, H.: "The chemistry of catalytic hydrocarbon conversions".
Academic Press New York, 1981.

14. Brouwer,D.M.; Hogeveen,H.: "Electrophilic substitutions at alkanes and in alkylcarbonium ions".
Prog. Phys. Org. Chem., 94, 179-240 (1972).

15. Sinfelt,J.H.: "Bifunctional Catalysis"
Advances in Chem. Eng., 5, 37-74 (1964).

16. Muller,J.M.; Gault,F.G.: "Mechanisms of dehydrocyclization on platinum and palladium catalysts".
J. Catal. 24, 361-365 (1972).

17. Maire,G.; Plouidy,G.; Prudhomme,J.C.; Gault,F.C.: "The mechanism of hydrogenolysis and isomerization of hydrocarbon on metals, I. Hydrogenolysis of cyclic hydrocarbons".
J.Catal., 4, 556-569 (1965)

18. Barron,Y.; Maire,G.; Muller,J.M.; Gault,F.G.: "The mechanism of hydrogenolysis and isomerization of hydrocarbons on acids II. Mechanisms of isomerization of hexanes on platinum catalysts".
J. Catal., 5, 428-446 (1966)

19. Delmon,B. "Characterization of catalyst deactivation. Industrial and laboratory time scales".
Applied Catalysis, 15, 1-16 (1985)

20. Wolf,E.E.; Alfani,F.: "Catalyst deactivation by coking"
Catal. Revs. Sci. Eng., 24(3), 329-371 (1982).

21. Menon,P.G.; Prasad,J. in "Proceedings, 6th international congress on catalysis, London, 1976", (G.C.Bond, P.B. Wells, and F.C. Tompkins, Eds.), paper B45. The Chemical Society London, 1977.

22. Davis,B.H.; Westfall,G.A.; Naylor,R.W.: "Paraffin Dehydrocyclization V. The influence of Pt loading on the aromatic selectivity"
J. Catal., 42, 238-246 (1976).

23. Davis,B.H., Westfall,G.A., Watkin,J.; Pezzanite,J.Jr.: "Paraffin Dehydrocyclization VI.
The influence of metal and gaseous promoters on the aromatic selectivity".
J.Catal., 42, 247-256 (1976)

24. Davis,B.H.: "Paraffin Dehydrocyclization VII.
Comparison of aromatic distribution from n-octane conversion over Pt at atmospheric and 200Psig."
J.Catal. , 42, 376-380 (1976).

25. Lester,G.R.: "Different mechanisms of aromatization of trimethylpentanes over chromia - alumina and platinum - alumina catalysts"
J. Catal., 13, 187-192 (1969)

26. Dautzenberg,F.M.; Platteeuw,J.C.: "Isomerization and dehydrocyclization of hexanes over monofunctional supported platinum catalysts".
J.Catal. 19, 41-48 (1970)

27. Ako,C.T.: "Kinetic analysis of C_8 dehydrocyclization reactions on mono- and bifunctional platinum-alumina catalyst."
Ph.D thesis, University of Lagos (1984).

28. Sinfelt,J.H.; Hurwitz,H.; Rohrer,J.C.: "Kinetics of n-pentane isomerization over Pt-Al_2O_3 catalyst".
J. Phys, Chem. 64, 892 - 894 (1960).

29. Keulemans,A.I.M.; Voge,H.H.: "Reactivities of naphthenes over a platinum reforming catalyst by a gas chromatographic technique".
J. Phys. Chem. 63, 476-480 (1959)

30. Starnes,W.C.; Zabor,R.C.: Symp. div. of petrol chem. of the Am. Chem. Soc.; Boston, Massachusetts, April 5-10, 1959.

31. Keulemans,A.I.M.; Schuit,G.C.A.: "The mechanism of heterogenous catalysis", Elsevier, Amsterdam, 1960.

32. Hosten,L.H.; Froment,G.H.: "Isomerization of n-pentane"
Ind. Eng. Chem. Proc. Des. Dev.; 10(2) 280-287 (1971)

33. Jossens,L.H.; Petersen,E.E.: "Fouling of a platinum - rhenium reforming catalysts using model reforming reactions".
J. Catal., 26, 265-276 (1982)

34. Dartigues,J.M.; Chambellam,A.; Gault,F.G., J.Am. Chem. Soc., 98, 856, 1978.

35. De Jougste,H.C.; Ponec,V.; Gault,F.G.: "Influence of alloying Pt with Cu on the reaction mechanisms of hydrocarbon reforming reactions".
J. Catal., 63, 395-403 (1980)

36. Smith,R.L.; Naro,P.A.; Silvestri,A.J.: "Reaction paths for decyclization of methylcyclopentane over Pt/Al_2O_3 catalyst"
J.Catal.,20, 359-366 (1971)

37. Cusumano,J.A.; Dembinski,G.W.; Sinfelt,J.H.: "
"Chemisorption and catalytic properties of supported platinum"
J. Catal., 5, 471-479 (1966)

38. Maatman,R.W.; Mahaffy,P., Hoekstra,P.; Addink,C.: "The preparation of Pt-Alumina Catalyst and its role in cyclohexane dehydrogenation"
J. Catal., 23, 105 - 117 (1971)

39. Paal,Z.; Tetenyi,P.: "Investigation of dehydrocyclization on metal catalysts IV. Parallelism of the dehydrogenation of cyclohexane and dehydrocyclization"
Acta Chim. Acad. Sci. 55(3) 273-286 (1968)

40. Paal,Z.; Rozengart,I.: "Changes in the dehydrocyclizing activity of nickel catalysts during use".
Acta. Chim. Acad. Sci. Hung.54(3-4) 287-293 (1967)

41. Donnis,B.B.: "Platinum - Alumina catalysts in reforming methylcyclopentane".
Ind. Eng. Pro. Des. Dev.15(4), 254-258 (1976)

42. Hindin S.G.; Weller,S.W.; Mills, G.A.: "Mechanically mixed dual function catalysts".
J. Phys. Chem., 62, 244-245 (1958)

43. Kramer,R.; Zuegg,H.: "The hydrogenolysis of methylcyclopentane on platinum model catalysts: Particle size effects due to a reaction occuring at the phase boundary metal support".
J. Catal., 80, 446 - 456 (1983)

44. Barron,Y.; Maire,G.; Muller,J.M.; Gault,F.G.: "The mechanism of hydrogenolysis and isomerization of hydrocarbons on metals II. Mechanisms of isomerization of hexanes on platinum catalysts".
J. Catal. 5, 428-446 (1966)

45. Maire,G.; Corolleur,C.; Juttard,D.; Gault,F,G.
"Comments on a dispersion effect in hydrogenolysis of methylcyclopentane and isomerization of hexanes over supported platinum catalysts".
J. Catal. 21, 250-253 (1971)

46. Bragin,O.V.; Karpinski,Z.; Matusek,K.; Paal,Z.;Tetenyi,P.
"Comparative study of various platinum catalyst in skeletal reactions of C_6 hydrocarbons."
J. Catal. 56, 219-228 (1978)

47. Glassl,H.; Hayek,K.; Kramer,R.: "Electron microscopy of Pt/Al_2O_3 model catalysts.III. The hydrogenolysis of methylcyclopentane as a function of particle size".
J. Catal., 68, 397-405 (1981)

48. Gault,F.G. in "Advances in Catalysis and Related Subjects", Vol. 30, P.I. Academic Press, New York, London, 1981.

49. Cooper,B.J.; Trimm,D.L. in Catalyst Deactivation (Delmon,B.; Froment,G.F. (Eds))."The coking of Pt/Al_2O_3 reforming catalysts". Elsevier Scientific Publishing Co., Amsterdam P63-71, 1980.

50. Corella,J.; Asua,J.M.: "Kinetics of deactivation of a solid catalyst in a nonsimple reaction. Isobutene oxidation in gaseous phase by a parallel reaction network"
Ind. Eng. Chem. Pro. Des. Dev. 21, 551-558 (1982)

51. Froment,G.F.: Proc. VI Internat. Congress on Catal.1, 10-13, (1976).

52. Omoleye,J.A.: "Mortality of mono-and bimetallic reforming catalysts and the existence of stability states.Ph.D thesis, University of Lagos, 1987

53. Hougen,O.A.; Watson,K.M.: "Chemical Process Principles", Vol.III, Wiley, New York (1947)

54. Froment,G.F.: "Model discrimination and parameter estimation in heterogenous catalysis".
A.I. Ch.E. J. 21, 1041-1057 (1975)

55. Nelder,J.A.; Mead, R.: "A simplex method for function minimization"
Computer J., 7, 308-313 (1965)

56. Himmelblau,D.M. "Applied Nonlinear Programming"
McGraw-Hill, Inc., New - York, PP 190-217, 1982

57. Lewis,M.J.; Wills,G.B.: "Estimation of nonlinear kinetic parameters for propylene disproportionation"
J. Catal., 20, 182-189 (1971)

58. Rossini,R.D.; Pitzer,K.S.; Arnett,R.L.; Braun,R.M.; Pimentel,G.C.: "Selected values of physical and thermodynamic properties of hydrocarbons and related compounds"
A.P.I. Research Project 44, Carnegie Press, Pittsburg, Pa., 1953.

59. Butt,J.B. :"Analysis of non-selective poisoning. Reaction selectivity and reactor performance in some nontrivial polyfunctional systems".
Chem. Eng. Sci., 25, 801 - 808 (1970)

60. Butt,J.B.; Wachter,C.K.; Billimor,R.M.: "Separability of catalytic deactivation kinetics".
Chem. Eng. Sci. 33(10), 1321-1329 (1978)

61. Sinfelt,J.H.; Rohrer,J.C.: "Kinetics of the catalytic isomerization dehydroisomerization of methylcyclopentane"
J. Phys. Chem. 65, 978-981 (1961)

62. Hegedus,L.L.; McCabe,R.W. in Delmon,B. and Froment,G.F. (Eds). "Catalyst Poisoning". Catalyst Deactivation. Elsevier Scientific publishing Company, Amsterdam p471-505, 1980

63. Froment,G.F. in Delmon, B. and Froment, G.F. (Eds). "A quantitative approach of catalyst deactivation by coke formation ". Catalyst Deactivation. Elsevier Scientific Publishing Company, Amsterdam, p1-19 (1980)

64. Voorhies,A. Jr.: "Carbon formation in catalytic cracking"
Ind. Eng. Chem., 37, 318-322 (1945).

65. Eberly, P.E.; Kimberli, C.N.; Miller,W.H.; Drushel,V.H. "Coke formation on silica-alumina cracking catalysts". Ind. Eng. Chem. Proc. Des. Dev. 5, 193 (1966)

66. Dumez,F.J.; Froment,G.F.: "Dehydrogenation of 1-butene into butadiene - kinetics, catalyst coking, and reactor design"
Ind. Eng. Chem. Proc. Des. Dev. 15(2), 291-301 (1976)

67. Levenspiel,O.: "Experimental search for simple rate equation to describe deactivating porous catalyst particles".
J.Catal., 25, 265-272 (1972)

68. Corella,J.; Asua, J.M.: "Kinetic equations of mechanistic type with nonseparable variables for catalyst deactivation by coke. Models and data analysis methods".
Ind. Eng. Chem. Proc. Des. Dev.,21, 55-61 (1982

69. Barbier,J.; Marecott,P.; Martin, N.; Elassal; Maurel,R. in Delmon,B. and Froment,G.F.(Eds). :"Selective poisoning by coke formation on Pt/Al_2O_3". Catalyst Deactivation. Elsevier Scientific Publishing Company, Amsterdam p53-62 (1980)

70. Tarman,M.; Kriz,J.F. in Delmon,B. and Froment,G.F.(Eds). "Some effects of catalyst composition on deactivation and coke formation when hydrocracking Athabasca bitumen". Catalyst Deactivation. Elsevier Scientific Publishing Company, Amsterdam, p 283-293 (1980)

71. Trimm, D.L.: Catal. Revs. Sci. Eng. 16(2), 155-189 (1977)

72. John,T.M.; Pachovsky,R.A.; Wojiechowski,B.W.: "Coke and deactivation in catalytic cracking"
Adv. Chem. Sci., 133, 422-430 (1974).

73. Lanhorst,P.P.; De Jougste, H.C.; Ponec,V. in Delmon,B and Froment, G.F.(Eds). "Particle size and carbon deposition effects in the hexane reforming reactions". Catalyst Deactivation. Elsevier Scientific Publishing Company, p43-52 (1980).

74. Bolivar,H.; Charcosset,R.; Frety,M.; Primet,L.; Tournayan, C.; Betizeau,G.; Lectercq; Maurel,R. "Platinum - rhenium/alumina catalysts. I. Investigation of reduction by hydrogen". J. Catal.,39, 249-259 (1975)

75. Freel,M.: Preprints of Div. Pet. Chem., Am. Chem. Soc. Dallas Mtg.; April, 8-13, 1974. Cited by Isaacs,B.H.; Petersen,E.E. Surface area measurement of platinum/ rhenium/alumina.I. Stoichiometry of hydrogen-oxygen chemisorptions and titrations J.Catal.,85, 1-7 (1984)

76. Betizeau,C.; Leclercq,G.;Maurel,R.; Bolivar,C.; Charcosset,H.; Frety,R.; Tournayan,L.: "Platinum-rhenium-alumina catalyst. III. catalytic properties" J. Catal., 179-188 (1976)

77. Bolivar,C.; Charcosset,H.; Frety,R.;Tournayan,L.; Proc. 5th Ibero-Amer. Sympo. Catal. 2, 188 (1970)

78. Jossens,L.W.: Ph.D thesis, University of California at Berkely (1981).

79. Isaacs,B.H.; Petersen,E.E.: "Surface area measurement of platinum/rhenium/alumina. II. Effect of catalyst pretreatment" J. Catal. 85, 8-15 (1984)

80. Dowell,D.A.: Chem. Soc. Spec. Publ. Catalysis 2, 1-27, 1978.

81. Bertolacini,R.J.; Pellet,R.J. in Delmon, B. and Froment, G.F.(Eds)." The function of rhenium in bimetallic reforming catalysis". Catalyst Deactivation. Elsevier Scientific Publishing Company, Amsterdam, P1-19 (1980)

82. Perry,R.H.; Chilton,C.H. (Eds). Chemical Engineer's Handbook. Fifth Edition. McGraw Hill Books.

83. Paal,Z.; Dobrovolszky,M.; Tetenyi, P.: "Transformations of 3-methylpentane and 3-methylpentenes over platinum black catalysts" J. Catal. 45, 189-197 (1976)

84. Sinfelt,J.H.: "Catalytic reforming of hydrocarbons" in Catalysis Science and Technology Vol.I (Anderson,J.R.; Boudart,M.Eds) p257-300, 1981.

85. Paal,Z.; Menon,P.G.: "Hydrogen effects in metal catalysts" Catal. Rev.- Sci. Eng. 25, 229-324 (1983)

86. Paal,Z.: "Metal catalyzed cyclization reactions of hydrocarbons". Adv. Catal., 29, 273-334 (1980)

87. Paal,Z.; Szekely,G.; Tetenyi,P.: "Thermodynamics and kinetic effects in platinum catalyzed n-hexane transformations"
J. Catal.,73, 30-44 (1982)

88. Biloen,P.; Helle,J.N.; Verbeek,H,; Dautzenberg,F,M.; Sachtler,W.M.H.
"The role of rhenium and sulfur in platinum-based hydrocarbon-conversion catalysts"
J. Catal. 63, 112-121 (1980)

89. Brandenberger,S.G.; Callender,W.L.; Meerbott,W,K.
"Mechanism of methylcyclopentane ring opening over platinum - alumina catalysts"
J. Catal. 42, 282-287 (1976)

90. Usov,Y.N.; Zubanova,L.G.; Kuvshino,N.I.: "Kinetics of dehydrogenating cyclohexane over an alumino-platinum catalyst under pulsed conditions".
Intn. Chem. Engr. 14(2), 222-228 (1974)

91. Susu,A.A.; Enoh,F.E.; Ogunye,A.F.: "Cyclohexane dehydrogenation kinetics on a platinum - rhenium/alumina oxide catalyst with hydrogen and inert diluents".
J. Chem. Tech. Biotechnol. 30, 735-747 (1980)

92. Gault,F.G.; Amirebra, V.; Garin,F.; Parayre,P; Weisang,F.
"Skeletal rearrangement of hydrocarbons on metals".
Bult. Soc. Chim. Belg. 88(7-8), 475-495 (1979)

93. Van-Hardeveld,R.: Hartog,F.: "Statistics of surface atoms and surface sites on metal crystals".
Surf. Sci., 15, 189-197 (1969)

94. Burtron,J.J. in Catalysis Reviews (H. Hienemann and J.J. Carberry, Eds), Vol. 9, P 209, Dekker New York 1974.

95. Moraweck,B.; Glugnet,G.; Renouprez,A.J.: "Contraction and relaxation of interatomic distances in small platinum particles from extended x-ray adsorption fine structure (EXAFS) spectroscopy".
Surf. Sci., 81(2),L631 - L634 (1979)

96. Gordon,M,B.; Cyrot-Lackmann,F.; Desjonqueres,M.
"Influence of size and roughness on electronic structure of transition metal surfaces"
Surf. Sci. 68(1), 359 - 367 (1977)

97. Omoleye,J.A.; Susu,A.A.: "Reforming Catalyst Mortality. I. Coking levels on fresh and spent Pt/Al_2O_3 "
N.S.Ch.E. J., Vol.5 No.2, 24-29 (1986)

98. Albright,L.F.; Tsai,T.C. in Albright,L.F.; Crynes,B.L. and Corcocan,W.A. (Eds) Pyrolysis.
Theory and Industrial Practice, Academic Press, New York 1983 , P 233-254.

99. Baker R.T.K.; Harris, P.S.:
Chem. Phys. Carbon 14, 83 (1978).

100. Araki,M.; Ponec,V.: "Methanation of carbon monoxide on nickel and nickel copper alloys".
J. Catal., 44,439-448 (1976)

101. Mc Carty,J.A.; Wise,H.: "Hydrogenation of surface carbon on alumina - supported nickel"
J. Catal. 57(3), 406-416 (1979)

102. Ponec,V.: "Some aspects of mechanism of methanation and Fischer - Tropsch synthesis".
Catal. Rev., 18(1), 151 - 171 (1978)

103. Cardner,D.C.; Bartholomew,C.H.: "Kinetics of carbon deposition during methanation of CO."
Ind. Eng. Prod. Res. Dev., 20(1), 80-87 (1981)

104. Moeller,A.D.; Bartholomew,C.H.: "Deactivation by carbon of nickel, nickel - ruthenium, and nickel - molybdenium methanation catalysts".
Ind. Eng. Prod. Res. Dev., 21(3), 390-397 (1982)

105. Corolleur,G.; Gault,F.G.; Juttard,D.; Maire,G.; Muller,J.M. "Effect of the metal particle size in supported catalysts on the selectivity and the reaction mechanisms".
J. Catal., 27, 466-468 (1972)

106. O'cinneide,A.; Gault,F.G.: "Reactions of hexanes. Unlabeled and labeled with ^{13}C, on alumina - supported palladium - gold and platinum - gold alloys".
J. Catal., 37, 311 - 323 (1975)

107. Anderson,J.R.; Avery, N.R.: "The isomerization of aliphatic hydrocarbons over evaporated films of platinum and palladium".
J. Catal. 5, 446 - 463 (1966).

APPENDIX A

Table A.1

Vapour Pressure of Normal Octane Versus Temperature

Vapour Pressure (mmHg)	Temperature [°C]
1	-14
5	+ 8.3
10	19.2
20	31.5
40	45.1
60	53.8
100	65.7

From the above data, a plot of vapour pressure versus temperature is shown in Fig.A.1.

The graph enables us to find the vapour pressure of N-octane for the temperatures of interest during each experimental run. From the vapor pressure and the knowledge of the total pressure of the system, the partial pressure of the gas bubbled through the saturator at a particular temperature can be determined.

Table A.2

Vapour Pressure of Iso Octane (2,2,4 Trimethyl Pentane) Versus Temperature[82]

Vapour Pressure (mmHg)	Temperature (°C)
1	-36.5
5	- 15
10	- 4.3
20	7.5
40	20.7
60	29.1
100	40.7

From the above data, a plot of vapor pressure versus temperature is shown in Fig.A2.

The graph enables us to find the vapor pressure of iso-octane for the temperature of interest during each experimental run. From the vapor pressure and the knowledge of the total pressure of the system, the partial pressure of the gas bubbled through the saturator at a particular temperature can be determined.

Table A.3

Vapour Pressure of MCP Versus Temperature[82]

Vapour Pressure (mmHg)	Temperature (°C)
1	-53.7
5	-33.8
10	-23.7
20	-12.8
40	- 6.0
60	+ 7.2
100	19.9
200	34.0

From the above data, a plot of Vapor pressure versus temperature is shown in Fig.A3.

The graph enables us to find the vapor pressure of MCP for the temperatures of interest during each experimental run. From the vapor pressure and the knowledge of the total pressure of the system, the partial pressure of the gas bubbled through the saturator at a particular temperature can be determined.

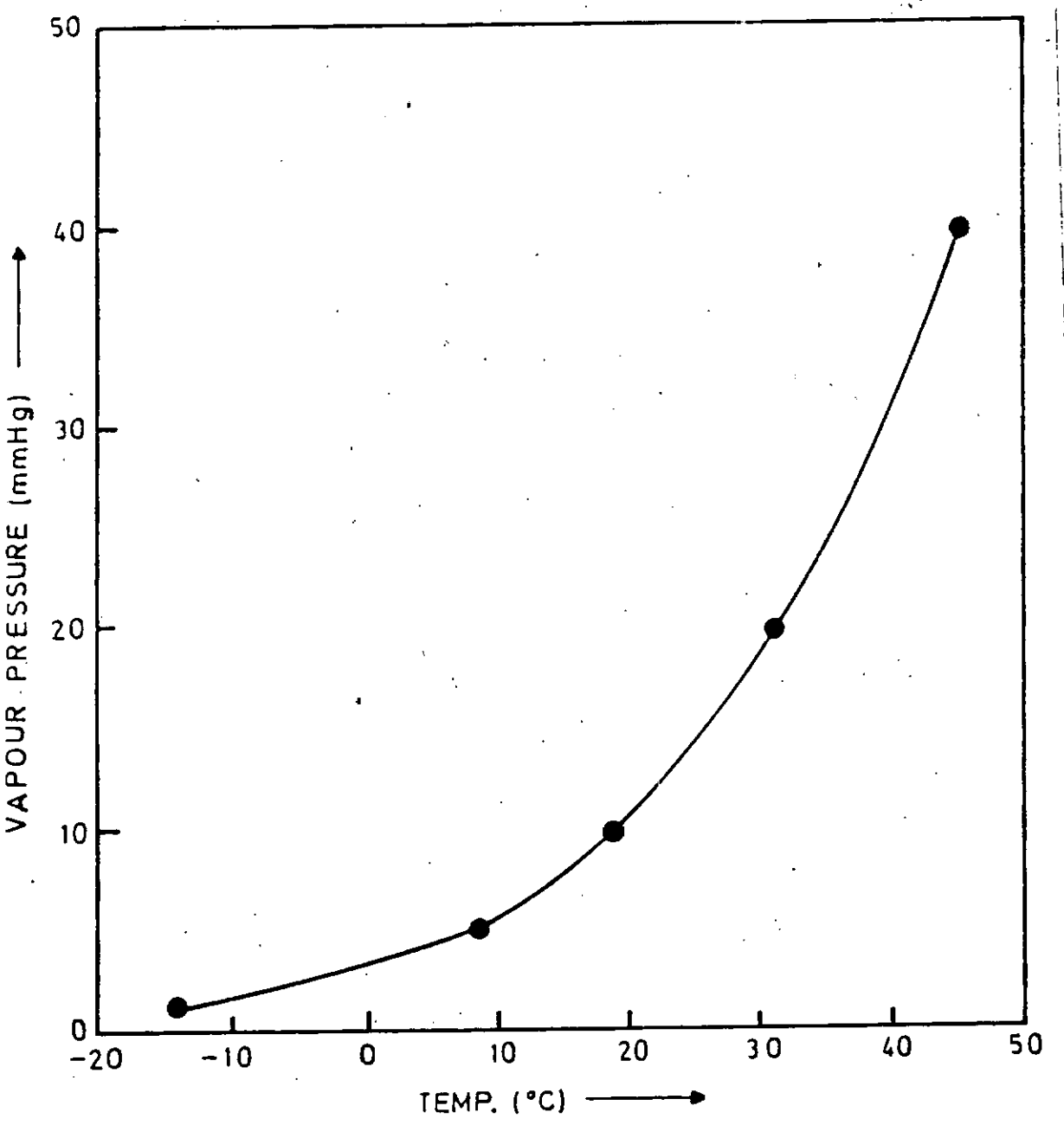

Fig. A.1: Vapor Pressure of n-octane versus temperature.

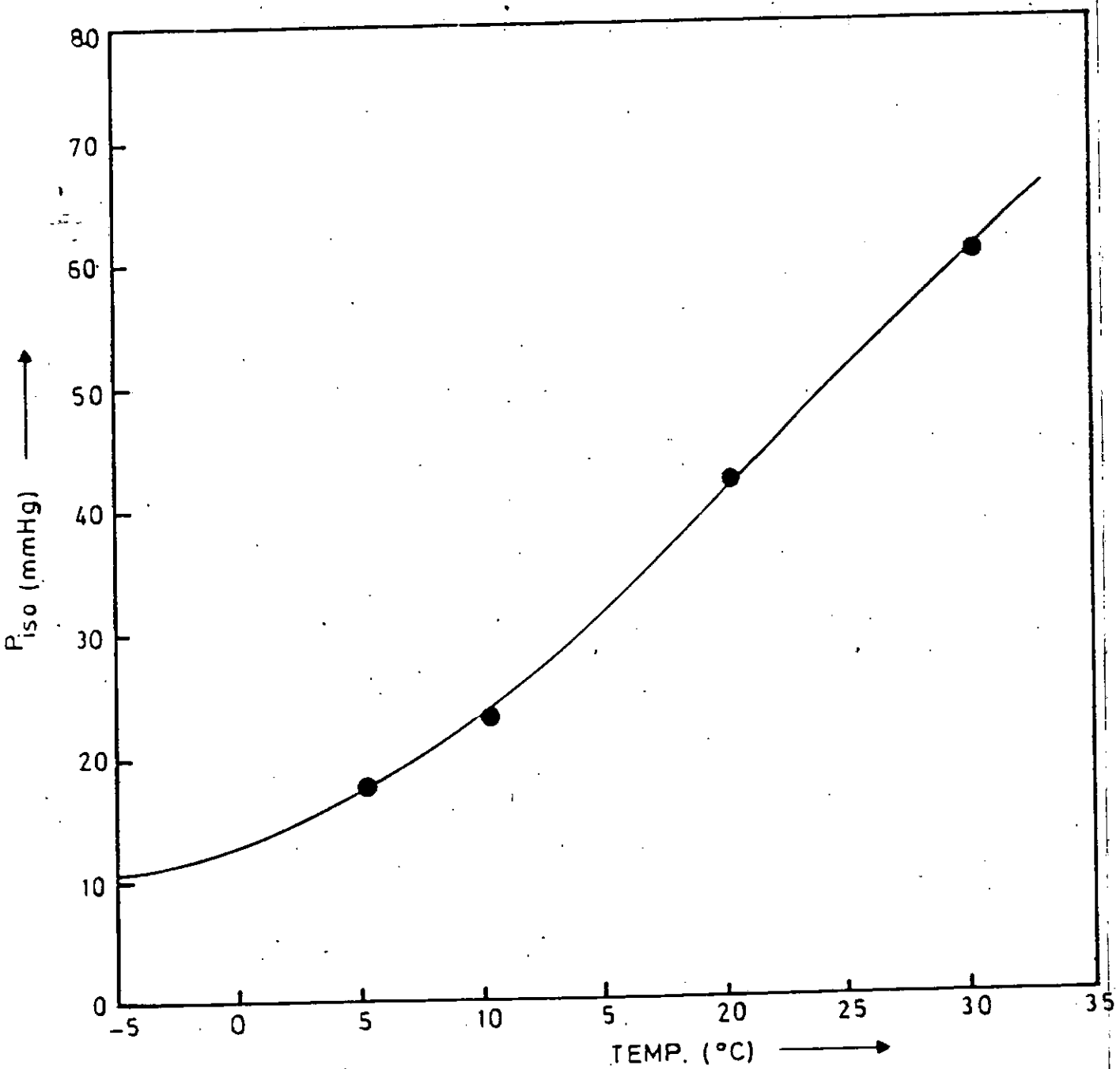

Fig. A.2: Vapor pressure of iso-octane versus temperature.

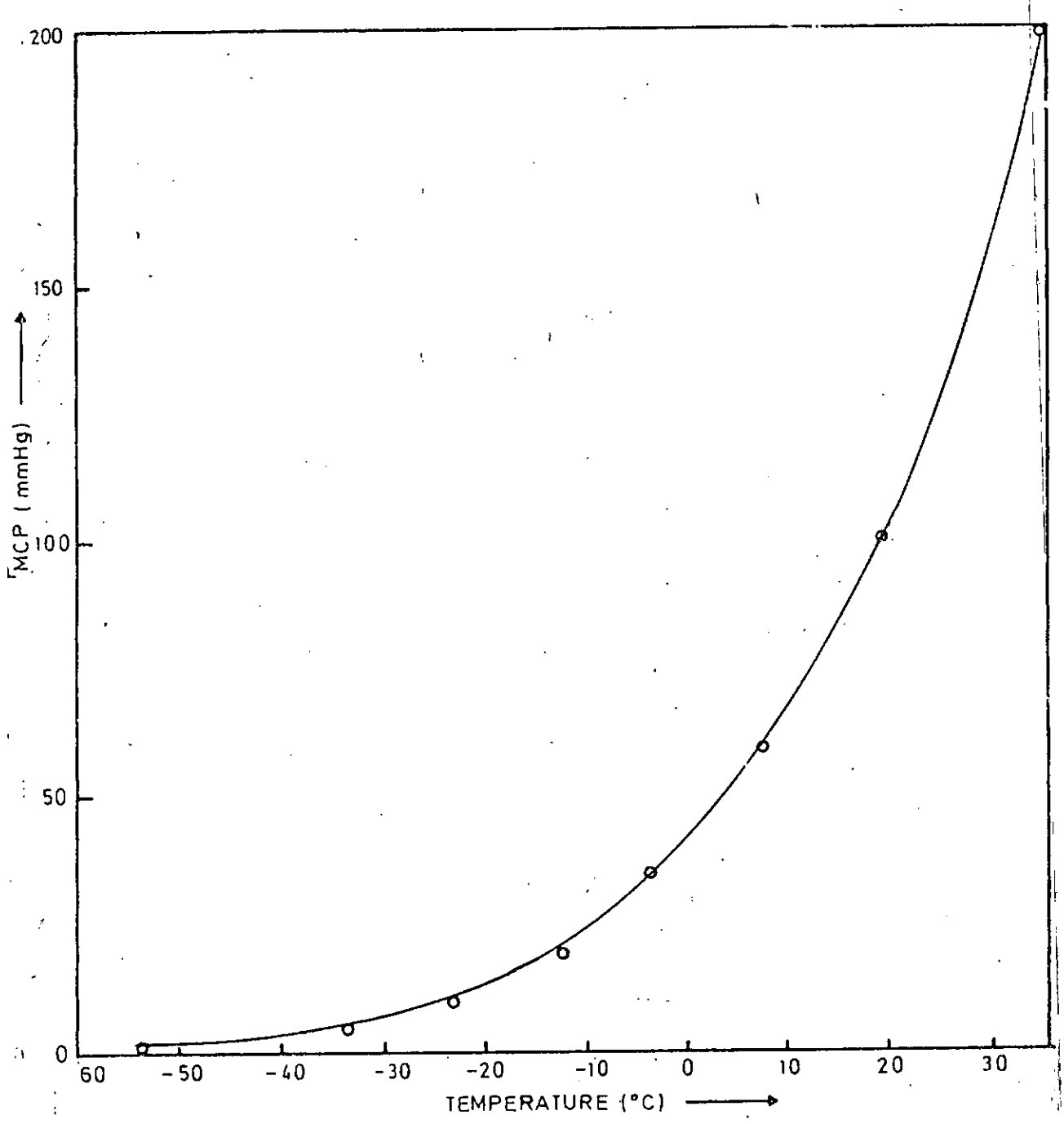

Fig. A.3: Vapor pressure of MCP versus temperature.

APPENDIX B

Table B.1

Calibration of Chromatograph for Products of n-Octane reactions. Weight Fractions of Compounds

SAMPLE	1	2	3	4	5	7	8	9	10	11	12	13	14
Iso Octane	0.0863	0.053	0.0516	0.0492	0.052	0.398	0.799	0.2	0.0518	0.2	0.2	0.1	0.0514
Normal Octane	0.086	0.0502	0.101	0.095	0.0525	0.398	0.052	0.596	0.798	0.1966	0.197	0.102	0.0536
Ethyl Benzene	0.2186	0.0487	0.40	0.57	0.796	0.101	0.0492	0.0502	0.0498	0.199	0.1	0.1	0.0484
Para. Xylene	0.5212	0.8013	0.3971	0.19	0.0496	0.0502	0.0487	0.1014	0.0498	0.2035	0.102	0.1	0.518
Ortho Xylene	0.0876	0.0503	0.0498	0.0955	0.0497	0.0522	0.0507	0.052	0.051	0.2	0.399	0.595	0.795

Table B.2

Calibration of Chromatograph for Products of n-octane reactions. Area fractions from chromatograph

SAMPLES	1	2	3	4	5	6	7	8	9	10	11	12	13	14
Iso Octane	0.1032	0.058	0.0571	0.0517	0.0413	0.611	0.366	0.76	0.234	0.0477	0.251	0.247	0.13	0.0558
Normal Octane	0.106	0.048	0.103	0.1033	0.0467	0.184	0.428	0.0673	0.624	0.84	0.218	0.197	0.115	0.041
Ethyl Benzene	0.222	0.049	0.415	0.58	0.822	0.0489	0.083	0.066	0.033	0.039	0.182	0.094	0.0947	0.04
Para Xylene	0.49	0.807	0.386	0.1766	0.0506	0.045	0.0625	0.053	0.063	0.037	0.171	0.0895	0.0911	0.042
Ortho Xylene	0.079	0.037	0.038	0.086	0.039	0.074	0.065	0.051	0.033	0.035	0.177	0.371	0.64	0.82

Table B.3

Calibration of Chromatograph for products of MCP reactions.—Mole-fractions of Compounds

SAMPLES	1	2	3	4	5	6	7	8	9	10	11	12	13	14	15
2Methylpentane	0.081	0.0754	0.0769	0.07	0.01678	0.072	0.0734	0.075	0.1531	0.1536	0.2336	0.289	0.4021	0.4895	0.5416
Methylcyclo-pentane	0.0955	0.1779	0.1816	0.2497	0.05935	0.2543	0.3466	0.4434	0.4511	0.543	0.4590	0.4258	0.3797	0.2888	0.2130
Cyclohexane	0.099	0.1854	0.2836	0.26	0.0824	0.353	0.3609	0.3694	0.2838	0.1887	0.1913	0.1775	0.099	0.1	0.111
Benzene	0.724	0.5613	0.458	0.4199	0.0998	0.3209	0.2191	0.1121	0.114	0.1144	0.116	0.1075	0.12	0.1216	0.1346

Table B.4

Calibration of Chromatograph for products of MCP reactions. Area fractions from Chromatograph

SAMPLES	1	2	3	4	5	6	7	8	9	10	11	12	13	14	15
2Methylpentane	0.0668	0.073	0.073	0.0696	0.0605	0.081	0.0725	0.067	0.145	0.1518	0.239	0.309	0.363	0.526	0.595
Methylcyclo-pentane	0.0777	0.175	0.157	0.225	0.185	0.2415	0.3715	0.414	0.438	0.57	0.464	0.422	0.445	0.277	0.193
Cyclohexane	0.0874	0.188	0.278	0.273	0.346	0.358	0.3726	0.423	0.291	0.188	0.197	0.1712	0.095	0.097	0.0996
Benzene	0.768	0.564	0.492	0.432	0.408	0.3196	0.1833	0.096	0.126	0.089	0.1	0.097	0.096	0,1	0.111

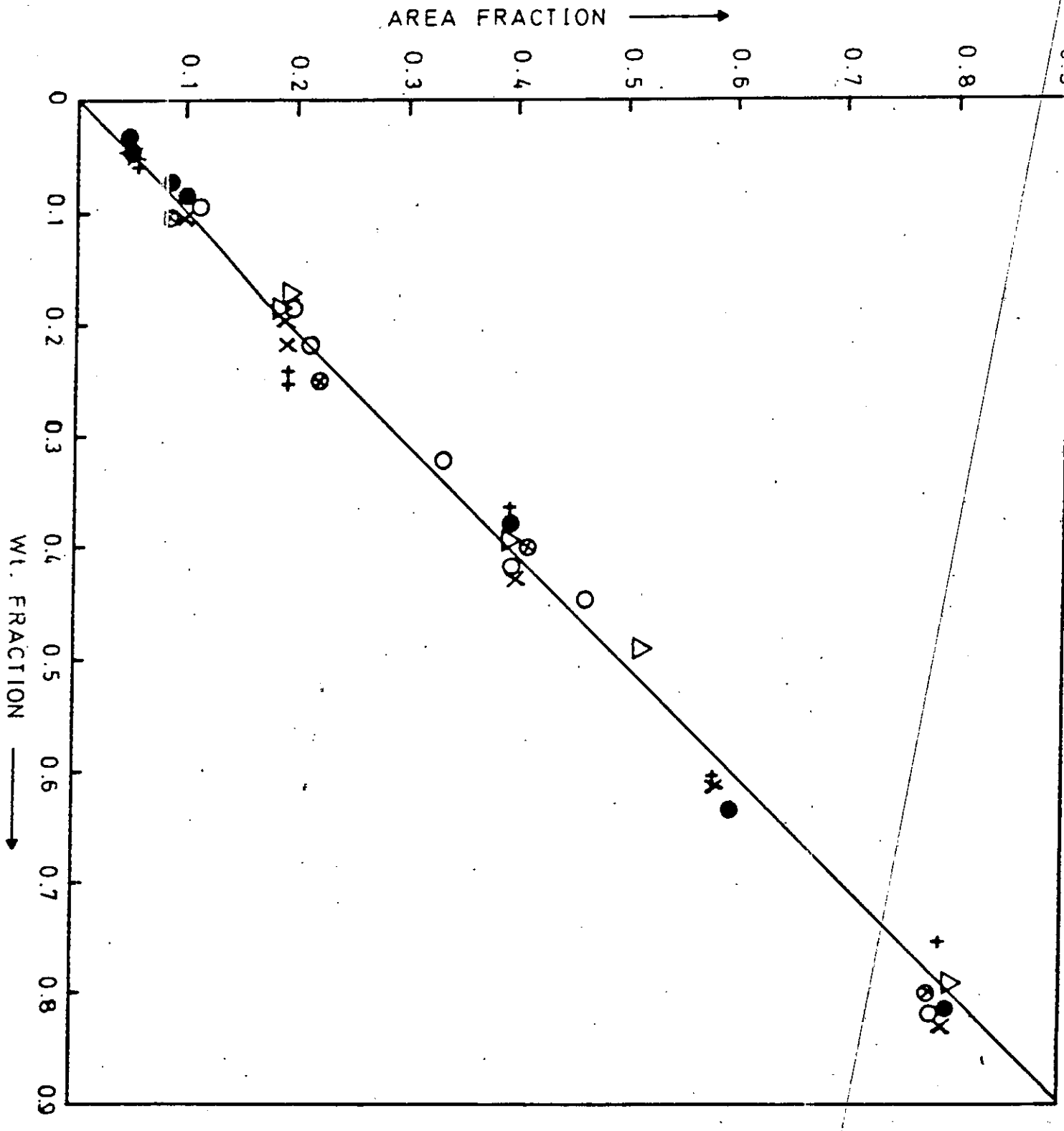

Fig. B.1: Weight fraction of sample of n-octane reaction products versus area fraction of chromatogram.

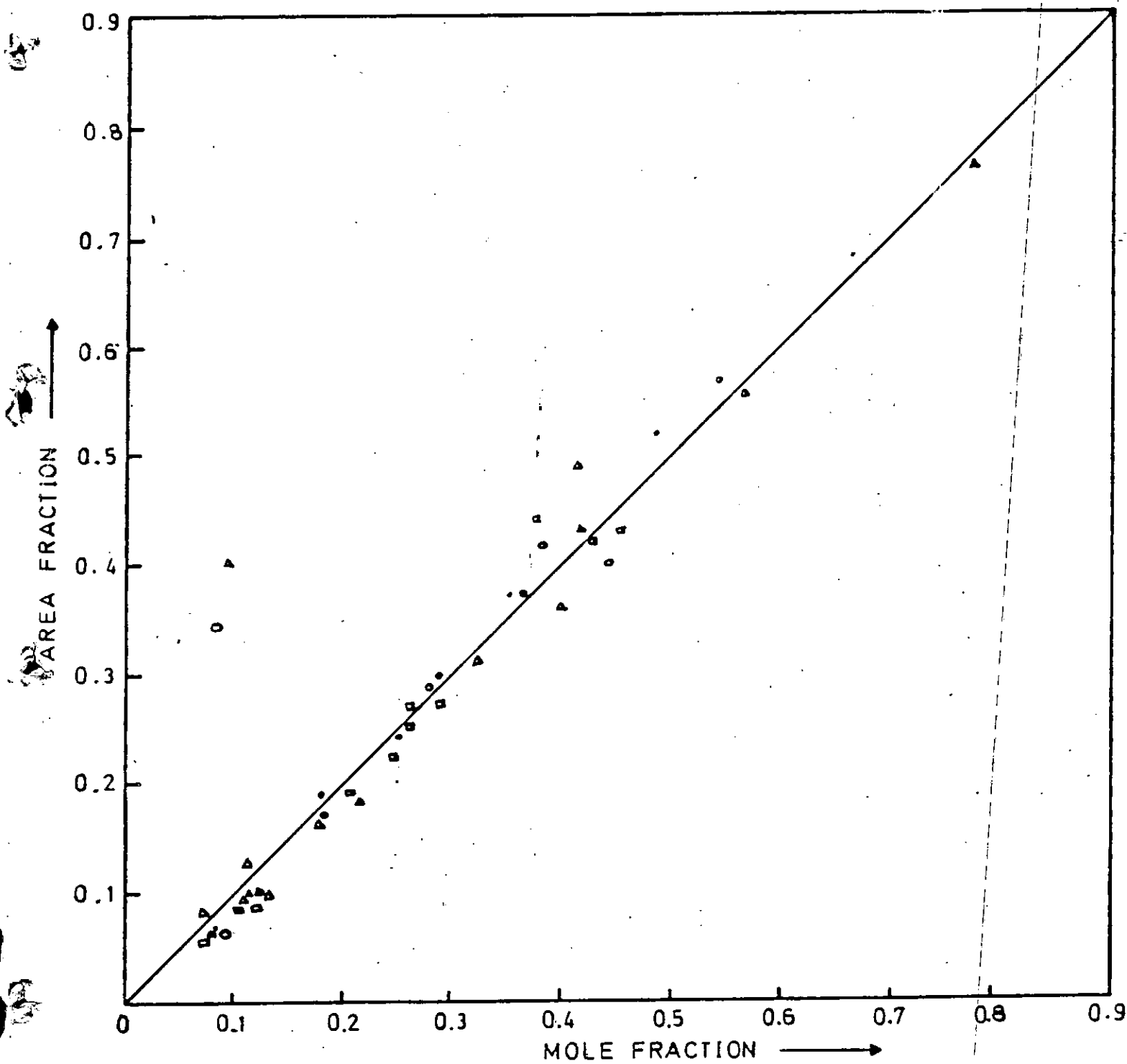

Fig. B.2: Weight fraction of sample of MCP reaction products versus area fraction of chromatograph.

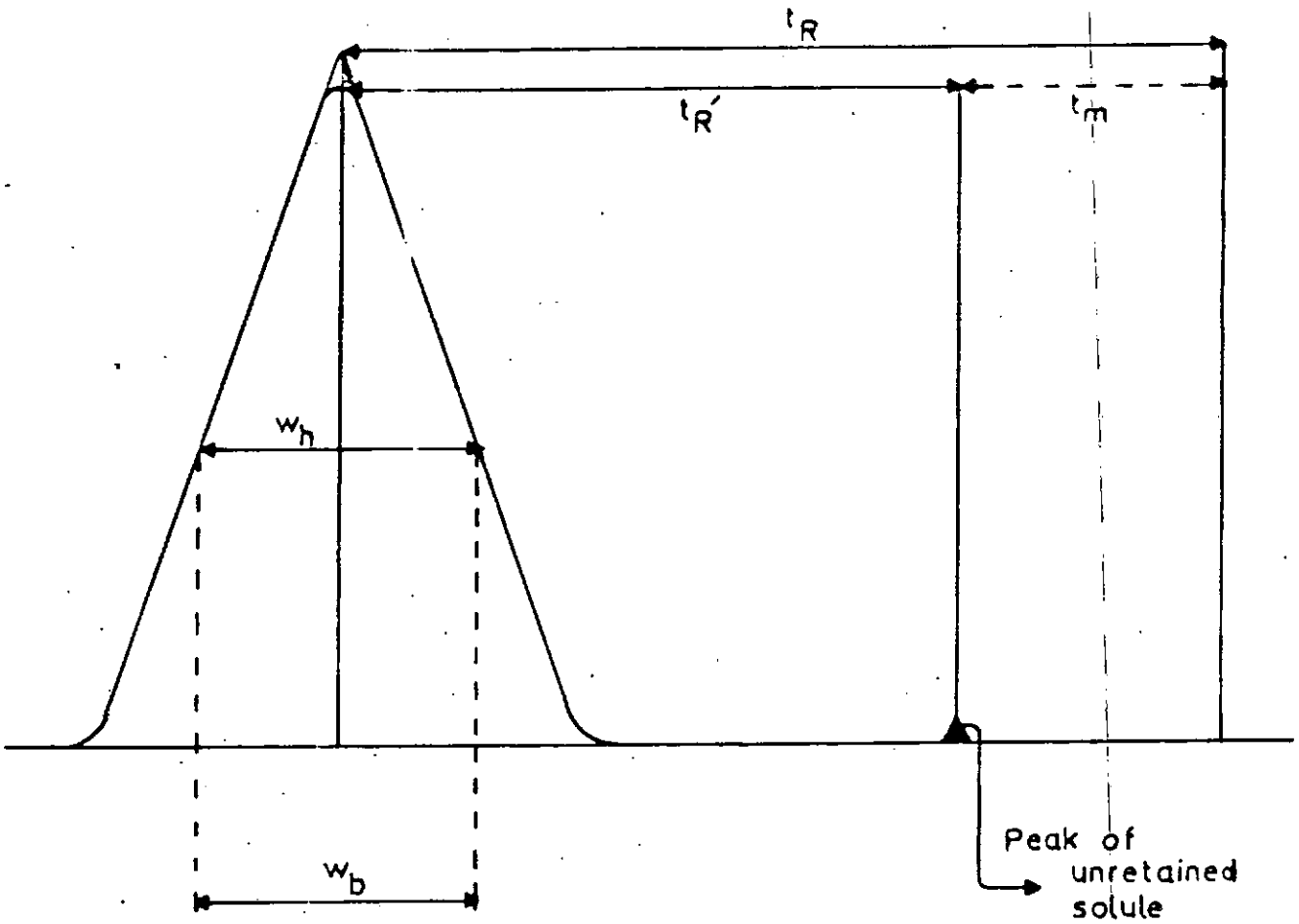

t_R = retention time

t_m = observed retention time of an unretained solution ("air peak time")

t'_R = adjusted retention time

W_h = Peak width of half height

W_b = Peak width of base (the intercept of the two tangents drawn to the inflexion points from the base line)

Fig.B.3: Basic terms describing a chromatogram.

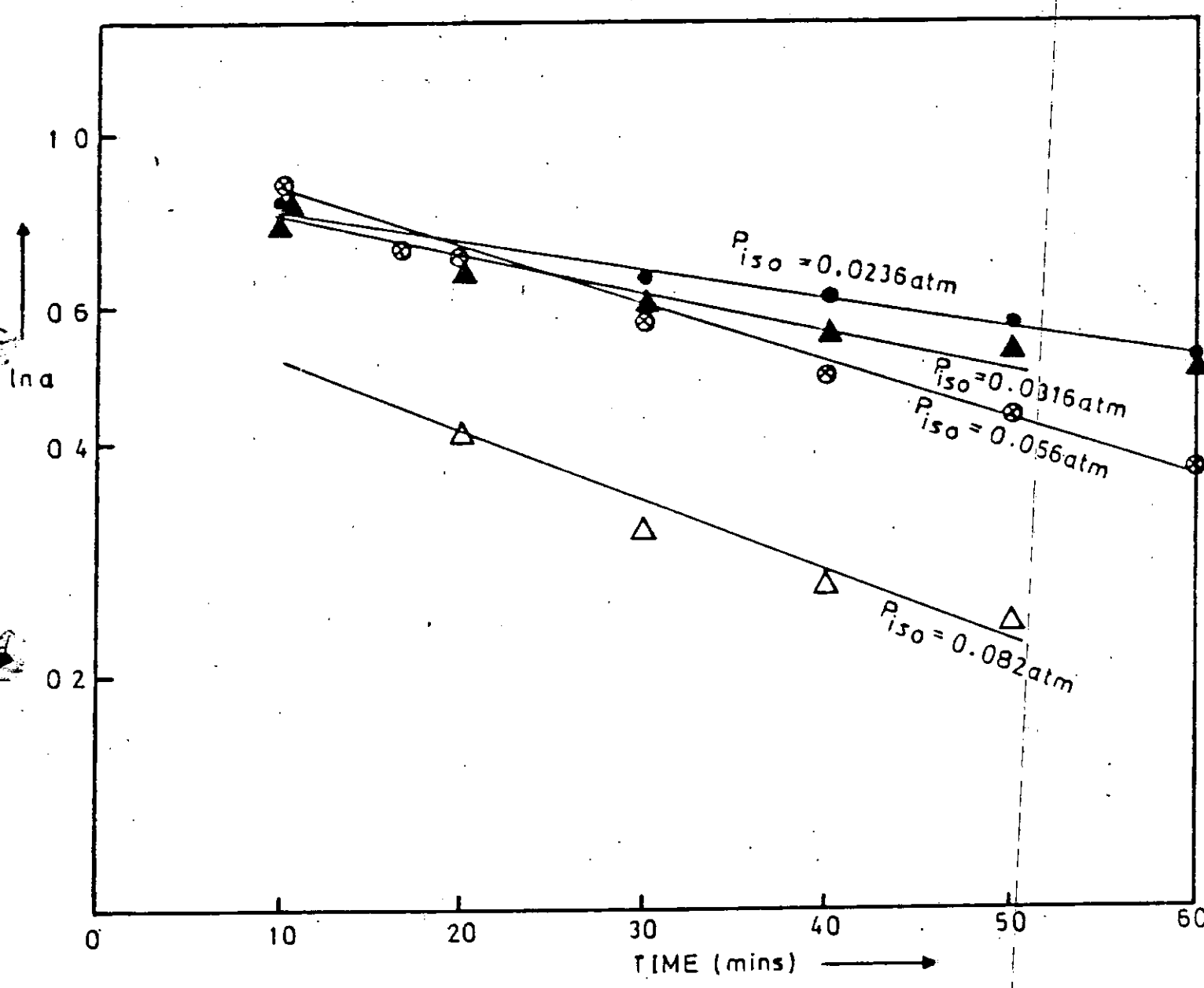

Fig. C.1: $\ell n a$ versus time for 0.3%Pt/Al_2O_3 catalyst at various P_{iso} = 0.5atm; W/F = 0.11gmincm^{-3} and 410°C.

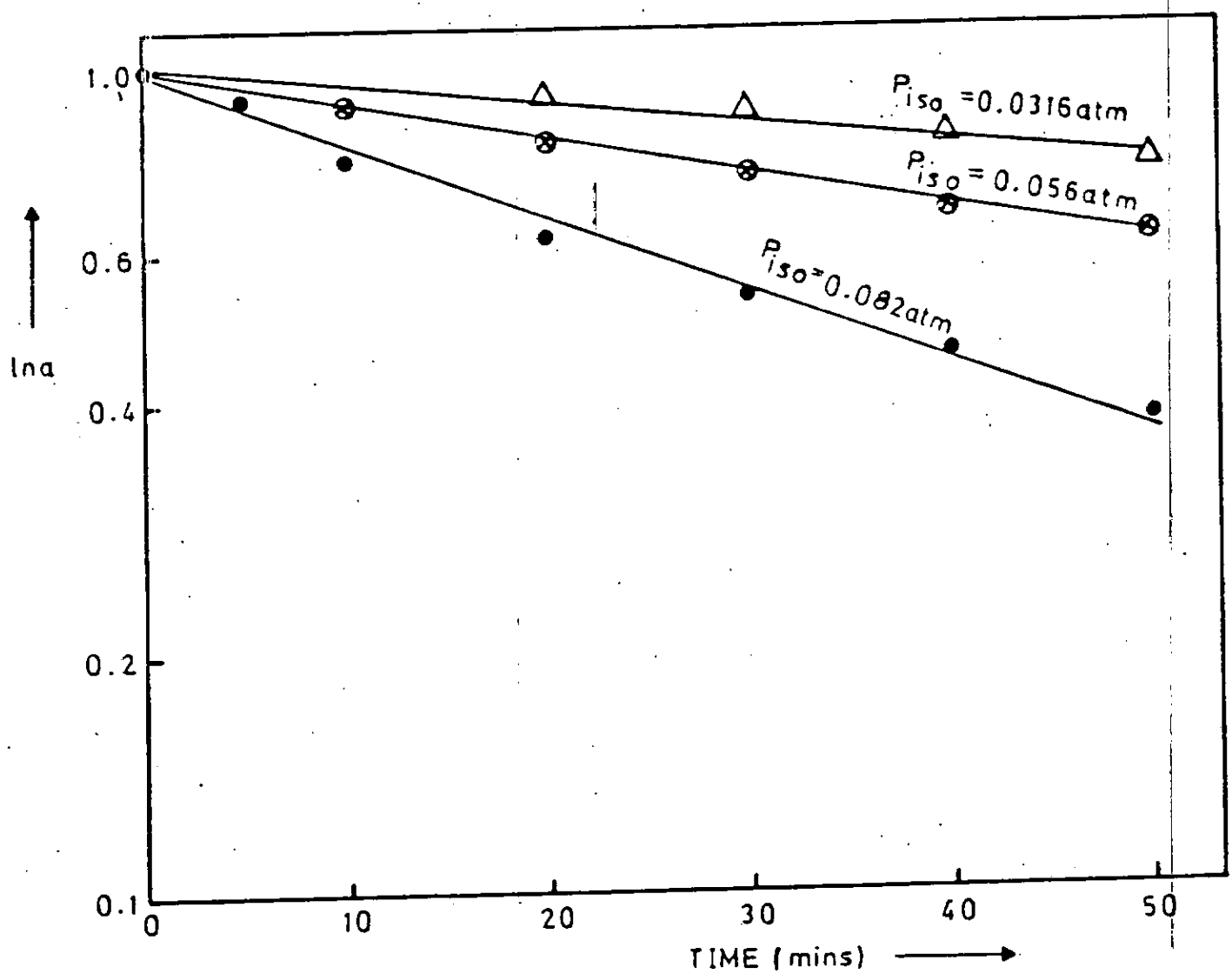

Fig. C.2: ℓna versus time for 0.6%Pt/Al_2O_3 catalyst at various P_{iso} = 0.5atm; W/F = 0.11gmincm^{-3} and 410°C.

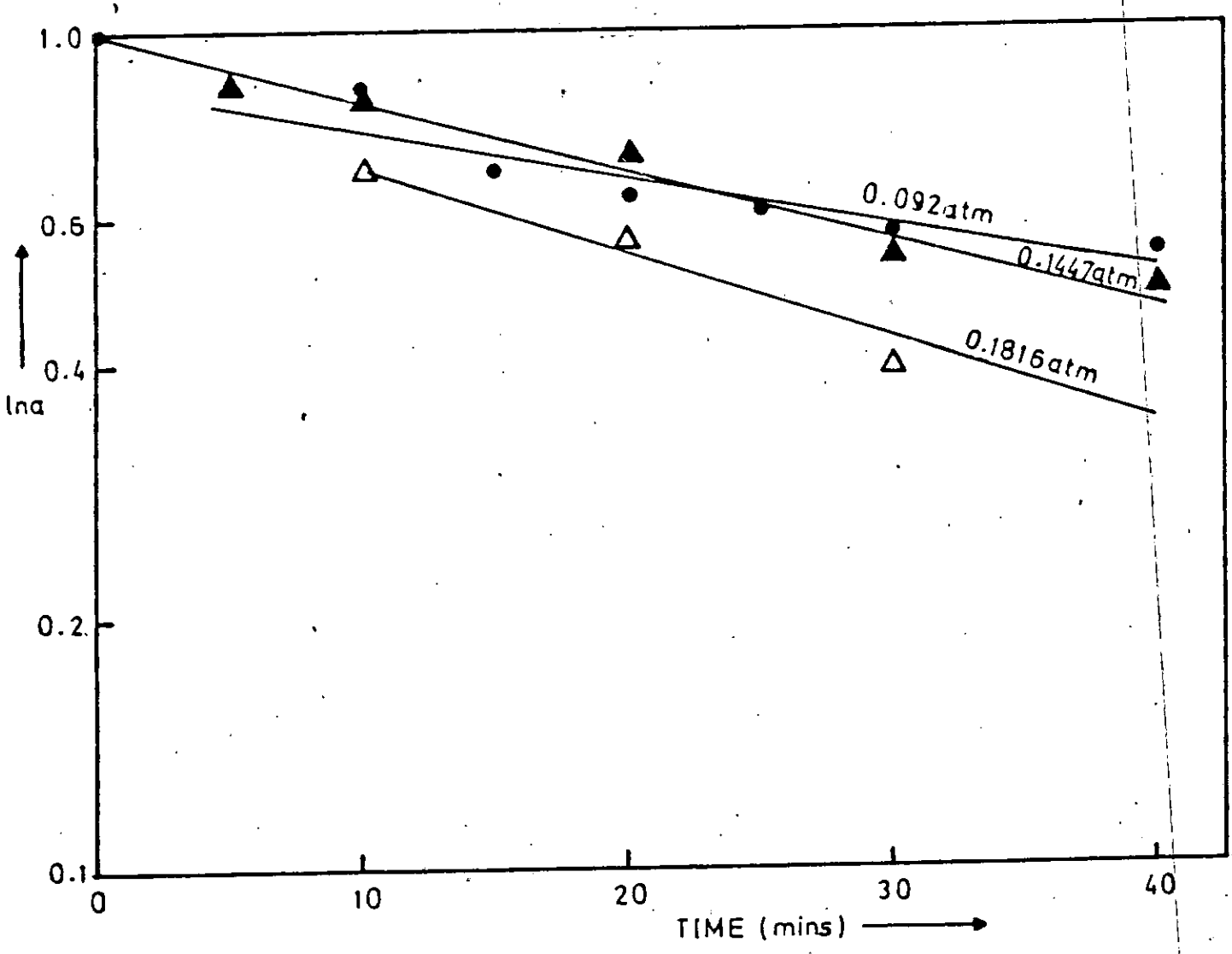

Fig. C.3: ℓna versus time for Pt/Al_2O_3 catalyst at various P_{MCP} & P_{H_2} = 0.5atm; W/F = 0.11gmincm^{-3} and 400°C.

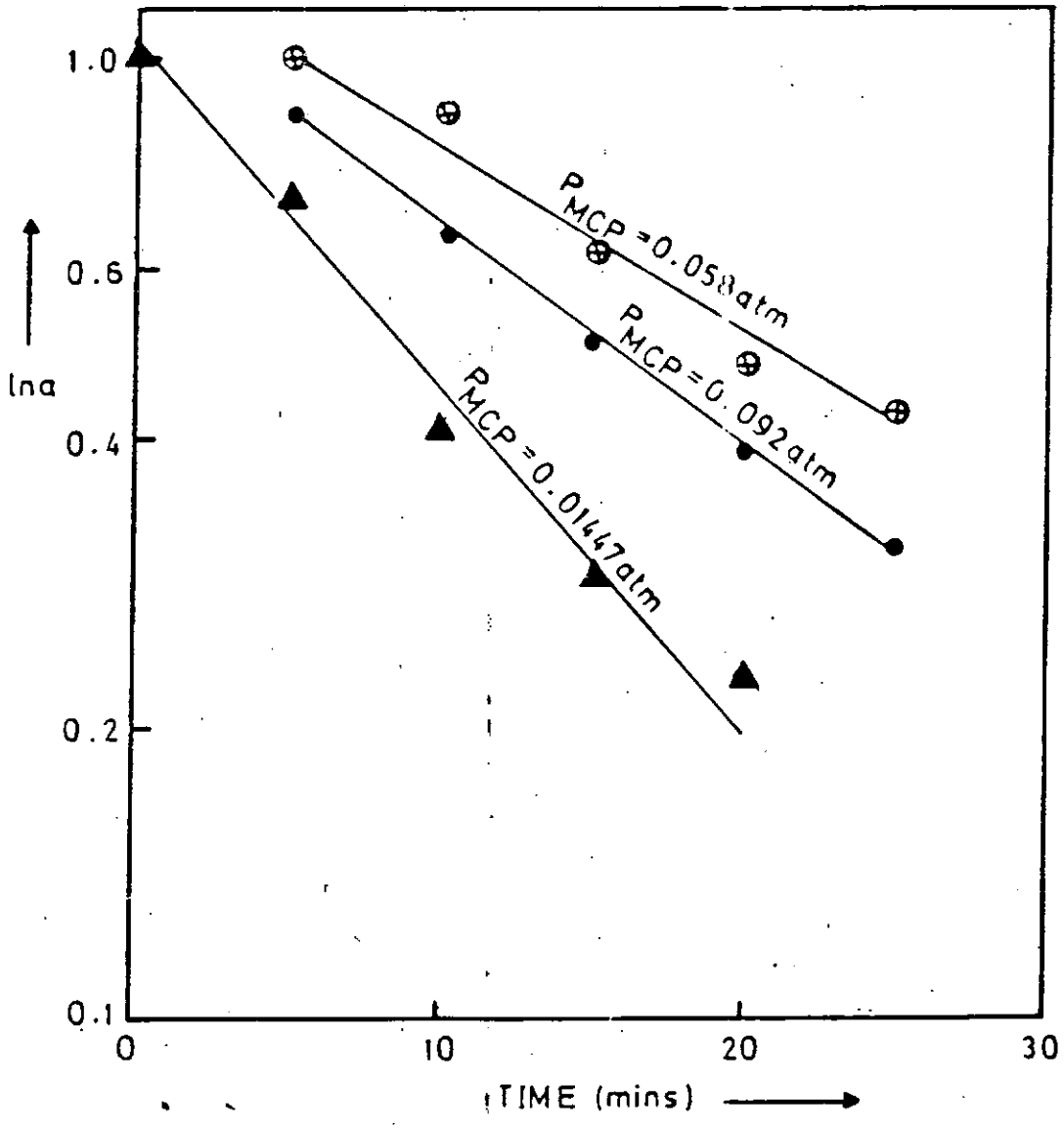

Fig. C.4: ℓna versus time for Pt-Re/Al_2O_3(DRIED) catalyst at various P_{MCP}; P_{H_2} = 0.5atm; W/F = 0.11gmincm^{-3} and 410°C .

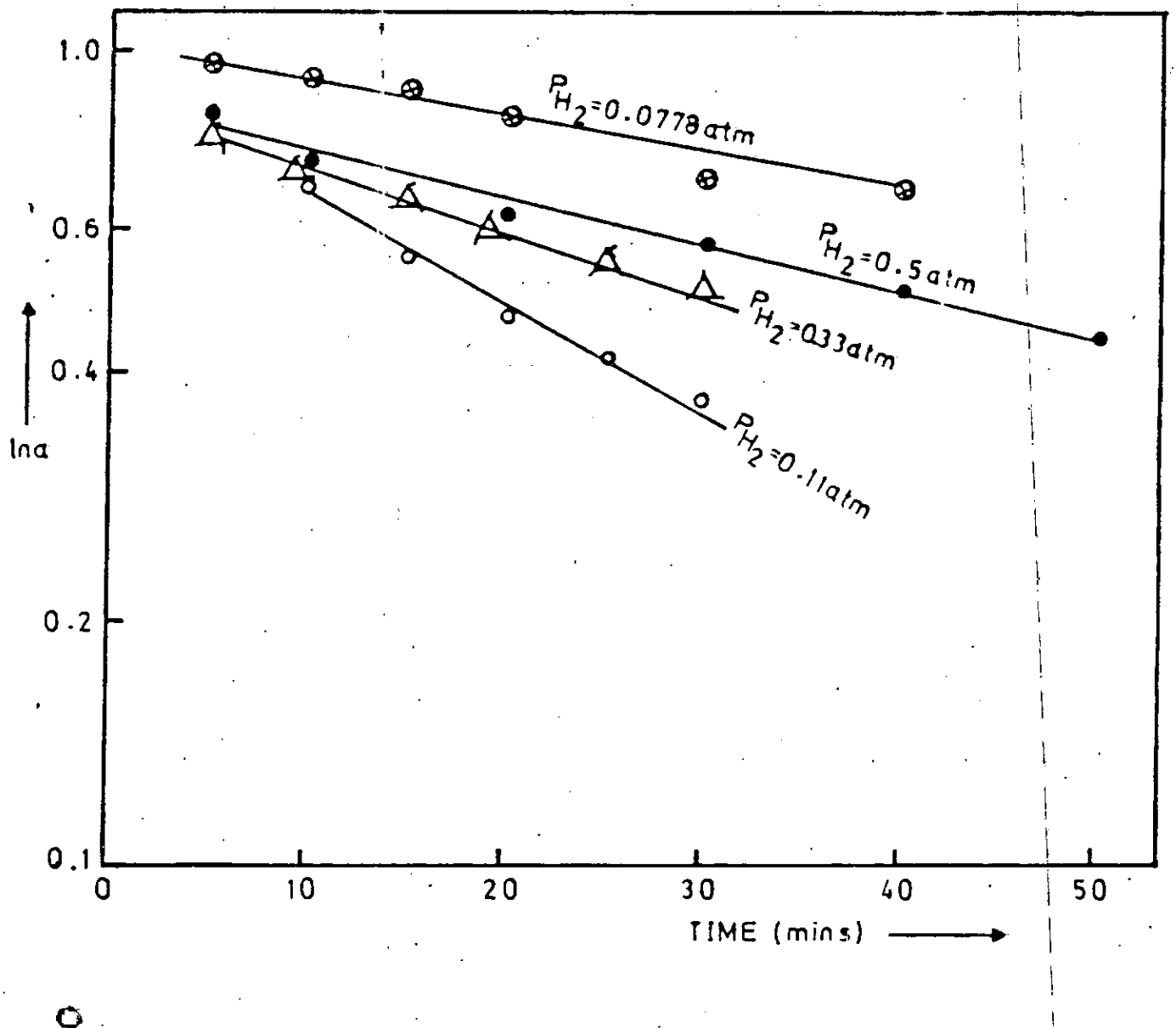

Fig. C.5: ℓna versus time for 0.3%Pt/Al_2O_3 catalyst at various P_{H_2}, P_{iso} = 3.16×10^{-2}atm; W/F = 0.11 gmincm^{-3} and 390°C.

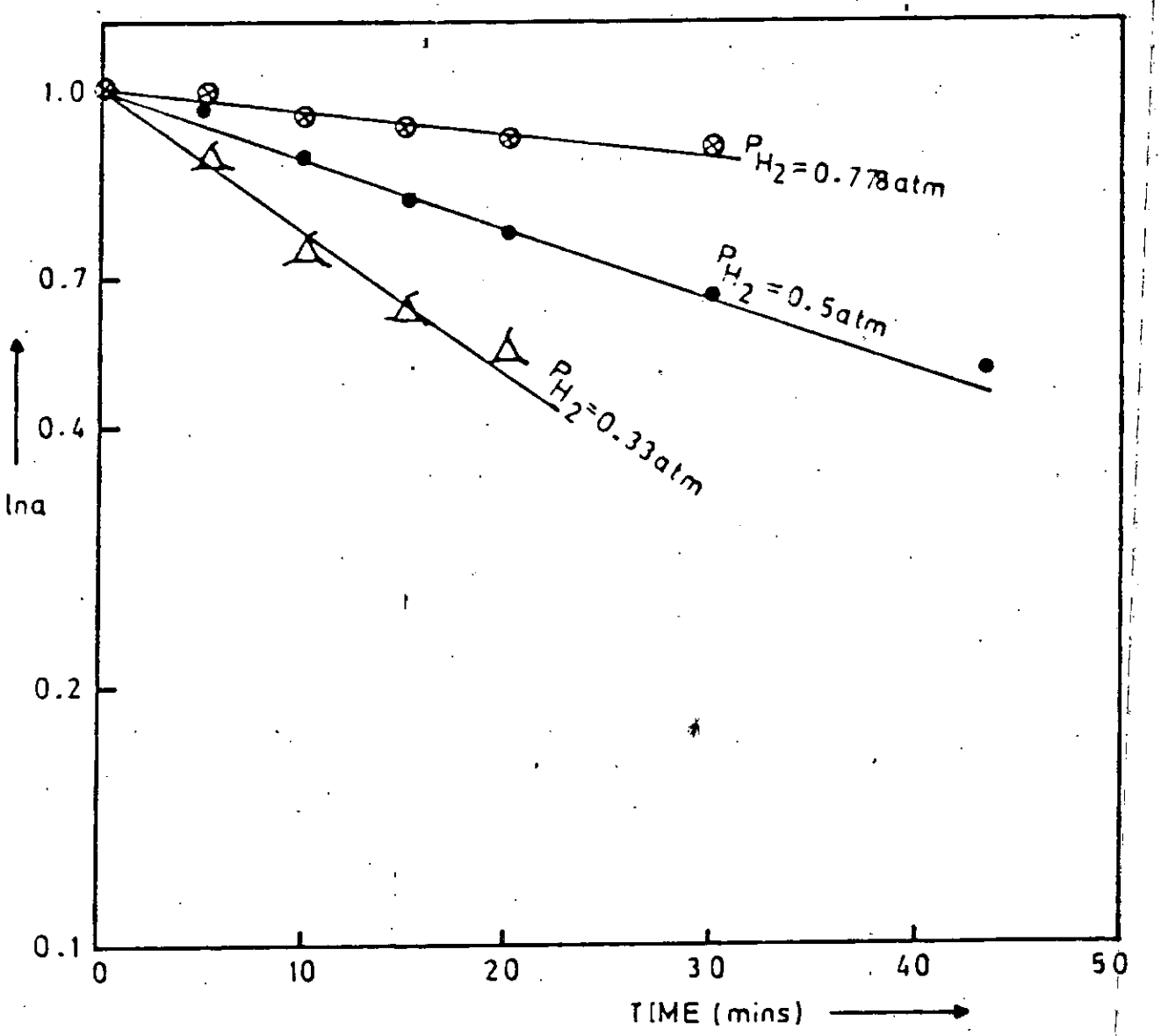

Fig. C.6: ℓna versus time for 0.3%Pt/Al_2O_3 catalyst at various P_{H_2} ; P_{iso} = 3.16×10^{-2}atm; W/F = 0.11gmincm^{-3} and 410°C.

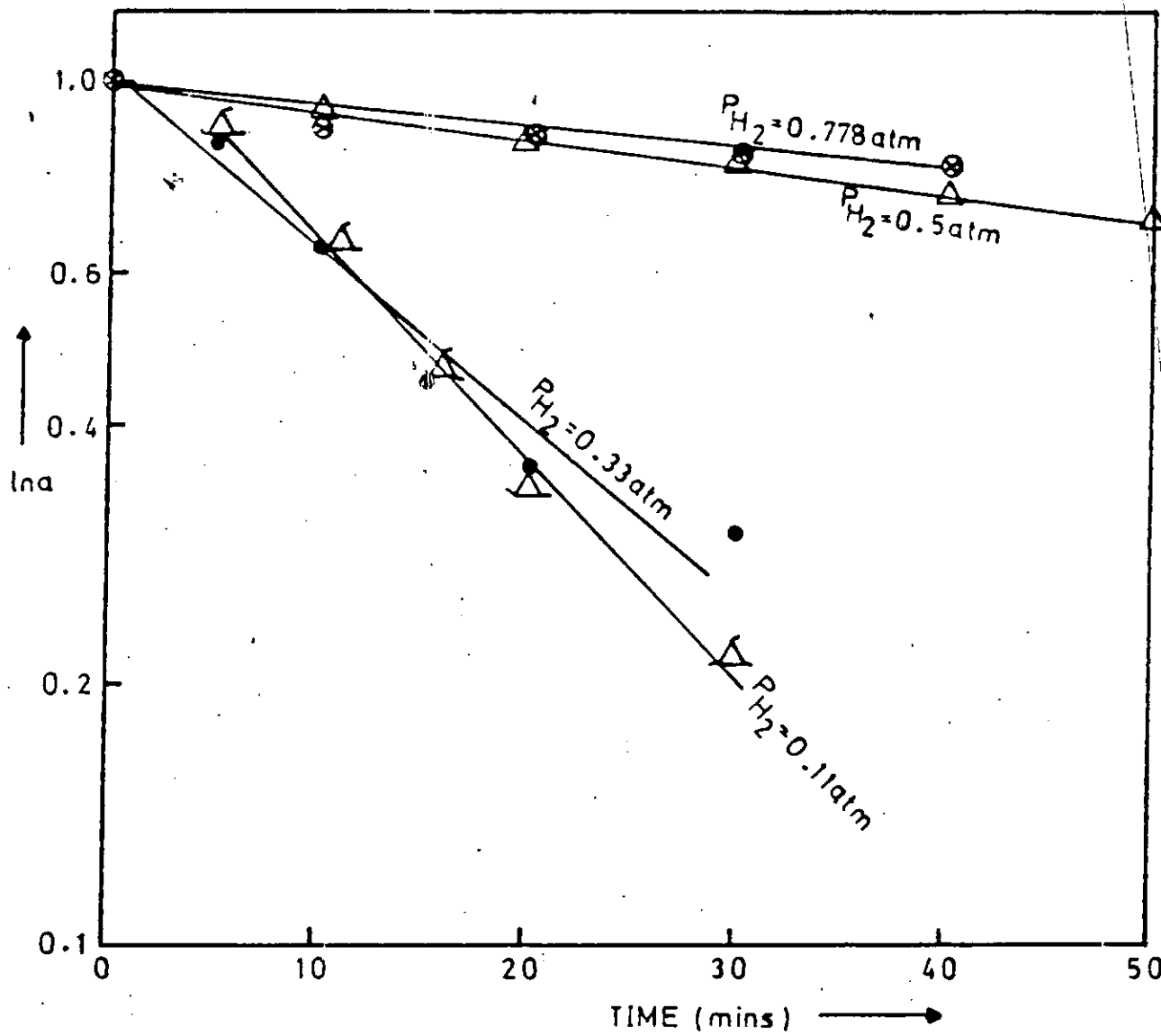

Fig. C.7: &na versus time for 0.3%Pt/Al_2O_3 catalyst at various P_{H_2}, P_{iso} = 3.16×10^{-2}atm; W/F = 0.11gmincm^{-3} and 430°C.

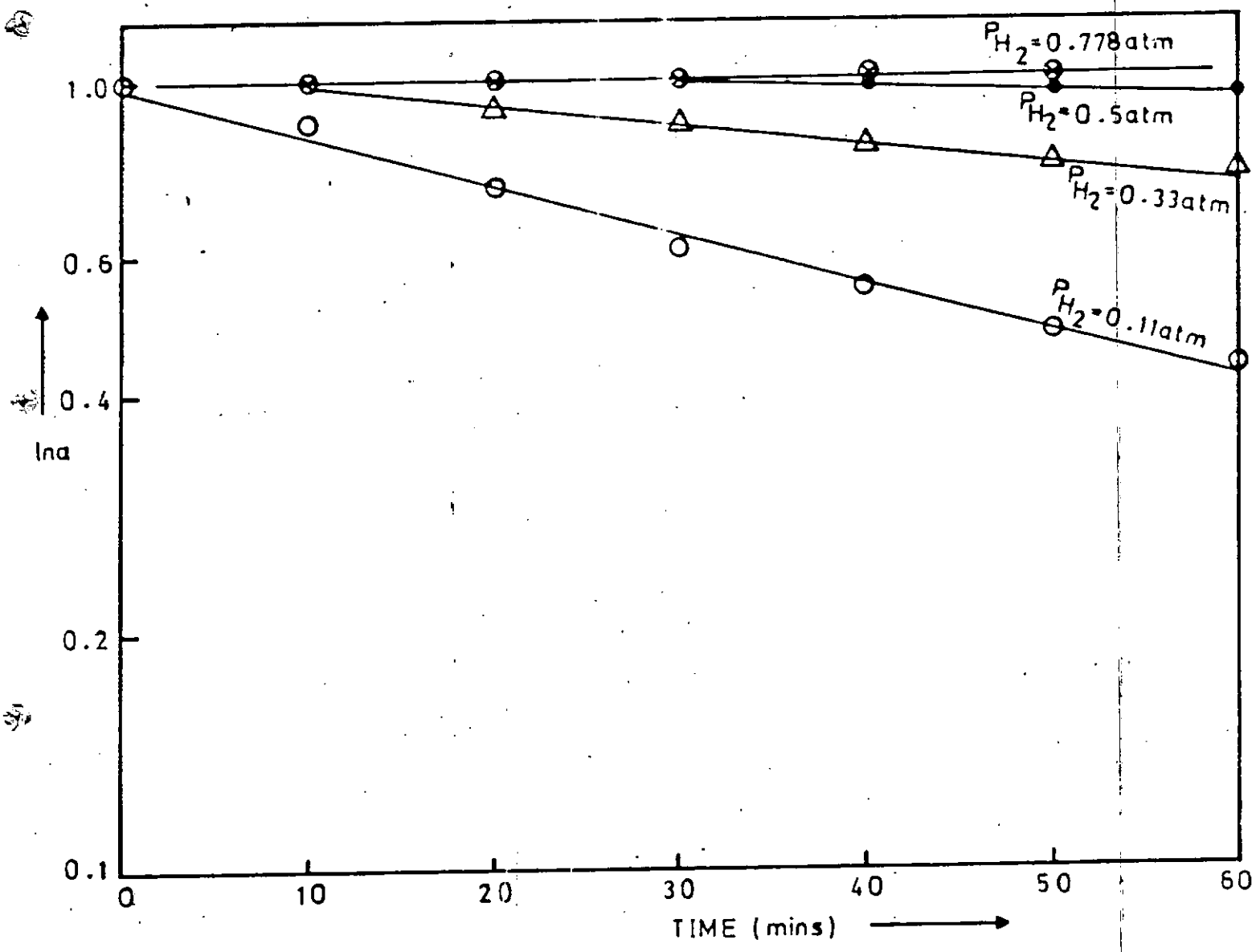

Fig. C.8: ℓna versus time for 0.6%Pt/Al_2O_3 catalyst at various P_{H_2}; P_{iso} = 3.16×10^{-2}atm; W/F = 0.11gmincm^{-3} and 390°C.

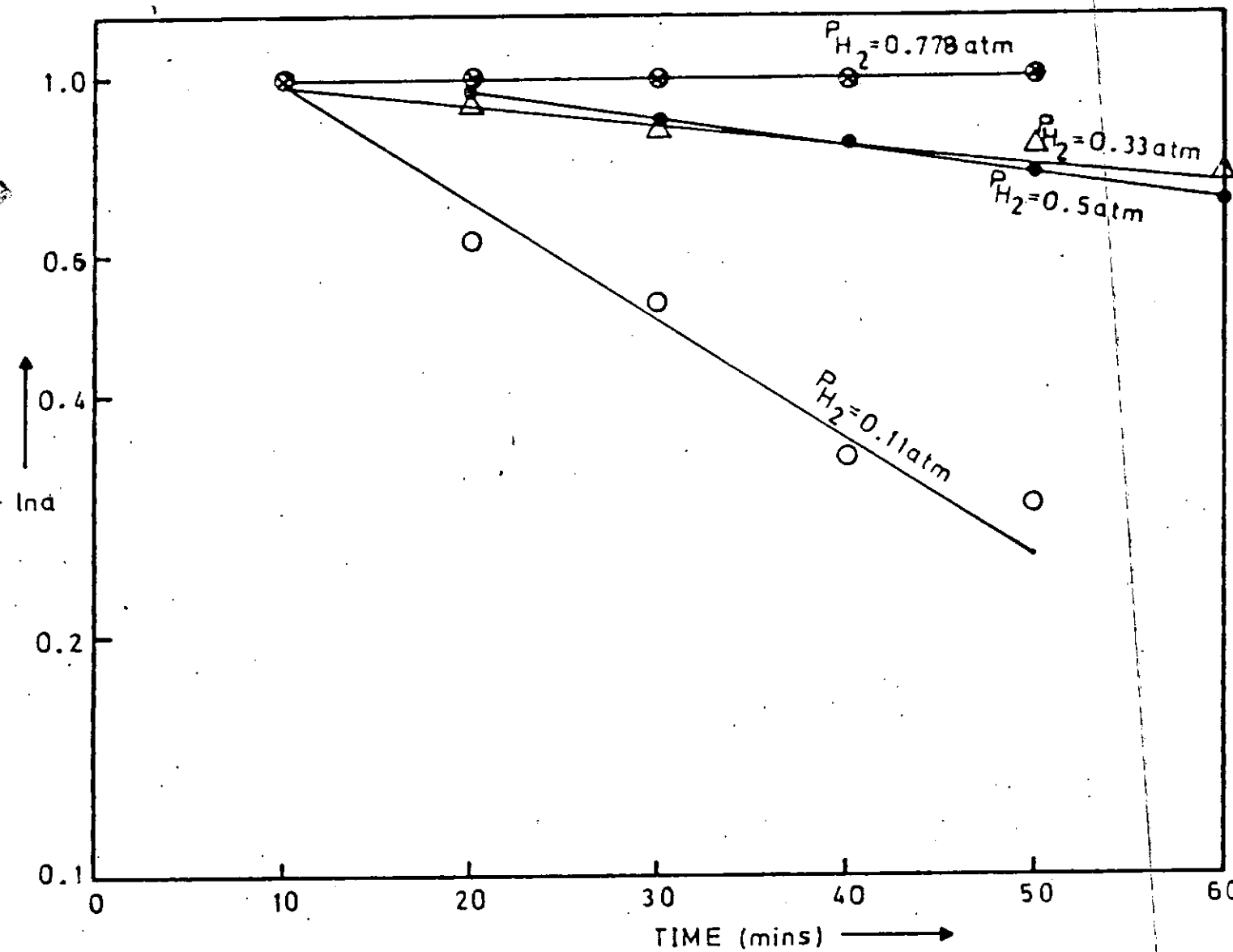

Fig. C.9: ℓna versus time for 0.6%Pt/Al_2O_3 catalyst at various P_{H_2}; P_{iso} = 3.16×10^{-2} atm; W/F = 0.11 gmincm^{-3} and 410°C

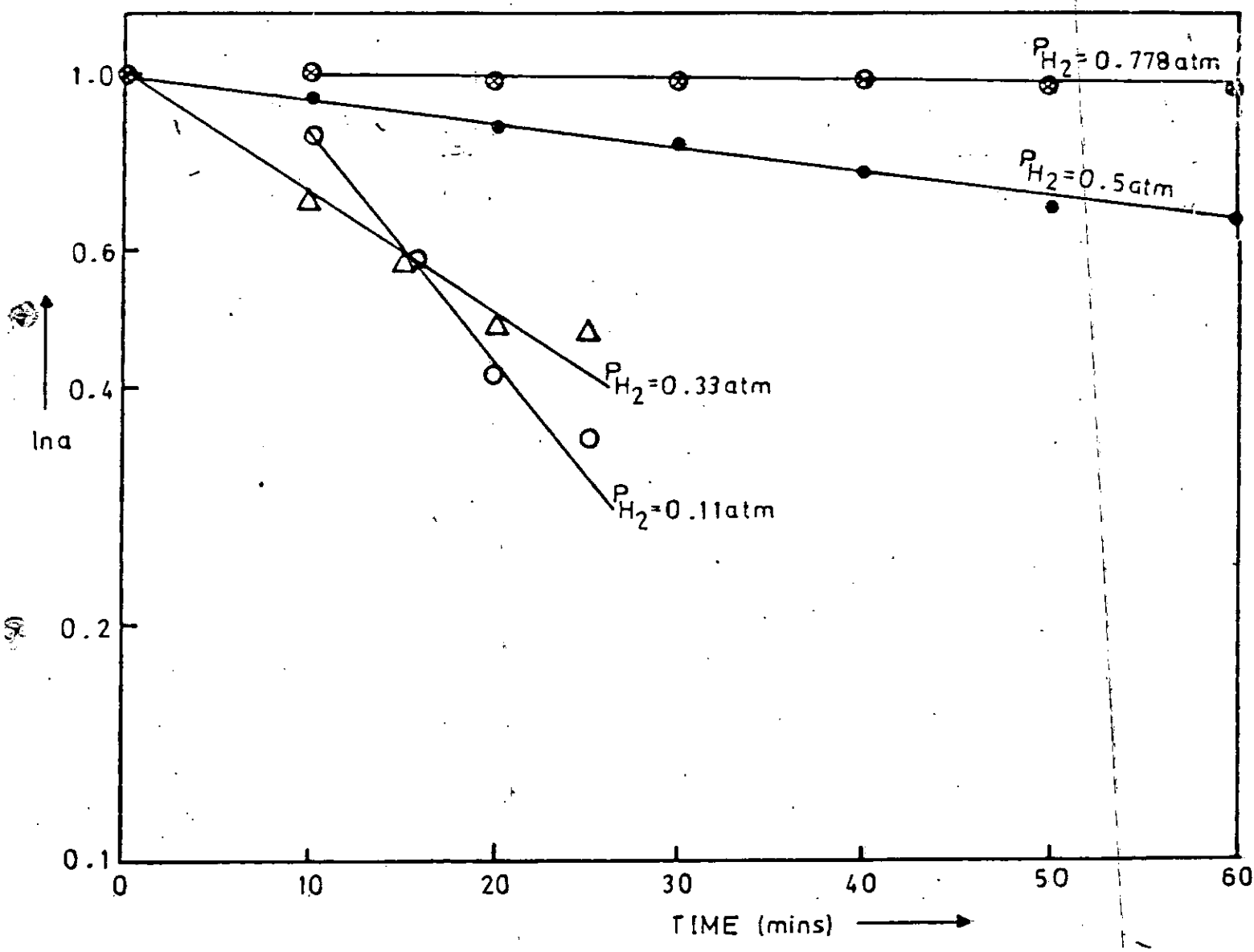

Fig. C.10: ℓna versus time for 0.6%Pt/Al_2O_3 catalyst at various P_{H_2}; P_{iso} = 3.16×10^{-2}atm; W/F = 0.11gmincm^{-3} and 430°C

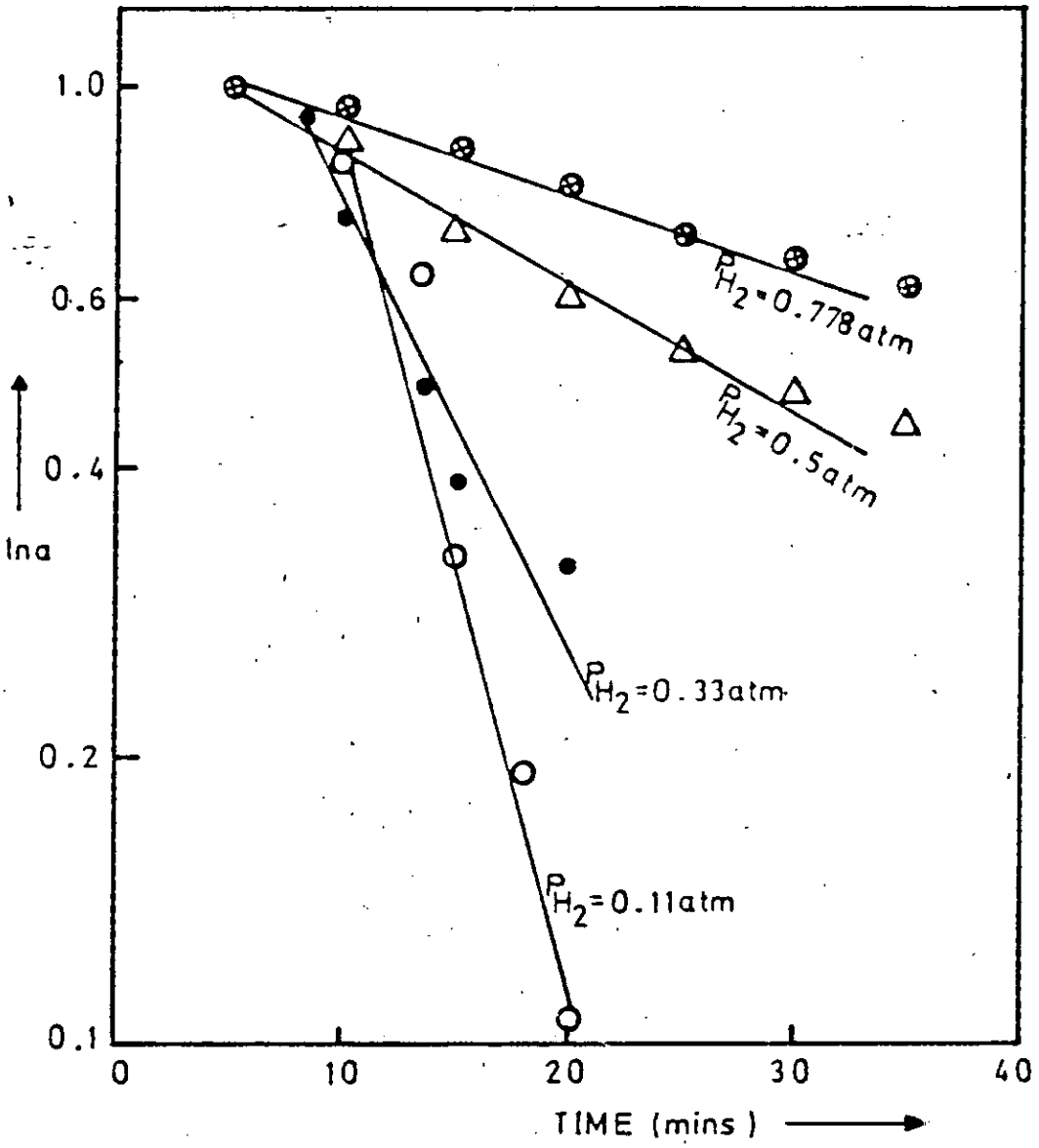

Fig. C.11: ℓna versus time for Pt/Al_2O_3 catalyst at various P_{H_2}; $P_{MCP} = 9.2 \times 10^{-2}$ atm; $W/F = 0.11$ gmincm^{-3} and 390°C.

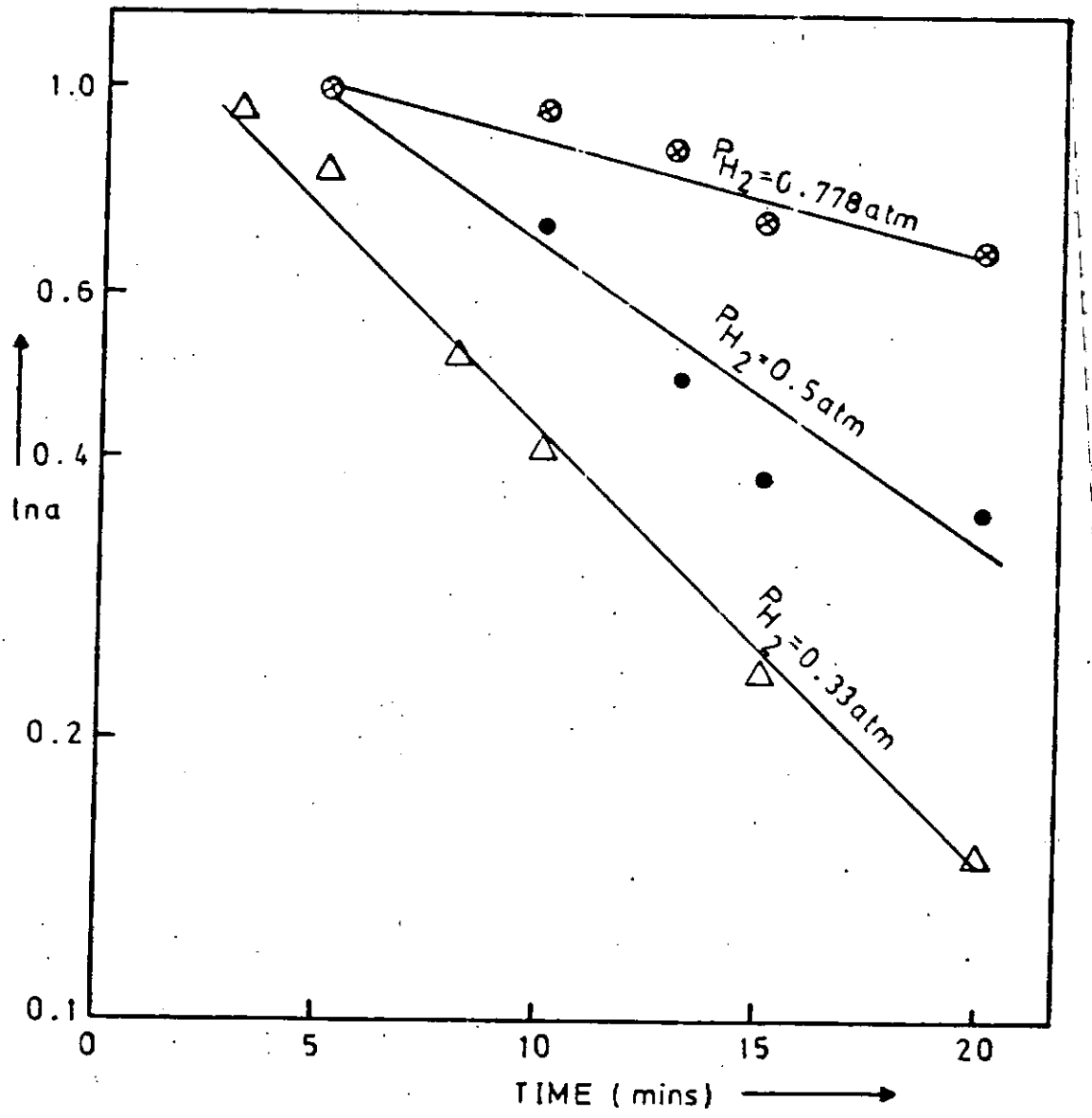

Fig. C.12: &na versus time for Pt/Al_2O_3 catalyst at various P_{H_2}; $P_{MCP} = 9.2 \times 10^{-2}$atm; W/F = 0.11gminc$m^{-3}$ and 400°C

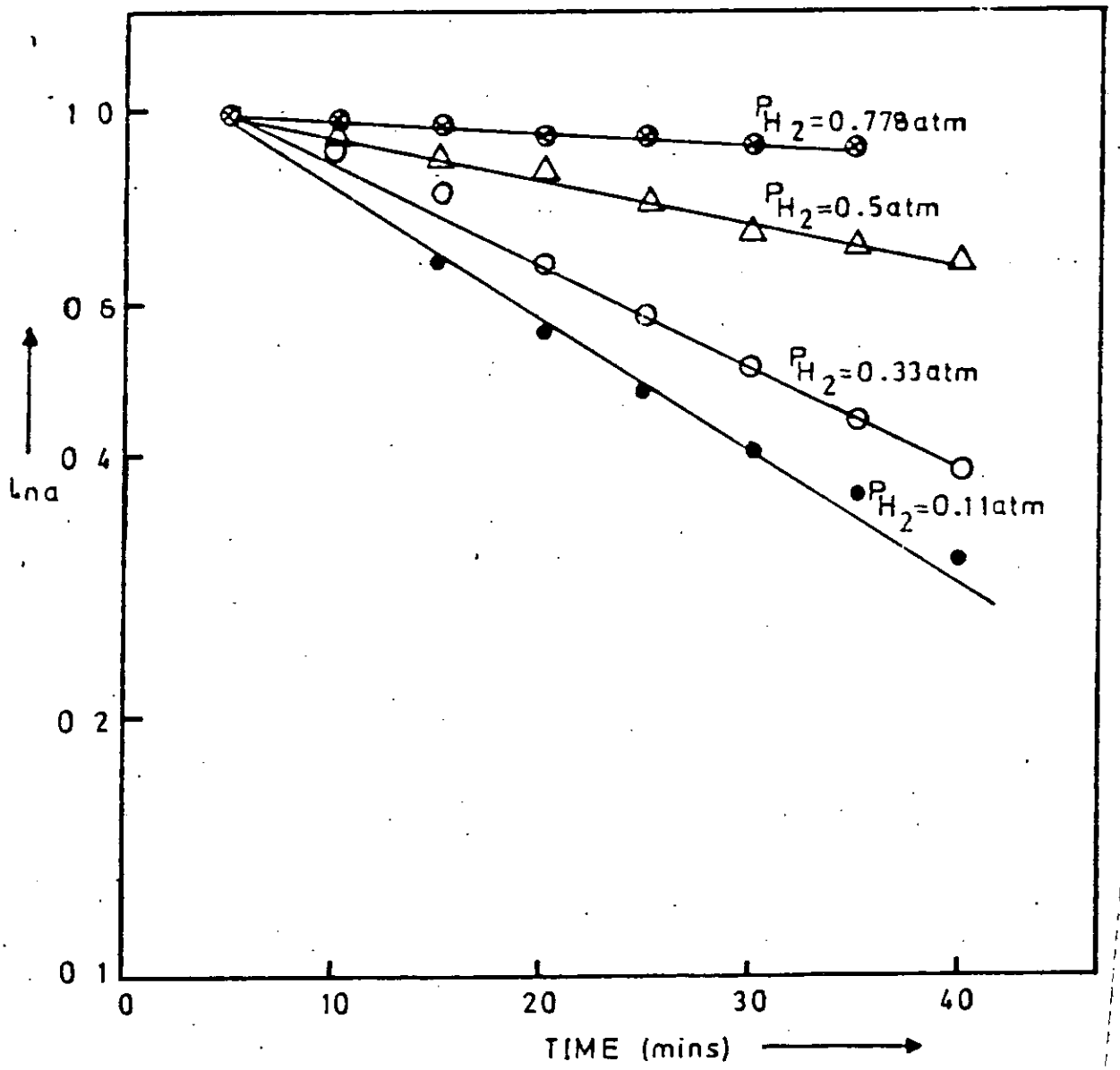

Fig. C.13: ℓna versus time for Pt-Re/Al_2O_3(DRIED) catalyst at various P_{H_2}; P_{MCP} = 9.2×10^{-2}atm; W/F = 0.11gmincm^{-3} and 390°C.

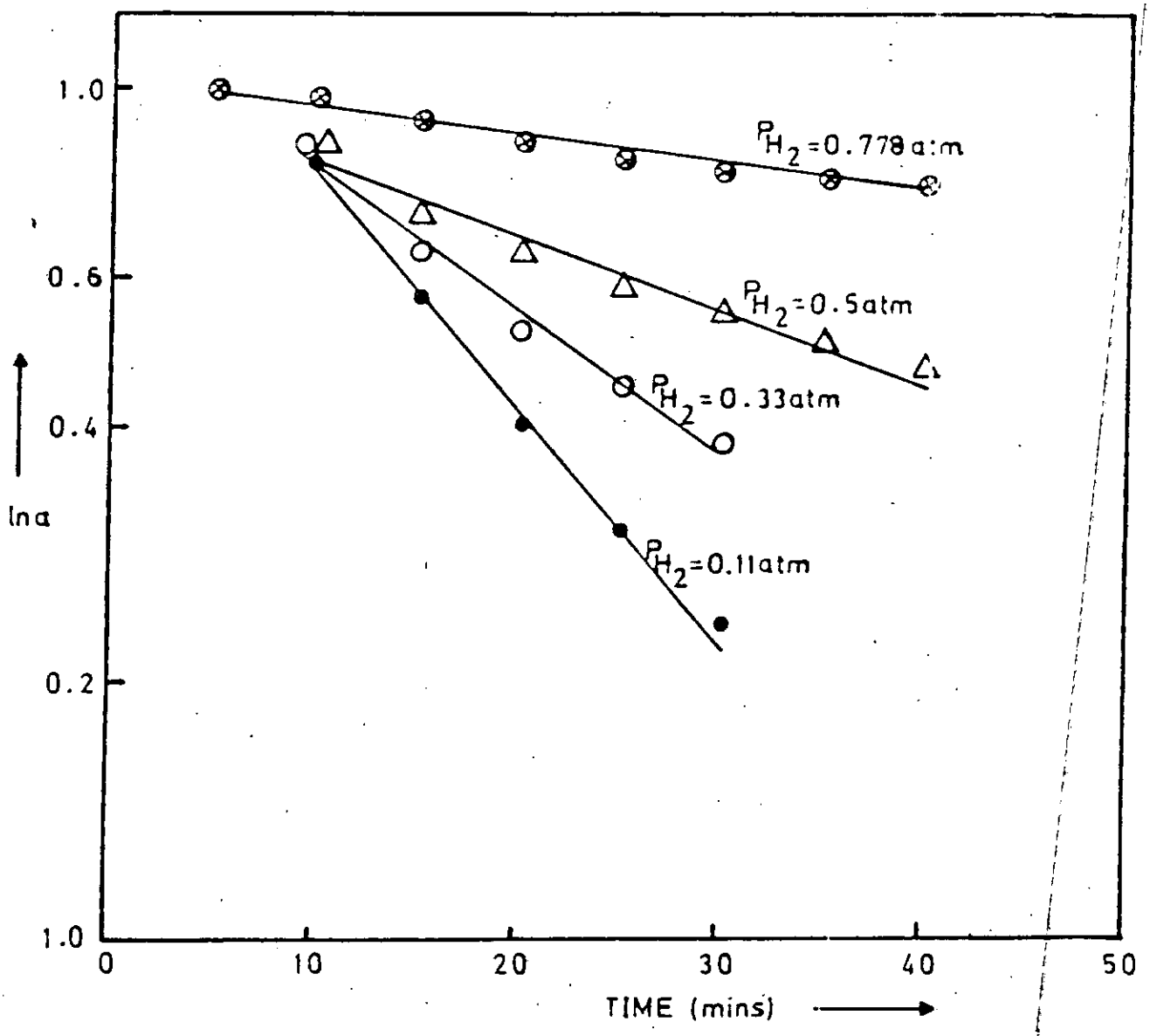

Fig. C.14: ℓna versus time for Pt-Re/Al_2O_3(DRIED) catalyst at various P_{H_2}; P_{MCP} = 9.2×10^{-2}atm; W/F = 0.11gmincm^{-3} and 400°C.

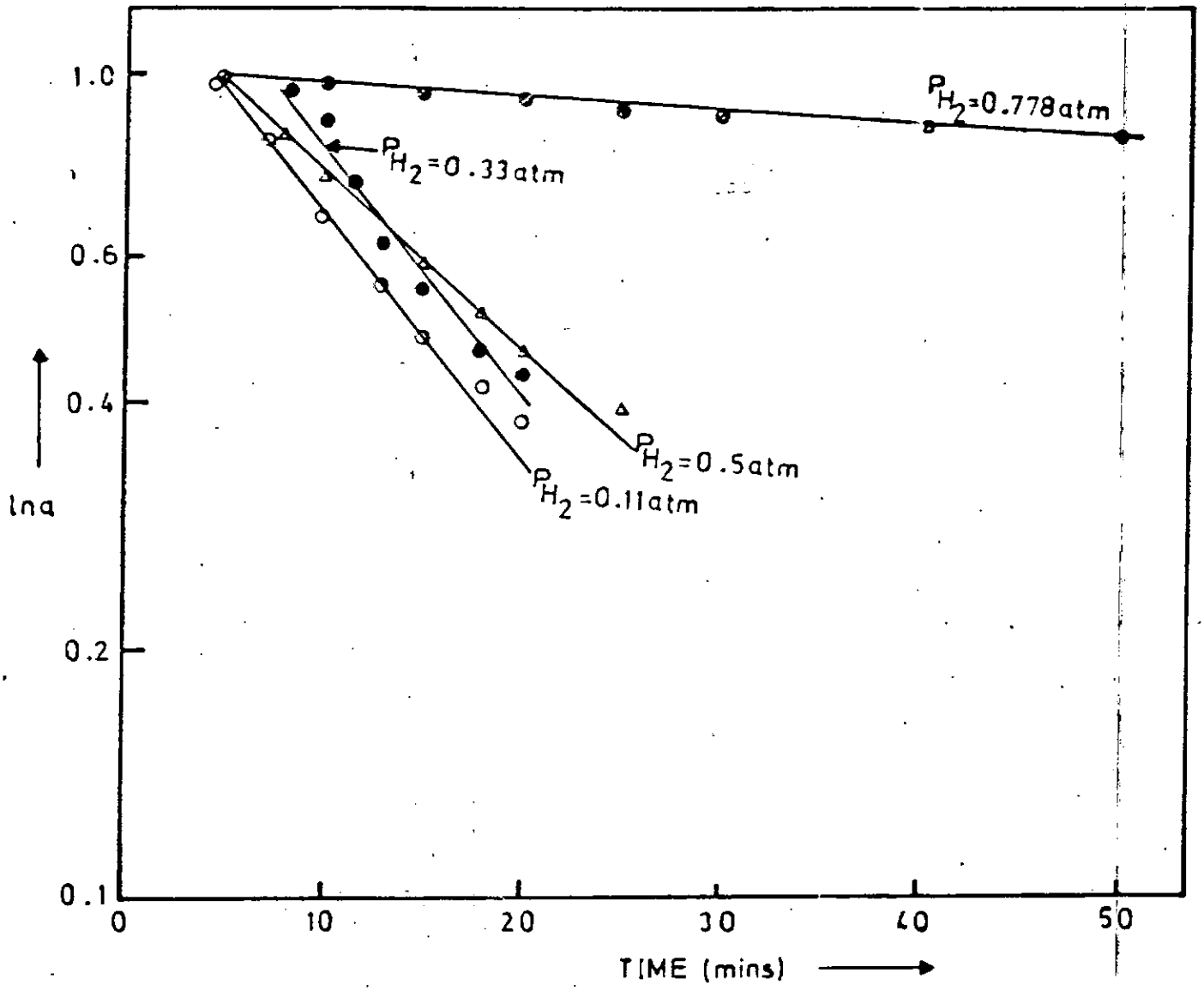

Fig. C.15: ℓna versus time for Pt-Re/Al_2O_3(DRIED) catalyst at various P_{H_2}; P_{MCP} = 9.2×10^{-2}atm; W/F = 0.11gmincm^{-3} and 410°C.

APPENDIX D

Table D.1: Deactivation Function of 0.3%Pt/Al_2O_3 and 0.6%Pt/Al_2O_3 Catalysts at Various Iso-octane Partial Presure and 410°C

P_{iso}[atm]	$\psi_{01}(P_i,T)$	
	0.3%Pt/Al_2O_3	0.6%Pt/Al_2O_3
0.0236	0.0084	-
0.0316	0.01138	0.0059
0.056	0.0167	0.0097
0.082	0.021	0.0202

Table D.2 : Deactivation function of Pt/Al_2O_3 and Pt-Re/Al_2O_3 (DRIED) Catalyst at various MCP partial pressure

P_{MCP}	$\psi_{01}(P_i,T)$	
	Temp = 400°C 0.3%Pt/Al_2O_3 P_{H_2} = 0.778atm	Temp 410°C 0.3%Pt-Re/Al_2O_3(DRIED) P_{H_2} = 0.5atm
0.058	-	0.042
0.092	0.01266	0.051
0.1447	0.01888	0.0665
0.1816	0.0223	-

Table D.3 : Deactivation function of Pt/Al_2O_3 catalyst at P_{iso} = 0.0316 atm; W/F = 0.11gmincm^{-3} and at various P_{H_2} and temperature

P_{H_2} [atm]	$\psi_{01}(P_i,T)$		
	390°C	410°C	430°C
0.11	0.0325	-	0.058
0.33	0.0186	0.0388	0.0446
0.5	0.0128	0.019	0.007
0.778	0.01	0.006	0.0052

Table D.4: Deactivation function of 0.6%Pt/Al_2O_3 catalyst at P_{iso} = 0.0316 atm, W/F = 0.11gmincm^{-3} and at various P_{H_2} and temperature.

P_{H_2} [atm]	$\psi_{01}(P_i,T)$		
	390°C	410°C	430°C
0.11	0.015	0.0347	0.0433
0.33	0.006	0.0054	0.0347
0.5	0.0017	0.0085	0.007
0.778	0	0	0.0015

Table D.5: Deactivation function of Pt/Al_2O_3 catalyst at P_{MCP} 0.092atm, W/F = 0.11gmincm^{-3} and at various P_{H_2} and temperature

P_{H_2} (atm)	$\psi_{01}(P_i,T)$	
	390°C	400°C
0.11	0.197	—
0.33	0.11	0.1046
0.5	0.032	0.076
0.778	0.0185	0.028

Table D.6: Deactivation function of Pt-Re/Al_2O_3 (DRIED) catalyst at P_{MCP} = 0.092atm, W/F = 0.11gmincm^{-3} and at various P_{H_2} and temperature.

P_{H_2} (atm)	$\psi_{01}(P_i,T)$		
	390°C	400°C	410°C
0.11	0.036	0.066	0.07
0.33	0.0276	0.0384	0.068
0.5	0.0114	0.02	0.051
0.778	0.00314	0.00743	0.0036

APPENDIX E

METHOD OF LEAST SQUARE FIT

Definition:

Suppose that we have $E(r) = ax + h$

Let (X_1,Y_1), (X_2,Y_2), ... ,(X_n,Y_n) be a random sample of Y

The Least square estimates of the parameters a and b are those values of a and b which minimize

$$\sum_{i=1}^{n} [Y_i - (ax_i + b)]^2 \qquad (E.1)$$

For each pair (x_i,Y_i) we compute the discrepancy between Y_i, the observed value, and $ax_i + b$, the expected value. In order to obtain the required estimates for a and b we proceed as follows:

$$\text{Let } f(a,b) = \sum_{i=1}^{n} [Y_i - (ax_i + b)^2] \qquad (E.2)$$

To minimize f(a,b), we must solve the equations

$$\frac{\partial f}{\partial a} = o \qquad (E.3)$$

and

$$\frac{\partial f}{\partial b} = o \qquad (E.4)$$

differentiating f with respect to a and b, we obtain

$$\frac{\partial f}{\partial a} = \sum_{i=1}^{n} 2(Y_i - (ax_i + b)) - (X_i)$$

$$= -2 \sum_{i=1}^{n} (X_i Y_i - a x_i^2 - b x_i) \qquad (E.5)$$

and

$$\frac{\partial f}{\partial b} = \sum_{i=1}^{n} 2(Y_i - (ax_i + b))(-1)$$

$$\frac{\partial f}{\partial b} = -2 \sum_{i=1}^{n} (Y_i - ax_i - b) \qquad (E.6)$$

Thus $\frac{\partial f}{\partial a} = 0$, $\frac{\partial f}{\partial b} = 0$ May be written respectively as follows:

$$a \sum_{i=1}^{n} X_i^2 + b \sum_{i=1}^{n} X_i = \sum_{i=1}^{n} X_i Y_i \qquad (E.7)$$

$$a \sum_{i=1}^{n} X_i + nb = \sum_{i=1}^{n} Y_i \qquad (E.8)$$

Solving the two linear equations

$$a = \frac{\sum_{i=1}^{n} Y_i (X_i - \bar{X})}{\sum_{i=1}^{n} (X_i - \bar{X})^2} \qquad (E.9)$$

where

$$\bar{X} = \frac{1}{n} \sum_{i=1}^{n} X_i \qquad (E.10)$$

and

$$b = \bar{Y} - a\bar{x} \qquad (E.11)$$

where

$$\bar{Y} = \frac{1}{n} \sum_{i=1}^{n} Y_i \qquad (E.12)$$

APPENDIX F

SAMPLE CALCULATION OF OXIDIZABLE COKE LEVEL

By titration 20ml of unreacted $Ba(OH)_2$ solution against a 0.105N HC1, 32.3ml of the acid was found to neutralize the $Ba(OH)_2$ solution completely.

$N_1V_1 = N_2V_2$

$N_1 = ?$

$V_1 = 20ml$

$N_2 = 0.105, \quad V_2 = 32.3ml$

$$\therefore \quad N_1 = \frac{0.105 \times 32.3}{20} = 0.1697N$$

i.e the strenght of the unreacted $Ba(OH)_2$ solution

= 0.1697N.

Molecular weight of $Ba(OH)_2$ = 171g

$\therefore$ Wt of $Ba(OH)_2$ in 150ml of 0.1697 N excess solution

$$= \frac{0.1697}{1} \times \frac{171}{2} \times \frac{150}{1000}$$

$$= 2.1769g$$

wt of $Ba(OH)_2$ in 150ml of 0.1734N sample solution.

$$= \frac{0.1734}{1} \times \frac{171}{2} \times \frac{150}{1000} = 2.2238g$$

$\therefore$ Amount reacted

$$= 2.2238 - 2.1769$$

$$= 0.0469g$$

Stoichiometry of reaction

$$Ba(OH)_2 + CO_2 \longrightarrow BaCO_3 + H_2O$$

171g of $Ba(OH)_2$ ⟶ 197g $BaCO_3$

$\therefore$ 0.0469g of $Ba(OH)_2$ produces

$$0.0469 \times \frac{197}{171} = 0.054g \text{ of } BaCO_3$$

gram Carbon in 197g of $BaCO_3$ = 12g

$\therefore$ in 0.054g $BaCO_3$

$$C = \frac{12}{197} \times 0.054$$

Coke level = 3.29×10^{-3}g C

Appendix G

Programme for the flexible polygon search of Nelder and Mead

```
#OPTIONS X,S=250,L=250
        DIMENSION X1(50,50) ,X(50) , SUM(50)
        COMMON/ERR/X,X1,NX,STEP,K1,SUM,IN
        COMMON/CONC/C(15,15),WDF(15),EC(15),CC(15)
        NX=4
        WRITE(1,*)'ENTER INITIAL GUESS OF RATE CONSTANTS'
        XNX=4
        DO 131 I=1,NX
             ACCEPT'NEXT GUESS',X(I)
131           CONTINUE
             ACCEPT'ENTER INITIAL STEP SIZE',STEP
         WRITE(1,*) 'INITIAL STEP SIZE IS ',STEP
       CALL OPEN (4,'B:DOMO3')
       DO 132 J=1,2
       DO 132 I=1,10
       READ(4,*)  C(J,I)
132    CONTINUE
              ALFA=1.0
       BETA=.5
       GAMA=2.0
       DIFER=0.0
       IN=1
       CALL SUMR
       WRITE(1,*) SUM(IN),(X(I),I=1,NX)
       K1=NX+1
       K2=NX+2
       K3=NX+3
       K4=NX+4
       CALL START
       DO 3 I= 1,K1
       DO 4 J= 1,NX
    4  X(J)=X1(I,J)
       IN=I
       CALL SUMR
    3  CONTINUE
C SELECT LARGEST VALUE OF SUM(I) IN SIMPLEX
   28  SUMH=SUM(1)
       INDEX=1
       DO 7 I=2,K1
       IF (SUM(I).LE.SUMH) GOTO 7
       SUMH=SUM(I)
       INDEX=I
    7  CONTINUE
C  SELECT MINIMUM VALUE OF SUM(I) IN SIMPLEX
       SUML=SUM(1)
```

```
      KOUNT=1
      DO 8 I=1,K1
      IF(SUML.LE.SUM(I)) GOTO 8
      SUML=SUM(I)
      KOUNT=I
    8 CONTINUE
C   FIND CENTROID OF PTS WITH I DIFFERNT FROM INDEX
      DO 9 J= 1,NX
      SUM2=0.
      DO 10 I=1,K1
   10 SUM2=SUM2 +X1(I,J)
      X1(K2,J)= 1.0/(XNX)*(SUM2-X1(INDEX,J))
C   FIND REFLECTION OF HIGH PT THROUGH CENTROID
      X1(K3,J)=(1.+ALFA)*X1(K2,J)-ALFA*X1(INDEX,J)
    9 X(J)=X1(K3,J)
      IN=K3
      CALL SUMR
      IF(SUM(K3).LT.SUML) GOTO 11
C   SELECT SECOND LARGEST VALUE IN SIMPLEX
      IF(INDEX.EQ.1) GOTO 38
      SUMS=SUM(1)
      GOTO 39
   38 SUMS=SUM(2)
   39 DO 12 I=1,K1
      IF((INDEX-I).EQ.0) GOTO 12
      IF(SUM(I).LE.SUMS) GOTO 12
      SUMS=SUM(I)
   12 CONTINUE
      IF(SUM(K3).GT.SUMS) GOTO 13
      GOTO 14
C   FORM EXPANSION OF NEW MINIMUM IF REFLECTION HAS PRODUCED ONE MI
   11 DO 15 J= 1,NX
      X1(K4,J) =(1.0-GAMA)*X1(K2,J) + GAMA*X1(K3,J)
   15 X(J)= X1(K4,J)
      IN=K4
      CALL SUMR
      IF (SUM(K4).LT.SUML) GOTO 16
      GOTO 14
   13 IF (SUM(K3).GT.SUMH) GOTO 17
      DO 18 J= 1,NX
   18 X1(INDEX,J)=X1(K3,J)
   17 DO 19 J= 1,NX
      X1(K4,J)=BETA*X1(INDEX,J)+(1.-BETA)*X1(K2,J)
```

```
   19  X(J)=X1(K4,J)
       IN=K4
       CALL SUMR
       IF(SUMH.GT.SUM(K4)) GOTO 16
C  REDUCE SIMPLEX BY HALF IF REFLECTION HAPPENS TO PRODUCE LARGER
C  UE THAN THE MAXIMUM
       DO 20 J=1 ,NX
       DO 20 I=1,K1
   20  X1(I,J)=.5*(X1(I,J)+X1(KOUNT,J))
       DO 29 I=1,K1
       DO 30 J=1,NX
   30  X(J)=X1(1,J)
       IN=I
       CALL SUMR
   29  CONTINUE
       GOTO 26
   16  DO 21 J= 1,NX
       X1(INDEX,J)=X1(K4,J)
   21  X(J)= X1(INDEX,J)
       IN=INDEX
            CALL SUMR
       GOTO 26
   14  DO 22 J= 1,NX
       X1(INDEX,J)=X1(K3,J)
   22  X(J)=X1(INDEX,J)
       IN=INDEX
       CALL SUMR
   26  DO 23 J=1,NX
   23  X(J)=X1(K2,J)
       IN=K2
       CALL SUMR
       DIFER=0.
       DO 24 I=1,K1
   24  DIFER=DIFER +(SUM(I)-SUM(K2))**2
       DIFER =1./XNX*SQRT(DIFER)
       TYPE
       TYPE'VALUES OF CALCULATED CONSTANTS'
       TYPE
WRITE(1,501) (I,X1(KOUNT,I),I=1,3)
WRITE(1,501) (I,X1(KOUNT,I),I=4,6)
WRITE(1,501) (I,X1(KOUNT,I),I=7,9)
WRITE(1,501) (I,X1(KOUNT,I),I=10,12)
501 FORMAT(1X,20(1X,'K(',I3,')=',1X,F8.4))
       TYPE
```

```
      TYPE 'SUM OF ERRORS SQUARED',SUML
      IF(DIFER.GE.0.000001 )GOTO 28
      CALL EXIT
      END
$OPTIONS X
      SUBROUTINE START
      DIMENSION A(50,50),X1(50,50),X(50), SUM(50)
      COMMON/ERR/ X,X1,NX,STEP,K1,SUM,IN
      COMMON/CONC/C(15,15),WDF(15),EC(15),CC(15)
      VN=NX
      STEP1=STEP/(VN*SQRT(2.))*(SQRT(VN+1.)+VN-1.)
      STEP2=STEP/(VN*SQRT(2.))*(SQRT(VN+1.)-1.)
      DO 1 J=1,NX
    1 A(1,J)=0.
      DO 2 I=1,K1
      DO 2 J=1,NX
      A(I,J)=STEP2
      L=I-1
      A(I,L)=STEP1
    2 CONTINUE
      DO 3 I= 1,K1
      DO 3 J= 1,NX
    3 X1(I,J)=X(J)+A(I,J)
      RETURN
      END
$OPTIONS X
      SUBROUTINE SUMR
      DIMENSION X1(50,50),X(50),SUM(50)
      DIMENSION R1(15),R1E(15),DIFF(15)
      COMMON/ERR/ X;X1,NX,STEP,K1,SUM,IN
      COMMON/CONC/C(15,15),WDF(15),EC(15),CC(15)
      R1E(1)=10.6; WDF(1)=0.025
      R1E(2)=7.6; WDF(2)=0.05
      R1E(3)=6.07; WDF(3)=0.075
      R1E(4)=5.15; WDF(4)=0.1
      R1E(5)=4.48; WDF(5)=0.125
      R1E(6)=3.95; WDF(6)=0.15
      R1E(7)=3.57; WDF(7)=0.175
      R1E(8)=3.275; WDF(8)=0.2
      R1E(9)=2.82; WDF(9)=0.25
      R1E(10)=2.23; WDF(10)=0.336
      DO 123 I=1,14
```

```
      RNUM=(X(1)*X(3)*C(1,I))-(X(2)*C(2,I)/X(5))
      DNUM=1+X(3)*C(1,I)+C(2,I)/X(5)


          R1(I)=RNUM/DNUM
      DIFF(I)=(R1E(I)-R1(I))**2
123   CONTINUE
C     CALCULATE EXPER CONVERSION,EC=R1E(I)*WDF(I)
C     CALCULATE COMPUTED CONVERSION,CC=R1(I)*WDF(I)
TYPE
TYPE'        W/F                EXP. CONVR.          CAL. CONVR.
DO 478 I=1,10
EC(I)=R1E(I)*WDF(I)
CC(I)=R1(I)*WDF(I)
478    CONTINUE
C      WRITE OUT RESULTS ON SCREEN
DO 480 I=1,10
480TYPE WDF(I),EC(I),CC(I)
      SUM(IN)=0.0
      DO 124 I=1,10
 124  SUM(IN)=SUM(IN)+DIFF(I)


        RETURN
SUM(IN)=-X(1)*X(11)*X(2)*X(3) +X(4)*(X(1)*X(2) +2*X(2)*X(3))
SUM(IN)=SUM(IN)+X(4)*(2*X(1)*X(3)-108.0)
SUM(IN)=SUM(IN)-AMDA*(X(1)+X(2)+X(3)+X(4))
      RETURN
      END
```

```
C     PROGRAMME TO DETERMINE THE MODEL OF CATALYST COKING DEACTIVATION
C     ----------------------------------------------------------------
C    ****************************************************************
C         DEACTIVATION STUDIES USING N-OCTANE * BY ONUKWULI,O.D *
C       ----------------------------------------------------------
          REAL XT(30),YT(30),ACT(30),YACT(30),CN(30),CP(30),MX(30)
          REAL CIS(30),EB(30),DEFC(30),ERROR(30),XAREA(30),CONC(30)
          REAL PX(30),OX(30)
          OPEN(UNIT=1,FILE='ONU1.DAT')
          OPEN(UNIT=2,FILE='CON')
 1000     READ(1,50) ITIME,ND,LRUN
          IF(ITIME.EQ.0) GO TO 31
C  READ THE VALUES OF TOTAL CONVERSION AND YIELD IN REGULAR TIME
C  INTERVALS  STARTING WITH THE VALUES AT TIME EQUAL TO ZERO
          DO 111 N=1,ND
          READ(1,55) XT(N),CN(N),CP(N),CIS(N),EB(N),MX(N),PX(N),OX(N)
 111      CONTINUE
          WRITE(2,61)LRUN
          DO 10 K=1,ND
          YT(K)=XT(K)
C  CALCULATE ACTIVITY FROM TOTAL CONVERSION
          ACT(K)=YT(K)/YT(1)
          WRITE(2,62)YT(K),ACT(K)
 10       CONTINUE
          DO 11 L=1,3
          DO 12 M=1,6
          DO 13 IH=1,3
          N=L-1
C CHECK ON DIVISION BY ZERO DURING CALCULATION OF DEACTIVATION FUNCTION
          INDEX=N-IH-1
          IF(INDEX.EQ.0)GO TO 13
C  SET THE INITIAL TOTAL AREA UNDER THE CURVE EQUAL TO ZERO AS WELL AS
C  THE SUMMATION OF THE PRODUCT OF YT AND XT
          YMSUM=0.0
          XMSUM=0.0
          AREL=0.0
          XYS1=0.0
          XYS2=0.0
          XSQS1=0.0
          XSQS2=0.0
          XS1=0.0
          XS2=0.0
          YS1=0.0
          YS2=0.0
          DO 14 MN=1,ND
          X=M
C  CALCULATE CONCENTRATION OF THE PRODUCTS TO THE APPROPRIATE POWER
          CNUM=(27.782*(CN(MN)**(N+IH))-(0.267*(EB(MN)**(N+IH))))
          CDEN1=1.0+0.7174*CN(MN)+(CIS(MN)/4.94)+(CP(MN)/1.3123)+1.0/5.35
          CDEN2=(EB(MN)/4.46)+(OX(MN)/9.9)+(MX(MN)/7.0)+(PX(MN)/12.22)
          CDEN=(CDEN1+CDEN2)**FLOAT(IH)
          CONC(MN)=CNUM/CDEN
          IF(N.EQ.1)GO TO 110
          YACT(MN)=ACT(MN)**(FLOAT(INDEX)/X)
          GO TO 120
```

```
 110     YACT(MN)=1/(ACT(MN)**(FLOAT(IH)/X))
C  FIND AREA UNDER THE CURVE USING SIMPSON'S RULE
 120     J=MN-1
         IF(J.EQ.0)GO TO 14
         XAREA(MN)=AREL+(ITIME*(CONC(MN)+CONC(J)))/((ND-1)*2)
         AREL=XAREA(MN)
C  PARAMETERS TO DETERMINE THE SLOPE AND INTERCEPT OF THE GRAPH
C  USING LEAST SQUARE FIT METHOD
         XY2=XAREA(MN)*YACT(MN)
         XYS2=XYS2+XY2
         XS2=XS2+XAREA(MN)
         YS2=YS2+YACT(MN)
         XSQ2=XAREA(MN)**2
         XSQS2=XSQS2+XSQ2
  14     CONTINUE
C  CALCULATE INTERCEPT AND SLOPE
         SINT=(XYS2*XS2-YS2*XSQS2)/(XS2**2-(ND-1)*XSQS2)
         SLOPE=((ND-1)*XYS2-XS2*YS2)/((ND-1)*XSQS2-XS2**2)
C  NOW TEST FOR PERCENTAGE LINEARITY USING LEAST SQUARE METHOD
         XMEAN=XS2/(ND-1)
         YMEAN=YS2/(ND-1)
         DO 15 IL=1,ND
         IF(IL.EQ.1) GO TO 15
         XMSUM=XMSUM+((XAREA(IL)-XMEAN)**2)/FLOAT(ND)
         YMSUM=YMSUM+((YACT(IL)-YMEAN)**2)/FLOAT(ND)
  15     CONTINUE
         XSTDV=SQRT(XMSUM)
         YSTDV=SQRT(YMSUM)
         TEST=(SLOPE*XSTDV/YSTDV)*100.0
C  PICK MODELS WITH 99.9% LINEARITY OR BETTER
         IF(SLOPE.LT.0.0)GO TO 13
         IF(TEST.GT.99.8.OR.TEST.LT.-99.8)GO TO 130
         GO TO 13
 130     IF(IH.GT.1)GO TO 140
         WRITE(2,63)
         GO TO 150
 140     WRITE(2,64)
 150     WRITE(2,65)N,M,IH
         WRITE(2,66)TEST,SLOPE,SINT
         WRITE(2,67)
C  NOW USE THE MODEL TO PREDICT ACTIVITY AND THE PERCENTAGE ERROR
         DO 16 J=1,ND
         IF(J.EQ.1)GO TO 16
         XM=SLOPE*XAREA(J)+SINT
         IF(XM.LE.0.0) GO TO 16
         DEFC(J)=(SLOPE*XAREA(J)+SINT)**(X/FLOAT(INDEX))
         ERROR(J)=(ACT(J)-DEFC(J))*100.0/ACT(J)
         WRITE(2,68)DEFC(J),ERROR(J)
  16     CONTINUE
C        GO TO 13
  13     CONTINUE
  12     CONTINUE
  11     CONTINUE
         GO TO 1000
  61     FORMAT(4X,'***RUN NO. ',I3,'**** ',/2X,'TOTAL CONVERSION',4X,
```

```
     $   'EXP. ACTIVITY').
  62     FORMAT(6X,F7.5,12X,F7.5)
  63     FORMAT(4X,'SINGLE-SITE COKING STEP',/4X,23('-'),/)
  64     FORMAT(4X,'DOUBLE-SITE COKING STEP',/4X,23('-'),/)
  65     FORMAT(4X,'NO. OF UNADSORBED GAS MOLECULES REACTING (N)= ',I2,//
     $4X,'NO. OF ACTIVE SITES PARTICIPATING IN MAIN RXN. (M) =',I2,//
     #4X,'NO. OF ACTIVE SITES PARTICIPATING IN COKING RXN (H)= ',I2)
  66     FORMAT(4X,'PERCENTAGE LINEARITY = ',F7.3,'%',4X,'SLOPE = ',
     $   E10.3,/4X,'INTERCEPT = ',E10.3)
  67     FORMAT(/4X,'PREDICTED ACTIVITY',6X,'% ERROR')
  68     FORMAT(8X,F10.5,11X,F9.5)
  50     FORMAT(3I3)
  55     FORMAT(8F6.3)
  31     STOP
         END
```

```
C     PROGRAMME TO DETERMINE THE MODEL OF CATALYST COKING DEACTIVATION
C     ---------------------------------------------------------------
C    ***************************************************************
C        DEACTIVATION STUDIES USING ISO-OCTANE  * BY ONUKWULI,O.D *
C      -------------------------------------------------------------
         REAL XT(30),YT(30),ACT(30),YACT(30),CA(30),CB(30)
         REAL DEFC(30),ERROR(30),XAREA(30),CONC(30)
         OPEN(UNIT=1,FILE='ONU3.DAT')
         OPEN(UNIT=2,FILE='PRN')
 1000    READ(1,50) ITIME,ND,LRUN
         IF(ITIME.EQ.0) GO TO 31
C  READ THE VALUES OF TOTAL CONVERSION AND YIELD IN REGULAR TIME INTERVALS
C  STARTING WITH THE VALUES AT TIME EQUAL TO ZERO
         DO 111 N=1,ND
         READ(1,55) XT(N)
 111     CONTINUE
         WRITE(2,61)LRUN
         DO 10 K=1,ND
         YT(K)=XT(K)
         CB(K)=XT(K)
         CA(K)=1.0-XT(K)
C  CALCULATE ACTIVITY FROM TOTAL CONVERSION
         ACT(K)=YT(K)/YT(1)
         WRITE(2,62)YT(K),ACT(K)
 10      CONTINUE
         DO 11 L=1,3
         DO 12 M=1,6
         DO 13 IH=1,3
         N=L-1
C  CHECK ON DIVISION BY ZERO DURING CALCULATION OF DEACTIVATION FUNCTION
         INDEX=N-IH-1
         IF(INDEX.EQ.0)GO TO 13
C  SET THE INITIAL TOTAL AREA UNDER THE CURVE EQUAL TO ZERO AS WELL AS
C  THE SUMMATION OF THE PRODUCT OF YT AND XT
         YMSUM=0.0
         XMSUM=0.0
         AREL=0.0
         XYS1=0.0
         XYS2=0.0
         XSQS1=0.0
         XSQS2=0.0
         XS1=0.0
         XS2=0.0
         YS1=0.0
         YS2=0.0
         DO 14 MN=1,ND
         X=M
C  CALCULATE CONCENTRATION OF THE PRODUCTS TO THE APPROPRIATE POWER
         CNUM=(272.20*(CA(MN))**(N+IH))-(0.977*(CB(MN))**(N+IH))
         CDEN=(1.0+11.960*CA(MN)+(3.52E-04*CB(MN)))**FLOAT(IH)
         CONC(MN)=CNUM/CDEN
         IF(N.EQ.1)GO TO 110
         YACT(MN)=ACT(MN)**(FLOAT(INDEX)/X)
         GO TO 120
 110     YACT(MN)=1/(ACT(MN)**(FLOAT(IH)/X))
```

```
C  FIND AREA UNDER THE CURVE USING SIMPSON'S RULE
 120     J=MN-1
         IF(J.EQ.0)GO TO 14
         XAREA(MN)=AREL+(ITIME*(CONC(MN)+CONC(J)))/((ND-1)*2)
         AREL=XAREA(MN)
C  PARAMETERS TO DETERMINE THE SLOPE AND INTERCEPT OF THE GRAPH
C  USING LEAST SQUARE FIT METHOD
         XY2=XAREA(MN)*YACT(MN)
         XYS2=XYS2+XY2
         XS2=XS2+XAREA(MN)
         YS2=YS2+YACT(MN)
         XSQ2=XAREA(MN)**2
         XSQS2=XSQS2+XSQ2
  14     CONTINUE
C  CALCULATE INTERCEPT AND SLOPE
         SINT=(XYS2*XS2-YS2*XSQS2)/(XS2**2-(ND-1)*XSQS2
         SLOPE=((ND-1)*XYS2-XS2*YS2)/((ND-1)*XSQS2-XS2**2)
C  NOW TEST FOR PERCENTAGE LINEARITY USING LEAST SQUARE METHOD
         XMEAN=XS2/(ND-1)
         YMEAN=YS2/(ND-1)
         DO 15 IL=1,ND
         IF(IL.EQ.1) GO TO 15
         XMSUM=XMSUM+((XAREA(IL)-XMEAN)**2)/FLOAT(ND)
         YMSUM=YMSUM+((YACT(IL)-YMEAN)**2)/FLOAT(ND)
  15     CONTINUE
         XSTDV=SQRT(XMSUM)
         YSTDV=SQRT(YMSUM)
         TEST=(SLOPE*XSTDV/YSTDV)*100.0
C  PICK MODELS WITH 99.9% LINEARITY OR BETTER
         IF(SLOPE.LT.0.0)GO TO 13
         IF(TEST.GT.87.0.OR.TEST.LT.-99.8)GO TO 130
         GO TO 13
 130     IF(IH.GT.1)GO TO 140
         WRITE(2,63)
         GO TO 150
 140     WRITE(2,64)
 150     WRITE(2,65)N,M,IH
         WRITE(2,66)TEST,SLOPE,SINT
         WRITE(2,67)
C  NOW USE THE MODEL TO PREDICT ACTIVITY AND THE PERCENTAGE ERROR
         DO 16 J=1,ND
         IF(J.EQ.1)GO TO 16
         XM=SLOPE*XAREA(J)+SINT
         IF(XM.LE.0.0) GO TO 16
         DEFC(J)=(SLOPE*XAREA(J)+SINT)**(X/FLOAT(INDEX))
         ERROR(J)=(ACT(J)-DEFC(J))*100.0/ACT(J)
         WRITE(2,68)DEFC(J),ERROR(J)
  16     CONTINUE
C        GO TO 13
  13     CONTINUE
  12     CONTINUE
  11     CONTINUE
         GO TO 1000
  61     FORMAT(4X,'***RUN NO. ',I3,'**** ',/2X,'TOTAL CONVERSION',4X,
     $   'EXP. ACTIVITY')
```

```
62     FORMAT(6X,F7.5,12X,F7.5)
63     FORMAT(4X,'SINGLE-SITE COKING STEP',/4X,23('-'),/)
64     FORMAT(4X,'DOUBLE-SITE COKING STEP',/4X,23('-'),/)
65     FORMAT(4X,'NO. OF UNADSORBED GAS MOLECULES REACTING (N)= ',I2,//
    $4X,'NO. OF ACTIVE SITES PARTICIPATING IN MAIN RXN. (M) =',I2,//
    #4X,'NO. OF ACTIVE SITES PARTICIPATING IN COKING RXN (H)= ',I2)
66     FORMAT(4X,'PERCENTAGE LINEARITY = ',F7.3,'%',4X,'SLOPE = ',
    $  E10.3,/4X,'INTERCEPT = ',E10.3)
67     FORMAT(/4X,'PREDICTED ACTIVITY',6X,'% ERROR')
68     FORMAT(8X,F10.5,11X,F9.5)
50     FORMAT(3I3)
55     FORMAT(F6.3)
31     STOP
       END
```

NOMENCLATURE

MCP	Methylcyclopentane
$MCP^{=}$	Methylcyclopentene
$CH^{=}$	Cyclohexene
CH	Cyclohexane
ΣC_6	Hydrogenolysis products
$\Sigma C_6^{=}$	Olefinic hydrogenolysis products
B_z	Benzene
S	Active Site
MCPS	Adsorbed Methylcyclopentane
$MCP^{=}S$	Adsorbed Methylcyclopentene
$CH^{=}S$	Adsorbed Cyclohexene
CHS	Adsorbed Cyclohexane
$\Sigma C_6 S$	Adsorbed hydrogenolysis Products
$\Sigma C_6^{=}S$	Adsorbed Olefinic Hydrogenolysis Products
k	Rate Constant
K	Equilibrium Constant
r	Rate of reaction
B_{zs}	Adsorbed benzene

N		Normal Octane
CP	=	Hydrocracked Products
I	=	Iso Octane
EB	=	Ethyl Benzene
MX	=	Meta Xylene
OX	=	Ortho Xylene
PX	=	Para Xylene
NS	=	Adsorbed Normal Octane
IS	=	Adsorbed Iso Octane
EBS	=	Adsorbed Ethyl Benzene
OXS	=	Adsorbed Ortho Xylene
S	=	Free Active Site of Catalyst
MXS	=	Adsorbed Meta Xylene
PXS	=	Adsorbed Para Xylene
P_{H_2}	=	Hydrogen partial pressure

N-OCTANE REACTION PRODUCTS

1. Iso-Octane
2 Hydrocracked products
3. Ethylbenzene
4. O-xylene
5. P- xylene
6. M- xylene
7. Toluene

A = ISO_1 = Iso Octane (Reactant)

M = Iso_1 = Iso Octene (Formed from reactant)

N = Iso_2 = Iso Octene (That which formed Product)

B = Iso_2 = Iso Octane (Product)

1 = active site (metal)

S = active site (acidic)

Al = Adsorbed Iso Octave (Reactant) on metal site.

Ml = Adsorbed iso octane (formed from reactant) on metal site

Nl = Adsorbed iso Octene (That which formed product) on metal site.

Bl = Adsorbed iso Octane (That which forms product) on metal site)

MS = Adsorbed iso octene (formed from reactant) on acidic site

NS = Adsorbed iso octene (That which formed product) on acidic site).

P_N = Methylcyclopentane partial pressure

P_{iso} = Iso-octane partial pressure

k_i = rate constant

K_i = equilibrium constant

A = Reactant

M = Reactant that forms coke precursor (If only one reactant A is present A=M)

ℓ = active site

$C_{A\ell}$ $C_{R\ell}$, $C_{M\ell}$ = Concentration of the species $M\ell$, $A\ell$ and $R\ell$ on the surface of the catalyst.

C_ℓ = Concentration of vacant active site

n = number of molecules in gaseous phase which react with h molecules adsorbed to give the coke precusor

ψ = deactivation function

m = number of active sites involved in the controlling step of the main reaction

P_1 = Coke precusor

P_2, P_3 = forms of coke

P_m = Partial pressure of m

a = Catalyst activity

k_d = deactivation constant

K_A, K_R, K_m = equilibrium constants of A, R. M

K_m' = $K_1\ K_2\ K_m$

K_m'' = $K_1 K_A + K_1 K_2 K_A$

γ = Relates the micropores in which deactivation takes place by both the site coverage and poreblockage

δ/V = number of sites per micropore

S (Froment) = Activity of catalyst at time t ,

δ = Standard deviation